SCUOLA DI DOTTORATO
UNIVERSITÀ DEGLI STUDI DI MILANO-BICOCCA

Dipartimento di / Department of BIOTECHNOLOGY AND BIOSCIENCES

Dottorato di Ricerca in / PhD program:
BIOLOGY AND BIOTECHNOLOGY
Ciclo / Cycle: XXXII

INVESTIGATION OF MOLECULAR AND CELLULAR MECHANISMS UNDERPINNING Cd-INDUCED CARCINOGENESIS THROUGH *IN VITRO* AND *IN SILICO* APPROACHES.

Cognome / Surname: OLDANI Nome / Name: MONICA

Matricola / Registration number: 729318

Tutore / Tutor: PAOLA ALESSANDRA FUSI

Coordinatore / Coordinator: PAOLA BRANDUARDI

ANNO ACCADEMICO / ACADEMIC YEAR:
2018/2019

CONTENTS

ABSTRACT

Cadmium (Cd) is a heavy metal, commonly found in the earth's crust combined with other elements such as oxygen, chlorine, or sulfur. However, having been released into the environment for decades by anthropogenic activities (Thevenod, 2009), Cd is now considered one of the most common environmental contaminants. In particular, Cd can occur in air, water, soil and subsoil. Workers are mainly exposed to the inhalation of Cd-containing particles. The non-occupational population absorbs low concentrations of Cd through cigarette smoking, ingestion of contaminated water and food. In 1993, Cd was classified by the World Health Organization's International Agency for Research on Cancer (IARC) as a human carcinogen (Group 1). However, the molecular mechanisms underpinning Cd carcinogenicity are still not fully understood. As a non-genotoxic agent, it cannot directly cause DNA mutations; it can instead act through the alteration of epigenetic mechanisms and gene expression, the induction of oxidative stress, the inhibition of DNA repair mechanisms and the interaction with proteins involved in cell cycle control, apoptosis and cellular defense system. Moreover, Cd can interfere with the homeostasis of many essential metals, such as zinc, calcium and iron; it is able to displace zinc from zinc-finger proteins, impairing their functionality. To better investigate Cd-induced carcinogenesis, we decided to use the Cell Transformation Assay (CTA), one of the most advanced *in vitro* tests to screen the carcinogenic potential and to understand the mechanism of action of chemical substances. Indeed, these assays offer several advantages in comparison to the *in vivo* bioassays in rodents, especially their ability to reproduce key stages of *in vivo* transformation.

In this context, the purposes of this thesis work were: i) to investigate the mechanisms by which cadmium induces cellular transformation; ii) to implement one of the most promising *in vitro* assays to assess the potential of chemical carcinogenesis.

We exploited the use of CTA by jointly applying different techniques. We first carried out a transcriptomic analysis to evidence deregulated pathways in C3H10T1/2Cl8 after 24h of Cd treatment and in *foci*-derived transformed cells. These two conditions have allowed to analyze early events inducing the malignant phenotype and the features of transformed cells. Consequently, we focused on metabolic rewiring and modifications of mitochondrial structure and function caused by Cd. We applied Seahorse assays, enzyme activity and metabolite assays to the first aim; to the second purpose, we applied laser scanning confocal

fluorescence microscopy, image analysis and flow cytometry technique. Finally, we compared the transcriptome of two different human cell lines: hepatocellular carcinoma HepG2 cells and neuroblastoma SHSY5Y cells, in the search for genes deregulated in both the cell lines.

Due to the limits of the current methods in adequately addressing the identification of non-genotoxic chemicals, the scientific and regulatory community has recognised the need to develop the so-called Integrated Approach to Testing and Assessment (IATA) (Corvi et al., 2017). This approach considers all the existing information, including environmental and epidemiological data, traditional and alternative toxicity tests, to analyse multiple endpoints related to cancer hallmarks and to improve the assessment of the carcinogenic potential of a substance. In this perspective, the present thesis project included mechanistic studies and i*n vitro* assays on the basis of an integrated approach which, using multiple sources, is able to provide many useful information for the understanding of the carcinogenesis process and the underlying mechanisms.

RIASSUNTO

Il cadmio (Cd) è un metallo pesante che si può trovare sulla crosta terrestre associato con altri elementi più comuni, come l'ossigeno, il cloro e lo zolfo. Tuttavia, essendo stato massicciamente rilasciato nell'ambiente dall'uomo, il Cd è attualmente considerato uno dei più comuni inquinanti ambientali. Infatti, è presente in tutti i comparti (aria, acque, suolo e sottosuolo). I lavoratori sono maggiormente esposti all'inalazione di particelle contenenti Cd, mentre la popolazione non occupazionalmente esposta entra in contatto con il Cd attraverso il fumo di sigaretta e l'ingestione di acque e cibi contaminati. Nel 1993, il Cd è stato classificato come cancerogeno (gruppo 1) per l'uomo dall'Agenzia Internazionale per la Ricerca sul Cancro (IARC), ma i meccanismi molecolari alla base della sua cancerogenesi sono ancora poco noti. Sappiamo però che il Cd è un agente non genotossico. Questo metallo non provoca direttamente mutazioni del DNA, ma può agire mediante l'alterazione dei meccanismi epigenetici e dell'espressione genica, l'induzione di stress ossidativo, l'inibizione dei meccanismi di riparo del DNA e l'interazione con proteine coinvolte nel controllo del ciclo cellulare, nell'apoptosi e nelle difese cellulari. Il Cd può inoltre interferire con l'omeostasi di molti metalli essenziali, tra cui lo zinco, il calcio e il ferro. In particolare, il Cd sembra essere in grado di sostituire lo zinco nelle proteine che possiedono motivi zinc-finger, compromettendone la funzionalità. Per studiare più approfonditamente la carcinogenesi indotta da Cd, abbiamo deciso di utilizzare il Cell Transformation Assay (CTA), uno dei test in vitro più avanzati per lo screening del potenziale di cancerogenesi e per comprendere il meccanismo d'azione delle sostanze chimiche. In effetti, questi saggi sono in grado di riprodurre le fasi chiave delle trasformazioni neoplastiche in vivo. In questo contesto, gli scopi di questo lavoro di tesi sono stati: i) studiare i meccanismi attraverso cui il Cd induce la trasformazione cellulare; ii) implementare uno dei test in vitro più avanzati per valutare il potenziale della carcinogenesi chimica. Abbiamo prima analizzato il transcrittoma delle C3H10T1 / 2Cl8 dopo 24 ore di trattamento con Cd e di cellule completamente trasformate (foci). Poi ci siamo concentrati sulle modifiche metaboliche e/o nella morfologia e nella funzione dei mitocondri causate dal Cd. Abbiamo applicato la tecnica del Seahorse, saggi enzimatici e dei metaboliti per verificare la prima ipotesi; la microscopia confocale a fluorescenza a scansione laser, l'analisi d iimmagine e la citometria a flusso per la seconda. Alla fine, abbiamo confrontato il transcrittoma di due diverse linee cellulari umane: le HepG2 e SHSY5Y. La prima è una linea cellulare di carcinoma

epatico, la seconda è una linea cellulare di neuroblastoma. L'OECD ha stabilito che il CTA rappresenta il saggio centrale per la valutazione della cancerogenesi nell'ambito di un approccio integrato. In particolare, a causa dei limiti delle attuali metodologie nell'affrontare adeguatamente l'identificazione di sostanze chimiche non genotossiche, la comunità scientifica e normativa ha riconosciuto la necessità di sviluppare il cosiddetto Integrated Approach to Testing and Assessment (IATA). Tale approccio considera tutte le informazioni disponibili, incluse quelle derivanti da dati ambientali ed epidemiologici per analizzare più endpoint cellulari e molecolari correlati agli hallmark del cancro e migliorare la valutazione del potenziale di cancerogenicità di una sostanza. In quest'ottica, si è inserito il presente progetto di tesi, in cui studi di tipo meccanicistico, tra cui quelli in silico, sono stati affiancati da saggi in vitro sulla base di un approccio integrato che è in grado di fornire numerose informazioni utili alla comprensione del processo di cancerogenesi e dei meccanismi sottostanti.

LIST OF ABBREVIATIONS

α-KG α-keto-glutarate

AACR American Association for Cancer Research

ADI Acceptable Daily Intake

AO Adverse Outcome

AOPs Adverse Outcome Pathways

ALS Amyotrophic Lateral Sclerosis

ATSDR Agency for Toxic Substances and Disease Registry

BCF BioConcentration Factor

BER Base Excision Repair

CADD Computer Aided Drug Design

CLCE Chronic low doses Cd exposure

CNS Central Nervous System

CONTAM the Scientific Panel on Contaminants in the Food Chain

CTA Cell Transformation Assay

CVD CardioVascular Disease

DOM Dissolved Organic Matter

DRAs Drug Regulatory Authorities

DRP Detailed Review Paper

EC European Commission

ECHA European CHemicals Agency

ECM Extracellular Matrix

EFc crustal Enrichment Factors

EFSA European Food and Safety Authority

EMA The European Medicines Agency

EMT Epithelial–Mesenchymal Transition

ENTPD5 Ectonucleoside Triphosphate Diphosphohydrolase 5

ETC Electron Transfer Chain

EU European Union

EURL ECVAM European Union Reference Laboratory for the Validation of Alternative Methods

FAO Food and Agriculture Organization

FDA Food and Drug Administration

GI GastroIntestinal

GG-NER Global Genome Repair

GSSG Oxidised Glutathione

HK2 Hexokinase 2

IARC International Agency of Research on Cancer

IATA Integrated Approach to Testing and Assessment

ICH International Council on Harmonisation of Technical Requirements for Registration of Pharmaceuticals for Human Use

IMT Intima-Media Thickness

KEs Key Events

JECFA Joint Expert Committee on Food Additives and Contaminants

LH Luteinizing Hormone

LMWP Low Molecular Weight Proteins

MAPK Mitogen-Activated Protein Kinases

MIE Molecular Initiating Event

MMR Mismatch Repair

MTs Metallothionein

NCI National Cancer Institute

NGTxC Non-Genotoxic Carcinogens

NER Nucleotide Excision Repair

NOAEL No Observed Adverse Effect Level

NTP National Toxicology Program

OECD Organisation for Economic Co-operation and Development

OXPHOS Mitochondrial Oxidative Phosphorylation

PTWI Provisional Tolerable Weekly Intake

PVC Polyvinyl Chloride Polymers

QSAR Quantitative Structure Activity Relationship

RBP Retinol-Binding Protein

RCBs Rodent Cancer Bioassays

REACH Registration, Evaluation and Authorisation of Chemicals

ROS Reactive Oxygen Species

RND Regulatory Notice Document

SA Structure-Activity

SARs Structure Activity Relationship

SHE Syrian Hamster Embryo

SMR Standardised Mortality Ratio

TCA Tricarboxylic Acid Cycle

TPA 12-O-tetradecanoylphorbol-13-acetate

VICH International Cooperation on Harmonisation of Technical Requirements for Registration of Veterinary Medicinal Products

WHO World Health Organization

Introduction

Chapter 1

1. Cancer

❖ 1.1.Introduction

"Cancer is a growing public health concern which requires increased attention, prioritization and funding" (WHO Assembly Resolution, 2017)

Cancer is the name given to a collection of heterogeneous diseases that arise when some of the body's cells begin to divide uncontrollably and spread into surrounding tissues (NIH NCI, 2018). When human cells are old or damaged, new cells take their place, while, in cancer development this orderly process breaks down. With these simplistic premises, at the end of the 19th century, the level of optimism in the field of cancer research was high: the American Association for Cancer Research (AACR) in 1907 stated that the discovery of the cause of cancer was "just around the corner" (Weinstein et al., 2008). However, cancer has continued to circumvent our complete understanding and therapies so far: cancer remains one of the leading causes of morbidity and mortality worldwide, with 18,1 million new cases and 9,6 million cancer-related deaths in 2018 (Bray et al., 2018). More in detail, one in five men and one in six women develop cancer during their lifetime, while one in eight men and one in eleven women die from this disease (IARC, 2018). It is also estimated that this tendency is on the rise: the number of new expected cases is projected to increase to 24.1 million per year no later than 2030, and up to 29.5 million in 2040 (Madia et al., 2019). The principal challenge in cancer research was and keeps on being the vast catalogue of cancer genotypes and target organs. In addition, it is known that tumorigenesis is not the consequence of a single event or mutation, but it is a multistep process, in which each step, from pre-cancerous lesions to fully malignant phenotypes, is critical for its investigating and treating. For instance, in each foremost step of carcinogenesis (initiation, promotion and progression), a succession of randomly changes in cell genomes and epigenomes occur to confer advantageous cell phenotypes (Figure 1.1). Hence, this process that mimics the Darwinian evolution in the microcosm of a tissue, also mimics all the difficulties in understanding the rules and criteria of evolution (Chaffer et al., 2015). In an evolutionary point of view, cancer can be considered as a result of an adaptive response of species to rapid changes in the environment (Aktipis et al., 2013). On the other hands, in 2000, Hanahan

and Weinberg published their influential review to order the complexities of cancer biology into main alterations shared by all types of tumour cells: the hallmarks of cancer (henceforth termed Hallmarks I and showed in green in Figure 1.2). The six described hallmarks were self-sufficiency in growth signals, insensitivity to anti-growth signals, evasion of the apoptosis, limitless replicative potential, sustained angiogenesis, and tissue invasion and metastasis. A decade later, an updating review supplemented the first cancer features with two other innovative hallmarks and two qualifying features. The dysregulation of energy metabolism and the avoidance of the immune response became Hallmarks II, while genome instability and tumour-promoting inflammation were new traits (Hanahan and Weinberg, 2011; Fouad et al, 2017). Connected with the dysregulation of energy metabolism (Hallmarks II), the Warburg effect needs to be cited: it can be described as the reverse of the Pasteur effect (the inhibition of fermentation by O_2) (Koppenol et al., 2011). Indeed, in 1920, Warburg and Cori demonstrated that cancer avidly consumes glucose and excrete lactate, although oxygen was present (Cori et al., 1925; Warburg et al., 1927). Subsequently, they have proven that this phenomenon of aerobic glycolysis was shared by several tumor types, such as breast, lung and glioblastoma (Wu et al., 2007; Lai et al., 2013). However, the observations that cancer cells may concurrently oxidise and ferment glucose has engendered uncertainty over the role of mitochondrial respiration in the Warburg effect. Warburg himself promoted the erroneous idea that damaged respiration was the *sine qua non* that increased glucose fermentation in cancers (Koppenol et al., 2011). Today, it is more evident that the increment in glycolysis under aerobic conditions is connected with a mitochondrial dysfunction, but not with the complete damage of cell respiration. Moreover, Fantin et al. (2006) and Bui et al. (2006) stated that both oxidative phosphorylation and glycolysis were active in cancer cells. Indeed, in the experiments in which glycolysis is suppressed, most tumor cells are able to produce ATP with the oxidative phosphorylation. On the other hand, it has been shown that mitochondria dysfunctions contribute to the development and progression of cancer and other relevant diseases (Czarnecka et al., 2007). The importance of these two cancer features (mitochondria dysfunction and Warburg effect) is extensively outlined in Chapter 3, being one of the critical issues of the presented research.

Figure 1.1. Graphical representation of the three-phase process of carcinogenesis upon carcinogen administration (Burgio et al., 2014).

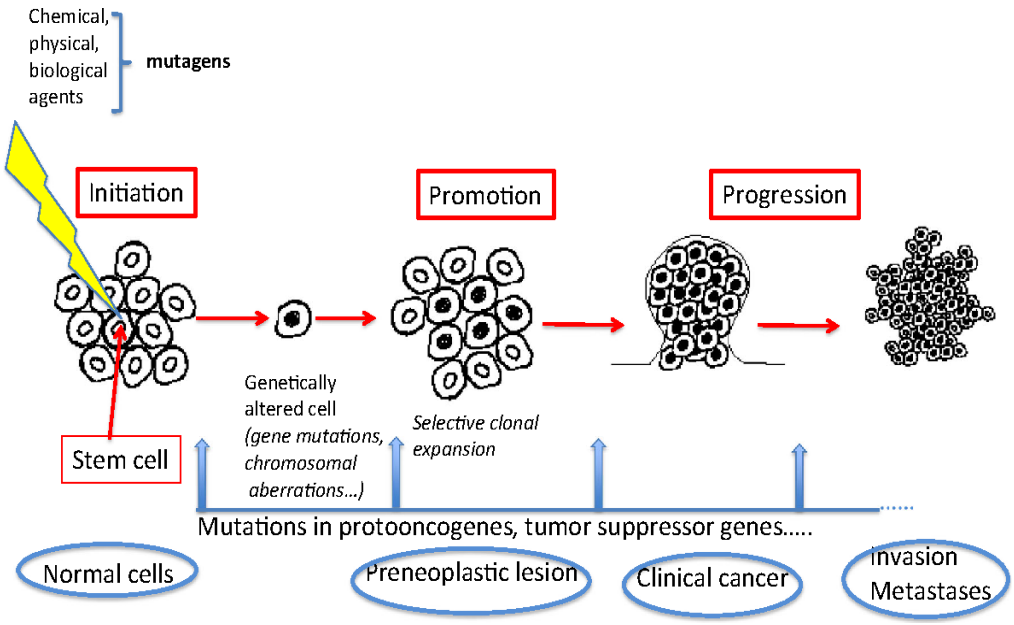

Figure 1.2. Graphical representation of the hallmarks of cancer (modified from Broertjes et al., 2015).

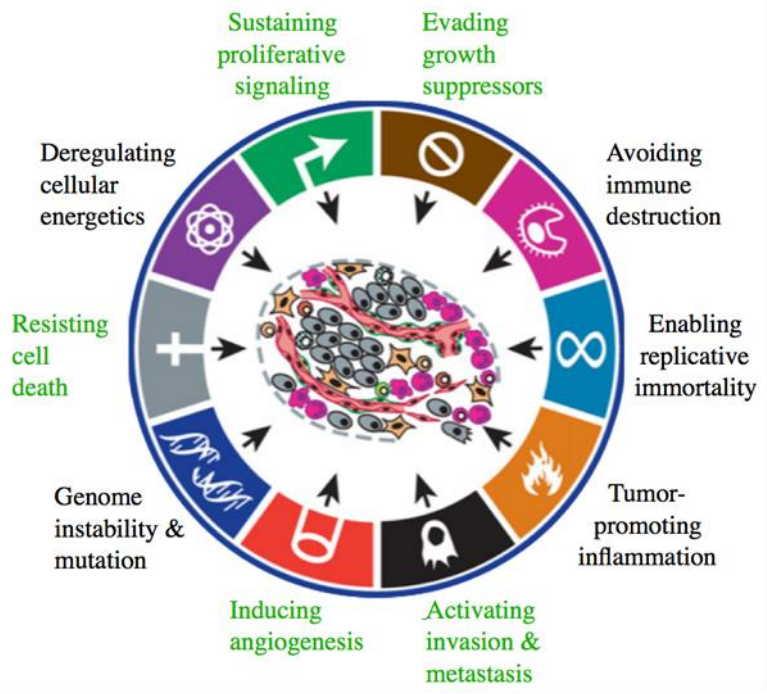

❖ 1.2 The multitude and diversity of cancer risk factors

"[…] *to ensure healthy lives and promote well-being for all at all ages*",
"[…] *to substantially reduce the number of deaths and illnesses from hazardous chemicals and air, water and soil pollution and contamination*" (United Nations, 2015).

It is usually not possible to know exactly why one person develops cancer, but research has shown that risk factors may increase a person's chances of developing this disease. Indeed, lifestyle, growth and ageing of the population, and individual genetic factors cannot fully explain the present growing incidence of cancer. Both genetic and environmental factors influence cancer development, including marked regional and socioeconomic disparities, the resources dedicated to preventive medicine, hygiene levels, and the occupational and environmental control of hazardous chemicals (Bray et al., 2012; Madia et al., 2019). Environmental factors such as microorganisms (including viruses), radiations (including UV and pulsed electromagnetic fields) and exposure to chemical agents may play a more critical role in carcinogenesis than it is expected (Belpomme et al., 2007; Wu et al., 2016). For this reason, the exposure to recognised or potentially chemical carcinogens, that is an inevitable consequence of modern society and environmental pollution, has become an issue of concern in many countries. Of primary concerns are substances contained in outdoor air, indoor air and tobacco smoke such as particulate matter, formaldehyde and volatile organic compounds (benzene); alternatively, there are food additives and contaminants such as nitrates, pesticides, carcinogenic metals, metalloids, pharmaceutical medicines and cosmetics (Belpomme et al., 2007). This long list of possible carcinogenic and mutagenic factors supports the hypothesis and concerns according to which the recent modifications of our environment may induce cancer. The most reliable evidence of the correlation between cancer occurrence and chemical exposure is related to occupational exposure. The identification and classification of carcinogens are, therefore, other tasks in public health risk assessment. In particular, international organizations, such as the World Health Organization, have established guidelines for the use and consumption of hazardous chemicals and set appropriate thresholds for human exposure at workplace, home, and clinic. To draw up these regulatory policies, the

International Agency of Research on Cancer (IARC) program, opened in 1969 by Lorenzo Tomatis (1929-2007) and colleagues, classified chemical agents or complex mixtures of substances into different carcinogenic categories (Figure 1.3), considering evidence acquired through humans studies, animal experiments, and other relevant data (IARC, 2006).

Figure 1.3. Schematic representation of IARC classification of different categories of carcinogens.

❖ 1.3 Genotoxic and non-genotoxic carcinogens

The terms “genotoxic or non-genotoxic carcinogens” were coined in 1980 during the United States National Toxicology Program (NTP), based on the DNA reactivity, mutagenicity in *Salmonella* (Ames test), and carcinogenicity in rodents of 222 chemicals. Indeed, the report indicated that rodent carcinogens were not all equal. Among 115 substances that were recognised as carcinogens in rodents, only 71 were DNA reactive and *Salmonella* positive. The remaining 44 chemicals were structure alert negative and *Salmonella* negative (Ashby et al., 1988). As a result, the agents in the former group that were able to exert carcinogenicity via the induction of direct DNA damage were classified as “genotoxic carcinogens”. The latter group, that was represented by chemicals capable of producing cancer by secondary mechanisms not related to direct gene damage, was called the “non-genotoxic carcinogens” (NGTxC) class (Hayashi, 1992). In addition, owing to their DNA interaction properties, each group was subjected to different regulatory policies, that are currently maintained. For genotoxic chemicals, that are not considered to have a safe threshold or dose, strict regulatory policies are globally accepted. The Environmental Health Criteria set by the World Health Organization (WHO) stated also that “substances that are both genotoxic and carcinogenic would generally not be considered acceptable for use as food additives, pesticides or veterinary drugs” (FAO/WHO, 2009). For non-genotoxic carcinogens, “the dose makes the poison” (Nohmi, 2018). A chemical can be toxic if the exposition dose exceeds a specific threshold; on the contrary, a substance can be considered non-toxic if the dose is below a determined threshold. For NGTxC, the threshold level is the acceptable daily intake (ADI), based on the no observed adverse effect level (NOAEL) (Nohmi, 2018). Consequently, the aim of authorities is to find the appropriate level of exposure for each chemical that could come into contact with humans, especially if non-genotoxic carcinogens are to be used in the market. At this point, some crucial definitions need to be specified. The ADI of a substance is the daily intake level which does not allow to observe adverse effects, even if a person used this chemical for his/her entire life (Truhaut, 1991). The NOAEL is the highest dose used in toxicological assays at which no significant adverse effects can be examined (Zarn et al., 2011). Thus, the distinction between genotoxic and non-genotoxic compounds is of critical importance in the regulation of chemicals. However, the strict

distinction between these two groups and no carcinogenic substances is really complicated, considering the molecular effect of chemicals. Indeed, some mechanisms of action that are typically associated with non-genotoxic compounds, are also shared by genotoxic carcinogens or are symptomatic of other diseases. In particular, non-genotoxic carcinogens (NGTxC) act through secondary mechanisms such as epigenetic changes (DNA methylation and/or histone modifications and/or alterations in levels of non-coding RNAs), peroxisome proliferation, immune suppression, inflammatory responses, oxidative stress, disruption of cellular signaling connected with cell proliferation, growth suppression and contact inhibition that are not exclusive of cancer (Thomson et al., 2014). The induction of oxidative stress, for example, by both genotoxic and non-genotoxic carcinogens induce cell damage, but it can also be related with other adverse outcomes such as inflammation. Hence, genotoxic substances are more identifiable than non-genotoxic compounds (Paragraph 4.4). These agents can induce direct mutagenicity, described as the induction of permanent and transmissible changes in the genetic material of cells; or genotoxicity, that is similar to mutagenicity except that genotoxic effects are not necessarily associated with mutations. In particular, a genotoxic compound can cause changes in a single base pair in single or multiple genes or chromosomes, create a stable (transmissible) deletion, duplication or rearrangement of chromosome segments, change (gain or loss) in chromosome number, and mitotic recombination (OECD, 2015a). Thus, the evaluation of chemical carcinogenicity, defined as the ability for a chemical substance or a mixture of substances to cause cancer or increase its incidence, need to be improved.

Connected with this claim to support cancer hazard identification, an IARC international group of experts identified 10 key characteristics commonly shared by established human carcinogens (Madia et al. 2019). These 10 properties are distinct from the hallmarks of cancer, but reflect carcinogen mechanisms (at least two of them always present) (Smith et al., 2016). Namely, a carcinogen:

- is electrophilic or can be metabolically activated;
- is genotoxic;
- alters DNA repair or cause genomic instability;
- induces epigenetic alterations;

- induces oxidative stress;
- induces chronic inflammation;
- is immunosuppressive;
- modulates receptor-mediated effects;
- causes immortalization; and
- alters cell proliferation, cell death, or nutrient supply

The above mentioned are the 10 key characteristics of carcinogens form the basis of current IARC mechanistic evaluations (Madia et al. 2019) (Paragraph 1.5).
Lastly, a particular class of carcinogens (metal compounds) request an additional description of their mechanisms of actions. However, only cadmium (Cd) and Cd-induced carcinogenesis will be discussed in this thesis (Chapters 2 and 3).

❖ 1.4 Assays to detect genotoxic carcinogens

Although regulatory requirements vary according to the product sector and regulatory jurisdiction, the carcinogenicity of chemicals needs multiple assays to be validated. More in detail, the standard regulatory approach for carcinogenicity study continues to be a combination of genotoxicity tests and rodent cancer bioassays (RCBs). *In vitro* studies are employed firstly. Subsequently, if i*n vitro* positive results are obtained, *in vivo* assays and *in vivo* mammalian testings are recommended for further confirmation of the carcinogenicity of tested compounds (Jacobs et al., 2016). For an adequate evaluation of the mutagenic potential of chemicals, the bacterial reverse mutation assay (Ames test) and the mammalian gene mutation assays are the *in vitro* assays required. Conversely, to investigate structural and numerical chromosome aberrations, cytogenetic assays need to be employed. For example, the chromosome aberration assay in cultured mammalian cells or *in vitro* human lymphocytes, and the *in vitro* micronucleus assay can detect this kind of genotoxicity. Subsequently, the transgenic rodent gene mutation assay or the *in vivo* micronucleus assay ought to be used to the validation of data.

The Table 1.1 summarises commonly used *in vitro* and *in vivo* mutagenicity/genotoxicity studies for germ cells and somatic cells.

Table 1.1. Commonly *in vitro* and *in vivo* mutagenicity/genotoxicity studies for germ cells and somatic cells (Corvi et al., 2017a).

Type	Germ Cells	Somatic Cells
In Vitro	• **Bacterial reverse mutation test (OECD TG 471) - Ames test** • ***In vitro* mammalian chromosome aberration test (OECD TG 473)** • ***In vitro* mammalian cell gene mutation test using the *hprt* or *xprt* genes** • **(OECD TG 476)** • Genetic Toxicology: DNA Damage and Repair, Unscheduled DNA Synthesis in Mammalian Cells *In Vitro* (OECD TG 482) • *In vitro* mammalian cell micronucleus test (OECD TG 487) • ***In vitro* mammalian cell gene mutation tests using the thymidine kinase gene (OECD TG 490)**	
In Vivo	• Rodent dominant lethal mutation test (OECD TG 478) • Mouse heritable translocation assay (OECD TG 485) • Mouse specific locus test • Sister chromatid exchange analysis in spermatogonia • Unscheduled DNA synthesis test (UDS) in testicular cells • **Transgenic rodent somatic and germ cell gene mutation assay(OECD TG 488)**	• **Mammalian erythrocyte micronucleus test (OECD TG 474)** • **Mammalian bone marrow chromosome aberration test (OECD TG 475)** • **Liver Unscheduled DNA Synthesis (UDS) in vivo (OECD TG 486)** • **Transgenic rodent somatic and germ cell gene mutation assay(OECD TG 488)** • Mouse spot test (OECD TG 484) • Mammalian bone marrow Sister Chromatid Exchange (SCE)

All these assays can recognie most of the genotoxic carcinogens, however, they are not relevant for the identification of non-genotoxic carcinogens (NGTxC) that do not involve direct interaction with DNA. In conclusion, it appears simple to distinguish genotoxic and non-genotoxic carcinogens, but there are exceptions. For instance, estragole, leucomalachite green, dicyclanil, and ochratoxin A are all compounds whose mechanism of carcinogenesis remain to be clarified (Zeiger et al., 1987; Srivastava et al., 2004; Umemura et al., 2007; IARC, 1993).

1.4.1 In vivo cancer bioassays

Testing schemes and guidelines for evaluating the carcinogenic potential of substances vary on the basis of human health risk and the final use of each compound. Besides, the regulations, including prioritizing and selecting agents for carcinogenicity studies, change across various sectors: industrial chemicals, biocidal products, medicines for human and veterinary use, pesticides, and cosmetics (Madia et al., 2016). Information on current policies related to food and environmental safety legislation can be found on the European Commission (EC) website. Standard protocols on carcinogenicity testing are instead published by International Organizations for each specific type of research. The International Council on Harmonisation of Technical Requirements for Registration of Pharmaceuticals for Human Use (ICH) establishes guidelines for pharmaceutical research, and the Trilateral (EU-Japan-USA) Programme aim at harmonising technical requirements for veterinary product registration (VICH). The Organisation for Economic Co-operation and Development (OECD) have to be consulted for guidelines about chemicals testing. For existing and new industrial chemicals, specific information can be retrieved from the REACH (Registration, Evaluation and Authorisation of CHemicals) dossier in the European Chemicals Agency (ECHA) website. The European Medicines Agency (EMA) and the United States Food and Drug Administration (FDA) are the drug-regulatory agency designate for approving the safety and effective drugs for human and veterinary use. However, despite the multitude of models and guidelines, the two-year bioassays in rodents represent the “golden standard” for the evaluation of cancer hazard in all sectors, other than for the cosmetic ingredients and products (see Paragraph 1.4.1.1). In 2003, the 7thAmendment to the European Union (EU) Cosmetics Directive has restricted the use of animal tests for a variety of end points (Pauwels, 2004; Hartung, 2008). After, an initial ban on acute toxicity testing in animals, including *in vivo* genotoxicity testing, came into effect in 2009 (Bhattacharya, 2011). In the end, in 2013, the legislation prohibited to test cosmetic ingredients on animals (including repeat-dose studies, reproductive toxicity testing, and carcinogenicity bioassays) for the products designated for the European market. This has caused a profound concern to the evaluation of the carcinogenicity of new cosmetic ingredients, but it has also led to a new stimulus to develop alternative tests for screening

carcinogens without the use of animals (Adler et al., 2011; d'Yvoire et al., 2012) (Paragraph 1.5). In that context, the carcinogenic potential of cosmetic ingredients is now verified only with *in vitro* mutagenicity tests (European Union, 2009; SCCS, 2015; Corvi et al., 2017b).

The current regulatory background (Corvi et al., 2017b):

- For industrial chemicals, requirements applied to toxicity testing are based on a top-down approach under the REACH legislation. The toxicity information required for each compound is dictated primarily by the production volume (tonnage), to which potential exposure for human is linked (EC Regulation 1907, 2006). Carcinogenicity testing is also required only for mutagens category 3 (GHS category 3). Currently, also ECHA 2nd report on "The Use of Alternatives to Testing on Animals for the REACH Regulation" can be consulted.
- For biocides, the carcinogenicity testing is required in two different species for all new active substances, unless those are classified as mutagens category 1A and 1B (EU Regulation 528, 2012). A positive outcome in one or more of the *in vitro* genotoxicity tests requires confirmation by *in vivo* testing. If a substance is clearly negative in the *in vitro* battery, no further *in vivo* study is needed.
- For tracks of veterinary drugs in food for human consumption, if results from genotoxicity tests are negative, no structure alerts are identified and human exposure is negligible, animal testing can be overlooked (VICH GL28, 2005).
- For human medicines, carcinogenicity testing is required mainly for drugs with a foreseen chronic administration. ICH guideline M7 establishes the assessment and control of DNA reactive (mutagenic) impurities in pharmaceuticals. When levels of the impurity cannot be controlled, it is recommended that the impurity is tested in an *in vivo* gene mutation assay. Chemicals with positive results in these assays should be considered to have no safe threshold. Also, in the ICH Regulatory Notice Document (RND) posted by the Drug Regulatory Authorities (DRAs), alternative approaches to the 2-year rat carcinogenicity test are suggested for predicting the risk of human carcinogenicity of a pharmaceutical (ICH, 2016).

- For cosmetic ingredients, *in vivo* testing is banned since March 2013, see above (EC Regulation 1223, 2009).

1.4.1.1 The Two-Year Rodent Carcinogenesis Bioassay

The first model of Rodent Carcinogenesis Bioassay (RCBs) was proposed for the first time between the 1940s and 1950s, when a few classes of potent carcinogens had started to be evaluated in rodents. However, in 1971, the National Cancer Institute (NCI) improved the development of a new extensive evaluation procedure using 2 species of rodent exposed to a chemical for up to 2 yr. Unfortunately, the standardisation of this protocol was not put into place until the end of ’70s. Indeed, several decades ago, there was no standard bioassay for detecting chemical carcinogens. This had changed when the National Toxicology Program (NTP), under the leadership of the National Institute of Environmental Health Sciences, recognised that the vast database of studies conducted under standardised conditions permitted extensive comparisons across species, organ systems, and between genotoxic and nongenotoxic carcinogens. Currently, RCBs are detailed and described in two internationally accepted guidelines published by the OECD, the Test Guideline 451 (OECD, 2009a; OECD 2018), and the Test Guideline 453 (OECD, 2009b), that has remained almost unaltered from the first Test Guideline release in 1981. Otherwise, a scientific report prepared by the European Food and Safety Authority (EFSA) is available, in order to support the establishment of protocols for chronic toxicity and/or carcinogenicity studies in rodent with whole food/feed (EFSA, 2013). Consequently, for nearly half a century, many synthetic and natural chemicals have been tested by private and research institutes in 2-year rodent studies as part of a toxicity outline for human toxicity and carcinogenicity risk assessment.

Rodent Carcinogenesis Bioassay protocol:

- In the OECD Test Guideline 451, the recommended rodent species for the assay are rat and mice, although other species (e.g. dog, 4-6/sex/group) can be used if indicated as particularly relevant for the tested compound.
- At least three concentrations of the test compound are daily administrated in the diet, by gavage or by inhalation to groups consisting of 50/65 animals of each sex for up to 2 years.
- The highest dose chosen should be used to identify target organs of the compound, avoiding suffering, morbidity, or death of the animals.
- The animals are strictly observed during their life span, trying to note signs of toxicity and the development of neoplastic lesions.
- Animals are weighted, and their food and water consumption are measured along all the duration of the study.
- At the end of the assay, all the animals are subjected to a full necropsy, and fixed and stained samples examined by microscopy. A control group should be tested, as well.

In the OECD Test Guideline 453, called also chronic toxicity/carcinogenicity test, two parallel phases, the 1-year chronic phase, and the 2-years carcinogenicity study are both analysed. The second phase is defined by OECD 451 guideline.

In general, recommendations detailed in OECD TG 451 and OECD TG 453 are valid for a broad range of substances, but some details and requirements may differ for pharmaceuticals. For specifics, the International Conference on Harmonisation of Technical Requirements for Registration of Pharmaceuticals for Human Use is the reference document (ICH, 1997).

1.4.1.2 Critical aspects of the Two-Year Rodent Carcinogenesis Bioassay

During the 1970s, the original purpose of the RCBs was to identify potentially hazardous chemicals. The substances that did not show increased cancer incidence under these conditions were considered relatively safe and of low priority for further studies. While, positive chemicals were subjected to more accurate evaluations to determine whether the results could be replicated, or to select a threshold for a potential human use (Page, 1977). However, it soon became apparent that the cost and time-consuming of these studies could be limited only to the analyses of a small number of chemicals. In detail, approximately one million "*Euro*"/chemical and 5-8 yr needed to "select and obtain a chemical, conduct the necessary pre-chronic studies, select doses and determine the appropriate route of exposure, design the long-term study, select a contractor, conduct and monitor the studies, evaluate the laboratory findings, and report the results" (Boorman et al., 1994). Nonetheless, most animal experiments had also a limited sample size (Allen et al., 2004). At the same time, with an increasing number of pharmaceutical and agricultural chemicals to screen and identify possible carcinogens, the research into the mechanisms of toxicity and carcinogenesis needed to be intensified and improved. As a result, this massive amount of collected data and the additional research requested led to questions concerning the applicability of the standard 2-yr bioassay for evaluating the human risk assessment. Indeed, for years, the justification for using the 2-yr rodent systems in the evaluation of chemicals potential hazard was based on a paradox: if a carcinogen possessed an intrinsic property of producing cancer, positive results in one species should be sufficient to declare the carcinogenicity of this specific compound in all others. Nevertheless, it was shown that some carcinogenic activity could be species-specific, increasing doubt that the rodent models could be an optimal surrogate to study putative carcinogens effects on humans (Wittenau et al., 1983). Consequently, it was decided that human carcinogens should be tested for their potential carcinogenicity in more than one species (Wilbourn et al., 1986; Tomatis et al., 1989; Corvi et al., 2017a). These assays were also criticised for their high incidence of false-positive results, related to naturally occurring tumours of rats and mice, depending on sex, age and strain or stock (Knight et al., 2006a,b). In this regard, two practices were created to validate the results

of these assays. The most common strains and stocks of mice (CD-1, B6C3F1) and rats (F344, Sprague-Dawley) used in toxicology had to be characterised as regards the incidence and pathology including natural history (Ward, 2007). Tumours arising after 18-24 months of exposure had to be subjected to additional investigations, because they could not be connected with the treatment (Paules et al., 2011). In addition, the limited accuracy and predictability of these assays for human toxicity (detection limit of approximately 10 %, see Cohen and Ellwein, 1990) was considered to be an outcome of the use of rodents, that cannot develop some of the most prevalent tumours in humans, including colon and prostate cancer. This is in part due to differences in genetics, diet, specific natural chemical exposures and infectious agents that occur between these two different species (Knight et al., 2006a,b). Otherwise, this mismatch between rodents and humans could be due to a combination of several factors, including the variable stress caused by handling and restraint, or the stressful routes of administration common to carcinogenicity bioassays. Currently, beyond all these concerns, another problem of RBCs is connected with the lack of mechanistic information about carcinogenesis. RCBs rely on the observation of effects on a phenomenological level (tumours formation), but they do not provide information either on the mechanism of action of a specific compound or on the step of the biological response to the exposure (d'Yvoire et al., 2012). In the pharmaceutical sector, the concern is further underscored by the assertion that animal models cannot mimic human pathophysiology. Differences in rates of absorption and transport mechanisms between test routes of administration and human routes of exposure could be responsible for a different response between rodents and humans. There are rodent-specific mechanisms of carcinogenicity and differences in metabolism that can alter the interpretation of carcinogenicity studies (Friedrich et al., 2011, Sistare et al., 2011). Furthermore, the selected doses in the assay can be more elevated respect to those destined to be used clinically: animals often do not tolerate the chemical agent ,modifying their biological processes and producing artifacts (Meer et al.,2012; Bourcier et al., 2015). The last critical gap of current practice is that some non-genotoxic carcinogens remain unidentified, especially if they are not classified for any other hazardous property (Jacobs et al., 2016).

❖ 1.5 Alternative methods and 3Rs concept

The inadequacy of animal models for carcinogenicity and toxicity studies (Paragraph 1.4.1.2) led towards a new concept of research, in which the pioneering concept of "Alternative Methods to animal testing" was evident.
In 1978, Smyth defined this new paradigm for toxicity testing as:

"*All procedures that can completely replace the need of animal experiments, reduce the number of animals required, or diminish the amount of pain or distress suffered by animals in meeting the essential needs of man and other animals.*"

However, this definition referred to another concept introduced by Russel and Burch in their revolutionary book "The Principles of Humane Experimental Technique" (1959): the 3Rs concept. In this book, they stated that every effort should have been made to Replace or avoid the use of animals with non-sentient alternatives, to Reduce the number of animals utilised, and to Refine the conditions of animals in the experiments decreasing, animal pain and distress. Currently, the "3Rs" of animal research have influenced both research workers who use animals and who oppose their use. Indeed, it has been recognised that the adoption of the 3Rs can improve the quality of science: experiments that provide optimal living conditions and minimise unnecessary stress or pain of animals, often produce more reliable data (Flecknell, 2002). Besides, it has been shown that the use and creation of new alternative methods, including in vitro 2D and 3D cells cultures, non-testing methods such as *in silico* analyses ([Q]SAR and the adverse outcome pathway (AOP) approach), Physiologically Based Pharmacokinetic (PBPK) modelling, and epidemiology studies can sometime speed up the process of the analysis and investigate the mechanisms of action of the tested substances. Indeed, the rapid increase in the amount and heterogeneity of new substances to which humans are exposed need testing procedures and regulatory requirements as detailed and fast as possible (Hendry et al., 2007; Madia et al., 2019). For example, the amount of any substances of concern, such as non-genotoxic in the environment, and the use of nanomaterials, pesticides and pharmaceuticals with unknown properties (e.g. biologicals, cell and gene therapies) are expected to increase (Madia et al., 2019). Moreover, it has been estimated that more than 100,000 chemicals in use have not been tested for their safety (Rohrbeck et al., 2010). Therefore, the transformation of the

chemical exposure scenarios has raised additional difficulties for risk assessment and risk management.

1.5.1 Integrated approach to testing and assessment (IATA)

"A structured approach used for hazard identification (potential), hazard characterization (potency) and/or safety assessment (potential/potency and exposure) of a chemical or group of chemicals, which strategically integrates and weights all relevant data to inform regulatory decision regarding potential hazard and/ or risk and/or the need for further targeted testing and therefore optimising and potentially reducing the number of tests that need to be conducted" (OECD, 2015b).

A strategic plan to avoid and reduce animal use in genotoxicity testing is described by EURL ECVAM (Figure 1.4; Corvi et al., 2017a):

Figure 1.4. EURL ECVAM strategy plan in genotoxicity testing.

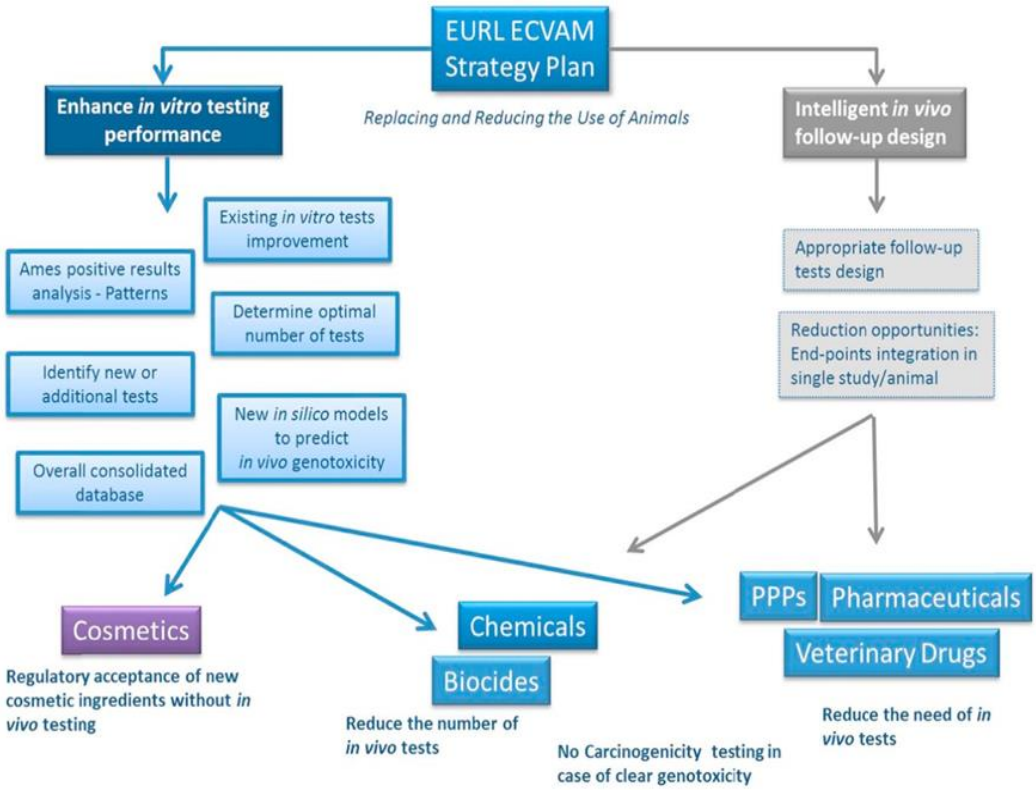

Due to the limitations of the current approaches to the identification of non-genotoxic chemicals, the scientific and regulatory community developed an integrated approach to testing and assessment (IATA) for studying the non-genotoxic carcinogens (Corvi et al., 2017a) (Figure 1.5).

Figure 1.5. A conceptual overview of an IATA for NGTxC from Jacobs et al., (2016). The figure depicts the levels of organisation of the NGTxC IATA, with increasing levels of complexity that are related with the hallmarks of NGTxC. Epigenetic machinery is described as the epicentre of the NGTxC hallmark wheel. The blue lines with connecting nodes are symbolic causality network, where key events (KE) and key event relationships (KER) can be identified based on the in silico studies (Paragraph 1.5.3/4) and verified with in vitro models.

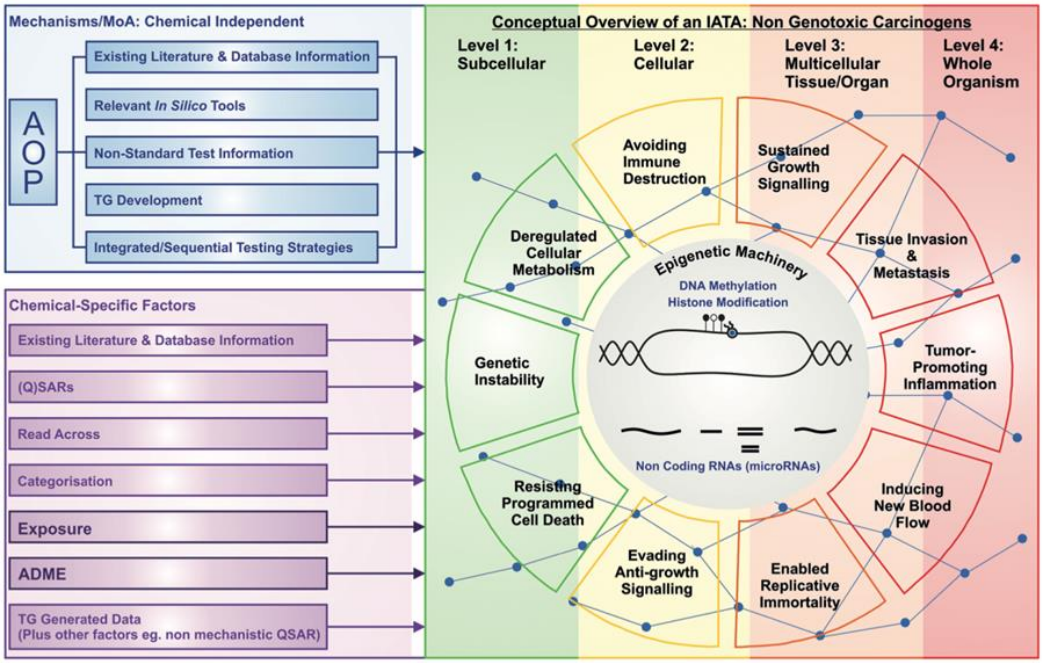

In this integrated approach, the cell transformation assay (CTA) can be considered as one of the possible building blocks of the IATA, as an *in vitro* model for carcinogenicity studies. Indeed, relating to their promising properties (see details in paragraph 1.5.2), several studies have revealed an additional value to exploit CTA: the assay may be used to study unknown mechanisms of *in vitro* carcinogenesis induced by a compound, or by a mixture of compounds. In particular, C3H10T1/2 CTA is remarkably exploited for mechanistic studies, hence it is considered a model useful to elucidate molecular mechanisms of cell transformation at the genomic and transcriptomic level (Vasseur et al., 2012). Moreover, CTAs offer a good phenotypic anchoring, which links the initial

molecular key events occurring after the chemical exposure to the onco-transformation (Corvi et al., 2017a,b). Consequently, CTAs gained the attention of the regulatory agencies to create standard protocols for studying carcinogenicity. The OECD published a Detailed Review Paper (DRP) on Cell Transformation Assays as a method for the detection of chemical carcinogens (OECD, 2007), and in 2012 and 2013, the European Union Reference Laboratory for alternatives to animal testing (EURL ECVAM) published two Recommendations for Cell Transformation Assays, using BALB/c 3T3, SHE and Bhas 42 systems (EURL ECVAM, 2012; 2013). Also, CTAs were proposed as an alternative method for genotoxocity/carcinogenicity testing for cosmetics (Adler et al., 2011). However, in 2014, the OECD concluded that CTA should not be used as a stand-alone assay to predict carcinogenesis, but it should be integrated with other test information, such as 'Omic' technologies (Paragraph 1.5.3). Thus, it was clarified that only the integration of Omics analysis and laboratory work can provide a global insight into the carcinogenesis process. To conclude, OECD recently published also two Guidance documents for SHE and Bhas 42 CTAs (OECD, 2015b; 2016), that can now be used for IATA approches.

1.5.2 Cell Transformation Assay

In vitro cell transformation assay can be described as a method that can mimic *in vivo* neoplastic process, in which idiosyncratic *in vitro* events appear to be similar to the progression of different phases of carcinogenesis in vivo. The most common cellular alterations include: (a) acquisition of infinite lifespan (immortality), (b) phenotypic modifications such as (i) cellular morphological changes (e.g. acquisition of spindle-shaped morphology and intense basophilic staining), and (ii) cellular growth changes (e.g. criss-cross, multi-layered, disorganised and misoriented cellular array patterns), (c) aneuploidy and genetic instability, (d) anchorage-independent growth (e.g. growth in semi-solid agar), and (e) the ability to induce tumours *in vivo* (Schechtman, 2012). Other cellular and sub-cellular alterations are constituted by alteration in oxidative balance, DNA stability and repair changes, DNA methylation changes, cell cycle deregulation, signal transduction pathway modulation, oncogene activation, tumor suppressor gene inactivation, and apoptosis inhibition (Schechtman, 2012). The chance to mimic the multi-phase process of

tumorigenesis of CTAs derives from the use of cultured cells with low incidence of spontaneous transformation rate, but, at the same time, sensitive to the neoplastic transformation after the exposure to a carcinogen. In this regard, three *in vitro* CTAs have been developed and accepted using rodent cell lines: BALB/c 3T3 and C3H10T1/2 cells, that are mouse immortalized fibroblasts, or Syrian Hamster Embryo (SHE) cells, that are primary or secondary normal cells (DiPaolo et al., 1972; Landolph, 1985; LeBoeuf et al., 1999; OECD, 2007, Corvi et al., 2012). In 2015, Bhas 42 cells were also established as a possible alternative cell line for the assay based on their sensitivity to 12-O-tetradecanoylphorbol-13-acetate (TPA) (Sasaki et al., 2015). The Bhas 42 cell line was obtained by transfecting mouse BALB/c 3T3 A31-1-1 cells with the *v-Ha-ras* gene (Sakai et al., 2011). In more details, the SHE assay was developed by Berwald and Sachs (1963) that used primary cells obtained by a Syrian hamster embryo at 13 days of gestation. After, two different SHE assays were improved changing the pH of the test media and considered based equivalent: pH > 7 to mimic the physiological conditions or pH 6.7 to increase the cell susceptibility to transformation (Vasseur et al., 2012). The BALB/c 3T3 assay is based on the malignant transformation of BALB/c 3T3 aneuploid cells. The test was first set up by Kakunaga (1973) and was reviewed by an international scientific committee which published guidelines to develop a standard reference protocol (IARC/NCI/EPA Working Group, 1985). Several improvements to the basic protocol were proposed during the years to enhance the specificity and sensitivity of the test. For example, several improvements were related to the number of cells seeded, the exposure time of the tested substance, as well as the possibility of tumoral promoter use to reduce the duration of the assay (27-28 days) or increase the cell transformation frequency (e.g. TPA) (Tsuchiya et al., 1995; Matthews, 1993). The last methods, developed by Reznikoff et al. (1973), is the protocol used in here presented work and that involved the C3H10T1/2 cell lines. In the C3H10T1/2 CTA, that is similar to BALB/c 3T3 CTA, a cytotoxicity test or dose-range finding phase is followed by the transformation assay. The cytotoxicity test is first applied to select the optimal range of test chemical concentrations for the transformation assays; after, at least five doses selected are tested in the transformation assays, with positive and negative controls test as well. In more details, the standard C3H/10T1/2 test starts with the low density (1000-2000 cells per dish) seeding of cells into culture dishes for a 24 hr for

attachment period. After, the tested chemicals are added for 24 or 48 hr. At the end of the treatment, the medium is removed and replaced with fresh medium without the test agent until the end of the experiments. The cells are maintained in culture for up to six weeks or longer, then fixed with methanol and stained with 10% Giemsa (OECD, 2007). At the end of CTA, the relevant data obtained is the fraction of dishes in a treatment group with one or several foci and the number of Type II and Type III foci in the total number of dishes counted for each group. In this regard, three types of foci can be distinguished (I, II, III) using a stereomicroscope, although it is likely that a continuum of focal phenotypes exists (Landolph, 1985) (Figure 1.6). Type I foci are cells more densely packed than a normal monolayer and slightly basophilic. Type II foci display massive piling up into virtually opaque multilayers, in which cells are moderately polar and criss-crossing is not pronounced. Type III foci are highly polar, fibroblastic, multilayered, criss-crossed arrays of densely stained cells. Only the Type I does not give rise to neoplastic growths upon injection into irradiated mice.

Figure 1.6. Representative images of contact-inibithed normal cells (Normal), Type I, Type II and Type III foci (Urani et al., 2009)

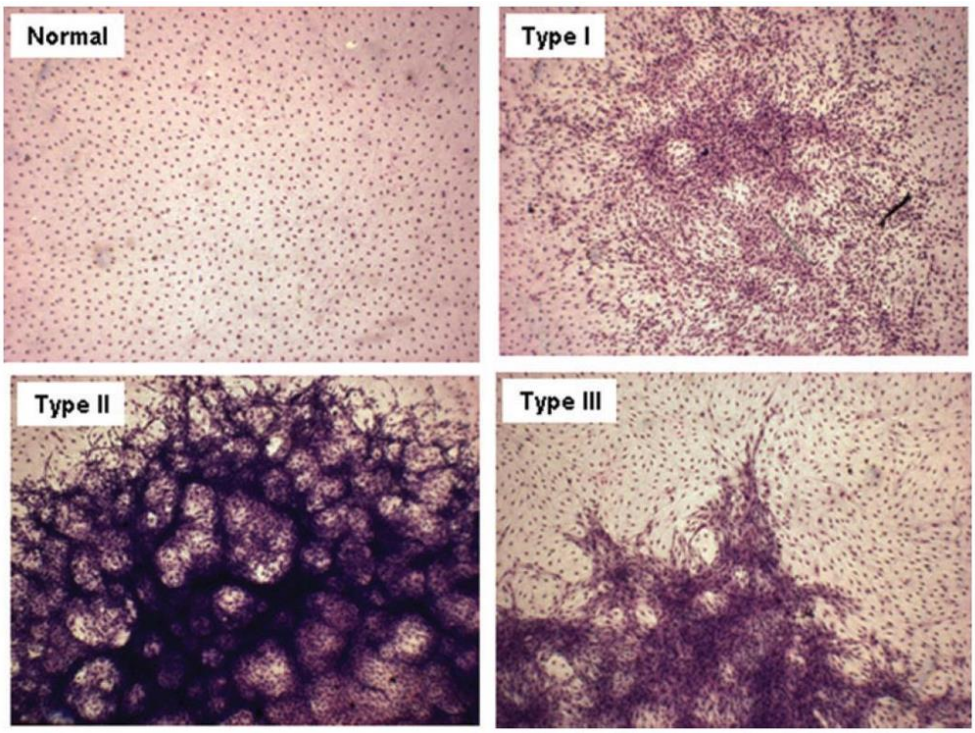

Urani et al. (2009) described in details the outline of the cytotoxicity assay and of the *in vitro* cell transformation assay, on which this research relies. Briefly, C3H were seeded at a density of 800 cells/dish in 100 mm diameter Petri dishes, and exposed 24 hr after seeding to different CdCl2 concentration (0.1, 0.5, 1, 2 µM) for 24 hr. As a result, Urani et al., (2009) demonstrated that 1 µM CdCl2, which was below the cytotoxicity threshold (IC50 of 2.4 µM), was able to induce the formation of transformed foci. Subsequently, Forcella M. et al. (2016) have used the Urani et al. (2009) CTA protocol with a single concentration of (1 µM) CdCl2 with the only aim to obtain transformed cells to be further characterised. In this case, they have performed a two-step CTA, in which all samples treated with CdCl2 were also exposed 4 days after the treatment to 0.1 µg/ml TPA, a known tumor promoter. The new cell lines obtained and used in this thesis for mechanistic studies of Cd carcinogenesis was called: CTR (cells from a normal monolayer of sample exposed to complete medium only), TPA (cells from a monolayer exposed to TPA alone), F1 (cells from a fully transformed focus (Type III) after exposure to 1µM CdCl2), F2 (cells from a focus classified as intermediate between Type II and III after exposure to 1µM CdCl2), and F3 (cells from a fully transformed focus (Type III) after exposure to 1µM CdCl2) (Figure 1.7).

Figure 1.7. An outline of the experimental design (Forcella et al., 2016)

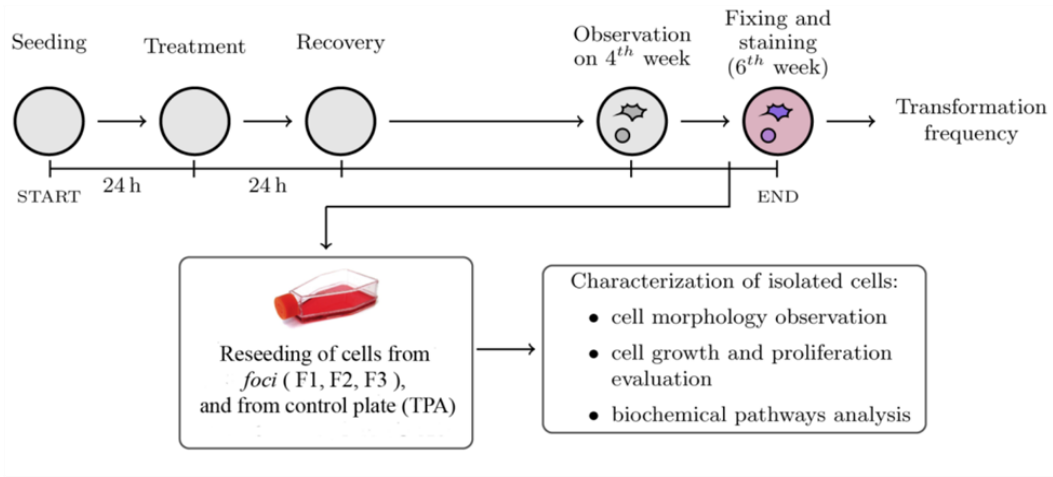

1.5.3 Cross-Omic approaches

“Omics” approaches, including genomics, transcriptomics, proteomics, epigenomics and metabolomics, have become the new mantra in molecular research (Mousumi et al., 2010). Indeed, Omics permit both to simultaneously analyse many thousands of macro and small molecules in their dynamic functions and interactions, and to deepen the knowledge of mechanisms underpinning carcinogenicity (Kroeger, 2006). In particular, genomics reveals the static sequences of genes, transcriptomics and proteomics reveal the biological function of the gene product, while, metabolomics examines the metabolic profiles in biological samples. More in details, through this technique, it is possible to acquire qualitative and quantitative information concerning the changing in metabolites levels in normal circumstances and after a perturbation. At the end, epigenomics investigates epigenomic changes, such DNA methylation patterns or/and histone modification of treated or tumour cells respect to control. However, considering a large amount of biological data obtained from these technologies, the interpretation of the results cannot always be straightforward, especially when different “omic” results are combined. Currently, to utilise the CTA within an IATA for carcinogenesis, Mascolo et al. (2018) have suggested and developed the "transformics method”, in which transcriptomics was used to highlight the molecular steps leading to *in vitro* malignant transformation. In particular, they suggested to analyse transcripts at different time points along with the process of *in vitro* transformation (24hr, 72hr and after 32 days). Consequently, gene signatures, indicative of concentration-related events, can be identified and anchored to the phenotypic endpoint. This approach is similar to the one used in this thesis (Chapter 6 and 7). In more details, in Chapter 6, transcriptomics analyses carried out after 24 hr of Cd treatment have revealed the triggering eventsthat have induced the final malignant phenotype; in Chapter 7, the features of transformed cells are fully described. The "transformics" approach has hence demonstratedto be a relevant asset that connect an easily recognisable phenotypic endpoint of oncotransformation, as provided by the CTA (Sasaki et al., 2012), with the corresponding gene signature, in a context of chemical carcinogenicity hazard assessment.

1.5.4 Improving performance, objectivity and mechanistic understanding in the CTA assay

Although CTAs have been used for several decades, and a considerable amount of data have demonstrated their robustness, some concerns have limited the widespread acceptability of these assays so far. The principal issues of CTAs have concerned the assay reproducibility between laboratories, the subjectivity of scoring transformed cells (relying on a judgement of the operator using coded morphological criteria), the absence of mechanistic understanding, and the use of mouse cell lines to predict the carcinogenic potential of chemical compounds in humans. So, trying to reduce the concerns related to these procedures, and, having seen the advantages of these techniques in the 3Rs contest (Paragraph 1.5.2), significant effort has been invested to further characterise and improve the in vitro CTAs. For examples, a prevalidation study of the CTAs using the BALB/c 3T3 and C3H10T1/2 cell line, SHE cells at pH 6.7, and SHE cells at pH 7.0 was coordinated by the European Centre for the Validation of Alternative Methods (ECVAM) for obtaining the standardisation of protocols, test method transferability and within- and between-laboratory reproducibility (Corvi et al., 2012). Besided, the performance of the various methods has recently been collected in the Detailed Review Paper (DRP) by the Organisation for Economic Co-operation and Development (OECD) (See Table 1.2), to which is added the Figure 1.8.

Table 1.2. Performances of different CTAs from Creton et al., 2012 and in agreement with rodent carcinogenicity.

	SHE pH 6.7	**SHE pH 7.0**	**BALB/c 3T3**	**C3H10T1/2**
Concordancea (%)	74	85	68	84
Sensitivity (%)	66	92	75	72
Specificity (%)	85	66	53	80
Positive predictivity	88	88	77	95
Negative predictivity	62	75	50	34
False-positive rate	15	34	47	20
False-negative rate	33	8	25	28
Number of chemicals	88	204	149	96
Number of carcinogens (%)	54 (61)	142 (74)	100 (68)	81 (84)

Figure 1.8. Performances of CTAs based on different cellular systems are displayed in radar-charts, where at each axis corresponds one parameter of classification, namely, concordance, sensitivity, specificity, positive and negative instances predictivity, and false positive and negative. These data are detailed in EURL ECVAM, 2012; OECD, 2007 and Sakai et al., 2010.

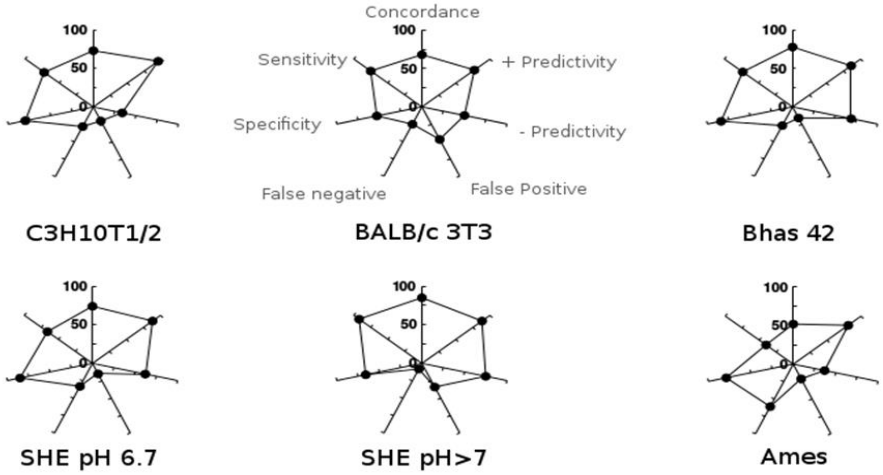

Many other studies, instead, are converged on the improvement of the final phase of the CTA protocol (namely, visual scoring of the transformed morphologies), in which worker subjectivity can mainly condition the results. Indeed, the classification of the transformed colonies/foci is surely based on accepted morphological criteria, but a trained expert identifies transformed cells into positive instances (finally registered for the in vitro carcinogenicity assessment) and negative instances based on own visual scoring. Consequently, some intermediate *foci*, that show a transition degree of coded morphological criteria, can not be clearly classified into a specific Type of *foci* (Landolph, 1985; Sasaki et al., 2012b). The morphological criteria are based on the characteristic of the transformed cells. These cells:

- are deeply basophilic stained;
- acquire a spindle shape;
- grow into multilayers (piling up of cells);
- are randomly oriented at the edge of the focus;
- are invasive into the background monolayer (Landolph, 1985; Sasaki et al., 2012).

Moreover, this method of classification can be supported by specifically designed photo catalogues (Sasaki et al., 2012; Maire et al., 2012c; Bohnenberger et al., 2012; OECD, 2016). However, as a notable alternative, new image analysis of transformed colonies seems a very promising road to overcome the subjectivity issues (Poth, 2009; Urani et al. 2013; Callegaro et al., 2015). On the other hand, several studies, including this thesis, focalised their attention to exploit CTAs to study unknown mechanisms of in vitro carcinogenesis induced by a compound, or by a mixture of compounds. In particular, C3H10T1/2 CTA was mainly used for mechanistic studies in IATA approaches or tiered approach taking advantage of *in silico* methods as well as statistical methods, as described above. For this reason, in Paragraph 1.1.5.1 are illustrated some *in silico* methods for a possible implementation of CTAs. All these methods are not mutually exclusive, and can be used depending upon the experimental questions. As an example, Benigni and colleagues (Benigni et al., 2013) showed that an approach consisting in Ames and SHE CTA assays, combined with structure-activity (SA) could be able to identify almost all IARC human carcinogens, consisting in genotoxic and non-genotoxic carcinogens. Concerning the final CTAs disadvantage (the use of mouse cell lines to predict human carcinogens), more studies are needed. The solution seems to create a human-cell based CTAs, in which one or many protocols based on different cell lines can be an ideal system to identify carcinogens in a more physiological context. However, many problems occur. First, the number of genetic events required to transform human cells is greater than in rodents. Moreover, it has been shown that telomerase expression is more robust in rodent, suggesting that the differences in telomere biology between humans and rodents also contribute to the threshold variation for rodent and human cell transformation cells (Calado et al., 2013). These differences between human and mouse cell lines and the complexities of the carcinogenesis process can explain why a CTA based on human cells has not yet been established for routine use. However, new alternative methods were created to study several mechanisms involved in growth and development of cancer, as illustrated in Paragraph 1.1.5.2.

1.5.5 Other alternative approaches to the in vivo bioassay for studying carcinogenesis

Various alternative methods are proposed to avoid animal use in experimentation and possible unethical procedures. The advantages associated are time efficienct and cost-effective. However, these approaches are not described in detail, as they do not represent the focus of this research, although they are extremely important in the 3Rs context (Doke et al., 2015).

1.5.5.1 Non-testing methods

- Specialised computer models and software programs can help to generate useful simulations to predict various biological and toxic effects of a chemical or potential drug without animal studies. For example, the software Computer Aided Drug Design (CADD) can be used to predict the receptor binding site for a potential drug molecule, and to avoid testing of chemicals having no biological activity (Vedani, 1991). Another popular tool with a similar purpose is the Structure Activity Relationship (SARs) computer program.
- Quantitative Structure Activity Relationship (QSAR) is the mathematical description of the relationship between physicochemical properties of a drug molecule and its biological activity (Knight et al., 2006c). The carcinogenicity and mutagenicity of a potential drug candidate are well predicted by the computer database (Benigni, 2014; Benigni et al., 2011; 2013). QSARs for non-genotoxic carcinogenicity are still in an early stage of development.
- Adverse outcome pathways (AOPs) enable users to organise information from diverse sources (*in silico*, *in vitro*, *in vivo*, etc.) in a logical framework, facilitating the knowledge of the processes examined (Madden et al., 2014; Jacobs et al., 2016). In more details, an AOP describes existing information on the toxicity mechanisms of a compound leading to a description of a possible adverse human and/or environmental health effect, at different levels of biological organisation (OECD, 2013; Tollefesen et al., 2014; Villeneuve et al., 2014). In AOPs terms, some biological changes that are called key events (KEs) befall in response to a molecular initiating event (MIE) leading to an adverse

outcome (AO). MIEs, KEs and AOs are linked with key event relationships (KERs). The MIE and the adverse outcome need to be the two defining anchor points. To develop an AOP, mechanistic information is not essential *a priori*, but, when information becomes available, it can be used as further supporting evidence. At a global level, OECD has recognized the importance of the AOP approach, launching its programme for the development of AOPs in 2012. Some IATA approaches are based on AOPs (Tollefesen et al., 2014; Jacobs et al., 2016).

1.5.5.2 In Vitro Models and Alternative organisms

- Lower vertebrates are an attractive option for the genetic relatedness to the higher vertebrates. One example of a possible alternative is the *Danio rerio*, commonly called zebrafish. Indeed, this model is an important system to study vertebrate development because of the rapid, external development and transparency of the zebrafish embryo, but also cancer as a genetic disease. A comparison of the human genome sequence and zebrafish genome sequence demonstrates the conservation of cell-cycle genes, tumour suppressors, and oncogenes (Amatruda et al., 2002).
- Invertebrate organisms, that are used to study various diseases like neuronal diseases, muscle dystrophy, cell ageing, programmed cell death, and toxicological testing (Lagadic et al., 1998), can be also used to investigate the processes of apoptosis and autophagy in the development of cancer (Kyriakakis et al., 2015). For instance, experiments with *Caenorhabditis elegans*, a eukaryotic nematode selected as a model organism by Nobel laureate Brenner (Strange, 2007), can be transferred to humans and have led to the development and testing of therapeutic new agents (Artal-Sanz et al., 2006; Nass et al., 2008).
- 3D spheroids mimic some features of solid tumours, such as their spatial architecture, physiological responses, secretion of soluble mediators, gene expression patterns and drug resistance mechanisms. These unique characteristics are currently used as *in vitro* models for screening new

anticancer therapeutics, both at a small and a large scale (Costa et al., 2016).

- 3D Organoids are cell aggregates derived from primary tissue or stem cells that are capable of self-renewal, self-organisation and exhibit organ functionality. Organoid technology can be used to model human organ development and various human pathologies 'in a dish." Additionally, patient-derived organoids hold promise to predict drug response in a personalised fashion (Clevers, 2016).
- At least, microfluidic 3D cancer models can be used to investigate the effect of continuous flow on cancer development and progression in more complex microenvironments. In microfluidic 3D systems, many microenvironmental factors such as the number of cell types and ECM properties become more controllable. Furthermore, the continued integration of microfabrication, 3D biology, and microfluidics has also led to the development of organs-on-a-chip, such as a 3D microfluidic cell culture device that mimics some of the functions of a biological organ. Otherwise, the body-on-chip, that incorporates key organs onto a single screening microfluidic platform, can recreate *in vivo*-like structures and functions for a more extensive understanding of complex interactions in the tumour microenvironment (Sung et al., 2013; Sung et al., 2014).

References

- Adler S., Basketter D., Creton S., Pelkonen O., et al., *Alternative (non- animal) methods for cosmetics testing: current status and future prospects- 2010.*, In: Archives of Toxicology (2011), Vol. 85, pp 367–485
- Aktipis C.A., Nesse R.M.**,** *Evolutionary foundations for cancer biology.,* Evolutionary Applications (2013), Vol. 6, pp 144-159
- Allen D.G., Pearse G., Haseman J.K., Maronpot R.R., *Prediction of Rodent Carcinogenesis: An Evaluation of Prechronic Liver Lesions as Forecasters of Liver Tumors in NTP Carcinogenicity Studies.,* Toxicologic Pathology (2004), Vol. 32, pp 393–401
- Amatruda J.F., Shepard J.L., MStern H., Izon L., *Zebrafish as a cancer model system., Cancer Cell (2002) Vol. 1, pp 229-231*
- Artal-Sanz M., de Jong L., Tavernarakis N., *Caenorhabditis elegans: a versatile platform for drug discovery.,* Journal of Biotechnology (2006), Vol. 1, pp1405-1418
- Ashby J., Tennant R.W., *Chemical structure, Salmonella mutagenicity and extent of carcinogenicity as indicators of genotoxic carcinogenesis among 222 chemicals tested in rodents by the U.S. NCI/NTP.,* Mutat Res. (1988), Vol. 204, pp 17–115
- Belpomme D., Irigaray P., Hardell L., Clapp R., Montagnier L., Epstein S., Sasco A.J., *The multitude and diversity of environmental carcinogens.,* Environmental Research (2007), Vol. 105, pp 414-429
- Benigni R., *Predicting the carcinogenicity of chemicals with alternative approaches: recent advances.*, Expert Opinion on Drug Metabolism & Toxicology (2014), Vol. 10, pp 1199–1208
- Benigni R., Bossa C., *Alternative strategies for carcinogenicity assessment: an efficient and simplified approach based on in vitro mutagenicity and cell transformation assays.*, Mutagenesis (2011), Vol 26, pp 455–460
- Benigni R., Bossa C., Tcheremenskaia O., *In vitro cell transformation assays for an integrated, alternative assessment of carcinogenicity: a data-based analysis.*, Mutagenesis (2013), Vol. 28, pp 107–116
- Berwald Y., Sachs L., *In Vitro Cell Transformation with Chemical Carcinogens*. In: Nature (1963), Vol. 200, pp. 1182–1184
- Bhattacharya S. Zhang Q., Carmichael P.L., Boekelheide K., Andersen M.E., *Toxicity Testing in the 21st Century: Defining New Risk Assessment Approaches Based on Perturbation of Intracellular Toxicity Pathways.,* PLosOne (2011), Vol. 6, e20887
- Bohnenberger S., Bruce S.W., Kunkelmann T., Pant K., Perschbacher S., Schwind K.R., Sly J., Poth A., *Photo catalogue for the classification of cell colonies in the Syrian hamster embryo (SHE) cell transformation assay at pH 6.7.*, Mutation Research (2012), Vol. 744, pp 82-96
- Boorman G.A.,Maronpot R.R., Eustis S.L., *Rodent Carcinogenicity Bioassay: Past, Present, and Future.,* Toxicologic Pathology (1994), Vol. 22, pp 105-111
- Bourcier T., McGovern T., Stavitskaya L., Kruhlak N., Jacobson-Kram D., *Improving Prediction of Carcinogenicity to Reduce, Refine, and Re- place the Use of Experimental Animals.*, In: Journal of the American Association for Laboratory Animal Science : JAALAS (2015), Vol. 54, pp 163–169 F.

- Bray F., Jemal A., Grey N., Ferlay J., Forman D., *Global cancer transitions according to the Human Development Index (2008–2030): A population-based study,* Lancet Oncology (2012), Vol 13, pp 790-801
- Bray F., Ferlay J., Soerjomataram I., Siegel R.L., Torre L.A., Jemal A., *Global cancer statistics 2018: GLOBOCAN estimates of incidence and mortality worldwide for 36 cancers in 185 countries.*,CA Cancer Journal for Clinicians (2018), Vol. 0, pp 1-31
- Broertjes J., *The Ten Hallmarks of Cancer in Cutaneous Malignant Melanoma*., The UNAV Journal for Medical Students (2015), Vol. 1, pp 6-12
- Bui T., Thompson C.B., *Cancer's sweet tooth*., Cancer Cell (2006), Vol. 9, pp 419- 420
- Burgio E., Migliore L., *Towards a systemic paradigm in carcinogenesis: linking epigenetics and genetics.,* Molecular Biology Reports (2014), Vol. 42, pp 777-790
- Calado R.T., Dumitriu B., *Telomere dynamics in mice and humans.,* Seminars in Hematology (2013), Vol. 50, pp 165-174
- Callegaro G., Stefanini F.M., Colacci A., Vaccari M., Urani C., Toxicology in Vitro (2015), Vol. 29, pp 1839-1850
- Chaffer C.L., Weinberg R.A., *How does multistep tumorigenesis really proceed?*, Cancer Discovery (2015), Vol. 5, pp 22-24
- Clevers H., *Modeling Development and Disease with Organoids.,* Cell (2016), Vol. 165, pp 1586-1597
- Cohen S.M., Ellwein L.B., *Proliferative and genotoxic cellular effects in 2-acetylaminofluorene bladder and liver carcinogenesis: biological modeling of the ED01 study.*, In: Toxicology and Applied Pharmacology (1990), Vol. 104, pp 79–93
- Cori C.A., Cori G.T, *The carbohydrate metabolism of tumors.*, Journal of Biological Chemistry (1925), Vol. 65, pp 397-405
- Corvi R., Aardema M.J., Gribaldo L., Hayashi M., Hoffmann S., Schechtman L., Vanparys P., *ECVAM prevalidation study on in vitro cell transformation assays: general outline and conclusions of the study.,* Mutation Research (2012), Vol. 744, pp 12-19
- Corvi R., Madia F., *In vitro genotoxicity testing–Can the performance be enhanced?.,* Food and Chemical Toxicology (2017a), Vol. 106, pp 600-608
- Corvi R., Madia F., Guyton K. Z., Kasper P., Rudel R., Colacci A., Kleinjans J., Jennings P., *Moving forward in carcinogenicity assessment: Report of an EURL ECVAM/ESTIV workshop.,* Toxicology in Vitro (2017b), Vol. 45, pp 278-286
- Costa E.C., Moreira A.F., de Melo-Diogo D., Gaspar V.M., Carvalho M.P., Correia I.J., *3D tumor spheroids: an overview on the tools and techniques used for their analysis.,* Biotechnology Advances (2016), Vol. 34, pp 1427-1441
- Creton S., Aardema M.J.,Carmichael P.L., Harvey J.S., Martin F.R., Newbold R.F., O'Donovan M.R., Pant K., Poth A., Sakai A., Sasaki K., Scott A.D., Schechtman L.M., Shen R.R, Tanaka N., Yasaei H., *Cell transformation assays for prediction of carcinogenic potential: state of the science and future research needs.,* Mutagenesis (2012), Vol. 27, pp 93–101
- Czarnecka A.M., Gammazza A.M., Di Felice V., Zummo G., Cappello F., *Cancer as a "Mitochondriopathy".,* Journal of Molecular Cancer (2007), Vol. 3, pp 71-79

- DiPaolo J. A., Takano K., Popescu N. C., *Quantitation of chemically induced neoplastic transformation of BALB-3T3 cloned cell lines.*, In: Cancer research (1972)., Vol. 32.12, pp. 2686–2695
- Doke S.K., Dhawale S.C., *Alternatives to animal testing: A review.,* Saudi Pharmaceutical Journal (2015), Vol. 23, pp 223-229
- d'Yvoire M.B., Bremer S., Casati S., Ceridono M., Coecke S., Corvi R., Eskes C., Gribaldo L., Griesinger C., Knaut H., Linge J.P., Roi A., Zuang V., *ECVAM and new technologies for toxicity testing.,* In: *New Technologies for Toxicity., Testing*. Springer (2012), pp 154–180
- ECHA website, https://echa.europa.eu/regulations/reach/registration/information-requirements
- EC Regulation 1907**,** *Regulation (EC) no 1907/2006 of the European parliament and of the council of 18 December 2006 concerning THE registration, evaluation, authorisation and restriction of chemicals (REACH), establishing a European chemicals agency, amending directive 1999/4.,* Official Journal of the European Union (2006), Vol. 396, pp. 1-849
- EC Regulation 1223, *Regulation (EC) no 1223/2009 of the European Parliament and of the Council of 30 November 2009 on cosmetic products.,* Official Journal of the European Union (2009), Vol. 342, pp 59-209
- European Food Safety Autority (EFSA). *Considerations on the applicability of OECD TG 453 to whole food/feed testing*., In: EFSA Journal (2013) 11.7
- EURL ECVAM. EURL-ECVAM -Recommendation on three Cell Trans- formation Assays. (2012).
- EURL ECVAM Recommendation Bhas-CTA 2013. (2013)
- EU Regulation 528, *Regulation (EU) no 528/2012 of the European Parliament and of the Council of 22 May 2012 concerning the making available on the market and use of biocidal products,* Official Journal of the European Union (2012), Vol. 167, pp 1-123
- Fantin V.R., St-Pierre J., Leder P., *Attenuation of LDH-A expres- sion uncovers a link between glycolysis, mithocondrial physiology and tumor maintenance.,* Cancer Cell (2006), Vol. 9, pp 425-434
- Flecknell P., *Replacement, reduction and refinement.,* ALTEX (2002), Vol. 19, pp 73-78
- Fouad Y.A., Aanei C., *Revisiting the hallmarks of cancer.,* American Journal of Cancer Research (2017), Vol. 7, pp 1016–1036
- Forcella M., Callegaro G., Melchioretto P., Gribaldo L., Frattini M., Stefanini F.M., Fusi P., Urani C., *Cadmium-transformed cells in the in vitro cell transformation assay reveal different proliferative behaviors and activated pathways.*, Toxicology In vitro (2016), Vol. 36, pp 71-80
- Friedrich A., Olejniczak K.**,** *Evaluation of carcinogenicity studies of medicinal products for human use authorised via the European centralised procedure* (1995-2009), Regulatory Toxicology and Pharmacology (2011), Vol. 60, pp 225-248
- Hayashi Y., *Overview of genotoxic carcinogens and non-genotoxic carcinogens.,* Experimental and Toxicologic Pathology (1992), Vol. 44, pp 465-471
- Hanahan D., Weinberg R.A., *The hallmarks of cancer.*, Cell (2000)
- Hanahan D., Weinberg R.A., *Hallmarks of cancer: the next generation.,* Cell (2011)

- Hartung T., *Food for thought … on alternative methods for cosmetics safety testing.,* ALTEX (2008), Vol. 25, pp 147-62
- Hendry A.P., Farruggia T.J., Kinnison M.T., *Human influences on rates of phenotypic change in wild animal populations.,* Molecular Ecology (2007), Vol. 17, pp 20-29
- International Agency for Research on Cancer (IARC), *Ochratoxin A*., IARC Monographs on the Evaluation of Carcinogenic Risks to Humans (1993), Vol. 56, pp 489–521
- International Agency for Research on Cancer (IARC), IARC Monographs on the Evaluation of Carcinogenic Risks to Humans (2006)
- IARC/NCI/EPA Working Group., *Cellular and Molecular Mechanisms of Cell Transformation and Standardization of Transformation Assays of Established Cell Lines for the Prediction of Carcinogenic Chemicals: Overview and Recommended Protocols.,* Cancer Research (1985), Vol. 5, pp 2395-2399
- ICH (1997). *ICH Harmonized Tripartite Guideline - Testing for Carcinogenicity of Pharmacauticals S1B.*
- ICH (2016), *Regulatory notice document Proposed Change to Rodent Carcinogenicity Testing of Pharmaceuticals*
- Jacobs M.N., Colacci A., Louekari K., Luijten M., Hakkert B.C., Paparella M., Vasseur P., *"International regulatory needs for development of an IATA for non-genotoxic carcinogenic chemical substances".*, ALTEX-Alternatives to Animal Experimentation (2016), Vol. 33, pp 359–392
- Kakunaga T., *A quantitative system for assay of malignant transformation by chemical carcinogens using a clone derived from BALB-3T3.*, International journal of cancer (1973), Vol. 12.2, pp. 463–473
- Kyriakakis E., Markaki M., Tavernarakis N., *Caenorhabditis elegans as a model for cancer research.*, Molecular and Cellular Oncology (2015), Vol. 2, e975027
- Knight A., Bailey J., Balcombe J., *Animal carcinogenicity studies: 1. Poor human predictivity.,* Alternatives to Laboratory Animals : ATLA (2006a), Vol. 34, pp 19-27
- Knight A., Bailey J., Balcombe J., *Animal carcinogenicity studies: 2. Obstacles to extrapolation of data to humans.,* Alternatives to laboratory animals: ATLA (2006b). Vol 34, pp 29–38
- Knight A., Bailey J., Balcombe J., *Animal carcinogenicity studies: alternatives to the bioassay.*, Atla Nottingham (2006c), Vol. 34, p. 39
- Koppenol W.H., Bounds P.L., Dang C.V., *Otto Warburg's contributions to current concepts of cancer metabolism.,* Nature Reviews, Cancer (2011), Vol. 11, pp 325-337
- Kroeger M., *How omics technologies can contribute to the '3R' principles by introducing new strategies in animal testing.*, Trends in Biotechnology (2006), Vol. 24, pp 343-346
- Lai J.H., Jan H.J., Liu L.W., Lee C.C, Wang S.G., Hueng D.Y., Cheng Y.Y., Lee H.M., Ma H.I., *Nodal regulates energy metabolism in glioma cells by inducing expression of hypoxia-inducible factor 1α.,* Neuro-Oncology (2013), Vol. 15, pp 1330–1341
- Lagadic L., Caquet T., *Invertebrates in testing of environmental chemicals: are they alternatives?.,* Environmental Health Perspectives (1998), Vol. 106, pp 593
- Landolph J.R., *Chemical transformation in C3H 10T1/2 Cl 8 mouse embryo fibroblasts: historical background, assessment of the transformation assay, and evolution and*

optimization of the transformation assay protocol., IARC scientific publications (1985), Vol. 67, pp. 185–203

- LeBoeuf R.A., Kerckaert K.A., Aardema M.J., Isfort R.J., *Use of Syrian hamster embryo and BALB/c 3T3 cell transformation for assessing the carcinogenic potential of chemicals.*, IARC scientific publications (1999), Vol. 146, pp. 409–425
- Madden J.C., Rogiers V., Vinken M., *Application of in silico and in vitro methods in the development of adverse outcome pathway constructs in wildlife.,* Philosophical Transactions of the Royal Society B (2014), Vol. 369
- Madia F., Worth A., Whelan M., Corvi R., *Carcinogenicity assessment: Addressing the challenges of cancer and chemicals in the environment.,* Environment International (2019), Vol. 128, pp 417-429
- Madia F., Worth A., Corvi R., *Analysis of carcinogenicity testing for regulatory purposes in the European Union.,* European Commission (2016), EUR, 27765
- Maire M.-A., C. Rast C., Vasseur P., *Photo catalogue for the classification of cell colonies in the Syrian hamster embryo (SHE) cell transformation assay at pH 7.0.,* Mutation Research/Genetic Toxicology and Environmental Mutagenesis. International Prevalidation Study on Cell Transformation Assays (2012), Vol. 744, pp 97–110
- Mascolo M.G., Perdichizzi S, Vaccari M., Rotondo F., Zanzi C., Grilli S., Martin Paparella M., Jacobs M.N., Colacci A., *The transformics assay: first steps for the development of an integrated approach to investigate the malignant cell transformation in vitro.,* Carcinogenesis (2018), Vol. 39, pp 955–967
- Matthews E.J., *Transformation of BALB/c-3T3 cells: I. Investigation of experimental parameters that influence detection of spontaneous transformation.*, Environmental Health Perspectives (1993). Vol. 101 (Suppl 2), pp. 277– 291
- Meer P.J.K.v., Kooijman M., Gispen-de Wied C.C., Moors E.H.M., Schellekens H., *The ability of animal studies to detect serious post marketing adverse events is limited.,* Regulatory Toxicology and Pharmacology (2012), Vol. 64, pp 345–349
- Mousumi D., Prasad G.B.K.S., Bisen P.S., *Omics Technology.*, In: Molecular Diagnostics: Promises and Possibilities (2010), Dordrech Heidelberg London, Springer, pp 11-31
- Nass R., Merchant K.M., Ryan T., *Caenorhabditis elegans in Parkinson's disease drug discovery: addressing an unmet medical need.,* Molecular Interventions (2008), Vol. 8, pp 284-293
- NIH NCI, https://www.cancer.gov/about-cancer/understanding/what-is-cancer (2018)
- Nohmi T., *Thresholds of Genotoxic and Non-Genotoxic Carcinogens.,* Toxicological Research (2018), Vol. 34, pp 281–290
- OECD website, http://www.oecd.org/env/ehs/testing/oecdguidelinesforthetestingof chemicals.htm
- OECD., Detailed Review Paper on Cell Transformation Assays for detection of chemical carcinogens - series on testing and assessment Number 31 (2007).
  - Test Guideline 451 – Carcinogenicity studies. OECD Guidelines for the Testing of Chemicals (2009a).
  - Test Guideline 453 - Combined Chronic Toxicity/Carcinogenicity Studies. OECD Guidelines for the Testing of Chemicals (2009b).

- Guidance Document for developing and assessing Adverse Outcome Pathways (AOPs) - Series on Testing and Assessment No. 184 (2013).
- Genetic Toxicology Guidance Document (2015a)
- Guidance Document on the in vitro Syrian Hamster Embryo (SHE) Cell Transformation Assay - Series on Testing & Assessment No. 214. (2015b)
- Guidance Document on the in vitro Bhas 42 Cell Transformation Assay Series on Testing & Assessment No. 231. (2016)
- Guidelines for the Testing of Chemicals. Test Guideline 451 - Carcinogenicity studies. (2018)

- Page N., *Concept of a bioassay program in environmental carcinogenesis.,* In: Advances in Medical Toxicology (1977), H.F. Kraybill and H.A. Mehlman (ed). Wiley and Sons, New York pp. 87-171
- Paules R.S., Aubrecht J., Corvi R., Garthoff B., Kleinjans J.C., *Moving forward in human cancer risk assessment.*, In: Environmental health perspectives (2011). Vol. 119, pp 739–743
- Pauwels M,, Rogiers V., *Safety evaluation of cosmetics in the EU. Reality and challenges for the toxicologist.,* Toxicoly Letters (2004), Vol. 151, pp 7–17
- Poth A., *Cell transformation assay -past-present-future*., ALTEX: Abstracts 7th World Congress Rome (2009), Vol. 26
- Reznikoff C.A., Brankow D.W., Heidelberger C., *Establishment and characterization of a cloned line of C3H mouse embryo cells sensitive to postconfluence inhibition of division.*, In: Cancer Research (1973) Vol. 33.12, pp. 3231– 3238
- Rohrbeck A., Salinas G., Maaser K., Linge J., Salovaara S., Corvi R., Borlak J., *Toxicogenomics applied to in vitro carcinogenicity testing with Balb/c 3T3 cells revealed a gene signature predictive of chemical carcinogens.*, In: Toxicological Sciences (2010) Vol. 118, pp. 31–41
- Russel, W. and R. Burch., *The Principles of Humane Experimental Technique.* (1959)
- Sakai A.,Sasaki K.,Hayashi K.,Muramatsu D.,Arai S.,Endou N.,Kuroda S.,Poth A., Bohnenberger S., Kunkelmann T., Asakura M., Hirose H., Ishii N., Mizuhashi F., Kasamoto S., Nagai M., Pant K., Bruce S.W., Sly J.E., Yamazaki S., Umeda M., Tanaka N., *An international validation study of a Bhas 42 cell transforma- tion assay for the prediction of chemical carcinogenicity*, Mutation Research (2011), Vol. 725, pp 57–77
- Sasaki K., Bohnenberger S., Hayashi K., Kunkelmann T., Muramatsu D., Poth A., Sakai A., Salovaara S., Tanaka N., Thomas B.C., Umeda M., *Photo catalogue for the classification of foci in the BALB/c 3T3 cell transformation assay.,* Mutation Research (2012), Vol. 744, pp 42-53
- Sasaki, K., Umeda M., Sakai A., Yamazaki S., Tanaka N., *Transformation assay in Bhas 42 cells: a model using initiated cells to study mechanisms of carcinogenesis and predict carcinogenic potential of chemicals.*, In: Journal of Environmental Science and Health. Part C, Environmental Carcinogenesis & Ecotoxicology Reviews (2015), Vol. 33, pp 1–35
- SCCS, *SCCS's Notes of Guidance for the Testing of Cosmetic Ingredients and Their Safety Evaluation* (2015), SCCS/1564/15
- Schechtman L.M., *Rodent cell transformation assays—A brief historical perspective.,in* Mutation Research: Mutation Research/Genetic Toxicology and Environmental Mutagenesis (2012), Vol. 744, pp 3–7

- Sistare F.D., Morton D., Alden C., Christensen J., Keller D., De Jonghe S., ..., DeGeorge J.J.**,** *An analysis of pharmaceutical experience with decades of rat carcinogenicity testing: support for a proposal to modify current regulatory guidelines.*, Toxicologic Pathology (2011), Vol. 39, pp 716-744
- Smyth, D., Alternatives to animal experiments. London: Scholar Press (1978)
- Smith M.T., Guyton K.Z., Gibbons C.F., Fritz J.M., Portier C.J., Rusyn I., DeMarini D.M., Caldwell J.C., Kavlock R.J., Lambert P.F., Hecht S.S, Bucher J.R., Stewart B.W, Baan R.A., Cogliano V.J., Straif K., *Key characteristics of carcinogens as a basis for organizing data on mechanisms of carcinogenesis.,* Environmental Health Perspectives (2016), Vol. 124
- Srivastava S., Sinha R., Roy D., *Toxicological effects of malachite green.,* Aquatic Toxicology (2004), Vol. 66, pp 319–329
- Strange K., *Revisiting the Krogh principle in the post-genome era: Caenorhabditis elegans as a model system for integrative physiology research.,* Journal of Experimental Biology (2007), Vol. 210, pp 1622-1631
- Sung K.E., Su X., Berthier E., Pehlke C., Friedl A., Beebe D.J., *Understanding the Impact of 2D and 3D Fibroblast Cultures on In Vitro Breast Cancer Models.,* PlosOne (2013), Vol. 8, pp e76373
- Sung K.E., Beebe D.J., *Microfluidic 3D models of cancer.,* Advanced Drug Delivery Reviews (2014), Vol. 0, pp 68–78
- The Food and Agricultural Organization of the United Nations and the World Health Organization (FAO/WHO), *Chapter 7: risk characterization in Environmental Health Criteria 240: Principles and Methods for Risk Assessment of Chemicals in Food.(*2009), pp 1–18
- Thomson J.P., Moggs J.G., Wolf, C.R., Meehan R.R., *Epigenetic profiles as defined signatures of xenobiotic exposure.*, Mutation Research - Genetic Toxicology and Environmental Mutagenesis (2014), Vol. 764-765, 3-9
- Tollefsen K.E., Scholz S., Cronin M.T., Edwards S.W., de Knecht J., Crofton K., Garcia-Reyero N., Hartung T., Worth A., Patlewicz G., *Applying Adverse Outcome Pathways (AOPs) to support Integrated Approaches to Testing and Assessment (IATA).,* Regulatory Toxicology and Pharmacology (2014), Vol. 70, pp 629-640
- Tomatis L., Aitio A., Wilbourn J., Shuker L., *Human carcinogens so far identified.,* Japanese journal of cancer research (1989), Vol. 80, pp 795-807
- Truhaut R., *The concept of the acceptable daily intake: an historical review.,* Food Additives and Contaminants(1991), Vol. 8, pp 151-162
- Tsuchiya T., Umeda M., *Improvement in the efficiency of the in vitro transformation assay method using BALB/3T3 A31-1-1 cells*, Carcinogenesis (1995), Vol.16, pp 1887-1894
- Umemura T., Kuroiwa Y., Tasaki M., Okamura T., Ishii Y., Kodama Y., Nohmi T., Mitsumori K., Nishikawa A., Hirose M., *Detection of oxidative DNA damage, cell proliferation and in vivo mutagenicity induced by dicyclanil, a non-genotoxic carcinogen, using gpt delta mice.,* Mutation Research (2007), Vol. 633, pp 46–54
- United Nations, *Transforming our world: the 2030 agenda for sustainable development,* Gen. Assem. 70 Sess, 16301 (2015), pp. 1-35

- Urani C., Stefanini F.M., Bussinelli L., Melchioretto P., Crosta G F., *Image analysis and automatic classification of transformed foci.*, In: Journal of microscopy (2009). Vol. 234, pp. 269–279
- Urani C., Corvi R., Callegaro G., Stefanini F.M., *Objective scoring of transformed foci in BALB/c 3T3 cell transformation assay by statistical image descriptors*., Toxicology in Vitro (2013), Vol. 27, pp 1905-1912
- Vasseur P., Lasne C., *OECD Detailed Review Paper (DRP) number 31 on "Cell Transformation Assays for Detection of Chemical Carcinogens": main results and conclusions.*, In: Mutation Research/Genetic Toxicology and Environmental Mutagenesis (2012), Vol. 744, pp. 8–11
- Vedani A., *Computer-aided drug design: an alternative to animal testing in the pharmacological screening*, ALTEX (1991), Vol. 8, pp 39
- VICH GL28, *Studies to evaluate the safety of residues of veterinary drugs in human food: carcinogenicity testing.,* Guidance for Industry, Revision(Step 9) (2005), pp 1-5
- Villeneuve D.L., Crump D., Garcia-Reyero N., Hecker M., Hutchinson T.H., LaLone C.A., Landesmann B., Lettieri T., Munn S., Nepelska M., Ottinger M.A., Vergauwen L., Whelan M., *Adverse Outcome Pathway (AOP) Development I: Strategies and Principles.,* Toxicological Sciences (2014), Vol. 142, pp 312–320
- Warburg O., Wind F., Negelein E., *The metabolism of tumors in the body., Journal of General Physiology* (1927), Vol.8, pp 519-530
- Ward J.M., *The Two-Year Rodent Carcinogenesis Bioassay - Will It Survive?,* Toxicologic Pathology (2007); Vol. 20, pp 13–19
- Weinstein B., Case K., *The History of Cancer Research: Introducing an AACR Centennial Series,* 2008
- Wilbourn J., Haroun L., Heseltine E., Kaldor J., Partensky C., Vainio H., *Response of experimental animals to human carcinogens: an analysis based upon the iarc monographs programme.*, Carcinogenesis (1986), Vol. 7 , pp 1853-1863
- von Wittenau M.S., Estes P.C., *The redundancy of mouse carcinogenicity bioassays.* Fundamental and Applied Toxicology (1983), Vol, 3, pp 631-639
- WHO Assembly Resolution**,** *IARC Statement on the Adoption of the New Cancer Resolution by the World Health Assembly*, (2017)
- World Health Organization's International Agency for Research on Cancer (2018). Latest global cancer data: Cancer burden rises to 18.1 million new cases and 9.6 million cancer deaths in 2018. Available at www.iarc.fr/wp-content/uploads/2018/09/pr263_E.pdf
- Wu M., Neilson A., Swift A.L., Moran R., Tamagnine J., Parslow D., Armistead S., Lemire K., Orrell J., Teich J., Chomicz S., Ferrick D.A., *Multiparameter metabolic analysis reveals a close link between attenuated mitochondrial bioenergetic function and enhanced glycolysis dependency in human tumor cells.*, The American Journal of Physiology-Cell Physiology (2007), Vol. 292, C125-C136
- Wu S., Powers S., Zhu W., Hannun Y.A., *Substantial contribution of extrinsic risk factors to cancer development.*, Nature (2016), Vol. 529, pp 43-47
- Zarn J.A., Engeli B.E., Schlatter J.R., *Study parameters influencing NOAEL and LOAEL in toxicity feeding studies for pesticides: exposure duration versus dose decrement, dose*

spacing, group size and chemical class., Regulatory Toxicology and Pharmacology (2011), Vol. 61, pp 243-250

- Zeiger E., Anderson B., Haworth S., Lawlor T., Mortelmans K., Speck W., *Salmonella mutagenicity tests: III. Results from the testing of 255 chemicals.,* Environmental Mutagen Research (1987); Vol. 9, pp 1–109

Chapter 2

2. Biogeochemistry of Cadmium and its speciation in the Environment

❖ 2.1 Preamble

Cadmium (Cd) is a silver-white, soft and malleable metal that constitutes one of the trace elements in earth's crust, along with Copper (Cu), Lead (Pb), Nickel (Ni) and Zinc (Zn). As shown Table 2.1, as a member of Group 12 (d block and period 5) of the Periodic System of the Chemical Elements, Cd shares many chemical and physical properties with zinc and, to a lesser extent, with mercury (Waalkes, 2003). This metal was discovered in 1817 as an impurity of Zn ores; F. Strohmeyer identified cadmium in the smithsonite (ZnCO3), and K. S. L. Hermann e J. C. H. Roloff in a specimen of zinc oxide (ZnO) (Bashir et al., 2014; Moulis et al., 2016). Furthermore, the highest concentrations of Cd are associated with the Zn sulfides (e.g., sphalerite and wurtzite), Zn silicates and Zn carbonates. Low levels of cadmium are also observed as a byproduct of lead and copper sulfides (e.g., galena (PbS), metacinnabar (HgS), and chalcopyrite (CuFeS2)) (Sharma et al., 2015; Cullen et al., 2013). Consequently, high concentrations of Cd are more commonly found in areas characterised by deposits of zinc, lead, and copper. Cd is present in crustal materials and soils as a mixture of eight stable isotopes (Table 1) and artificial radioisotopes; these are ^{103}Cd, ^{104}Cd, ^{105}Cd, ^{107}Cd, ^{109}Cd, ^{115}Cd, ^{117}Cd, ^{118}Cd and ^{119}Cd with a half-life of 10 min, 57 min, 55 min, 6.5 h, 450 days, 53.5 h, 2.4 h, 49 min and 2.7 min, respectively (Cullen et al., 2013). Overall, Cd exists in complexes with either inorganic or organic substances. The prevalent Cd compounds and mineral forms are CdS (greenockite and hawleyite), cadmoselite (CdSe), monteponite (CdO), otavite ($CdCO_3$), cadmian metacinnabar ((Hg,Cd)S), cadmium-sulfate ($CdSO_4$), cadmium-chloride ($CdCl_2$) and cadmium-nitrate ($Cd(NO_3)_2$) (Bashir et al., 2014, Cullen et al., 2013). Among these, greenockite is the most common mineral of cadmium that, due to its light-yellow or orange-coloured and its solubility in water of approximately 0.13 mg/100 g at 18 °C, is used as a pigment for soaps, fireworks, textiles, paper, and in printing inks.

Table 2.1. Relevant physical, chemical and geochemical properties of cadmium. (Sharma et al., 2015, Cullen et al., 2013)

Physical properties	Chemical properties	Geochemical properties
Insoluble in water	Atomic number is 48	Strong chalcophilic Element
Inflammable	Atomic weight is 112.40 g mol^{-1}	Abundance in earth crust is 0.15-0.2 ppm (µg/g)
Density is 8.642 g/cm^{-3} at 25°C	Cd has 8 stable isotopes: ^{106}Cd,1.22%; ^{108}Cd, 0.88%; ^{110}Cd, 12.39%; ^{111}Cd, 12.75%; ^{112}Cd, 24.07%; ^{113}Cd, 12.26%; ^{114}Cd, 28.86%; ^{116}Cd, 7.58%(abundance)	Low concentration in igneous rocks
Vapor pressure at 400°C is 1.4 mm and at 500°C is 16 mm	As a transition metal belongs to Group II b of the periodic table	Ratio of Zn/Cd varies in all igneous rocks
Forms CdO in air as vapor is very reactive	Electronic configuration is [Kr] $4d^{10}$ $5s^{2}$	Cadmium concentration is high in oceanic shale and lacustrine sediments, oceanic manganese and nodules phosphorites
Melting point is 321.069 °C, 609.92 4 °F, 594.219 K	Oxidation state is +2 but few compounds show +1 oxidation state	The most common cadmium mineral is greenockite (CdS).
Boiling point is 767 °C, 1413 °F, 104 K	Has a tendency to form covalent bonds with sulphur	Cadmium may accumulate in sedimentary rocks, and marine phosphates often contain about 15 mg cadmium/kg (GESAMP, 1984).
CAS number is 7440-43-9	forms soluble complexes with cyanine's and ammines,	
	For fourfold coordination, cadmium ionic radius is 0.88A°	
	For six-fold coordination, cadmium ionic radius is 1.03A°	

❖ 2.2 Cadmium Compounds and their Sources

The mobilization of cadmium in the biosphere depends on both natural and anthropogenic activities. 60% of natural Cd emissions into the environment occur via episodic volcanic eruptions (100-500 mt/yr) (Nriagu et al., 1988), and the remaining 40% are a combination of wind-borne dust, marine biogenic aerosols, and burning of plant biomass (Cullen et al., 2013). However, the variability in Cd content and the unpredictability of the eruptions make it hard to have an accurate quantification of the global Cd fluxes coming from these natural sources. Nevertheless, Cd concentrations around volcanoes remain elevated, as in the case of the plume of Mount Etna that contains about 90 ng/m^3 of this metal (Buatmenard et al., 1978). Physical and chemical weathering of rocks represents the main flux of large quantities of cadmium to the world's oceans (15,000 mt/yr) (GESAMP, 1987). In particular, regions of the United Kingdom and United States (USA) are characterized by soil and aquatic contaminations because of the erosion of shale and minerals deposits containing elevated Cd levels (Lund et al., 1981). Analysis of ice core provides a historical report of pollutants in atmospheric precipitation. The Arctic ice deposits contain on average 5 pg/g Cd, while the Antarctic contains 0.3 pg/g (Wolff et al., 1985). To sum up, in a year, 25,000 tons of cadmium are comprehensively released into the environment through natural sources (Bashir et al., 2014). Moreover, anthropogenic activities also represent an important source of Cd release into air, land, and water (WHO, 2010). The principal Cd releasing activities are the smelting and refining of non-ferrous metals, fossil fuel combustion, electric and electronic scraps incineration, and the industrial application and creation of Cd-containing products (WHO, 2007). Other anthropogenic sources are the mining of ores, phosphate fertilizers, and remobilization of historical waste sediments, such as the contaminated water close to mines and landfill sites. Cd production is strongly related to the extraction of Zn minerals. It is calculated that the extraction and the processing of one ton of Zn generate 3 kg of Cd (Moulis et al., 2016). Consequently, the high commercial demand of Zn products has led to an increase in Cd pollution, amounting to ca. 20,000 tons/yr.

❖ 2.3 Cadmium Compounds and their Uses

Since the industrial revolution, Cd has been widely used in many types of manufacturing applications, and its commercial demand has continued to increase. The first use of Cd was in the form of pigment. Many painters, such as Claude Monet, Vincent Van Gogh, Cezanne and Matisse started to utilise the Cd yellows and reds in oils, acrylics and watercolours. Later, Cd was broadly used in coatings and printing industries, and also in toys, soap, ceramics, glasses and enamels (Bandow et al., 2016). However, concerns about human health and economic factors have led to a considerable reduction in the use of Cd as a pigment and to its replacement with safe paints. Nickel/cadmium (NiCd) batteries remain the primary industrial application for cadmium, also considering the growth of their use from 8% of the total market in 1970 to 70% in 2016 (Moulis et al., 2016). These types of batteries are more versatile than other rechargeable accumulators, because of their long life, larger capacitance, higher energy density and tolerance to physical and electrical stress (Cullen et al., 2013). Cd is also used for coating materials in marine and aerospace applications, for improving the resistance of alloys in electroplating and as a stabiliser in polyvinyl chloride polymers (PVC), owing to its good resistance to corrosion (WHO, 1992; Wilson, 1988). The ability of some Cd crystals to convert light energy into electricity has made Cd an economical option in photovoltaics cells. Cd has also been employed in phosphate fertilisers, fungicides, detergents, sprinkler systems, refined petroleum products and in nuclear reactors to control atomic fission (Moulis et al., 2016; Wilson, 1988). More recently, the introduction of stringent limits and restrictions on Cd consumption has led to a decline in Cd applications in certain countries. For example, member states of European Union (EU) curbed the emissions of cadmium from 485 mt/yr in 1990 to 257 mt/yr in 2003 and 172 mt/yr in 2016 (WHO, 2007; EEA, 2018; Crea et al., 2013). Further, some countries have implemented recycling initiatives. The replacement of Cd in industrial products that require harsh processing conditions, such as in special alloys development, is less straightforward. The main cadmium user countries remain Canada, USA, Australia, Mexico, Japan, and Peru; East Asia has increased Cd emissions in the last 40 years (Bashir et al., 2014); this reflects the industrial development and the less stringent emission control of this area (Cullen et al., 2013).

❖ 2.4 Cadmium in the Environment

2.4.1 Cadmium in the Atmosphere

The release of cadmium in nature by human actions has altered the biogeochemical cycle of this metal in each environmental compartment. In the atmosphere, Cd emissions are predominantly triggered by anthropogenic sources, such as combustion processes and steel production. In particular, the main Cd compounds discharged in the air are oxides (CdO), chlorides (CdCl2), sulfides (CdS and CSO_4) and the elemental form. Elemental cadmium (Cd) is a by-product of organic fossil fuel combustion; non-ferrous metal production creates sulfides, and waste incineration is a source of cadmium chloride (Crea et al., 2013). Cadmium and its salts enter into the atmosphere as particles with sizes ranging from 0.6 to 1.3 μm; Cd can be included into the particulate ($PM_{2.5}$ and PM_{10}) (Molnar et al., 1995; Dillner et al., 2005). Molnar et al. (1995) have also identified a rare particle of approximately 0.1 μm. The "lifetime" of pollutant particles in the atmosphere (the time needed to reduce the concentration of a particular compound of 37% of its original concentration) depends on the particle density and on meteorological condtions. For example, a climate with little rainfall leads to a longer lifetime of Cd in the air (also 3–7 weeks), implying a long-range atmospheric transport (Godt et al., 2006). In any case, because of the particles small size, Cd can be quickly dispersed by the wind. Analysis of Cd deposition by measuring the crustal enrichment factors (EF_c) in several areas of the planet has shown a latitudinal gradient of pollution (Cullen et al., 2013; Lee et al., 2008). Nevertheless, concentrations of cadmium persist in being more elevated near metal industries (Hirata, 1981). In Europe, Cd air concentrations are ca. 0.05–0.2 ng/m^3 in Northern Europe, 0.2–0.5 ng/m^3 in central Europe and 0.06–0.12 ng/m^3 in southern Europe in 2003 (Aas et al., 2005). In particular, cadmium concentrations are 1–10 ng/m^3 in urban areas, and 100 ng/m^3 in the proximity of industrial area, such as Belgium (WHO, 1992). However, Cd pollution in EU decreased to a half in the period 1990–2003. In the USA, the levels of atmospheric Cd range from 0.001 μg/m^3 in remote areas to 0.005-0.04 μg/m^3 in urban areas, to 7 μg/m^3 in industrial areas (Davidson et al., 1985; EPA, 1981; Saltzman et al., 1985; Schroeder et al., 1987). In these conditions, if a person breathes 20 m^3 of air per day and spends 10% of time outdoors, he or she could likely assume 0.1-0.8 μg/day of Cd in urban

cities and 0.02 µg/day in rural areas. Indoor, Cd is found in house dust in a concentration of ca. 15 µg/g in rural areas, 40 µg/g in urban areas, and 140 µg/g in industrial areas (Friberg et al., 1974). However, these concentrations could increase with contributions of other indoor sources, such as smoking. From the atmosphere, Cd relocates in soils and waters by dry and wet depositions of its particles.

2.4.2 Cadmium in soils

Cd concentration in soils depends on the content of this metal in parent rocks and anthropogenic activities. Still, the anthropogenic sources dominate the mobilisation of terrestrial cadmium in this environmental compartment. Besides the atmospheric deposition described in Paragraph 1.4.1, phosphate fertilizers and biosolids are direct sources of Cd pollution. As a result, Cd levels in arable soils are more elevated respect to non-agricultural soils. Mean Cd concentrations vary between 0.06 and 0.6 mg/kg in EU (Lado et al., 2008) and between 0.1 and 1.0 mg/kg in the USA (Page et al., 1987). In Western Africa values ranging from 1.6 to 2.55 mg/kg have been observed (Hutton, 1982). The employment of municipal sewage sludge as a fertilizer has also increased Cd levels in soils, but, national and regional regulations have limited this practice in many industrialized countries (Davis, 1984). Estimations have shown that polluted soils can contain Cd levels of 57 mg/kg for a long-term continuous application of sludge, 160 mg/kg close to metallurgical industries, and 468 mg/kg in non-ferrous metal mining areas (Fleischer et al., 1974). Metals and Cd are relatively immobile in the soil (clay soils retaining more Cd than sandy soils), and consequently, their contamination is highest next to the source and diminishes with distance. However, pH and cation exchange are the principal factors regulating Cd solubility and absorption in soils, Cd being more soluble in acidic soils; besides, soils that are rich in hydrous oxides of manganese and iron, organic matter, and calcium carbonate decrease their levels of Cd in solution (WHO, 1992). As a consequence, Cd availability to plants decreases as soil pH increases, while only Cd in solution can be directly available. Moreover, Cd incorporation into solid soil phases occurs in decades in the top 15 cm via chemicals reactions (e.g. ion exchange) (Cullen et al., 2013; ATSDR, 1999). The most common forms in soils are Cd^{2+} and aqueous sulfate species at pH < 8,

$Cd(OH)_2$ and $CdCO_3$ in basic conditions, and Cd-cyanine complexes (Crea et al., 2013). Fortunately, soil pollution can be monitored and controlled by direct removal of Cd from contaminated soil. This procedure is implemented by adding non-toxic materials to lessen Cd solubility and by plants phytoremediation (Paragraph 2.5.3).

2.4.3 Cadmium in natural waters

Air and soil pollution influence Cd levels in freshwaters and oceans. On one side, Cd can contaminate fresh and marine waters through the precipitation of atmospheric particulate; on the other side, Cd in agricultural land (Paragraph 1.4.2) can be dissolved in irrigation waters and transported in large quantities into the rivers, groundwaters, and oceans (Yamagata et al.,1970). Furthermore, rivers can lead to extensive contamination downstream of Cd source by the dumping of dredged sediments or by flooding (Forstner, 1980). However, Cd and its compounds change their mobility and toxicity depending on pH, ionic strength, the concentration of competing cations and the amount of organic matter in the aquatic environment. For example, in a freshwater and at pH 9, 90% of Cd speciation are represented by $CdCO_3$ and Cd^{2+}, with $Cd(OH)^+$ representing only 7%. At pH 7, instead, Cd^{2+} is the predominantly dissolved form. The chloride forms dominate in seawaters. At pH 8, Cd is present for 45% as $CdCl_2$, 36,6% as $CdCl^+$, 14,4% as $CdCl^-_3$ and 3.1% as a free ion. In hypersaline waters, all the cadmium is distributed as soluble chloro complexes (Crea et al., 2013). This depends on the interactions between Cd^{2+} and the main inorganic component of waters. Free Cd^{2+} ions can also bind different organic matter changing the levels of $[Cd^{2+}]$free/[Cd]Tot. The value of this ratio can switch from 0.01-0.03 in eutrophic lakes to 0.05-0.09 in rivers (Cao et al., 2006). Acidification of lakes leads to an increase of Cd levels in waters (WHO, 1986), but the organic complexation in oligotrophic or acidic lakes (pH < 7.3) reaches a value of 0.8 (Sigg et al., 2005). The levels of Cd pollution around the sources remain more elevated: Cd concentrations in unpolluted waters are below 1 µg/l (Friberg et al., 1986), while the maximum value recorded is around 100 µg/l in the Rio Rimao in Peru (WHO, 1989). The predominant anthropogenic activities leading to Cd accumulation in aquatic environments are non-ferrous metal mining, as well as the processing and the smelting of ores. In particular,

Cd release is influenced by specific industrial waste management policies (e.g. the control and purification of discharge waters) (WHO, 1992). The natural mobilization of Cd in the waters depends on the coastal erosion or the pitting of minerals bodies. Natural decontamination of waters can occur using some medicinal plants, such as the seeds of *Moringa oleifera*, peanuts (*Arachis hypogaea*), cowpeas (*Vigna unguiculata*), urad (*Vigna mungo*) and corn (*Zea mays*) (Rahimzadeh et al., 2017) (Paragraph 2.5.3).

❖ 2.5 Cadmium and its Toxicity

The massive Cd release into the environment has a destructive impact on various ecosystems. Cd does not have a biological role in almost any living organisms and it is toxic to many forms of life; moreover, biological systems are unable to prevent its uptake, because of its similariry to Zn, which does not allow cells to discriminate between the two (Moulis et al., 2016). Cd can cross cell membranes by what has been named a "Trojan horse strategy": Cd ions easily replace Zn and other divalent cations in channels and transporters. The implication is that Cd^{2+} accumulates inside the cells of many organisms, enter into the food chain and represent a serious threat for animal and human health (Paragraph 1.5.3). Once inside the cell, Cd ions substitute other ions in their biological functions, leading to an unbalance in metals homeostasis or disrupting metabolic pathways of cells (Chapter 4). Cd^{2+} can replace iron as shown by Bonomi et al. (1994) in the reduced *Clostridium pasteurianum* ferredoxin, copper as illustrated by Iguchi and Sano (1985) and zinc as described in the research of Tang et al. (2014). Otherwise, manganese (Mn), selenium (Se) and cobalt (Co) are also fundamental for the regulation of several enzymes and could be targets of Cd replacement. Besides, cells inability to excrete Cd, leads to its accumulation and progressively induces more severe dysfunctions in organs. In 1976, the Task Group on Metal Toxicity defined the terms of "critical concentration" and "critical organ". The first definition is the metal concentration to which functional changes, reversible or irreversible, appear into one of the cells of an organ. The critical concentration varies by species. The "critical organ" is the organ in which the first damage of the critical concentration occurs. The first adverse change was identified as the "critical effect”. In case of Cd, it has not yet been clarified.

2.5.1 Cadmium toxicity in acquatic organisms

The poisoning of the aquatic organisms depends principally on the presence of high levels of Cd^{2+} in the waters, while the formation of Cd complexes with inorganic or organic ligands leads to a decrease in the toxicity of this metal (Campbell, 1995). An elevated dissolved organic matter (DOM) content can therefore protect the whole ecosystem by removing Cd in solution. The uptake of Cd in water organisms can also decrease with increasing water hardness, H^+ concentration and salinity (Peterson et al. 1984; Mayer et al. 1989). Consequently, Cd varies its toxicity in fresh and salt waters. In the oceans, where this metal concentration ranges from 5 ng/L to 1 µg/L and in surface waters is less than 5 ng/L, its distribution resembles Zn distribution and other essential nutrients profile (WHO,1992). The highest Cd concentrations are estimated in the ocean bottom, and an impoverishment towards the water surface occurs because of phytoplankton absorption (Xu et al., 2013; Cullen et al., 2013). This vertical profile is a possible demonstration that Cd can have a physiological role as a nutrient and has beneficial effects on marine phytoplankton. This theory was later confirmed in several experiments. Indeed, in some culture studies, the growth rate of phytoplankton under conditions of Zn limitation has almost mimed the growth standard profile with the addition of Cd to the medium (Price et al., 1990). Quite conceivably, Cd replaces Zn in many proteins maintaining their biological functions. Moreover, Cd is less efficient in carrying out the biological role of Zn and Cd becomes toxic in Zn depletion conditions (Xu et al., 2013). The only protein, discovered so far, that uses Cd^{2+} in the catalytic site is Carbonic anhydrase from diatomea, catalysing the reversible hydration of HCO_3^- to form CO_2 required by ribulose-1,5-biphosphate carboxylase in the Calvin cycle (Xu et al., 2008). In general, CA relies on Zn for its activity; however, when the concentration of Zn in the medium is close to 2–50 pM, Cd can substitute for Zn in TWCA1 or increase the expression of Cd-specific form of CA (Lane et al., 2000). This is an exception, Cd ions being toxic also for marine organisms. The toxicity depends on the competition of Cd for the same uptake system of Mn and Fe and the inability of the individual species to detoxify this metal (Xu et al., 2013). The uptake of Cd by phytoplankton is directly proportional to dissolved Cd concentrations and indirectly proportional to dissolved Zn and Mn concentrations. Under low Mn and low Zn, the upregulation of a high affinity Mn transporter and the Cd/Co

transport system carry Cd inside cells. Cd toxicity in phytoplankton is similar to its toxicity in plants (Paragraph 1.5.2.). In freshwater, Cd is more toxic and bioavailable to a wide range of organisms, but in particular, fish and invertebrates are the most sensitive (Wright et al., 2011). O'Hara (1973) has demonstrated that the mortality of fiddler crabs *Uca pugilator* was higher at low salinities. Voyer and Modica (1990) found the same results with the shrimp Mysidopsis bahia. Sub-lethal effects of Cd could be a reduction of growth and reproduction of aquatic invertebrates and structural defects on invertebrate gills. In fish, Cd^{2+} is accumulated in gills, kidney, intestine, muscles and skin. However, kidney and liver are the critical organs for all fish species, while gills, intestine and muscle are secondarily damaged after Cd long-term exposure (Oluwatosin et al., 2015). In the kidney, Cd disrupts calcium metabolism; in the liver, Cd induces engorgement of blood vessels, necrosis of hepatocytes, and change in fatty metabolism (Kumar et al., 2010). Sub-lethal effects in fish are evident as malformations of the spine, gills and kidney (Kumar et al., 2010; Oluwatosin et al., 2015). At the molecular level, Cd inhibits ion transport systems and induces metallothionein (MTs) synthesis. MTs enables fish to detoxify this and other metals. Fish are thus used as biological indicators of metal contamination through the bioconcentration factor (BCF). This value is a measure of chemical partitioning between fish tissue and water and is measured in mol/kg of fish or mol/l of water. Fish in polluted areas can have a BCF in the range of 50,000-200,000, while 2,000 being a typical value in uncontaminated regions. Otherwise, if Cd accumulates in sediments, the target of this metal becomes the benthic biota. Cadmium levels are approximatively 5 mg/kg in river and lake sediments and vary from 0.03 to 1 mg/kg in marine sediments (Korte, 1983). The value of Cd that allows 95% of surviving of aquatic biota is 0.2 µg/L in freshwater with a hardness of 30 mg/L $CaCO_3$, and 5.5 µg/L in marine waters (ANZECC & ARMCANZ, 2000).

2.5.2 Cadmium toxicity in plants

The pollution of the soils is strongly connected with an increase in the uptake of Cd by plants. However, the variety of cultivated plants or the type, pH and organic matter content of soils can modify the levels of absorption; considering that only soluble Cd in soil is available. An enrichment in hydrous oxides of manganese and iron, organic matter, and calcium carbonates results in a reduction of Cd accumulation by plants, but soil pH is the most critical factor governing the levels of Cd in the soil solution (Page et al., 1987). In particular, the crops planted at acid pH are more susceptible to Cd uptake. Acid rains could influence the pH of the soils increasing the levels of Cd uptake by plants. Still, since the transfer of Cd from the soils to vegetables may increase the dietary Cd exposure for the general population, it is not only essential to assess those soil factors, but also to choose the best species of plants to be cultivated in a specific agricultural land. For this reason, plants are distributed into three categories according to their capacity to uptake heavy metals from the soils, and successively, used for different purposes. The classification in ecotypes relies on the bioaccumulation coefficient (or bioconcentration factor), that is the ratio between the concentration of a specific metal inside the plant tissues and its content in the soil (Küpper et al., 2013). The first group includes the "Excluder" plants; the plants that belong to the second group are denominated "Indicator", and the third group includes the "Hyperaccumulator" plants (Küpper et al., 2013). A plant is a hyperaccumulator when both its shoot/root quotient (level of heavy metal in the shoot divided by level in the root) and the extraction coefficient (level of heavy metal in the shoot divided by total level of the same metal in the soil) are greater than 1. The mean Cd level in plants is less than 0.1 mg/kg, but mushrooms, seeds with lipid reserves, cereal kernels, legumes, rise, tobacco and cocoa beans can accumulate Cd to an average of 2 mg/kg in their tissues. A plant with a shoot/root quotient lower than 1 is classified as an excluder, even if it is characterised by high levels of heavy metals in its roots (e.g. Cyperus articulatus L. for Cd). The excluder plants are resistant to the toxicity of heavy metals and are unable to accumulate them. The indicator plants (e.g. Ludwigia stolonifera for Cd) have a direct proportionality between the level of the amassed metal and the concentration of the metal in the environment. The hyperaccumulators plants store heavy metals in their tissues (Baker et al., 1989), avoiding being eaten by the

herbivores; in a hyperaccumulator heavy metals levels are 10-500 times higher than excluder plants (Mganga et al., 2011). The first group is used for re-vegetation of toxic sites (e.g. soils close to non-ferrous metal mining or lands that were subjected to sewage sludge applications). The second group is utilised for monitoring environmental pollution. The last group is employed for phytoremediation, i.e., the decontamination of polluted soils and water by plants (Chaney R.L., 1983; Shah K., 2017), or phytomining (Baker et al., 1989). Indeed, the hyperaccumulators plants can grow at high concentrations of Cd in natural soil and survive better than the other ecotypes. Instead, Cd can produce biochemical and morphological alterations in the other two plants groups, because of its toxicity. Cd can repress root and shoot development; at higher levels it can Cd inhibit photosynthesis, plant metabolism or the functions of many enzymes, generate free radicals and induce mutations in the genome (Shah K., 2017; Andrersen et al., 2013). Cd enters through the roots, is accumulated in root vacuoles, and it is translocated to the leaves using metal (Fe^{2+}, Zn^{2+} and Mn^{2+}) transporters and channels, as well as Ca^{2+} channels (Moulis et al., 2016). Unfortunately, the role of a specific transporters/channels changes among plant species and single mechanisms involved, are still to be fully elucidated (Marwa et al., 2019; Küpper et al., 2013). In *Arabidopsis thaliana* and rice, IRT1, a member of the ZIP transporter family, allows accumulation Mn, Zn and Cd under low Fe conditions (Vert et al., 2002; Nakanishi et al., 2006); ZIP transporters such as *Arabidopsis* ZIP1, 2, 3 and rice OsZIP1 can transport Cd (Grotz et al., 1998; Ramesh et al., 2003). OsNRAMP5, constitutively expressed in roots, takes up Cd in rice (Sasaki et al., 2012). Another source of Cd accumulation for plants is the deposition of contaminated dust on leaves. Indeed, in controlled laboratory conditions, the uptake of Cd from the leaves can attain 50% of the total. In real conditions, the percentage of Cd absorbed from air dust is hard to be determined. After absorption, plant cells sequester Cd in the vacuole using different transporter, like CAtion/H1 eXchangers (CAX) or P_{1B}-type ATPases (Moulis et al., 2016). A schematic representation of the anthropogenic and natural sources of cadmium together with its biogeochemical cycle is represented in Figure 2.1.

Figure 2.1. A schematic representation of the anthropogenic and natural sources of cadmium together with its biogeochemical cycle (Sebastian et al., 2014).

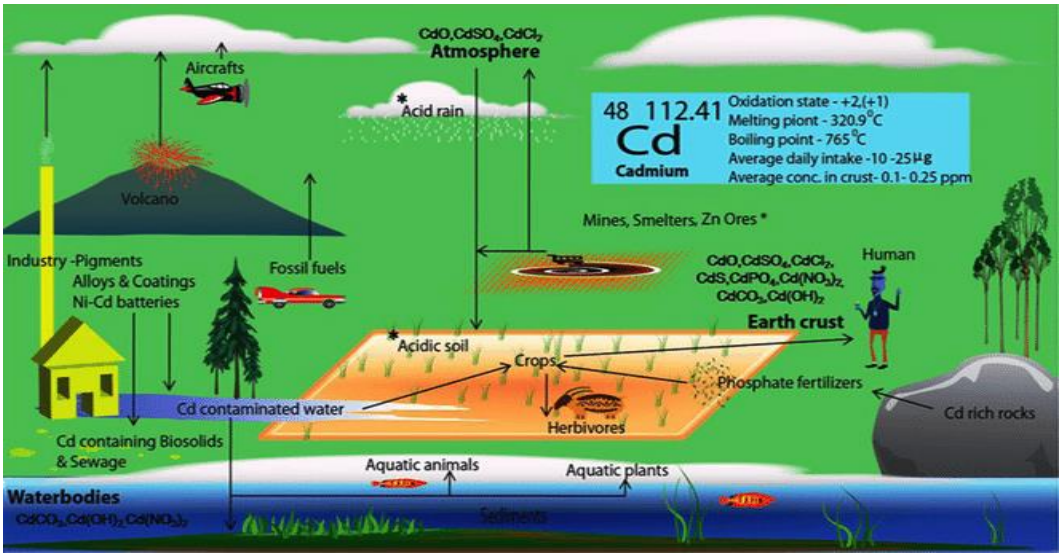

2.5.3 Cadmium Toxicity in Animals and Humans

To conclude the overview of Cd toxicity, this paragraph focuses on harmful effects of Cd in ‘‘animals’’, and more restrictively in ‘‘humans’’. This choice has been based on the necessity to emphasize the dangerous threat that Cd pollution poses for human health. Furthermore, because the probability of human exposure has risen proportionally with environmental contamination, Cd and its compounds have become a serious issue of public concern. It should also be taken into consideration that Cd, having a biological half-life of 10-30 tears, increases its concentration in human body with age. Indeed, there are no known mechanisms that make Cd metabolisation possible. Cd has no beneficial effects in humans.

2.5.3.1 Human Exposure

Workers of various occupational settings can mainly absorb Cd compounds by inhalation or to a lesser extent by contaminated food and waters. For the general population, dietary intake and smoking are the major sources of Cd exposure. In more details, the non-smoking general population accumulates Cd principally by food, and only 10% of total exposure is due to inhalation of Cd content from atmospheric dust and to drinking contaminated water (WHO, 2008). The main categories of food that contribute to Cd exposure are cereals and vegetables, while potatoes, peas, meat and fish contain fewer Cd amounts. In particular, meat, fish, and fruit contain similar Cd levels of 5-10 μg/kg wet weight; Cd concentrations in plant-based foodstuffs remain around 25 μg/kg fresh weight (WHO, 1992). Food preparation can reduce Cd content in vegetables. The milling of wheat grain removes approximately half of Cd in white flour (Linnman et al., 1973). The peeling and cooking of clods can also help to decrease Cd contamination, although it is not extremely effective. On the other hand, the use of plastic or ceramic containers with cadmium-plated surfaces to store or cook foodstuffs can increase Cd contamination, particularly in the case of acidic liquid foods (WHO, 1992). Cd amount in animal commodities depends on the type of feeding stuff used. Cd levels are usually lower than 0.01 mg/kg fresh weight in the meat of cattle, pigs, sheep, rabbits and poultry. On the contrary, offals can register high cadmium concentrations (WHO, 2008). In the liver and kidneys, the organs in which Cd tends to accumulate, Cd concentrations can fluctuate from 0.2 mg/kg to a maximum of 3 mg/kg. Crustaceans and bivalve molluscs, with a Cd amount of 0.09 and 0.38 mg/kg, respectively, are other foods of animal origin rich in cadmium. In the light of the foregoing, the average daily intake of Cd through food could change among countries, the dietary habits and age of the individuals. Teenagers consume the highest Cd concentrations since they have the highest caloric diet (Kjellström et al., 1978). In non-industrialized rural area, Cd intake by ingestion amounts to 10-60 μg per day (μg/d); in Cd polluted areas, such as Japan, values could be several hundreds μg/d (Friberg et al., 1974). Although it is relatively less important than the dietary intake, drinking-water is another way of assuming Cd. For instance, if drinking-water contains approximately 1 μg/L Cd, a person that weighs 60 kg and consumes 2 L of water daily could ingest 0.233 μg/kg of Cd per week (WHO, 2007). Contamination of drinking-water could

derive by the corrosion of the galvanised pipes, water heaters, water coolers and taps. Cd uptake in the gut represents only 5% of Cd ingested with water and food; however, a poor diet, lacking vitamins, calcium and trace elements can increase Cd uptake. People with low iron stocks, such as people with anaemia or with a chronic iron deficit, show a 6% higher Cd uptake (Godt et al., 2006). Another route for Cd uptake is the hand-to-mouth route. This path leads to an uptake of 0.02-0.01 μg of ingested Cd per day per 1 μg/g of soil for adults and about 0.7 μg daily for young children (Culbard et al., 1988); while 0.002-0.12 μg Cd are dermally adsorbed per day per 1 μg/g of soil. The ingestion and dermal uptake of Cd via house dust are both about 0.3 μg/d in rural areas, 0.8 μg/d in urban areas, and 3 μg/d in industrial areas. Assuming that air Cd concentration is about 10 ng/m^3 and the daily inhalation rate (IR) is 20 m^3 for an adult (Paragraph 1.4.1), the intake of Cd from the atmosphere is 0.15 μg, of which 25% is absorbed by lungs. Besides, for the general population who lives in unpolluted areas, Cd uptake is about 0.04 μg/d (Friberg et al., 1974). In polluted areas, in which Cd levels in air become 0.5 μg/m^3, Cd inhalation and absorption are 7.5 μg/d and 2 μg/d, respectively. Smokers may absorb more Cd by inhalation than from food. In more details, if one cigarette contains 1-2 μg Cd (Friberg et al., 1974), but only 0.1-0.2 μg are inhaled (Elinder et al., 1983), a person of 60 kg who smokes 20-40 cigarettes per day inhales 0.23-0.93 μg/kg of Cd per week (EFSA, 2009). For workers, the inhalation of workplace air with a Cd concentration of 10-50 μg/m^3 in 10 m^3 of breathed air, leads to a daily Cd intake of about 100-500 μg and daily Cd uptake of about 25-125 μg. Smoking raises Cd accumulation in the lungs (WHO, 1992).

To minimise the risk of adverse effects on human health, the Scientific Panel on Contaminants in the Food Chain (CONTAM) has established a Tolerable Weekly Intake (TWI) for Cd of 2.5 μg/kg of body weight per week (EFSA, 2009). However, CONTAM believes that this value should be further reduced because Cd remains a risk factor for the health of vegetarians, children and people living in contaminated areas (EFSA, 2009). Indeed, comparing the Cd intake via different routes of exposure, it could be noticed that children absorption of Cd is more elevated than adults, and a vegetarian diet more than doubles the intake of Cd respect to an omnivorous diet. All values are reported in μg/kg of body weight per week and are summarised in Table 5. For children, it was considered a daily inhalation volume of 7 m^3 and a body weight of 15 kg.

Table 2.2. Average population intake (µg/kg of body weight per week) in different exposure pathways

Exposure pathways	Adults	Children
Food	Omnivores: 1,89-2,46 Vegetarian: 5,47	2.56-3.46
Drinking water	0.002-0.23	0.009-0.93
Outdoor air	Rural areas: 0.0002-0.01 Urban areas: 0.005-0.035 Industrial areas: 0.035-0.35	Rural areas: 0.0003-0.02 Urban areas: 0.0065-0.05 Industrial areas: 0.05-0.5
Indoor air	0.08	0.61
Smoking	0,23-0,35	/

2.5.3.2 Entry pathways, transport, and trafficking

Lungs and the gastrointestinal (GI) tract absorb Cd with different efficiencies. In the respiratory system, the size of the airborne Cd particles may determine the site of damage: smaller particles penetrate deeper into the broncho-alveolar region; while large particles (> 10 µm in diameter) remain in the upper airways (Thévenod et al., 2013). However, irrespective of the place of deposition, the particulate material can induce inflammation, which influences the uptake mechanism and the organ sensitivity to Cd. Indeed, under inflammatory conditions, Cd is more efficiently uptaken by alveolar macrophages than type II alveolar epithelial cells, leading to its detoxification in loco but increasing its systemic absorption (Hart et al., 1995). Alternatively, free Cd cations are intaken transcellularly via ion channels and transporters through the plasma membrane of lung cells. For instance, Zrt-,Irt-like protein 8 (ZIP8 or SCL39A8) and SLC11A2 (DMT1) can contribute to apical Cd uptake in lung cells, while the precise involvement of ZIP8 in the physiological trafficking of this metal remain unclear, partly because of its complex regulation (Moulis et al., 2016). In addition, a contribution of paracellular permeation of Cd may also be observed. Cd is able to decrease the number of cadherins (calcium-dependent adhesion proteins) in the epithelial alveolar cells and vascular endothelial cells, leading to the disruption of cell-cell interactions and its permeation through the lung epithelium (Jumarie, 2002). Other parameters that influence Cd absorption in the lungs are the mucociliary and alveolar clearance (Task Group on Lung Dynamics, 1966). Cd uptake into epithelial cells, interstitium or the systemic

circulation hence depends on physical and biochemical processes in the respiratory tract after deposition (e.g., mechanical clearance, solubilization, and transport) (Bressler et al., 2004). In humans, 50% of the Cd inhaled via cigarette smoke could be absorbed (Elinder et al., 1976). Moreover, $CdCl_2$ penetrates more effectively than cadmium oxide and sulfide. From lung, inhaled Cd particles may additionally be transported and accumulated along the primary olfactory nerves in the olfactory bulb (Martelli et al., 2006). Still, although Cd intake in the lungs is more effective than in the gut, Cd absorption from GI tract remains the principal route of Cd contamination and depends on several factors: type of Cd compound, dose, frequency of administration, and interactions of this metal with various nutrients. For example, after a single exposure, the absorption of Cd nitrate or chloride varies from 0.5 to 8% in several animals, but it settles around 5% in humans (Friberg et al., 1974). Furthermore, diets with low levels of calcium and protein, as also iron-deficiency, promote Cd absorption (Friberg et al., 1974; Gunshin et al., 1997). DMT1 is involved in Cd apical transport in human intestinal cells, along with members of the ZIP family, such as ZIP8 and one form of ZIP14, or Ca^{2+} selective channel TRPV6 (Martelli et al., 2006; Bridges et al., 2005). Cd export through the base-lateral membrane of enterocytes into the blood is less efficient than absorption. In this case, Cd can be transported into the bloodstream by Fe export transporter ferroportin 1 (FPN1, IREG1 and MTP1). Cd absorption via GI tract is amplified in pregnant women: in fact, they lower iron levels and a higher density of DMT1 to optimize the absorption of micronutrients (Leazer et al., 2002; Martelli et al., 2006). After absorption, Cd is distributed in various tissues and organs through the blood. The mechanism by which Cd reaches the circulation is not completely clarified, although Cd probably uses transporters or channels dedicated to other ions and biomolecules, both in cationic form or bound to chelating agents such as glutathione and cysteine (Martelli et al., 2006). So, once taken up by systemic circulation, about 50% Cd accumulates in the kidneys and 15% in the liver due to the abundance of Metallothioneins (MTs), reaching values in the range of hundreds of µmol/L (EFSA, 2009; Hartwig et al., 2002). MTs are low molecular weight proteins (about 7 kDa) that participate in a series of protective responses to stress (Babula et al., 2012). In particular, physiological functions of MTs embrace homeostasis of essential metals (Zn, Cu), protection against the cytotoxicity of toxic metals, and scavenging free radicals generated in oxidative stress (Sabolić et al., 2010). The

main route of Cd excretion is urine. However, daily Cd excretion represents only a small portion of that absorbed (approximately 0.007-0.015% of the total body burden). Instead, unabsorbed Cd is removed from the GI tract in feces (approximately 0.03% of the body burden). The slow rate of Cd excretion is due both to the lack of an active biochemical mechanism for elimination and to renal reabsorption (Satarug et al., 2004).

2.5.3.3 Health effects

Exposure to Cd via different pathways leads to an increase in Cd concentrations in body fluids. As a result, Cd adverse are well documented in many organs, although a fatal outcome has been reported in sporadic cases. Human clinical symptoms are thus tightly associated with Cd organs and tissues distribution. Cd can also cause acute or chronic toxicity in humans, depending on the exposition time and on the concentrations to which individuals are subjected. Acute Cd toxicity is less common than chronic exposure. In acute, high-dose Cd intoxication, depending upon the route of exposure (by ingestion and inhalation), the main impact occurs in the lungs and gastrointestinal tract. Indeed, the principal symptom of an acute Cd poisoning (0.01-0.15 mg/m^3 for 9 hrs) via inhalation is the irritation of the upper respiratory tract, although an asymptomatic period of 4-8 hours can occur. Other manifestations of intoxication depend on the dose inhaled. 0.5 mg/m^3 Cd is the threshold established by WHO as "safe" dose, while 1-5 mg/m^3 Cd inhaled for 8 hrs or shorter period was identified as ‘immediately dangerous’ to humans. This amount may lead to extensive fluid loss, metabolic acidosis, pulmonary oedema, hypotension, anorexia, nausea, oliguria, altered metabolism of calcium and zinc and multiorgan failure (HPA, 2010). Higher Cd concentrations are lethal. For instance, 5 mg/m^3 Cd may be lethal after 8 hrs of exposition. The highest dose estimated after post mortem lungs examinations was 2900 mg/m^3 of CdO (Barrett et al., 1947). Acute cadmium poisoning is common among workers that are exposed to Cd containing fumes. Cd acute ingestion can occur accidentally by swallowing contaminated food or beverages. Symptoms begin 60 minutes after exposure and include vomiting, abdominal cramps, diarrhoea, fatigue, sleep disturbances, sensory and motor function disturbances, anorexia, peripheral neuropathy (HPA, 2010). These clinical disorders occur when doses around 15 mg/kg body weight, whereas doses of 20-30 mg/kg body weight

(350 and 8900 mg Cd) are fatal in 24 hours (Bernard et al., 1986). In this case, the liver is the primary target organ of Cd toxicity and hepatic dysfunction causes the death of the patient. Other fatal symptoms are acute renal failure, cardiac damage and hemorrhagic necrosis of gastrointestinal tract. In non-fatal cases, the recovery is complete (Thévenod et al., 2013). Chronic low doses Cd exposure (CLCE) affects a more substantial part of the world population than acute Cd exposure and can target different organs. In particular, kidneys and bones are the principal and general targets of Cd poisoning (Bernard, 2008); while lungs diseases are prevalent among industrial workers and smokers. The reason for these chronical diseases is the very long half-life of Cd after absorption. Indeed, it has been estimated that half-life of this metal in the body is about 13.4 years, 6.2 years in the liver and 17.6 years in the kidney (Thévenod et al., 2013). The exceptional residence time of this metal in the body reflects the fact that Cd can escape detoxification. Hence, Cd exposure in a child can create health problems during the growth. CLCE also increases the risk of mortality in the injured population.
The principal adverse effects of Cd chronic poisoning are listed below and organised by target organs.

Kidney is the chief organ showing Cd toxic impact. In particular, Cd deposition occurs preferentially in the kidney tubule region, and tubular proteinuria is the earliest sign of Cd toxicity. Indeed, proteins with a molecular weight of 10.000 to 40.000 are used as biomarkers of the disease for their increased urinary excretion (Butler et al., 1958). The most common low molecular weight proteins (LMWP) monitored for the diagnosis of Cd-induced tubular proteinuria are ß2-microglobulin (B2M), lysozyme (muramidase), ribonuclease, immunoglobin chains, retinol-binding protein (RBP), and alpha1-microglobulin (A1M) (Satarug et al., 2000). In some circumstances, proteinuria remains the only clinical symptom of the poisoning; in other situations, i.e. when the levels of Cd absorbed are elevated, additional kidney dysfunctions, such as hypercalciuria, phosphaturia, polyuria, glucosuria, and aminoaciduria, become manifest (WHO, 1992). Moreover, in severe cases of Cd intoxication, the renal damage progresses to a reduction in glomerular filtrations and becomes irreversible. In this case, albumin, transferrin, tubular antigens, glucose,

calcium and phosphate are considered as typical biomarkers of glomerular lesion (Thévenod et al., 2013). The disorders of calcium metabolism may be also connected with bone demineralization and the formation of renal stones (Bernard, 2008). An exposure-response relationship is therefore evident, in which renal dysfunction and damage are proportionate to the quantity of Cd stored in cells. In this regard, in 1989, the Food and Agriculture Organization (FAO) and World Health Organization (WHO) Joint Expert Committee on Food Additives and Contaminants (JECFA) established, among several chemical compounds, the safe Cd dietary intake guideline and the urinary Cd threshold limit (FAO/WHO 1989). The original Provisional Tolerable Weekly Intake (PTWI) for Cd was 400–500 μg per person per week. In 1993, the PTWI for Cd was revised to 7 μg/kg body weight per week (70 μg/day for a 70-kg person) (FAO/WHO 1993). Both these values were based on biological models in which the daily Cd intake was about 140-260 μg, and 2000 mg of Cd was accumulated over a lifetime. Currently, the tolerable Cd intake is set at 25 μg/kg body weight per month (0.83 μg/kg body weight/day or 58 μg/day for a 70-kg person), while a urinary Cd threshold level is 5.24 μg/g creatinine (FAO/WHO 2010). The thresholds have been defined upon epidemiological studies of renal failure in which only 10% of the general population has developed renal alterations in above mentioned conditions: 180–200 μg/g Cd wet kidney weight, which corresponds to a Cd concentration of about 10 μg/g of creatinine in urine (Thévenod et al., 2013). About 50% of people show renal tubular proteinuria when Cd concentration achieves 300 mg/kg in the kidney cortex. Proteinuria may also occur following an annual inhalation of 25-134 μg/m^3 of cadmium for at least ten years (corresponding to 1.12-6.01 μg/kg of body weight per week for 70-kg person who inhales 20 m^3 of air per day) (HPA, 2010). The symptoms of renal dysfunction reflect, at the molecular level, that the main Cd binding proteins (metallothioneins) and the antioxidant defence mechanisms (GSH, GR, etc) are overwhelmed. Also, in vitro evidence has shown that free Cd can damage transport proteins and mitochondria, leading to apoptosis or necrosis of tubular cells (Satarug, 2018). Cd may potentiate diabetes-induced effects on the kidney (EFSA, 2009).

Bone is another target organ of Cd toxicity, and several data support this statement. For instance, one study in Belgium (Buchet et al., 1990), another in Sweden (Jarup et al., 1998) and one more in China (Wu et al., 2001) have demonstrated that Cd induces a prolonged urinary excretion of Ca^{2+} (Satarug et al., 2004). Moreover, Cd can impair Vitamin D, parathyroid hormone and collagen metabolism with deleterious impact on bone (Nogawa et al., 1987; Bernhoft, 2013). Cd can thus contribute with these effects to the development of osteomalacia and/or osteoporosis. The correlation between Cd exposure and skeletal demineralisation was also underlined by the Itai-Itai disease, whose symptoms combine intense bone pain with osteoporosis, renal tubular dysfunction, anaemia, and calcium malabsorption. Indeed, in the 1960s and 1970s, the Japanese population began to develop malformation and fractures of bones and, after epidemiological studies, it was reported that tissues of people with Itai-Itai disease contained high concentrations of Cd (Hagino et al., 1961; WHO, 1992). It was also discovered that patients developed Itai-Itai syndrome as a consequence of the ingestion of Cd contaminated rice. Hence, in 1989, Itai-Itai disease has been officially recognized as a pollution-related disease (WHO, 1992).

Cd toxicity on the bone does not depend solely on indirect Cd effects on the kidney, but, has been demonstrated by *in vitro and in vivo* experiments. *In vivo* studies have proved that bone damage may appear well before kidney dysfunctions after Cd exposure to 5 µg/mL (Ogoshi et al., 1989); *in vitro* experiments on the mouse osteoblast-like cell line, MC3T3- E1, have shown that mechanisms of Cd toxicity in bone include an unbalance between bone formation and resorption (Iwami et al., 1993). In particular, Cd concentration that varies from 0.1 to 1 µM decreases osteoblast differentiation down-regulated alkaline phosphatase activity; while 1 µM Cd can activate osteoclast via a MAPK-dependent pathway (Bhattacharyya, 2009).

Liver is the main organ storing Cd in vivo, although the effects of Cd chronic toxicity are moderate. In this organ, Cd stimulates *de novo* synthesis of MTs that efficiently bind and sequester free Cd ions, and it is assumed that toxicity in the cells starts when the buffering capacity of intracellular MTs is overwhelmed. Urani et al. (2005) also confirmed that Cd is highly cytotoxic to human hepatoma cells (HepG2) and the genes coding for MT are up-regulated in the presence of sub-lethal Cd concentration (2-10 μM) after 24 hours of exposure, in a dose-dependent way (Fabbri et al., 2012). Moreover, absorbed Cd can partially be secreted into the biliary tract in the form of Cd-Glutathione conjugates, further reducing Cd toxicity. When hepatocyte necrosis and apoptosis occur, Cd-MT complexes are transported into sinusoidal blood and reach the proximal tubule cells. In the kidney, Cd-MT complexes are filtered, endocytosed, and degraded in lysosomes. Consequently, kidneys remain the main targets of Cd toxicity also in chronic liver intoxication. As a confirmation of this hypothesis, Chan et al. (1993) tried to transplant livers of Cd-exposed rats into normal rats showing that, with time after surgery, Cd-MT levels decreased in the liver and increased in the kidney in each animal. The same evidence is true for humans. In human kidney, Cd concentrations, that are close to zero at birth, increase linearly with age up to 40-50 mg/kg (fresh weight) in 50-60 years. In the liver, the amount of Cd increases from birth to around 20-25 years to typical values of 1-2 mg/kg (fresh weight) (Sumino et al., 1975; Hartwig et al., 2002; EFSA, 2009).

Respiratory System manifests symptoms of Cd intoxication depending on exposure time and metal dosage. However, lung diseases are preferentially correlated with acute Cd poisoning; instead chronic injury rarely occurs after long-term occupational exposure to Cd fumes. The clinical manifestation of chronic intoxication are anosmia and/or chronic inflammation of the nose, pharynx, and larynx in the upper respiratory system (Thévenod et al., 2013). In the lower respiratory system, dyspnoea, bronchitis, emphysema, and chronic obstructive respiratory diseases, such as functional lung impairment with an increase in residual volume and a reduction in working capacity, are frequently seen in Cd workers (WHO, 1992). Excess mortality from

emphysema or dyspnea thus becomes a possible outcome for Cd workers. To prevent toxic effects on the respiratory system, the WHO declared that workers should not be exposed to a Cd concentration exceeding 20 $\mu g/m^3$ in 40 hours working week (WHO, 2010). Smoking induces all or most symptoms described before in cigarette smokers; hence, Cd in tobacco could be an additional harmful environmental agent causing respiratory disorders (Satarug et al., 2004). Indeed, a 50-year-old average non-smoker has a Cd body burden of 15 mg; a comparable life-long smoker shows a value of 30 mg (Godt et al., 2016). Experimental observations have confirmed the relation between Cd exposure and lung dysfunctions. For instance, interstitial pneumonitis and emphysema were found in rabbits after a treatment of 8 mg/m^3 CdO for 4-8 months (Richerson et al., 1978). Snider et al. (1973) observed signs of emphysema in rats after 10 days of exposure to $CdCl_2$ aerosol (10 mg/m^3). According to the Agency for Toxic Substances and Disease Registry (ATSDR), Cd exposure may also enhance the incidence of lung cancer, but the risk is higher in polluted areas (Lampe et al., 2008).

Long-term exposure to cadmium through air, water, soil, and food also leads to cancer and organ system toxicity in reproductive, cardiovascular, and both central and peripheral nervous. Animal studies on Cd toxicity in the reproductive system are limited to male reproductive organs: Cd decreases density, volume and number of sperms, and increases immature sperm forms, leading to infertility (Pizent et al., 2012). In females, both the function of ovary and the development of oocytes seem to be inhibited, but these hypotheses are controversial (Rahimzadeh et al., 2017). However, the production of progesterone and testosterone seems to be the principal target of Cd toxicity. Low Cd doses stimulates ovarian progesterone biosynthesis, while high doses inhibit it (Godt et al., 2006). Nevertheless, it has been reported in experimental animals that Cd compounds may induce adverse effects on the embryo, such as embryonic death or abnormal development of one or more body systems (Thompson J., 2008). Moreover, Cd is deleterious to maternal health. Teratogenic effects (exencephaly, hydrocephaly, cleft lip and palate, microphthalmia, micrognathia, etc) can occur when Cd transported across the placenta is transferred to the embryo in the early stages of gestation

(Thévenod et al., 2013). The literature also supports that Cd affects the cardiovascular system in several ways: i.e., Cd can induce hypertension, atherosclerosis, diabetes, increase systolic pressures or destroy the monolayer of vascular endothelial cells (Navas-Acien et al., 2004; Everett et al., 2008; Eum et al., 2008). Otherwise, epidemiological evidence connects Cd with cardiovascular disease (CVD), cardiac death, peripheral arterial disease, increased carotid intima-media thickness (IMT), and myocardial infarction. Proposed mechanisms of Cd toxicity in cardiovascular system include the disruption of calcium homeostasis in cells and the inhibition of endothelial nitric oxide synthase and acetylcholine, resulting in vasoconstriction (Rahimzadeh et al., 2017; Bernhoft, 2013). In the blood, Cd is transported and accumulated in erythrocytes leading to a decrease in haemoglobin concentration. Hemolysis, Fe^{2+} deficiency, and renal damage may be other factors in leading to Cd-associated anaemia (Thévenod et al., 2013). Neurotoxicity of Cd has been recently reported (Ismail et al., 2015). Oxidative stress, lipid peroxidation, cell death, disturbance of cell signaling pathways, and depletion of glutathione, superoxide dismutase 2, catalase, glutathione peroxidase, and glutathione-S-transferase are foremost mechanisms of Cd toxicity in the central nervous system (CNS) (Lopez et al., 2003; Kim et al., 2005; Shagirtha et al., 2011). The clinical and subclinical brain disorders connected with Cd exposure are olfactory dysfunction, neurobehavioral defects in attention, disorder in psychomotor activity, and memory deficits (Leal et al., 2012). Cd poisoning is also related with Parkinson, Alzheimer, and Huntington's diseases, and amyotrophic lateral sclerosis (ALS) (Vinceti et al., 2017; Rahimzadeh et al., 2017). Viaene et al. (2000) have also suggested that the CNS may be at least as sensitive as the kidneys to Cd toxicity. Lastly, Cd also accumulates in the spleen, heart, thymus, salivary glands, epididymis and prostate (WHO, 2011).

To conclude, Cd and its compounds were classified as carcinogenic in humans by the International Agency for Research on Cancer (IARC), and many epidemiological studies have been published to emphasise the connection between Cd and cancer. The evidence and the possible cellular and molecular mechanisms underpinning cadmium carcinogenicity are treated in details in Chapter 3 of this thesis.

References

- Aas W., Breivik K., Heavy metals and POP measurements 2003. Kjeller, Norwegian Institute for Air Research (EMEP-CCC Report #9/2005). (2005)
- Andresen E., Küpper H., *Cadmium toxicity in plants.,* Metals ions in Life Sciences (MILS)(2013), Vol. 11, Cadmium: From Toxicity to Essentiality pp 395-414
- ANZECC & ARMCANZ., *Australian and New Zealand Guidelines for Fresh and Marine Water Quality.*, Australian and New Zealand Environment and Conservation Council and Agriculture and Resource Management Council of Australia and New Zealand (2000), Canberra.
- ATSDR, *Toxicological profile for mercury – update.* Atlanta, GA, Agency for Toxic Substances and Disease Registry (1999) (http://www.atsdr.cdc.gov/ toxprofiles/tp46.html, accessed 18 September 2007)
- Babula P., Masarik M., Adam V., *Mammalian metallothioneins: properties and functions.*, Metallomics (2012)., Vol. 4, pp 739-750
- Bandow N., Simon F.G., *Significance of cadmium from artists' paints to agricultural soil and the food chain.,* Environmental Sciences Europe (2016), Vol. 28, pp 1:12
- Baker A.J.M.,Brooks R.R., *Terrestrial Higher Plants whichHyper- accumulate Metallic Elements - A Review of their Distribution, Ecology and Phytochemistry,* Biorecovery (1989), Vol. 1, pp. 81-126
- Barrett H.M., Card B.Y., *Studies on the toxicity of inhaled cadmium. II. The acute lethal dose of cadmium oxide for man.*, Journal of industrial hygiene and toxicology (1947), Vol. 29, pp 286-293
- Bashir N., Manoharan V., Prabu S.M., *Cadmium toxicity: Oxidative Stress and Organ Dysfunction.* Research & Reviews: A Journal of Toxicology. (2014), Vol. 4, pp 14-3
- Bernard A., *Cadmium and its adverse effects on human health.,* Indian Journal of Medical Research Indian (2008), Vol.128, pp 557-564
- Bernard A., Lauwerys R., *Present status and trends in biological monitoring of exposure to industrial-chemicals.*, Journal of Occupational and Environmental Medicine (1986), Vol. 28, pp 558-562
- Bernhoft R.A., *Cadmium Toxicity and Treatment.,* The Scientific World Journal (2013)
- Bhattacharyya M.H.*, Cadmium Osteotoxicity in Experimental Animals: Mechanisms and Relationship to Human Exposures.,* Toxicology and Applied Pharmacology (2009), Vol. 238, pp 258–265
- Bonomi F., Ganadu M.L., Lubinu G., Pagani S., *Reversible and non-denaturing replacement of iron by cadmium in Clostridium pasteurianum ferredoxin.,* Eur J Biochemistry (1994), Vol. 222, pp 639-44
- Bridges C.C., Zalups R.K., *Molecular and ionic mimicry and the transport of toxic metals.,* Toxicology and Applied Pharmacology (2005), Vol. 204, pp 274-308

- Bressler J.P., Olivi L., Cheong J.H., Kim Y., Bannona D., *Divalent metal transporter 1 in lead and cadmium transport*., Annals of the New York Academy of Sciences (2004), Vol 1012, pp 142-152
- Buatmenard P., Arnold M., *Heavy-metal chemistry of atmospheric particulate matter emitted by Mount Etna volcano.*, Geophysical Research Letters (1978), Vol. 5, pp 245-248
- Buchet J.P., Lauwerys R., Roels H., Bernard A., Bruaux P., Claeys F., et al., *Renal effects of cadmium body burden of the general population.* Lancet (1990), Vol.336, pp 699–702
- Butler E.A., Flynn F.V., *The proteinuria of renal tubular disorders.,* Lancet (1958), Vol. 2, pp 978-980
- Campbell PGC, *Interactions between trace metals and aquatic organisms: A critique of the free-ion activity model.,* In Metal speciation and bioavailability in aquatic systems (1995), eds A Tessier & DR Turner, John Wiley & Sons, Chichester, pp 45-102
- Cao J., Xue H., Sigg L., *Effects of pH and Ca competition on complexation of cadmium by fulvic acids and by natural organic ligands from a river and a lake.,* Acquatic Geochemistry (2006), Vol. 12, pp 375-387
- Chan H.M., Zhu L.F., Zhong R., Grant D., Goyer R.A., Cherian M.G., *Nephrotoxicity in Rats Following Liver Transplantation from Cadmium-Exposed Rats.,* Toxicology and Applied Pharmacology (1993), Vol. 123, pp 89-96
- Chaney R.L., *Toxic element accumulation in soils and crops: protecting soil fertility and agricultural food-chain.*, in Land treatment of hazardous waste, Eds Parr J.E., Marsh P.B., Kla J.M., Noyes Data Corp., Park Ridge (1983), pp 50-76
- Crea F., Foti C., Milea D., Sammartano S., *Speciation of Cadmium in the Environment.,* Metals ions in Life Sciences (MILS)(2013), Vol. 11, Cadmium: From Toxicity to Essentiality pp 63-84
- Culbard E.B., Thornton I., Watt J., Wheatley M., Moorcroft S., Thompson M., *Metal contamination in British urban dusts and soils.*, Journal of environmental Quality (1988), Vol. 17, pp 227-234
- Cullen J.T., Maldonado M.T., *Biogeochemistry of Cadmium and Its Release to the Environment.,* Metals ions in Life Sciences (MILS)(2013), Vol. 11, Cadmium: From Toxicity to Essentiality pp 31-62
- Davis R.D., *Cadmium - a complex environmental problem. Part II. Cadmium in sludges used as fertilizer.,* Experientia (1984), Vol. 40, pp 117-126
- Davidson C.I., Goold W.D., Mathison T.P., Wiersma G.B., Brown K.W., Reilly M.T., *Airborne trace elements in Great Smoky Mountains, Olympic, and Glacier National Parks.,* Environmental Sciences Technology (1985), Vol. 19, pp 27-35
- Dillner A.M., Schauer J.J., Christensen W.F., Cass G.R., *A quantitative method for clustering size distributions of elements.,* Atmospheric Environment (2005), Vol. 39, pp 1525–1537

- Elinder C.-G., Kjellström T., Lind B., Linnman L., *Cadmium concentration in kidney cortex, liver, and pancreas among autopsied Swedes.*, Archives of Environmental & Occupational Health (1976), Vol. 31, pp 292-302
- Elinder C.G., Kjellström T., Piscator M., Sundstedt K., *Cadmium exposure from smoking cigarettes:variations with time and country where purchased.,* Environmental Research (1983), Vol. 32, pp 220-227
- EPA (U.S. Environmental Protection Agency), *Health assessment document for cadmium.* EPA-600/8-81-023. Research Triangle Park, N.C.: U.S. Environmental Protection Agency, Environmental Criteria and Assessment Office (1981)
- Eum K.D., Lee M.S., Paek D., *Cadmium in blood and hypertension.,* Science of the Total Environment (2008), Vol. 407, pp 147–153
- European Environment Agency (2018). Heavy metal emissions.
- European Food Safety Autority (EFSA), *Cadmium in food. Scientific Opinion of the Panel on Contaminants in the Food Chain.*, The EFSA Journal (2009), Vol. 980, pp 1-139
- Everett C.J., Frithsen I.L., *Association of urinary cadmium and myocardial infarction.,* Environmental Research (2008), Vol. 106, pp 284–286
- Fabbri M., Urani C., Sacco M.G., Procaccianti C., Gribaldo L., *Whole Genome Analysis and MicroRNAs Regulation in HepG2 Cells Exposed to Cadmium.,* ALTEX (2012), Vol. 29, pp 173-82
- Fleischer M., Adel F. Sarofim A.F., Fassett D.W., Hammond P., Shacklette H.T., Nisbet I.C.T., Epstein S., *Environmental Impact of Cadmium: A Review by the Panel on Hazardous Trace Substances.*, Environmental Health Perspectives (1974), pp 253-323
- Food and Agriculture Organization of the United Nations (FAO) World Health Organization (WHO), *Evaluation of Certain Food Additives and Contaminants (Thirty-third Report of the Joint FAO/WHO Expert Committee on Food Additives).,* Geneva: World Health Organization (1989), WHO Technical Report Series No. 776
- Food and Agriculture Organization of the United Nations (FAO) World Health Organization (WHO), *Evaluation of Certain Food Additives and Contaminants: Forty-First Report of the Joint FAO/WHO Expert Committee on Food Additives.*, WHO; Geneva, Switzerland (1993), WHO Technical Report Series No. 837
- Food and Agriculture Organization of the United Nations (FAO) World Health Organization (WHO) Summary and Conclusions; Proceedings of the Joint FAO/WHO Expert Committee on Food Additives Seventy-Third Meeting; Geneva, Switzerland (2010)
- Forstner U., *Cadmium in the environment, Part I.* In: Nriagu J.O., ed. Cadmium in polluted sediments, New York (1980), Chichester, John Wiley & Sons, pp. 305-363
- Friberg, L., Piscator, M., Nordberg, G. F., and others., *Cadmium in the Environment*, 2nd Ed. Boca Raton, Fla.: CRC (1974)

- Friberg, L., Elinder C.G., Kjellström T., Nordberg G.F., *Cadmium and health, a toxicological and epidemiological appraisal. Vol. II. Effects and response*, Cleveland, Ohio, CRC Press, 303 pp. (1986)
- GESAMP, The Joint Group of Experts on the Scientific Aspects of Marine pollution (GESAMP) held its fourteenth session at IAEA Headquarters, Vienna from 26-30 March (1984).
- Godt J., Scheidig F., Grosse-Siestrup C., Esche V., Brandenburg P., Reich A., Groneberg D.A., *The toxicity of cadmium and resulting hazards for human health.,* Journal Occupational Medicine and Toxicology (2006); Vol. 1, pp 1- 22
- Grotz N., Fox T., Connolly E., Park W., Guerinot M.L., Eide D., *Identification of a family of zinc transporter genes from Arabidopsis that respond to zinc deficiency.,* Proceedings of the National Academy of Sciences (1998), Vol. 9, pp 7220-7224
- Gunshin H., Mackenzie B., Berger U.V., et al., *Cloning and characterization of a mammalian proton-coupled metal-ion transporter.,* Nature (1997), Vol. 388, pp 482-488
- Hagino N., Yoshioka K., *A study on the etiology of Itai-Itai disease.*, Journal of the Japanese Clinical Orthopaedic Association (1961), Vol. 35, pp 812-815
- Hart B.A., Gong Q., Eneman J.D., Durieuxlu C.C., *In Vivo Expression of Metallothionein in Rat Alveolar Macrophages and Type II Epithelial Cells Following Repeated Cadmium Aerosol Exposures.,* Toxicology and Applied Pharmacology (1995), Vol. 133, pp 82-90
- Hartwig A., Asmuss M., Blessing H., Hoffmann S., Jahnke G., Khandelwal S., Pelzer A., Bürkle A., I*nterference by toxic metal ions with zinc-dependent proteins involved in maintaining genomic stability.,* Food and Chemical Toxicology. (2002), Vol 40, pp 1179-1184
- Hirata H., *Annaka: land polluted mainly by fumes and dust from a zinc smelter.* In: Kitagishi, K. & Yamane, I., ed. Heavy metal pollution in soils of Japan, Tokyo, Japan Scientific Societies Press (1981), pp 149-163
- Health Protection Agency (2010). Cadmium Toxicological overview. US EPA.
- Hutton M., *Cadmium in the European Community: a prospective assessment of sources, human exposure, and environmental impact.*, London (1982), Monitoring and Assessment Research Centre, Chelsea College, University of London, 100 pp (MARC Report Number 26)
- Iguchi H., Sano S., *Cadmium- or zinc-binding to bone lysyl oxidase and copper replacement.,* Connect Tissue Research (1985), Vol. 14, pp 129-39
- IPCS (1992)., *Cadmium.,* Geneva, World Health Organization, International Programme on Chemical Safety; Environmental Health Criteria 134 (http://www.inchem.org/documents/ehc/ehc/ehc134.htm)
- Ismail S.M., Ismail H.A., Al-Sharif G.M., *Neuroprotective effect of barley plant (Hardeum Valgara) against the changes in MAO induced by lead and cadmium administration in different CNS regions of male guinea pig.,* International Journal of Life science and Pharma Research (2015);Vol. 2, pp 53–60

- Iwami K., Moriyama T., *Comparative effect of cadmium on osteoblastic cells and osteoclastic cells.,* Archives of Toxicology (1993), Vol. 67, pp 352-357
- Jarup L., Berglund M., Elinder C., Nordberg G., Vahter M., *Health effects of cadmium exposure—a review of literature and a risk estimate.,* Scandinavian Journal of Work, Environment and Health (1998), Vol. 24 (suppl 1), pp 1–52
- Jumarie C., *Cadmium transport through type II alveolar cell monolayers: contribution of transcellular and paracellular pathways in the rat ATII and the human A549 cells.,* Biochemistry Biophysics Acta (2002), Vol 1564, pp 487-99
- Kim S.D., Moon C.K., Eun S.Y., Ryu P.D., Jo S.A., *Identification of ASK1, MKK4, JNK, c-Jun, and caspase-3 as a signaling cascade involved in cadmium-induced neuronal cell apoptosis.,* Biochemical and Biophysical Research Communications (2005), Vol. 328, pp 326–34.
- Kjellström T., Nordberg G.F., *A kinetic model of cadmium metabolism in the human being.,* Environmental Research (1978), Vol. 16, pp 248-269
- Korte F., *Ecotoxicology of cadmium: general overview*., Ecotoxicology and Environmental Safety (1983), Vol. 7, pp 3-8
- Kumar P., Singh A., *Cadmium toxicity in fish: An overview.,* GERF Bulletin of Biosciences (2010), Vol. 1, pp 41-47
- Küpper H., Leitenmaier B., *Cadmium-accumulatiing plants.,* Metals ions in Life Sciences (MILS)(2013), Vol. 11, Cadmium: From Toxicity to Essentiality pp 373-393
- Lado L.R., Hengl T., Reuter H.I., *Heavy metals in European soils: a geostatistical analysis of the FOREGS geochemical database.,* Geoderma (2008), Vol. 148, pp 189–199
- Lampe B.J., Park S.K., Robins T., Mukherjee B., Litonjua A.A., Amarasiriwardena C., Weisskopf M., Sparrow D., Hu H., *Association between 24-hour urinary cadmium and pulmonary function among community-exposed men: the VA Normative Aging Study.*, Environmental Health Perspectives, (2008), Vol. 116, pp 1226-1230
- Lane T.W., Morel F.M.M., *A biological function for cadmium in marine diatoms.,* Biochemistry (2000), Vol.97, pp 4627-4631
- Leal R.B., Rieger D.K., Peres T.V., Lopes M.W., Gonçalves C.A.S., *Cadmium Neurotoxicity and Its Role in Brain Disorders.,* in Metal Ion in Stroke (2012), Part of the Springer Series in Translational Stroke Research book series (SSTSR), pp 751-766
- Leazer T.M., Liu Y., Klaassen C.D., *Cadmium absorption and its relationship to divalent metal transporter-1 in the pregnant rat.*, Toxicology and Applied Pharmacology (2002), Vol. 185, pp 18-24
- Linnman L., Andersson A., Nilsson K.O., Lind B., Kjellström T., Friberg L., *Cadmium uptake by wheat from sewage sludge used as a plant nutrient source.*, Archives of environmental Health (1973), Vol. 27, pp 45-47
- Lee K., Do Hur S, Hou S., Hong S., Qin X., Ren J., Liu Y., Rosman K.J.R., Barbante C., Boutron C.F., Atmospheric pollution for trace elements in the remote high-altitude atmosphere in

central Asia as recorded in snow from Mt. Qomolangma (Everest) of the Himalayas., Science of the total environment (2008), Vol. 404, pp 171-181

- Lopez E., Figueroa S., Oset-Gasque M.J., Gonzalez M.P., *Apoptosis and necrosis: two distinct events induced by cadmium in cortical neurons in culture.* British Journal of Pharmacology (2003); Vol. 138, pp 901–911
- Lund L.J., Betty E.E., Page A.L., Elliott R.A., *Occurrence of naturally high cadmium levels in soils and its accumulation by vegetation.,* Journal of Environmental Quality (1981), Vol. 10, pp 551-556
- Martelli A., Rousselet E., Dycke C., et al., Cadmium toxicity in animal cells by interference with essential metals., Biochimie (2006), Vol. 88, pp 1807-1814
- Marwa A.I., Elyamine A.M, Moussa M.G., Cai M., Zhao X., Hu C., *Cadmium in plants: uptake, toxicity, and its interactions with selenium fertilizers.,* Metallomics (2019),Vol. 11, pp 255-277
- Mayer F.L., Marking L.L., Pedigo L.E., Brecken J.A., Physicochemical factors affecting toxicity: pH, salinity, and temperature. I. Literature review. (1989), EPA/600/X-89/033, United States Environmental Protection Agency, Washington DC
- Mganga N., Manoko M.L.K., Rulangaranga Z.K., *Classification of Plants According to Their Heavy Metal Content around North Mara Gold Mine, Tanzania: Implication for Phytoremediation.,* Tanzania Journal of Science (2011), Vol. 37, pp 109-119
- Molnar A., Mészáros E., Polyák K., Borbély-Kiss I., Koltay E., Szabó Gy., Horváth Zs., *Atmospheric budget of different elements in aerosol particles over Hungary.,* Atmospheric Environment (1995), Vol. 29, pp 1821–1828
- Moulis J.M., Bourguignon J., Catty P., *Cadmium* in *Binding, Transport and Storage of Metal Ions* in *Biological Cells.* Edited by Maret W., Wedd A. RCS Metallobiology Series n. 2. The Royal Society of Chemistry (2016), Chapter 23, pp 695-746
- Nakanishi H., Ogawa I., Ishimaru Y., Mori S., Nishizawa N.K., *Iron deficiency enhances cadmium uptake and translocation mediated by the Fe^{2+} transporters OsIRT1 and OsIRT2 in rice.,* Soil Science Plant Nutrition (2006), Vol. 52, pp 464-469
- Navas-Acien A., Selvin E., Sharrett A.R., Calderon-Aranda E., Silbergeld E., Guallar E., *Lead, cadmium, smoking, and increased risk of peripheral arterial disease.,* Circulation (2004), Vol. 109, pp 3196–3201
- Nogawa K., Tsuritani I., Kido T., Honda R., Yamada Y., Ishizaki M., *Mechanism for bone disease found in inhabitants environmentally exposed to cadmium: decreased serum 1alpha,25-dihydroxyvitamin D level.*, International Archives of Occupational and Environmental Health (1987), Vol. 59, pp 21-30
- Nriagu J.O., Pacyna J.M., *Quantitative assessment of worldwide contamination of air, water and soils by trace metals.*, Nature (Lond.) (1988), Vol. 333, pp 134-139
- O'Hara J., *The influence of temperature and salinity on the toxicity of cadmium to the fiddler crab, Uca pugilator.,* Fishery Bulletin *(1973),* Vol. 71, pp 149-153

- Oluwatosin E.A., Godwin O.O., *Distribution of three non-essential trace metals (Cadmium, Mercury and Lead) in the organs of fish from Aiba Reservoir, Iwo, Nigeria.,* Toxicology Reports (2015), Vol. 2, pp 896-903
- Ogoshi K., Moriyama T., Nanzai Y., *Decrease in the mechanical strength of bones of rats administered cadmium.,* Archives of Toxicology (1989), Vol. 63, pp 320-324
- Page A.L., Chang A.C., El-Amamy M., *Chapter 10: cadmium levels in soils and crops in the cadmium levels in soils and crops in the United States.* In: Hutchinson TC, Meema KM, editors. Lead, mercury, cadmium and arsenic in the environment. (1987) New York: Wiley
- Peterson H.G., Healey F.P. , Wagemann R., *Metal toxicity to algae: A highly pH dependent phenomenon.,* Canadian Journal of Fisheries and Aquatic Sciences (1984), Vol. 41, pp 974–978
- Pizent A., Tariba B., Zivkovic T., *Reproductive toxicity of metals in men.,* Arh Hig Rada Toksikologiju (2012), Vol. 63, pp 35–46
- Price N.M., Morel F.M.M., *Cadmium and cobalt substitution for zinc in a marine diatom.,* Nature (1990), Vol. 344, pp 658-660
- Rahimzadeh M.R., Kazemi S., Moghadamnia A., *Cadmium toxicity and treatment: An update,* Caspian Journal of Internal Medicine (2017), Vol. 8, pp 135–145
- Ramesh S.A., Shin R., Eide D.J., Schachtman D.P., *Differential metal selectivity and gene expression of two zinc transporters from rice.,* Plant Physiology (2003), Vol. 133, pp 126-134
- Richerson H.B., Seidenfeld J.J., Ratajczak H.V., Richards D.W., *Chronic experimental interstitial pneumonitis in the rabbit.*, The American review of respiratory disease (1978), Vol. 117, pp 5-13
- Sabolić I., Breljak D., Skarica M., Herak-Kramberger C.M., *Role of metallothionein in cadmium traffic and toxicity in kidneys and other mammalian organs.*, Biometals (2010) Vol. 23, pp 897-926
- Saltzman B.E., Cholak J., Schafer L.J., *Concentrations of six metals in the air of eight cities.*, Environmental Sciences Technology. (1985), Vol. 19, pp 328-333
- Shagirtha K., Muthumani M., Prabu S.M., Melatonin abrogates cadmium induced oxidative stress related neurotoxicity in rats., European Review for Medical and Pharmacological Sciences (2011), Vol. 15, pp 1039–1050
- Shah K., Mankad A.U., Reddy M.N., *Cadmium accumulation and its effects on growth and biochemical parameters in Tagetes erecta L.,* Journal of Pharmacognosy and Phytochemistry (2017), Vol. 6, pp 111-115
- Sharma H., Rawal N., Mathew B.B., *Cadmium: Toxicity effect and its mechanism.,* International Journal of Nanotechnology and Nanoscience. (2015); Vol. 3, pp 1-9
- Satarug S., Haswell-Elkins M.R., Moore M.R., *Safe levels of cadmium intake to prevent renal toxicity in human subjects.,* British Journal of Nutrition (2000), Vol. 84, pp 791-802

- Satarug S., Moore M.R., *Adverse Health Effects of Chronic Exposure to Low-Level Cadmium in Foodstuffs and Cigarette Smoke.,* Environmental Health Perspectives (2004), Vol. 112, pp 1099-1103
- Sasaki A., Yamaji N., Yokosho K., Ma J.F., *Nramp5 is a major transporter responsible for manganese and cadmium uptake in rice.,* Plant Cell (2012), Vol. 24, pp 2155-2167
- Satarug S., *Dietary Cadmium Intake and Its Effects on Kidneys.,* Toxics (2018), Vol. 6, pp 1-15
- Schroeder W.H., Dobson M., Kane D.M., *Toxic trace elements associated with airborne particulate matter: A review.*, JAPCA (1987), Vol. 37, pp 1267-1285
- Sebastian J.R., Sebastian D.J., Beck K.G., (2014), Feral Rye Control in Colorado. Western Society of Weed Science Progress Report, Colorado Springs, CO
- Sigg L., Behra R., in *Metal Ions Biological Systems*, Vol 44, Eds A. Sigel, H. Sigel, R. K. O. Sigel, Taylor & Francis Ltd, Boca Raton, FL, (2005), pp. 47–73
- Snider G.L., Hayes J.A., Korthy A.L., Lewis G.P., *Centrilobular Emphysema Experimentally Induced by Cadmium Chloride Aerosol.,* American Review of Respiratory Disease (1973), Vol. 108, pp 40-48
- Sumino K., Hayakawa K., Shibata T., Kitamura S., *Heavy metals in normal Japanese tissues. Amounts of 15 heavy metals in 30 subjects.,* Archives of Environmental & Occupational Health (1975), Vol. 30, pp 487-494
- Tang L., Qiu R., Tang Y., Wang S., *Cadmium-zinc exchange and their binary relationship in the structure of Zn-related proteins: a mini review.,* Metallomics (2014), Vol. 6, pp 1313-1323
- TASK GROUP ON LUNG DYNAMICS, *Deposition and retention models for internal dosimetry of the human respiratory tract.*, Health Physics (1966), Vol. 12, pp 173-208
- TASK GROUP ON METAL TOXICITY, *Conceptual considerations: critical organ, critical concentration in cells and organs, critical effect, subcritical effect, dose-effect and dose-response relationships.* In: Nordberg, G.F., ed. Effects and dose-response relationships of toxic metals (1976), Amsterdam, Oxford, New York, Elsevier Science Publishers, pp 10-13
- Thévenod F., Lee W., *Toxicology of cadmium and its damage to mammalian organs.*, Metals ions in Life Sciences (MILS)(2013), Vol. 11, Cadmium: From Toxicity to Essentiality pp 415-490
- Thompson J., Bannigan J., *Cadmium: toxic effects on the reproductive system and the embryo.,* Reproductive Toxicology (2008), Vol. 25, pp 304–315
- Urani C., Melchioretto P., Canevali C., Crosta G.F., *Cytotoxicity and induction of protective mechanisms in HepG2 cells exposed to cadmium.,* Toxicology in Vitro (2005), Vol. 21, pp 314-319
- Vert G., Grotz N., Dédaldéchamp F., Gaymard F., Guerinot M.L., Briat J.F., Curie C., *IRT1, an Arabidopsis transporter essential for iron uptake from the soil and for plant growth.,* Plant Cell (2002), Vol. 14, pp 1223-1233

- Viaene M.K., Masschelein R., Leenders J., De Groof M., Swerts L.J.V.C., Roels H.A., *Neurobehavioural eVects of occupational exposure to cadmium: a cross sectional epidemiological study.,* Occupational and Environmental Medicine (2000), Vol. 57, pp 19–27
- Vinceti M., Filippini T., Mandrioli J., Violi F., Bargellini A. , Weuve J., Fini N., Grill P., Michalke B., *Lead, cadmium and mercury in cerebrospinal fluid and risk of amyotrophic lateral sclerosis: A case-control study., Journal of Trace Elements in Medicine and Biology (2017),* Vol. 43, pp 121-125
- Voyer R.A., Modica G., *Influence of salinity and temperature on acute toxicity of cadmium to Mysidopsis bahia Molenock.,* Archives of Environmental Contamination and Toxicology *(1990), Vol.* 19, pp 124-131
- Waalkes M.P., *Cadmium carcinogenesis.,* Mutation Research/Fundamental and Molecular Mechanisms of Mutagenesis. (2003); Vol. 533, pp 107-120
- Wilson D.N., *Cadmium-market trends and influences.* Cadmium Vol. 87, Proceedings of the 6th International Cadmium Conference, London (1988), Cadmium Association, pp 9-16
- Wright D.A., Welbourn P. M., *Cadmium in the aquatic environment: A review of ecological, physiological, and toxicological effects on biota.,* Environmental Reviews (2011), Vol. 2, pp 187-214
- Wolff E.W., Peel D.A., *The record of global pollution in polar snow and ice.*, Nature (Lond.) (1985), Vol. 313, pp 535-540
- World Health Organization (1986), Health impact of acidic deposition. Science of the Total Environment, Vol. 52, pp 157-187
- World Health Organization (1989), *Indoor air quality: Organic pollutants.,* Environmental Technology Letters, Vol. 10, pp 855-858
- World Health Organization (1992). Environmental Health Criteria 134. Cadmium. Available at www.inchem.org/documents/ehc/ehc/ehc134
- World Health Organization (2007). Health risks of heavy metals from long-range transboundary air pollution. 5-33. Available at www.euro.who.int/data/assets/pdf_file/ 0007/78649/E91044.pdf
- World Health Organization (2008). Guidelines for Drinking-water Quality., WHO Library Cataloguing-in-Publication Data Guidelines for drinking-water quality [electronic resource]: incorporating 1st and 2nd addenda, Vol.1, Recommendations. – 3rd ed.
- World Health Organization (2010). Exposure to cadmium: a major public health concern. Available at www.who.int/ipcs/features/air_pollution.pdf
- Wu X., Jin T., Wang Z., Ye T., Kong Q., Nordberg G., *Urinary calcium as a biomarker of renal dysfunction in a general population exposed to cadmium.,* Journal of Occupational and Environmental Medicine (2001), Vol. 43, pp 898–904
- Yamagata N., Shigematsu I., *Cadmium pollution in perspective.,* Bulletin of the High Institute of Public Health, Tokyo (1970), Vol. 19, pp 1-27

- Xu Y., Feng L., Jeffrey P.D., Shi Y., Morel F.M.M., *Structure and metal exchange in the cadmium carbonic anhydrase of marine diatoms.,* Nature (2008), Vol. 452, pp 56-62
- Xu Y., Morel F.M.M., *Cadmium in marine phytoplankton.*, Metals ions in Life Sciences (MILS)(2013), Vol. 11, Cadmium: From Toxicity to Essentiality pp 509-528

Chapter 3

3. Cadmium and Cancer

❖ 3.1 State of Art

The International Agency for Research on Cancer (IARC) classified cadmium (Cd) and its inorganic compounds as carcinogen to humans (IARC, 1993a,b). In particular, Cd was inserted in Group 1 of IARC classification, basing on the evidence of carcinogenicity in humans and experimental animals (Hartwig, 2013). The most convincing data of a correlation between Cd and cancer are occupational data, showing that workers within the electroplating, battery production, and pigment industries have shown an increased incidence of lung cancer respect the general population (Hartwig, 2013a). Several studies conducted in Belgium, Canada, Sweden, Finland, Germany, Great Britain, and the United States have confirmed this hypothesis. For instance, Kazantzis et al. (1992) illustrated that the mortality from lung cancer of Cd-processing workers of 17 plants in United Kingdom was elevated, with visible positive trends with the duration of employment and with the intensity of exposure. At the same time, in the United Kingdom and Sweden, an increase in standardised mortality ratio (SMR) for lung cancer was also manifested by Ni-Cd battery workers (Elinder et al., 1985; Sorahan et al., 1987). However, some essential criticism about the correlation between Cd and cancer raised because of the limited number of collected observations and the lack of historical data. Furthermore, cigarette smoking and the simultaneous exposure of workers to nickel and arsenic created an additional uncertainty about the possibility that Cd caused cancer: both these factors could modify the results of carcinogenicity studies increasing the lung cancer incidence on their own (German MAK Commission, 2006; IARC, 2012; Park et al., 2012). Since that time, new data have confirmed Cd hazardous nature. Indeed, several data have associated Cd not only with lung cancer, but also with breast, endometrial, pancreas, kidney, liver, hematopoietic system, stomach and prostate cancer (Shigematsu et al., 1982; Kriegel et al., 2006; McElroy et a.l, 2006; Åkesson et al., 2008). In support of human data, Cd and its compounds were tested on animals to provide other evidence of Cd-induced carcinogenicity. Two studies on cadmium chloride in rats were exhaustive. In the first, the oral administration of cadmium chloride to Wistar rats increased the incidence of leukaemia, prostatic, and testis

tumours (Waalkes et al., 1992); in the second, the researchers have shown the development of prostatic hyperplasia in the treated animals (Waalkes et al., 1999). Moreover, it has been demonstrated that inhalation exposure to cadmium chloride, cadmium sulfide/sulfate, and cadmium oxide fume could induce the development of malignant lung tumours in rats, including adenocarcinomas, after systemic or direct exposure (Glaser et al., 1990). Instead, single or multiple subcutaneous administration of cadmium chloride, cadmium sulfide, cadmium sulfate and cadmium oxide caused local sarcomas in rats (Shirai et al., 1993; Waalkes et al., 2000). Mice, that were less susceptible than rats to induction of local tumours by Cd compounds, exhibited injection-site sarcomas as well (Waalkes et al., 1994). Thus, accumulated data have indicated that Cd is a multi-route, multi-site and multi-species carcinogen in rodents (Waalkes, 2003). Although all these experiments have confirmed that Cd induces carcinogenesis, the molecular mechanism or mechanisms of Cd toxicity continue to be unknown. The only clear *in vivo* Cd mechanism of action is defined for the development of testicular tumors in rodents, that, unfortunately, does not seem to be relevant for human. In this case, Cd appears to induce testicular necrosis, in which rare interstitial cells in the degenerate tissue are overstimulated by LH and produce tumors (Waalkes et al., 1997).

To improve understanding of Cd carcinogenicity, this thesis proposes a possible mode of action of this carcinogen. Indeed, there is no real reason to assume that Cd cancer inducing mechanisms are the same in all target tissues. Moreovere, a better understanding of Cd mechanisms would allow better assessment of the risk associated with this common environmental contaminant.

❖ 3.2 Cadmium general effects

Various *in vitro* model systems have been developed to define potential molecular events associated with Cd-induced carcinogenesiss, and the principal results can be listed as follows cells (Tapisso et al., 2009; IARC, 1997; IARC, 2012):

- Cd, as other metals except for chromium (VI), has shown low mutagenicity in classical bacterial assays and standard mammalian mutagenicity tests.
- Cd exerts clastogenic activity, leading to chromosomal aberrations and micronuclei, in mammalian
- Cd and Cd salts are not able to cause direct DNA damage but preferably interact with proteins.

As a result, Cd was classified as a non-genotoxic compound (IARC, 1993a,b), and as such, its toxicity and/or carcinogenicity was described as mediated by non-genotoxic mechanisms of action (Paragraph 1.3). Among the 10 key characteristics of carcinogens of current IARC mechanistic evaluations (Paragraph 1.3), the induction of oxidative stress and interactions with the DNA damage response systems seem to be more relevant in cadmium-induced carcinogenicity. In more details, Cd seems to modify the production of Reactive Oxygen Species (ROS), connected with an inhibition of the antioxidant defense, such as the antioxidant enzymes catalase, superoxide dismutase, glutathione reductase, and glutathione peroxidase (Hartwig, 2013a,b). Moreover, Cd has been shown to impair almost all major DNA repair pathways, e.g. nucleotide excision repair, base excision repair, and mismatch repair (Hartwig, 2013a).

3.2.1 Oxidative stress and recruitment of stress signaling pathways

In normal conditions, ROS, such as superoxide anion ($O_2^{\cdot -}$), hydrogen peroxide (H_2O_2), and hydroxyl radical (HO·), are generated by incomplete reduction of oxygen to H_2O during cellular respiration. Simultaneously, a complex antioxidant network converts highly reactive oxygen species to less harmful ones to minimise oxygen-derived toxicity. When the equilibrium between ROS generation and their detoxification is disrupted, oxidative stress occurs, leading to the generation of elevated DNA and macromolecules damage. The possible DNA damage induced by ROS, including DNA base modifications, DNA single- and double-strand breaks, DNA-protein crosslinks, and abasic sites may hence act as initiators in carcinogenesis. Pyrimidine bases are the most sensitive to oxidative stress: cytosine and thymine can undergo saturation or hydroxylation of their single ring, causing distortions in the geometry of DNA. On the other hand, one of the most frequent oxidative alterations of purine bases concerns the oxidation of guanosine in position 8 and the detachment of nitrogenous bases from sugars (Urso et al., 2003). It has been demonstrated that transition metals (iron, copper, cobalt, or nickel) can play an essential role in the induction of oxidative DNA damage. Indeed, transition metals are able to converted superoxide anions or hydrogen peroxide into highly reactive hydroxyl radicals using Fenton-type reactions ($Me^{ox} + O_2\bullet - \rightarrow Me^{rid} + O2$, $Me^{rid} + H_2O_2 \rightarrow Me^{ox} + OH\bullet + OH-$). The net result of these reactions is also known as the Haber-Weiss reaction. Subsequently, the increase of reactive hydroxyl radical generates conspicuous damage in various cellular macromolecules, due to its extreme reactivity towards biomolecules and the lack of endogenous inactivation mechanisms. For example, reactive hydroxyl radicals can damage proteins, nucleic acids, glycosaminoglycans and above all, the polyunsaturated fatty acids of membrane phospholipids. However, Cd ions, that do not participate in Fenton-type chemical reactions, generate oxidative stress interfering with cellular redox regulation. Oxidative DNA damage by Cd is assumed to be also due to a modification in the activities of the antioxidant enzymes catalase, such as glutathione reductase, and glutathione peroxidase. One other mechanism proposed consists in the displacement of redox-ctive metal ions (Fe^{2+}) in metallothionein, giving rise to Fenton reactions (Stohs et

al., 2001; Thevenod, 2009). In literature, increased levels of ROS after Cd exposure have been observed both *in vitro* and *in vivo.* For instance, in mammalian cells, the involvement of ROS in Cd toxicity is underlined by the decrease of DNA strand breaks and chromosomal aberrations with the introduction of antioxidants and antioxidant enzymes (Valko et al., 2006). Thus, ROS may be involved in Cd-induced genotoxicity and Cd-induced carcinogenicity (Figure 3.1). Furthermore, since mitochondria are the primary site of ROS production, these organelles and their functions seem to be implied in Cd-induced carcinogenesis (Paragraph 3.4).

Figure 3.1. Cd and Oxidative stress. Cadmium and oxidative stress. Cadmium does not belong to redox-active metals. Chronic Cd(II) exposure can induce expression of metallothionin (MT) and triggers adaption mechanisms towards oxidative stress, thus limiting the role of ROS in carcinogenesis (Henkler et al., 2010).

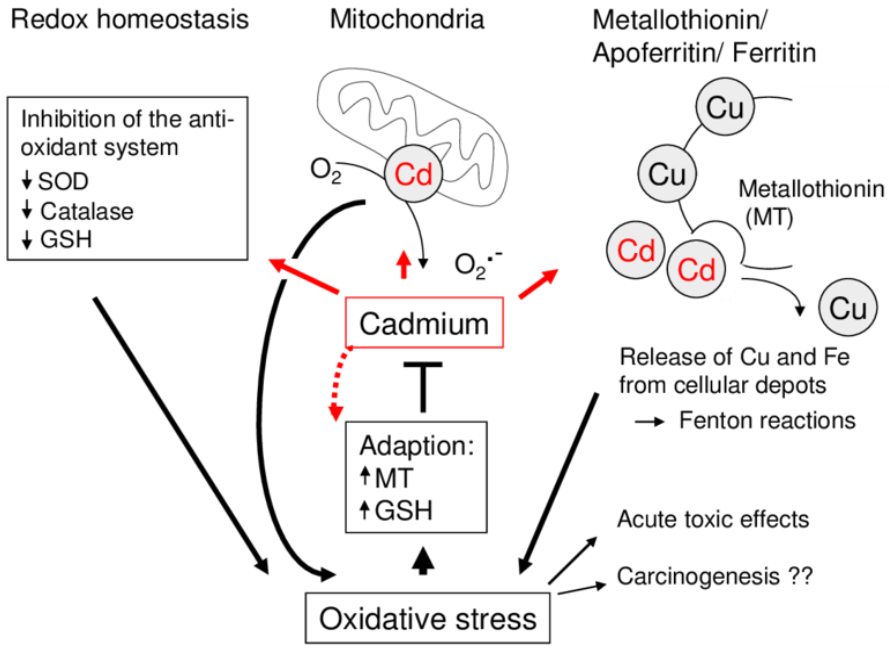

3.2.2 Cadmium interactions with the DNA Damage Response System

Maintenance of genetic information is essential for all cellular processes and the prevention of tumour development. However, Cd has been shown to impair almost all major DNA repair pathways, especially in non-cytotoxic concentrations (Koedrith et al., 2011; Hartwig, 2013a). In more details, convincing evidence is available for Cd interference with nucleotide excision repair (NER), base excision repair (BER), and mismatch repair (MMR). For example, among the Nucleotide Excision Repair (NER) pathways, Cd has been shown to inhibit the global genome repair (GG-NER) in several studies (Hartmann et al., 1996; Schwerdtle et al., 2010). GG-NER is the repair system involved in the removal of unrelated bulky bases which produce significant helical distortions (Hartmann et al., 1996; Schwerdtle et al., 2010). One possible molecular mechanism related to the inactivation of NER can be the displacement of zinc by Cd in zinc-binding proteins (Paragraph 3.5) (Asmuss et al., 2000). Moreover, Cd seems to inhibit many glycosylases implied in Base Excision Repair (BER), such as the murine 8-oxoguanine DNA glycosylase 1 (mOgg1) and the human 8-oxoguanine glycosylase (hOGG1) (Zharkov et al., 2002; Potts et al., 2003). Cd inhibition of the repair of oxidative DNA damage is also evident *in vivo*: for example, in rat testis, in which a gradual decrease in 8-oxo-dGTPase activity was observed (Bialkowski et al., 1999). In the end, in human cells, low Cd concentrations inhibit some proteins involved in the initial step of the Mismatch Repair (MMR), such as MSH2, MSH3, MSH6. One possible explanation can be that Cd interferes with the ATP binding and hydrolysis of MMR enzymes, reducing their DNA binding activity (Lutzen et al., 2004; Giaginis et al., 2006). It is essential to emphasise that cells with a shortage in MMR pathways can increase their incidence of spontaneous mutations, as also the risk to develop different types of cancer.

❖ 3.3 Cadmium and Warburg effect

Over six decades ago, the innovative work of Otto Warburg revealed a modification of metabolism in cancer cells (Warburg, 1956). In more details, Warburg emphasised that cancer cells avidly fermented glucose, even if oxygen was present. This phenomenon, that was repeatedly confirmed *in vitro* and *in vivo*, was called aerobic glycolysis or, in honour of its discoverer, the Warburg effect. Besides, Warburg originally attributed aerobic glycolysis to impaired mitochondrial function (Warburg, 1956; Fan et al., 2013). Since that time, this fundamental effect has changed the belief that cancer is a purely genetic disease, for the provocative suggestion that cancer can be principally a metabolic disease. In this regard, in a series of experiments, Israel and Schaeffer have demonstrated that the malignancy of cells could be suppressed in 100% of samples when the cytoplasm of enucleated normal cell was fused with a single nucleus of a tumor cell to form cybrid cell (Israel et al., 1987; Seyfried, 2012; Seyfried, 2015). In contrast, tumors formed in 97% of mice implanted if the cybrid cells were obtained by fusion of malignant cells cytoplasm with non-tumorigenic nuclei from normal cells (Seyfried, 2015). The consequence of their work underlined that a normal nuclear gene expression was unable to suppress malignancy; while the cytoplasm of the tumor cell could reprogram the nucleus of a normal cell to become tumorigenic (Figure 3.2).

Figure 3.2. Role of the nucleus and mitochondria in the origin of tumours (Seyfried, 2015).

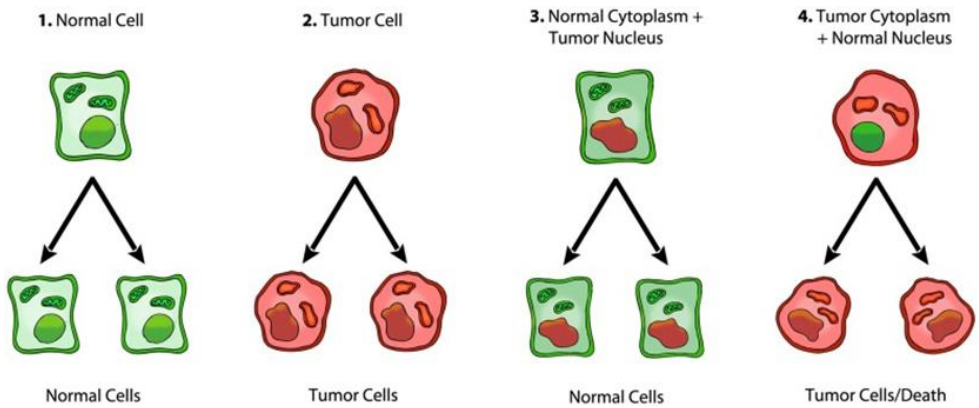

The discovered role of cytoplasm in tumorogenesis supported the Warburg's theory, in particular, if it is considered that dysfunctional mitochondria are a possible cause of aerobic glycolysis. "If tumor cell mitochondria are defective, as Warburg postulated (1956), then, the suppression of the malignancy could result from the introduction of mitochondria from normal cells into cybrids" (Howell et al., 1978). Currently, as announced by Weinhouse in 1956, it needs to be considered that mitochondrial respiration in cancer cells is functional, but suppressed because of the heightened glycolytic flux in the cytosol (Crabtree, 1929). Inhibition of mitochondrial respiration, due to the higher cellular glucose uptake, is called the reversed Pasteur effect or, more often, the Crabtree effect. For example, the loss of Pasteur effect can be seen in tumors associated with a mutation of p53. Indeed, the gain of function of mutated p53 promotes the translocation of glucose transporter 1 to the cytoplasmic membrane, increasing the uptake of glucose in cells (Zhang et al., 2013). In addition, if c-Myc is simultaneously upregulated, this protooncogene can also induce the hexokinase 2 (HK2) with the conversion of glucose to glucose-6-phosphate (Kim et al., 2004; Kim et al., 2007), intensifying glycolytic flux in the cytoplasm (Figure 3.3). In literature, Cd is able to modify the expression level of both these genes (Paragraph 3.5; Tokumoto et al., 2011; Hartwig, 2013a,b; Urani et al., 2014). Consequently, the metabolic alterations caused by this heavy metal are still to be fully elucidated. Furthermore, the role of PKM2 isoform of pyruvate kinase in Cd-induced carcinogenicity was also studied (Cheon et al., 2016; Tanaka et al., 2018; Christofk et al., 2008) (Figure 3.3). In particular, PKM2 has not only a metabolic function in glycolysis but also a non-metabolic function, leading to EMT and promoting cancer cell invasion. Recent studies also suggested that PKM2 is upregulated by c-Myc (Kim et al., 2004; Xu et al., 2015). The Warburg effect can be associated with a decoupling between pyruvate metabolism and glycolytic flux; while glutaminolytic and glycolytic fluxes are coupled in cancer cells (Kim, 2015). In other words, the Krebs cycle seems to favour carbon usage for anabolic reactions. Indeed, cancer cells can use glutamate, that enters the Krebs cycle as α-keto-glutarate (α-KG), another important carbon source for anaplerosis. Besides, through its oxidation in the Krebs cycle, glutamate can provide hydrogen/electrons for mitochondrial oxidative phosphorylation (OXPHOS). Instead, carbons from glutamate can leave the Krebs cycle as malate, and generate pyruvate and NADPH. The latter can be used for anabolic reactions (DeBerardinis et al., 2007), while, pyruvate is

reduced to lactate and transported out of the cell. In general, in this condiction, Krebs cycle intermediates can serve to create macromolecules for growth and proliferation. For example, oxaloacetate can leave the mitochondria as aspartate for *de novo* synthesis of amino acids (Hunnewell et al., 2010). Or, citrate may serve as a carbon source for *de novo* synthesis of fatty acids. Hence, the catabolic degradation of glucose and glutamine are increased to supply the cancer cells demands for *de novo* synthesis of nucleotides, proteins and lipids.

Figure 3.3. The Warburg effect in cancer cells (Fu et al., 2017).

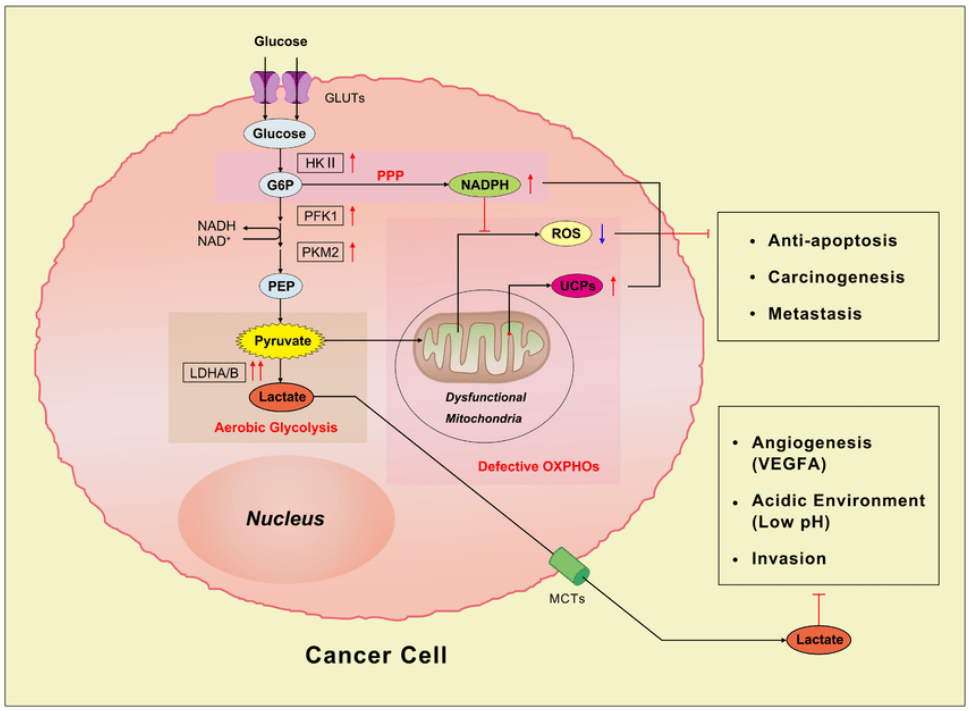

❖ 3.4 Cadmium and mitochondria

Cancer is a multiple disease principally characterised by uncontrolled growth. Hence, the metabolism requests of cancer cells must be satisfied, usually with aerobic glycolysis, to sustain this rapid proliferation. Nonetheless, the field is not able to reach agreement on the issue of mitochondria: are mitochondria the culprits of aerobic glycolysis in cancer or innocent bystanders (Kim, 2015)? As a consequence, mitochondria in cancer attracted researchers attention from a new metabolic perspective. In particular, it has become clear that mitochondrial circuitries can readjust, with considerable metabolic plasticity, their bioenergetic or anabolic functions in malignant cells (Wise et al., 2011; Fendt et al., 2013). To understand the role of these organelles in cancer energy metabolism, it needs to be considered that mitochondria are not damaged, but merely dysfunctional (Weinhouse, 1956; Koppenol et al., 2011). Indeed, mitochondrial functions, including oxidative phosphorylation (OXPHOS), the Krebs cycle, β-oxidation of fatty acids, calcium handling are not enduringly changed, but try to accommodate the metabolic demands of the tumor. The first strategy implies that Krebs cycle can be decoupled from OXPHOS. However, it should be kept in mind that the elevated aerobic glycolysis is not the consequence of an insufficient ATP production by impaired mitochondrial respiration. On the contrary, cancer cells may deliberately decrease mitochondrial OXPHOS to exploit the Krebs cycle intermediates for anabolic reactions (Kim, 2015). For example, cytosolic ATP can be rapidly be hydrolysed to AMP to replenish the UTP pool for the regeneration of UDP-glucose. In this case, the high expression levels of ectonucleoside triphosphate diphosphohydrolase 5 (ENTPD5), that hydrolyses UDP to UMP and Pi, and the increase of lactate production via glycolysis are not connected with altered mitochondrial respiration (Fang et al., 2010). The increase of ENTPD5 is needed to properly execute N-glycosylation reactions, in which glycolytic flux maintains nucleotide and hexosamine synthesis (Shirato et al., 2011). A second possibility is that electron transfer chain (ETC) complexes can be decoupled from ATP production in cancer cells. Mitochondrial respiration involves the reduction of oxygen molecules to water, whereas ATP production refers to the formation in ADP to ATP. In general, the magnitude of proton-motive force across the mitochondrial inner membrane is directly coupled to the electron transfer rate.

Recent studies have suggested that ETC complexes in mitochondrial OXPHOS could be required to guarantee rapid proliferation of cancer cells (Vander Heiden et al., 2010; Fang et al., 2010; Sullivan et al., 2015; Birsoy et al., 2015). Indeed, ETC complexes can be used to oxidise NADH to maintain the NAD^+/NADH ratio (Sullivan et al., 2015; Birsoy et al., 2015). In any case, cancer cells can modify their metabolism with particular attention to the intensification of anabolic reactions, with mitochondria playing a central role in the control of cellular metabolism. The strategies can be different: "cancer cells couple glycolytic and glutaminolytic fluxes, decouple pyruvate metabolism from the glycolytic flux, and decouple ATP production from ETC complexes, but couple the Krebs cycle with ETC complexes" (Kim, 2015). Notwithstanding, mitochondria regulation in cancer cells does not come down to a simple decoupling between Krebs cycle and OXPHOS (etc.), but it is also important to consider the tumor microenvironment and/or the mitochondrial dynamics in a single cell. Pokorný et al. (2014) have suggested two different types of mitochondrial dysfunction: cancer cells with normal and with reverse Warburg effect. In normal Warburg effect, cancer cells have dysfunctional and depolarised mitochondria, with oxidative metabolism reduced by the inhibition of the pyruvate transfer. In reverse Warburg effect, cancer cells have fully functional mitochondria, but they receive the energy-rich metabolites (pyruvate, lactate, glutamine, etc.) from the associated stromal fibroblasts with the mitochondrial dysfunction. Cancer cells of this type have high aggressiveness and a high probability of metastatic activity. Hence, cancer cells have a growth advantage over normal cells because they strategically manipulate metabolic fluxes to supply proper amounts of macromolecules following circumstances (Figure 3.4). On the other hand, considering a single cell, these organelles are not inert, but dynamic in controlling their health and role in several functions (Figure 3.5). The main dynamic processes are fusion, fission (the division of a single organelle into two), transport, and mitophagy (targeted destruction via the autophagic pathway) (Mishra et al., 2016). Consequently, it is not surprising that the dynamic properties of mitochondria can influence mitochondrial bioenergetics. For example, mitochondrial fusion, that consists of outer membrane fusion, mediated by mitofusins, followed by inner membrane fusion, mediated by Opa1, can be observed when the cellular conditions require an increase in ATP production (Mitra et al., 2009; Tondera et al., 2009). Indeed, some observations have suggested that high OXPHOS

activity is correlated with mitochondrial fusion. Hence, the creation of mitochondrial networks can lead to a higher efficiency in energy generation and distribution through long distances (Amchenkova et al., 1988; Skulachev, 2001). Otherwise, the opposite can also be valid: an increase in OXPHOS activity can stimulate mitochondrial fusion. In the case of Cd, high oxidative stress and high levels of oxidised glutathione (GSSG) can facilitate the creation of disulfide bonds between mitofusin of different organelles, enhancing outer-membrane fusion (Chapter 7). On the contrary, fission of mitochondria is related to an inhibition of mitochondrial OXPHOS. Indeed, the use of drugs that repress mitochondrial respiration, such as mitochondrial uncouplers (e.g., CCCP and FCCP), results in a rapid and dramatic fragmentation of the organellar network in multiple cell types. This process is mediated by the Dynamin-related Protein 1 (Drp1), that is able to induce the scission of the single organelle in two, in a GTP-dependent manner. Fission is implicated in the facilitation of mitochondrial transport, mitophagy, and apoptosis. In the liver, Xu et al. (2013) have demonstrated that mitochondria are critical targets for Cd toxicity. In particular, Cd was able to induce Drp1-dependent mitochondrial fragmentation by disturbing calcium homeostasis. Thus, manipulation of Drp1 may be the potential avenue for developing novel strategies to protect against cadmium-induced hepatotoxicity. In conclusion, these dynamic mitochondrial behaviours could be linked with normal physiology, but also with disease states, including cancer induced by Cd (Labbé et al., 2014; Mishra et al., 2014). The connection between mitochondrial structure, position in the cytoplasm and function has led to the novel concept of ‘‘mitochondrial morphofunction” (Bulthius et al., 2019). Moreover, mitochondria seem to have an intrinsic ability to sense their state of health and, when stressed, shall implement a compensatory quality-control mechanism to address the problem.

Figure 3.4. The Warburg effect and the reverse Warburg effect. "A. In normal tissues, glucose is bio-transformed to pyruvate and carried into the mitochondria for the oxidative phosphorylation (OXPHOS). B. Most types of cancer engage themselves in glycolysis, irrespective to the presence of oxygen (aerobic glycolysis or Warburg Effect). C. Some cancer cells reprogram cancer associated fibroblasts (CAFs) to undergo aerobic glycolysis (WE) and to secrete energy-rich nutrients that feed into mitochondrial oxidative metabolism in cancer cells" (Paolicchi et al., 2016).

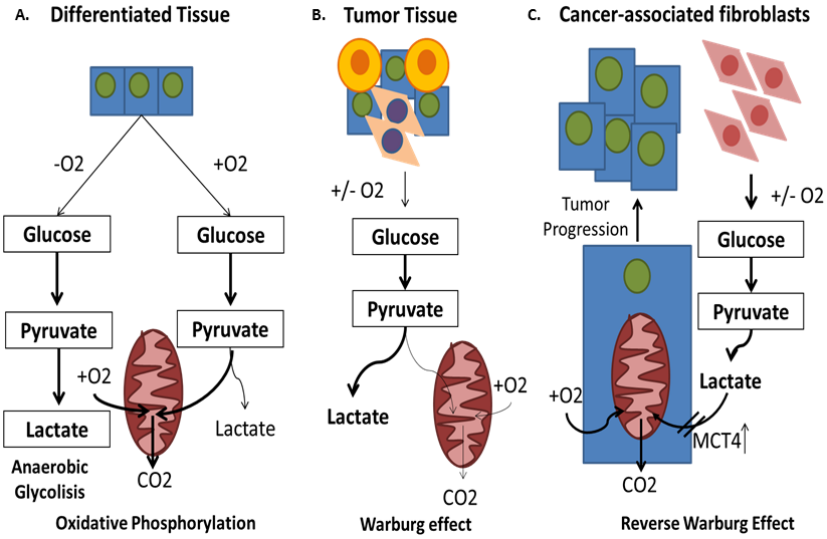

Figure 3.5. Mitochondrial dynamics. Under normal physiological conditions, mitochondria exist in a dynamic equilibrium by continuous fusion and fission events. Fission is regulated by dynamin-related protein 1 (Drp1), fission 1 protein (Fis1), and mitochondrial fission factor (Mff), whereas fusion is regulated by optic atrophy 1 (Opa1) and mitofusin (Mfn) 1 and 2. Fission leads to formation of small, rounded mitochondria, whereas fusion forms elongated, tubular interconnected mitochondrial networks. An imbalance of mitochondrial dynamics can compromise mitochondrial membrane potential (ΔΨ), mitochondrial DNA (mtDNA) function, and oxidative phosphorylation (adapted from Balong et al., 2016).

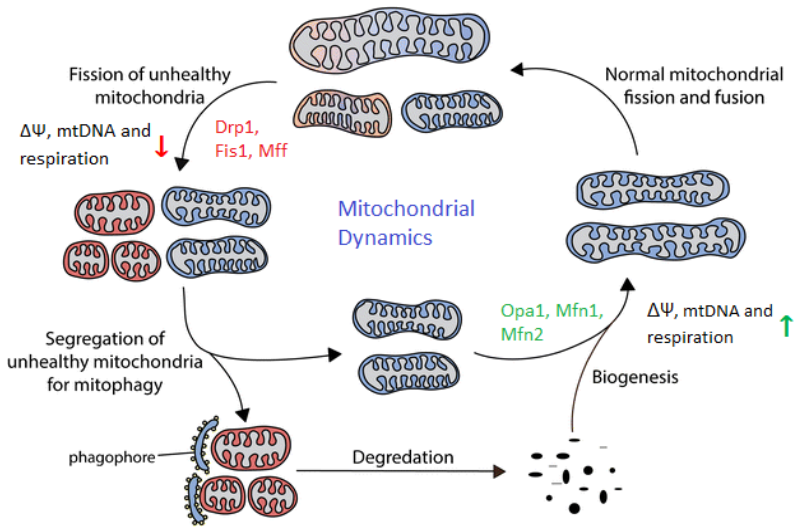

❖ 3.5 Cadmium and genetic dysregulation

Analysis of transcriptome data from various species has indicated that Cd exposure alters the expression of hundreds of genes (Cui et al. 2007; Hsiao et al., 2009; Fabbri et al., 2012; Oono et al., 2016). More recently, Callegaro et al. (2018) analysed the early response of the C3H/10T1/2 cell line to Cd exposure. As a result, transcriptomic profiling revealed that only a limited number of genes (only 13) were differentially expressed after 24 hour of Cd treatment. For example, three members of the GSTα family, that were all upregulated, could be needed as a protection towards oxidative stress and metal toxicity. The upregulation of Pip5k1a, Mt1, Mt2, Slc30a1, Man2c1, Gdf15, RHOV, and several olfactory receptors genes suggest that Cd interferes with zinc (and on divalent ions) homeostasis, in accordance with previous works by our group (Urani et al., 2010; Urani et al., 2015) and other authors (Meplan et al., 1999; Babula et al., 2012). In conclusion, results suggest that the disruption of zinc homeostasis is another important Cd effect leading to cancer (Costello et al., 2012; Grattan et al., 2012). It is currently believed that Cd is potentially able to alter the 3-dimensional structure and the specific function of proteins that contain zinc in one of their domains, including transcription factors, tumor suppressor proteins and DNA repair proteins. Alternatively, among the early response genes, other studies have proven that Cd induces the expression of protooncogenes, such as c-fos, c-jun and c-myc, by activating, in turn, several genes involved in growth and cell division (Takiguchi et al., 2003; Hartwig, 2013a,b). In HepG2 human liver cells, instead, it has been shown that a family of genes related to cancer development are up-regulated in the presence of non-cytotoxic concentrations of Cd (Fabbri et al., 2012). More in details, Fabbri et al, (2012) showed that some genes coded for proteins involved in the Mitogen-Activated Protein Kinases (MAPK) pathway, and linked to proliferation, differentiation and cell migration, were upregulated; Cd could also induce genes involved in the avoidance of apoptosis, the induction of DNA damage, angiogenesis and insensitivity to growth-inhibiting signals. The genes coding for heat shock proteins (hsp), such as hsp70 and hsp22, were also up-regulated (Fabbri et al., 2012). Furthermore, Cd modified the expression of genes encoding integrins, actin and proteins involved in focal adhesions, that play an essential role in critical biological processes, including cell motility, proliferation, differentiation, survival and regulation of gene expression (Fabbri

et al., 2012). Hsp family proteins, that are linked to various types of stress, including metal toxicity, are involved in the repair or degradation of other damaged proteins (Kiang et al., 1998). Focal adhesions, along with invadopodia and podosomes, are instead involved in cancer invasiveness (Albiges-Rizo et al., 2009). In 2015, Urani et al. showed that Snail1 was up-regulated after Cd treatment. This gene, coding for a protein belonging to a superfamily of transcription factors containing a zinc-finger domain, is involved in the loss of cellular adhesion and the acquisition of invasive and migratory properties during tumor progression (Nieto, 2002). Other proteins implicated in the loss of adherence, whose genes were up-regulated after Cd exposure (Urani et al., 2015), are the MET tyrosine kinase receptor, which promotes the growth and metastasis of cancer by transmitting proliferative, antiapoptotic and promigratory signals (Trusolino et al., 2010), and the Transforming Growth Factor Receptor (TGF-βR), involved in cell proliferation, cell migration and Snail1 activation (Massagué, 2008). To sum up, Cd seems to principally influence two classes of genes, i.e., stress-response genes such as metallothioneins (MTs), heme oxygenase, and heat shock proteins (hsps), and apoptosis-related genes (see also Chapter 5,6,9,10). However, Cd can also modify the expression of many other genes involved in cell metabolism and both intracellular and extracellular signalisation (see also Chapter 5,6,9,10). Finally, Cd can upregulate the Rac and cdc42 genes that promote the formation of lamellipodia and filopodia, regulating cell migration through cytoskeletal remodelling (Sadok et al., 2014).

In contrast, Cd can downregulate microRNA family (miRNA), that, although miRNAs are small molecules of non-coding RNA (18-25 nucleotides), play essential roles in gene regulation. Indeed, they can signal mRNAs both for degradation and for suppression of their translation modulating several cellular processes, including differentiation, proliferation and apoptosis (Bartel, 2009). After Cd exposure, for example, the miRNA let-7, miR-15b, miR-34a and miR-200a are all down-regulated (Fabbri et al., 2012). The miRNAs belonging to the let-7 family have been described as tumor suppressors and, according to their function, are down-regulated in many tumors (Boyerinas et al., 2010). MiR-15b has also been reported as a tumor suppressor because it regulates apoptosis (Gu et al., 2009). Downregulation of miRNAs belonging to the miR-34 family contributes to the abnormal expression of Snail1: usually, this protein is antagonised by members of the miR-34 family, their lack leading to a

pathological expression of nail1 and, consequently, to the epithelial-mesenchymal transition of tumor cells (Kim et al., 2011). The down-regulation of miR-200a also contributes to this transition since in normal conditions, the miRNAs of the miR-200 family suppress it (Xiong et al., 2012).

References

- Albiges-Rizo C., Destaing O., Fourcade B., Planus E., Block M.R., Actin machinery and mechanosensitivity in invadopodia, podosomes and focal adhesions., Journal of Cell Science (2009), Vol. 122, pp 3037-3049
- Åkesson A., Julin B., Wolk A., Long-term dietary cadmium intake and postmenopausal endometrial cancerincidence:apopulation-basedprospectivecohort study., Cancer Research (2008), Vol. 68, pp 6435–6441
- Amchenkova A.A., Bakeeva L.E., Chentsov Y.S., Skulachev V.P., Zorov D.B., Coupling membranes as energy-transmitting cables. I. Filamentous mitochondria in fibroblasts and mitochondrial clusters in cardiomyocytes. Journal of Cell Biology (1988), Vol. 107, pp 481–495
- Asmuss M., Mullenders L.H., Hartwig A., Interference by toxic metal compounds with isolated zinc finger DNA repair proteins., Toxicology Letters (2000), Vol. 112–113, pp 227–231
- Babula P., Masarik M., Adam V., Eckschlager T., Stiborova M., Trnkova L., Skutkova H., Provaznik I., Hubalek J., Kizek R., Mammalian metallothioneins: properties and functions., Metallomics (2012) Vol. 4, pp739–750
- Balong J., Mehta S.L., Vemuganti R., *Mitochondrial fission and fusion in secondary brain damage after CNS insults.*, Journal of Cerebral Blood Flow & Metabolism (2016), Vol. 36, pp 2022–2033
- Bartel D.P., MicroRNAs: target recognition and regulatory functions., Cell (2009), Vol. 136, pp 215-233
- Bialkowski K., Bialkowska A., Kasprzak K.S., Cadmium(II), unlike nickel(II), inhibits 8-oxo-dGTPase activity and increases 8-oxo-dG level in DNA of the rat testis, a target organ for cadmium(II) carcinogenesis., Carcinogenesis (1999), Vol. 20, pp 1621-1624
- Birsoy K., Wang T., Chen W.W., Freinkman E., Abu-Remaileh M., Sabatini D.M., An essential role of the mitochondrial electron transport chain in cell proliferation is to enable aspartate synthesis., Cell (2015), Vol. 162, pp 540–551
- Boyerinas B., Park S.M., Hau A., Murmann A.E., Peter M.E., The role of let-7 in cell differentiation and cancer., Endocrine-Related Cancer (2010), Vol. 17, pp 19-36
- Bulthius E.P., Adjobo-Hermans M.J.W., Willems P.H.G.M., Koopman W.J.H., Mitochondrial Morphofunction in Mammalian Cells, ANTIOXIDANTS & REDOX SIGNALING (2019), Vol. 30, pp 2066-2109
- Cheon J.H., Kim S.Y., Son J.Y., Kang Y.R., An J.H.,Kwon J.H., Song H.S.,Moon A., Lee B.M., Kim H.S., Pyruvate Kinase M2: A Novel Biomarker for the Early Detection of Acute Kidney Injury., Toxicological Research (2016), Vol. 32, pp 47–56

- Christofk H.R., Vander Heiden M.G., Harris M.H., Ramanathan A., Gerszten R.E., Wei R., Fleming M.D., Schreiber S.L., Cantley L.C., The M2 splice isoform of pyruvate kinase is important for cancer metabolism and tumour growth., Nature (2008), Vol. 452, pp 230-233
- Costello, C.L., Franklin, R.B., Cytotoxic/tumor suppressor role of zinc for the treatment of cancer: an enigma and an opportunity., Expert Review of Anticancer Therapy (2012), Vol. 12, pp 121–128
- Crabtree H.G., Observations on the carbohydrate metabolism of tumours., Biochemical Journal (1929), Vol. 23, pp 536-545
- Cui Y., McBride S.J., Boyd W.A., Alper S., Freedman J.H., Toxicogenomic analysis of Caenorhabditis elegans reveals novel genes and pathways involved in the resistance to cadmium toxicity., Genome Biology (2007), Vol 8: R122
- DeBerardinis R.J., Mancuso A., Daikhin E., Nissim I., Yudkoff M., Wehrli S., Thompson C.B., Beyond aerobic glycolysis: transformed cells can engage in glutamine metabolism that exceeds the requirement for protein and nucleotide synthesis., Proceedings of the National Academy of Sciences of the United States of America (2007), Vol. 104, pp 19345–19350
- Elinder C.-G.,Jellström T.K., Hogstedt C., Andersson K.,Spång G., Cancer mortality of cadmium workers., British Journal of Industrial Medicine (1985), Vol. 42, pp 651-655
- Fabbri M., Urani C., Sacco M.G., Procaccianti C., Gribaldo L., Whole Genome Analysis and MicroRNAs Regulation in HepG2 Cells Exposed to Cadmium., ALTEX (2012), Vol. 29, pp 173-82
- Fan J., Kamphorst J.J., Mathew R., Chung M.K., White E., Shlomi T., Rabinowitz J.D., Glutamine-driven oxidative phosphorylation is a major ATP source in transformed mammalian cells in both normoxia and hypoxia., Molecular Systems Biology (2013), Vol. 9, pp 1-11
- Fang M., Shen Z., Huang S., Zhao L., Chen S., Mak T.W., Wang X., The ER UDPase ENTPD5 promotes protein N-glycosylation, the Warburg effect, and proliferation in the PTEN pathway., Cell (2010), Vol. 143, pp 711–724
- Fendt S.M., Bell E.L., Keibler M.A., Olenchock B.A., Mayers J.R., Wasylenko T.M., Vokes N.I., Guarente L., Vander Heiden M.G., Stephanopoulos G., Reductive glutamine metabolism is a function of the alpha-ketoglutarate to citrate ratio in cells., Nature Communications (2013), Vol. 4, pp 2236
- Fu Y., Liu S., Yin S., Niu W., Xiong W., Tan M., Li G., Zhou M.,*The reverse Warburg effect is likely to be an Achilles' heel of cancer that can be exploited for cancer therapy.,* Oncotarget. (2017), Vol. 8, pp 57813-57825
- German MAK Commission. Cadmium and Its Compounds (in the form of inhable dusts/aerosols) in The MAK collection for occupational health and safety. Edited by Greim H. Vol. 22. Weinheim, Germany: Wiley-VCH
- Giaginis C., Gatzidou E., Theocharis S., DNA repair systems as targets of cadmium toxicity., Toxicology and Applied Pharmacology (2006), Vol. 213, pp 282–290

- Glaser U., Hochrainer D., Otto F.J., Oldiges H., Carcinogenicity and toxicity of four cadmium compounds inhaled by rats., Toxicological & Environmental Chemistry (1990), Vol. 27, pp 153-162
- Grattan B.J., Freake H.C., Zinc and cancer: implications for LIV-1 in breast cancer., Nutrients (2012), Vol. 4, pp 648–675
- Gu C.-J., Pan Q., Li D.-G., Sun H., Liu B.W., miR-15b and miR-16 are implicated in activation of the rat hepatic stellate cell: An essential role for apoptosis. Journal of Hepatology (2009), Vol. 50, pp 766-778
- Hartmann A., Speit G., Effect of arsenic and cadmium on the persistence of mutagen-induced DNA lesions in human cells., Environmental and Molecular Mutagenesis (1996), Vol. 27, pp 98–104
- Hartwig A., Cadmium and Cancer in Cadmium: From Toxicity to Essentiality. Edited by Sigel A., Sigel H., Sigel R.K. Vol. 11. Dordrecht: Springer Netherlands. (2013a). pp 491-507
- Hartwig, A., Metal interaction with redox regulation: an integrating concept in metal carcinogenesis?, Free Radical Biology and Medicine (2013b) Vol. 55, pp 63–72
- Henkler F., Joep B., Luch A., *The Role of Oxidative Stress in Carcinogenesis Induced by Metals and Xenobiotics.,* Cancers (2010), Vol. 2, pp 376-396
- Howell A.N., Sager R., Tumorigenicity and its suppression in cybrids of mouse and Chinese hamster cell lines., Proceedings of the National Academy of Sciences of the United States of America (1978), Vol. 75, pp 2358–2362
- Hsiao C.J., Stapleton S.R., Early sensing and gene expression profiling under a low dose of cadmium exposure., Biochimie (2009), Vol. 91, pp 329–343
- Hunnewell M.G., Forbes N.S., Active and inactive metabolic pathways in tumor spheroids: determination by GC-MS., Biotechnology Progress (2010), Vol. 26, pp 789–796
- IARC (1993a). Beryllium, cadmium, mercury, and expo- sures in the glass manufacturing industry. Working Group views and expert opinions, Lyon, 9–16 February 1993. IARC Monogr Eval Carcinog Risks Hum, Vol. 58, pp 1-415
- IARC (1993b). Cadmium and cadmium compounds. IARC Monogr Eval Carcinog Risks Hum, Vol. 58, pp 119-237
- IARC (1997), Supplement: Cadmium and Cadmium compounds,
- IARC (2012), A Review of Human Carcinogens; Part C: Arsenic, Metals, Fibres, and Dusts,, pp. 121–145
- Israel B.A., Schaeffer W.I., Cytoplasmic suppression of malignancy., In Vitro Cellular & Developmental Biology (1987), Vol. 23, pp 627-32
- Kazantzis G., Blanks R.G., Sullivan K.R., Is cadmium a human carcinogen?, IARC Scientific Publications (1992), Vol. 118, pp 435-446
- Kiang J.G., Tsokos G.C., Heat shock protein 70 kDa: molecular biology, biochemistry and physiology., Pharmacology and Therapeutics (1998), Vol. 80, pp 183-201.

- Kim A., Mitochondria in Cancer Energy Metabolism:Culprits or Bystanders?, Toxicological Research (2015), Vol. 31, pp 323–330
- Kim J.W., Zeller K.I., Wang Y., Jegga A.G., Aronow B.J., O'Donnell K.A., Dang C.V. , Evaluation of myc E-box phylogenetic footprints in glycolytic genes by chromatin immunoprecipitation assays., Molecular and Cellular Biology (2004), Vol. 24, pp 5923-5936
- Kim J.W., Gao P., Liu Y.C., Semenza G.L., Dang C.V., Hypoxia-inducible factor 1 and dysregulated c-Myc cooperatively induce vascular endothelial growth factor and metabolic switches hexokinase 2 and pyruvate dehydrogenase kinase 1., Molecular and Cellular Biology (2007), Vol. 27, pp 7381-7393
- Kim N.H., Kim H.S., Li X.-Y., Choi H.S., Kang S.E., Cha S.Y., Ryu J.K., Yoon D., Fearon E.R., Rowe R.G., Lee S., Maher C.A., Weiss S.J., Yook J.I., A p53/miRNA-34 axis regulates Snail1-dependent cancer cell epithelial-mesenchymal transition., Journal of Cell Biology (2011), Vol. 195, pp 417-433
- Koedrith P., Seo Y.R., Advances in carcinogenic metal toxicity and potential molecular markers., The International Journal of Molecular Sciences (IJMS) (2011), Vol. 12, pp 9576–9595
- Koppenol W.H., Bounds P.L., Dang C.V., Otto Warburg's contributions to current concepts of cancer metabolism., Nature Reviews Cancer (2011), Vol. 11, pp 325-337
- Kriegel A.M., Soliman A.S., Zhang Q., El-Ghawalby N., Ezzat F., Soultan A., Abdel-Wahab M., Fathy O., Ebidi G., Bassiouni N., Hamilton S.R., Abbruzzese J.L., Lacey M.R., Blake D.A. Serum cadmium levels in pancreatic cancer patients from the East Nile Delta region of Egypt., Environ Health Perspect (2006), Vol. 114, pp 113–119
- Labbé K., Murley A., Nunnari J., Determinants and functions of mitochondrial behavior. The Annual Review of Cell and Developmental Biology (2014), Vol. 30, pp 357–391
- Lutzen A., Liberti S.E., Rasmussen L.J., Cadmium inhibits human DNA mismatch repair in vivo., Biochemical and Biophysical Research Communications (2004), Vol. 321, pp 21–25
- Massagué J., TGFβ in cancer., Cell (2008), Vol. 134, pp 215-230
- McElroy J.A., Shafer M.M., Trentham-Dietz A., Hampton J.M., Polly A. Newcomb P.A., Cadmium exposure and breast cancer risk., The Journal of the National Cancer Institute (JNCI) (2006), Vol. 98, pp 869–873
- Meplan, C., Mann, K., Hainaut, P., Cadmium induces conformational modifications of wild-type p53 and suppresses p53 response to DNA damage in cultured cells., The Journal of Biological Chemistry (1999), Vol. 274, pp 31663–31670
- Mishra, P., Chan D.C., Mitochondrial dynamics and inheritance during cell division, development and disease., Nature Reviews Molecular Cell Biology (2014), Vol. 15, pp 634–646
- Mishra P., Chan D.C., Metabolic regulation of mitochondrial dynamics, The journal of cell Biology (2016), Vol. 212, pp 379-387

- Mitra K., Wunder C., Roysam B., Lin G., Lippincott-Schwartz J., A hyperfused mitochondrial state achieved at G1-S regulates cyclin E buildup and entry into S phase. Proceedings of the National Academy of Sciences of the United States of America (2009), Vol. 106, pp 11960-11965
- Nieto M.A., The Snail superfamily of zinc-finger transcription factors., Nature Reviews Molecular Cell Biology (2002), Vol. 3, pp 155-166
- Onoo Y., Yazawa T., Kanamori H., Sasaki H., Mori S., Handa H., Matsumoto T., Genome-Wide transcriptome analysis of cadmium stress in rice., BioMed Research International (2016)
- Paolicchi E., Gemignani F., Krstic-Demonacos M., Dedhar S., Mutti L., Landi S., *Targeting hypoxic response for cancer therapy.,* Oncotarget (2016), Vol. 7, pp 13464-13478
- Park R.M,1 Stayner L.T., Petersen M.R, Finley-Couch M., Hornung R., Rice C., Cadmium and lung cancer mortality accounting for simultaneous arsenic exposure.,Occupational and Environmental Medicine (2012); Vol. 69, pp 303–309
- Pokorný J., Pokorný J., Kobilková J., Jandová A., Vrba J., Vrba J. Jr., Targeting Mitochondria for Cancer Treatment – Two Types of Mitochondrial Dysfunction., Prague Medical Report (2014), Vol. 115, pp 104–119
- Potts R.J., Watkin R.D., Hart B.A., Cadmium exposure down-regulates 8-oxoguanine DNA glycosylase expression in rat lung and alveolar epithelial cells., Toxicology (2003), Vol. 184, pp 189–202
- Sadok A., Marshall C.J., Rho GTPases—masters of cell migration., Small GTPases (2014), Vol. 5, pp 1-7
- Schwerdtle T., Ebert F., Thuy C., Richter C., Mullenders L.H., Hartwig A., Genotoxicity of soluble and particulate cadmium compounds: impact on oxidative DNA damage and nucleotide excision repair., Chemical Research in Toxicology (2010), Vol. 23, pp 432–442
- Seyfried T.N., Cancer as a mitochondrial metabolic disease., Frontiers in Cell and Developmental Biology (2015), Vol. 3, pp 43
- Seyfried T. N., Mitochondria: the ultimate tumor suppressor, In: Cancer as a Metabolic Disease: On the Origin, Management, and Prevention of Cancer. (Hoboken N.J. : John Wiley & Sons) (2012), pp 195–205
- Sorahan T., Mortality from lung cancer among a cohort of nickel cadmium battery workers: 1946-84., British Journal of Industrial Medicine (1987), Vol. 44, pp 803–809
- Shigematsu I., Kitamaru S., Takeuchi J. et al., A retrospective mortality study on cadmium-exposed populations in Japan., Edited Proceedings of the Third International Cadmium Conference, Miami, FL, 3–5 February 1981. Wilson D, Volpe RA, editors. (1982), London/ New York: Cadmium Association/Cadmium Council, pp 115–118
- Shirai T., Iwasaki S., Masui T. Mori T., Kato T., Ito N., Enhancing effect of cadmium on rat ventral prostate carcinogen- esis induced by 3,2′-dimethyl-4-aminobiphenyl., Japanese Journal of Cancer Research (1993), Vol. 84, pp 1023–1030

- Shirato K., Nakajima K., Korekane H., Takamatsu S., Gao C., Angata T., Ohtsubo K., Taniguchi N., Hypoxic regulation of glycosylation via the N-acetylglucosamine cycle., Journal of Clinical Biochemistry and Nutrition (2011), Vol. 48, pp 20–25
- Skulachev V.P., Mitochondrial filaments and clusters as intracellular power-transmitting cables., Trends in Biochemical Sciences (2001), Vol. 26, pp 23–29
- Stohs S.J., Bagchi D., Hassoun E., Bagchi M., Oxidative mechanisms in the toxicity of chromium and cadmium ions., The Journal of Environmental Pathology, Toxicology, and Oncology (2001), Vol. 20, pp 77–88
- Sullivan L.B., Gui D.Y., Hosios A.M., Bush L.N., Freinkman E., Vander Heiden M.G., Supporting aspartate biosynthesis is an essential function of respiration in proliferating cells., Cell (2015), Vol. 162, pp 552–563
- Takiguchi M., Achanzar W.E., Qu W., Li G., Waalkes M.P., Effects of cadmium on DNA-(Cytosine-5) methyltransferase activity and DNA methylation status during cadmium-induced cellular transformation., Experimental Cell Research (2003), Vol. 286, pp 355-365
- Tanaka F., Yoshimoto S., Okamura K., Ikebe T., Hashimoto S., Nuclear PKM2 promotes the progression of oral squamous cell carcinoma by inducing EMT and post-translationally repressing TGIF2., Oncotarget (2018), Vol. 9, pp 33745–33761
- Tapisso J.T., Marques C.C., Mda M.L., Mda R.G., Induction of micronuclei and sister chromatid exchange in bone-marrow cells and abnormalities in sperm of Algerian mice (Mus spretus) exposed to cadmium, lead and zinc., Mutation Research (2009), Vol.678, pp 59-64
- Thevenod F., Cadmium and cellular signaling cascades: to be or not to be?., Toxicology and Applied Pharmacology (2009), Vol. 238, pp 221–239
- Tokumoto M., Fujiwara Y., Shimada A., Hasegawa T., Seko Y., Nagase H., Satoh M., Cadmium toxicity is caused by accumulation of p53 through the down-regulation of Ube2d family genes in vitro and in vivo., The Journal of Toxicological Sciences (2011), Vol. 36, pp 191-200
- Tondera D., Grandemange S., Jourdain A., Karbowski M., Mattenberger Y., Herzig S., Da Cruz S., Clerc P., Raschke I., Merkwirth C., Merkwirth C., Ehses S., Krause F., Chan D.C., Alexander C., Bauer C., Youle R., Langer T., Martinou J.C., SLP-2 is required for stress-induced mitochondrial hyperfusion., EMBO J. (2009), Vol. 28, pp 1589-1600
- Trusolino L., Bertotti A., Comoglio P.M., MET signalling: principles and functions in development, organ regeneration and cancer., Nature Reviews Molecular Cell Biology (2010), Vol. 11, pp 834-848
- Urani C., Melchioretto P., Gribaldo L., Regulation of metallothioneins and ZnT-1 transporter expression in human hepatoma cells HepG2 exposed to zinc and cadmium., Toxicology in Vitro (2010), Vol. 24, pp 370-374
- Urani C., Melchioretto P., Fabbri M., Bowe G., Maserati E., Gribaldo L., Cadmium Impairs p53 Activity in HepG2 Cells., ISRN Toxicology (2014)

- Urani C., Melchioretto P., Bruschi M., et al., Impact of Cadmium on Intracellular Zinc Levels in HepG2 Cells: Quantitative Evaluations and Molecular Effects., BioMed Research International (2015)
- Urso M.L., Clarkson P.M., Oxidative stress, exercise, and antioxidant supplementation., Toxicology (2003), Vol. 189, pp 41-54
- Valko M., Rhodes C.J., Moncol J., Izakovic M., Mazur M., Free radicals, metals and antioxidants in oxidative stress-induced cancer., Chemico-Biological Interactions (2006), Vol. 160, pp 1–40
- Vander Heiden M.G., Locasale J.W., Swanson K.D., Sharfi H., Heffron G.J., Amador-Noguez D., Christofk H.R., Wagner G., Rabinowitz J.D., Asara J.M., Cantley L.C., Evidence for an alternative glycolytic pathway in rapidly proliferating cells., Science (2010), Vol. 329, pp 1492–1499
- Warburg O., On the origin of cancer cells., Science (1956), Vol. 123, pp 309–314
- Waalkes M.P., Cadmium carcinogenesis., Mutation Research/Fundamental and Molecular Mechanisms of Mutagenesis. (2003); Vol. 533, pp 107-120
- Waalkes M.P., Rehm S., Carcinogenicity of oral cadmium in the male Wistar (WF/NCr) rat: effect of chronic dietary zinc deficiency., Fundamental and Applied Toxicology (1992), Vol.19, pp 512-520
- Waalkes M.P., Rehm S., Chronic toxic and carcinogenic effects of cadmium chloride in male DBA/2NCr and NFS/NCr mice: strain-dependent association with tumors of the hematopoietic system, injection site, liver, and lung., Fundamental and Applied Toxicology (1994), Vol. 23, pp 21–31
- Waalkes M.P., Anver M.R., Diwan B.A., Chronic toxic and carcinogenic effects of oral cadmium in the Noble (NBL/Cr) rat: induction of neoplastic and proliferative lesions of the adrenal, kidney, prostate, and testes., Journal of Toxicology and Environmental Health (1999), Vol.58, pp 199-214
- Waalkes M.P., Rehm S., Cherian M.G., Repeated cadmium exposures enhance the malignant progres- sion of ensuing tumors in rats., Toxicological Sciences (2000), Vol. 54, pp 110-120.
- Waalkes M.P., Rehm S., Devor D.E., The effects of continuous testosterone exposure on spontaneous and cadmium-induced tumors in the male Fischer (F344/ NCr) rat: loss of testicular response., Toxicology and Applied Pharmacology (1997), Vol. 142, pp 40–46
- Weinhouse S., On respiratory impairment in cancer cells., Science(1956), Vol. 124, pp 267-269
- Wise D.R., Ward P.S., Shay J.E., Cross J.R., Gruber J.J., Sachdeva U.M., Platt J.M., DeMatteo R.G., Simon M.C., Thompson C.B., Hypoxia promotes isocitrate dehydrogenase-dependent carboxylation of alpha-ketoglutarate to citrate to support cell growth and viability., Proceedings of the National Academy of Sciences of the United States of America (2011); Vol. 108, pp 19611–19616

- Xiong M., Jiang L., Zhou Y.,Qiu W., Fang L., Tan R., Wen P., Yang J., The miR-200 family regulates TGF-β1-induced renal tubular epithelial to mesenchymal transition through smad pathway by targeting ZEB1 and ZEB2 expression., The American Journal of Physiology - Renal Physiology (2012), Vol. 302, pp 369-379
- Xu S., Pi H., Chen Y., Zhang N., Guo P., Lu Y., He M., Xie J., Zhong M., Zhang Y., Yu Z., Zhou Z., Cadmium induced Drp1-dependent mitochondrial fragmentation by disturbing calcium homeostasis in its hepatotoxicity, Cell Death and Disease (2013), Vol. 4, pp 1-10
- Xu X., Li J., Sun X., Guo Y., Chu D., Wei L., Li X., Yang G., Liu X., Yao L., Zhang J., Shen L., Tumor suppressor NDRG2 inhibits glycolysis and glutaminolysis in colorectal cancer cells by repressing c-Myc expression.,Oncotarget (2015), Vol. 6, pp 26161-26176
- Zharkov D.O., Rosenquist T.A., Inactivation of mammalian 8-oxoguanine-DNA glycosylase by cadmium(II): implications for cadmium genotoxicity., DNA Repair (Amst) (2002), Vol. 1, pp 661–670
- Zhang C., Liu J., Liang Y., Wu R., Zhao Y., Hong X., Lin M., Yu H., Liu L., Levine A.J., Hu W., Feng Z., Tumour-associated mutant p53 drives the Warburg effect., Nature Communications (2013), Vol. 4, pp 2935
- Zhang H., Reynolds M. , Cadmium exposure in living organisms: A short review., Science of the Total Environment (2019), Vol. 678, pp 761-767

Chapter 4

"Objective of the thesis"

The objectives of the thesis were:

i) the investigation of the mechanisms through which Cd, a non-genotoxic environmental contaminant, induces carcinogenesis;

ii) the implementation of Cell Transformation Assay (CTA), one of the most advanced *in vitro* biological assays for evaluation of chemical carcinogenesis. For these purposes, the process of cells transformation has been studied by *in vitro* experiments supplemented by bioinformatics analyses.

The use of CTA improved with *in silico* models to evaluate the carcinogenic potential of a chemical substance and its mechanism of action is extremely important because they are examples of application of the "3R" principles (Reduction, Refinement and Replacement) of Russell and Burch and of alternative methods to animal experimentation, whose diffusion is fundamental for ethical, economic and scientific reasons.

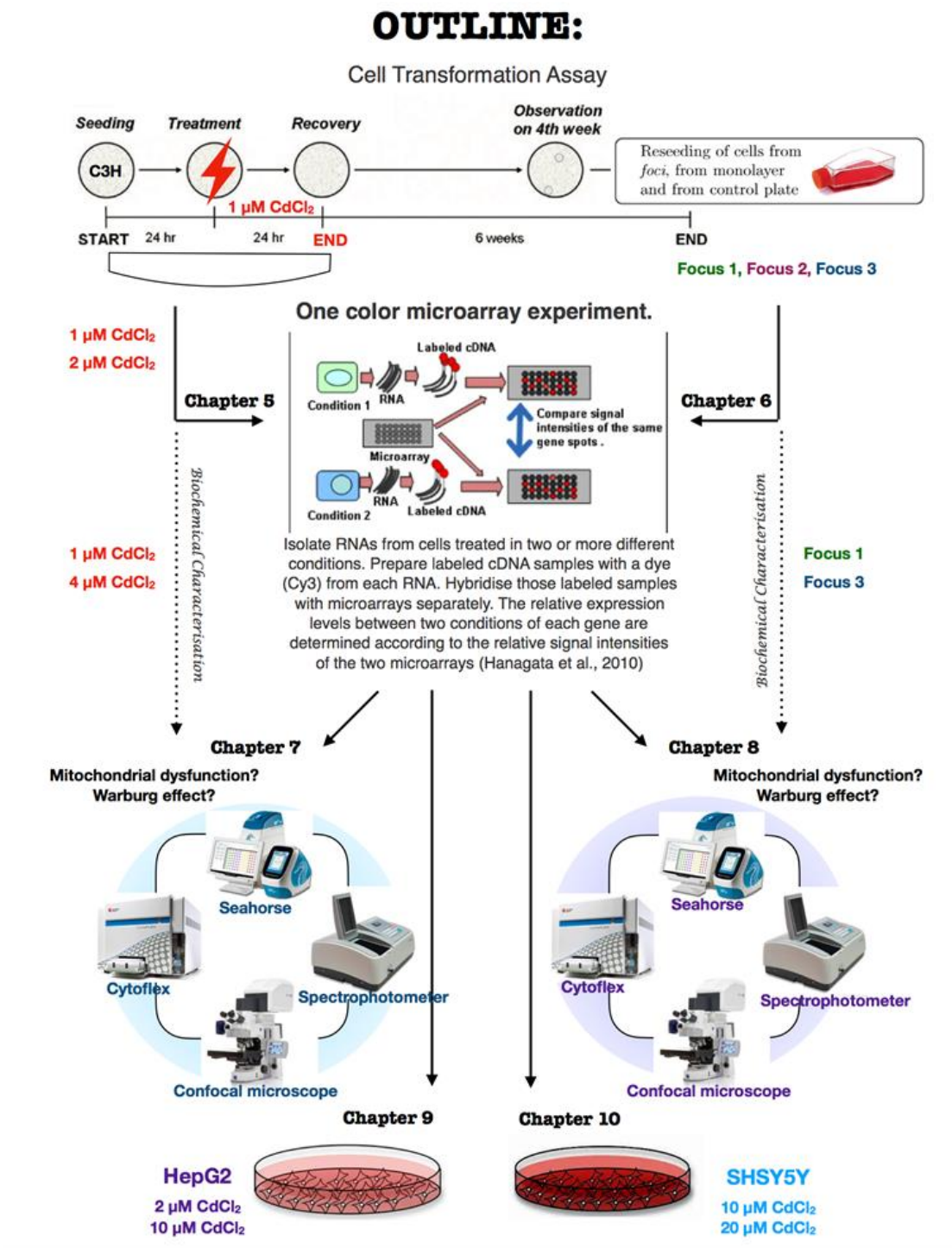

Hanagata N., Takemura T., Takashi Minowa T., *Global gene expression analysis for evaluation and design of biomaterials, Sci Technol Adv Mater. (2010), Vol. 11(1): 013001.*

Chapter 5

"A toxicogenomic study reveals early events in cadmium toxicity."

ABSTRACT

Cadmium is a non-essential metal that is widespread in all the environmental compartments (air, soils and water). However, since this heavy metal is a very pollutant agent, the continuous dissemination of Cd in the ecosystems as a consequence of natural and anthropogenic activities is a source of concern for human health, especially for industrial workers and populations living in polluted areas. In this regard, the principal source of Cd exposure for the general population can be food, drinking water and tobacco smoke. Moreover, Cd absorption is eased and promoted by its ability to mimic essential ions: Cd enters the cells through a variety of channels and transport pathways, in what has been named a "Trojan horse mechanism".

After the uptake in human tissues, Cd can lead to the development of different diseases, including cancer, although Cd mechanisms of action are still not fully elucidated. In this work, in order to investigate Cd effects in more depth, we performed a toxicogenomic study based on whole-genome microarray analysis of gene modulation induced by Cd treatment in C3H10T1/2 cells. In more details, we have chosen to use two different concentrations of this metal (1 and 2 μM $CdCl_2$ 24 hr) to elucidate the dose-effects of Cd in this particular cell line. C3H10T1/2 cells are one of the cell lines suggested by OECD as a model for carcinogenicity studies in the Cell Transformation Assay (CTA). In addition, C3H10T1/2 CTA is considered, among CTA protocols, the best model useful to elucidate molecular mechanisms of cell transformation at the genomic and transcriptomic level. We have carried out exploratory analyses using Principal Component Analysis (PCA). We have applied combinations of differential expression analyses using generalized linear models; on the DE genes as well as on the log(FC) calculated by limma approach, we have subsequently performed downstream analyses, such as Gene Ontology (GO) and pathway enrichment analysis, along with weighted coexpression network analyses. Our data suggest that in the first 24 hrs, the up-regulation of metallothioneins and glutathione S-transferase (Gstα 1–3) are not fully efficient in preventing damages caused by cadmium. In particular, at the end of the analysis, the results have shown that dysfunctions of mitochondria can be one of the main causes of Cd-induced carcinogenesis. Indeed, this study links Cd toxicity with dysregulation of genes coding for mitochondrial proteins, including several genes that encode for proteins of the respiratory chain. Moreover, knowing that cadmium leads to Zn

release, we hypothesize a mechanism of Zn replacement with Cd. In this regard, we are currently trying to identify genes that encode for Zinc(Zn)-binding proteins, and analyze their level of expression after Cd exposure. To conclude, although CTA use has been limited so far to the detection of chemically-induced transformation, with this work we propose that it can also be a valuable tool to study the mechanisms involved in carcinogenesis.

❖ 5.1. Introduction

Cadmium (Cd) is a heavy metal that is commonly found in low concentrations in the earth's crust combined with other elements such as oxygen (cadmium oxide), chlorine (cadmium chloride), or sulfur (cadmium sulfate, cadmium sulfide). However, due to the several Cd uses in the industrial sector, anthropogenic activity has dramatically increased Cd levels into the environment. For example, Cd can be used in the production of batteries, pigments, metal coatings, and plastics. Consequently, since the industrial revolution, Cd has become a dangerous environmental pollutant. In this regard, it has been shown that, when released into the environment, Cd leads to ecosystems destruction, also at much lower doses than most toxic metals (Jaishankar et al., 2014). Furthermore, it has been known that Cd dispersed in the environment can persist in soils and sediments for decades, exacerbating the potential environmental damage (Wuana et al., 2011). For these reasons, Cd remains a source of concern for human health, especially for industrial workers and populations living in polluted areas. The occupational exposure to Cd primarily occurs by inhalation and ingestion. The principal source of Cd exposure for the general population can be food, tobacco smoke, drinking water, and air (WHO, 1992); according to the route of exposure, Cd can hence cause acute and chronic intoxications in different organs. Once absorbed, due to its exceptionally long half- life in the human body, Cd irreversibly accumulates in kidneys, lungs or liver and can induce several diseases, including cancer (Bernard, 2008; Thévenod et al., 2013). In this regard, Cd was classified as a human carcinogen (Group 1) by the World Health Organization's International Agency for Research on Cancer (IARC) and by the German MAK Commission. However, Cd mechanisms of action, especially at the molecular level, are still not completely understood (IARC, 1993). For this reason, valid therapies against Cd intoxication are not currently available. Based on many data obtained by the literature, Cd effects can be divided into two main categories: Cd can control cell proliferation (Asara et al., 2013), whereas elevated concentrations of this metal result to be cytotoxic (Waisberg et al., 2003). In more details, Cd induces tissue injury through oxidative stress increase (Henkler et al., 2010), epigenetic changes in DNA expression (Wang et al., 2012), inhibition or upregulation of transport pathways (Yang et al., 2015), modification in the

homeostasis of other divalent cation (Zn2+ and Ca2+), and inhibition of heme synthesis (Schauder et al., 2010). Otherwise, several studies suggested that Cd toxicity could be related to mitochondrial damage (Sanni et al., 2008; Cannino et al., 2009; Xu et al., 2013). In fact, following Cd uptake in cells, some free metal ions or some Cd-metallothioneins complexes not only remain in the cytosol but could also penetrate the mitochondria (Waku, 1984). Subsequently, in these organelles, high concentrations of Cd can lead to the inhibition of mitochondrial functions (Vergilio et al., 2013) either by inhibiting the activity of complexes II and III of the electron transport chain (Wang et al., 2004) or by inducing the activation of apoptotic signalling (Kumar et al., 2016; Yuan et al., 2018). It has been shown that Cd can alter gene expression (Zhou et al., 2004), acting as a transcriptional regulator for normal and pathological cell types (Bertin et al., 2006). For example, Callegaro et al. (2018) have demonstrated that Cd intake can upregulate the expression of several genes (those coding for metallothioneins, glutathione and heat shock proteins) (Callegaro et al., 2018). Whereas, other gene expression analyses have proved that chronic Cd exposure can change the expression of genes connected with inflammation, metabolism, or can lead to the deregulation of onco- or tumour suppressor genes and transporters (Koizumi et al., 2003). Considering that several mechanisms appear to contribute to Cd-induced carcinogenesis, in this study we performed a whole-genome transcriptomics analysis to test the acute toxicity of Cd in C3H10T1/2 clone 8 mouse embryonic fibroblasts (C3H). In particular, C3H cells were treated with two sub-lethal concentration of Cd for 24 h (1 and 2 µM). The lowest cadmium concentration (1 µM) was selected because it was able to induce foci formation in in vitro Cell Transformation Assay, as described in our previous study (Forcella et al., 2016). The highest concentration (2 µM) was used to investigate the dose- dependent effect of this metal. Thus, the purpose of this research was both to identify early markers of Cd-induced carcinogenesis and to gain a deeper understanding its molecular mechanisms, in order to allow better assessment of associated risks and insights into possible therapies against Cd intoxication.

❖ 5.2. Materials and Methods

2.1. Cells and culture conditions

The experiments were achieved using C3H10T1/2 clone 8 (C3H from here on) mouse embryonic fibroblasts (cell line ATCC, CCL 226 lot. n. 58078542), because this cell line is characterized by high sensitivity to carcinogenic compounds and low spontaneous transformation rates. This cell line also represents one of the finest and suitable cell models used in the in vitro carcinogenicity studies (Cell Transformation Assays, CTAs) (OECD, 2007). Cells were cultured in Basal Medium Eagle (BME, Sigma Chemical Co., St. Louis, MO, USA) enriched with 10% heat- inactivated fetal bovine serum (FBS, Euroclone, Pero, Italy), 1% glutamine, 0.5% HEPES 2M and 25 µg/mL gentamicin (all purchased from Sigma) at 37°C in a humidified incubator supplied with a constant flow of 5% CO2 in air throughout each experiment. Cells were routinely seeded in 100 mm Ø Petri dishes, the medium was changed every 3 days and cells grown until 80% confluence maximum was reached. The cells were stored in ampoules, frozen at –80°C with 10% sterile DMSO as a preservative.

2.2. RNA extraction and purification

For RNA extraction, the cells were seeded at a density of 106 cells/ dish in 100 mm Ø Petri dishes, two Petri dishes for each treatment. After 24 h, the cells were exposed to 1 or 2 µM CdCl2 (Cd) for 24 h, by replacing the basal medium with an enriched medium with the appropriate concentrations of CdCl2. The stock solution (1mM) of CdCl2 (97% purity BDH Laboratory, Milan, Italy) was prepared in ultra-pure water (0.22 µm filtered Milli-Q water, Millipore, Vimodrone, Milan, Italy) and stored at 4 °C. Previous experiments performed by our group (Urani et al., 2009; Forcella et al., 2016) have demonstrated that 1 µM CdCl2, which is below the cytotoxicity threshold (IC50 of 2.4 µM), is able to induce the formation of transformed colonies of cancerous cells (foci) in the Cell Transformation Assay. At the end of treatments, all cell clones were harvested by trypsinization at 80% confluence and lysed in 300 µl RLT buffer (Qiagen, Germantown, MD, USA) added with 1:100 β-mercaptoethanol. Homogenates were obtained by

passing 5 times through a blunt 20-gauge needle fitted to a syringe. Samples were stored at -80°C until RNA extraction was carried out. RNA was purified from cell clones using the RNeasy Plus kit (Qiagen, Germantown, MD, USA). RNA was quantified using a ND-1000 UV-Vis Spectrophotometer (NanoDrop Technologies), and the integrity of the RNA was assessed with the Agilent 2100 Bioanalyzer (Agilent), according to the manufacturer's instructions. RNA samples used in this study all had a 260/280 ratio above 1.9 and RNA Integrity Number (RIN) above 9.0.

2.3. Microarray expression profiling

In the microarray experiments, all sample-labelling, hybridization, washing, and scanning steps were conducted following the manufacturer's specifications. In brief, Cy3-labeled cRNA was generated from 500 ng input total RNA using Quick Amp Labeling Kit, One-color (Agilent). Three independent replicates were used for treatments and controls. For every sample, 1.65 µg cRNA from each labelling reaction (with a specific activity above 9.0) was hybridized using the Gene Expression Hybridization Kit (Agilent) to the SurePrint G3 Mouse GE 8x60K Microarray (G4852, Agilent), which is a 8 x 60k 60mer slide format. After hybridization, the slides were washed and then scanned with the Agilent G2565BA Microarray Scanner (Agilent). The fluorescence intensities on scanned images were extracted and preprocessed by Agilent Feature Extraction Software (v10.5.1.1). Quality control and array normalization was performed in the R statistical environment using the Agi4x44PreProcess package downloaded from the Bioconductor web site (Gentleman et al., 2004). The normalization and filtering steps were based on those described in the Agi4x44PreProcess reference manual. After that, all duplicated genes were eliminated using the function collapseRows of the WGCNA package (Langfelder et al., 2008). The function has allowed to collapse the rows of the processed matrix, forming a representative row for each group of rows that have the same name. As a result, a sub-matrix of about 22.000 genes was obtained.

2.4. Biostatistical and bioinformatic analyses

We carried out a first exploration of the data using Principal Component Analysis (PCA) with the built-in R function prcomp. This allowed us to verify that the groups of interest were sufficiently separated to perform differential expression analyses (DEA). We used the linear model implemented in the Limma R/Bioconductor package (Ritchie et al. Nucleic Acids Research 2015) for DEA. We considered as significant the DE genes with a Log Fold Change (LogFC) ≥ 1 (up-regulated) or ≤ -1 (down-regulated), and with a false discovery rate (FDR) < 0.05 (Smyth, 2004). The analysis is based on the investigation of three different pairwise comparisons: 1 µM Cd versus control (1vsC), 2 µM Cd versus control (2vsC) and 2 µM Cd versus 1 µM Cd (2vs1). We estimated the intersections between the up- and downregulated genes in the three different comparison using the UpsetR package (Conway et al., 2017). We illustrated the DE genes using a volcano plot through the TCGAanalyze_DEA function of the TCGAbiolinks package.

2.5. Pathway enrichment analysis and Gene Ontology enrichment analysis

To determine the functions of the DE genes, the pathway enrichment analyses were performed using two different databases as a reference, KEGG and Reactome Pathway Database. The first is the Kyoto Encyclopedia of Genes and Genomes (KEGG; http://www.genome.jp/kegg) database, that consists of a collection of online databases of genomes, enzymatic pathways and biological chemicals. The KEGG analysis was accomplished with the up- and down-regulated genes separately and a threshold of p.value < 0.05. Secondly, ReactomePA version 1.18.1, an R package for Reactome Pathway Analysis (Fabregat et al. 2018; Milacic et al. 2012) was applied with an adjusted p-value cutoff of 0.05. GO classification was performed to study the biological process or cellular component categories of DEGs (Ashburner et al., 2000). GO functional enrichment analysis was done using topGo R/Bioconductor package. GO results are represented in circular plots generated by the GOplot (Wencke et al., 2015) R/Bioconductor package. These plots display the relation between the most significant GO terms and the DE genes.

❖ 5.3. Results

5.3.1. Cadmium administration for 24 hours shows dose dependent effects

A first exploration of the gene expression data was carried out using principal component analysis (PCA), as reported in Figure 5.1. In our dataset, the first principal component (PC1) explained the 75.0% of the samples variance, while the second principal component (PC2) accounted for the 8.8%. The projections of the data along the first two PCs suggest that 2 µM Cd concentration is enough to change C3H cells gene expression, compared to the other conditions (1 µM treated cells and control cells). Indeed, 1 µM Cd treated cells and the control samples feature a high overlap in the PCA space. Considering PCA results, we performed the analysis on transcriptomics data using a statistical framework for differential expression analysis (DEA) (Ritchie et al., 2015). In particular, we took into consideration three pairwise comparisons: 1 µM Cd and 2 µM Cd each versus control (1vsC and 2vsC) and 2 µM Cd versus 1 µM Cd (2vs1).

Figure 5.1. Principal-Component Analysis. PCA was performed on all genes of the dataset to summarize the hidden trends of the transcriptomics data by fitting the whole matrix to orthogonal axes. The principal components PC1 is shown along the x-axis and the PC2 is shown along the y-axis. The green circle represents 2 µM Cd, the red circle represents 1 µM Cd and the little blue circle represents control samples.

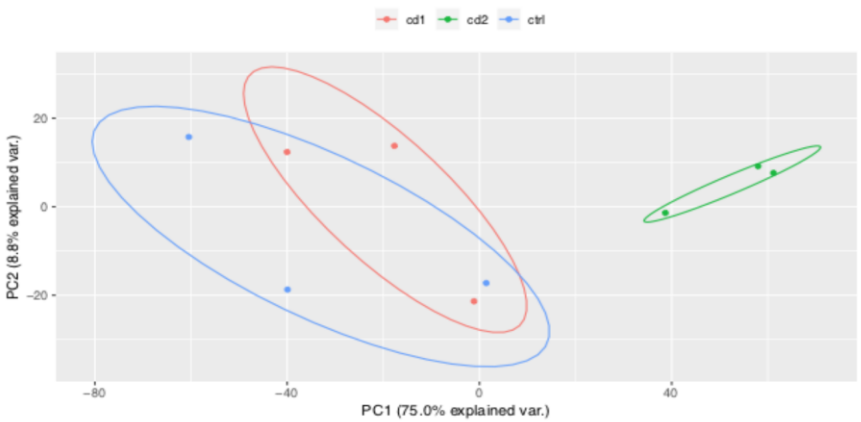

5.3.2. A concentration of 2 µM $CdCl_2$ modulates the level of expression of ca. 2000 genes

To represent a summary of the DEA calculations, we decided to generate a UpSetR plot in which the rows represented gene sets, and the columns correspond to their intersections (Figure 5.2). The plot illustrated 17 up-regulated genes after the treatment with the lowest concentration of CdCl2 (1 µM). Of these, 9 genes were up-regulated in all the conditions (1vsC, 2vsC, and 2vsC) and 8 common genes were shared between the first and the second comparisons (1vsC and 2vsC). At the same time, any down-regulated gene after 1 µM Cd exposure occurred. On the other hand, about 2000 Differentially Expressed Genes (DEGs) were analysed by increasing the treatment with a concentration of Cd from 1 to 2 µM. 554 up- and 389 down-regulated genes characterised the intersection between 2vsC and 2vs1, respectively; whereas 554 up-regulated and 444 down-regulated genes were exclusively differentiated in 2vsC comparison. Al least, 41 up- and 20 down-regulated genes were distinctive of the third situation (2vs1).

Figure 5.2. An UpSetR plot to visualize an effective representation of associated data. Data for UpsetR plot are based on the SurePrint G3 Mouse GE 8x60K Microarray experiments normalized using the Agi4x44PreProcess package. Each row corresponds to a set of genes obtained in a specific comparison, and each column corresponds to an intersection, as indicated in the figure. Cells in light-gray indicate that set is not part of that intersection; black dots show that the set is participating in the intersection.

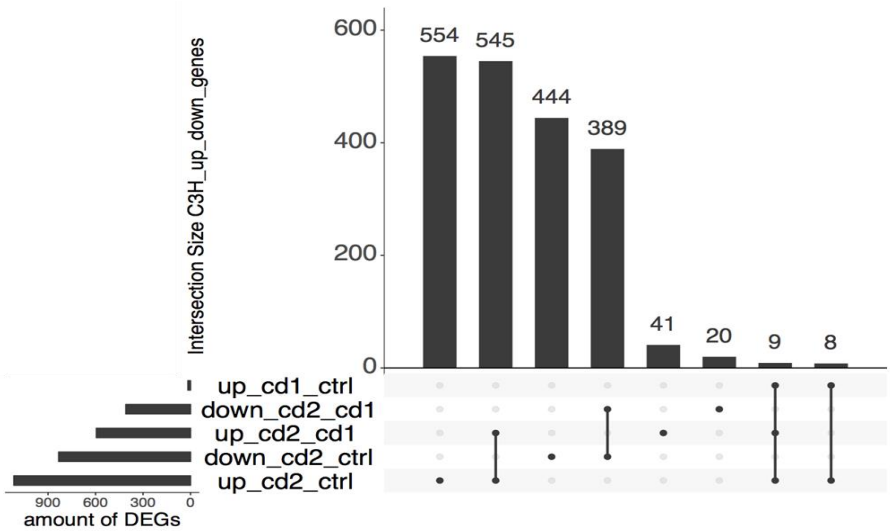

5.3.3. 2 µM $CdCl_2$ modulates genes related to inflammation and metastasis

When we investigated the identity of the 17 DEGs achieved in the first comparison (1vsC), we recognised the genes annotated by Callegaro et al. (2018). However, we also found other five upregulated genes, after 24 hours treatment with 1 µM Cd (Table 5.1). For example, we identified LOC625953, a predictive gene similar to Glutathione S-transferase Ya chain (GST class-alpha) coding gene, the Carboxylesterase 5A (Ces5) coding gene, responsible for the hydrolysis of various xenobiotics, and three genes not yet identified. The complete list of the DE genes with their respective Log fold change (LogFC) is shown in Table 5.1. On the contrary, given the large amount of DEGs in 2vsC comparison, we decided to present the data of the second condition with a Volcano plot, represented in Figure 5.3. The Volcano plot highlights the top 20 DE genes, among the up- or down-regulated genes detected after treatment with a higher cadmium concentration (2vsC). Results obtained in the 1vsC comparison match those obtained in the 2vsC comparison (Table 5.1). For example, MTs and GST were upregulated in both conditions. Moreover, although the number of up- and downregulated genes were equivalent, all the top 20 DEGs were upregulated. After treatment with 2 µM Cd, the genes coding for Paralemmin-3 (PALM3), solute carrier family 11 member 1 (SLC11A1), Angiopoietin-2 (ANG2), aldehyde dehydrogenase family 1, subfamily A7 (ALDH1A7), serine (or cysteine) peptidase inhibitor, clade B, member 1b (SERPINB1B) and Purinergic Receptor P2X 7 (P2RX7) were all upregulated. More in details, PALM3, localised in the lipid rafts of the plasmamembrane, is correlated with tumour progression and metastasis (Hultqvist et al., 2012), and it can be involved in LPS-Toll-like receptor 4 (TLR4) signalling (Chen et al., 2017). SLC11A1 is linked to cancer, causing chronic inflammation (Agnes A Awomoyi, 2007). P2RX7, that mediates Nlrp3-inflammasome activation, generally contributes to the development of neural disorders (Albalawi et al., 2017). ANG2 and ALDH1A7 are both implicated in metastasis progression (Van den Hoogen et al., 2010; Ramanathan R et al., 2017), while ANG2 is described as a hallmark of cancer (Ramanathan R et al., 2017). In conclusion, the top 20 DEGs annotated in the Volcano plots showed that 2 µM CdCl2 increases the expression of genes related to inflammation and metastasis.

Figure 5.3. Volcano plot of the DEGs obtained in the second comparison (2vsC). This type of scatter-plot summarises changes in the gene expression levels in our large data sets composed of replicate data. The graph plots the significance (the negative log of the p-value on the y) versus logFC on the y- and x-axes, respectively. Modulated genes were chosen using cutoffs for Log fold change (LogFC) as >= 1 or <=-1, and a cutoff of 0.05 for false discovery rate (FDR). Genes in red are up-regulated, in green down-regulated. In addition, the names of the twenty highlighted genes in each comparison are shown in yellow.

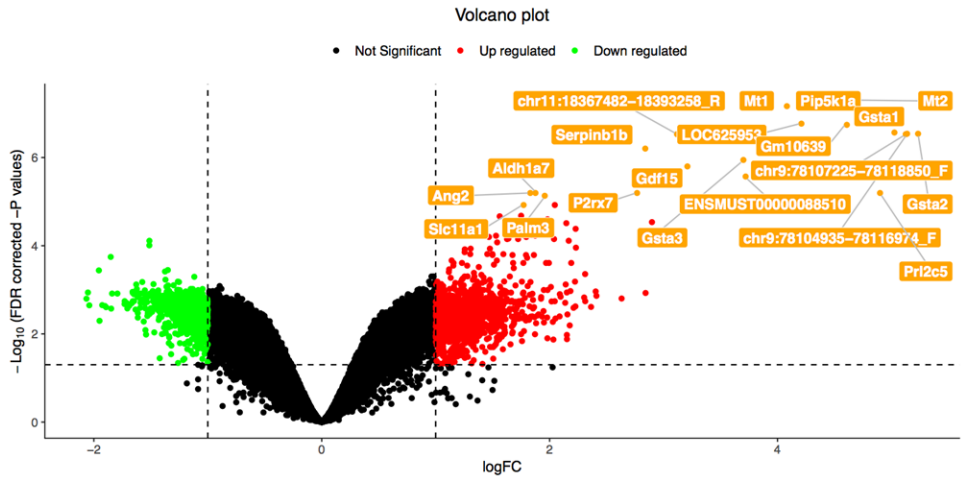

Table 5.1. Upregulated genes in 1vsC comparison

	logFC	AveExpr	t	P.Value	Adj.P.Val
Mt2	4,6993109	15,779222	36,419610	2,27E-12	4,98E-08
Mt1	4,08241614	16,0159052	32,1403186	8,33E-12	6,84E-08
Pip5k1a	4,25171859	14,0724961	31,7805332	9,36E-12	6,84E-08
LOC625953	4,20969077	7,77317537	28,3032316	3,11E-11	1,70E-07
Gm10639	4,60857904	9,4531497	27,5330155	4,14E-11	1,81E-07
Gsta1	5,02599002	10,9518814	26,0222922	7,41E-11	2,71E-07
Gsta2	5,23367512	10,30356	25,4523789	9,31E-11	2,88E-07
chr9:78104935-78116974_F	5,13744258	10,3921202	25,1509822	1,05E-10	2,88E-07
chr11:18367482-18393258_R	3,118093	8,30815119	24,7761942	1,23E-10	2,96E-07
chr9:78107225-78118850_F	5,12546889	10,9288314	24,5544658	1,35E-10	2,96E-07
Serpinb1b	2,83934671	6,44615368	22,6144679	3,15E-10	6,27E-07
Gsta3	3,70075072	8,24143651	21,1645324	6,21E-10	1,13E-06
Gdf15	3,2092265	9,24490198	20,3227909	9,41E-10	1,59E-06
ENSMUST00000088510	3,72035715	7,97739757	19,1581734	1,72E-09	2,69E-06
P2rx7	2,76758811	6,42915379	17,4385947	4,48E-09	6,37E-06
Aldh1a7	1,87563029	8,858225	17,2758215	4,93E-09	6,37E-06

5.3.4. Cadmium alters specific gene expression of several ECM components

To investigate the cell response to cadmium toxicity, we focused on the study of the pathways and biological processes in which the DEGs were involved. ReactomePA and topGO packages (Fabregat et al. 2018; Milacic et al. 2012) were used to carry out pathway enrichment and Gene Ontology (GO) enrichment analysis, respectively. The comparison 1vsC was initially analyzed; however, since it did not lead to any additional information respect to results obtained in Callegaro et al. (2018), we decided to describe in more details the 2vsC comparison. To carry out Reactome analyses, up- and down-regulated genes were considered together. Hence, the dot plot of Figure 5.4 and in Table 5.1S illustrates the most significant pathways and their correlated genes modified after the treatment with 2 µM CdCl2. We found that several collagen-encoding genes, that were down-regulated (see Table 5.1S), characterised all the pathways presented in Figure 5.4, except for the "post-translational protein phosphorylation", "signalling by ROBO receptors" and "signalling by Leptin" pathways. Not surprisingly, collagen not only has been recognised as a physical barrier against cancer invasion and tumor cells migration, but it has become a significant factor involved in promoting tumour migration, infiltration and angiogenesis (Fang et al., 2014). Thus, a decrease in matrix cross-linking and a modification in ECM protein arrangement induced by Cd may be symptoms that this metal can alter of cells growth, reduce the adhesive properties of cells and enhance epithelial-mesenchymal transition (EMT) process. GO results (data not shown) confirm the outcomes of Reactome analysis.

Figure 5.4. Pathway enrichment analysis of DEGs obtained in the second comparison (2vsC). Enriched terms are displayed in a dot plot. On the y-axis, the names of deregulated pathways are annotated, while on the x-axis the Gene Ratio is illustrated. The amount of DEGs inside a specific pathway is connected with the size of dots in the panel. The colour of the dots reflects the p. Adjust value of each pathway: blue for the less significant values and red for the more significant values.

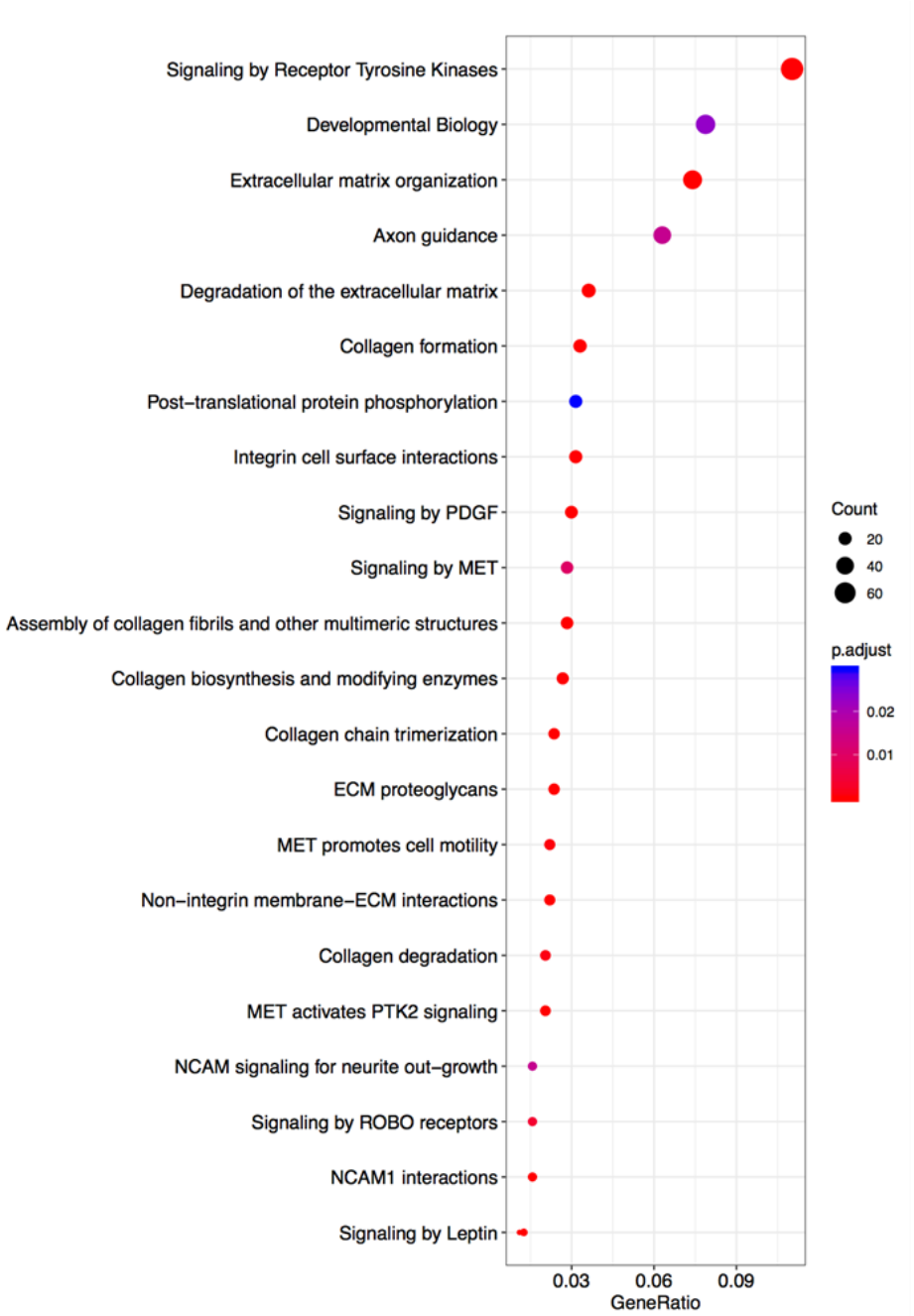

5.3.5. Cadmium arrests cell cycle and influences cell morphology

In order to carry out a more in-depth investigation on the early Cd effects on C3H cells, we also carried out KEGG pathway enrichment analysis (Luo et al., 2013) (Figure 5.5 and 5.6). Notably, the down-regulation of genes involved in PI3K-AKT signaling pathway (Figure 5.5) and in Focal Adhesion (Figure 5.6) was observed, as well as the deregulation of genes involved in ECM-receptor interaction pathway, as described in Paragraph 5.3.4 (data not shown). Consequently, Cd appeared to block the cell cycle, through the down-regulation of the PI3K-AKT pathway, mainly involved in cell survival and motility (Osaki et al., 2004), and the down-regulation of the cyclin D (CycD) and Jun Proto-Oncogene, AP-1 Transcription Factor Subunit (c-Jun) (Fig 5.6). Indeed, c-Jun is required for induction of cyclin D and progression of cell cycle (Wisdom et al., 1999). On the other hand, after Cd treatment, the cells apparently tend to lose their morphology, considering that a diverse group of cytoskeletal proteins, for instance, Vinculin, Actin, Actinin, Zyxin and Filamin, were down-regulated (Fig 5.6). Downregulation of Protein kinase C (PKC) and Glycogen Synthase Kinase 3 Beta (GSK3B), instead, could underlie an unbalance in the control of glucose homeostasis.

Figure 5.5. PI3K-AKT signaling pathway KEGG map. Representation of the KEGG map for PI3K-AKT signaling pathway. Genes in red are up-regulated, those in green are down-regulated.

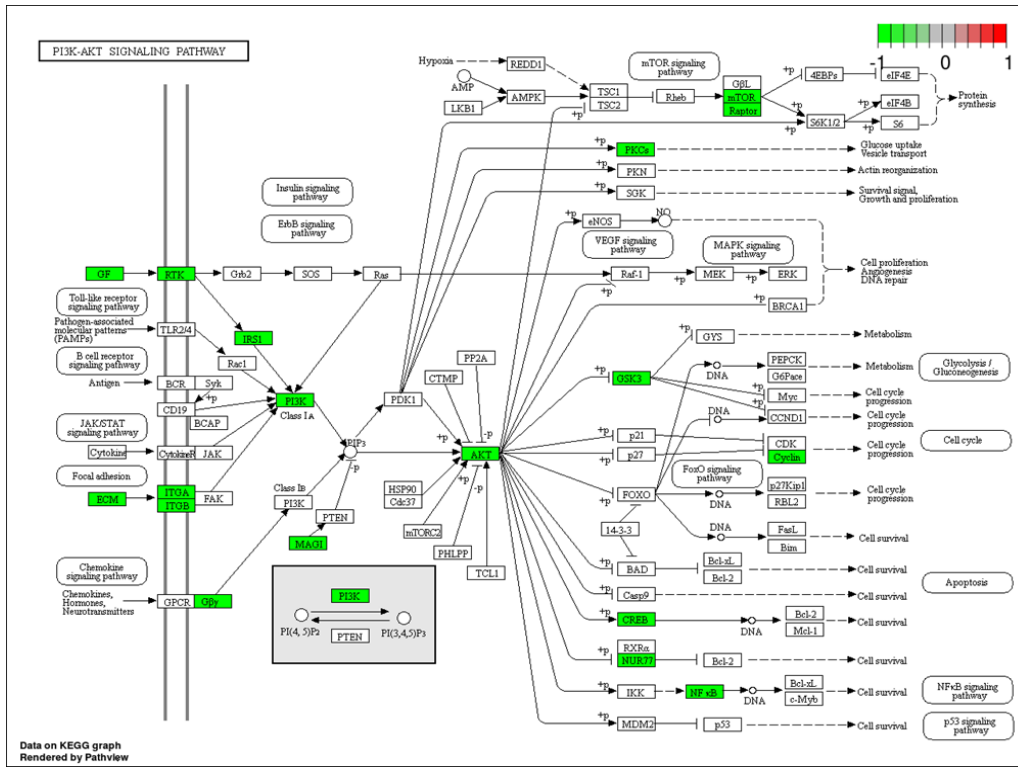

Figure 5.6. Focal Adhesion KEGG map. Representation of the KEGG map for focal adhesion. Genes in red are up-regulated, those in green are down-regulated.

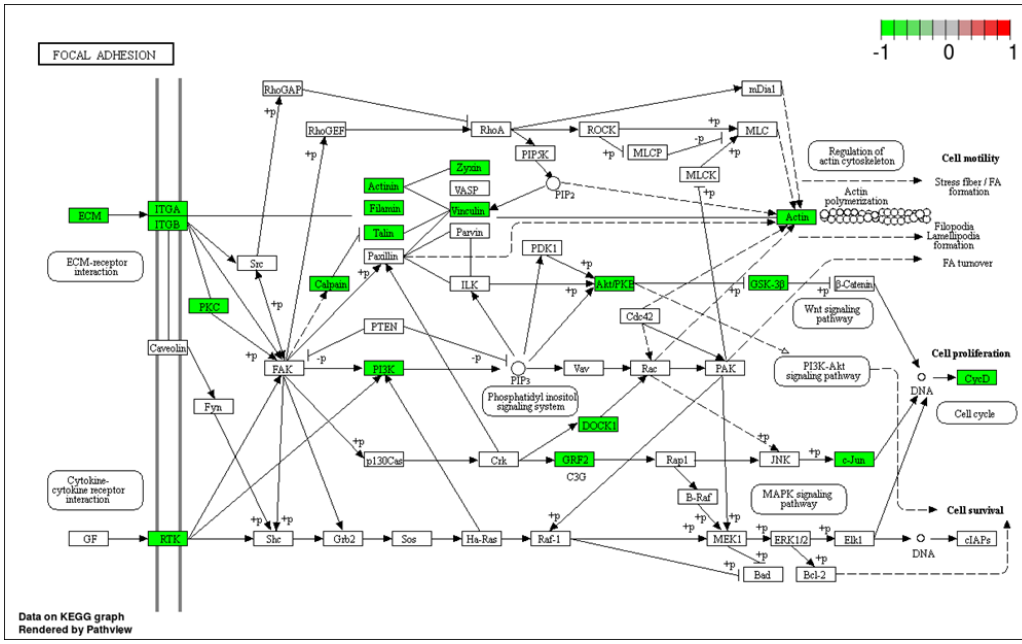

5.3.6. Many genes coding for mitochondrial proteins are dysregulated by cadmium

A Gene Ontology Cellular Component (GOCC) analysis, performed on the up-regulated genes identified in the 2vsC comparison, showed many genes coding for mitochondrial proteins, endowed with different functions (Figure 5.7). For example, the most highly expressed gene was the gene coding for the inner mitochondrial membrane peptidase subunit 1 (IMMP1L), that, together with IMMP2L, is essential for the activity of the mitochondrial inner membrane peptidase (IMP) complex. Moreover, many genes coding for mitochondrial ribosomal proteins (MRPL) were upregulated (Fig 5.7). Based on these data, we used MitoCarta2.0 for comparing all DEGs annotated in the 2vsC comparison with a list of genes coding for mitochondrial proteins (Calvo et al., 2016). The results of the analysis are shown in Table 5.2. In addition, we have implemented our analyses to reveal the hidden-patterns of genes in our transcriptomic dataset. To this purpose, we used the fuzzy c-means algorithm (Kumar et al., 2007), allowing to define groups of co-expressed genes. The results showed 6 gene clusters (data not shown): the first includes about 1430 genes, the second 300, the third 1000, the fourth 680, the fifth 380 and the sixth 2100 genes with similar expression profiles. However, only cluster 3 and cluster 6 produced a significant result when the pathway enrichment analyses was applied. In particular, the Reactome plot of cluster 3 displayed information connected with mitochondrial functions (Table 5.3), such as the up-regulation of genes coding for proteins involved in electron transport and ATP synthesis, like ATP Synthase (ATP)5h, ATP5k, ATP5e, cytochrome c (Cycs), many NADH:Ubiquinone Oxidoreductases (NUDF) and Ubiquinol-Cytochrome C Reductase (UQCR). Results reported in Table 5.3 also emphasised the up-regulation of Proteasome (PSM) Gene Family (Psmc5, Psma1, Psme2, Psma3, Psma5, Psma7, and Psmb10), confirming the down-regulation of NF-κB (Figure 5.6). In fact, PSM can control the degradation of transcription factors NF-κB and c-Jun, leading to cell cycle arrest (Almond et al., 2002). The dot plot of cluster 6 was correlated with Figure 5.4, and, at the same time, revealed that the metabolism of carbohydrates decreased after 2 µM Cd.

Figure 5.7. *Cellular Component enriched category of Gene Ontology on up-regulated genes in 2vsC. A circular plot generated by topGo function represent GO results. The plot display the relation between the most significant 6 GO Terms and the up-regulated genes that belong to the second comparison (2vsC). For each gene is also shown the log(FC) calculated by limma approach from 1 to 2, as well as illustrated in the legend logFC. The names of the GO Terms are collected in the second legend with a color code: each environment is represented with a specific color (i.e yellow indicates the mitochondrial intermembrane space).*

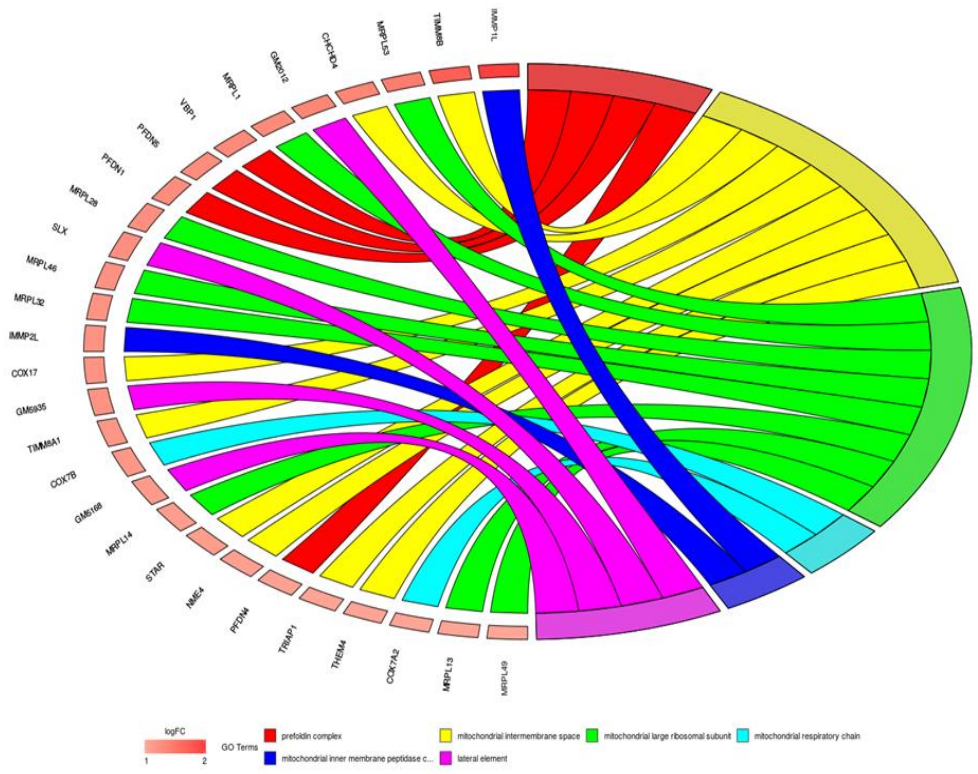

Table 5.2. List of DEGs annotated in the 2vsC comparison coding for mitochondrial proteins

Gene	comparison	direction	Description
1110001A16Rik	cd2-ctrl	up	RIKEN cDNA 1110001A16 gene
1110058L19Rik	cd2-ctrl	up	RIKEN cDNA 1110058L19 gene
1700071K01Rik	cd2-ctrl	up	RIKEN cDNA 1700071K01 gene
1810043H04Rik	cd2-ctrl	up	RIKEN cDNA 1810043H04 gene
2410015M20Rik	cd2-ctrl	up	RIKEN cDNA 2410015M20 gene
2610507B11Rik	cd2-ctrl	down	RIKEN cDNA 2610507B11 gene
Acn9	cd2-ctrl	up	ACN9 homolog (S. cerevisiae)
Acot13	cd2-ctrl	up	acyl-CoA thioesterase 13
Acyp2	cd2-ctrl	up	"acylphosphatase 2, muscle type"
Aldh1a7	cd2-ctrl	up	"aldehyde dehydrogenase family 1, subfamily A7"
Alkbh1	cd2-ctrl	up	"alkB, alkylation repair homolog 1 (E. coli)"
Apoo	cd2-ctrl	up	apolipoprotein O
Atp5e	cd2-ctrl	up	"ATP synthase, H+ transporting, mitochondrial F1 complex, epsilon subunit"
Atp5f1	cd2-ctrl	up	"ATP synthase, H+ transporting, mitochondrial F0 complex, subunit B1"
Atxn2	cd2-ctrl	down	ataxin 2
Bnip3	cd2-ctrl	up	BCL2/adenovirus E1B interacting protein 3
C330018D20Rik	cd2-ctrl	up	RIKEN cDNA C330018D20 gene
Ccdc90b	cd2-ctrl	up	coiled-coil domain containing 90B
Chchd1	cd2-ctrl	up	coiled-coil-helix-coiled-coil-helix domain containing 1
Chchd4	cd2-ctrl	up	coiled-coil-helix-coiled-coil-helix domain containing 4
Cisd2	cd2-ctrl	up	CDGSH iron sulfur domain 2
Cmc1	cd2-ctrl	up	COX assembly mitochondrial protein 1
Cox16	cd2-ctrl	up	cytochrome c oxidase assembly protein 16
Cox17	cd2-ctrl	up	cytochrome c oxidase assembly protein 17
Cox6a2	cd2-ctrl	up	cytochrome c oxidase subunit VIa polypeptide 2
Cox7a2	cd2-ctrl	up	cytochrome c oxidase subunit VIIa 2
Cox7b	cd2-ctrl	up	cytochrome c oxidase subunit VIIb
Cs	cd2-ctrl	down	citrate synthase
Dnajc15	cd2-ctrl	up	"DnaJ (Hsp40) homolog, subfamily C, member 15"
Dnajc19	cd2-ctrl	up	"DnaJ (Hsp40) homolog, subfamily C, member 19"

Echs1	cd2-ctrl	up	"enoyl Coenzyme A hydratase, short chain, 1, mitochondrial"
Efhd1	cd2-ctrl	down	EF hand domain containing 1
Fam136a	cd2-ctrl	up	"family with sequence similarity 136, member A"
Fkbp10	cd2-ctrl	down	FK506 binding protein 10
Fxn	cd2-ctrl	up	frataxin
Gm2382	cd2-ctrl	up	predicted gene 2382
Gm561	cd2-ctrl	up	predicted gene 561
Gpx4	cd2-ctrl	up	glutathione peroxidase 4
Guk1	cd2-ctrl	up	guanylate kinase 1
Hibch	cd2-ctrl	up	3-hydroxyisobutyryl-Coenzyme A hydrolase
Hint3	cd2-ctrl	up	histidine triad nucleotide binding protein 3
Hk1	cd2-ctrl	down	hexokinase 1
Hrsp12	cd2-ctrl	up	heat-responsive protein 12
Hscb	cd2-ctrl	up	HscB iron-sulfur cluster co-chaperone homolog (E. coli)
Hspe1	cd2-ctrl	up	heat shock protein 1 (chaperonin 10)
Immp1l	cd2-ctrl	up	IMP1 inner mitochondrial membrane peptidase-like (S. cerevisiae)
Immp2l	cd2-ctrl	up	IMP2 inner mitochondrial membrane peptidase-like (S. cerevisiae)
Isca2	cd2-ctrl	up	iron-sulfur cluster assembly 2 homolog (S. cerevisiae)
Lamc1	cd2-ctrl	down	"laminin, gamma 1"
Lonp1	cd2-ctrl	down	"lon peptidase 1, mitochondrial"
Lyplal1	cd2-ctrl	up	lysophospholipase-like 1
Lyrm1	cd2-ctrl	up	LYR motif containing 1
Lyrm2	cd2-ctrl	up	LYR motif containing 2
Lyrm5	cd2-ctrl	up	LYR motif containing 5
Mcee	cd2-ctrl	up	methylmalonyl CoA epimerase
Mgst1	cd2-ctrl	up	microsomal glutathione S-transferase 1
Mrpl1	cd2-ctrl	up	mitochondrial ribosomal protein L1
Mrpl13	cd2-ctrl	up	mitochondrial ribosomal protein L13
Mrpl14	cd2-ctrl	up	mitochondrial ribosomal protein L14
Mrpl28	cd2-ctrl	up	mitochondrial ribosomal protein L28
Mrpl32	cd2-ctrl	up	mitochondrial ribosomal protein L32
Mrpl46	cd2-ctrl	up	mitochondrial ribosomal protein L46
Mrpl49	cd2-ctrl	up	mitochondrial ribosomal protein L49
Mrpl53	cd2-ctrl	up	mitochondrial ribosomal protein L53
Mrps17	cd2-ctrl	up	mitochondrial ribosomal protein S17
Mrps18c	cd2-ctrl	up	mitochondrial ribosomal protein S18C
Mtcp1	cd2-ctrl	up	mature T cell proliferation 1

Mthfs	cd2-ctrl	up	"5, 10-methenyltetrahydrofolate synthetase"
Mtrf1	cd2-ctrl	up	mitochondrial translational release factor 1
Ndufa4	cd2-ctrl	up	"NADH dehydrogenase (ubiquinone) 1 alpha subcomplex, 4"
Ndufb2	cd2-ctrl	up	"NADH dehydrogenase (ubiquinone) 1 beta subcomplex, 2"
Ndufb4	cd2-ctrl	up	NADH dehydrogenase (ubiquinone) 1 beta subcomplex 4
Ndufb6	cd2-ctrl	up	"NADH dehydrogenase (ubiquinone) 1 beta subcomplex, 6"
Ndufs4	cd2-ctrl	up	NADH dehydrogenase (ubiquinone) Fe-S protein 4
Nit2	cd2-ctrl	up	"nitrilase family, member 2"
Nme3	cd2-ctrl	up	NME/NM23 nucleoside diphosphate kinase 3
Nme4	cd2-ctrl	up	NME/NM23 nucleoside diphosphate kinase 4
Nudt2	cd2-ctrl	up	nudix (nucleoside diphosphate linked moiety X)-type motif 2
Pabpc5	cd2-ctrl	up	"poly(A) binding protein, cytoplasmic 5"
Pstk	cd2-ctrl	up	phosphoseryl-tRNA kinase
Ptrh2	cd2-ctrl	up	peptidyl-tRNA hydrolase 2
Pts	cd2-ctrl	up	6-pyruvoyl-tetrahydropterin synthase
Rpl34	cd2-ctrl	up	ribosomal protein L34
Rpl35a	cd2-ctrl	up	ribosomal protein L35A
Sdhaf2	cd2-ctrl	up	succinate dehydrogenase complex assembly factor 2
Sfxn3	cd2-ctrl	down	sideroflexin 3
Slc25a14	cd2-ctrl	up	"solute carrier family 25 (mitochondrial carrier, brain), member 14"
Slc25a24	cd2-ctrl	down	"solute carrier family 25 (mitochondrial carrier, phosphate carrier), member 24"
Slc25a33	cd2-ctrl	up	"solute carrier family 25, member 33"
Spg7	cd2-ctrl	down	spastic paraplegia 7 homolog (human)
Star	cd2-ctrl	up	steroidogenic acute regulatory protein
Tfb1m	cd2-ctrl	up	"transcription factor B1, mitochondrial"
Them4	cd2-ctrl	up	thioesterase superfamily member 4
Timm10	cd2-ctrl	up	translocase of inner mitochondrial membrane 10
Timm8a1	cd2-ctrl	up	translocase of inner mitochondrial membrane 8A1
Timm8b	cd2-ctrl	up	translocase of inner mitochondrial membrane 8B
Tmem126a	cd2-ctrl	up	transmembrane protein 126A
Tmem70	cd2-ctrl	up	transmembrane protein 70
Tomm20	cd2-ctrl	up	translocase of outer mitochondrial membrane 20 homolog
Tomm5	cd2-ctrl	up	translocase of outer mitochondrial membrane 5 homolog
Triap1	cd2-ctrl	up	TP53 regulated inhibitor of apoptosis 1
Ttc7b	cd2-ctrl	down	tetratricopeptide repeat domain 7B
Uqcr10	cd2-ctrl	up	"ubiquinol-cytochrome c reductase, complex III subunit X"
Usmg5	cd2-ctrl	up	upregulated during skeletal muscle growth 5

Table 5.3. List of pathway in cluster 3

ID	Description	pvalue	p.adjust	geneID
R-MMU-163200	Respiratory electron transport, ATP synthesis by chemiosmotic coupling, and heat production by uncoupling proteins.	1,81E+06	8,49E+07	Atp5h/Atp5k/Atp5e/Cycs/Ndufb4/Gm3244/Gm3873/Ndufs5/Ndufa7/Ndufb9/Ndufb2/Ndufs4/Ndufb10/Ndufv2/Uqcrh/Uqcr11/Uqcrc2/Uqcrq
R-MMU-72689	Formation of a pool of free 40S subunits	2,24E+06	8,49E+07	Eif3e/Eif1ax/Rpl41/Rpl19/Rpl15/Rpl26/Rpl38/Rpl35a/Rpl11/Rps17/Rpl34/Rpl34-ps1/Rpl12/Rps27/Rps21/Rplp0/Rpl13a/Rpl36
R-MMU-611105	Respiratory electron transport	1,03E+07	2,28E+09	Cycs/Ndufb4/Gm3244/Gm3873/Ndufs5/Ndufa7/Ndufb9/Ndufb2/Ndufs4/Ndufb10/Ndufv2/Uqcrh/Uqcr11/Uqcrc2/Uqcrq
R-MMU-156827	L13a-mediated translational silencing of Ceruloplasmin expression	1,51E+07	2,28E+09	Eif3e/Eif1ax/Rpl41/Rpl19/Rpl15/Rpl26/Rpl38/Rpl35a/Rpl11/Rps17/Rpl34/Rpl34-ps1/Rpl12/Rps27/Rps21/Rplp0/Rpl13a/Rpl36
R-MMU-72766	Translation	1,77E+06	2,28E+09	Chchd1/Eif3e/Eif1ax/Mrpl30/Mrpl14/Mrpl11/Mrps28/Mrps31/Mrpl55/Mrpl33/Mrps33/Mrps26/Rpl41/Rpl19/Rpl15/Rpl26/Rpl38/Rpl35a/Rpl11/Rps17/Rpl34/Rpl34-ps1/Rpl12/Rps27/Rps21/Rplp0/Rpl13a/Rpl36
R-MMU-72706	GTP hydrolysis and joining of the 60S ribosomal subunit	1,80E+06	2,28E+09	Eif3e/Eif1ax/Rpl41/Rpl19/Rpl15/Rpl26/Rpl38/Rpl35a/Rpl11/Rps17/Rpl34/Rpl34-ps1/Rpl12/Rps27/Rps21/Rplp0/Rpl13a/Rpl36
R-MMU-1799339	SRP-dependent cotranslational protein targeting to membrane	3,07E+07	2,92E+09	Rpl41/Rpl19/Rpl15/Rpl26/Rpl38/Rpl35a/Rpl11/Rps17/Rpl34/Rpl34-ps1/Rpl12/Rps27/Rps21/Rplp0/Rpl13a/Rpl36
R-MMU-975956	Nonsense Mediated Decay (NMD) independent of the Exon Junction Complex (EJC)	3,07E+07	2,92E+09	Rpl41/Rpl19/Rpl15/Rpl26/Rpl38/Rpl35a/Rpl11/Rps17/Rpl34/Rpl34-ps1/Rpl12/Rps27/Rps21/Rplp0/Rpl13a/Rpl36

R-MMU-72613	Eukaryotic Translation Initiation	5,71E+07	4,34E+08	Eif3e/Eif1ax/Rpl41/Rpl19/Rpl15/Rpl26/Rpl38/Rpl35a/Rpl11/Rps17/Rpl34/Rpl34-ps1/Rpl12/Rps27/Rps21/Rplp0/Rpl13a/Rpl36
R-MMU-72737	Cap-dependent Translation Initiation	5,71E+07	4,34E+08	Eif3e/Eif1ax/Rpl41/Rpl19/Rpl15/Rpl26/Rpl38/Rpl35a/Rpl11/Rps17/Rpl34/Rpl34-ps1/Rpl12/Rps27/Rps21/Rplp0/Rpl13a/Rpl36
R-MMU-1428517	The citric acid (TCA) cycle and respiratory electron transport	4,65E+08	0.000321258895371191	Atp5h/Atp5k/Atp5e/Cycs/Ndufb4/Gm3244/Gm3873/Ndufs5/Ndufa7/Ndufb9/Ndufb2/Ndufs4/Ndufb10/Ndufv2/Sdhd/Uqcrh/Uqcr11/Uqcrc2/Uqcrq
R-MMU-927802	Nonsense-Mediated Decay (NMD)	6,05E+08	0.000353830647738423	Rpl41/Rpl19/Rpl15/Rpl26/Rpl38/Rpl35a/Rpl11/Rps17/Rpl34/Rpl34-ps1/Rpl12/Rps27/Rps21/Rplp0/Rpl13a/Rpl36
R-MMU-975957	Nonsense Mediated Decay (NMD) enhanced by the Exon Junction Complex (EJC)	6,05E+08	0.000353830647738423	Rpl41/Rpl19/Rpl15/Rpl26/Rpl38/Rpl35a/Rpl11/Rps17/Rpl34/Rpl34-ps1/Rpl12/Rps27/Rps21/Rplp0/Rpl13a/Rpl36
R-MMU-6799198	Complex I biogenesis	4,89E+09	0.002656784761062 62	Ndufb4/Gm3244/Gm3873/Ndufs5/Ndufa7/Ndufb9/Ndufb2/Ndufs4/Ndufb10/Ndufv2
R-MMU-6791226	Major pathway of rRNA processing in the nucleolus and cytosol	6,52E+09	0.002912828587210 54	Exosc7/Rcl1/Rpl41/Rpl19/Rpl15/Rpl26/Rpl38/Rpl35a/Rpl11/Rpl34/Rpl34-ps1/Rpl12/Rplp0/Rpl13a/Rpl36/Tbl3
R-MMU-72312	rRNA processing	6,52E+09	0.002912828587210 54	Exosc7/Rcl1/Rpl41/Rpl19/Rpl15/Rpl26/Rpl38/Rpl35a/Rpl11/Rpl34/Rpl34-ps1/Rpl12/Rplp0/Rpl13a/Rpl36/Tbl3
R-MMU-8868773	rRNA processing in the nucleus and cytosol	6,52E+09	0.002912828587210 54	Exosc7/Rcl1/Rpl41/Rpl19/Rpl15/Rpl26/Rpl38/Rpl35a/Rpl11/Rpl34/Rpl34-ps1/Rpl12/Rplp0/Rpl13a/Rpl36/Tbl3
R-MMU-187577	SCF(Skp2)-mediated degradation of p27/p21	0.000269161161314 75	0.011364582366622 8	Cdk4/Cdkn1b/Psmc5/Psma1/Psme2/Psma3/Psma5/Psma7/Psmb10/Skp1a
R-MMU-351202	Metabolism of polyamines	0.000706058493716625	0.025552593105935	Ass1/Enoph1/Mtap/Psmc5/Psma1/Psme2/Psma3/Psma5/Psma7/Psmb10
R-MMU-69202	Cyclin E associated events during G1/S transition	0.000706058493716625	0.025552593105935	Cdk4/Cdkn1b/Psmc5/Psma1/Psme2/Psma3/Psma5/Psma7/Psmb10/Skp1a
R-MMU-69656	Cyclin A:Cdk2-associated events	0.000706058493 71	0.025552593105 93	Cdk4/Cdkn1b/Psmc5/Psma1/Psme2/Psma3/Psma5/Psma7/Psmb10/Skp1a

	at S phase entry	6625	5	
R-MMU-8953854	Metabolism of RNA	0.00115795959438913	0.04000224053344427	Bud31/Cnot8/Exosc7/Gle1/Nxt1/Polr2g/Psmc5/Psma1/Psme2/Psma3/Psma5/Psma7/Psmb10/Rcl1/Rpl41/Rpl19/Rpl15/Rngtt/Rpl26/Rnmt/Rpl38/Rpl35a/Rpl11/Rps17/Rpl34/Rpl34-ps1/Rpl12/Rps27/Rps21/Rplp0/Rpl13a/Rpl36/Snrpb2/Snrnp48/Snrpb/Tbl3/Wdr61/Zrsr1
R-MMU-69229	Ubiquitin-dependent degradation of Cyclin D1	0.00156483880776 15	0.04955322891244 76	Cdk4/Psmc5/Psma1/Psme2/Psma3/Psma5/Psma7/Psmb10
R-MMU-75815	Ubiquitin-dependent degradation of Cyclin D	0.00156483880776 15	0.04955322891244 76	Cdk4/Psmc5/Psma1/Psme2/Psma3/Psma5/Psma7/Psmb10

❖ 5.4 Discussion

C3H10T1/2Cl8 mouse embryo fibroblasts are a useful model to elucidate the molecular mechanisms, underpinning the process of cell transformation, especially at the genomic and transcriptomic levels. Moreover, C3H10T1/2Cl8 cell line is one of the suitable cells used in the cell transformation assays (CTAs) (OECD, 2007), the most biologically relevant in vitro model for the identification of potential carcinogens. Indeed, these assays have been shown to involve a multistage process that closely mimics the critical stages of in vivo carcinogenesis (Corvi et al., 2017). For this purpose, we have chosen C3H10T1/2Cl8 cells to investigate the deregulated pathways and the alterations in gene expression, after Cd treatment for 24 hrs, with the aim of unravelling the early markers of Cd-induced-carcinogenesis. In fact, gene expression changes are considered the first and most sensitive biomarkers of cells response to chemicals.

In this work, not yet complete, the results have shown that Cd could use different mechanisms to induce cancer development: e.g., it can alter the expression of genes involved in the control of the oxidative stress, block cell growth or interfere with the homeostasis of essential metals, as previously suggested (Martelli et al., 2006; Urani et al., 2015). Concerning the earliest Cd effects, this metal toxicity has been since a long time correlated with oxidative stress: Kukongviriyapan et al., (2016) showed that Cd can increase reactive oxygen species formation, by depleting antioxidants in cells cytosol; Kiran Kumar et al., (2016) showed that lung cells treated with Cd showed a decrease in the activity of the antioxidant enzymes superoxide dismutase (SOD) and glutathione peroxidase (GSH-Px) enzymes. In accordance with our results, Won et al. (2011) and Yim et al. (2015) suggested that GST activity increased after Cd exposure, and proposed that GST could be considered a molecular biomarker for Cd toxicity. Furthermore, we showed that Cd binds metalloproteins (Pinter et al., 2015). Indeed, among the large number of biological functions that have been proposed for MTs, the storage and detoxification of certain metals, as well as their antioxidant properties, are the most relevant. Cd binding to MTs appears to be strongly related to its replacement of Zn. Hence, cadmium-zinc exchange in many other proteins can be one of the most important element of Cd biological toxicity. Cadmium can disrupt Zn homeostasis, leading to an increase of intracellular free zinc. Subsequently, high levels of free Zn in the

cytosol can play an essential role in cancer etiology and outcome (Costello and Franklin, 2012; Grattan and Freake, 2012). Overall, many data from literature support the theory that Cd interferes with zinc-proteins and displaces zinc from the zinc-proteome. Regarding the possible cell cycle arrest induced by Cd, recent data have illustrated that this metal can decrease cell proliferation in various cell types by p53-dependent and -independent mechanisms (Chen et al., 2019). However, the arrest of cell cycle induced by Cd was often connected with the apoptosis of treated cells. For example, Chatterjee et al. (2009) have revealed that, although ROS and p21 were involved in Cd cell cycle arrest in a p53 independent manner, after few hours, cells activated the apoptotic response through the p53 up-regulation, loss of mitochondrial transmembrane potential (MTP), down-regulation of Bcl-xl, activation of caspase-3 and release of cytochrome c (Cyt c). On the contrary, in our results, p53 was not found deregulated, while MTP increased after Cd treatment (see Chapter 7). Therefore, in our experiments, Cd cannot be connected with the activation of the apoptotic pathway. Furthermore, the analysis of genes related to cell cycle showed that Cd influenced the downregulation of the Cyclin D, which synthesis initiates during the G1 phase. As a conclusion, we suggest that cell cycle arrest caused by Cd is probably connected with the downregulation of Cyclin D and with the DNA damage caused by ROS production. For this reason, cells that escape the control mechanisms in G1 phase could acquire an abnormal proliferative capacity and undergo the process of carcinogenesis. Concerning DNA damage and cell proliferation, Cd can have many effects on the microtubular cytoskeleton in the cell. Indeed, Cd affects the mechanisms controlling the organisation of cytoskeleton, as well as tubulin assembly/disassembly processes. Cd can induce the formation of abnormal MT arrays and irregular nuclear disorder. Furthermore, it has been reported that, with increased Cd concentration and duration of treatment, microtubules depolymerised more severely, the frequency of abnormal cell increased and the mitotic index decreased progressively (Xu et al., 2009).

The induction of genes connected with inflammation is another Cd mechanism of action to induce carcinogenesis. In the peripheral nervous system, for example, Cd promotes interleukin-6 (IL-6) and IL-8 production and release. Upregulation of IL-6 expression is linked to the pathogenesis of neurodegenerative diseases, while IL-8 plays a role in angiogenesis of gliomas (Phuagkhaopong et al., 2017). Kundu et al. (2009 and 2011) showed that low

Cd concentrations triggered lung cells proliferation, severe inflammation and cancer. The novelty of this study lies in the connection of Cd toxicity with dysregulation of genes coding for mitochondrial proteins. Indeed, although several previous studies have proven that mitochondria can accumulate Cd (Waku, 1984; Vergilio et al., 2013), we suggest the possibility of selective mitochondrial damage, following cadmium uptake. Moreover, although CTA use has been limited so far to the detection of chemically-induced transformation, we have demonstrated with this work that it can also be a valuable tool to study the mechanisms involved in carcinogenesis.

References

- Awomoyi A.A., The human solute carrier family 11 member 1 protein (SLC11A1): linking infections, autoimmunity and cancer?, FEMS Immunol Med Microbiol. (2007), Vol. 49(3), pp 324-9
- Asara Y., Marchal J.A., Carrasco E., Boulaiz H., Solinas G., Bandiera P., Garcia M.A., Farace C., Montella A., Madeddu R., Cadmium Modifies the Cell Cycle and Apoptotic Profiles of Human Breast Cancer Cells Treated with 5-Fluorouracil, Int J Mol Sci. (2013), Vol. 14(8), pp 16600-16616
- Ashburner M., Ball C.A., Blake J.A., Botstein D., Butler H., Cherry J.M., Davis A.P., Dolinski K., Dwight S.S., Eppig J.T., Harris M.A., Hill D.P., Issel-Tarver L., Kasarskis A., Lewis S., Matese J.C., Richardson J.E., Ringwald M., Rubin G.M., Sherlock G., Gene ontology: tool for the unification of biology. The Gene Ontology Consortium., Nat Genet. (2000), Vol 25(1), pp 25-9
- Bernard A., Lauwerys R., Present status and trends in biological monitoring of exposure to industrial-chemicals., Journal of Occupational and Environmental Medicine (1986), Vol. 28, pp 558-562
- Bertin G., Averbeck D., Cadmium: cellular effects, modifications of biomolecules, modulation of DNA repair and genotoxic consequences (a review), Biochimie. (2006), Vol. 88(11), pp 1549-59
- Calvo S.E., Clauser K.R., Mootha V.K., MitoCarta2.0: an updated inventory of mammalian mitochondrial proteins., Nucleic Acids Res. (2016), Vol. 44(D1):D1251-7
- Cannino G., Ferruggia E., Luparello C., Rinaldi A.M., Cadmium and mitochondria, Mitochondrion (2009), Vol. 9, pp 377-384
- Chatterjee S., Kundu S., Sengupta S., Bhattacharyya A., Divergence to apoptosis from ROS induced cell cycle arrest: effect of cadmium., Mutat Res. (2009), Vol. 663(1-2), pp 22-31
- Chen Q.Y., DesMarais T., Costa M., Metals and Mechanisms of Carcinogenesis., Annu Rev Pharmacol Toxicol. (2019), Vol. 59, pp 537-554
- Conway J.R., Lex A., Gehlenborg N., UpSetR: an R package for the visualization of intersecting sets and their properties., Bioinformatics. (2017), Vol. 33(18), pp 2938-2940
- Corvi R., Madia F., Guyton K.Z., Kasper P., Rudel R., Colacci A., Kleinjans J., Jennings P., Moving forward in carcinogenicity assessment: Report of an EURL ECVAM/ESTIV workshop., Toxicol In Vitro. (2017), Vol. 45(Pt 3), pp 278-286
- Costello L.C., Franklin R.B., Cytotoxic/tumor suppressor role of zinc for the treatment of cancer: an enigma and an opportunity., Expert Rev Anticancer Ther. (2012); Vol. 12(1), pp 121-8
- Forcella M., Callegaro G., Melchioretto P., Gribaldo L., Frattini M., Stefanini F.M., Fusi P., Urani C., Cadmium-transformed cells in the in vitro cell transformation assay reveal different proliferative behaviours and activated pathways., Toxicol In Vitro. (2016), Vol. 36, pp 71-80
- Callegaro G., Forcella M., Melchioretto P., Frattini A., Gribaldo L., Fusi P., Fabbri M., Urani C., Toxicogenomics applied to in vitro Cell Transformation Assay reveals mechanisms of early response to cadmium., Toxicol In Vitro. (2018), Vol. 48, pp 232-243

- Chen X.X., Tang L., Fu Y.M., Wang Y., Han Z.H., Meng J.G., Paralemmin-3 contributes to lipopolysaccharide-induced inflammatory response and is involved in lipopolysaccharide-Toll-like receptor-4 signaling in alveolar macrophages., Int J Mol Med. (2017), Vol. 40(6), pp 1921-1931
- Fabregat A., Jupe S., Matthews L., Sidiropoulos K., Gillespie M., Garapati P., Haw R., Jassal B., Korninger F., May B., Milacic M., Roca C.D., Rothfels K., Sevilla C., Shamovsky V., Shorser S., Varusai T., Viteri G., Weiser J., Wu G., Stein L., Hermjakob H., D'Eustachio P., The Reactome Pathway Knowledgebase. Nucleic Acids Res. (2018), Vol. 46(D1):D649-D655
- Fang M., Yuan J., Peng C., Li Y., Collagen as a double-edged sword in tumor progression., Tumour Biol. (2014), Vol. 35(4), pp 2871-82
- Grattan B.J., Freake H.C., Zinc and cancer: implications for LIV-1 in breast cancer., Nutrients. (2012), Vol. 4(7), pp 648-75
- Henkler F., Joep B., Luch A., The Role of Oxidative Stress in Carcinogenesis Induced by Metals and Xenobiotics., Cancers (2010), Vol. 2, pp 376-396
- Hultqvist G., Ocampo Daza D., Larhammar D., Kilimann M.W., Evolution of the vertebrate paralemmin gene family: ancient origin of gene duplicates suggests distinct functions., PLoS One. (2012), Vol. 7(7), e41850
- IARC (1993). Cadmium and cadmium compounds. IARC Monogr Eval Carcinog Risks Hum, Vol. 58, pp 119-237
- Jaishankar M., Tseten T., Anbalagan N., Mathew B.B., Beeregowda K.N., Toxicity, mechanism and health effects of some heavy metals., Interdiscip Toxicol. (2014); Vol. 7(2), pp 60–72
- Kiran Kumar K.M., Naveen Kumar M., Patil R.H., Nagesh R., Hegde S.M., Kavya K., Babu R.L., Ramesh G.T., Sharma S.C., Cadmium induces oxidative stress and apoptosis in lung epithelial cells., Toxicol Mech Methods. (2016), Vol. 26(9), pp 658-666
- Koizumi S., Yamada H., DNA microarray analysis of altered gene expression in cadmium-exposed human cells., J Occup Health.(2003), Vol. 45(6), pp 331-4
- Kukongviriyapan U., Apaijit K., Kukongviriyapan V., Oxidative Stress and Cardiovascular Dysfunction Associated with Cadmium Exposure: Beneficial Effects of Curcumin and Tetrahydrocurcumin., Tohoku J Exp Med. (2016), Vol. 239(1), pp 25-38
- Kumar L., Futschik M., Mfuzz: a software package for soft clustering of microarray data., Bioinformation. (2007), Vol. 2(1), pp 5-7
- Kundu S., Sengupta S., Chatterjee S., Mitra S., Bhattacharyya A., Cadmium induces lung inflammation independent of lung cell proliferation: a molecular approach., J Inflamm (Lond). (2009), 6:19
- Kundu S., Sengupta S., Bhattacharyya A., EGFR upregulates inflammatory and proliferative responses in human lung adenocarcinoma cell line (A549), induced by lower dose of cadmium chloride., Inhal Toxicol. (2011), Vol. 23(6), pp 339-48
- Langfelder P., Horvath S., WGCNA: an R package for weighted correlation network analysis., BMC Bioinformatics. (2008), 9:559

- Luo W., Brouwer C., Pathview: an R/Bioconductor package for pathway-based data integration and visualization., Bioinformatics.(2013), Vol. 29(14), pp 1830-1
- Martelli A., Rousselet E., Dycke C., Bouron A., Moulis J.M., Cadmium toxicity in animal cells by interference with essential metals., Biochimie. (2006), Vol. 88(11), pp 1807-14
- Milacic M., Haw R., Rothfels K., Wu G., Croft D., Hermjakob H., D'Eustachio P., Stein L., Annotating cancer variants and anti-cancer therapeutics in reactome., Cancers (Basel). (2012), Vol. 4(4), pp 1180-211
- OECD, Detailed review paper on cell transformation assays for detection of chemical carcinogens, Development, O.f.e.c.-o.a. (Ed). OECD Environment, health and safety publications, (2007) 1-164
- Osaki M., Oshimura M., Ito H., PI3K-Akt pathway: its functions and alterations in human cancer., Apoptosis. (2004), Vol. 9(6), pp 667-76
- Pinter T.B., Irvine G.W., Stillman M.J., Domain Selection in Metallothionein 1A: Affinity-Controlled Mechanisms of Zinc Binding and Cadmium Exchange., Biochemistry. (2015), Vol. 54(32), pp 5006-16
- Phuagkhaopong S., Ospondpant D., Kasemsuk T., Sibmooh N., Soodvilai S., Power C., Vivithanaporn P., Cadmium-induced IL-6 and IL-8 expression and release from astrocytes are mediated by MAPK and NF-κB pathways., Neurotoxicology. (2017), Vol. 60, pp 82-91
- Ramanathan R., Olex A.L., Dozmorov M., Bear H.D., Fernandez L.J., Takabe K., Angiopoietin pathway gene expression associated with poor breast cancer survival., Breast Cancer Res Treat. (2017), Vol. 162(1), pp 191-198
- Ritchie M.E., Phipson B., Wu D., Hu Y., Law C.W., Shi W., Smyth G.K., Limma powers differential expression analyses for RNA-sequencing and microarray studies., Nucleic Acids Res. (2015), Vol. 43(7):e47
- Schauder A., Avital A., Malik Z., Regulation and gene expression of heme synthesis under heavy metal exposure--review., J Environ Pathol Toxicol Oncol.(2010), Vol. 29(2), pp 137-158
- Thévenod F., Lee W., Toxicology of cadmium and its damage to mammalian organs., Metals ions in Life Sciences (MILS)(2013), Vol. 11, Cadmium: From Toxicity to Essentiality, pp 415-490
- Urani C., Stefanini F.M., Bussinelli L., Melchioretto P., Crosta G.F., Image analysis and automatic classification of transformed foci., J Microsc. (2009), Vol. 234(3), pp 269-79
- Urani C., Melchioretto P., Bruschi M., Fabbri M., Sacco M.G., Gribaldo L., Impact of Cadmium on Intracellular Zinc Levels in HepG2 Cells: Quantitative Evaluations and Molecular Effects., Biomed Res Int. (2015);2015:949514
- van den Hoogen C., van der Horst G., Cheung H., Buijs J.T., Lippitt J.M., Guzmán-Ramírez N., Hamdy F.C., Eaton C.L., Thalmann G.N., Cecchini M.G., Pelger R.C., van der Pluijm G., High aldehyde dehydrogenase activity identifies tumor-initiating and metastasis-initiating cells in human prostate cancer., Cancer Res. (2010), Vol. 70(12), pp 5163-73

- Vergilio Cdos S., de Melo EJ., Autophagy, apoptosis and organelle features during cell exposure to cadmium., Biocell. (2013), Vol. 37(2), pp 45-54
- Waisberg M., Joseph P., Hale B., Beyersmann D., Molecular and cellular mechanisms of cadmium carcinogenesis., Toxicology. (2003), Vol. 192(2-3), pp 95-117
- Waku K., The chemical form of cadmium in subcellular fractions following cadmium exposure., Environ Health Perspect. (1984), Vol. 54, pp 37-44
- Wang Y., Fang J., Leonard S.S., Rao K.M., Cadmium inhibits the electron transfer chain and induces reactive oxygen species., Free Radic Biol Med. (2004), Vol. 36(11), pp 1434-1443
- Wang B., Li Y., Shao C., Tan Y., Cai L., Cadmium and its epigenetic effects., Curr Med Chem. (2012); Vol. 19(16), pp 2611-2620
- Wencke W., Sánchez-Cabo F., Ricote M. GOplot: an R package for visually combining expression data with functional analysis., Bioinformatics (2015), Vol. 31(17), pp 2912-2914
- Wisdom R., Johnson R.S., Moore C., c-Jun regulates cell cycle progression and apoptosis by distinct mechanisms, EMBO J. (1999), Vol. 18(1), pp 188-97
- World Health Organization (1992). Environmental Health Criteria 134. Cadmium. Available at www.inchem.org/documents/ehc/ehc/ehc134
- Won E.J., Kim R.O., Rhee J.S., Park G.S., Lee J., Shin K.H., Lee Y.M., Lee J.S., Response of glutathione S-transferase (GST) genes to cadmium exposure in the marine pollution indicator worm, Perinereis nuntia., Comp Biochem Physiol C Toxicol Pharmacol. (2011), Vol. 154(2), pp 82-92
- Wuana R.A., Okieimen F.E., Heavy Metals in Contaminated Soils: A Review of Sources, Chemistry, Risks and Best Available Strategies for Remediation., International Scholarly Research Network Ecology (2011), Article ID 402647
- Yang H, Shu Y., Cadmium Transporters in the Kidney and Cadmium-Induced Nephrotoxicity., Int J Mol Sci. (2015), Vol 16(1), pp 1484–1494
- Yim B., Kim H., Jung M-J., Lee Y.-M., Cadmium modulates the mRNA expression and activity of glutathione S-transferase in the monogonont Rotifer Brachionus koreanus., Toxicology and Environmental Health Sciences (2015), Vol. 7(3), pp 217–223
- Yuan Y., Zhang Y., Zhao S., Chen J., Yang J., Wang T., Zou H., Wang Y., Gu J., Liu X., Bian J., Liu Z., Cadmium-induced apoptosis in neuronal cells is mediated by Fas/FasL-mediated mitochondrial apoptotic signaling pathway, Scientific Reports (2018), Vol. 8, Article number: 8837
- Xu S., Pi H., Chen Y., Zhang N., Guo P., Lu Y., He M., Xie J., Zhong M., Zhang Y., Yu Z., Zhou Z., Cadmium induced Drp1-dependent mitochondrial fragmentation by disturbing calcium homeostasis in its hepatotoxicity, Cell Death and Disease (2013), Vol. 4, pp 1-10
- Xu P., Liu D., Jiang W., Cadmium effects on the organization of microtubular cytoskeleton in interphase and mitotic cells of Allium sativum., Biologia Plantarum (2009), Vol. 53(2), pp 387-390

- Zhou T., Jia X., Chapin R.E., Maronpot R.R., Harris M.W., Liu J., Waalkes M.P., Eddy E.M., Cadmium at a non-toxic dose alters gene expression in mouse testes., Toxicol Lett. (2004), Vol. 154(3), pp 191-200

Supplementary

Table 5.1S. List of pathways in 2vsC comparison

ID	Description	pvalue	p.adjust	geneID
R-MMU-1474244	Extracellular matrix organization	4,13E+05	4,49E+08	Adam8/Adamts2/Adam15/Adam19/App/Capn2/Col1a2/Col5a3/Col5a2/Col4a2/Col4a1/Col3a1/Col11a1/Col6a2/Col6a1/Col14a1/Col5a1/Col16a1/Col27a1/Col1a1/Col2a1/Ddr1/Dag1/Eln/Efemp2/Fbn1/Fn1/Fbln5/Fbn2/Furin/Itga11/Itga6/Hspg2/Itga9/Itgb5/Lamb2/Lamc2/Lamc1/Ltbp3/Matn4/Nid2/Pcolce/Plec/Prkca/Pxdn/Timp2/Vcan
R-MMU-2022090	Assembly of collagen fibrils and other multimeric structures	1,28E+06	6,96E+08	Col1a2/Col5a3/Col5a2/Col4a2/Col4a1/Col3a1/Col11a1/Col6a2/Col6a1/Col14a1/Col5a1/Col27a1/Col1a1/Col2a1/Itga6/Lamc2/Plec/Pxdn
R-MMU-3000178	ECM proteoglycans	8,63E+06	3,13E+09	App/Col1a2/Col5a3/Col5a2/Col3a1/Col6a2/Col6a1/Col5a1/Col1a1/Col2a1/Fn1/Itga9/Itgb5/Matn4/Vcan
R-MMU-8948216	Collagen chain trimerization	1,51E+07	4,10E+09	Col1a2/Col5a3/Col5a2/Col4a2/Col4a1/Col3a1/Col11a1/Col6a2/Col6a1/Col14a1/Col5a1/Col16a1/Col27a1/Col1a1/Col2a1
R-MMU-1474290	Collagen formation	2,45E+07	5,33E+08	Adamts2/Col1a2/Col5a3/Col5a2/Col4a2/Col4a1/Col3a1/Col11a1/Col6a2/Col6a1/Col14a1/Col5a1/Col16a1/Col27a1/Col1a1/Col2a1/Itga6/Lamc2/Pcolce/Plec/Pxdn
R-MMU-186797	Signaling by PDGF	3,84E+07	6,39E+09	Col5a3/Col5a2/Col4a2/Col4a1/Col3a1/Col6a2/Col6a1/Col5a1/Col2a1/Furin/Nck1/Pdgfra/Pdgfrb/Pik3r2/Rapgef1/Stat5b/Stat3/Stat5a/Thbs3
R-MMU-3000171	Non-integrin membrane-ECM interactions	4,11E+07	6,39E+09	Col1a2/Col5a3/Col5a2/Col4a2/Col4a1/Col3a1/Col5a1/Col1a1/Col2a1/Ddr1/Fn1/Hspg2/Itgb5/Prkca
R-MMU-8874081	MET activates PTK2 signaling	6,44E+07	8,76E+09	Col1a2/Col5a3/Col5a2/Col3a1/Col11a1/Col5a1/Col27a1/Col1a1/Col2a1/Fn1/Lamb2/Lamc2/Lamc1
R-MMU-419037	NCAM1 interactions	8,63E+07	9,56E+09	Col5a3/Col5a2/Col4a2/Col4a1/Col3a1/Col6a2/Col6a1/Col5a1/Col2a1/Ncam1

R-MMU-1474228	Degradation of the extracellular matrix	8,78E+07	9,56E+09	Adam8/Adam15/Capn2/Col1a2/Col5a3/Col5a2/Col4a2/Col4a1/Col3a1/Col11a1/Col6a2/Col6a1/Col5a1/Col1a1/Col2a1/Eln/Fbn1/Fn1/Fbn2/Furin/Hspg2/Lamc2/Timp2
R-MMU-2586552	Signaling by Leptin	1,19E+08	0.000117586882116953	Irs2/Irs1/Lepr/Lep/Sh2b1/Stat5b/Stat5a
R-MMU-9006934	Signaling by Receptor Tyrosine Kinases	1,38E+08	0.000125676815296865	Actb/Akt1/Atp6v1c2/Atp6v0a1/Arhgef2/Arhgef12/Atp6v0b/Arhgef17/Arhgdia/Col1a2/Col5a3/Col5a2/Col4a2/Col4a1/Ctnnd1/Cyfip1/Col3a1/Col11a1/Cyba/Col6a2/Col6a1/Col5a1/Col27a1/Col1a1/Col2a1/Ctnna1/Dusp7/Egfr/Dock1/Epn1/Fgfr4/Fn1/Fgd3/Fgf6/Flt1/Furin/Grb10/Hgs/Irs2/Hnrnpm/Irs1/Lamb2/Lamc2/Lamc1/Mapk7/Nedd4/Nck1/Mtor/Pcsk6/Pdgfra/Pdgfrb/Pde3b/Pik3r4/Plekhg2/Pik3r2/Polr2k/Prkca/Polr2d/Rapgef1/Rps6ka3/Rela/Sh2b3/Stat5b/Stat3/Stat5a/Spint2/Them4/Thbs3/Ubc/Wasf2
R-MMU-216083	Integrin cell surface interactions	1,60E+08	0.000133614317755986	Col1a2/Col5a3/Col5a2/Col4a2/Col4a1/Col3a1/Col6a2/Col6a1/Col5a1/Col16a1/Col1a1/Col2a1/Dag1/Fbn1/Fn1/Itga11/Itga6/Hspg2/Itga9/Itgb5
R-MMU-2586551	Signaling by Leptin	2,14E+08	0.000166437430504148	Irs2/Irs1/Lepr/Lep/Sh2b1/Stat5b/Stat3/Stat5a
R-MMU-1650814	Collagen biosynthesis and modifying enzymes	3,52E+08	0.000255897200025099	Adamts2/Col1a2/Col5a3/Col5a2/Col4a2/Col4a1/Col3a1/Col11a1/Col6a2/Col6a1/Col14a1/Col5a1/Col16a1/Col27a1/Col1a1/Col2a1/Pcolce
R-MMU-8875878	MET promotes cell motility	9,77E+08	0.000665027119097559	Col1a2/Col5a3/Col5a2/Col3a1/Col11a1/Col5a1/Col27a1/Col1a1/Col2a1/Fn1/Lamb2/Lamc2/Lamc1/Rapgef1
R-MMU-1442490	Collagen degradation	1,73E+09	0.001108107230329080	Col1a2/Col5a3/Col5a2/Col4a2/Col4a1/Col3a1/Col11a1/Col6a2/Col6a1/Col5a1/Col1a1/Col2a1/Furin
R-MMU-376176	Signaling by ROBO receptors	6,09E+09	0.003684586401823890	Abl1/Abl2/Cxcl12/Dag1/Evl/Gpc1/Myo9b/Pfn2/Prkca/Ubc
R-MMU-6806834	Signaling by MET	0.000174813754561788	0.010019588353567700	Col1a2/Col5a3/Col5a2/Col3a1/Col11a1/Col5a1/Col27a1/Col1a1/Col2a1/Fn1/Hgs/Lamb2/Lamc2/Lamc1/Rapgef1/Stat3/Spint2/Ubc

R-MMU-375165	NCAM signaling for neurite out-growth	0.00030070896214 7423	0.01570490 51872202	Col5a3/Col5a2/Col4a2/Col4a1/Col3a1/Col6a2/Col6a1/Col5a1/Col2a1/Ncam1
R-MMU-422475	Axon guidance	0.00030284941132 3805	0.01570490 51872202	Abl1/Abl2/Actb/Arhgef12/Col5a3/Col5a2/Col4a2/Col4a1/Col3a1/Col6a2/Col6a1/Col5a1/Cxcl12/Col2a1/Dcc/Dag1/Dpysl3/Dpysl2/Efnb1/Egfr/Dock1/Evl/Git1/Gpc1/Grb10/Gsk3b/Irs2/Itga9/Kirrel/Mapk7/Ncam1/Myo9b/Nck1/Pfn2/Plxna2/Prkca/Plxna3/Sema5a/Tln1/Ubc
R-MMU-1266738	Developmental Biology	0.00046524987016 6637	0.02302986 85732485	Abl1/Abl2/Actb/Akt1/Arhgef12/Cdon/Cdh2/Col5a3/Col5a2/Col4a2/Col4a1/Col3a1/Col6a2/Col6a1/Col5a1/Cxcl12/Col2a1/Ctnna1/Dcc/Dag1/Dpysl3/Dpysl2/Efnb1/Egfr/Dock1/Evl/Foxo1/Furin/Git1/Gpc1/Grb10/Gsk3b/Irs2/Itga9/Lgi4/Krt2/Kirrel/Mapk7/Ncam1/Myo9b/Nck1/Pfn2/Pcsk6/Plxna2/Prkca/Plxna3/Sema5a/Smad3/Tln1/Ubc
R-MMU-8957275	Post-translational protein phosphorylation	0.00062881773318 3903	0.02977315 26711857	App/Aplp2/C3/Cdh2/Csf1/Cyr61/Fbn1/Fn1/Fam20a/Fstl1/Gas6/Il6/Igfbp5/Lamb2/Lamc1/Mfge8/Rcn1/Sparcl1/Tmem132a/Vcan

Chapter 6

"In vitro and bioinformatics mechanistic-based approach for cadmium carcinogenicity understanding."

ABSTRACT

Cadmium is a toxic metal able to enter the cells through channels and transport pathways dedicated to essential ions, leading, among others, to the dysregulation of divalent ions homeostasis. Despite its recognized human carcinogenicity, the mechanisms are still under investigation. A powerful tool for mechanistic studies of carcinogenesis is the Cell Transformation Assay (CTA). We have isolated and characterized by whole genome microarray and bioinformatics analysis of differentially expressed genes (DEGs) cadmium-transformed cells from different foci (F1, F2, and F3) at the end of CTA (6 weeks). The systematic analysis of up- and down-regulated transcripts, and the comparison of DEGs in transformed cells evidence different functional targets and the complex picture of cadmium-induced transformation. Only 34 in common DEGs are found in cells from all foci, and among these, only 4 genes are jointly up-regulated (Ccl2, Ccl5, IL6 and Spp1), all responsible for cytokines/chemokines coding. Most in common DEGs are down-regulated, suggesting that the switching-off of specific functions plays a major role in this process. In addition, the comparison of dysregulated pathways immediately after cadmium treatment with those in transformed cells provides a valuable means to the comprehension of the overall process.

Monica Oldani, Marco Fabbri, Pasquale Melchioretto, Giulia Callegaro, Paola Fusi, Laura Gribaldo, Matilde Forcella and Chiara Urani

This chapter is an extract of the accepted paper in Toxicology in vitro, 2020

❖ 6.1.Introduction

Cadmium (Cd) is a toxic metal massively released into the environment (~ 30,000 tons/year) due to anthropogenic activities. Besides occupational exposure, Cd contamination in humans can occur through food, drinking water, inhalation of air particles, and cigarette smoking. It has been estimated that daily intake of Cd from food is generally between 8 and 25 µg (Jarup and Akesson, 2009). Cadmium ions (Cd^{2+}) enter the cells through channels and transport pathways dedicated to essential ions, in what has been named a "Trojan horse mechanism" (Martelli et al., 2006). Once absorbed, Cd is trapped in the body and evades detoxification leading to an estimated biological half-life of more than 26 years. The accumulation of this metal contributes to the increase of oxidative stress and to the alteration of divalent ions homeostasis, primarily Zn^{2+} and Ca^{2+} (Choong et al., 2014); (Thevenod, 2010); (Urani et al., 2015); (Callegaro et al., 2018). Notably, about 3200 proteins (~ 10% of the human proteome) require zinc to properly function, and, along with the ability of Cd to replace Zn in zinc-finger regions or zinc-domains functionally important for many proteins and enzymes (Meplan et al., 1999); (Tang et al., 2014), these features suggest a role for Cd in essential metal dyshomeostasis, leading to alterations of physiological processes.

Cd is involved in global and site-specific DNA methylation, according to studies performed on model organisms (Hwang et al., 2019) as well as in humans (Ray et al., 2014). Cd-associated epigenetic effects have also been studied in the context of other exposures such as smoking (Virani et al., 2016). Last but not least, Cd is a well-known carcinogen as classified by the International Agency for Research on Cancer, but the mechanisms underpinning the molecular processes are not completely clarified.

Cadmium carcinogenicity has been well demonstrated both in in vitro biological systems (Urani et al., 2009) (Ao et al., 2010), such as the Cell Transformation Assays (CTAs), and in humans and animal models (Hartwig, 2013). The CTA is the most advanced in vitro assay for human carcinogenicity prediction induced by chemicals (Vanparys et al., 2012). It has been shown to closely model some in vivo key stages of the conversion of normal cells into malignant ones, and it is a powerful tool for mechanistic studies of carcinogenesis. Suitable cell lines are exposed to suspected carcinogens and, as a consequence of cell

transformation, foci of transformed cells are formed after 3-6 weeks (OECD, 2007).

The CTA offers the unique advantage of studying in a standardized and controlled environment the signals that trigger chemical-induced carcinogenesis, and the biochemical processes and pathways deregulated in transformed cells (*foci*). Furthermore, these assays are extremely important in the context of the 3Rs as they provide a means to reduce the use of animals, as CTA can be used to pre-screen for the potential of human carcinogens. Up to now, the use of alternative non-animal approaches, such as the CTA, in the context of carcinogenesis has been limited for different reasons, among which the lack of a complete comprehension of the carcinogenesis processes. Finally, even though the CTA should not be used as a stand-alone assay to predict carcinogenesis in the regulatory context, these assays are proposed as one of the building blocks in an integrated approach (Corvi and Madia, 2017); (Corvi et al., 2017), thus stressing their importance in mechanistic studies and in hazard assessment.

The aim of this work is to investigate, through a toxicogenomic approach based on whole genome microarray analysis of gene expression and on a bioinformatics study, the differentially regulated genes in transformed cells from different foci obtained at the end of the in vitro cell transformation upon exposure of C3H10T1/2 cells to the same stimulus (1 μM CdCl2 24 h treatment). The systematic analysis of deregulated genes and pathways in transformed cells, along with the comparison to what has previously been obtained by our group after the analysis of early responses to CdCl2 exposure in the same cell model (Forcella et al., 2016) (Callegaro et al., 2018), will provide a picture of triggering signals, of specific signatures and mechanistic processes in cadmium-induced cell transformation. Furthermore, these methods could represent a step forward in the development of a mechanistic-based approach for carcinogenesis alternatives methods.

❖ 6.2. Materials and Methods

6.2.1 Cells and culture conditions

The experiments were performed using the cells collected from Cd-transformed *foci* obtained at the end of Cell Transformation Assays (CTAs) on C3H10T1/2 clone 8 mouse embryonic fibroblasts (cell line ATCC, CCL 226 lot. n. 58078542). This cell line was chosen for its high sensitivity to carcinogenic compounds, its low spontaneous transformation rates, and because it represents one of the three cell lines suggested in the Detailed Review Paper on Cell Transformation Assay to be used for detection of chemical carcinogens (OECD, 2007) . Cells with passages from 9 to 12 were used for cell transformation studies (OECD, 2007). C3H cells were seeded at a density of 800 cells/dish in 100 mm diameter Petri dishes, and exposed 24 h after seeding to 1 µM $CdCl_2$ for 24 h. Previous Cell Transformation Assays performed by our group (Urani et al.,2009) on a wide range of $CdCl_2$ concentrations demonstrated that 1 µM $CdCl_2$, which is below the cytotoxicity threshold (IC_{50} of 2.4 µM), is able to induce the formation of transformed *foci*. Samples treated with $CdCl_2$ were exposed 4 days after the treatment to 0.1 µg/ml TPA (12-O-tetradecanoylphorbol-13-acetate), a known tumour promoter, in DMSO. TPA addition was maintained throughout all the experiments. Cells exposed to 0.1 µg/ml TPA alone were used as reference control. After 24 h of treatment, the cells were rinsed twice with phosphate buffered saline (PBS) and fresh medium was added. The medium was changed weekly. Upon confluence (around the 3rd week), high serum (10% FBS) medium was substituted with low (5% FBS) serum medium. The samples were observed weekly under a light microscope throughout the duration of the assay (6 weeks) to check healthy cells' status and *foci* formation.

Different cell types were collected at the end of the CTAs, and the derived cell clones were cultured and processed for further analyses, as described in the following sections. The new cell clones were derived from three different fully transformed *foci,* all obtained after the initial exposure (24 h) to1 µM $CdCl_2$, and classified as F1, F2, and F3. Cells were cultured in Basal Medium Eagle (BME, Sigma Chemical Co., St. Louis, MO, USA) enriched with 10% heat-inactivated foetal bovine serum (FBS, Euroclone, Pero, Italy), 1% glutamine, 0.5% HEPES 2M and 25 µg/mL gentamicin (all purchased from Sigma) at 37°C in

a humidified incubator supplied with a constant flow of 5% CO_2 in air throughout each experiment. Cells were routinely seeded in 100 mm Ø Petri dishes, the medium was changed every 3 days and cells grown until 80% confluence maximum was reached. The cells were stored in ampoules, frozen at –80°C with 10% sterile DMSO as a preservative.

6.2.2 RNA extraction and purification

All cell clones were harvested by trypsinization at 80% confluence and lysed in 300 µl RLT buffer (Qiagen, Germantown, MD, USA), with 1:100 β-mercaptoethanol added. Homogenates were obtained by passing 5 times through a blunt 20-gauge needle fitted to a syringe. Samples were stored at -80°C until RNA extraction was carried out. RNA was purified from cell clones using the RNeasy Plus kit (Qiagen, Germantown, MD, USA). RNA was quantified using a ND-1000 UV-Vis Spectrophotometer (NanoDrop Technologies), and RNA integrity was assessed with the Agilent 2100 Bioanalyzer (Agilent), according to the manufacturer's instructions. RNA samples used in this study all had a 260/280 ratio above 1.9 and an RNA Integrity Number (RIN) above 9.0.

6.2.3 Microarray expression profiling and exploratory statistical analyses of the three foci

In the microarray experiments, all sample-labelling, hybridization, washing, and scanning steps were conducted following the manufacturer's specifications. In brief, Cy3-labeled cRNA was generated from 500 ng input total RNA using Quick Amp Labeling Kit, One-colour (Agilent). For every sample, 1.65 µg cRNA from each labelling reaction (with a specific activity above 9.0) was hybridized using the Gene Expression Hybridization Kit (Agilent) to the SurePrint G3 Mouse GE 8x60K Microarray (G4852, Agilent), which is an 8 x 60k 60mer slide format. After hybridization, the slides were washed and then scanned with the Agilent G2565BA Microarray Scanner (Agilent). The fluorescence intensities on scanned images were extracted and pre-processed by Agilent Feature Extraction Software (v10.5.1.1). Quality control and array normalization was performed in the R statistical software environment using the Agi4x44PreProcess package downloaded from the Bioconductor web site (Gentleman et al., 2004). The normalization and filtering steps were based on those described in the Agi4x44PreProcess reference manual. In order to detect differences in gene expression among different cell populations a moderate *t*-test was applied. Moderated *t* statistics were generated by the Limma Bioconductor package. Modulated genes were chosen as those with a fold change greater than 1 or smaller than -1 and a false discovery rate (Benjamini and Hochberg's method) corrected p-value smaller than 0.05 (Smyth, 2004).

6.2.4 Quantitative real time-PCR

RNA was reverse-transcribed using SuperScript® II RT (Invitrogen, Carlsbad, CA, USA), oligo dT and random primers, according to the manufacturer's protocol.
The SYBR Green method was used for quantitative real-time PCR (Q-PCR). Briefly, 50 ng cDNA was amplified with SYBR Green PCR Master Mix (Applied Biosystems, Foster City, CA, USA) and specific primers (100 nM), using an initial denaturation step at 95°C for 10 min, followed by 40 cycles of 95°C for 15 sec and 59°C annealing for 1 min. Each sample was analyzed for Interleukin 6 expression and normalized for total RNA content using β-actin gene as an internal reference control. The relative expression level was calculated with the

Livak method (2[-ΔΔC(T)]) (Livak and Schmittgen, 2001) and was expressed as a fold change ± standard deviation. The accuracy was monitored by the analysis of melting curves. The following primers were used: Interleukin 6 Fw 5'-AGCCAGAGTCCTTCAGAGAGA-3' and Rv 5'-TGGTCTTGGTCCTTAGCCAC-3'; β-actin Fw 5'-CCACCATGTACCCAGGCATT-3' and Rv 5'-CGGACTCATCGTACTCCTGC-3'.

6.2.5 Functional enrichment analysis

Differentially Expressed Genes (DEGs), namely up-regulated and down-regulated genes, were analyzed with WebGestalt (WEB-based Gene SeT AnaLysis Toolkit, http://www.webgestalt.org), to identify genes with similar functions (Wang et al., 2013). Enrichment analyses were conducted studying the Gene Ontology categories with a p-value lower than 0.05 in a hypergeometric test. The method used for enrichment analysis was the Over-Representation Analysis (ORA). WebGestalt gene tables summarization and volcano plots were used to summarize and visualize the enrichment results.

❖ 6.3. Results

One of the purposes of the study was the identification of specific transcriptomic signatures able to unravel cadmium-induced carcinogenesis. In this regard, cDNA microarrays were used to analyze the modulation of gene expression induced by 1 μM cadmium chloride ($CdCl_2$) at the end of Cell Transformation Assay (CTA) (Callegaro et al., 2018), using TPA-treated cells as a reference control. Thus, we performed a systematic analysis of the functions of up- and down-regulated genes in cells derived from three *foci* (F1, F2, and F3) to figure out a picture of cadmium promoted pathogenic mechanisms leading to cells transformation.

6.3.1 Differentially expressed genes (DEGs) in F1 focus

Among the top 15 up-regulated genes in F1 *focus*, listed in Table 1, we found a series of genes involved in inflammation, such as *Cfh* gene coding for complement factor H, a major regulator of the alternative pathway of the complement system, which is able to bind neutrophiles, macrophages and monocytes with a proinflammatory effect (Jozsi et al., 2018). In addition, through a function not related to its complement-regulatory capacity, receptor-bound factor H can mediate or regulate cell adhesion.

Another gene involved in inflammation is *Spp1* gene coding for Osteopontin (also known as optineurin), a cytokine and cell attachment phosphoprotein expressed by various tissues and cell types and involved in multiple functions such as inflammation, cell adhesion, migration and tumour invasion. In particular, osteopontin is known to up-regulate MMP-2 expression and activity in tumour cells (Zhang et al., 2011) and may act as a potent angiogenic factor (Zhao et al., 2018). Another transcript related to inflammation is the T-cell specific GTPase 2 isoform X1, coded by *Tgtp2*, which has been demonstrated to be involved in systemic inflammatory response syndrome (SIRS) (Mastronardi et al., 2007), as well as in antiviral response (Carlow et al., 1998).

Lumican, coded by up-regulated *Lum* gene, is a member of the small leucine-rich proteoglycan family, expressed in the extracellular matrix of different tissues, where it plays a critical role in collagenous matrix assembly, protecting collagen from cleavage by matrix metalloproteinase-9 (MMP-9) (Malinowski et al., 2012). Its ability to down-regulate the proteolytic activity associated with

endothelial cell membranes, particularly MMP-14 and MMP-9, gives Lumican angiostatic properties.

Other up-regulated genes code for proteins involved in cell proliferation, migration and invasion, like FBJ osteosarcoma oncogene B (coded by *Fosb* gene) which promotes cell survival, and Histone deacetylase (coded by *Hdac9* gene), a negative regulator of adipogenic differentiation, whose over-expression has been documented in several malignancies.

Capn6, encoding for Calpain 6 (CAPN6), was also found to be up-regulated in cells from F1 *focus*. Unlike the other members of the family, CAPN6 is not a proteolytic enzyme (Dear et al., 1997), since it lacks the active-site catalytic cysteine residue. Instead, it has been shown to modulate osteoclasts and stabilize microtubules (Tonami et al., 2011).

Among the 15 top down-regulated genes in cells from F1 *focus* (also listed in Table 1) we found *Rspo3* gene, a homolog of Xenopus laevis R-spondin 3 gene. R-spondins (RSPO) are agonists of the Wnt pathway, interfering with the clearance of Wnt receptors from the plasma membrane (Fischer et al., 2017). RSPO3 expression has been shown to cause rapid development of adenoma and adenocarcinoma in the intestine, establishing RSPO3 as an efficient, causal driver of intestinal cancer (Hilkens et al., 2017).

Another interesting down-regulated gene, *Slc17 a3*, coding for a member of solute carrier family 17 (sodium phosphate), isoform CRA_c, is a member of the Major Facilitator Superfamily (MFS), a large and diverse group of secondary transporters that includes uniporters, symporters, and antiporters.

Mest gene, which was down-regulated in cells from all the three *foci*, codes for mesoderm-specific transcript protein isoform 1 precursor (MEST), a putative alpha/beta hydrolase, although the substrate of this enzyme has not yet been identified (Kaneko-Ishino et al., 1995). A functional role related to oncofetal angiogenesis has been suggested for the MEST proteins (Mayer et al., 2000).

PEP-19/pcp4 is a neuron-specific peptide in the adult brain, binding to the C-domain of calmodulin; a role for PEP-19/pcp4 as a regulator of synaptic plasticity in the mouse striatum, in the context of spatial learning, has recently been proposed (Aerts et al., 2017).

Gas6 gene, coding for growth arrest specific 6 protein, was found to be down-regulated also in cells from F2 and F3 *foci*. *Gas6* protein activates STAT3 signalling and stimulates the molecular process of differentiation or myelination in the adult optic nerve (Goudarzi et al., 2016). Moreover, other

authors (Ray et al., 2017) found that the complete deletion of the *Gas6* signalling pathway significantly impacted resolution of inflammation, axonal integrity and remyelination. *Gas6* therefore seems to have an anti-inflammatory effect and a role in cell differentiation, its down-regulation likely leading to loss of differentiation and inflammation. *Slit3* gene, also down-regulated in F1 *focus*, codes for a member of the Slits proteins, large matrix proteins that are secreted by endothelial cells. *Slit3* was reported to enhance monocyte migration *in vitro*, as well as myeloid cell recruitment *in vivo* and to induce the activation of RhoA, a member of the Rho family of small GTPases (Geutskens et al., 2010).

Mgmt gene codes for O-6-methylguanine-DNA methyltransferase (MGMT), a DNA alkyl transferase; a role in the development of certain kinds of human tumours is suggested by the observation that Mgmt gene is silenced by promoter methylation in gliomas, colorectal tumours, non-small-cell lung carcinoma, lymphomas and head and neck cancers (Mari-Alexandre et al., 2017). Heparan sulfate 6-O-sulfotransferase 2 (HS6ST2), transcript variant 2, coded by Hs6st2 gene, belongs to the HS6ST family, comprising different isoforms with distinct substrate preferences. HS6ST-1-deficiency is lethal to mice mostly at later embryonic stages, leading to various malformations in muscle development (Habuchi and Kimata, 2010).

Smpdl3a gene codes for sphingomyelin phosphodiesterase acid-like 3A (SMPDL3A), a di-zinc-dependent enzyme, which, in contrast to sphingomyelinase, is inactive against sphingomyelin and can instead hydrolyze nucleoside diphosphates and triphosphates, which may play a role in purinergic signalling (Gorelik et al., 2016).

TMF-1 regulated nuclear protein 1 (TRNP1), coded by *Trnp1* gene, is a basic protein which accumulates in an insoluble nuclear fraction in mammalian cells, that can accelerate cell cycle progression (Volpe et al., 2006).

Another down-regulated gene in cells from F1 *focus* is Thbd, coding for thrombomodulin (TM), a protease with a role in TM dependent protein C activation, essential for mitochondrial function and myelination in CNS (Wolter et al., 2016). Loss of TM-dependent PC generation impairs primarily mitochondrial function and not mitochondrial biogenesis, suggesting a protective role for TM in CNS against oxidative stress.

Two more genes, Mt2 and Hspb1 coding for metallothionein 2 and heat shock protein 1 respectively, are down-regulated in cells from F1 *focus*.

6.3.2 Differentially expressed genes (DEGs) in F2 focus

Table 2 lists the top 15 up-regulated and down-regulated genes in cells from F2 *focus*. Among the most up-regulated genes, we found *Efemp1*, coding for the glycoprotein fibulin-3, which is normally expressed along the primary olfactory pathway and produced by olfactory epithelium cells *in vitro* (Vukovic et al., 2009). Fibulin-3 belongs to a small family of glycoproteins that normally have widespread distribution in extracellular matrix structures such as basement membranes, microfibrils and elastic fibres (Argraves et al., 1990); (Timpl et al., 2003); (de Vega et al., 2009). Based on its interaction with the tissue inhibitor of metalloproteinases-3 (TIMP-3) (Klenotic et al., 2004), a critical role for fibulin-3 in regulating matrix metalloproteinase (MMP) activity has been proposed (McLaughlin et al., 2007). Manipulation of fibulin-3 expression in cultured olfactory epithelium cells has been shown to alter both proliferation and migration (Vukovic et al., 2009).

Ras-activating protein-like 3 (RASAL3), encoded by *Rasal 3* up-regulated gene, is a T cell-specific Ras GTPase-activating protein, that negatively regulates T cell receptor (TCR)-induced activation of Ras/MAPK pathway. Collectively, Rasal3 controls the magnitude of inflammatory responses through the survival of both naive T cells and activated T cells *in vivo* (Muro et al., 2018).

Follistatin-like 4, a SPARC-related protein-containing immunoglobulin domains 1 (SPIG1) encoded by *Fstl4* gene, was identified as one of the dorsal-retina-specific molecules expressed in the developing chick retina. SPIG1 negatively regulates Brain Derived Neurotrophic Factor maturation, thereby suppressing axonal branching and spine formation, (Suzuki et al., 2014).

Other up-regulated genes in cells from F2 *focus* are *Chat*, coding for choline acetyltransferase, *Xlr3b*, coding for X-linked lymphocyte-regulated 3B, and *Resp18*, coding for Regulated endocrine-specific protein,18 kDa; the latter is a unique endoplasmic reticulum resident protein with an unknown function, first identified as a dopaminergic drugs-regulated intermediate pituitary transcript.

Also related to immunological signalling is *Ccl2* gene, coding for chemokine (C-C motif) ligand 2 (previously named MCP-1), one of the most important members of the CC chemokines family, involved in the regulation of oriented migration and the infiltration of mainly reticuloendothelial system cells, specifically monocyte/macrophage phenotypes. Fundamental roles are played by CCL2 and its related receptor (the CCR2) in brain tumours and in migration of monocytes

from the bloodstream through the vascular endothelium (Vakilian et al., 2017). CCL2 is a potent monocyte-attracting chemokine and greatly contributes to the recruitment of blood monocytes into sites of inflammatory responses and tumours. Although tumour cells are considered to be the main source of CCL2, various non-tumour cells in the tumour stroma also produce CCl2 in response to stimuli.

Spp1 gene coding for Osteopontin is up-regulated also in cells from F2 *focus*. The last up-regulated gene with a known function, *Olfml2a*, codes for olfactomedin-like 2A, belonging to the OLF (olfactomedin)-family, a major component of the extracellular mucus matrix of olfactory neuroepithelium (Furutani et al., 2005).

Among the top 15 down-regulated genes in cells from F2 *focus* we found many genes which are also down-regulated in F1 *focus*, such as *Slc17a3*, *Mest*, *Rspo3*, *Thbd*, *Mgmt*, *Hspb1*, as well as *Gm5493* gene, whose product is unknown.

Among the genes exclusively up-regulated in F2 *focus* we found *Scrn1*, coding for Secernin 1, a brain cytosolic protein, with a putative dipeptidase activity, also capable of regulating exocytosis in permeabilized mast cells (Way et al., 2002), and *Fbln7*, coding for fibulin-7 (FBLN7), also called TM14, a cell adhesion molecule that interacts with extracellular matrix molecules in teeth (de Vega et al., 2007). Argraves and coworkers (Argraves et al., 1990) described the first member of this family, fibulin-1, as a binding partner for the fibronectin receptor integrin and an important regulator of cell adhesion. So far, 5 other members (fibulins 2–6) have been identified, modulating cell morphology, growth, adhesion, and motility. In addition, it has been demonstrated that the dysregulation of some fibulins is linked to cancer, and both tumour suppressive and pro-oncogenic roles have been proposed for members of the fibulin family (Gallagher et al., 2005).

6.3.3. Differentially expressed genes (DEGs) in F3 focus

As shown in Table 3, among the 15 top up-regulated genes in F3 *focus*, we found a series of genes coding for 2'-5' oligoadenylate synthetases (OAS), such as *Oas1a*, *Oas1f*, *Oas2* and *Oasl2*. OAS proteins are interferon (IFN) inducible pathogen recognition receptors expressed in different cell types. Upon activation by the pathogen-associated molecular pattern (PAMP) double-stranded viral RNA, certain OAS proteins synthesize 2'-5'- oligoadenylate (2-5A), which activates RNase L (Silverman and Weiss, 2014). In mice, there are 8 *Oas1* genes (Mashimo et al., 2003) (Perelygin et al., 2006) (Kristiansen et al., 2011); however, only *mOAS1a* and *mOAS1g* are believed to be enzymatically active. Mice have four additional *Oas* genes, which produce 3 enzymatically active proteins (mOAS2, mOAS3 and mOASL2), and one inactive (mOASL1) protein (Kakuta et al., 2002).

With two exceptions, namely *Usp18* and *Rtp4*, all other genes up-regulated in cells from F3 *focus* code for proteins involved in IFN mediated antiviral response: *Ifi44*, coding for interferon-induced protein 44; *Sp110*, coding for Sp110 nuclear body protein, an interferon induced transcriptional coactivator with a bound zinc atom highly expressed in leukocytes; *Mx1*, coding for myxovirus resistance 1 protein; *Isg15*, coding for ISG15 ubiquitin-like modifier; H2-K1, histocompatibility K region; *Ifi27l2a*, coding for interferon alpha-inducible protein27 like 2A, and *Tgtp2*, coding for T cell specific GTPase 2. Ifi2712a belongs to a family of small interferon induced hydrophobic proteins, the ISG12 proteins; the expression of *ISG12b1*, also called *IFI27*, has been reported to be up-regulated in the mouse brain after intracerebral virus infection. Moreover, *ISG12b1* has been identified as an adipose-specific gene, localized in mitochondria: current studies demonstrate that its overexpression in 3T3-L1 cells inhibits mitochondrial biogenesis and lipid accumulation in adipocytes (Li et al., 2009).

Usp18 codes for ubiquitin-specific protease 18, a deubiquitinating enzyme (DUB) catalysing the deconjugation of ubiquitin chains from ubiquitinated proteins (Komander et al., 2009). Many studies have demonstrated that some DUBs are the signalling targets of cellular stress such as oxidative stress. In mouse, *Usp18* was found to be induced by oxidative stress, in a dose- and time-dependent manner, while its depletion could stimulate an increase in p53 and caspase 3 protein levels. This suggests that *Usp18* protects the cells from

oxidative stress-induced apoptosis, likely through the regulation of p53 and caspase 3 (Lai et al., 2017). DUBs can regulate p53 signalling pathway *via* different mechanisms within different cellular compartments in response to different kinds of stresses (Kwon et al., 2017).

Rtp4 codes for receptor transporter protein 4, a member of the RTP protein family specifically expressed in olfactory neurons. These proteins are normally associated with olfactory receptors (OR) proteins and enhance OR responses to odorants (Saito et al., 2004).

Among the top 15 genes down-regulated in cells from F3 *focus*, also listed in Table 3, we found the *Mest* gene, which is found among the 15 top down regulated genes of cells from F1 and F2 *foci*. Two genes coding for collagen, *Col2a1* and *Col11a1* are also down regulated in this *focus*, as well as *Pcp4* gene, which is one of the most strongly down-regulated genes in F1 *focus*. Interestingly, *Fos* gene, promoting cell survival, was found to be down-regulated in F3 *focus*, while it is found among the most up-regulated genes in F1 *focus*. The same is true for *Igf1* gene, coding for insulin-like growth factor 1, which plays a key role in the development and progression of many human cancers. Moreover, a large amount of data supports that insulin-like growth factor 1 (IGF-1) deficiency increases insulin resistance, impairs lipid metabolism, promotes oxidative damage, and dysregulates the GH/IGF-1 axis (Gonzalez-Guerra et al., 2017).

Another down-regulated gene in cells from F3 *focus* is *Plxdc2* gene, coding for plexin domain containing 2. Direct molecular activity of Plxdc2 has been demonstrated in the control of proliferation, its expression being altered in various kinds of cancer; in particular, Plxdc2 has been shown to act as a mitogen in the developing nervous system (Miller-Delaney et al., 2011).

Arxes2 gene, coding for adipocyte-related X-chromosome expressed sequence 2, is required for fat cells differentiation and is transactivated by adipogenic transcription factors.

Sorl1 gene codes for sortilin-related receptor, an LDLR class A receptor with a cysteine-rich repeat that plays a central role in mammalian cholesterol metabolism, as well as in cell migration and metabolic regulation (Schmidt et al., 2016).

Speer2 gene codes for spermatogenesis associated glutamate (E)-rich protein 2, a new group of haploid sperm-specific nuclear factors (Spiess et al., 2003).

RPE65, the product of *Rpe65* gene, is an enzyme involved in vitamin A metabolism in retinal pigment epithelium (RPE) cells (Redmond et al., 1998), where it is necessary for production of 11-cisvitamin A in the retinal visual cycle. Mutations in *Rpe65* are associated with several retinal disorders. Pyakurel and coworkers demonstrated that the disruption of ERK1/2 specifically in RPE cells leads to a marked decrease of RPE65 expression, while the activation of ERK1/2 is associated with the activation of the Wnt/□-catenin pathway, which plays a key role in the expression of the RPE-specific transcription factors (Pyakurel et al., 2017).

Two more genes were found down-regulated in cells from F3 *focus*: *Papss2*, coding for 3'-phosphoadenosine 5'-phosphosulfate synthase 2, and *Ppp1r1b* encoding protein phosphatase, inhibitor subunit 1b, a bifunctional signal transduction molecule.

6.3.4 Cytokines encoding genes are up-regulated in cells from all foci

The Venn Diagram in Figure 1A shows the number of the differentially expressed genes (DEGs) in the cells from the three *foci*. On the whole, cells from F3 *focus* undergo the highest gene expression deregulation, with 1091 DEGs, while cells from F2 seem to be the less changed by Cd treatment, with only 126 DEGs; the cells from F1 *focus* present an intermediate situation with 255 DEGs. Only 34 genes are deregulated in all three *foci*, although not to the same extent, and are all listed in Table 4 and graphically represented in Figure 1B. Table 4 shows that the only genes up-regulated in all three *foci* are genes coding for cytokines: *Ccl2*, *Ccl5*, *Il6* and *Spp1*. Among the 34 DEGs common in all *foci*, the majority (23) appears to be down-regulated in all *foci*, while only 4 are down-regulated in both F1 and F2 *foci* and up-regulated in F3 *focus*; only one gene (*Marcksl1*, coding for MARCKS-like 1 protein) is up-regulated in both F1 and F2 *foci* and down-regulated in F3 *focus*, while *Thy1* gene, coding for thymus cell antigen 1, is down-regulated in F1 *focus* and up-regulated in both F2 and F3 *foci*.

The validation through RT-PCR confirmed *Il-6* gene up-regulation in all three *foci*. The relative quantification of Interleukin-6 mRNA was carried out through real-time quantitative PCR in cells from all three *foci*, using β-actin as internal reference control, and TPA-treated cells as a calibrator. The results, reported in Figure 2, showed *Il-6* gene to be up-regulated in all three *foci*, with a higher fold change in F1 *focus*, compared to both F2 and F3 *foci*.

Figure 6.1. Differentially expressed genes (DEGs) in the three different foci (F1, F2, and F3) analysed. A) Venn Diagram of DEGs (both up and down) for the three foci; B) Plot of fold change (FC) on y-axis of the genes differentially expressed in all the three foci (see Table 4). Colours represent the three different foci. Genes are ordered by the comparison F1 vs TPA.

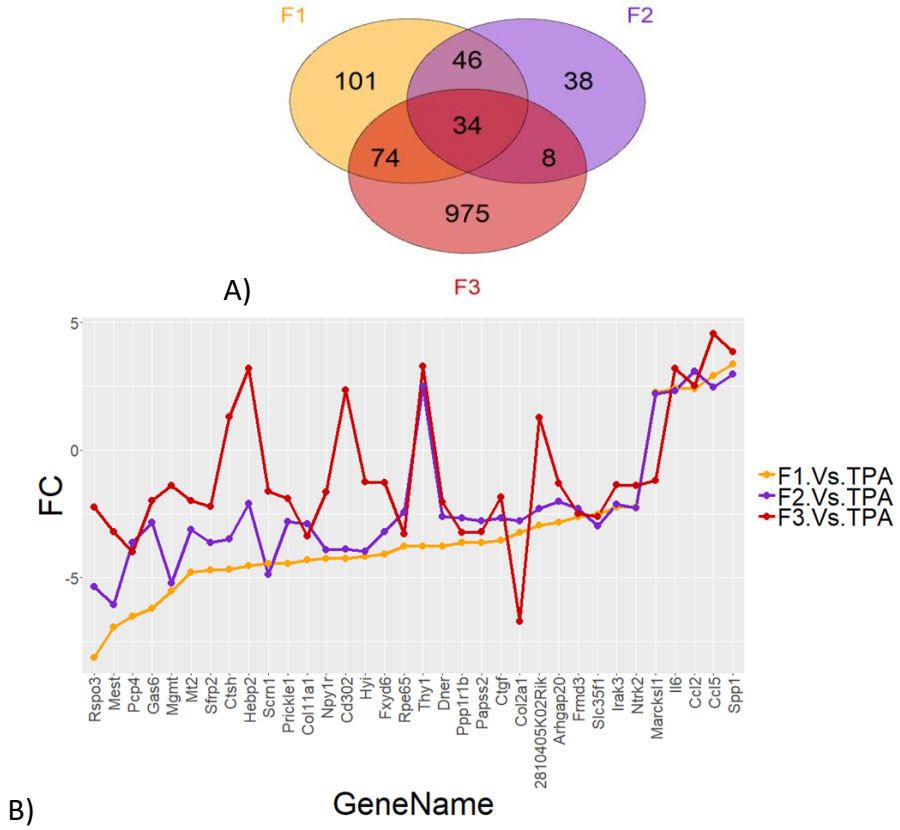

Figure 6.2. Relative quantification of Interleukin-6 mRNA levels by real-time quantitative PCR in F1, F2, F3 cell clones. The relative expression level was calculated with the Livak method (2[−ΔΔC(T)]) and was expressed as a fold change ± SD, using β-actin gene as internal reference control and the TPA-treated cell clone as calibrator. *** P < 0.001 (Dunnett's test).

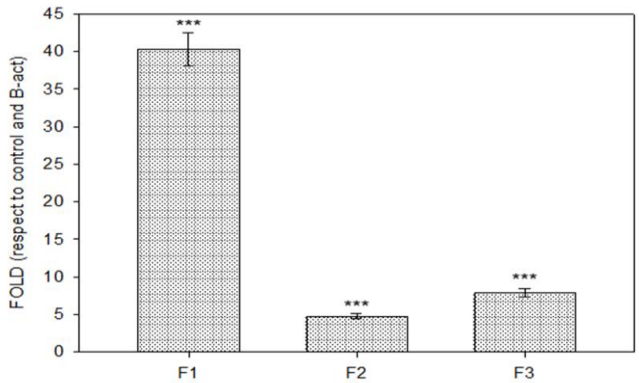

6.3.5 Gene Ontology enrichment analysis

The DEGs detected in microarrays from the three *foci* were subjected to a Gene Ontology (GO) enrichment analysis, as described in Materials and Methods. Results reported in Figure 3 show the presence, in all *foci,* of dysregulated gene expression in the "angiogenesis" category, which includes some up-regulated genes, like *Spp1*, coding for osteopontin, or down-regulated genes, like *Mest* and *Plxdc2*. Other categories showing dysregulated genes in all *foci* concern organ and tissue morphogenesis, as well as extracellular organization; however, none of these categories is common to all *foci*. Dysregulated genes in "extracellular structure organization" are found in F2 and F3 *foci* (Figure 3B and 3C), but not in F1 (Figure 3A). However, F1 *focus* shows dysregulated genes in connective tissue, muscle organ and skeletal system development, as well as in "regulation of animal morphogenesis", "extracellular organization" and "tissue morphogenesis" (Figure 3A). Moreover, only F1 *focus* shows dysregulation of genes related to negative regulation of growth, a category including many growth factors, as well as different chemokines and interleukins, leading to a loss of growth regulation.

Apart from genes involved in regulation of cell morphogenesis, skeletal system development and extracellular structure organization, most of dysregulated genes in F3 *focus* belong to categories related to immune defence, like "regulation of innate immunity response", "response to virus", "positive regulation of defence response" "response to beta and gamma interferons" (Figure 3C).

As shown in Figure 3B, some dysregulated genes related to immune response are also found in F2 *focus* in the "chemiotaxis" category, including chemokines coding genes, as well as *Gas6* and *Fgf4* genes.

Figure 6.3. Functional enrichment analysis

Each volcano plot shows the log of False Discovery Rates (FDR) against enrichment ratio for all the Gene Ontology categories. The gene set name showed in the volcano plot are representative of the TOP 10 categories based on the FDR. For example, the most significant categories are shown in the upper part of the plots. The size and colour of the dots are proportional to the size of the category. Volcano plots represent the Enrichment results of F1 (A), of F2 (B), and of F3 cell clones (C). Figure in the next page.

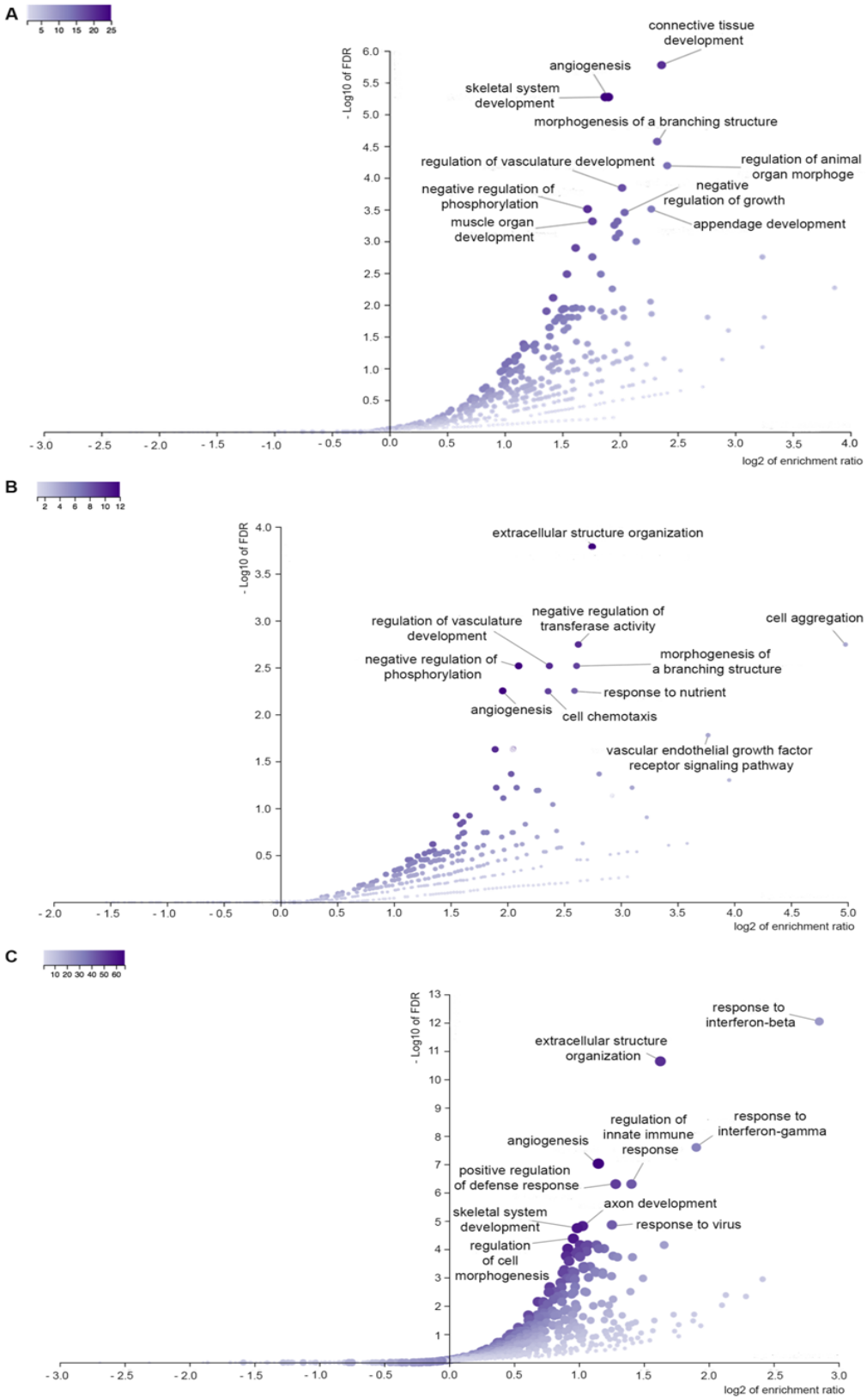
A
5 10 15 20 25
connective tissue development
angiogenesis
skeletal system development
morphogenesis of a branching structure
regulation of vasculature development
regulation of animal organ morphoge
negative regulation of phosphorylation
negative regulation of growth
muscle organ development
appendage development
- Log10 of FDR
log2 of enrichment ratio
B
2 4 6 8 10 12
extracellular structure organization
regulation of vasculature development
negative regulation of transferase activity
cell aggregation
negative regulation of phosphorylation
morphogenesis of a branching structure
response to nutrient
angiogenesis
cell chemotaxis
vascular endothelial growth factor receptor signaling pathway
- Log10 of FDR
log2 of enrichment ratio
C
10 20 30 40 50 60
response to interferon-beta
extracellular structure organization
regulation of innate immune response
response to interferon-gamma
angiogenesis
positive regulation of defense response
axon development
skeletal system development
response to virus
regulation of cell morphogenesis
- Log10 of FDR
log2 of enrichment ratio

❖ 6.4. Discussion

Comparing the lists of differentially expressed genes (DEGs) in the cells from the three *foci*, it is evident that a common stimulus (1□M $CdCl_2$ for 24h) administered to the healthy C3H10T1/2 cells elicits different cellular responses, as preliminarily shown in a work by our group (Forcella et al., 2016). Most of the cells treated with $CdCl_2$ have efficient defence mechanisms, demonstrated by the up-regulation of metallothioneins and Hsp70 in the first hours after cadmium administration, followed by their down-regulation (Callegaro et al., 2018). However, a few cells, cannot efficiently counteract the insult and develop different metabolic alterations (Forcella et al., 2016), leading to cell transformation and *foci* formation in the weeks following cadmium treatment.

DEGs analysis, performed in this work, confirms these differences, showing only 34 common DEGs in cells from the different *foci*; among these, only 4 genes are up-regulated in all *foci*: *Ccl2*, *Ccl5*, *IL6* and *Spp1*, all coding for chemokines. Although chemokines were first discovered as mediators of migration of immune cells to sites of inflammation and injury, they are now known to play multiple roles in organ development, angiogenesis, and tumorigenesis. In particular, recent data show that CCl2 production regulates the interactions between tumour cells and macrophages, promoting tumour progression (Yoshimura, 2018).

Gene Ontology (GO) enrichment analysis, performed on all DEGs in the three *foci,* shows that inflammation, and therefore cytokines production, is involved in many of the identified pathways, like ”cell chemiotaxis”, ”positive regulation of defence response”, ”response to viruses” and ”regulation of immune innate response”. The up-regulation of inflammatory pathways is less evident in F1 *focus*, where genes connected with up-regulation of cell growth and extracellular matrix rearrangement prevail, in accordance with its highly proliferative behaviour; this confirms data from a previous work by our group (Forcella et al., 2016), showing that, while the ERK proliferative pathway is activated in F1 *focus*, the survival pathway mediated by Akt is activated in F3 *focus*. The down-regulation of both *Fosb* and *Igf1* genes in F3 *focus*, as well as the up-regulation of *Fosb* gene in F1 *focus*, likely accounts for this difference in proliferation.

On the other hand, we found that most common DEGs are down-regulated; among these, are genes coding for proteins of the extracellular matrix, like

Mest, *Col11a1*, *Col2a1* and *Ctgf*, and genes coding for proteins involved in cell growth arrest, such as *Gas6*, *Rspo3* and *Mgmt*. suggesting major rearrangements of the extracellular matrix leading to cell cycle progression. A major rearrangement of extracellular matrix is confirmed also by GO analyses, showing "regulation of animal morphogenesis", "connective tissue development", as well as "regulation of cell morphogenesis" and "extracellular structural organization" among the most deregulated pathways.

On the whole gene expression dysregulation induced by $CdCl_2$ seems to be achieved more through gene down-regulation than up-regulation: in F1 *focus*, apart from the most up-regulated gene (showing a fold change higher than 12), the other top up-regulated genes show an average fold of 4, in contrast with the top down-regulated genes, all showing folds higher than 5. The same is true for F2 *focus*, although with smaller overall fold values, showing higher values for top down-regulated genes than for up-regulated ones. In contrast, in F3 *focus*, the top 15 up- and down-regulated genes show similar fold values.

F1 and F2 *foci* are more similar to each other than to F3 *focus*, showing 8 identical top down-regulated genes out of 15. An intriguing feature of F2 *focus* is the down-regulation of two genes coding for olfactory receptors (OR); many other OR encoding genes were previously found to be down-regulated upon 24 hours treatment with cadmium (Callegaro et al., 2018). Although the meaning of this down-regulation is not clear, about 1500 genes coding for olfactory receptors are present in mouse genome and these receptors are also expressed in a variety of non-olfactory tissues (Zhang et al., 2016); (Ichimura et al., 2008); (Pluznick et al., 2013). Moreover, several predicted mammalian OR genes are solely expressed in non-olfactory tissues, raising the possibility that the receptors have functions other than odour recognition. Although still debated, OR are probably either Zn or Cu binding proteins, their dysregulation being due to Zn/metals homeostasis disruption.

Although significant differences are observed when comparing F1 and F2 top up-regulated genes, the only common DEG being *Spp1*, on the whole, the same pattern of cell matrix rearrangement and inflammatory response up-regulation emerges in cells from both *foci*, involving genes such as *Mest*, *Lum*, *Slit3* and *Hs6st2*, *Efemp1*, *Fbln7*, coding for cell matrix proteins, and *Spp1*, *Cfh*, *Tgtp2*, *Rasal3*, *Resp18*, *Ccl2* and *Xlr3b*, involved in inflammation. Moreover, many proteins encoded by DEGs have been previously reported to be oncogenic, like

Fosb, Hdac9 and *Gas6,* dysregulated in F1 *focus*, and *Mgmt, Rspo3* and *Thbd,* dysregulated in both F1 and F2 *foci*.

A completely different picture emerges from the top up- and down-regulated genes in F3 *focus*; in particular, 13 out of the 15 top up-regulated genes are involved in an interferon mediated antiviral response, which can be triggered by either viral DNA or viral RNA. Efficient elimination of viral infection relies on both detection of the virus by pattern recognition receptors (PRRs) and inhibition of viral replication by antiviral restriction factors. Retinoic acid-inducible gene-I (*RIG-I*) is a PRR that upon activation by primarily 5'-triphosphate RNA induces a signalling cascade leading to interferon (IFN) gene expression.

The 2'-5' oligoadenylate synthetases (OASs) are a family of IFN- and virus-induced antiviral restriction factors that provide protection against a wide spectrum of RNA and DNA viruses. Initial virus detection induces the expression of OASL, which, upon subsequent virus detection, can promote RIG-I signalling thereby enhancing the antiviral response (Ibsen et al., 2015). However, a similar response has been shown to be triggered also by mitochondrial damage releasing mtDNA into the cytosol. *Thbd* gene down-regulation in both F1 and F2 *foci* also suggests mitochondrial damage, loss of Thrombomodulin-dependent PC activation impairing mitochondrial functionality. GO enrichment analysis confirms the strong up-regulation of inflammatory response in F3 *focus*, showing pathways like "response to viruses", "positive regulation of defence response", "regulation of immune innate response" and "response to interferon gamma" are among the most dysregulated.

❖ 6.5. Conclusions

Our previous work on up- and down-regulated genes and functions, immediately after 24 hours exposure to 1 µM $CdCl_2$ and after a period of recovery, showed that the cells respond mainly by activating defence mechanisms, that decrease in the following recovery period. These defence mechanisms are generally very efficient, however a few cells evade them and proliferate or survive in an uncontrolled manner (Forcella et al., 2016); (Callegaro et al., 2018). This leads to the formation of *foci* derived from different transformed cell clones. The features of deregulated genes in each *focus,* analyzed in this work, suggest that different functional targets (proteins and/or processes) are involved in the complex mechanism of cell transformation. However, it is noteworthy that the only genes in common to all analyzed *foci* are those responsible for cytokine/chemokines coding. These genes are involved in the inflammatory response, which is a known feature of carcinogenesis (see for example (Coussens and Werb, 2002); (Suarez-Carmona et al., 2017). In addition, in F3 *focus* the inflammatory response is likely related to mitochondrial damage.

Thus, it appears that the significant signal triggering the process of Cd-induced transformation in C3H cells is mainly represented by the deregulation of zinc homeostasis. The interference of Cd on Zn homeostasis has previously been demonstrated by our group and is also described in the literature (Callegaro et al., 2018); (Urani et al., 2015); (Martelli et al., 2006). Moreover, our present work stresses the relevance of the cell transformation assays (CTAs) not only as *in vitro* methods for the evaluation of the carcinogenesis potential of chemicals, but also as powerful tools for the comprehension of the mechanisms underlying the process of cell transformation.

The *in vitro* and bioinformatics mechanistic-based approach of this work, along with novel integrated *in vitro* carcinogenicity test on multiple cellular endpoints (Wilde et al., 2018) is in agreement with the just published suggestions (Madia et al., 2019) on performing *ad hoc* studies sorted on the basis of cancer's hallmarks, and organised in the form of Integrated Approaches to Testing and Assessment (IATA). This would provide a better understanding of cancer induction by environmental contaminants, also in view of its prevention, and could progress the exploit of *in vitro* carcinogenicity evaluation.

Further, although our work is preliminary and further studies will be necessary, the identification of specific structures/processes deregulated in transformed cells could represent an important starting point for the development of anti-tumour agents targeting specific cell functions in transformed cells. In this context, the use of CTAs represents an invaluable means to perform preliminary studies in a controlled and relatively simple environment, in comparison to the *in vivo* situation.

Acknowledgements

The authors acknowledge the European Commission. CU acknowledges the partial support by Fondo di Ateneo (University of Milano - Bicocca, 2016-ATE-0411); PF acknowledges the partial support by Fondo di Ateneo (University of Milano - Bicocca, 2017-ATE-0273). The authors acknowledge Gerard Bowe for manuscript revisions.

Table 6.1. List of top 15 up- and down-regulated genes in cells from F1 *focus*. DEGs are listed in descending order of fold change compared to TPA-treated cell clone.

GeneName	Description	Fold change
chr10:119960546-119979696_F	lincRNA: chr10:119960546-119979696 forward strand	12,34
Cfh	complement component factor h (Cfh)	5,27
Pddc1	Parkinson disease 7 domain containing 1	4,56
Tgtp2	T cell specific GTPase 2	4,25
Lum	lumican	3,96
Hdac9	histone deacetylase 9 (Hdac9), transcript variant 2	3,88
Capn6	calpain 6	3,84
ENSMUST00000099684	Unknown	3,73
ENSMUST00000099050	Unknown	3,52
Fosb	FBJ osteosarcoma oncogene B	3,48
H2-K1	histocompatibility 2, K1, K region, transcript variant 1	3,44
Spp1	secreted phosphoprotein 1, transcript variant 5	3,36
ENSMUST00000099042	Unknown	3,34
Ear2	eosinophil-associated, ribonuclease A family, member 2	3,27
A_55_P1987086	Unknown	3,25
Mt2	metallothionein 2	-4,78
Thbd	thrombomodulin	-4,89
Trnp1	TMF1-regulated nuclear protein 1	-5,21
Hspb1	heat shock protein 1	-5,23
Smpdl3a	sphingomyelin phosphodiesterase, acid-like 3A	-5,26
Mest	mesoderm specific transcript, transcript variant 1	-5,28
Hs6st2	heparan sulfate 6-O-sulfotransferase 2	-5,34
Gm5493	9 days embryo whole body cDNA, RIKEN full-length enriched library, clone: D030063M22 product: weakly similar to Hypothetical KRAB box containing protein	-5,41
Mgmt	O-6-methylguanine-DNA methyltransferase	-5,53
Slit3	slit homolog 3 (*Drosophila*)	-5,90
Gas6	growth arrest specific 6	-6,20
Pcp4	Purkinje cell protein 4	-6,53
Mest	mesoderm specific transcript, transcript variant 2	-6,94
Slc17a3	solute carrier family 17 (sodium phosphate), member 3	-7,66
Rspo3	R-spondin 3 homolog (*Xenopus laevis*)	-8,13

Table 6.2. List of top 15 up- and down-regulated genes in cells from F2 *focus*. DEGs are listed in descending order of fold change compared to TPA-treated cell clone.

GeneName	Description	Fold change
Efemp1	epidermal growth factor-containing fibulin-like extracellular matrix protein 1	4,1
Rasal3	RAS protein activator like 3	4,04
Fstl4	follistatin-like 4	3,97
ENSMUST00000188511	tc|Q5SR98_MOUSE (Q5SR98) Ortholog of human Ras association (RalGDS\/AF-6) and pleckstrin homology domains 1 RAPH1 (Fragment), complete [TC1598183]	3,86
chr14:26093652-26208156_R	lincRNA: chr14:26093652-26208156 reverse strand	3,61
Chat	choline acetyltransferase	3,51
chr18:63480341-63480899_R	lincRNA: chr18:63480341-63480899 reverse strand	3,51
D6Ertd527e	DNA segment, Chr 6, ERATO Doi 527, expressed, transcript variant 1	3,45
ENSMUST00000181143	RIKEN cDNA B230104I21 gene (B230104I21Rik), misc_RNA	3,25
Xlr3b	X-linked lymphocyte-regulated 3B	3,24
Resp18	regulated endocrine-specific protein 18	3,14
Ccl2	chemokine (C-C motif) ligand 2	3,08
Spp1	secreted phosphoprotein 1, transcript variant 5	2,97
Olfml2a	olfactomedin-like 2A	2,96
chr2:150496011-150496503_R	lincRNA: chr2:150496011-150496503 reverse strand	2,93
2610008E11Rik	RIKEN cDNA 2610008E11 gene	-3,97
Hyi	hydroxypyruvate isomerase homolog (*E. coli*), transcript variant 1	-3,98
Gstt3	glutathione S-transferase, theta 3	-4,14
Olfr464	olfactory receptor 464	-4,30
Mest	mesoderm specific transcript, transcript variant 1	-4,71
Fbln7	fibulin 7	-4,75
Scrn1	secernin 1	-4,88
Hspb1	heat shock protein 1	-4,96
Gm5493	9 days embryo whole body cDNA, RIKEN full-length enriched library, D030063M22 product: weakly similar to Hypothetical KRAB box containing protein (Fragment) [Mus musculus], full insert sequence	-5,12
Mgmt	O-6-methylguanine-DNA methyltransferase	-5,21
Thbd	thrombomodulin	-5,35
Rspo3	R-spondin 3 homolog (*Xenopus laevis*) (Rspo3),	-5,37
ENSMUST00000019268	mRNA for mKIAA0193 protein	-5,63
Mest	mesoderm specific transcript, transcript variant 2	-6,06
Slc17a3	solute carrier family 17 (sodium phosphate), member 3, transcript variant 1	-7,88

Table 6.3. List of top 15 up- and down-regulated genes in cells from F3 *focus*. DEGs are listed in descending order of fold change compared to TPA-treated cell clone.

GeneName	Description	Fold change
Oas1a	2'-5' oligoadenylate synthetase 1A	7,68
Oas1f	2'-5' oligoadenylate synthetase 1F	6,31
Oas2	2'-5' oligoadenylate synthetase 2	6,09
Ifi44	interferon-induced protein 44	5,58
Gm9706	predicted gene 9706	5,54
Sp110	Sp110 nuclear body protein	5,48
Mx1	myxovirus (influenza virus) resistance 1	5,39
Oasl2	2'-5' oligoadenylate synthetase-like 2	5,38
Isg15	ISG15 ubiquitin-like modifier	5,30
H2-K1	histocompatibility 2, K1, K region	5,30
LOC100041034	Sp110 nuclear body protein-like	5,30
Ifi27l2a	interferon, alpha-inducible protein 27 like 2A	5,24
Tgtp2	T cell specific GTPase 2	5,19
Usp18	ubiquitin specific peptidase 18	4,97
Rtp4	receptor transporter protein 4	4,90
Papss2	3'-phosphoadenosine 5'-phosphosulfate synthase 2	-3,20
Mest	mesoderm specific transcript	-3,21
Ppp1r1b	protein phosphatase 1, regulatory (inhibitor) subunit 1B	-3,23
Rpe65	retinal pigment epithelium 65	-3,28
Col11a1	collagen, type XI, alpha 1	-3,37
Speer2	spermatogenesis associated glutamate (E)-rich protein 2	-3,42
1190002H23Rik	RIKEN cDNA 1190002H23 gene	-3,47
Sorl1	sortilin-related receptor, LDLR class A repeats-containing	-3,65
4933402N22Rik	RIKEN cDNA 4933402N22 gene	-3,67
Arxes2	adipocyte-related X-chromosome expressed sequence 2	-3,72
Plxdc2	plexin domain containing 2	-3,82
Pcp4	Purkinje cell protein 4	-4,01
Igf1	insulin-like growth factor 1	-4,54
Fos	FBJ osteosarcoma oncogene	-4,56
Col2a1	collagen, type II, alpha 1	-6,72

Table 6.4. Differentially expressed genes in all cell clones from F1, F2, and F3 *foci*

Gene name	Description	Fold change		
		F1	F2	F3
2810405K02Rik	RIKEN cDNA 2810405K02 gene	-2.94	-2.31	1.27
Arhgap20	Rho GTPase activating protein 20	-2.85	-2.02	-1.32
Ccl2	chemokine (C-C motif) ligand 2	2.41	3.08	2.50
Ccl5	chemokine (C-C motif) ligand 5	2.92	2.45	4.54
Cd302	CD302 antigen	-4.24	-3.89	2.33
Col11a1	collagen, type XI, alpha 1	-4.32	-2.90	-3.37
Col2a1	collagen, type II, alpha 1	-3.24	-2.77	-6.72
Ctgf	connective tissue growth factor	-3.55	-2.66	-1.85
Ctsh	cathepsin H	-4.69	-3.48	1.30
Dner	delta/notch-like EGF-related receptor	-3.76	-2.60	-2.05
Frmd3	FERM domain containing 3	-2.60	-2.31	-2.50
Fxyd6	FXYD domain-containing ion transport regulator 6	-4.07	-3.21	-1.27
Gas6	growth arrest specific 6	-6.20	-2.85	-1.98
Hebp2	heme binding protein 2	-4.54	-2.11	3.18
Hyi	hydroxypyruvate isomerase homolog (*E. coli*)	-4.17	-3.98	-1.26
Il6	interleukin 6	2.39	2.32	3.18
Irak3	interleukin-1 receptor-associated kinase 3	-2.25	-2.13	-1.37
Marcksl1	MARCKS-like 1	2.27	2.19	-1.19
Mest	mesoderm specific transcript	-6.94	-6.06	-3.21
Mgmt	O-6-methylguanine-DNA methyltransferase	-5.53	-5.21	-1.40
Mt2	metallothionein 2	-4.78	-3.12	-1.99
Npy1r	neuropeptide Y receptor Y1	-4.26	-3.92	-1.65
Ntrk2	neurotrophic tyrosine kinase, receptor, type 2	-2.25	-2.27	-1.40
Papss2	3'-phosphoadenosine 5'-phosphosulfate synthase 2	-3.62	-2.79	-3.20
Pcp4	Purkinje cell protein 4	-6.53	-3.63	-4.01
Ppp1r1b	protein phosphatase 1, regulatory (inhibitor) subunit 1B	-3.64	-2.68	-3.23
Prickle1	prickle homolog 1 (*Drosophila*)	-4.46	-2.80	-1.89
Rpe65	retinal pigment epithelium 65	-3.78	-2.45	-3.28
Rspo3	R-spondin 3 homolog (*Xenopus laevis*)	-8.13	-5.37	-2.23
Scrn1	secernin 1	-4.46	-4.88	-1.61
Sfrp2	secreted frizzled-related protein 2	-4.72	-3.64	-2.21
Slc35f1	solute carrier family 35, member F1	-2.54	-2.98	-2.60
Spp1	secreted phosphoprotein 1	3.36	2.97	3.83
Thy1	thymus cell antigen 1, theta	-3.78	2.48	3.28

References

- Aerts, J., Laeremans, A., Minerva, L., Boonen, K., Harshavardhan, B., D'Hooge, R., Valkenborg, D., Baggerman, G., Arckens, L., 2017. MS imaging and mass spectrometric synaptosome profiling identify PEP-19/pcp4 as a synaptic molecule involved in spatial learning in mice. Biochim Biophys Acta Proteins Proteom 1865, 936-945. doi:10.1016/j.bbapap.2016.10.007
- Ao, L., Liu, J.Y., Liu, W.B., Gao, L.H., Hu, R., Fang, Z.J., Zhen, Z.X., Huang, M.H., Yang, M.S., Cao, J., 2010. Comparison of gene expression profiles in BALB/c 3T3 transformed foci exposed to tumor promoting agents. Toxicol In Vitro 24, 430-438. doi:10.1016/j.tiv.2009.10.006
- Argraves, W.S., Tran, H., Burgess, W.H., Dickerson, K., 1990. Fibulin is an extracellular matrix and plasma glycoprotein with repeated domain structure. J Cell Biol 111, 3155-3164.
- Callegaro, G., Forcella, M., Melchioretto, P., Frattini, A., Gribaldo, L., Fusi, P., Fabbri, M., Urani, C., 2018. Toxicogenomics applied to in vitro Cell Transformation Assay reveals mechanisms of early response to cadmium. Toxicol In Vitro 48, 232-243. doi:10.1016/j.tiv.2018.01.025
- Carlow, D.A., Teh, S.J., Teh, H.S., 1998. Specific antiviral activity demonstrated by TGTP, a member of a new family of interferon-induced GTPases. J Immunol 161, 2348-2355.
- Choong, G., Liu, Y., Templeton, D.M., 2014. Interplay of calcium and cadmium in mediating cadmium toxicity. Chem Biol Interact 211, 54-65. doi:10.1016/j.cbi.2014.01.007
- Corvi, R., Madia, F., 2017. In vitro genotoxicity testing-Can the performance be enhanced? Food Chem Toxicol 106, 600-608. doi:10.1016/j.fct.2016.08.024
- Corvi, R., Madia, F., Guyton, K.Z., Kasper, P., Rudel, R., Colacci, A., Kleinjans, J., Jennings, P., 2017. Moving forward in carcinogenicity assessment: Report of an EURL ECVAM/ESTIV workshop. Toxicol In Vitro 45, 278-286. doi:10.1016/j.tiv.2017.09.010
- Coussens, L.M., Werb, Z., 2002. Inflammation and cancer. Nature 420, 860-867. doi:10.1038/nature01322
- de Vega, S., Iwamoto, T., Nakamura, T., Hozumi, K., McKnight, D.A., Fisher, L.W., Fukumoto, S., Yamada, Y., 2007. TM14 is a new member of the fibulin family (fibulin-7) that interacts with extracellular matrix molecules and is active for cell binding. J Biol Chem 282, 30878-30888. doi:10.1074/jbc.M705847200
- de Vega, S., Iwamoto, T., Yamada, Y., 2009. Fibulins: multiple roles in matrix structures and tissue functions. Cell Mol Life Sci 66, 1890-1902. doi:10.1007/s00018-009-8632-6
- Dear, N., Matena, K., Vingron, M., Boehm, T., 1997. A new subfamily of vertebrate calpains lacking a calmodulin-like domain: implications for calpain regulation and evolution. Genomics 45, 175-184. doi:10.1006/geno.1997.4870
- Fischer, M.M., Yeung, V.P., Cattaruzza, F., Hussein, R., Yen, W.C., Murriel, C., Evans, J.W., O'Young, G., Brunner, A.L., Wang, M., Cain, J., Cancilla, B., Kapoun, A., Hoey, T., 2017. RSPO3

antagonism inhibits growth and tumorigenicity in colorectal tumors harboring common Wnt pathway mutations. Sci Rep 7, 15270. doi:10.1038/s41598-017-15704-y

- Forcella, M., Callegaro, G., Melchioretto, P., Gribaldo, L., Frattini, M., Stefanini, F.M., Fusi, P., Urani, C., 2016. Cadmium-transformed cells in the in vitro cell transformation assay reveal different proliferative behaviours and activated pathways. Toxicol In Vitro 36, 71-80. doi:10.1016/j.tiv.2016.07.006
- Furutani, Y., Manabe, R., Tsutsui, K., Yamada, T., Sugimoto, N., Fukuda, S., Kawai, J., Sugiura, N., Kimata, K., Hayashizaki, Y., Sekiguchi, K., 2005. Identification and characterization of photomedins: novel olfactomedin-domain-containing proteins with chondroitin sulphate-E-binding activity. Biochem J 389, 675-684. doi:10.1042/BJ20050120
- Gallagher, W.M., Currid, C.A., Whelan, L.C., 2005. Fibulins and cancer: friend or foe? Trends Mol Med 11, 336-340. doi:10.1016/j.molmed.2005.06.001
- Gentleman, R.C., Carey, V.J., Bates, D.M., Bolstad, B., Dettling, M., Dudoit, S., Ellis, B., Gautier, L., Ge, Y., Gentry, J., Hornik, K., Hothorn, T., Huber, W., Iacus, S., Irizarry, R., Leisch, F., Li, C., Maechler, M., Rossini, A.J., Sawitzki, G., Smith, C., Smyth, G., Tierney, L., Yang, J.Y., Zhang, J., 2004. Bioconductor: open software development for computational biology and bioinformatics. Genome Biol 5, R80. doi:10.1186/gb-2004-5-10-r80
- Geutskens, S.B., Hordijk, P.L., van Hennik, P.B., 2010. The chemorepellent Slit3 promotes monocyte migration. J Immunol 185, 7691-7698. doi:10.4049/jimmunol.0903898
- Gonzalez-Guerra, J.L., Castilla-Cortazar, I., Aguirre, G.A., Munoz, U., Martin-Estal, I., Avila-Gallego, E., Granado, M., Puche, J.E., Garcia-Villalon, A.L., 2017. Partial IGF-1 deficiency is sufficient to reduce heart contractibility, angiotensin II sensibility, and alter gene expression of structural and functional cardiac proteins. PLoS One 12, e0181760. doi:10.1371/journal.pone.0181760
- Gorelik, A., Heinz, L.X., Illes, K., Superti-Furga, G., Nagar, B., 2016. Crystal Structure of the Acid Sphingomyelinase-like Phosphodiesterase SMPDL3B Provides Insights into Determinants of Substrate Specificity. J Biol Chem 291, 24054-24064. doi:10.1074/jbc.M116.755801
- Goudarzi, S., Rivera, A., Butt, A.M., Hafizi, S., 2016. Gas6 Promotes Oligodendrogenesis and Myelination in the Adult Central Nervous System and After Lysolecithin-Induced Demyelination. ASN Neuro 8. doi:10.1177/1759091416668430
- Habuchi, H., Kimata, K., 2010. Mice deficient in heparan sulfate 6-O-sulfotransferase-1. Prog Mol Biol Transl Sci 93, 79-111. doi:10.1016/S1877-1173(10)93005-6
- Hartwig, A., 2013. Cadmium and cancer. Met Ions Life Sci 11, 491-507. doi:10.1007/978-94-007-5179-8_15
- Hilkens, J., Timmer, N.C., Boer, M., Ikink, G.J., Schewe, M., Sacchetti, A., Koppens, M.A.J., Song, J.Y., Bakker, E.R.M., 2017. RSPO3 expands intestinal stem cell and niche compartments and drives tumorigenesis. Gut 66, 1095-1105. doi:10.1136/gutjnl-2016-311606

- Hwang, S.H., Yeom, H., Eom, S.Y., Lee, Y.M., Lee, M., 2019. Genome-wide DNA methylation changes in transformed foci induced by non-genotoxic carcinogens. Environ Mol Mutagen. doi:10.1002/em.22285
- Ibsen, M.S., Gad, H.H., Andersen, L.L., Hornung, V., Julkunen, I., Sarkar, S.N., Hartmann, R., 2015. Structural and functional analysis reveals that human OASL binds dsRNA to enhance RIG-I signaling. Nucleic Acids Res 43, 5236-5248. doi:10.1093/nar/gkv389
- Ichimura, A., Kadowaki, T., Narukawa, K., Togiya, K., Hirasawa, A., Tsujimoto, G., 2008. In silico approach to identify the expression of the undiscovered molecules from microarray public database: identification of odorant receptors expressed in non-olfactory tissues. Naunyn Schmiedebergs Arch Pharmacol 377, 159-165. doi:10.1007/s00210-007-0255-6
- Jarup, L., Akesson, A., 2009. Current status of cadmium as an environmental health problem. Toxicol Appl Pharmacol 238, 201-208. doi:10.1016/j.taap.2009.04.020
- Jozsi, M., Schneider, A.E., Karpati, E., Sandor, N., 2018. Complement factor H family proteins in their non-canonical role as modulators of cellular functions. Semin Cell Dev Biol. doi:10.1016/j.semcdb.2017.12.018
- Kakuta, S., Shibata, S., Iwakura, Y., 2002. Genomic structure of the mouse 2',5'-oligoadenylate synthetase gene family. J Interferon Cytokine Res 22, 981-993. doi:10.1089/10799900260286696
- Kaneko-Ishino, T., Kuroiwa, Y., Miyoshi, N., Kohda, T., Suzuki, R., Yokoyama, M., Viville, S., Barton, S.C., Ishino, F., Surani, M.A., 1995. Peg1/Mest imprinted gene on chromosome 6 identified by cDNA subtraction hybridization. Nat Genet 11, 52-59. doi:10.1038/ng0995-52
- Klenotic, P.A., Munier, F.L., Marmorstein, L.Y., Anand-Apte, B., 2004. Tissue inhibitor of metalloproteinases-3 (TIMP-3) is a binding partner of epithelial growth factor-containing fibulin-like extracellular matrix protein 1 (EFEMP1). Implications for macular degenerations. J Biol Chem 279, 30469-30473. doi:10.1074/jbc.M403026200
- Komander, D., Clague, M.J., Urbe, S., 2009. Breaking the chains: structure and function of the deubiquitinases. Nat Rev Mol Cell Biol 10, 550-563. doi:10.1038/nrm2731
- Kristiansen, H., Gad, H.H., Eskildsen-Larsen, S., Despres, P., Hartmann, R., 2011. The oligoadenylate synthetase family: an ancient protein family with multiple antiviral activities. J Interferon Cytokine Res 31, 41-47. doi:10.1089/jir.2010.0107
- Kwon, S.K., Saindane, M., Baek, K.H., 2017. p53 stability is regulated by diverse deubiquitinating enzymes. Biochim Biophys Acta Rev Cancer 1868, 404-411. doi:10.1016/j.bbcan.2017.08.001
- Lai, K.P., Cheung, A.H.Y., Tse, W.K.F., 2017. Deubiquitinase Usp18 prevents cellular apoptosis from oxidative stress in liver cells. Cell Biol Int 41, 914-921. doi:10.1002/cbin.10799
- Li, B., Shin, J., Lee, K., 2009. Interferon-stimulated gene ISG12b1 inhibits adipogenic differentiation and mitochondrial biogenesis in 3T3-L1 cells. Endocrinology 150, 1217-1224. doi:10.1210/en.2008-0727

- Livak, K.J., Schmittgen, T.D., 2001. Analysis of relative gene expression data using real-time quantitative PCR and the 2(-Delta Delta C(T)) Method. Methods 25, 402-408. doi:10.1006/meth.2001.1262
- Madia, F., Worth, A., Whelan, M., Corvi, R., 2019. Carcinogenicity assessment: Addressing the challenges of cancer and chemicals in the environment. Environ Int 128, 417-429. doi:10.1016/j.envint.2019.04.067
- Malinowski, M., Pietraszek, K., Perreau, C., Boguslawski, M., Decot, V., Stoltz, J.F., Vallar, L., Niewiarowska, J., Cierniewski, C., Maquart, F.X., Wegrowski, Y., Brezillon, S., 2012. Effect of lumican on the migration of human mesenchymal stem cells and endothelial progenitor cells: involvement of matrix metalloproteinase-14. PLoS One 7, e50709. doi:10.1371/journal.pone.0050709
- Mari-Alexandre, J., Diaz-Lagares, A., Villalba, M., Juan, O., Crujeiras, A.B., Calvo, A., Sandoval, J., 2017. Translating cancer epigenomics into the clinic: focus on lung cancer. Transl Res 189, 76-92. doi:10.1016/j.trsl.2017.05.008
- Martelli, A., Rousselet, E., Dycke, C., Bouron, A., Moulis, J.M., 2006. Cadmium toxicity in animal cells by interference with essential metals. Biochimie 88, 1807-1814. doi:10.1016/j.biochi.2006.05.013
- Mashimo, T., Glaser, P., Lucas, M., Simon-Chazottes, D., Ceccaldi, P.E., Montagutelli, X., Despres, P., Guenet, J.L., 2003. Structural and functional genomics and evolutionary relationships in the cluster of genes encoding murine 2',5'-oligoadenylate synthetases. Genomics 82, 537-552.
- Mastronardi, C., Whelan, F., Yildiz, O.A., Hannestad, J., Elashoff, D., McCann, S.M., Licinio, J., Wong, M.L., 2007. Caspase 1 deficiency reduces inflammation-induced brain transcription. Proc Natl Acad Sci U S A 104, 7205-7210. doi:10.1073/pnas.0701366104
- Mayer, W., Hemberger, M., Frank, H.G., Grummer, R., Winterhager, E., Kaufmann, P., Fundele, R., 2000. Expression of the imprinted genes MEST/Mest in human and murine placenta suggests a role in angiogenesis. Dev Dyn 217, 1-10.
- McLaughlin, P.J., Bakall, B., Choi, J., Liu, Z., Sasaki, T., Davis, E.C., Marmorstein, A.D., Marmorstein, L.Y., 2007. Lack of fibulin-3 causes early aging and herniation, but not macular degeneration in mice. Hum Mol Genet 16, 3059-3070. doi:10.1093/hmg/ddm264
- Meplan, C., Verhaegh, G., Richard, M.J., Hainaut, P., 1999. Metal ions as regulators of the conformation and function of the tumour suppressor protein p53: implications for carcinogenesis. Proc Nutr Soc 58, 565-571.
- Miller-Delaney, S.F., Lieberam, I., Murphy, P., Mitchell, K.J., 2011. Plxdc2 is a mitogen for neural progenitors. PLoS One 6, e14565. doi:10.1371/journal.pone.0014565
- Muro, R., Nitta, T., Kitajima, M., Okada, T., Suzuki, H., 2018. Rasal3-mediated T cell survival is essential for inflammatory responses. Biochem Biophys Res Commun 496, 25-30. doi:10.1016/j.bbrc.2017.12.159

- OECD, 2007. Detailed review paper on cell transformation assays for detection of chemical carcinogens. Development, O.f.e.c.-o.a. (Ed). OECD Environment, health and safety publications, 1-164.
- Perelygin, A.A., Zharkikh, A.A., Scherbik, S.V., Brinton, M.A., 2006. The mammalian 2'-5' oligoadenylate synthetase gene family: evidence for concerted evolution of paralogous Oas1 genes in Rodentia and Artiodactyla. J Mol Evol 63, 562-576. doi:10.1007/s00239-006-0073-3
- Pluznick, J.L., Protzko, R.J., Gevorgyan, H., Peterlin, Z., Sipos, A., Han, J., Brunet, I., Wan, L.X., Rey, F., Wang, T., Firestein, S.J., Yanagisawa, M., Gordon, J.I., Eichmann, A., Peti-Peterdi, J., Caplan, M.J., 2013. Olfactory receptor responding to gut microbiota-derived signals plays a role in renin secretion and blood pressure regulation. Proc Natl Acad Sci U S A 110, 4410-4415. doi:10.1073/pnas.1215927110
- Pyakurel, A., Balmer, D., Saba-El-Leil, M.K., Kizilyaprak, C., Daraspe, J., Humbel, B.M., Voisin, L., Le, Y.Z., von Lintig, J., Meloche, S., Roduit, R., 2017. Loss of Extracellular Signal-Regulated Kinase 1/2 in the Retinal Pigment Epithelium Leads to RPE65 Decrease and Retinal Degeneration. Mol Cell Biol 37. doi:10.1128/MCB.00295-17
- Ray, A.K., DuBois, J.C., Gruber, R.C., Guzik, H.M., Gulinello, M.E., Perumal, G., Raine, C., Kozakiewicz, L., Williamson, J., Shafit-Zagardo, B., 2017. Loss of Gas6 and Axl signaling results in extensive axonal damage, motor deficits, prolonged neuroinflammation, and less remyelination following cuprizone exposure. Glia 65, 2051-2069. doi:10.1002/glia.23214
- Ray, P.D., Yosim, A., Fry, R.C., 2014. Incorporating epigenetic data into the risk assessment process for the toxic metals arsenic, cadmium, chromium, lead, and mercury: strategies and challenges. Front Genet 5, 201. doi:10.3389/fgene.2014.00201
- Redmond, T.M., Yu, S., Lee, E., Bok, D., Hamasaki, D., Chen, N., Goletz, P., Ma, J.X., Crouch, R.K., Pfeifer, K., 1998. Rpe65 is necessary for production of 11-cis-vitamin A in the retinal visual cycle. Nat Genet 20, 344-351. doi:10.1038/3813
- Saito, H., Kubota, M., Roberts, R.W., Chi, Q., Matsunami, H., 2004. RTP family members induce functional expression of mammalian odorant receptors. Cell 119, 679-691. doi:10.1016/j.cell.2004.11.021
- Schmidt, V., Schulz, N., Yan, X., Schurmann, A., Kempa, S., Kern, M., Bluher, M., Poy, M.N., Olivecrona, G., Willnow, T.E., 2016. SORLA facilitates insulin receptor signaling in adipocytes and exacerbates obesity. J Clin Invest 126, 2706-2720. doi:10.1172/JCI84708
- Silverman, R.H., Weiss, S.R., 2014. Viral phosphodiesterases that antagonize double-stranded RNA signaling to RNase L by degrading 2-5A. J Interferon Cytokine Res 34, 455-463. doi:10.1089/jir.2014.0007
- Smyth, G.K., 2004. Linear models and empirical bayes methods for assessing differential expression in microarray experiments. Stat Appl Genet Mol Biol 3, Article3. doi:10.2202/1544-6115.1027

- Spiess, A.N., Walther, N., Muller, N., Balvers, M., Hansis, C., Ivell, R., 2003. SPEER--a new family of testis-specific genes from the mouse. Biol Reprod 68, 2044-2054. doi:10.1095/biolreprod.102.011593
- Suarez-Carmona, M., Lesage, J., Cataldo, D., Gilles, C., 2017. EMT and inflammation: inseparable actors of cancer progression. Mol Oncol 11, 805-823. doi:10.1002/1878-0261.12095
- Suzuki, R., Matsumoto, M., Fujikawa, A., Kato, A., Kuboyama, K., Yonehara, K., Shintani, T., Sakuta, H., Noda, M., 2014. SPIG1 negatively regulates BDNF maturation. J Neurosci 34, 3429-3442. doi:10.1523/JNEUROSCI.1597-13.2014
- Tang, L., Qiu, R., Tang, Y., Wang, S., 2014. Cadmium-zinc exchange and their binary relationship in the structure of Zn-related proteins: a mini review. Metallomics 6, 1313-1323. doi:10.1039/c4mt00080c
- Thevenod, F., 2010. Catch me if you can! Novel aspects of cadmium transport in mammalian cells. Biometals 23, 857-875. doi:10.1007/s10534-010-9309-1
- Timpl, R., Sasaki, T., Kostka, G., Chu, M.L., 2003. Fibulins: a versatile family of extracellular matrix proteins. Nat Rev Mol Cell Biol 4, 479-489. doi:10.1038/nrm1130
- Tonami, K., Kurihara, Y., Arima, S., Nishiyama, K., Uchijima, Y., Asano, T., Sorimachi, H., Kurihara, H., 2011. Calpain-6, a microtubule-stabilizing protein, regulates Rac1 activity and cell motility through interaction with GEF-H1. J Cell Sci 124, 1214-1223. doi:10.1242/jcs.072561
- Urani, C., Melchioretto, P., Bruschi, M., Fabbri, M., Sacco, M.G., Gribaldo, L., 2015. Impact of Cadmium on Intracellular Zinc Levels in HepG2 Cells: Quantitative Evaluations and Molecular Effects. Biomed Res Int 2015, 949514. doi:10.1155/2015/949514
- Urani, C., Stefanini, F.M., Bussinelli, L., Melchioretto, P., Crosta, G.F., 2009. Image analysis and automatic classification of transformed foci. J Microsc 234, 269-279. doi:10.1111/j.1365-2818.2009.03171.x
- Vakilian, A., Khorramdelazad, H., Heidari, P., Sheikh Rezaei, Z., Hassanshahi, G., 2017. CCL2/CCR2 signaling pathway in glioblastoma multiforme. Neurochem Int 103, 1-7. doi:10.1016/j.neuint.2016.12.013
- Vanparys, P., Corvi, R., Aardema, M.J., Gribaldo, L., Hayashi, M., Hoffmann, S., Schechtman, L., 2012. Application of in vitro cell transformation assays in regulatory toxicology for pharmaceuticals, chemicals, food products and cosmetics. Mutat Res 744, 111-116. doi:10.1016/j.mrgentox.2012.02.001
- Virani, S., Rentschler, K.M., Nishijo, M., Ruangyuttikarn, W., Swaddiwudhipong, W., Basu, N., Rozek, L.S., 2016. DNA methylation is differentially associated with environmental cadmium exposure based on sex and smoking status. Chemosphere 145, 284-290. doi:10.1016/j.chemosphere.2015.10.123

- Volpe, M., Shpungin, S., Barbi, C., Abrham, G., Malovani, H., Wides, R., Nir, U., 2006. trnp: A conserved mammalian gene encoding a nuclear protein that accelerates cell-cycle progression. DNA Cell Biol 25, 331-339. doi:10.1089/dna.2006.25.331
- Vukovic, J., Marmorstein, L.Y., McLaughlin, P.J., Sasaki, T., Plant, G.W., Harvey, A.R., Ruitenberg, M.J., 2009. Lack of fibulin-3 alters regenerative tissue responses in the primary olfactory pathway. Matrix Biol 28, 406-415. doi:10.1016/j.matbio.2009.06.001
- Wang, J., Duncan, D., Shi, Z., Zhang, B., 2013. WEB-based GEne SeT AnaLysis Toolkit (WebGestalt): update 2013. Nucleic Acids Res 41, W77-83. doi:10.1093/nar/gkt439
- Way, G., Morrice, N., Smythe, C., O'Sullivan, A.J., 2002. Purification and identification of secernin, a novel cytosolic protein that regulates exocytosis in mast cells. Mol Biol Cell 13, 3344-3354. doi:10.1091/mbc.e01-10-0094
- Wilde, E.C., Chapman, K.E., Stannard, L.M., Seager, A.L., Brusehafer, K., Shah, U.K., Tonkin, J.A., Brown, M.R., Verma, J.R., Doherty, A.T., Johnson, G.E., Doak, S.H., Jenkins, G.J.S., 2018. A novel, integrated in vitro carcinogenicity test to identify genotoxic and non-genotoxic carcinogens using human lymphoblastoid cells. Arch Toxicol 92, 935-951. doi:10.1007/s00204-017-2102-y
- Wolter, J., Schild, L., Bock, F., Hellwig, A., Gadi, I., Al-Dabet, M.M., Ranjan, S., Ronicke, R., Nawroth, P.P., Petersen, K.U., Mawrin, C., Shahzad, K., Isermann, B., 2016. Thrombomodulin-dependent protein C activation is required for mitochondrial function and myelination in the central nervous system. J Thromb Haemost 14, 2212-2226. doi:10.1111/jth.13494
- Yoshimura, T., 2018. The chemokine MCP-1 (CCL2) in the host interaction with cancer: a foe or ally? Cell Mol Immunol 15, 335-345. doi:10.1038/cmi.2017.135
- Zhang, H., Kho, A.T., Wu, Q., Halayko, A.J., Limbert Rempel, K., Chase, R.P., Sweezey, N.B., Weiss, S.T., Kaplan, F., 2016. CRISPLD2 (LGL1) inhibits proinflammatory mediators in human fetal, adult, and COPD lung fibroblasts and epithelial cells. Physiol Rep 4. doi:10.14814/phy2.12942
- Zhang, R., Pan, X., Huang, Z., Weber, G.F., Zhang, G., 2011. Osteopontin enhances the expression and activity of MMP-2 via the SDF-1/CXCR4 axis in hepatocellular carcinoma cell lines. PLoS One 6, e23831. doi:10.1371/journal.pone.0023831
- Zhao, H., Chen, Q., Alam, A., Cui, J., Suen, K.C., Soo, A.P., Eguchi, S., Gu, J., Ma, D., 2018. The role of osteopontin in the progression of solid organ tumour. Cell Death Dis 9, 356. doi:10.1038/s41419-018-0391-6

Chapter 7

"Low doses of cadmium elicit alterations in mitochondrial morphology and functionality."

ABSTRACT

Background: *Cadmium is a widespread contaminant and a recognized carcinogen. We previously showed that the administration of low cadmium doses for 24hr treatment to healthy C3H10T1/2Cl8 cells at the beginning of Cell Transformation Assay (CTA), up regulates genes involved in metal scavenging and antioxidant defense, like metallothioneines, Glutathione S-transferases and heat shock proteins. Still, although most cells thrive normally in the following weeks, malignant transformation is triggered by cadmium and leads to foci appearance at the end of the CTA. In this work we aim at elucidating the early metabolic deregulation induced by cadmium, underlying healthy cell transformation into malignant cells.*

Methods: *respiratory metabolism was investigated through Seahorse Agilent assays in different conditions, while oxidative stress level was assessed through fluorescent probes; DNA damage was evaluated by Comet assay and mitochondrial morphology was analyzed in confocal microscopy.*

Results: *Results show that although initial response to cadmium is effective in balancing oxidative stress, through mitochondria rearrangement, SOD1 activity is inhibited, leading to increased O_2^- level, which in turn causes DNA strand breaks. From the metabolic point of view, cells increase their glycolytic flux, although all extra NADH produced is still efficiently reoxidized by mitochondria.*

Conclusions: *Our results confirm previously shown response against cadmium toxicity; new data about glycolytic increase and mitochondrial rearrangements suggests pathways leading to cell transformation.*

General significance: *in this work we exploit the widely used, well known CTA, which allows following healthy cells transformation into a malignant phenotype, to understand early events in cadmium-induced carcinogenesis.*

Monica Oldani, Marta Manzoni, Anna M. Villa, Federico Stefanini, Pasquale Melchioretto, Eugenio Monti, Chiara Urani, Paola Fusi, and Matilde Forcella

This chapter is an extract of the submitted paper in Biochimica et Biophysica Acta (BBA), 2019

❖ 7.1. Introduction

Cadmium (Cd) is a toxic heavy metal, normally present in the atmosphere, as a result of gradual erosion and abrasion of rocks and soils [1]. However, since industrialization, it is being massively released into the environment by anthropogenic activities, such as the manufacturing of pigments, stabilizers, alloys, electronic compounds, and especially of rechargeable nickel-cadmium batteries [2].

Human intoxication can take place through inhalation, absorption and ingestion of contaminated water, food and air particles. Apart from professional contact, one of the most widespread routes of exposure is cigarette smoke [3] which contains high amounts of Cd, due to the natural bioaccumulation in tobacco plants. In heavy metal polluted soils, a class of rare plants, called hyper accumulators, are able to accumulate exceptionally high concentrations of trace elements, like Cd, in their aerial parts without visible toxicity symptoms [4] .

Acute intoxication causes injuries to the testes, liver and lungs [5], while chronic exposure leads to obstructive airway diseases, emphysema, end-stage renal failures, diabetes and renal complications, deregulated blood pressure, bone disorders and immunosuppression [2] [6]. Therefore, Cd release into the environment, at a current rate of 30000 tons per year, represents a serious threat to human health.

Cadmium is also a group I carcinogen, recognized by the International Agency for Research on Cancer [7]. Its oncogenic potential can be assessed through the *in vitro* Cell Transformation Assay (CTA), a valuable tool for carcinogenicity evaluation and mechanistic studies in fundamental research and in regulatory context, in an integrated approach to testing and assessment [8]. Despite many studies on Cd toxicity, its pathogenic mechanism leading to cancer is still not fully elucidated. Cd similarity to zinc (Zn) has led to propose a “Trojan horse” mechanism of toxicity, in which Cd could enter the cells through Zn transporters and potentially substitute this essential metal in the nearly 3800 different Zn proteins in living cells.

Aging and many diseases including cancer, are related to malfunctioning of mitochondria [9]. These are dynamic organelles with highly variable shape and size, existing as large networks or as discrete organelles according to the predominance within the cell of either fusion or fission [10] [11]. Cells with a

high fusion to fission ratio contain few highly interconnected long shaped mitochondria [12]; conversely, cells with a low fusion to fission ratio have numerous fragmented mitochondria appearing as small spheres and/or short rods [11]. Metals, like manganese, iron, copper, and zinc play essential roles as cofactors in mitochondria, helping mitochondrial proteins functions in processes such as electron transfer and enzymatic catalysis. Since the overall concentration of metal ions in mitochondria is finely regulated by metallochaperones and metal transporters [13], any imbalance in metal homeostasis can lead to mitochondrial function impairment. In particular, an increase in Zn cytoplasmic concentration has been shown to impair tricarboxylic acid cycle through alpha-ketoglutarate dehydrogenase inhibition [14]. Moreover, redox-inactive Zn(II) hampers the proton transfer to ubiquinone and the proton translocation across the inner mitochondrial membrane by blocking the proton channels in complex I [15].

Mitochondria are the key intracellular targets for different stressors including Cd [16], but the mechanisms of metal-induced mitochondrial damage are still not fully understood. Moreover, cadmium has previously been shown to trigger ROS production at the mitochondrial level and eventually lead to cell death, caused by severe mitochondrial dysfunction, [17] [18].

In a previous work [19] we have used the CTA as a tool to study the pathogenetic mechanisms underlying Cd carcinogenicity, through a toxicogenomics approach. Exposure of C3H10T1/2Cl8 cells to Cd at non-cytotoxic concentrations ($<IC_{50}$) for 24 hours switched a series of detoxifying mechanisms such as up-regulation of metallothioneins, scavenging glutathione S-transferase (GSTα) and different members of the heat shock proteins (HSPs) family. However, although the cells seem to thrive healthily in the following recovery weeks of culture, after 4-6 weeks colonies of transformed cells (*foci*) inevitably appear, thus showing that Cd injuries were also present in apparently healthy cells.

In the search of mechanisms accounting for the biological effects leading to foci formation, we turned to early events triggered by Cd and in particular we focused on mitochondria as possible targets. In this study, we investigate the effect of 24 hours Cd administration to C3H10T1/2Cl8 healthy cells. We chose C3H cells since they are used in the widely accepted *in vitro* CTA for chemical carcinogenesis assessment. Cadmium was administered for 24

hours in order to observe early effects and at low doses to mimic chronic exposure, which is closer to the conditions of human exposure to environmental contaminants. Cadmium was added to cultured cells at 1 μM $CdCl_2$ concentration, which had previously been established to induce cell transformation and foci generation [20]. However, experiments were also performed with 4 μM $CdCl_2$, in order to assess whether some effects, which were repeatedly observed at 1 μM but without statistical significance, were actually caused by Cd administration. Moreover, $CdCl_2$ supplementation for 24 hours allowed comparison of the observed metabolic effects with data of a previous toxicogenomics study [19].

Our aim is the identification of early key events running in the powerhouses of the cells, triggering the carcinogenic transformation of the few cells that escape the multiple defense mechanisms.

❖ 7.2. Materials and methods

7.2.1 Cell and culture conditions

The experiments were performed using contact-sensitive C3H10T1/2 clone 8 (C3H from here on) mouse embryonic fibroblasts (cell line ATCC, CCL 226 lot. n. 58078542). These cells were chosen for their high sensitivity to carcinogenic compounds, their low spontaneous transformation rates, and the fact that are among the cell lines suggested to perform the Cell Transformation Assays [21]. Cells were stored in ampoules, frozen at –80 °C with 10% sterile DMSO as preservative. Cells were cultured in Basal Medium Eagle (BME, Sigma Chemical Co., St. Louis, MO) enriched with 10% heat-inactivated fetal bovine serum (FBS, EuroClone, Pero, Italy), 1% glutamine, 0.5% HEPES 2M and 25 µg/mL gentamicin (all from Sigma) at 37 °C in a humidified incubator supplied with a constant flow of 5% CO2 in air throughout each experiment. Cells were routinely seeded in 100 mm Ø Petri dishes, the medium was changed every 3 days and cells grown until 80% confluence maximum was reached.

7.2.2 Detection of Intracellular Reactive Oxygen Species (ROS)

The generation of intracellular reactive oxygen species (ROS) was detected by the oxidation of 2',7'-Dichlorofluorescin diacetate (H_2DCFDA) or Dihydroethidium (DHE). H_2DCFDA is an indicator for both reactive oxygen species and nitric oxide (•NO); the second probe measures the level of cytosolic superoxide anion (O^2-). The cells were plated at a density of 2.5 x 10^5 cells per well into six-well plates in complete culture medium. The day after the seeding, the cells were exposed to 1 or 4 µM $CdCl_2$ for 24 hours, by changing the normal medium with a medium enriched with $CdCl_2$. At the end of the treatment, cells were incubated with H_2DCFDA (5 µM final concentration in PBS) or DHE (10 µM final concentration in complete medium) for 20 min in the dark at 37 °C. At the end of incubation, cells were washed by warm PBS, trypsinized (500 µl of trypsin /well) and harvested by centrifugation (5 min at 2000 g) at room temperature. The pellet was resuspended in 500 µl/tube of PBD and ROS generation of 10.000 cells was measured by the fluorescence intensity. FL-1 channel (530 nm) was utilized

to detect the fluorescence intensity of DCF; DHE fluorescence can be measured at 585 nm, or FL-2 channel, band-pass filter. Logarithmic amplification was used to detect probe fluorescence. Flowcytometric data were analyzed using CytExpert 2.3 Software (Beckman Coulter, Inc.).

7.2.3 Enzymatic assays

For enzymatic assay sample preparation, the cells were seeded at 1×10^6 cells/100 mm dish and 24 hours after seeding were exposed to 1 or 4 µM $CdCl_2$ for 24 hours, by changing the medium with a $CdCl_2$ enriched medium. The $CdCl_2$ stock solution (1 mM, 97% purity BDH Laboratory, Milan, Italy) was prepared in ultra-pure water (0.22 µm filtered Milli-Q water, Millipore, Vimodrone, Milan, Italy) and stored at 4 °C. Previous experiments performed by our group [22] [20] demonstrated that 1 µM $CdCl_2$ is able to induce the formation of transformed colonies of cancerous cells (*foci*) in the Cell Transformation Assay. Cells were then rinsed with ice-cold PBS and lysed in 50 mM Tris/HCl 50, pH 7.4, 150 mM NaCl, 5 mM EDTA, 10 % glycerol, 1 % NP40 buffer, containing protease inhibitors and 1mM PMSF. After lysis on ice, homogenates were obtained by passing the cells 5 times through a blunt 20-gauge needle fitted to a syringe and then centrifuging at 15,000 g for 30 min at 4°C. The resulting supernatant was used to measure enzymatic activities. Enzymes were assayed using the following procedures. Lactate dehydrogenase (LDH) and gliceraldeide-3-phosphate dehydrogenase (GAPDH) were assayed according to [23] (1974); catalase (CAT) was assayed according to [24], using 12 mM H_2O_2 as substrate; glutathione-S-transferase (GST) as reported in Habig et al. [25]; glutathione peroxidase according to [26]; glutathione reductase according to Wang [27]. For superoxide dismutase1 (SOD1) cells were rinsed with ice-cold PBS and lysed in PBS, containing protease inhibitors and 1mM PMSF. After lysis on ice, homogenates were obtained by passing the cells 5 times through a blunt 20-gauge needle fitted to a syringe, incubating on ice for 15 min and sonicating 2 times (10 s cycle). The supernatant was obtained by centrifugation at 15,000 g for 10 min at 4°C and used to measure enzymatic activities according to [28]. All assays were performed in triplicate at 30 °C in a Cary3 Spectrophotometer and analyzed by the Cary Win UV application software

for Windows. Activity was expressed in international units and referred to protein concentration as determined by the Bradford method [29].

7.2.4 Glutathione detection

Cells were plated at a density of 1 x 10^6 cells/100 mm dish in complete culture medium. The day after seeding, the cells were exposed to 1 or 4 µM $CdCl_2$ for 24 hours, by changing the normal medium with a $CdCl_2$ enriched medium. At the end of the treatment, the cells were trypsinized and harvested by centrifugation at room temperature, for 10 min at 1200 g. The pellet was resuspended in 3 mL PBS, harvested by a centrifugation in the above conditions and weighted. Pellets were resuspended in 500 µl cold 5% 5-sulfosalicylic acid (SSA), lysed by vortexing and by passing 5 times through a blunt 20-gauge needle fitted to a syringe. All the samples were incubated for 10 minutes at 4 °C and then centrifuged at 14.000 g for 10 minutes at 4 °C. The supernatant was used for the analysis following the instructions of Glutathione Colorimetric Detection Kit (Invitrogen). The Kit is designed to measure oxidized glutathione (GSSG), total glutathione (GSH tot) and reduced glutathione (GSH tot – GSSG) concentrations. Therefore, it was possible to obtain GSH/GSSG ratio, a critical indicator of cell health. The absorbance was measured at 405 nm using a micro plate reader. The values of absorbance were compared to standard curves (GSH tot and GSSG, respectively) and normalized to mg of cells. Final concentrations were expressed in nmol/mg cells.

7.2.5 Comet Assay

Single Cell gel electrophoresis (SCGE) or Comet assay is a microgel electrophoresis technique to assess DNA damage at single cells level. The protocol under alkaline conditions (pH >13) allows to measure single and double-strand breaks, incomplete repair sites and alkali-labile sites. The procedure started with the degreasing of microscope slides and the preparation of 0.65% w/v normal melting point (NMPA) and 0.5% w/v low melting point agarose (LMPA) in PBS. A minimum of two slides must be prepared and maintained at 4°C for every single sample in each experiment

and pre-coated with NMPA the day before the experiments. The cells were seeded at a density of 1,65 x 10^5 cells/100 mm dish in complete culture medium. The day after seeding, the cells were exposed to 1 or 4 µM $CdCl_2$ for 24 hours. At the end of the treatment, the cells were trypsinized and harvested by centrifugation for 10 minutes at 1200 g at room temperature. Pellets were resuspended in 900 µl LMPA and 100 µl of this suspension was dropped on the solidified NMPA. A cover slip was placed over the gel and the slides solidified at 4°C for 10-15 min. The procedure was repeated with another layer of LMPA. Subsequently, in a darkroom, the cover slips were removed and the slides were covered with a cold lysis solution (2.5 M NaCl, 100mM Na2EDTA, 10mM Tris/HCl, 300 mM NaOH, 1% Triton and 10% DMSO at pH 10) for 1 hour, placing them in the electrophoresis system. The slides were dipped in cold alkaline buffer (300 mM of NaOH and 1mM of EDTA) for 15 min in order to unwind DNA strands. Electrophoresis was carried out for 15 min at 0.8 V/cm. The slides were treated with neutralizing buffer (400 mM Tris/HCl pH 7.5) for 10 min; 20 µL of DAPI staining solution were dropped on the slides. Alongside each experiment, cells treated with 50 µM H_2O_2 for 30 minutes were considered as positive control. Three biological replicates were performed. To visualize the stained slides, a Zeiss fluorescent microscope equipped with an excitation filter of 515-560 nm, with a barrier filter of 590 nm and a magnification of 200X, was used. About 30 cells for each treatment and for controls were analyzed with the Comet Imager 1.2.14 (MetaSystems) program. Four parameters were measured, as indicative of DNA damage: Tail Length (TL), %Tail DNA, Tail Moment (TM) and Olive Tail Moment (OTM) [30]. TL and %Tail DNA are able to quantify the extent of DNA damage; while TM, or rather OTM are considered to be particularly useful in describing heterogeneity within a cell population, as OTM can emphasize variations in DNA distribution within the tail.

7.2.6 Oxygen consumption rate and extra-cellular acidification rate measurements

Oxygen consumption rate (OCR) and extra-cellular acidification rate (ECAR) were measured in adherent C3H fibroblasts with Seahorse XFe24 Analyzer (Seahorse Bioscience, Billerica, MA, USA) using Seahorse XF Cell Mito Stress Test Kit and Agilent Seahorse XF Glycolytic Rate Assay Kit. The cells were seeded in Agilent Seahorse XF24 cell culture microplates at density of 30 × 10^3 cells/well in 250 µL of Basal Medium Eagle and 24 hours after seeding were exposed to 1 or 4 µM CdCl2 for 24 hours.

The day of the assay the growth medium was replaced with 525 µl/well of Seahorse XF Base Medium containing 1 mM pyruvate, 2 mM glutamine and 10 mM glucose for the Cell Mito Stress Test Kit or 1 mM pyruvate, 2 mM glutamine, 10 mM glucose and 5 mM Hepes for the Glycolytic Rate Assay Kit. Then the plate was incubated into 37°C non-CO_2 incubator for 1 h, before starting the experiment procedure.

The sensor cartridge was calibrated by Seahorse XFe24 Analyzer. Pre-warmed Oligomycin, FCCP, Rotenone and Antimycin A were loaded into injector ports A, B and C of sensor cartridge, to reach working concentration of 1 µM, 2 µM and 0.5 µM respectively, for the Cell Mito Stress Test Kit. Pre-warmed Rotenone and Antimycin A and 2-deoxy-D-glucose (2-DG) were loaded into injector ports A and B of sensor cartridge, to reach working concentration of 0.5 µM and 50 mM for the Glycolytic Rate Assay Kit.

OCR and ECAR were detected under basal conditions followed by the sequential addition of the drugs, to measure non-mitochondrial respiration, maximal respiration, proton leak, ATP respiration, respiratory capacity, coupling efficiency for the Cell Mito Stress Test Kit and basal glycolysis, basal proton efflux rate, compensatory glycolysis and post 2-DG acidification for the Glycolytic Rate Assay Kit.

7.2.7 Mitochondrial transmembrane potential (MTP) assay

MTP alterations were assessed flowcytometrically, using the potentially sensitive dye 3,3' -dihexyloxacarbocyanine Iodide. The cells were plated at a density of 2.5 x 10^5 cells per well into six-well plates in complete culture medium. The day after the seeding, the cells were exposed to 1 or 4 µM $CdCl_2$ for 24 hours, by changing the normal medium with a medium enriched with $CdCl_2$. At the end of the treatment the cells were harvested by centrifugation (5 min at 2000 g) at room temperature and stained with DiOC6 (40 nM in PBS, 20 min at 37 °C and 5% CO_2 in the dark). Loss in DiOC6 fluorescence indicates disruption of the mitochondrial inner transmembrane potential. The probe was excited at 488 nm and emission was measured through a 530 nm (FL-1 channel) band-pass filter. Logarithmic amplification was used to detect the fluorescence of the probe. Flowcytometric data were analyzed using CytExpert 2.3 Software (Beckman Coulter, Inc.).

7.2.8 Confocal microscopy

Mitochondria fluorescence was studied by laser scanning confocal microscopy, using a Bio-Rad MRC-600 confocal microscope equipped with a 25mW argon laser (Bio-Rad, Hemel Hempstead, UK). The scanning head was coupled with an upright epifluorescence microscope Nikon Optiphot-2 (Nikon, Tokyo, Japan) with a 60x oil immersion objective Nikon Planapochromat (N.A. = 1.4). The fluorescence was excited at 488 nm and the emission collected through a long pass filter above 515 nm. High sensitivity photon counting detection was used to minimize the excitation power (0.1mW at the entry of the optical head) and preserve cell viability.
Cells were plated in 35mm Petri dishes at a density of 6 x 10^4 cells and left to grow for 24 hours in culture medium. Then $CdCl_2$ was added to the medium to a final concentration of 1 or 4 µM $CdCl_2$. After 24 hours, the medium was removed, cells were washed twice with phosphate buffer saline (PBS) and incubated for 10 min in 1 µM Rhodamine 123 (R123) solution at 37 °C and 5% CO_2. After incubation, the cells were rinsed twice with PBS and few microliters of PBS were left in the Petri dish to avoid cell drying. A coverslip was placed over the cells that were immediately imaged by confocal microscope.

7.2.9 Images analysis

Original confocal microscope images in a TIFF format were imported into R after loading the EBimage R package [31]. We developed original R code using the EBimage application programming interface to segment each image into a number of regions of interests (ROIs), where a ROI refers to a cell nucleus and its surrounding regions populated by mitochondria. If two ROIs overlapped then they were excluded, together with their nuclei, from the analysis. Grey levels were normalized after estimating the average background by collecting pixel intensities well outside ROIs. At the end of the procedure, distances of each pixel from the center of the cell nucleus within each ROI were also stored (measurement unit: number of pixels) for further analysis. The algorithm produced a PDF file for each processed image in which every intermediate image was stored to allow visual inspection of each processing step. All elaborations were performed using the R software and the following packages: ggplot2, EBimage, coin, RVAideMemoire [32-35] [31].
The average distance of pixels (ADP) from nucleus was calculated for each ROI in three different experimental conditions: control cells, CdCl2 1 µM, CdCl2 4 µM. Statistical tests were performed to evaluate changes in the distribution of ADP under the three experimental conditions.

7.2.10 Statistical analysis

The distributions of ADP obtained from confocal microscope images under CD treatment were compared to the control treatment using the Kolgomorov-Smirnov nonparametric test [36]. The hypotheses were refined by Mood's median test for the equality of medians.
In all other experiments, samples were compared to their reference controls and the data were tested by Dunnett multiple comparison procedure. All calculations were conducted using the R software environment for statistical computing and graphics [32].

❖ 7.3. Results

7.3.1 Cadmium treatment increases the production of superoxide anion

Previous reports of cadmium mediated increase in cellular reactive oxygen species (ROS) production [17] prompted us to evaluate ROS content in Cd treated healthy C3H cells. Total cytoplasmic ROS were evaluated with cytoflex, using H_2DCFDA fluorescent probe, while superoxide anion (O^2-) was assessed through DHE fluorescent probe. Measurements of DCF fluorescence, reported in Fig. 7.1 showed that the overall ROS production decreased following $CdCl_2$ administration and that this reduction is more evident in cells treated with 4µM $CdCl_2$ (p value < 0.01) than in cells treated with 1 µM $CdCl_2$. On the other hand, DHE fluorescence was found higher in cells treated with 4 µM $CdCl_2$ (p value < 0.05), showing that this metal induces a remarkable increase in the production of superoxide anion (Fig. 7.2).

The activity of the enzymes involved in keeping oxidative stress under control was also assayed. Fig. 7.3A shows the results of activity assays of Glutathione-S-transferase (GST), Glutathione reductase (GR), Glutathione peroxidase (GPox), catalase (CAT) and superoxide dismutase 1 (SOD1). While both GST and GR activities were found to increase significantly upon treatment with 4 µM $CdCl_2$, catalase activity was found to be reduced following the same treatment. Interestingly, SOD1 activity was diminished following treatment with both 1 and 4 µM $CdCl_2$, thus likely accounting for the increase in superoxide anion concentration. The increase in GR and GST was paralleled by an increase in total cell glutathione in 4 µM $CdCl_2$ treated samples, as shown in Fig. 7.3B. However, the ratio between oxidized (GSSG) and reduced glutathione (GSH) remained constant in all conditions.

Figure 7.1. Flowcytometric analysis of cadmium–induced ROS production in C3H cells. A) Cells are exposed to 1 or 4 µM of cadmium chloride for 24 hours. After the treatment, cells are incubated with 5 µM H_2DCFDA and the level of fluorescence of treated-cells is compared to the controls. The results are shown in a dot plot overlay. The dot plot is representative of three independent experiments. B) The fluorescence intensity of all experiments is represented by a box plot. The dark line within a box represents the median value, while the upper and lower sides of a box are the third and first quartiles, respectively. Statistically significant Cd 4µM vs CTR: ** $p < 0.01$ (Dunnett's test).

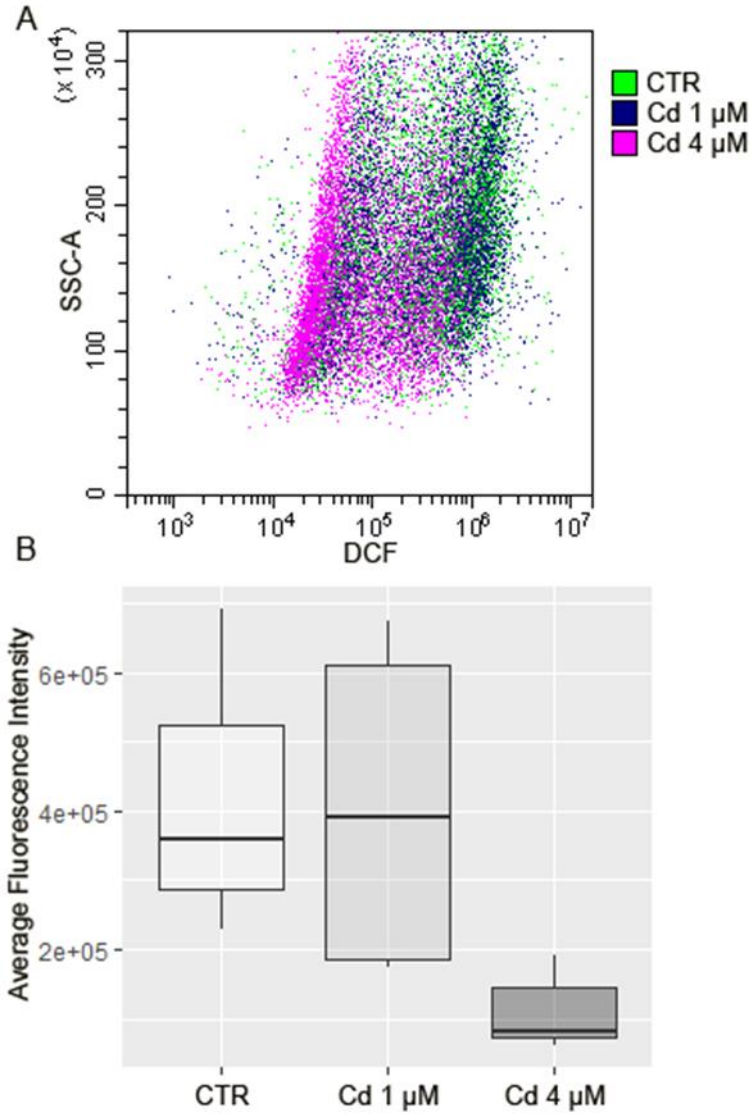

Figure 7.2. Flowcytometric analysis of cadmium–induced superoxide anion production in C3H cells. A) Cells are exposed to 1 or 4 µM of cadmium chloride for 24 hours. After the treatment, cells are incubated with 10 µM DHE and the level of fluorescence of treated-cells is compared to the controls. The results are shown in a dot plot overlay. The dot plot is representative of three independent experiments. B) The dark line within a box represents the median value, while the upper and lower sides of a box are the third and first quartiles, respectively. Statistically significant Cd 4µM vs CTR: * $p < 0.05$ (Dunnett's test).

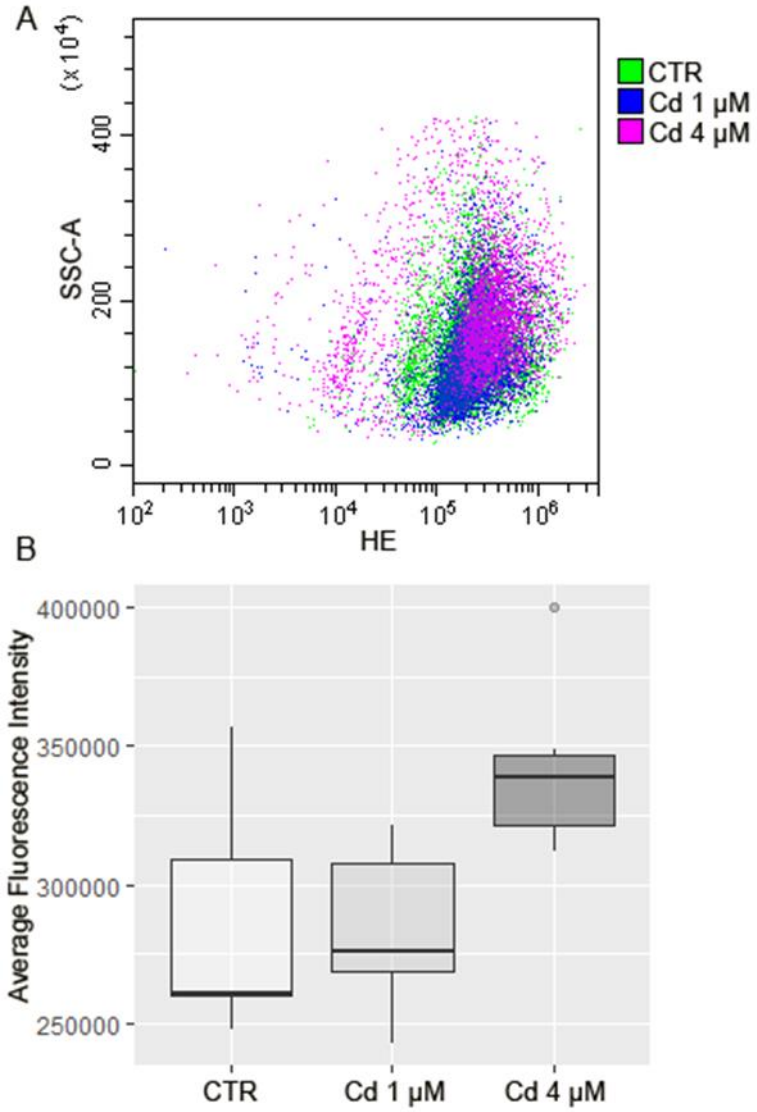

Figure 7.3. A) Enzymatic analysis in C3H cells exposed to 1 µM or 4 µM of cadmium chloride for 24 hours. The results are expressed as fold respect to untreated controls and are shown as mean ± SEM from three independent experiments. B) Glutathione level in C3H cells exposed to 1 µM or 4 µM of cadmium chloride for 24 hours. The results are expressed in µM and normalized respect to mg of cells. Statistically significant: * $p < 0.05$, ** $p < 0.01$, (Dunnett's test).

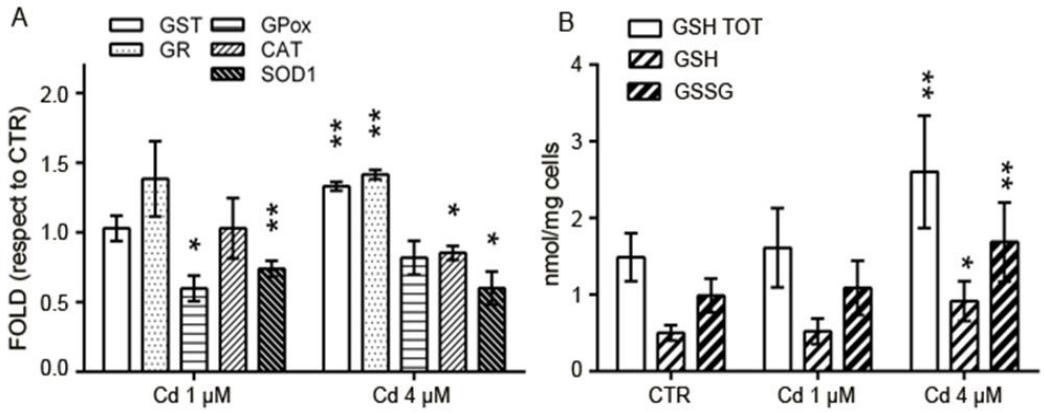

7.3.2 Comet assay reveals damage to nuclear DNA upon cadmium treatment

Although Cd is a non-genotoxic metal, it has been reported to damage DNA in an indirect way, through ROS production [37]. O^2- is recognized as the most effective ROS in inducing DNA damage, as well as the only ROS overproduced in our $CdCl_2$-treated cells; this prompted us to evaluate cadmium effect on nuclear DNA by Comet assay. Microscopy results obtained after treatment with 1 or 4 µM $CdCl_2$ for 24 hours are shown in Fig. 7.4. DNA integrity from untreated control cells appears as a sun (Fig. 7. 4A, left), while DNA of cells treated with 4 µM $CdCl_2$ appear as a comet (Fig. 7.4A, right), with DNA fragments in the so called tail region of the comet. Image analysis (Fig. 7.4B) showed that both the tail length and the percent DNA in tail were significantly increased in cells treated with cadmium. In particular, the first value increases fourfold after 4 µM $CdCl_2$ treatment while the percent DNA in tail gets triple respect to control cells. The lowest cadmium concentration shows all parameters comparable to those of

controls, thus revealing non-significant DNA damage. H_2O_2 treated cells, as expected by this positive control, show highly statistical values ($p<0.001$ Dunnett's test) of all parameters analyzed indicative of an extended DNA damage.

Figure 7.4. COMET assay for DNA damage evaluation in C3H cells exposed to 1 µM or 4 µM of cadmium chloride for 24 hours. A) Image of a sun (on the left) corresponding to typical undamaged control cells, and of a comet (on the right), stained with DAPI and detected by fluorescent microscopy. B) Analysis of different parameters for DNA damage quantification. Bars indicate the mean ± SEM of parameters in thirty cells analyzed for each sample condition, representative of three independent experiments. Statistically significant: * $p < 0.05$, *** $p < 0.001$ (Dunnett's test).

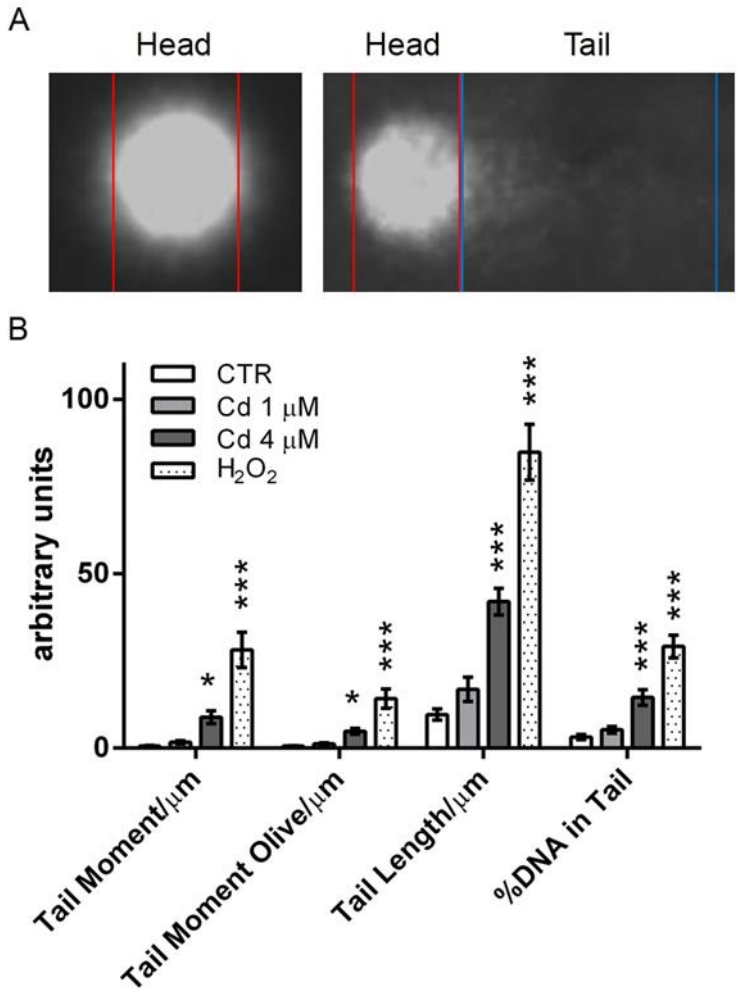

7.3.3 Mitochondria of cadmium treated cells show altered metabolism, with increased membrane potential

Respiratory metabolism was investigated measuring oxygen consumption rate (OCR), basal respiration, spare respiratory capacity, ATP synthesis and extracellular acidification rate (ECAR), through Agilent Seahorse analyses. Results are shown in Fig. 7.5: treatment with cadmium increased both basal respiration and spare respiratory capacity, although both parameters were found significantly increased only after treatment with 4 µM $CdCl_2$ (Fig. 7.5A, B and C). Moreover, the increase in spare respiratory capacity following 4 µM $CdCl_2$ treatment far exceeded the increase in basal respiration, suggesting a higher availability of oxidable substrates. ATP production (Fig. 7.5C) was also increased upon treatment with $CdCl_2$, although to a significant extent only in cells treated with 4 µM $CdCl_2$. ECAR measurement (Fig. 7.5D) revealed that cells treated with 4 µM $CdCl_2$ showed a higher level of acidification during basal respiration, which was not affected by ATPase inhibition. Since both treated and untreated cells showed fully coupled mitochondria (Fig. 7.5E), this stronger acidification seems to be due to glycolysis rather than to CO_2 produced by oxidative phosphorylation. Fig. 7.5D also shows that ECAR increase upon FCCP addition and mitochondria uncoupling was much higher 4 µM $CdCl_2$ treated cells than in untreated cells, again suggesting that it may be due to increased glycolysis. Moreover, after rotenone addition and electron transport inhibition, ECAR did not decrease to untreated cells level, confirming a substantial contribute of glycolysis. Moreover, all these rearrangements in oxidative phosphorylation were found perfectly reversible (data not shown) upon cadmium removal, after a period of recovery of 24 hours.

In accordance with Seahorse results, $\Delta\psi$ measured with cytoflex using DiOC6 fluorescent probe, was found to be increased (more negative) in cadmium treated cells. As shown in Fig. 7.6, cells treated with 1 µM $CdCl_2$ showed increased DiOC6 fluorescence, indicative of a more negative $\Delta\psi$ increase that was even more marked in cells treated with 4 µM $CdCl_2$ (p value < 0.05).

Figure 7.5. Seahorse mitostress analysis in C3H cells exposed to 1 µM or 4 µM of cadmium chloride for 24 hours. A) OCR traces, expressed as pmoles O2/min/mg proteins in control and Cd-treated C3H cells. The arrows indicate the time of oligomycin, FCCP and antimycinA/rotenone addiction. The OCR profile is representative of three independent experiments. B) The values at points 3, 6, 9 reflect OCR_B (basal), OCR_O (oligomycin) and OCR_F (FCCP). Bars indicate the mean ± SEM obtained in three independent experiments. C) Analysis of different parameters related with mitochondrial function. D) ECAR traces, expressed as mpH/min/mg proteins, in control and Cd-treated C3H cells. The arrows indicate the time of oligomycin, FCCP and antimycinA/Rotenone addiction. The ECAR profile is representative of three independent experiments. E) Coupling efficiency. Statistically significant: * $p < 0.05$, ** $p < 0.01$, (Dunnett's test).

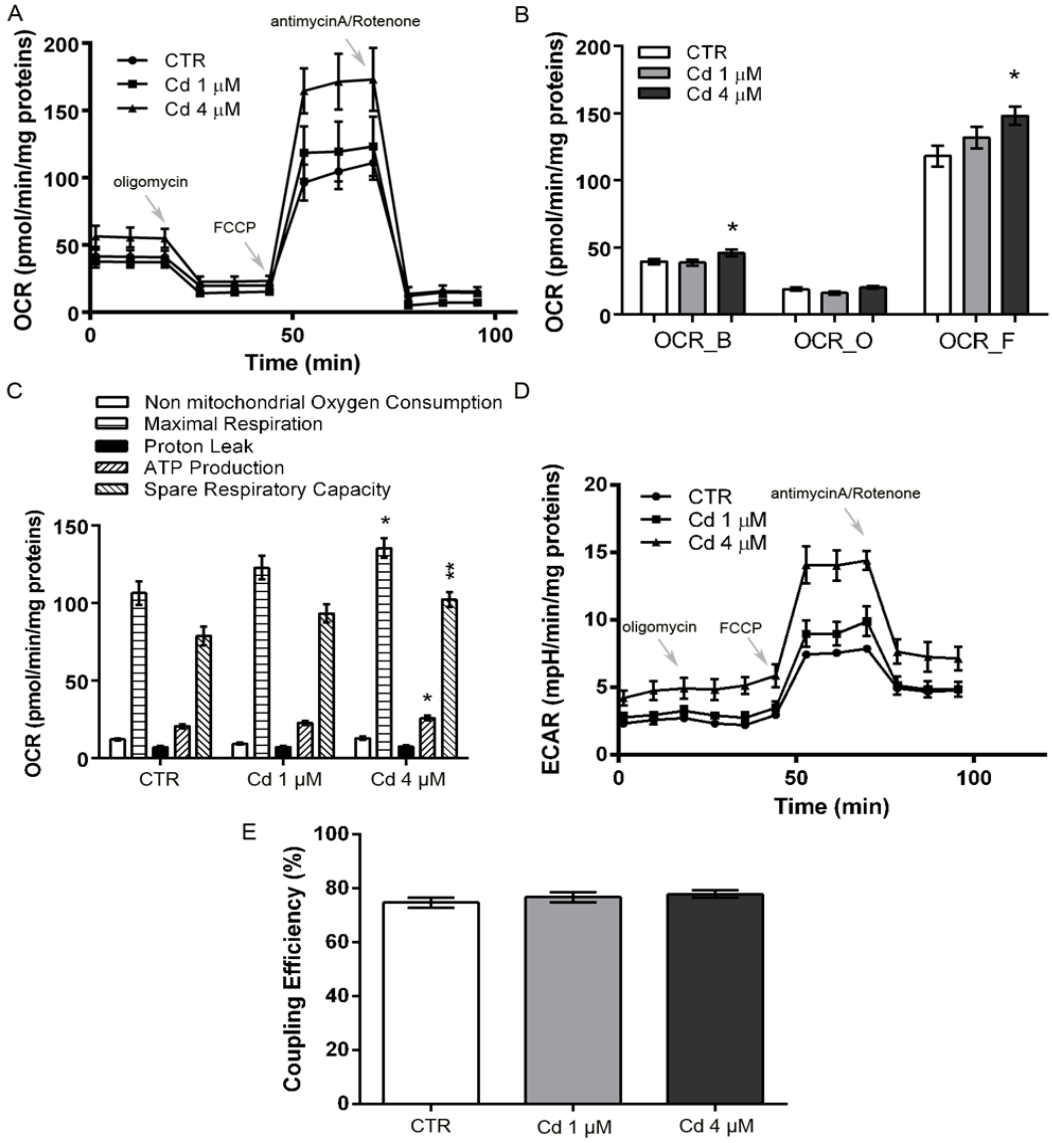

Figure 7.6. Flowcytometric analysis of mitochondrial Δψ in C3H cells. A) Cells are exposed to 1 or 4 µM of cadmium chloride for 24 hours. After treatment, the cells are incubated with 40 nM DiOC6 and the level of fluorescence of treated-cells is compared to the controls. The results are shown in a dot plot overlay. The results are representative of three independent experiments. B) The fluorescence intensity of all experiments is represented by a box plot. The dark line within a box represents the median value, while the upper and lower sides of a box are the third and first quartiles, respectively. Statistically significant Cd 4µM vs CTR: * $p < 0.05$ (Dunnett's test).

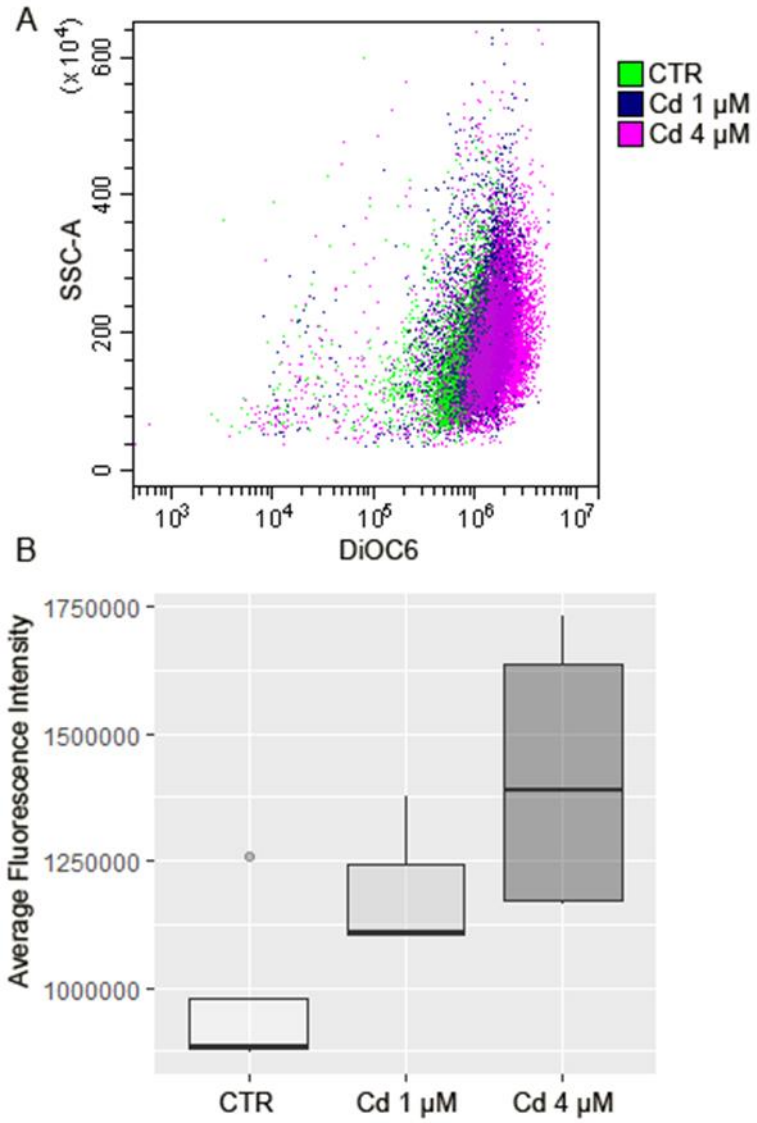

7.3.4 Cadmium treated mitochondria show increased glycolysis

Glycolytic contribution to extracellular acidification rate was determined through Seahorse, using the Glycolytic Assay kit (Fig. 7.7). In both control and 4 µM $CdCl_2$ treated cells, the proton efflux rate (PER) was found to be sustained by mitochondrial electron transport as well as by glycolysis, to almost the same extent. However, upon addition of rotenone and antimicin A, inhibiting complex III, cells treated with 4µM $CdCl_2$ showed a higher glycolytic compensation, thus confirming a higher glycolytic capacity, accounting for the higher spare respiratory capacity (Fig. 7.7B). The addition of hexokinase inhibitor 2-deoxyglucose (2-DG) completely abolished PER (Fig. 7.7A). However, neither lactate nor lactate dehydrogenase activities were significantly increased in our experiments (Fig. 7.7C), suggesting that the higher glycolytic compensation shown by 4µM $CdCl_2$ treated cells is obtained by a higher glycolytic NADH production.

Figure 7.7. Seahorse glycolytic analysis in C3H cells exposed to 4 µM of cadmium chloride for 24 hours. Analysis of different parameters related with glycolysis, Bars indicate the mean ± SEM obtained in three independent experiments. Statistically significant: ** $p < 0.01$, *** $p < 0.001$ (Student's t-test).

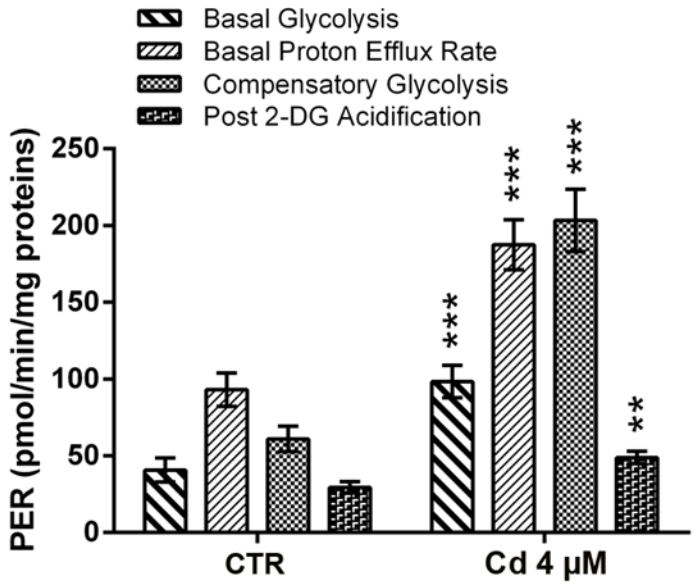

7.3.5 Confocal microscopy shows an altered morphology and intracellular distribution of mitochondria upon treatment with cadmium

Confocal microscopy images of control and $CdCl_2$ treated cells stained with R123 were collected to investigate mitochondria morphology and intracellular distribution.

As seen in Fig. 7.8A, mitochondria in control cells are distributed through the cytoplasm and extend from the nucleus to the cell periphery. A similar intracellular localization is observed when cells are treated with 1 µM $CdCl_2$ for 24 hours (Fig. 7.8B), while cells treated with 4 µM $CdCl_2$ for 24 hours (Fig. 8C) show mitochondria mainly crowded in the perinuclear region, with only sparse organelles at the cytoplasm periphery.

Enlarged views of Fig. 7.8A, 7.8B, and 7.8C allow to appreciate the details of mitochondria morphology. In control cells (Fig. 7.8A, inset 1, 2, 4), mitochondria are mainly filamentous and elongated, sometimes showing rod-like shape (Fig. 7.8A, inset 3). These elongated and well-separated mitochondria are organized in wide networks.

In contrast, in 1 µM $CdCl_2$ treated cells (Fig. 7.8B) mitochondria mainly show a less elongated shape, sometimes giving rise to a very dense network (Fig. 7.8B, inset 1) or presenting a swollen morphology (Fig. 7.8B, insets 2, 3), an indication of damaged organelles.

In 4 µM $CdCl_2$ treated cells, (Fig. 7.8C) the crowding of mitochondria in the perinuclear region does not allow to appreciate their morphology (Fig. 7.8C, insets 1, 2, 4). At the cell periphery, punctate and rod-like shaped mitochondria are observed (Fig. 7.8C, inset 3).

Figure 7.8. Representative confocal images of: A) C3H control cells with the typical mitochondrial network organization and filamentous features; B) C3H cells treated with CdCl2 1 µM for 24 hours, showing altered dense network and swollen morphology and C) C3H cells treated with CdCl2 4 µM for 24 hours showing a crowding of mitochondria in the perinuclear region. Enlarged views allow to appreciate the details of these morphological features. Figure in next page.

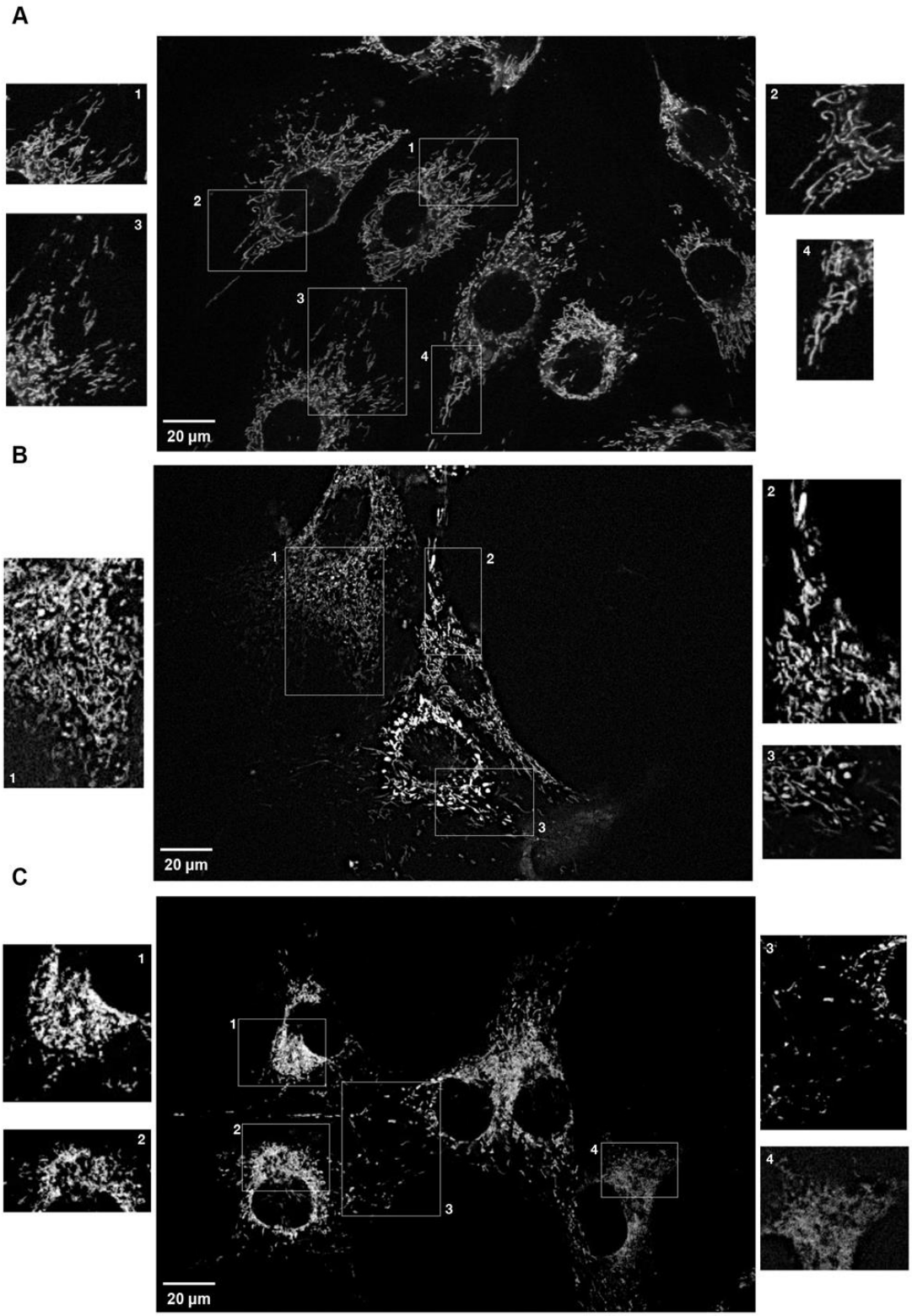
A
1
2
3
4
20 µm
B
1
2
3
20 µm
C
1
2
3
4
20 µm

Average distances acquired from digital image analysis in the first step of the analysis were summarized using a boxplot for each treatment, as reported in Fig. 7.9. The median, the first and the third quartiles of ADP were expressed in microns.

Fig. 7.9 also shows the presence of extreme values, in particular in control and 4 µM $CdCl_2$ treated cells, therefore the median was preferred to the mean for its well-known robustness features with respect to the presence of candidate outlying observations. For this reason, we preferred statistical tests for the distribution of ADP and for the equality of medians, without taking the Normal distribution as a reference.

The Kolgomorov-Smirnov tests [36] for the equality of probability distribution functions (cdfs, indicated as F) were performed on the ADP variable under different treatments: if cadmium has an effect then empirical distributions of ADP have to show (partially) different features over treatments. Both control cells vs 1 µM $CdCl_2$ and control vs 4 µM $CdCl_2$ comparisons were found statistically significant, with p-values of 0.0350 and 0.0267 respectively.

We also calculated the Bonferroni adjustment for multiple testing to protect the resulting three tests against false nulls rejection: the resulting working alpha value was 0.0166, thus after test protection the null hypotheses were not rejected anymore.

Mood median test for the refined hypothesis of median equality was performed and the p value of the test statistic comparing three medians was 0.0635 (control cells vs 1 µM $CdCl_2$, control vs 4 µM $CdCl_2$, as well as 1 µM $CdCl_2$ vs 4 µM $CdCl_2$).

Figure 7.9. Boxplots of average distance values. The distribution of ADP (average distance of pixels from their nucleus) is summarized by one boxplot for each treatment. The dark line within a box represents the median value, while the upper and lower sides of a box are the third and first quartiles, respectively. The so-called whiskers outside the box extend to 1.5 times the interquartile range from the box. Observations outside the two whiskers are considered candidate outliers with respect to a normal distribution.

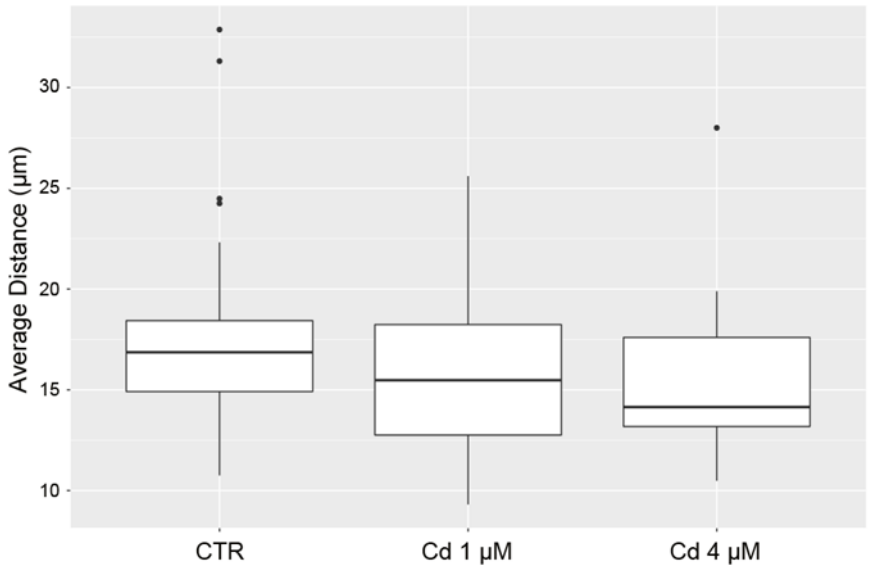

❖ 7.4. Discussion

In contrast to what believed in the past, recent epidemiological studies have provided numerous evidence that even low-level environmental exposure to cadmium, nowadays occurring in numerous economically developed countries, represents a risk for the health of the general population [38]. In particular, the study of cadmium carcinogenic mechanism is of the outmost importance, due to the fact that this heavy metal does not undergo biodegradation in the environment and limitation of exposure to this toxic metal is very difficult.

The information gathered over the past decades has strengthened the role of the mitochondria in normal physiology and in pathology. In particular, tumorigenesis *per se* was shown as a mitochondrial disease where metabolically hijacked mitochondria become highly dependent on glucose and glutamine [39], while oxidative metabolism antagonizes metastasis [40].

With the aim of understanding intracellular early effects of low doses of cadmium, which eventually trigger cell transformation, we turned to the study of oxidative stress and defense mechanism, as well as mitochondria morphology and metabolism.

Assessment of total ROS, estimated through H_2DCFDA fluorescent probe, showed an overall decrease in ROS content following cadmium administration. Although this may seem at first surprising, ROS have been shown to possess dual functions. Actually, low levels of ROS can activate various signaling pathways that stimulate cell proliferation and survival, whereas excess ROS irreversibly damage cellular macromolecular components (proteins, lipids, nucleic acids) and cause cell death (including apoptosis) [40]. In both healthy and pathological conditions, mitochondria generate ROS, which act as signaling and/or damaging molecules, in a hormetic way. In particular, ROS have been shown to regulate mitochondrial dynamics through acting on mitochondrial fusion and fission proteins, permitting (auto)regulation of mitochondrial morphology and function by redox-mediated signaling [41]. In our experiments, cadmium induced higher basal mitochondrial respiration, as well as increased $\Delta\psi$, ATP production and mitochondrial spare respiratory capacity, suggesting an overall improved mitochondrial metabolic efficiency. Moreover, no difference in mitochondrial coupling between electron transport and ATP synthesis was

observed following cadmium administration. This overall higher efficiency of mitochondrial respiration can be related to the change in morphology and subcellular localization, as observed by confocal microscopy, with mitochondria more densely packed around the nuclei in cadmium treated cells, so that a more efficient network can be realized, despite the occurrence of some mitochondria damage, as suggested by the presence of swollen mitochondria. Mitochondria perinuclear localization has been previously observed in many cancer cells [42]. Moreover, accumulating evidence suggests that cellular and mitochondrial redox homeostasis is linked to mitochondrial dynamics. This has led to the novel concept of ‘‘mitochondrial morphofunction”, a tight and multidirectional connection between mitochondrial internal structure, external structure, and function, although a comprehensive understanding is currently still lacking [43]. Moreover, mitochondria have an intrinsic ability to sense their state of health and, when stressed, induce compensatory quality-control mechanisms, such as fusion or fission and mitophagy of damaged mitochondria. Normally, high oxidative phosphorylation activity correlates with mitochondrial fusion and is consistent with the proposal that elongated mitochondrial networks are more efficient at energy generation. Increased ATP production also leads to fusion, with uncoupling leading to fusion inhibition [44]. However, in diseases such as cancer, mitochondria phenotypes have been shown to vary between tumors, showing a predominant punctuate (spherical), network or swollen morphology, and can be used to classify types of cancer [45]. Very similarly to what we observed, Giedt et al. [45] reported that, after 0.1 mM selenium administration, morphology of lung A459 cells showed a progressive shift from a networked to a punctuate and finally to a swollen phenotype. Swollen mitochondria were also observed in vivo in renal cortex [46] and in liver [47] of rats treated with cadmium.

Although cadmium has been reported to increase ROS in many previous studies, the overall reduction in ROS content observed in our experiments is likely due to the efficient response against oxidative stress induced by cadmium. This is confirmed by the increase of glutathione reductase activity, as well as of total cell glutathione. The increase in GST activity is also part of this defense mechanism, although this enzyme is more likely to be endowed with a scavenger role towards cadmium, as previously highlighted by

toxicogenomic data [19]. The reason why cadmium administration leads to an increase in GR activity probably lies in the fact that cytosolic SOD1 and peroxisomal catalase, which are primarily involved in O^2- detoxification, are less active, so that ROS detoxification is mainly achieved through glutathione. Both SOD1 and catalase are metalloenzymes, the former containing Zn and Cu in the catalytic site, the latter only Cu. The ability of cadmium to interfere with essential bioelements such as zinc, magnesium, selenium, calcium, and iron resulting in alteration of their homeostasis and disturbance in their biological functions has been well documented [48]. Prolonged low-level exposure to cadmium has been reported to decrease the activity of antioxidative enzymes (SOD1 and catalase) and the concentration of non-enzymatic antioxidants (reduced glutathione, –SH groups, vitamin C and E) in the liver, leading to the oxidative damage to the hepatocytes [9].

Although the overall ROS content was found diminished, the evaluation of superoxide anion (O^2-) showed that production of this ROS was significantly enhanced by 4 µM $CdCl_2$ administration, thus confirming the impaired ability to remove O^2- caused by SOD1 and catalase partial inactivation. Interestingly, O^2- accumulation leads to some extent of DNA fragmentation, which might be responsible for irreversible cell damage and could also account for the fraction of swollen mitochondria that are seen in confocal images of cells treated with 4 µM $CdCl_2$. The DNA damage observed and consequent genomic instability could contribute to the formation of transformed and cancerous foci from the cells able to escape the repair and protection mechanisms. In fact, it is reported that cadmium is able to impair almost all major DNA repair pathways and that this effect is likely due to inactivation of enzyme and tumor suppressors functions [37] [49] [50] [51].

Zinc is easily displaced by cadmium, from all zinc proteins, including the zinc buffering proteins, metallothioneines [52] [37] and this can alter zinc intracellular homeostasis. Interestingly, a study performed on neuronal cell cultures highlighted mitochondria as targets of Zn^{2+} [53]. These authors reported that upon loading of neocortical mice primary cultures with 300 µM $ZnCl_2$ (a condition which occurs during ischemia), cytosolic Zn^{2+} can enter mitochondria and induce effects including loss of mitochondrial membrane potential, mitochondrial swelling, and ROS generation. Since cadmium addition is known to displace zinc from zinc-proteins, the effect we observe

in C3H cells can be partially mediated by zinc release, a condition previously observed in C3H cells and human hepatoma cells [19] [52]. However, comparing our experiments with those reported by Ji and Weiss [53], the main difference lies in the concentrations of zinc used by the authors which cannot possibly be equaled by those of zinc released by 1 or 4 μM $CdCl_2$ used in our experiments. These concentrations still lie in a range where efficient defense mechanisms are available, so that we do not observe mitochondrial network disruption, but rather an increase in mitochondria efficiency. However, we do observe mitochondrial swelling, which could lead to irreversible damage, should cadmium persist in the medium. Mitochondrial impairment, reported by Belyaeva and colleagues [17], is also likely caused by the high $CdCl_2$ doses (500 μM) used by these authors.

Our results show that cells respond to cadmium treatment with an increase in $\Delta\psi$; although this can seem at first in contrast with other studies showing that cadmium induces mitochondrial damage involving a decrease in $\Delta\psi$ [17] [54], it can be explained by the low cadmium doses we have used, which allow the cells to build up an effective defense, and is in accordance with the overall frame of improved oxidative phosphorylation, revealed by Seahorse assays. In fact, a previous study [54], performed on hepatocytes, showed that $CdCl_2$ reduced ATP production as well as $\Delta\psi$ in a time-dependent manner. In addition to mitochondrial dysfunction, cell viability also underwent a time-dependent reduction. However, the $CdCl_2$ concentration of 12 μM used by the authors in hepatic cells is much higher than in our experiments and expected to lead to irreversible cell damages.

Taking a closer look at mitochondrial oxidative phosphorylation, our results show that, besides increased basal OCR and spare respiratory capacity, 4 μM $CdCl_2$ treatment induces an ECAR increase upon FCCP addition, which is due to increased proton pumping following increased electron transport rate, but also upon electron transport inhibition through rotenone and antimycin A. The latter can only be due to increased glycolysis, as it is also demonstrated by the measure of proton efflux rate (PER): during basal respiration, PER is maintained by both mitochondrial CO_2 production and glycolytic acidification, in both control and 4 μM $CdCl_2$ treated cells. However, when oxidative phosphorylation is inhibited, cadmium treated cells show an increase in PER, due to a higher glycolytic compensatory

capacity, as shown by the fact that it is abolished by 2-DG addition. This increase in glycolysis, sustaining both higher extracellular acidification and increased respiratory capacity, must yield more NADH, which can be oxidized by the electron transport chain to yield more ATP.

❖ 7.5. Conclusions

Our work shows that low doses of $CdCl_2$ trigger cells to increase the glycolytic flux, without increasing lactate production. NADH is effectively shuttled to mitochondria, where it can be oxidized, its removal from the cytosol preventing glycolysis inhibition. Still, as NADH increasingly accumulates, lactate production is likely to be activated. Moreover, increased NADH could lead to decreased histones deacetylation, which is linked to higher cell proliferation.

On the whole, what we see in our cells is an efficient defense mechanism against moderate cadmium concentrations, which upon cadmium removal allows most cells to grow normally, although, only a very few become transformed and give rise fully transformed foci, at the end of the CTA [20]. What we see is likely still a reversible condition: with the help of an efficient detoxification by MTs and GSTs, as previously detected [19], and despite O^{2-} increased generation, if cadmium is administered at low doses and removed and/or inactivated by protein chelation after 24 hours, most cells can regain their healthy state. However, there are a few metabolic rearrangements, triggered by cadmium, which may become irreversible in a small number of cells and lead to transformation and foci formation; these rearrangements include increased glycolysis, O^{2-}-induced DNA damages and mitochondrial impairment. Taken together, our results show how mitochondria represent key targets of this carcinogenic toxic metal. However, further studies will be necessary to establish the direct link between all the observed morpho-functional alterations and the induction of cell transformation.

References

- [1] L.B. Marcano, I.M. Carruyo, X.M. Montiel, C.B. Morales, P.M. de Soto, Effect of cadmium on cellular viability in two species of microalgae (Scenedesmus sp. and Dunaliella viridis), Biol Trace Elem Res, 130 (2009) 86-93.
- [2] L. Jarup, A. Akesson, Current status of cadmium as an environmental health problem, Toxicol Appl Pharmacol, 238 (2009) 201-208.
- [3] P. Richter, O. Faroon, R.S. Pappas, Cadmium and Cadmium/Zinc Ratios and Tobacco-Related Morbidities, Int J Environ Res Public Health, 14 (2017).
- [4] U. Kramer, Metal hyperaccumulation in plants, Annu Rev Plant Biol, 61 (2010) 517-534.
- [5] S. Kakuta, S. Shibata, Y. Iwakura, Genomic structure of the mouse 2',5'-oligoadenylate synthetase gene family, J Interferon Cytokine Res, 22 (2002) 981-993.
- [6] T. Jin, Q. Kong, T. Ye, X. Wu, G.F. Nordberg, Renal dysfunction of cadmium-exposed workers residing in a cadmium-polluted environment, Biometals, 17 (2004) 513-518.
- [7] IARC, TOXICOLOGICAL PROFILE FOR CADMIUM, U.S. Department of Health and Human Services, Public Health Service Agency for Toxic
- Substances and Disease Registry, (2012).
- [8] R. Corvi, M.J. Aardema, L. Gribaldo, M. Hayashi, S. Hoffmann, L. Schechtman, P. Vanparys, ECVAM prevalidation study on in vitro cell transformation assays: general outline and conclusions of the study, Mutat Res, 744 (2012) 12-19.
- [9] G. Cannino, E. Ferruggia, C. Luparello, A.M. Rinaldi, Cadmium and mitochondria, Mitochondrion, 9 (2009) 377-384.
- [10] H. Chen, D.C. Chan, Mitochondrial Dynamics in Regulating the Unique Phenotypes of Cancer and Stem Cells, Cell Metab, 26 (2017) 39-48.
- [11] S.A. Detmer, D.C. Chan, Functions and dysfunctions of mitochondrial dynamics, Nat Rev Mol Cell Biol, 8 (2007) 870-879.
- [12] E. Smirnova, L. Griparic, D.L. Shurland, A.M. van der Bliek, Dynamin-related protein Drp1 is required for mitochondrial division in mammalian cells, Mol Biol Cell, 12 (2001) 2245-2256.
- [13] P.A. Lindahl, M.J. Moore, Labile Low-Molecular-Mass Metal Complexes in Mitochondria: Trials and Tribulations of a Burgeoning Field, Biochemistry, 55 (2016) 4140-4153.
- [14] A.M. Brown, B.S. Kristal, M.S. Effron, A.I. Shestopalov, P.A. Ullucci, K.F. Sheu, J.P. Blass, A.J. Cooper, Zn2+ inhibits alpha-ketoglutarate-stimulated mitochondrial respiration and the isolated alpha-ketoglutarate dehydrogenase complex, J Biol Chem, 275 (2000) 13441-13447.
- [15] M. Schulte, D. Mattay, S. Kriegel, P. Hellwig, T. Friedrich, Inhibition of Escherichia coli respiratory complex I by Zn(2+), Biochemistry, 53 (2014) 6332-6339.

- [16] B. Sanni, K. Williams, E.P. Sokolov, I.M. Sokolova, Effects of acclimation temperature and cadmium exposure on mitochondrial aconitase and LON protease from a model marine ectotherm, Crassostrea virginica, Comp Biochem Physiol C Toxicol Pharmacol, 147 (2008) 101-112.
- [17] E.A. Belyaeva, D. Dymkowska, M.R. Wieckowski, L. Wojtczak, Reactive oxygen species produced by the mitochondrial respiratory chain are involved in Cd2+-induced injury of rat ascites hepatoma AS-30D cells, Biochim Biophys Acta, 1757 (2006) 1568-1574.
- [18] S. Nemmiche, Oxidative Signaling Response to Cadmium Exposure, Toxicol Sci, 156 (2017) 4-10.
- [19] G. Callegaro, M. Forcella, P. Melchioretto, A. Frattini, L. Gribaldo, P. Fusi, M. Fabbri, C. Urani, Toxicogenomics applied to in vitro Cell Transformation Assay reveals mechanisms of early response to cadmium, Toxicol In Vitro, 48 (2018) 232-243.
- [20] M. Forcella, G. Callegaro, P. Melchioretto, L. Gribaldo, M. Frattini, F.M. Stefanini, P. Fusi, C. Urani, Cadmium-transformed cells in the in vitro cell transformation assay reveal different proliferative behaviours and activated pathways, Toxicol In Vitro, 36 (2016) 71-80.
- [21] OECD, Detailed review paper on cell transformation assays for detection of chemical carcinogens, Development, O.f.e.c.-o.a. (Ed). OECD Environment, health and safety publications, (2007) 1-164.
- [22] C. Urani, F.M. Stefanini, L. Bussinelli, P. Melchioretto, G.F. Crosta, Image analysis and automatic classification of transformed foci, J Microsc, 234 (2009) 269-279.
- [23] G.K. Bergmeyer HU, Grassl M. , Enzymes as biochemical reagents, in: B. HU (Ed.) Methods of enzymatic analysis, vol. 1, Academic Press, New York, 1974, pp. 427-522.
- [24] G.M. Bergmeyer HU, Enzymes. Catalase, in: B. HU (Ed.) Methods of enzymatic analysis, vol. 2, New York: Academic Press, NewYork, 1983, pp. 165-166.
- [25] W.H. Habig, M.J. Pabst, W.B. Jakoby, Glutathione S-transferases. The first enzymatic step in mercapturic acid formation, J Biol Chem, 249 (1974) 7130-7139.
- [26] H.S. Nakamura W, Hayashi K. , Purification and properties of rat liver glutathione peroxidase, Biochim Biophys Acta, 358 (1974) 251-261.
- [27] Y. Wang, L.W. Oberley, D.W. Murhammer, Antioxidant defense systems of two lipidopteran insect cell lines, Free Radic Biol Med, 30 (2001) 1254-1262.
- [28] P.G. Vance, B.B. Keele, Jr., K.V. Rajagopalan, Superoxide dismutase from Streptococcus mutans. Isolation and characterization of two forms of the enzyme, J Biol Chem, 247 (1972) 4782-4786.
- [29] M.M. Bradford, A rapid and sensitive method for the quantitation of microgram quantities of protein utilizing the principle of protein-dye binding, Anal Biochem, 72 (1976) 248-254.
- [30] T.S. Kumaravel, A.N. Jha, Reliable Comet assay measurements for detecting DNA damage induced by ionising radiation and chemicals, Mutat Res, 605 (2006) 7-16.

- [31] G. Pau, F. Fuchs, O. Sklyar, M. Boutros, W. Huber, EBImage--an R package for image processing with applications to cellular phenotypes, Bioinformatics, 26 (2010) 979-981.
- [32] R.C. Team, R: A language and environment for statistical computing. , R Foundation for Statistical Computing Vienna, Austria, (2008).
- [33] W. H, ggplot2: Elegant Graphics for Data Analysis, (2016).
- [34] K.H. Torsten Hothorn, Mark A. van de Wiel, Achim Zeileis Implementing a Class of Permutation Tests: The coin Package, Journal of Statistical Software 28(8) (2008) 1-23.
- [35] R.D.M.M. Hervé, Testing and Plotting Procedures for Biostatistics, (2018).
- [36] P.H. Kvam, Non parametric statistic with applications to science and engineering, Wiley, 2007.
- [37] A. Hartwig, Cadmium and cancer, Met Ions Life Sci, 11 (2013) 491-507.
- [38] M. Mezynska, M.M. Brzoska, Environmental exposure to cadmium-a risk for health of the general population in industrialized countries and preventive strategies, Environ Sci Pollut Res Int, 25 (2018) 3211-3232.
- [39] M. Neagu, C. Constantin, I.D. Popescu, D. Zipeto, G. Tzanakakis, D. Nikitovic, C. Fenga, C.A. Stratakis, D.A. Spandidos, A.M. Tsatsakis, Inflammation and Metabolism in Cancer Cell-Mitochondria Key Player, Front Oncol, 9 (2019) 348.
- [40] J. Lu, M. Tan, Q. Cai, The Warburg effect in tumor progression: mitochondrial oxidative metabolism as an anti-metastasis mechanism, Cancer Lett, 356 (2015) 156-164.
- [41] W. Mayer, M. Hemberger, H.G. Frank, R. Grummer, E. Winterhager, P. Kaufmann, R. Fundele, Expression of the imprinted genes MEST/Mest in human and murine placenta suggests a role in angiogenesis, Dev Dyn, 217 (2000) 1-10.
- [42] L.W. Thomas, O. Staples, M. Turmaine, M. Ashcroft, CHCHD4 Regulates Intracellular Oxygenation and Perinuclear Distribution of Mitochondria, Front Oncol, 7 (2017) 71.
- [43] E.P. Bulthuis, M.J.W. Adjobo-Hermans, P. Willems, W.J.H. Koopman, Mitochondrial Morphofunction in Mammalian Cells, Antioxid Redox Signal, 30 (2019) 2066-2109.
- [44] P. Mishra, D.C. Chan, Metabolic regulation of mitochondrial dynamics, J Cell Biol, 212 (2016) 379-387.
- [45] R.J. Giedt, P. Fumene Feruglio, D. Pathania, K.S. Yang, A. Kilcoyne, C. Vinegoni, T.J. Mitchison, R. Weissleder, Computational imaging reveals mitochondrial morphology as a biomarker of cancer phenotype and drug response, Sci Rep, 6 (2016) 32985.
- [46] W. Tang, Z.A. Shaikh, Renal cortical mitochondrial dysfunction upon cadmium metallothionein administration to Sprague-Dawley rats, J Toxicol Environ Health A, 63 (2001) 221-235.
- [47] J.O. Ossola, M.L. Tomaro, Heme oxygenase induction by cadmium chloride: evidence for oxidative stress involvement, Toxicology, 104 (1995) 141-147.

- [48] B. Messner, A. Turkcan, C. Ploner, G. Laufer, D. Bernhard, Cadmium overkill: autophagy, apoptosis and necrosis signalling in endothelial cells exposed to cadmium, Cell Mol Life Sci, 73 (2016) 1699-1713.
- [49] A. Hartwig, M. Asmuss, H. Blessing, S. Hoffmann, G. Jahnke, S. Khandelwal, A. Pelzer, A. Burkle, Interference by toxic metal ions with zinc-dependent proteins involved in maintaining genomic stability, Food Chem Toxicol, 40 (2002) 1179-1184.
- [50] C. Urani, P. Melchioretto, M. Fabbri, G. Bowe, E. Maserati, L. Gribaldo, Cadmium Impairs p53 Activity in HepG2 Cells, ISRN Toxicol, 2014 (2014) 976428.
- [51] T. Fatur, T.T. Lah, M. Filipic, Cadmium inhibits repair of UV-, methyl methanesulfonate- and N-methyl-N-nitrosourea-induced DNA damage in Chinese hamster ovary cells, Mutat Res, 529 (2003) 109-116.
- [52] C. Urani, P. Melchioretto, M. Bruschi, M. Fabbri, M.G. Sacco, L. Gribaldo, Impact of Cadmium on Intracellular Zinc Levels in HepG2 Cells: Quantitative Evaluations and Molecular Effects, Biomed Res Int, 2015 (2015) 949514.
- [53] S.G. Ji, J.H. Weiss, Zn(2+)-induced disruption of neuronal mitochondrial function: Synergism with Ca(2+), critical dependence upon cytosolic Zn(2+) buffering, and contributions to neuronal injury, Exp Neurol, 302 (2018) 181-195.
- [54] S. Xu, H. Pi, Y. Chen, N. Zhang, P. Guo, Y. Lu, M. He, J. Xie, M. Zhong, Y. Zhang, Z. Yu, Z. Zhou, Cadmium induced Drp1-dependent mitochondrial fragmentation by disturbing calcium homeostasis in its hepatotoxicity, Cell Death Dis, 4 (2013) e540.

Chapter 8

"Different fully transformed foci induced by cadmium show different metabolic profiles."

ABSTRACT

***Background**: At the end of Cell Trasformation Assay (CTA), performed by treating healthy C3H10T1/2Cl8 mouse embryo fibroblasts with 1 μM $CdCl_2$ for 24 h, different foci are produced. Previous data, obtained in our laboratory, showed that, despite being all completely transformed type III foci, they show different morphology and proliferative behavior. Many differences were also observed in gene expression dysregulation, with on a few dysregulated genes in common. In this work we investigate the metabolic rearrangements underlying such differences in the two less similar foci (F1 and F3), with particular regards to mitochondria, which we have previously shown to be early targets of cadmium toxicity.*

***Methods**: Foci metabolism was investigated by Seahorse Agilent assays and through enzyme activity assays; mitochondria were studied in confocal microscopy and reactive oxygen species were detected by the use of fluorescent probes.*

***Results**: F1 focus showed metabolic hyperactivation, with higher glycolytic and TCA fluxes respect to F3 focus, and a more negative mitochondrial membrane potential (Dy); most ATP synthesis was performed through oxidative phosphorylation; confocal microscopy showed perinuclear mitochondria organized in a network. F3 focus showed lower metabolic rates, with ATP mainly produced by glycolysis; impairment of oxidative phosphorylation was confirmed by the presence of damaged mitochondria.*

***Conclusions**: both foci showed metabolic alterations, following cadmium treatment, leading to the loss of coordination of glycolytic, TCA and oxidative phosphorylation pathways; we suggest that these alterations are triggered by loss of Pasteur effect in F1 focus and by mitochondrial impairment in F3 focus.*

***General Significance**: cadmium is a widespread pollutant and a recognized carcinogen; the elucidation of its mechanism of action can be useful both to improve CTA and to yield insights into environmental carcinogenesis.*

Oldani Monica, Anna M. Villa, Manzoni Marta, Melchioretto Pasquale, Parenti Paolo, Monti Eugenio, Urani Chiara, Fusi Paola e Forcella Matilde

Manuscript in preparation

❖ 8.1. Introduction

Although cadmium (Cd) is a well-known carcinogen, classified by the International Agency for Research on Cancer as a category I carcinogen, the molecular mechanisms involved in cell transformation into a malignant phenotype are largely unknown. Still, cadmium is a widespread environmental contaminant, currently released by anthropogenic activities at a rate of 30000 tons per year. Contamination in humans is therefore very easy: besides occupational exposure, it can occur through food, drinking water, inhalation of air particles, and cigarette smoking. The absence of any excretory way for cadmium leads to its persistency inside the body, with a half-life of more than 26 years.

While being devoid of all biological roles, with the exception of a catalytic role in some algal enzymes [1], Cd^{2+} ions can easily displace Zn^{2+} ions, because of their similar charge and masses [2] [3] [4] [5]. This similarity also accounts for cadmium uptake by zinc channels and transporters, in what has been named a "Trojan horse mechanism" [6]. Moreover, cadmium can interfere with Zn binding proteins, whose estimated number within the cell is higher than 3000. The ability of cadmium to interfere with the homeostasis of other essential metals, like copper and calcium has been documented [7].

Cell Transformation Assays (CTAs), the most advanced *in vitro* test for the prediction of human chemical carcinogenicity, is also a powerful tool for mechanistic studies of carcinogenesis [8]. In addition to be widely used for the screening of potential carcinogenicity [9] [10], the CTA supports the 3Rs principles of Replacement, Reduction and Refinement of experimental animals. Moreover, it has been shown to closely model some key stages of the *in vivo* carcinogenic process [11]. In our experiments, the CTA based on the use of C3H10T1/2Cl8 mouse embryo fibroblasts was adopted, the latter being among the suitable cells suggested by standard protocols [12].

Foci, obtained at the end of the CTA, are recognized under a microscope and classified by morphological features, such as deep basophilic staining, multilayered growth, random cell orientation at the edge of the focus, and invasiveness of the surrounding monolayer of normal cells [11] [12] . These morphological features are related to molecular changes leading the cells to acquire fully malignant characteristics, which are demonstrated by their ability to develop tumors when injected into susceptible host animals [13] .

In a previous work [14], we found that morphological evaluations and proliferative assays confirmed the loss of contact inhibition and the higher proliferative rate of transformed clones. Moreover, biochemical analysis of EGFR pathway revealed that, despite the same initial carcinogenic stimulus (1 µM $CdCl_2$ for 24 h), different *foci* were characterized by the activation of different molecular pathways; in particular, F1 focus showed ERK activation and a high proliferation rate, while F3 focus showed Akt activation and a survival molecular profile. More recently (Oldani et al. 2019, manuscript under revision), a toxicogenomic study, performed by our group, showed that the two foci also developed distinct patterns of upregulated and downregulated genes, upon cadmium administration.

This work reports a further metabolic characterization of both F1 and F3 *focus*; with the aim of identifying metabolic alterations caused by gene dysregulation, we investigated oxygen consumption rate and ATP production, as well as mitochondrial morphology and defense mechanisms against oxidative stress. Results show different metabolic patterns in each focus, accounting for their different proliferation rates.

❖ 8.2. Materials and Methods

8.2.1 Cell and culture conditions

The experiments were performed using the cells collected from Cd-transformed foci obtained at the end of Cell Transformation Assays (CTAs) on C3H10T1/2 clone 8 mouse embryonic fibroblasts (cell line ATCC, CCL 226 lot. n. 58078542), as previously described [14]. This cell line was chosen for its high sensitivity to carcinogenic compounds, its low spontaneous transformation rates, and because it represents one of the three cell lines suggested in the Detailed Review Paper on Cell Transformation Assay to be used for detection of chemical carcinogens [12]. Cells with passages from 9 to 12 were used for cell transformation studies [12]. Different cell types were collected at the end of the CTAs, and the derived cell clones were cultured and processed for further analyses, as described in the following sections. The new cell clones were derived from different fully transformed foci, all obtained after 1 µM Cd exposure. Among these new cell lines, we have decided to analyze the F1 and F3 *focus*. Cells were cultured in Basal Medium Eagle (BME, Sigma Chemical Co., St. Louis, MO, USA) enriched with 10% heat-inactivated fetal bovine serum (FBS, Euroclone, Pero, Italy), 1% glutamine, 0.5% HEPES 2M and 25 µg/mL gentamicin (all purchased from Sigma) at 37°C in a humidified incubator supplied with a constant flow of 5% CO2 in air throughout each experiment. Cells were routinely seeded in 100 mm Ø Petri dishes, the medium was changed every 3 days and cells grown until 80% confluence maximum was reached. The cells were stored in ampoules, frozen at –80°C with 10% sterile DMSO as a preservative.

8.2.2 Enzyme and metabolite assays

For enzymatic assay sample preparation, both cell clones F1 and F3 were harvested by trypsinization at 80% confluence, rinsed with ice-cold PBS and lysed in 50 mM Tris/HCl, pH 7.4, 150 mM NaCl, 5 mM EDTA, 10 % glycerol, 1 % NP40 buffer, containing protease inhibitors and 1 mM PMSF. After lysis on ice, homogenates were obtained by passing the cells 5 times through a blunt 20-gauge needle fitted to a syringe and then centrifuging at 15,000 *g* for 30 min at

4°C. The resulting supernatant was used to measure enzymatic activities. Enzymes were assayed using the following procedures. Lactate dehydrogenase (LDH), pyruvate kinase (PK), malate dehydrogenase (MDH), glutamate dehydrogenase (GLDH), glucose-6-phosphate dehydrogenase (G6PDH), $NADP^+$ dependent isocitrate dehydrogenase (ICDH), malic enzyme (ME) were assayed according to Bergmeyer [15]; citrate synthase was assayed according to Shepherd [16]; catalase (CAT) was assayed according to [17], using 12 mM H_2O_2 as substrate; glutathione S-transferase (GST) as reported in [18]; glutathione peroxidase according to [19]; glutathione reductase according to [20]. For superoxide dismutase1 (SOD1) cells were rinsed with ice-cold PBS and lysed in PBS, containing protease inhibitors and 1mM PMSF; homogenates were obtained by passing the cells 5 times through a blunt 20-gauge needle fitted to a syringe, incubating on ice for 15 min and sonicating 2 times (10 s cycle). The supernatant was obtained by centrifugation at 15,000 *g* for 10 min at 4°C and used to measure enzymatic activity according to Vance [21]. All assays were performed in triplicate at 30 °C in a Cary3 Spectrophotometer and analyzed by the Cary Win UV application software for Windows. Activity was expressed in international units and referred to protein concentration as determined by the Bradford method [22].

For metabolite assay sample preparation, both cell clones were harvested by trypsinization at 80% confluence; the pellets were resuspended in 3 mL PBS, harvested by a centrifugation in the above conditions, weighted, and resuspended with 5 volumes of 5% perchloric. The suspension was passed 5 times through a blunt 20-gauge needle fitted to a syringe, incubated on ice for 15 min and centrifuged at 3,000 *g* at 4°C for 10 min. The resulting supernatant was neutralized with 2.5 M K_2CO_3 to pH 6.5 and then centrifuged at 3,000 *g* at 4°C for 10 min to eliminate potassium perchlorate. The resulting supernatant was kept at –80°C until further analysis of metabolite concentrations. Lactate and total intracellular ATP were measured using standard enzymatic tests according to [15]. All assays were performed in triplicate at 30 °C in a Cary3 Spectrophotometer and analyzed by the Cary Win UV application software for Windows. Metabolite concentrations were expressed in nmol/mg cells.

8.2.3 GSH assay

Both cell clones were harvested by trypsinization at 80% confluence; the pellets were resuspended in 3 mL PBS, harvested by a centrifugation in the above conditions and weighted. Pellets were resuspended in 500 µl cold 5% 5-sulfosalicylic acid (SSA), lysed by vortexing and by passing 5 times through a blunt 20-gauge needle fitted to a syringe. All the samples were incubated for 10 minutes at 4 °C and then centrifuged at 14,000 *g* for 10 min at 4 °C. The supernatant was used for the analysis following the instructions of Glutathione Colorimetric Detection Kit (Invitrogen). The Kit is designed to measure oxidized glutathione (GSSG), total glutathione (GSH tot) and reduced glutathione (GSH tot – GSSG) concentrations. Therefore, it was possible to obtain GSH/GSSG ratio, a critical indicator of cell health. The absorbance was measured at 405 nm using a micro plate reader. The values of absorbance were compared to standard curves (GSH tot and GSSG, respectively) and normalized to mg of cells. Final concentrations were expressed in nmol/mg cells.

8.2.4 SDS-PAGE and Western blotting

For western blot analysis sample preparation, both cell clones were harvested by trypsinization at 80% confluence. The cells were then rinsed with ice-cold PBS and lysed in RIPA buffer (50 mM Tris/HCl pH 7.5, 150 mM NaCl, 1% NP-40, 0.5% sodium deoxycholate, 0.1% SDS) containing protease and phosphatase inhibitors and 1 mM PMSF (phenylmethylsulfonyl fluoride). After lysis on ice, homogenates were obtained by passing 5 times through a blunt 20-gauge needle fitted t a syringe and then centrifuged at 15,000 g for 30 min. Supernatants were analyzed for protein content by the BCA protein assay (Smith et al., 1985). SDS-PAGE and Western blotting were carried out by standard procedures [23]. Sixty micrograms of proteins were separated on a 10 % acrylamide/bis-acrylamide SDS-PAGE, transferred onto a nitrocellulose membrane (Millipore, Billerica, MA, USA), probed with the appropriated antibodies and visualized using ECL detection system (Millipore). Protein levels were quantified by densitometry of immunoblots using Scion Image software (Scion Corp., Frederick, MD, USA). The following primary antibodies were used (all purchased by Cell Signaling Technology, Danvers, MA, USA): anti-PKM2 (dilution 1:1,000), anti-PFKFB3 (dilution 1:1,000), anti-GAPDH (dilution

1:10,000) and anti-vinculin (dilution 1:10,000). IgG HRP anti rabbit conjugated secondary antibodies (purchased by Cell Signalling Technology, Danvers, MA, USA) were diluted 1:10,000.

8.2.5 Detection of Intracellular Reactive Oxygen Species (ROS)

The generation of intracellular reactive oxygen species (ROS) was detected by the oxidation of 2',7'-Dichlorofluorescin diacetate (H_2DCFDA) or Dihydroethidium (DHE). H_2DCFDA is an indicator for both reactive oxygen species and nitric oxide (•NO); the second probe measures the level of cytosolic superoxide anion (O_2^-). The cells were plated at a density of 2.5 x 10^5 cells per well into six-well plates in complete culture medium and incubated 24 h after seeding with H_2DCFDA (5 µM final concentration in DPBS) or DHE (10 µM final concentration in complete medium) for 20 min in the dark at 37 °C. At the end of incubation, cells were washed by warm DPBS, trypsinized (500 µl of trypsin /well) and harvested by centrifugation (5 min at 2000 *g*) at room temperature. The pellet was resuspended in 500 µl/tube of PBS and ROS generation of 10,000 cells was measured by the fluorescence intensity. FL-1 channel (530 nm) was utilized to detect the fluorescence intensity of DCF; DHE fluorescence can be measured at 585 nm, or FL-2 channel, band-pass filter. Logarithmic amplification was used to detect probe fluorescence. Flowcytometric data were analyzed using CytExpert 2.3 Software (Beckman Coulter, Inc.).

8.2.6 Mitochondrial transmembrane potential (MTP) assay

MTP alterations were assessed flowcytometrically, using the potentially sensitive dye 3,3' -dihexyloxacarbocyanine Iodide. The cells were plated at a density of 2.5 x 10^5 cells per well into six-well plates in complete culture medium, harvested 24 h after seeding by centrifugation (5 min at 2000 *g*) at room temperature and stained with DiOC6 (40 nM in PBS, 20 min at 37 °C and 5% CO_2 in the dark). Loss in DiOC6 fluorescence indicates disruption of the mitochondrial inner transmembrane potential. The probe was excited at 488 nm and emission was measured through a 530 nm (FL-1 channel) band-pass filter. Logarithmic amplification was used to detect the fluorescence of the probe. Flowcytometric data were analyzed using CytExpert 2.3 Software (Beckman Coulter, Inc.).

8.2.7 Oxygen consumption rate and extra-cellular acidification rate measurements

Oxygen consumption rate (OCR) and extra-cellular acidification rate (ECAR) were measured in F1 and F3 *foci* with Seahorse XFe24 Analyzer (Seahorse Bioscience, Billerica, MA, USA) using Seahorse XF Cell Mito Stress Test Kit and Agilent Seahorse XF Glycolytic Rate Assay Kit. The cells were seeded in Agilent Seahorse XF24 cell culture microplates at density of 3 × 10^4 cells/well in 250 µL of Basal Medium Eagle and 24 hours after seeding the growth medium was replaced with 525 µl/well of Seahorse XF Base Medium containing 1 mM pyruvate, 2 mM glutamine and 10 mM glucose for the Cell Mito Stress Test Kit or 1 mM pyruvate, 2 mM glutamine, 10 mM glucose and 5 mM Hepes for the Glycolytic Rate Assay Kit. Then the plate was incubated into 37°C non-CO_2 incubator for 1 h, before starting the experiment procedure.
The sensor cartridge was calibrated by Seahorse XFe24 Analyzer. Pre-warmed Oligomycin, FCCP, Rotenone and Antimycin A were loaded into injector ports A, B and C of sensor cartridge, to reach working concentration of 1 µM, 2 µM and 0.5 µM respectively, for the Cell Mito Stress Test Kit. Pre-warmed Rotenone and Antimycin A and 2-deoxy-D-glucose (2-DG) were loaded into injector ports A and B of sensor cartridge, to reach working concentration of 0.5 µM and 50 mM for the Glycolytic Rate Assay Kit.

OCR and ECAR were detected under basal conditions followed by the sequential addition of the drugs, to measure non-mitochondrial respiration, maximal respiration, proton leak, ATP respiration, respiratory capacity, coupling efficiency for the Cell Mito Stress Test Kit and basal glycolysis, basal proton efflux rate, compensatory glycolysis and post 2-DG acidification for the Glycolytic Rate Assay Kit.

8.2.8 Confocal microscopy

Mitochondria fluorescence was studied by laser scanning confocal microscopy, using a Bio-Rad MRC-600 confocal microscope (Bio-Rad, Hemel Hempstead, UK) equipped with a 25mW argon laser. The scanning head was coupled with an upright epifluorescence microscope Nikon Optiphot-2 (Nikon, Tokyo, Japan) with a 60x oil immersion objective Nikon Planapochromat (N.A. = 1.4). The fluorescence was excited at 488 nm and the emission collected through a long pass filter above 515 nm. High sensitivity photon counting detection was used to minimize the excitation power (0.1 mW at the entry of the optical head) and preserve cell viability.

Cells were plated in 35mm Petri dishes at density of 6×10^4 cells/well and 24 hours after seeding the medium was removed, cells were washed twice with phosphate buffer saline (PBS) and incubated for 10 min in 1 μM Rhodamine 123 (R123) solution at 37 °C and 5% CO_2. After incubation, the cells were rinsed twice with PBS and few microliters of PBS were left in the Petri dish to avoid cell drying. A coverslip was placed over the cells that were immediately imaged by confocal microscope.

8.2.9 Statistical analysis

The data were tested by Student's test. All calculations were conducted using the R statistics programming environment (Team, 2015).

❖ 8.3. Results

8.3.1 The main ATP production route is oxidative phosphorylation in F1 focus and substrate level phosphorylation in F3 focus

Respiratory metabolism of both F1 and F3 *foci* was investigated, measuring oxygen consumption rate (OCR) and extracellular acidification rate (ECAR), through Mitostress assay in the Agilent Seahorse. Results are reported in Fig. 8.1: F1 *focus* showed higher basal and maximal respiration rates, as well as a higher spare respiratory capacity, compared to F3 *focus* (Fig. 8.1A and 1B). The higher basal OCR shown by F1 *focus* is reflected by a higher level of acidification, as shown by ECAR measurement, reported in Fig. 8.1D. Both F1 and F3 ECAR were only slightly decreased upon oligomycin addition and they were increased following FCCP addition; however, F1 ECAR increase was found to be much higher than F3 and remained high even after rotenone/antimycin addition, suggesting a contribution of glycolytic acidification. As shown in Fig. 8.1C, the proton leak was also found to be more consistent in F1 *focus*; as a consequence, this *focus* showed less efficiently coupled mitochondria (20% uncoupling) compared to F3 *focus*, as reported in Fig. 8.1E. Despite mitochondria uncoupling, F1 higher basal respiration rate sustained a higher mitochondrial ATP production, compared to F3 *focus* (Fig. 8.1C).

Mitochondrial membrane potential was measured through the green-fluorescent, lipophilic dye 3,3'-dihexyloxacarbocyanine iodide (DiOC6), which accumulates in mitochondria due to their negative membrane potential and can be applied to monitor the mitochondrial membrane potential using flow cytometric detection. As reported in Fig. 8.2, in accordance with its higher mitochondrial ATP production and higher OCR, F1 *focus* showed a higher DiOC6 fluorescence, compared to F3 *focus*, indicating a more negative $\Delta\psi$.

Figure 8.1. Seahorse Mitostress analysis. A) OCR traces, expressed as pmoles O_2/min/mg proteins in F1 and F3 *foci*. The arrows indicate the time of addiction of oligomycin, FCCP and antimycinA/Rotenone. The OCR profile is representative of three independent experiments. B) The values at points 3, 6, 9 reflect OCR_B (basal), OCR_O (oligomycin) and OCR_F (FCCP). Bars indicate the mean ± SEM obtained in three independent experiments. C) Analysis of different parameters related with mitochondrial function. D) ECAR traces, expressed as mpH/min/mg proteins, in F1 and F3 foci. The arrows indicate the time of addiction of oligomycin, FCCP and antimycinA/Rotenone. The ECAR profile is representative of three independent experiments. E) Coupling efficiency. Statistical significant: * $p < 0.05$, ** $p < 0.01$, *** $p < 0.001$ (Student's t-test).

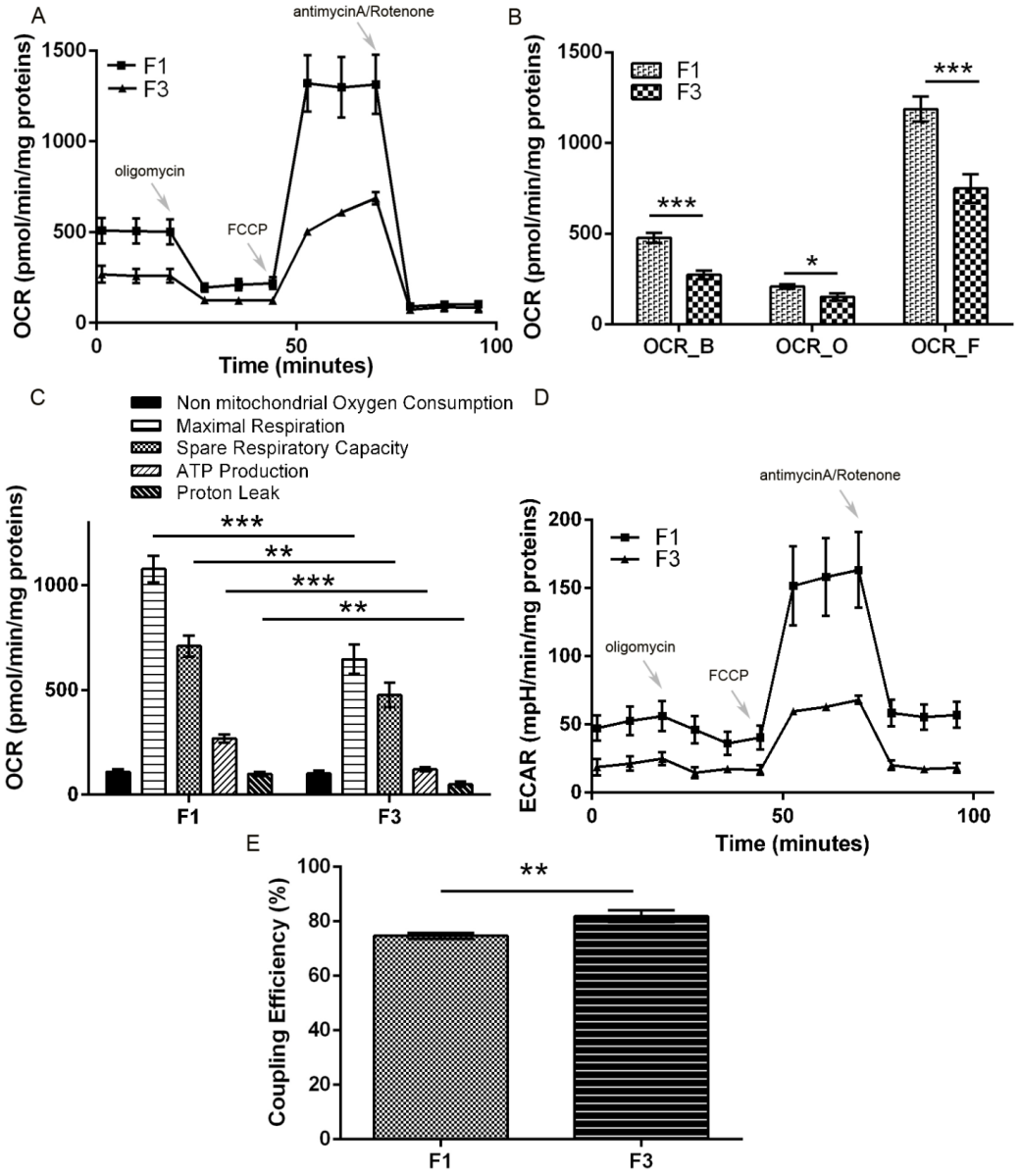

Figure 8.2. Flowcytometric analysis of Δψ mitochondrial in F1 and F3 *foci*. A) Cells are incubated with 40 nM DiOC6 and the level of fluorescence of cells is measured. The results are shown in a dot plot overlay. The dot plot is representative of three independent experiments. B) The fluorescence intensity of all experiments is represented by a box plot. The dark line within a box represents the median value, while the upper and lower sides of a box are the third and first quartiles, respectively. Statistically significant: * $p < 0.05$ (Student's t-test).

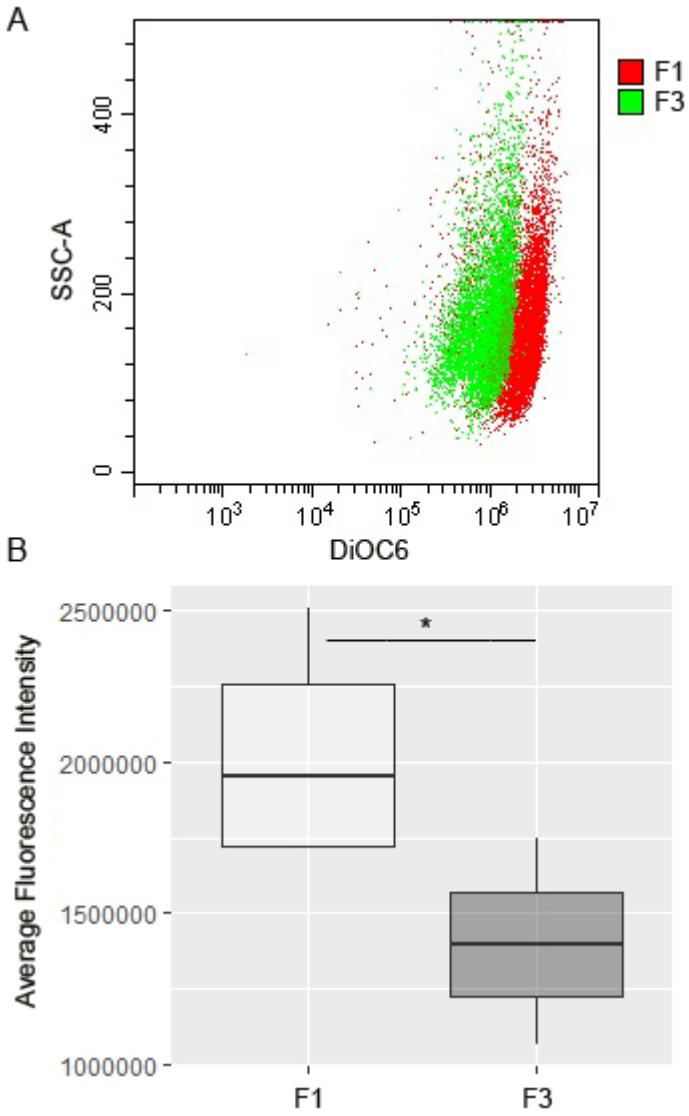

8.3.2 F1 focus shows hyperactivated glycolysis, TCA and lactic fermentation

The activities of a series of enzymes involved in sugar metabolism were assayed in both *foci*. Results are reported in Table 8.1: PK was found to be more active in F1 *focus* than in F3; moreover, both citrate synthase and malate dehydrogenase specific activities were also significantly higher in F1 *focus*.
On the contrary, a significant increase in glutamate dehydrogenase activity was detected in F3, compared to F1 *focus*, while no differences between the two *foci* were observed in specific activities of malic enzyme, G6PDH and $NADP^+$ dependent isocitrate DH. As shown in Fig. 8.3A, lactic dehydrogenase (LDH) was also found more active in F1 *focus*, suggesting that glycolytic NADH production exceeds mitochondrial reoxidative capacity leading to fermentation. This is confirmed by the increase in lactate production, shown by F1 *focus* (Fig. 8.3B).
In order to assess whether F1 *focus* metabolism is rewired into Warburg effect, we investigated the expression of PKM2 isoform of pyruvate kinase, which is often expressed in cancer cells, as well as the expression of the PFKFB3 isoform of the bifunctional PFK/FBP enzyme. PFKFB3 is endowed with a much higher kinase/phosphatase activity, compared to the normal enzyme, and allows cancer cells to maintain high glycolytic rates, by producing fructose 2,6 phosphate; the latter in turn activates phosphofructokinase activity of the bifunctional PFK1/FBP enzyme making it at the same time insensitive to ATP inhibition. As reported in Fig. 8.4, Western blots showed that PKM2 was expressed in both *foci*, although at higher levels in F1 *focus*. This is well in accordance with the fact that F1 *focus* produces more ATP through oxidative phosphorylation than through glycolysis: in fact, PKM2 can yield PEP without producing ATP.
PFKFB3 isoform and GAPDH were also found to be expressed at a higher level in F1 *focus* than in F3 focus, accounting for F1 higher glycolytic flux.

Table 8.1. Glycolytic metabolism and Krebs cycle enzymes activities in F1 and F3 *foci*. Results are expressed as U/mg and are shown as mean ± SEM obtained in three independent experiments. Statistically significant: * $p < 0.05$ (Student's t-test).

Enzyme	**F1**	**F3**	**p-value**
	U/mg	U/mg	
Pyruvate kinase	0.031 ± 0.001	0.028 ± 0.001	*
Citrate synthase	0.109 ± 0,009	0.087 ± 0,007	*
Malate dehydrogenase	0.296 ± 0,038	0.175 ± 0,022	*
Glutamate dehydrogenase	0.057 ± 0,003	0.068 ± 0.004	*
Malic enzyme	0.012 ± 0.001	0.014 ± 0.0001	
Glucose-6-phosphate dehydrogenase	0.012 ± 0,001	0.011 ± 0,0009	
Isocitrate dehydrogenase	0.031 ± 0,005	0.025 ± 0,004	

Figure 8.3. A) Lactate dehydrogenase activity analysis in F1 and F3 *foci*. The results are expressed as U/mg and are shown as mean ± SEM obtained in three independent experiments. B) ATP and lactate level in F1 and F3 foci. The results are expressed in nmol, normalized respect to mg of cells and are shown as mean ± SEM obtained in three independent experiments. Statistically significant: * $p < 0.05$, *** $p < 0.001$ (Student's t-test).

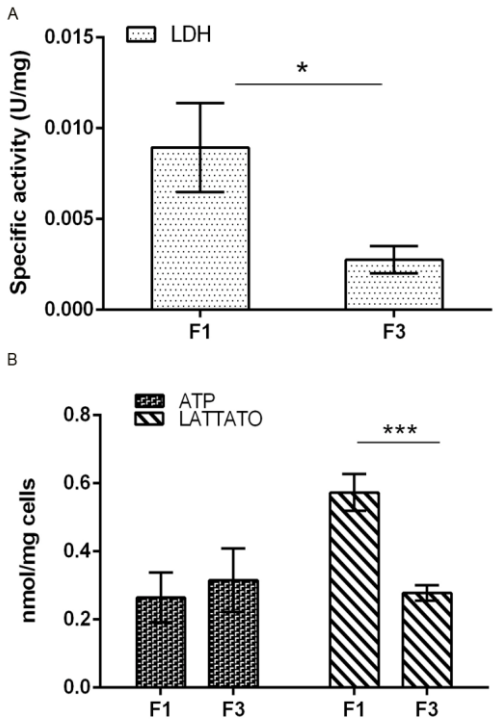

Figure 8.4. A) Representative Western-blot analysis performed on crude extracts, using anti-PKM2, anti-PFKFB3, anti-GAPDH antibodies. Vinculin was used as loading control. The experiments were performed in triplicate. B) Densitometric analysis was performed with Scion Image Software. Values are presented as means ± SEM. Statistically significant: * $p < 0.05$ (Student's t-test).

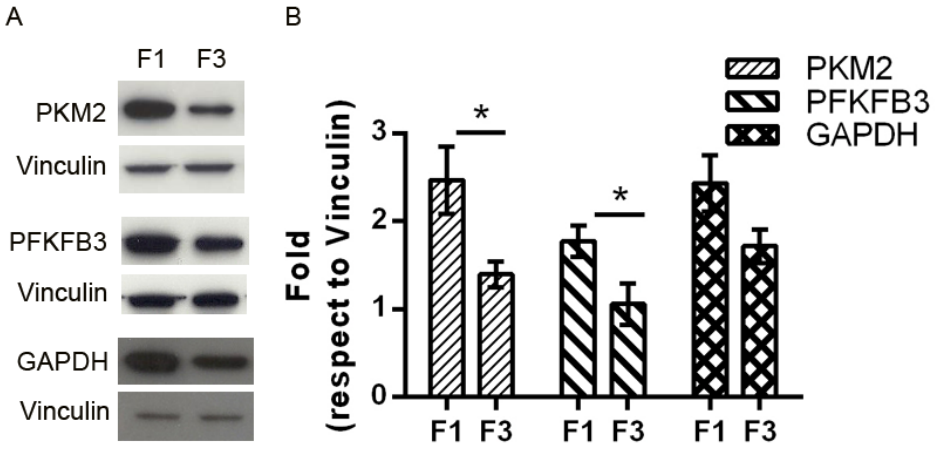

8.3.3 F3 focus show impaired oxidative phosphorylation

Although F1 *focus* showed a higher mitochondrial ATP production, total intracellular ATP was found to be the same in both *foci*, as shown in Fig. 3A, suggesting that F3 *focus* compensated with a higher ATP generation through substrate level phosphorylation. This was confirmed by OCR and ECAR measurements through Seahorse glycolytic assay, reported in Fig. 8.5; the Proton Efflux Rate (PER) was measured for each *focus* under different conditions. Results showed that, although basal PER was higher for F1 *focus*, F3 *focus* showed a higher basal glycolysis, as well as a higher compensatory glycolysis; moreover, the acidification level dropped to lower levels after glycolysis inhibition by 2-DG, confirming that F3 *focus* relies more on substrate level phosphorylation than on oxidative phosphorylation. Further confirmation comes from specific activity assays of glycolytic and TCA enzymes, reported in Table 8.1, showing that, while some TCA enzymes (like pyruvate kinase, citrate synthase and malate dehydrogenase) were found less active in F3 *focus*, compared to F1, glutamate dehydrogenase activity was found significantly higher; this suggests that F3 *focus* may use TCA in an anaplerotic way.

Figure 8.5. Seahorse glycolytic analysis in F1 and F3 *foci*. Analysis of different parameters related with glycolysis, Bars indicate the mean ± SEM obtained in three independent experiments. Statistically significant: * $p < 0.05$ (Student's t-test).

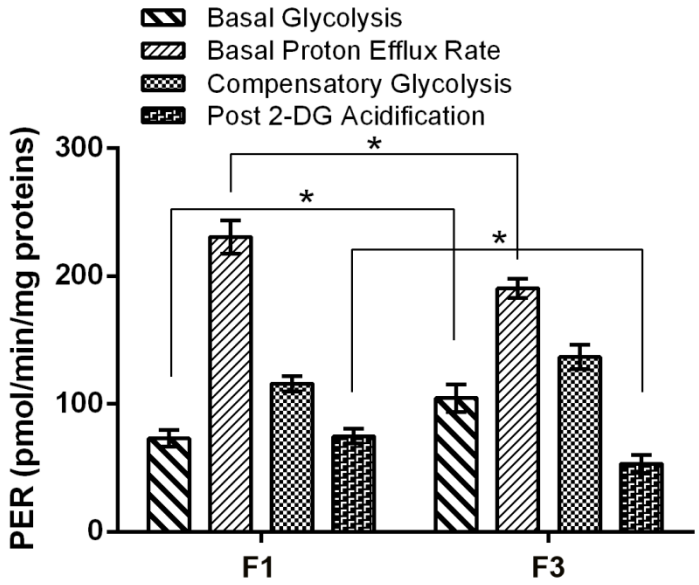

8.3.4 Although F3 focus generates more ROS, it produces less O_2^-, compared to F1 focus

Total ROS content was assayed in each *focus* through cell-permeant 2',7'-dichlorodihydrofluorescein diacetate (H_2DCFDA), which is oxidized to DCF fluorescent probe; results, reported in Fig. 8.6, showed that a higher ROS level was found in F3 *focus*; however, DHE fluorescent probe, measuring only O_2^-, showed that this particular ROS was more abundant in F1 *focus*, as reported in Fig. 8.7. These results were confirmed by the activity assays of the enzymes involved in oxidative stress defense, reported in Table 8.2; the levels of glutatione S-transferase and glutathione reductase specific activities were both found higher in F1 *focus* than in F3 *focus,* while glutathione peroxidase and catalase specific activities were more elevated in F3 *focus*. The level of SOD1 was similar in both *foci*. Glutathione assay showed that total glutathione level was significantly higher in F1 *focus* (Fig. 8.8), with most of in its oxidized (GSSG) form; F3 *focus* showed much lower total glutathione content, with a GSH/GSSG close to 1.

Figure 8.6. Flowcytometric analysis of cadmium –induced ROS production in F1 and F3 *foci*. A) Cells are incubated with 5 µM H_2DCFDA and the level of fluorescence is measured. The results are shown in a dot plot overlay, representative of three independent experiments. B) The fluorescence intensity of all experiments is represented by a box plot. The dark line within a box represents the median value, while the upper and lower sides of a box are the third and first quartiles, respectively. Statistically significant: * $p < 0.05$ (Student's t-test).

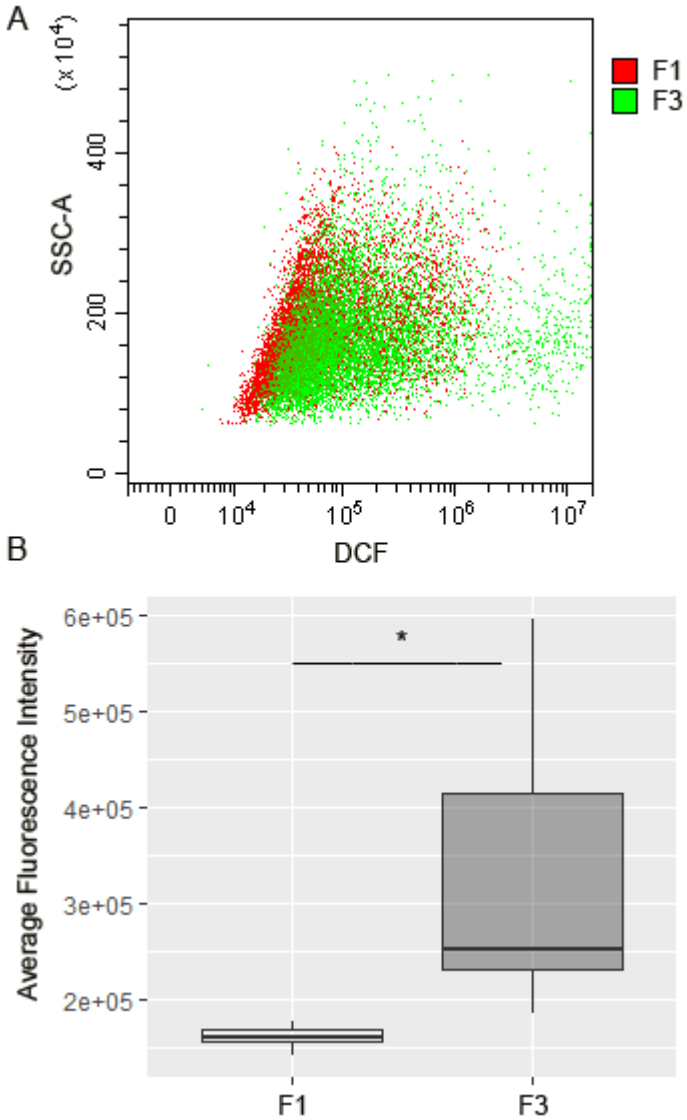

Figure 8.7. Flowcytometric analysis of cadmium –induced superoxide anion production in F1 and F3 *foci*. A) Cells are incubated with 10 µM DHE and the level of fluorescence of cells is measured. The results are shown in a dot plot overlay, representative of three independent experiments. B) The fluorescence intensity of all experiments is represented by a box plot. The dark line within a box represents the median value, while the upper and lower sides of a box are the third and first quartiles, respectively. Statistically significant: * $p < 0.05$ (Student's t-test).

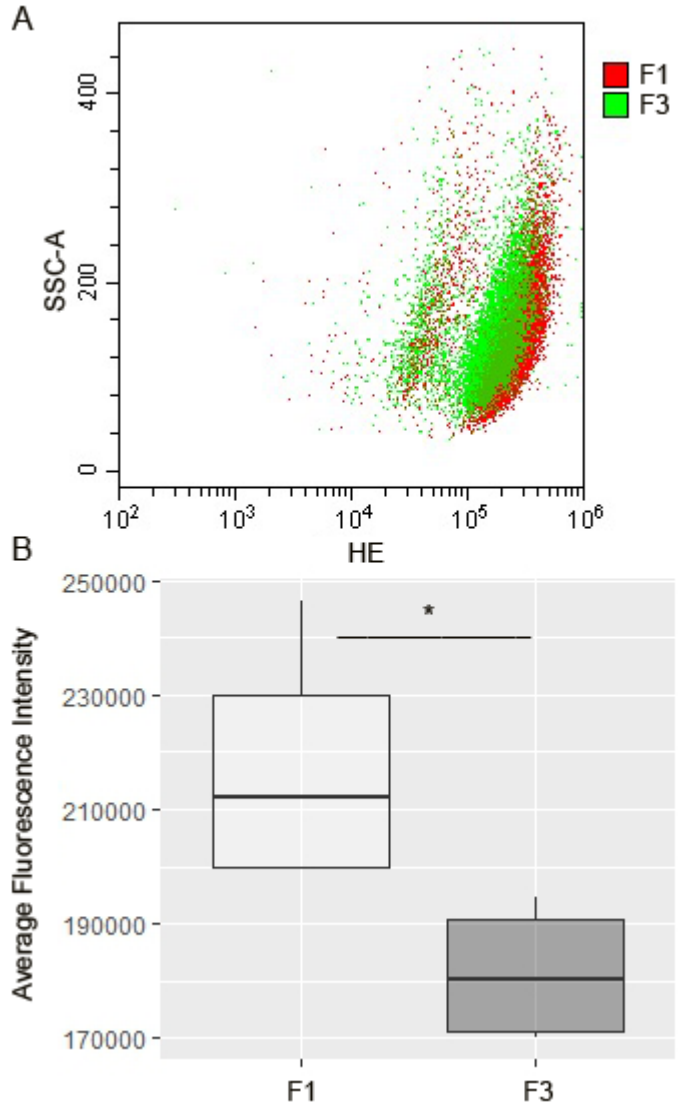

Table 8.2. Enzymes involved in oxidative stress defence in F1 and F3 *foci*. The results are expressed as U/mg and are shown as mean ± SEM obtained in three independent experiments. Statistically significant: * $p < 0.05$, ** $p < 0.01$ (Student's t-test).

Enzyme	**F1**	**F3**	**p-value**
	U/mg	U/mg	
Glutathione peroxidase	0.148 ± 0.015	0.211 ± 0.021	*
Glutathione reductase	0.016 ± 0.0005	0.012 ± 0.001	*
Glutathione S-transferase	0.066 ± 0.008	0.035 ± 0.007	*
Catalase	4.788 ± 0.594	7.354 ± 0.442	**
Superoxide dismutase 1	0.591 ± 0.050	0.559 ± 0.073	

Figure 8.8. Glutathione level in F1 and F3 *foci*. The results are expressed in nmol/mg and normalized respect to mg of cells. Statistically significant: * $p < 0.05$, ** $p < 0.01$ (t-test).

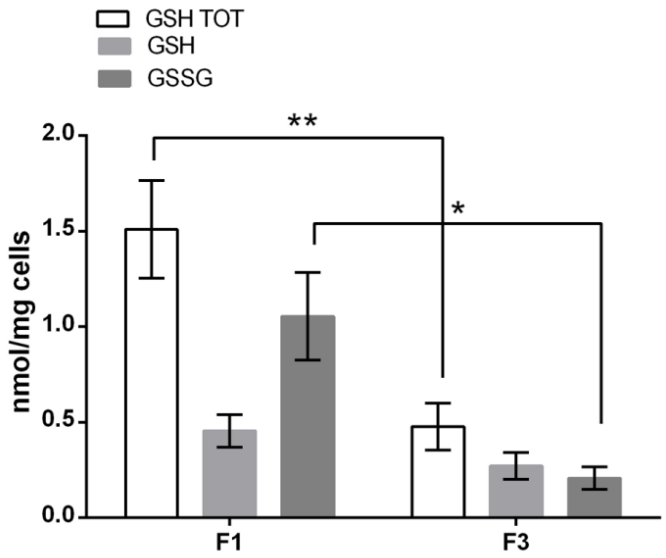

8.3.5 Mitochondria morphology analysis show different alterations in each focus

Confocal microscopy images of both *foci*, as well as control cells, stained with R123 were collected to investigate mitochondria morphology and intracellular distribution.

As already reported (Oldani et al. 2019, BBA submitted), mitochondria in control C3H cells are normally distributed through the cytoplasm and extend from the nucleus to the cell periphery (Fig. 8.9A). F1 *focus* showed mitochondria mainly crowded in the perinuclear region, with only sparse organelles at the cytoplasm periphery; although mitochondrial crowding around the nucleus does not allow to appreciate their morphology, punctate and rod-like shaped mitochondria are clearly observed at the cell periphery (Fig. 8.9B). A different picture is seen for F3 *focus* (Fig. 8.9C), showing less crowded mitochondria which are organized in an irregular network; swollen and punctuate mitochondria are observed, as well as dark areas, suggesting the presence of unfunctional mitochondria which are not stained by R123.

Figure 8.9. Representative confocal images of: A) C3H control cells B) *Focus* F1 and C) *Focus* F3. Enlarged views allow to appreciate the details of these morphological features.

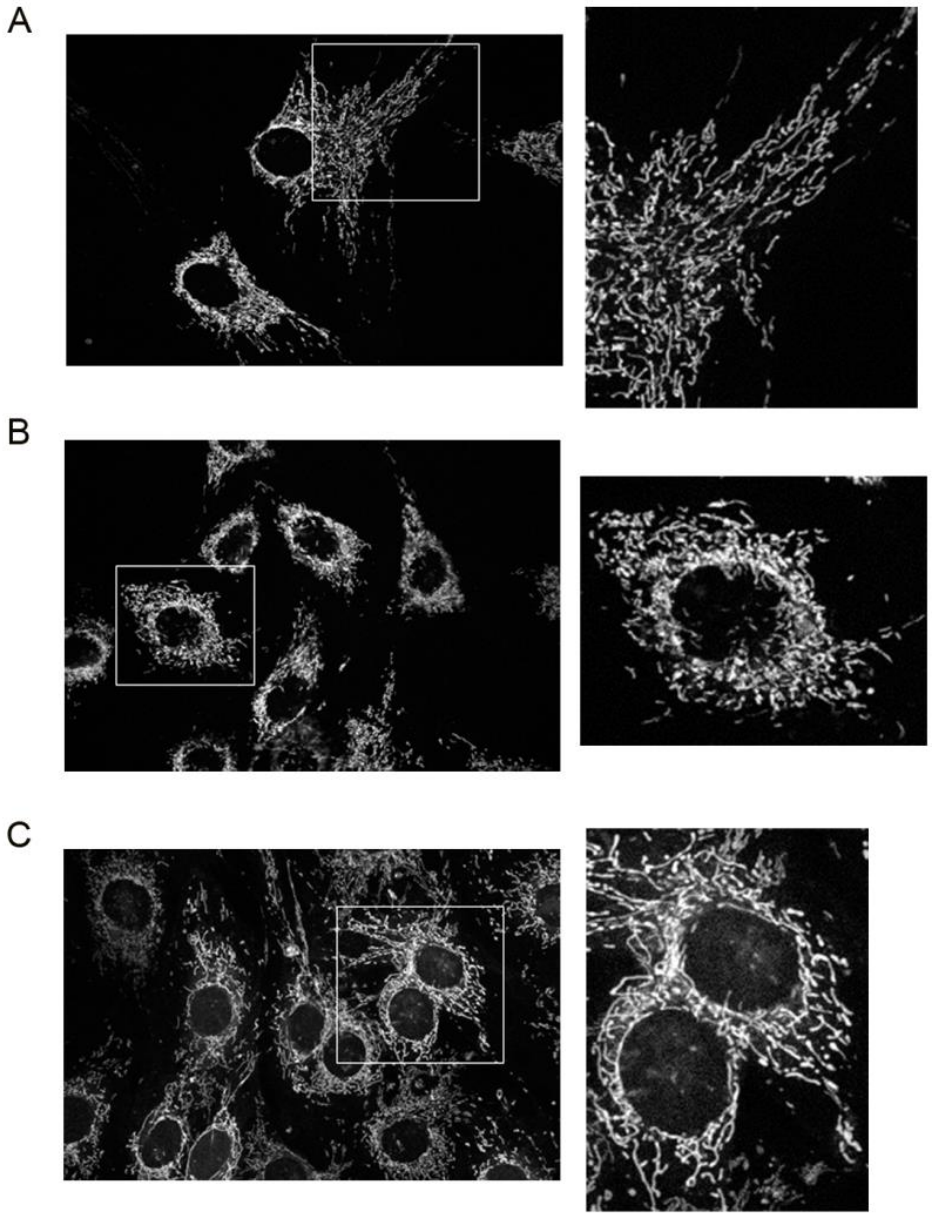

❖ 8.4. Discussion

The comparison between two different *foci*, obtained after CTA performed on C3H cells treated with cadmium for 24h, showed that differences at molecular level underlie previously observed differences in proliferative behavior [14] and in gene dysregulation (Oldani et al. 2019, TIV under revision); this in turn confirms that cadmium damages at molecular level can be unpredictable, because of the thousands of possible molecular targets, although they all eventually lead to malignancy.

In F1 *focus*, we observed higher glycolytic, TCA and oxidative phosphorylation rates, compared to F3 *focus*, which are well in accordance with its higher proliferative rate. This is likely accomplished through a mitochondrial reorganization in a tight network around the nucleus, as shown by confocal microscopy mitochondrial analysis, increasing mitochondrial functionality and supporting a high proliferative rate. This is very similar to what previously observed in C3H cells treated with $CdCl_2$ for 24 hours (Oldani et al. 2019, BBA submitted); however, while all NADH produced by Cd-treated C3H cells could be reoxidized on the electron transport chain so that no fermentation could be detected, in F1 *focus*, NADH production exceeds mitochondrial reoxidative capacity, so that NADH is partly reoxidized by LDH, producing lactate. Another interesting feature of F1 *focus* is the loss of Pasteur effect: although most ATP is produced through oxidative phosphorylation, glycolysis is not inhibited, while active glucose oxidation is generally not compatible with a high rate of glycolysis, because citrate inhibits PFK1 [24]. This is likely due PFKFB3 overexpression, which, unlike PFK1FBP, is not inhibited by ATP and is endowed with a much higher kinase/phosphatase activity, allowing cancer cells to maintain high glycolytic rates, by producing PFK1FBP allosteric activator fructose 2,6 phosphate. F1 high glycolytic rate also likely sustains other metabolic synthesis, through overexpression of PKM2 isoform, promoting PEP conversion into pyruvate without ATP synthesis; this can lead to the synthesis of many metabolites, essential to high proliferation rates, and particularly to glutathione synthesis, which is in fact more abundant in F1 *focus*, compared to F3. Glutamine is also required for glutathione synthesis and preliminary data, obtained in our laboratory, strongly suggest that F1 high proliferation rate is sustained by increased glutamine consumption.

F3 *focus* relies mostly on glycolysis for its ATP request, although this pathway is on the whole less active than in F1 *focus*; moreover, mitochondria are clearly dysfunctional in this *focus*, so that NADH produced in the glycolytic pathway is also reoxidized by LDH, yielding lactate. Although to a minor extent compared to F1 *focus*, in F3 *focus* glycolysis is hyperactivated to compensate for loss of mitochondrial ATP production; however, on the whole, the metabolic flux through glycolysis is reduced (as shown by lower PFKFB3, PKM2 and GAPDH expression), compared to F1 *focus*, justifying F3 lower proliferation rate.

On the whole, although in a different way, both F1 and F3 *foci* show uncoordinated glycolysis, TCA and oxidative phosphorylation, each pathway working independently; this is likely a consequence of the loss of Pasteur effect in F1 *focus* and of mitochondrial damage in F3 *focus*; two different pathways leading to the same fate: cell transformation into a malignant phenotype.

Regarding reactive oxygen species, which are normally produced by cadmium uptake, F3 *focus* showed a higher accumulation of total ROS, likely due to mitochondria dysfunction; however, O_2^- level was found much higher in F1 *focus*; the fact that GST and GR specific activities were found higher in this *focus*, together with total glutathione level, suggests that these represent the defense against O_2^- accumulation and seems to be confirmed by the higher ratio GSSG/GSH shown by F1 *focus*. Glutathione level is often increased in cancer cells, as a result of increased oxidative stress and glycolysis upregulation, leading to faster growth rates and resistance to a number of chemotherapeutic agents [25]. Besides, GSH has been shown to directly reduce O_2^- [26] and may therefore represent a defense mechanism against this ROS, apart from SOD.

An open question is why SOD1 activity is not increased in F1 *focus* in order to detoxify O_2^-; however previous data obtained in our laboratory (Oldani et al. 2019, BBA submitted) showed that SOD1 activity is impaired by 24 h treatment with $CdCl_2$, leading to O_2^- level increase; moreover, toxicogenomic data (Forcella et al. 2019, Neurotoxicology under revision) showed that SOD1 coding gene is not dysregulated by cadmium treatment in human SH-SY5Y neuroblastoma cells; in *foci*, the same level of SOD1 activity could be detected, despite the difference in O_2^- accumulation. In accordance with its higher level of total ROS, F3 *focus* showed higher specific activities of both GPox and catalase, suggesting an increased production of H_2O_2, which is inactivated by both enzymes. This in turn could be due to electron transfer impairment,

related to mitochondrial damage, as shown by confocal microscopy analysis. This is well in accordance with toxicogenomic data (Oldani et al. 2019, TIV under revision) showing that 13 out of the 15 top up-regulated genes in F3 *focus* are involved in an interferon mediated antiviral response, which can be triggered by either viral DNA or viral RNA. Numerous studies have demonstrated that bacterial RNA can be detected by cell type-specific endosomal and cytoplasmic receptors [27]. In both human and murine plasmacytoid dendritic cells, bacterial RNA induces type I IFN response mediated by TLR7 (ref), while in human monocytes bacterial RNA is detected by TLR8 resulting in IL-6 and TNF secretion. In our toxicogenomics study TLR8 gene was found to be upregulated, as well as IL-6 coding gene, suggesting that mtRNA is released from F3 damaged mitochondria and triggers an inflammatory response [28].

Another very interesting consideration is that each focus retains some of the alterations observed in C3H cells treated with $CdCl_2$ for 24h, suggesting that the different alterations did not originally occur in all treated cells, but that each cell reacted in its own peculiar way to cadmium intoxication. This definitely shows that, although C3H cells are all genetically identical, much of their fate upon cadmium intoxication depends on a plethora of microenvironmental and subcellular factors, like local MTs and GST expression, ROS defense enzyme activity etc., so that for the vast majority of cells cadmium is efficiently inactivated, while only a very small number of cells is damaged, each in a different way. Further research will address the question of how all these effects are irreversibly triggered by cadmium uptake, 4-6 weeks earlier than foci detection and collection. Recent data obtained in our laboratory suggest that an involvement of HIF-1α can be ruled out, since it does not appear to be stabilized in foci (Figure 8.10).

Figure 8.10. Representative Western-blot analysis performed on crude extracts using anti HIF-1a antibody. Tubulin was used as loading control. The experiments were performed in triplicate. The positive control was Cos7 cells treated with $CoCl_2$.

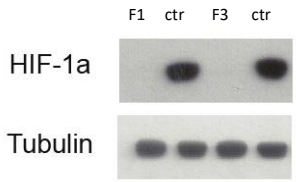

References

- [1] H. Strasdeit, The First Cadmium-Specific Enzyme, Angew Chem Int Ed Engl, 40 (2001) 707-709.
- [2] G. Choong, Y. Liu, D.M. Templeton, Interplay of calcium and cadmium in mediating cadmium toxicity, Chem Biol Interact, 211 (2014) 54-65.
- [3] F. Thevenod, Catch me if you can! Novel aspects of cadmium transport in mammalian cells, Biometals, 23 (2010) 857-875.
- [4] C. Urani, P. Melchioretto, M. Bruschi, M. Fabbri, M.G. Sacco, L. Gribaldo, Impact of Cadmium on Intracellular Zinc Levels in HepG2 Cells: Quantitative Evaluations and Molecular Effects, Biomed Res Int, 2015 (2015) 949514.
- [5] G. Callegaro, M. Forcella, P. Melchioretto, A. Frattini, L. Gribaldo, P. Fusi, M. Fabbri, C. Urani, Toxicogenomics applied to in vitro Cell Transformation Assay reveals mechanisms of early response to cadmium, Toxicol In Vitro, 48 (2018) 232-243.
- [6] A. Martelli, E. Rousselet, C. Dycke, A. Bouron, J.M. Moulis, Cadmium toxicity in animal cells by interference with essential metals, Biochimie, 88 (2006) 1807-1814.
- [7] B. Messner, A. Turkcan, C. Ploner, G. Laufer, D. Bernhard, Cadmium overkill: autophagy, apoptosis and necrosis signalling in endothelial cells exposed to cadmium, Cell Mol Life Sci, 73 (2016) 1699-1713.
- [8] P. Vanparys, R. Corvi, M.J. Aardema, L. Gribaldo, M. Hayashi, S. Hoffmann, L. Schechtman, Application of in vitro cell transformation assays in regulatory toxicology for pharmaceuticals, chemicals, food products and cosmetics, Mutat Res, 744 (2012) 111-116.
- [9] R.D. Combes, Cell transformation assays: are we barking up the wrong tree?, Altern Lab Anim, 40 (2012) 115-130.
- [10] R. Corvi, P. Vanparys, International prevalidation study on cell transformation assay. Preface, Mutat Res, 744 (2012) 1-2.
- [11] J.R. Landolph, Chemical transformation in C3H 10T1/2 Cl 8 mouse embryo fibroblasts: historical background, assessment of the transformation assay, and evolution and optimization of the transformation assay protocol, IARC Sci Publ, 67 (1985) 185-203.
- [12] OECD, Detailed review paper on cell transformation assays for detection of chemical carcinogens, Development, O.f.e.c.-o.a. (Ed). OECD Environment, health and safety publications, (2007) 1-164.
- [13] C.A. Reznikoff, D.W. Brankow, C. Heidelberger, Establishment and characterization of a cloned line of C3H mouse embryo cells sensitive to postconfluence inhibition of division, Cancer Res, 33 (1973) 3231-3238.
- [14] M. Forcella, G. Callegaro, P. Melchioretto, L. Gribaldo, M. Frattini, F.M. Stefanini, P. Fusi, C. Urani, Cadmium-transformed cells in the in vitro cell transformation assay reveal different proliferative behaviours and activated pathways, Toxicol In Vitro, 36 (2016) 71-80.

- [15] G.K. Bergmeyer HU, Grassl M. , Enzymes as biochemical reagents, in: B. HU (Ed.) Methods of enzymatic analysis, vol. 1, Academic Press, New York, 1974, pp. 427-522.
- [16] D. Shepherd, P.B. Garland, The kinetic properties of citrate synthase from rat liver mitochondria, Biochem J, 114 (1969) 597-610.
- [17] G.M. Bergmeyer HU, Enzymes. Catalase, in: B. HU (Ed.) Methods of enzymatic analysis, vol. 2, New York: Academic Press, NewYork, 1983, pp. 165-166.
- [18] W.H. Habig, M.J. Pabst, W.B. Jakoby, Glutathione S-transferases. The first enzymatic step in mercapturic acid formation, J Biol Chem, 249 (1974) 7130-7139.
- [19] H.S. Nakamura W, Hayashi K. , Purification and properties of rat liver glutathione peroxidase, Biochim Biophys Acta, 358 (1974) 251-261.
- [20] Y. Wang, L.W. Oberley, D.W. Murhammer, Antioxidant defense systems of two lipidopteran insect cell lines, Free Radic Biol Med, 30 (2001) 1254-1262.
- [21] P.G. Vance, B.B. Keele, Jr., K.V. Rajagopalan, Superoxide dismutase from Streptococcus mutans. Isolation and characterization of two forms of the enzyme, J Biol Chem, 247 (1972) 4782-4786.
- [22] M.M. Bradford, A rapid and sensitive method for the quantitation of microgram quantities of protein utilizing the principle of protein-dye binding, Anal Biochem, 72 (1976) 248-254.
- [23] U.K. Laemmli, Cleavage of structural proteins during the assembly of the head of bacteriophage T4, Nature, 227 (1970) 680-685.
- [24] A. Kim, Mitochondria in Cancer Energy Metabolism: Culprits or Bystanders?, Toxicol Res, 31 (2015) 323-330.
- [25] C.A. Lewis, S.J. Parker, B.P. Fiske, D. McCloskey, D.Y. Gui, C.R. Green, N.I. Vokes, A.M. Feist, M.G. Vander Heiden, C.M. Metallo, Tracing compartmentalized NADPH metabolism in the cytosol and mitochondria of mammalian cells, Mol Cell, 55 (2014) 253-263.
- [26] C.C. Winterbourn, D. Metodiewa, The reaction of superoxide with reduced glutathione, Arch Biochem Biophys, 314 (1994) 284-290.
- [27] S. Grazioli, J. Pugin, Mitochondrial Damage-Associated Molecular Patterns: From Inflammatory Signaling to Human Diseases, Front Immunol, 9 (2018) 832.
- [28] A.P. West, Mitochondrial dysfunction as a trigger of innate immune responses and inflammation, Toxicology, 391 (2017) 54-63.

Chapter 9

"Changes in gene expression in hepatic cells upon cadmium and copper exposure unveil mechanisms of metal carcinogenicity."

ABSTRACT

Metals are widely used in a large number of industrial activities and could be released in the environment at toxic levels for human health. Although metal toxicity has been studied, the underlying molecular mechanisms remain elusive. An example are the effects on biological processes induced by cadmium which is a non-essential metal ion known for its toxicity and carcinogenic potential. Another metal, copper, is on the contrary an essential trace metal that becomes toxic with higher concentrations but does not feature a carcinogenic effect. We here analysed transcriptomics data on a human hepatoma cell line, which was exposed to low (2 µM) and high (10 µM) concentrations of cadmium to help in the elucidation of the effects caused by cadmium at the cellular level, to identify cancer hallmarks related to cadmium exposure and to address dose-dependent effects. We also compared the changes induced by cadmium with the changes induced on the same cell lines upon exposure to low (100 µM) and toxic (400 µM) concentrations of copper. In this study, we used a combination of bioinformatic and biostatistics approaches. The transcriptomic signatures induced by copper exposure were used to discriminate between cancer-related changes and general toxic effects exerted by metal exposure since copper is known to be a non-cancerogenic metal. Our data unveiled a first protective response at low concentration of cadmium triggered thanks to the induction of metallothioneins, whereas high cadmium concentrations inhibited liver functions, promoted genes related to cellular migration and matrix organization, along with increased cellular stemness.

Monica Oldani, Isabelle da Piedade, Marta Lucchetta, Matilde Forcella, Chiara Urani, Paola Fusi, Elena Papaleo

Keywords: Cadmium; Hepatotoxicity; HepG2; human liver carcinoma cells; Toxicogenomics; Copper

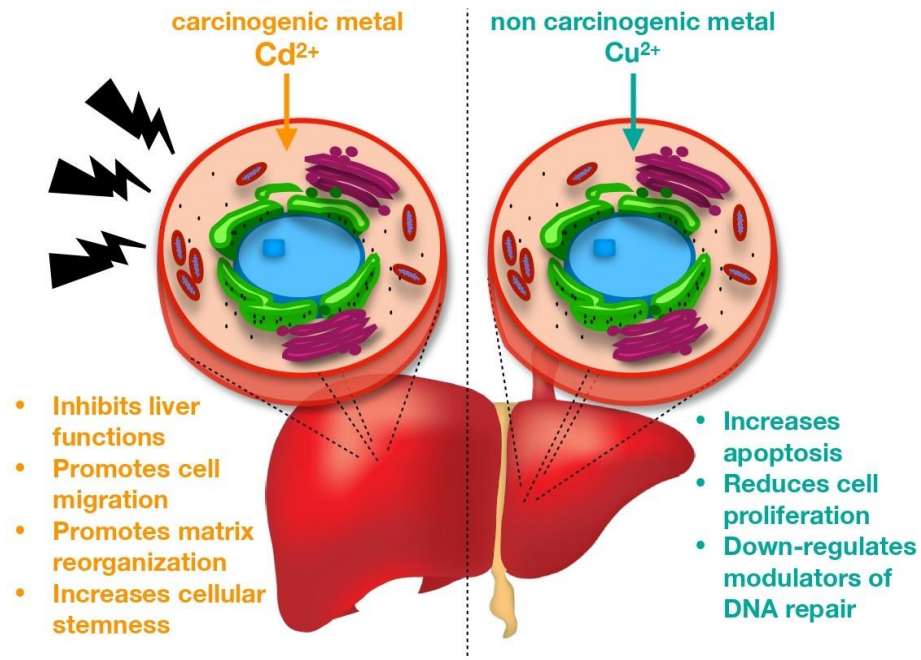

This chapter is an extract of the submitted paper in Metallomics, 2019

❖ 9.1.Introduction

Heavy metals belong to a group of chemical elements with a high atomic weight that find many applications in the industrial and agricultural sectors. However, all these metallic elements are classified as systemic toxicants or human carcinogens by the World Health Organization's International Agency for Research on Cancer [1]. Consequently, their largest release into the environment has increased the cancer risk for the general population [2]. Studying the mechanisms of metal toxicity is of strong interest for human health. Over the last forty years, several studies have shown that heavy metals toxicity depended on the dose, route and time of exposure and organs affected [3]. At the same time, different toxic effects of arsenic (As), cadmium (Cd), cobalt (Co), chromium (Cr), copper (Cu), lead (Pb), nickel (Ni) and mercury (Hg) are not completely understood. Among those heavy metals, cadmium is one of the most dangerous as it enters the food chain, e.g vegetables and cereals absorb cadmium from fertilizers or polluted soils. The accumulation of this metal in tobacco plants contributes to make smoking another source of cadmium exposure [4]. In addition, cadmium is able to accumulate in the human body and it is difficult to excrete [5]. The emergence of toxicogenomics [6], a combination of genomics and bioinformatics coupled with experimental validation, gives a global approach to investigate mechanisms and molecular pathways that are involved in metal intoxication, adaptive response of different tissues and increase of the risk of developing carcinogenesis. The integration of toxicogenomics analysis and bioinformatics tools combined with conventional laboratory work can provide better insight into the effect-response of cells after metal exposure such as cadmium or copper. For example, Benton and colleagues [7] compared for the first time the gene response of human lymphoblastoid cells to cadmium and arsenic. They were able to identify 167 differentially expressed genes that did not overlap between the two metals and were involved in tumorigenesis, inflammation, and cell signaling. Several studies [8] [9] showed that genes encoding for metallothioneins, antioxidant proteins, and heat shock proteins were induced upon exposure to lower doses of cadmium. Oxidative stress is also a common response to fight cellular toxicity upon exposure to nickel, chromium and cadmium in liver rat cells while retinoic acid signaling seems to be a unique response to cadmium [10]. More recently, Madejczyk and colleagues [11] identified common cadmium and

chromium induced responses such as oxidative stress, DNA damage, metabolism, cell cycle and inflammatory response pathways. Here, we aimed at using a combination of different bioinformatic tools to unveil the molecular mechanisms related to cadmium toxicity in cancer. The liver is the main organ subjected to cadmium accumulation and poisoning for its essential role in metal detoxification and homeostasis [12]. The liver contributes to the uptake of ingested metals from the circulating blood [13] and excretes them into the bile [14]. We thus selected the human hepatoma cell line HepG2 as a model system to screen the potential cytotoxicity of cadmium, as it was characterized by the absence of viral infection and the preservation of the genotypic and phenotypic features similar to normal liver cells [15]. We focused our attention to the analyses of transcriptomics data, considering that metals have been reported to modulate gene expression [16]. Specifically, it is well known that cadmium is a transcriptional regulator in different human tissues, in particular Cd increases expression of genes that encode for proteins related to stress-response such as metallothioneins (MTs) or heat shock proteins, apoptosis, cell metabolism, inflammation and extracellular organization [17 18 9 19].Cadmium can also replace zinc in the binding of several metal-binding proteins [20 21 22 23], such as zinc finger domains, which are often associated with transcription factors [24 25]. In more details, we studied the effects induced by 2 µM and 10 µM of cadmium, two sub-lethal concentrations of cadmium in comparison with unstressed cells [26]. In fact, Urani and colleagues [27] showed that the concentration of Cd required to produce 50% of lethal effect in HepG2 was about 25 µM after 24h. Hence, we wanted to evaluate a dose-dependent effect in genes modulation induced by cadmium, along with in the affected pathways and molecular processes in non-cytotoxic conditions). To better appreciate the specificity of the effects induced by cadmium and associated with its carcinogenic potential, we compared the changes in gene expression induced by cadmium with the corresponding effects induced by copper. Despite being both pollutants, copper is an essential element for humans and is not a carcinogenic metal. In light of these observations, copper thus is a suitable candidate to differentiate between changes in gene expression due to a general toxic effect induced by a metal ion and changes more tightly related to the cadmium cancerogenic potential. To this aim, we selected transcriptomics data, obtained from HepG2 cells, after exposure to low (100 µM) and high (400 µM) copper concentrations [28] to compare with our dataset, obtained after cadmium treatment of the same

cell line. Two µM Cd was compared with 100 µM Cu and 10 µM Cd with 400 µM Cu, across the two cellular models since 100 µM Cu and 2 µM Cd are both lethal doses (EC5) and 400 µM Cu and 10 µM Cd are both around EC30 at the same time in the same cell line.

❖ 9.2. Materials and Methods

9.2.1 Datasets

In this study, we are interested in the analysis of the modulation of gene expression in human hepatoma cell line HepG2 after cadmium and copper exposure. We downloaded the data from the National Center for Biotechnology Information's Gene Expression Omnibus (GEO) repository from [26] and from [76]. The data are accessible through GEO series Accession No. GSE31286 and GSE9539, respectively. We downloaded and used the probe level normalized matrix which was called GSE31286_probe_level_data.txt matrix: https://www.ncbi.nlm.nih.gov/geo/query/acc.cgi?acc=GSE31286. The corresponding annotation GPL4133 file called GPL4133_old_annotations.txt.gz is available at: https://www.ncbi.nlm.nih.gov/geo/query/acc.cgi?acc=GPL4133. We used the function collapseRows from WGCNA R package version 1.66 [104] to aggregate gene expression by genes. The expression matrix was restricted to protein coding genes using biomaRt R package to connect to Ensembl database and retrieve the human genome assembly GRCh38 [105]. In the cadmium dataset, about 20.000 genes from HepG2 cells treated for 24 hours with 2 and 10 µM Cd were collected in every single microarray data, six for each treatment condition. Three independent replicates were used for each type of stimuli. Song et al. have applied the global normalization to raw microarray data, per spot and per chip, through intensity dependent (Lowess) normalization [106]. Cells were treated with 100, 200, 400 or 600 µM Cu for 4, 8, 12 or 24 hours and they mentioned that the concentrations correspond to lethal dose between LD5 to LD50 after one day [28]. In 2005, Urani et al. showed that after the same time the concentration of Cd required to produce 50% of lethal effect was about 20 µM [27]. Consequently, we decided to merge cadmium microarray with copper microarray considering only 100 and 400 µM Cu after 24 hours. The choice was influenced by the fact that 100 µM Cu and 2 µM Cd are 5% of lethal dose and 400 µM Cu and 10 µM Cd are about LD30 for both compounds.

9.2.2 Principal component analysis

We performed a principal component analysis (PCA) to investigate the expression trends of the datasets using the built-in R function prcomp. Differential expression analyses (DEA) have been carried out using limma Bioconductor package [31] to detect up- or down-regulated genes after cadmium and copper treatments. Modulated genes were chosen using cutoffs for Log fold change (LogFC) as ≥ 1 or ≤-1, and a cutoff of 0.05 for false discovery rate (FDR). For the differentially expressed genes (DEGs), we used the UpsetR package [107] to visualize the representation of associated data, such as the number of elements in the aggregates and intersections. In addition, we obtained different volcano plots which showed the distribution of the genes according to the logFC and the LogFDR detected by the DEA and the top 20 most significant differentially expressed genes for all the comparisons using the TCGAVisualize_volcano function, incorporated into the TCGAbiolinks package [108]. All of the above computations were conducted using the R statistics programming environment.

9.2.3 Pathway enrichment analysis

The Kyoto Encyclopedia of Genes and Genomes (KEGG; http://www.genome.jp/kegg) database consists of a collection of online databases of genomes, enzymatic pathways and biological chemicals. A KEGG pathway enrichment analysis was performed to determine the function of DEGs with a threshold of $p<0.05$. We also used ReactomePA version 1.18.1, an R package for Reactome Pathway Analysis [109 110]. An adjusted p-value cutoff of 0.05 was set and the analysis was done by separating the up- and down-regulated genes and with all DEGs together.

9.2.4 Gene Ontology enrichment analysis

To identify altered biological functions in HepG2 after cadmium and copper treatments and understand the importance of DEGs, GO classifica-tion was performed including the following categories: biological process, cellular component and molecular functions [111 112]. GO functional enrichment analysis was done for DEGs using topGo R/Bioconductor package. We analyzed DEGs as up- and down-regulated genes first and using a list of all modulated genes together. GO results are represented in circular plots generated by the Goplot [113] R/Bioconductor package. These plots display the relation between the most significant GO terms and the DE genes that belong to as well as the log(FC) calculated by limma approach.

9.2.5 Stemness analysis

We used StemChecker [114] to estimate the stemness of the differentially expressed genes. The tool allows to estimate the significance of enrichment of genes included in a gene set in input for different classes of stem cell types. The composite gene sets for the different cell types are the unions of all selected stemness signatures of the corresponding cell type. The significance (p value) is calculated by a hypergeometric test, which assess the enrichment against the full annotated human genome. The adjusted p value is calculated by Bonferroni correction.

9.2.6 Merging cadmium and copper arrays

The Agilent cadmium microarray (GSE31286: 2µM vs 10µM) was merged with the copper microarray (GSE9539: 100µM vs 400µM for 24 hours). We downloaded the cadmium microarray from NCBI Gene Expression Omnibus (GEO) using GEOquery, R package release version (3.7) [115] to extract feature, pheno and expression matrix. We transformed the matrix into log2 and we aggregated by probe mean. We downloaded the raw data from the copper microarray. As there was a dye swap, each control and treatment took alternatively one channel (cy3 or cy5) but not always in the same order. The data were made of 6 replicates, 2 conditions i.e 12 samples and 24 channels (12 cy3 + 12 cy5). Target files have been created to extract the 12 samples with read.maimages. After extracting all the channels, background corrections have been performed with two LIMMA methods of normalization within arrays and between arrays. We calculated the ratio values (M = Log2(R/G), R = Red channel, G = Green channel) and the average values (A = Log2(R×G)/2) to obtain log2(R) and log2(G) values of normalized signals. We grouped all the treatments and controls following the dye swap order. We concatenated all the 12 treatments and 12 controls and aggregated them by probe ID mean. We extracted the features to have the names and the notation of all the unique probes with RGSgenes from Agilent. We duplicated the pheno matrix because of the separation of two channels (cy3 and cy5) to have the same dimension and we renamed the columns by the name of the samples. We merged the cadmium and copper matrices by probe mean using combat with two groups: 9 samples from cadmium and 24 from copper.

❖ 9.3. Results

9.3.1 Only the 10 µM concentration of Cd has a marked effect on gene expression

In this study, we aimed at comparing the effects induced on gene expression in a human hepatic cell line (HepG2) upon treatment with different Cd concentrations. The two concentrations of 2 µM and 10 µM Cd used in the study published by Fabbri and colleagues [26] were selected as they represent human relevant Cd concentrations [29 30]. However, it is known that Cd does not affect HepG2 cell viability when the cells are treated for 24 h with different $CdCl_2$ concentrations (0.1, 0.5, 1, 2, 5, and 10 µM) [27].

We initially carried out a general exploration using a dimensionality reduction technique based on principal component analysis (PCA) to extract the dominant patterns present in the data (Figure 9.1A). The first principal component (PC1) represents 52.5 % and the second principal component (PC2) 19.2% of the sample variance. Thus the genes that triggered the most pronounced effects upon Cd exposure were effectively captured into a two-dimensional space. We observed that only the 10 µM Cd was clearly separated from the other datasets. Indeed, 2 µM Cd samples and the controls were highly overlapping, suggesting that a low cadmium concentration had minor effects on gene expression and alterations of the related pathways. This first result suggests that there was a clear dose-dependent effect on gene expression. However, the lowest Cd concentration was not sufficient to rewire the transcriptome of HepG2 cells, whereas a higher concentration of Cd, corresponding to EC30, caused marked consequences.

In light of the PCA results, we then further analyzed the transcriptomics data using a robust statistical framework for differential expression analysis (DEA) based on linear models [31]. In particular, we took three different pairwise comparisons into consideration: 2 µM Cd versus control (2vsC), 10 µM Cd versus control (10vsC) and 10 µM Cd versus 2 µM Cd (10vs2).

9.3.2 Metallothioneins are the first response to Cd exposure in hepatic cells

When we compared 2 µM Cd versus control (2vsC), we identified nine upregulated metallothioneins (MTs) genes, (See Table 9.1, Figure 9.1B) as found in previous analyses [26]. MTs belong to a group of ubiquitous, small cysteine-rich heavy metal binding proteins. Mammalian genomes contain several MT genes, which encode for four members of the metallothioneins family (MT-1 to MT-4). MT-1 and MT-2 are the prevalent MT isoforms. Their roles have been extensively investigated in homeostasis of essential metals such as Zn and Cu, and in the defence against Cd toxicity in various organs in vivo and in vitro [32 33 34]. MTs are the only reported biomolecules in which Cd can naturally accumulate [33]. In acute Cd toxicity, the liver is the primary target and intracellular MTs bind to Cd to form a CdMT complex [34]. CdMT is released into the circulation and reaches the kidney giving rise to Cd-related renal dysfunctions [35]. In addition to being the earliest response of the cells against metal exposure [36], MTs are also known to be involved in zinc metabolism, and for their protective antioxidant role against hydroxyl free radicals [36 37 38]. MTs have been also associated with cell proliferation in breast, prostate, ovarian, head and neck, non-small cell lung cancer, melanoma, and soft tissue sarcoma [39]. Hepatic MTs have also been linked to hepatitis C and other liver diseases such as hepatitis B, hepatocellular carcinoma and liver fibrosis [37].

The overexpression of MTs upon exposure to mild Cd concentrations suggests that the cells can cope with low doses of this toxic agent to inhibit the Cd-induced acute hepatotoxicity by the direct binding of MTs to Cd. MTs interact with metals such as copper, calcium and zinc which are also divalent cations as cadmium. MTs have affinity for both Zn and Cd and they can form a CdMT complex. Cd accumulation could decrease zinc binding to MT thanks to the formation of CdMT complexes and thus disrupt zinc homeostasis [40]. Higher levels of MTs allow to sequester Cd efficiently and avoid these detrimental effects. Moreover, another protective mechanism could be related to the involvement of MT-1 and MT-2 in modulating early immune response [41].

For example, Subramanian Vignesh and Deepe have described that MTs can regulate the innate and adaptive immune system controlling the homeostasis of Zn and Cu, both involved in the development of the immune cells and their molecular function [42].

Table 9.1. Table of upregulated metallothioneins involved in the pairwise comparison between cadmium 2µM versus control.

Gene symbol	Gene description	logFC	FDR
MT1G	metallothionein 1G	3,46	0.00222970563603916
MT1B	metallothionein 1B	3,50	0.00222970563603916
MT1H	metallothionein 1H	3,37	0.00222970563603916
MT1A	metallothionein 1A	3,06	0.00222970563603916
MT1X	metallothionein 1X	3,41	0.00222970563603916
MT1E	metallothionein 1E	3,67	0.00251235851274546
MT1M	metallothionein 1M	3,50	0.0108192869130449
MT1F	metallothionein 1F	3,44	0.0127085833649553
MT2A	metallothionein 2A	2,15	0.0123155992628756

Figure 9.1. A) Principal Component Analysis (PCA) of the two concentrations of cadmium datasets (2µM and 10µM). The first two principal components (PC1 and PC2) account for 52.5% and 19.2% of the variance, respectively. The two-dimensional projections along these PCs allow to shed light on the similarities among the control (Ctrl) and the two cadmium datasets (2µM and 10µM). The colors indicate the different datasets: control (blue), 2µM cadmium (green) and 10 µM cadmium (red). B) Volcano plot for differentially expressed genes cadmium for the pairwise comparison between cadmium 2µM versus control (2vsC). The differential expression analysis was performed for 2vsC. The fold change is represented on the x-axis and the statistical significance i.e -log10 of the p-value on the y-axis. The upregulated genes are situated on the right part of the plot and colored in red. The downregulated genes are situated on the left part and are colored in green. The up- and downregulated genes found as a result are labeled in orange. Each single dot represents one gene with a detectable gene expression in both subtypes. The colored dots are statistically significantly ($p <= 0.05$) down-regulated and up-regulated genes respectively in green and red above the horizontal line that marks the threshold ($p < 0.05$). The vertical dashed lines represents a cutoff to retain significant DE genes with $|logFC| >= 1$.

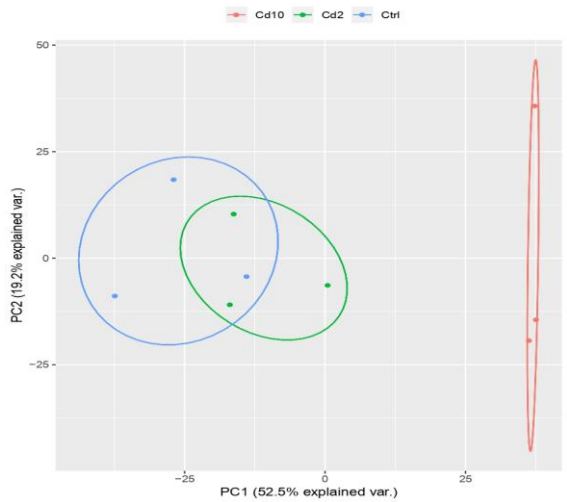

A)

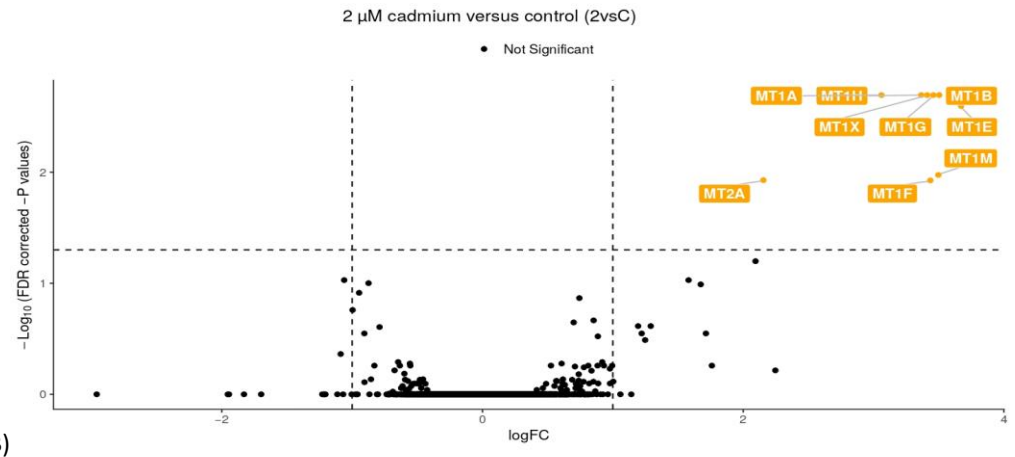

B)

9.3.3 Dose-dependent effect on gene expression upon Cd exposure

When the hepatic cells were treated with a higher concentration of Cd (10 µM), we identified 832 DE genes, i.e 468 up-regulated (Table 9.1SA) and 364 down-regulated (Table 9.1SB) genes (Figure 9.2A). The increased number of DE genes obtained compared to 2 µM Cd treatment confirmed the dose-dependent effect suggested by PCA analyses. We thus compared the changes in gene expression looking at the intersections between the different DEA comparisons (Figure 9.2B). The upregulation of the 9 metallothioneins (MTs) upon treatment with 2 µM Cd was a prolonged response still observable at 10 µM Cd concentration (Figure 9.1S). Moreover, new genes were up- and down-regulated following treatment with a higher Cd concentration for a total of 226 up- and 174 down-regulated genes compared with both the control and the 2 µM Cd treatment. Upon treatment with 10 µM Cd, 233 genes were up-regulated and 190 down-regulated compared to the control, suggesting a progressive adaptation of the cells to increased Cd concentrations (Figure 9.2B).

Figure 9.2. A) Volcano plot for differentially expressed genes cadmium for the pairwise comparison between cadmium 10µM versus control (2vsC). The differential expression analysis was performed for 10vsC. The fold change is represented on the x-axis and the statistical significance i.e -log10 of the p-value on the y-axis. The upregulated genes are situated on the right part of the plot and colored in red. The downregulated genes are situated on the left part and are colored in green. The up- and downregulated genes found as a result are labeled in orange. Each single dot represents one gene with a detectable gene expression in both subtypes. The colored dots are statistically significantly ($p <= 0.05$) down-regulated and up-regulated genes respectively in green and red above the horizontal line that marks the threshold ($p < 0.05$). The vertical dashed lines represents a cutoff to retain significant DE genes with $|logFC| >= 1$. B) Upset R plot shows intersection sizes between cadmium 2µM dataset versus control, cadmium 10µM dataset versus control and cadmium 2µM dataset versus cadmium 10µM dataset. Total set sizes are shown on the bottom left, overlaps are illustrated by links with a filled circle. The corresponding size of a specific overlap of DE gene sets are shown by bars above the links.

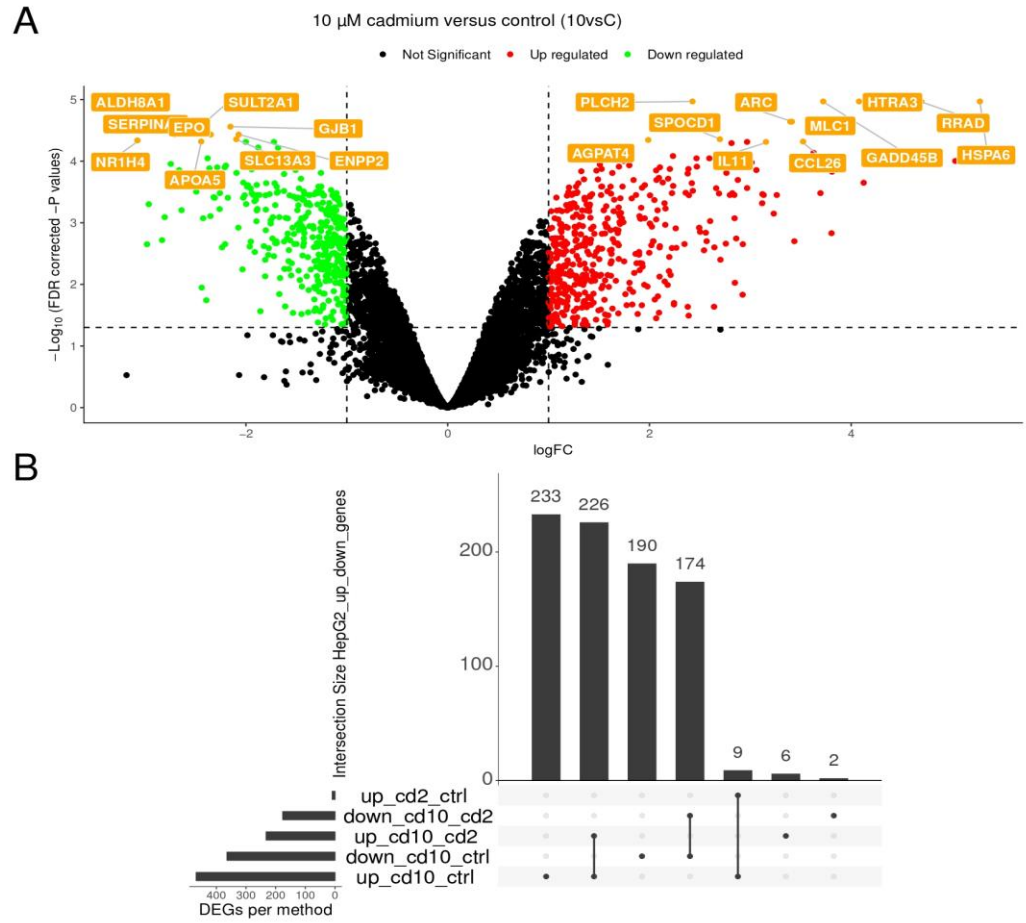

9.3.4 Toxic Cd concentrations inhibit liver functions and promote genes related to cellular migration and matrix reorganization

To illustrate the changes induced by a higher cadmium concentration (10vsC), we plotted a volcano plot to show the top 20 DE genes (Figure 9.2A). All down-regulated genes induced by 10 µM Cd were involved in liver functions (Figure 9.3). In more details, we identified the down-regulation of Nuclear Receptor Subfamily 1 Group H Member 4 (NR1H4) and Sulfotransferase Family 2A Member 1 (SULT2A1). NR1H4 is a receptor involved in bile acid synthesis (Figure 9.2A), with an important role in tumorigenesis, as either an oncogene or a tumour suppressor gene [43]. In mouse liver, NR1H4 deficiency is correlated with the activation of the Wnt/β-catenin pathway and the generation of spontaneous tumors [44]. SULT2A1 acts in the xenobiotics or endogenous compounds detoxification [45]. 1-phosphatidylinositol 4,5-bisphosphate phosphodiesterase η-2 (PLCH2), producing inositol 1,4,5-trisphosphate and diacylglycerol, and the 1-acylglycerol-3-phosphate O-acyltransferase 4 (AGPAT4), that converts lysophosphatidic acid to phosphatidic acid in de novo phospholipid biosynthesis, are both upregulated. HSPA6, CCL26 and GADD45B are implicated in the protection from stress, DNA damage and inflammation. Regarding GADD45B, several evidences suggest that GADD45 genes act as stress sensors related to cell cycle arrest, DNA repair, cell survival, senescence, or apoptosis [46]. For this reason, GADD45B may play a role in DNA excision repair induced by cadmium treatment. RRAD contributes to poor survival in patients because this protein acts as a positive regulator of the EGFR signalling pathway inducing a high proliferative capacity of the tumour cells. Cd inhibited genes that are involved in specific liver functions (Figure 9.3A and 9.4A) and, simultaneously, led to the up-regulation of genes related to the reorganization of the cellular matrix and cell migration (Figure 9.3B and 9.4B).

The three most significant down-regulated pathways and correlated genes belong to cholesterol biosynthesis, biological oxidations and complement cascade (Figure 9.3A). For the cholesterol biosynthesis, involving about 30 enzymes localized in the cytosol, ER membrane and peroxisomes, we found 11 down-regulated genes: ACAT2, DHCR24, FDFT1, HMGCR, HMGCS1, IDI1, LSS, MVD, MVK, SQLE, TM7SF2. Regarding the complement cascade, we identified 11 down-regulated genes: C1S, C3, C4BPA, C5, C8A, C8B, CFB, CFI, CPN2, MASP2, VTN. The down-regulation of both these pathways could suggest that cells were losing some of their typical functions to advantage the metastasis process. Losing the capacity to reduce the presence of reactive oxygen species (ROS) may increase the DNA damage which is another factor that enhances the

severity of the malignancy. Besides, we found low expression levels of cytochromes P450 (CYP19A1, CYP27A1, CYP2B6, CYP2W1, CYP4F12, CYP4F8, CYP8B1) and glutathione S-transferases (GSTA1, GSTA2, GSTA3, GSTA5 and GSTM4). CYP and GST are interesting predictors of cancer development, because both these enzyme families are involved in the detoxification and in the metabolism of toxic compounds [47]. The down-regulation of CYP and GST allows cadmium to remain in the cells as free ions and improves its biological effects [48]. The results of Gene Ontology analysis on the down-regulated genes confirmed the same results described above regarding the down-regulation of the cholesterol biosynthetic process and of plasminogen activation pathway (Figure 9.4A).

Figure 9.3. Dotplots for reactome pathway analysis for cadmium 10µM dataset versus control: downregulated genes (Figure 3A) and upregulated genes (Figure 3B).

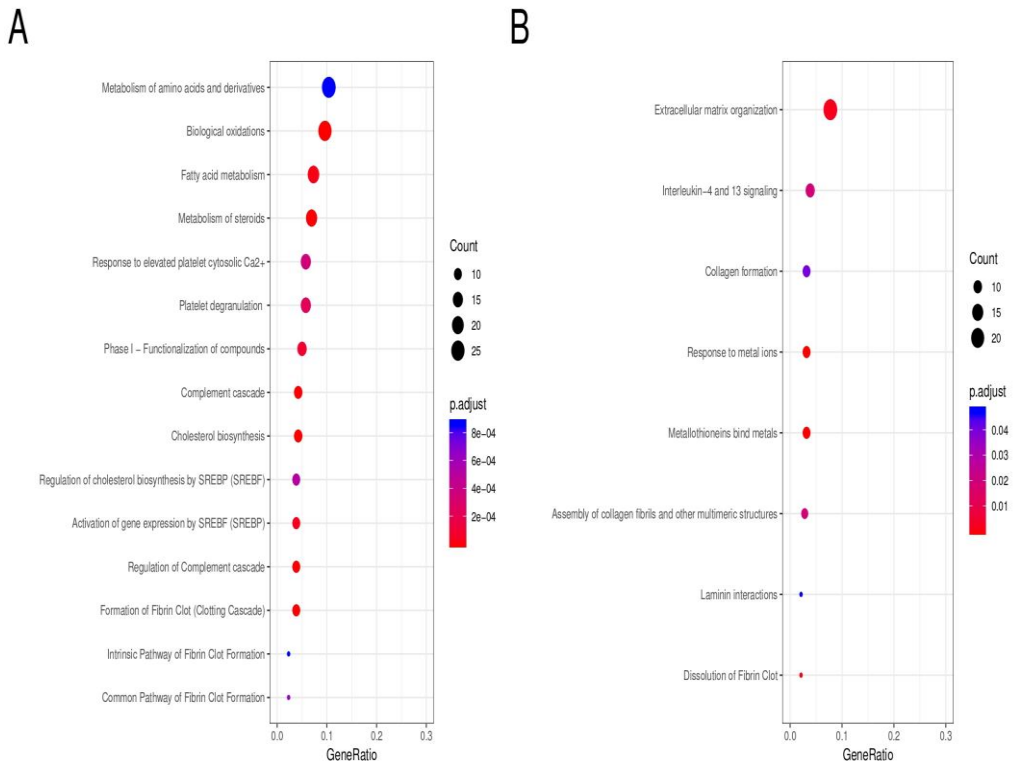

9.3.5 A high Cd concentration induces metastatic features in HepG2 cells

Subsequently, we investigated the functions of the up-regulated genes described in the Gene Ontology analysis (Figure 9.4B). Besides MTs, that remain up-regulated after 10 µM Cd treatment, we observed that the other significant up-regulated genes acted on the positive regulation of cell migration or on the extracellular matrix organization (Figure 9.4B). For example, we noticed the overexpression of SNAI1, a zinc finger transcriptional repressor that was a critical regulator of epithelial-mesenchymal transition (EMT) and cancer metastasis [49], and the up-regulation of CCL26, that is involved in proliferation, migration, invasion, and angiogenesis [50]. Also, Collagen type Iα1 (COL1A1) and collagen type IVα2 (COL4A2) are both reported to be oncoproteins in a variety of tumour tissues and cells [51 52]. COL6A1, ITGA2, ITGA3, and ITGA6 promote tumour cells invasion with poorer survival of the patients affected by cancer [53 51 54]. LAMB3 and COL7A1 are correlated with venous or lymphatic invasion [55 56]. Furthermore, the overexpression of urokinase plasminogen activator (PLAU) (Figure 9.4B) and the urokinase plasminogen activator surface receptor (PLAUR) (Table 9.2SA) also seem to improve migration, cell survival and proliferation of cancer cells inducing the remodelling of the extracellular matrix [57]. In fact, PLAUR is involved in the activation of matrix metalloproteases, such as MMP1 and MMP3 (Table 9.2SA) that generally allow cancer cells to leave the primary tumour as metastasis [58]. The assumption that cadmium causes metastatic features in the HepG2 was supported by the detection of other 3 genes, as well as MMP, involved in the extracellular matrix organization, such as SERPINE1, CYR61, and VCAN (Figure 9.4B) [59 60]. Other genes associated with the positive regulation of cell migration are: EDN1, that enhances cell viability and accelerates cell-cycle progression [61]; F2RL1, that facilitates neovascularization [62]; FAM110C, that regulates the migration of the hepatocyte [63]; Wnt11, that plays an essential role in CRC progression [64]; PREX1, that promotes motility and invasion of glioblastoma cells [65] and PAK1, that promotes NSCLC progression and metastasis through EMT [66]. Instead, MPLZ3 can protect human rectal cancer cell lines from ionizing radiation [67]. Among many genes leading to metastasization, we unexpectedly found the up-regulation of ICAM2 and SPOCK2, that seem to repress cell proliferation and invasion [68 69].

Figure 9. 4. Gene ontology plots for differentially expressed genes for the comparison cadmium 10 µM dataset versus control: downregulated genes (Figure 4A) and upregulated genes (Figure 4B).

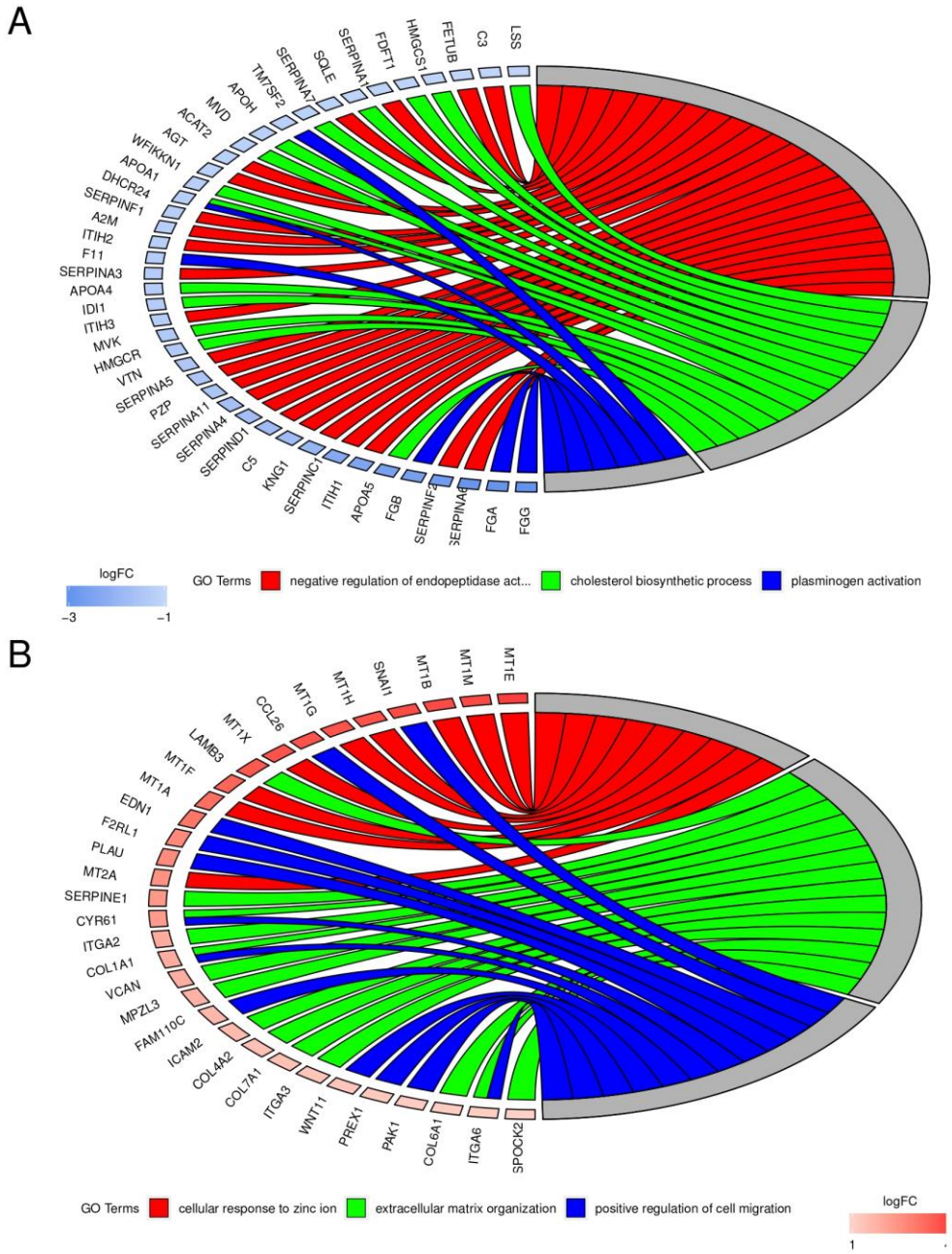

9.3.6 High cadmium concentrations cause dedifferentiation of hepatic cells with a marked stemness signature

Since we observed a down-regulation of genes associated with specialized liver functions upon exposure to high cadmium concentration, we wondered if another effect triggered by this toxic agent was to induce dedifferentiation. In fact, the evolution of cancer stem cells theory has opened new ground for the study of metal-induced carcinogenesis. We thus analyzed the up-regulated DE genes for their stemness signature (see Materials and Methods). We identified 33 genes (NFE2L3, VCAN, SDC4, GAL, PMAIP1, FAM46B, SLC39A10, TUBB2, RAB3B, SPRY4, GFPT2, F2RL1, MT1X, MT1F, UCHL1, MT1H, SERPINB9, DSP, BICD1, SLC2A1, HK1, GABARAPL1, SCHIP1, GGT5, ARID3B, GSTP1, SERPINB8, SLC6A6, MLLT11, KIF3C, SPINT2, STK17A, and MT1M) associated with embryonal carcinoma with significant adjusted p-values. We also evaluated the enrichment of genes included as transcription factor targets for a curation of 10 stemness-related transcription factor datasets, and we identified the SUZ12 transcription factor as dominant in our gene expression data after Cd exposure and a group of up-regulated genes associated with it (ZFP36L1, KLF5, DUSP6, TLE3, NFE2L3, ANKRD1, IER5L, COL7A1, VCAN, FAT, JUN, PPP1R2, RBP1, RGS10 ,SDC4, PPFIBP1, TMSB10, COTL1, TNFRSF12A, FXYD5, C6orf115, HSPBAP1, C9orf19, PAX6, BDH1, KLF6 ,CYP24A1, KRT12, RGS20, ADAMTS4, C2CD2L, LY96, PREX1, KRTAP3-1, ITPRIP, LETM2, and SH3RF2). No significant matches have been found on the down-regulated DEA genes.

9.3.7 Ten µM versus 2 µM Cd treatment comparison yields the same results as 10 µM versus control

The comparison 10 µM Cd vs. 2 µM Cd (10vs2) allowed to investigate the dose-dependent effect of cadmium in HepG2 cells. 232 up-regulated genes (Table 9.2SA) and 176 down-regulated genes were identified (Table 9.2SB).
However, taking into account the list of the top 20 DE genes in the volcano plot (Figure 9.2S), we noticed that only NPPC and CSGALNACT2 were specifically up-regulated genes in the 10 µM Cd vs. 2 µM Cd (10vs2) comparison; both genes are involved in skeletal differentiation or morphogenesis [70 71]. This result could be connected with the assumption that high Cd concentrations could severely damage bone quality when introduced into the human body. Cadmium effect on the skeleton has also been illustrated in the study of Engström et al. [72] in which a positive relationship between fracture risk and cadmium exposure was demonstrated. By contrast, no difference was observed in down-regulated genes underlined by volcano plot (Figure 9.2S) in the 10 µM Cd vs ctrl (10vsC) comparison, except Fibrinogen-like 1 (FGL1), a member of the fibrinogen family proteins. This protein may play a role in the development of hepatocellular carcinomas because FGL1 regulates the epithelial-mesenchymal transition (EMT) determining invasion and metastasis [51]. These data emphasize that sublethal Cd concentrations can be well tolerated by the cells, insomuch as 2 µM Cd and control seem to be comparable.
The results of up-regulated genes are similar to the above mentioned results (Table 9.2SA and Figure 9.2S).

9.3.8 Ten µM Cd modifies the expression level of transcription factors

To investigate if cadmium was able to change the expression levels of transcription factors and their targets, we extracted known transcription factors and their targets by comparing the TRRUST database [73], a manually curated database of human transcriptional regulatory networks with the list of DE genes after 10 µM Cd treatment. We identified 17 up- and 7 down-regulated transcription factors that created a network with different targets (Figure 9.5). Among the up-regulated transcription factors, the Fos gene family consisting of four members (FOS, FOSB, FOSL1, and FOSL2), was strongly represented. These genes dimerize with proteins of the proto-oncogenes JUN family, that were also up-regulated, forming the transcription factor complex AP-1 [74]. Subsequently, AP-1 proteins could control cell life and death modulating the expression of cell cycle regulators such as TP53 [75] or increase the transcription level of pro-inflammatory genes, i.e MMP-1 and MMP-3 (Figure 9.5).

Figure 9.5. Transcription factor- target analysis representation

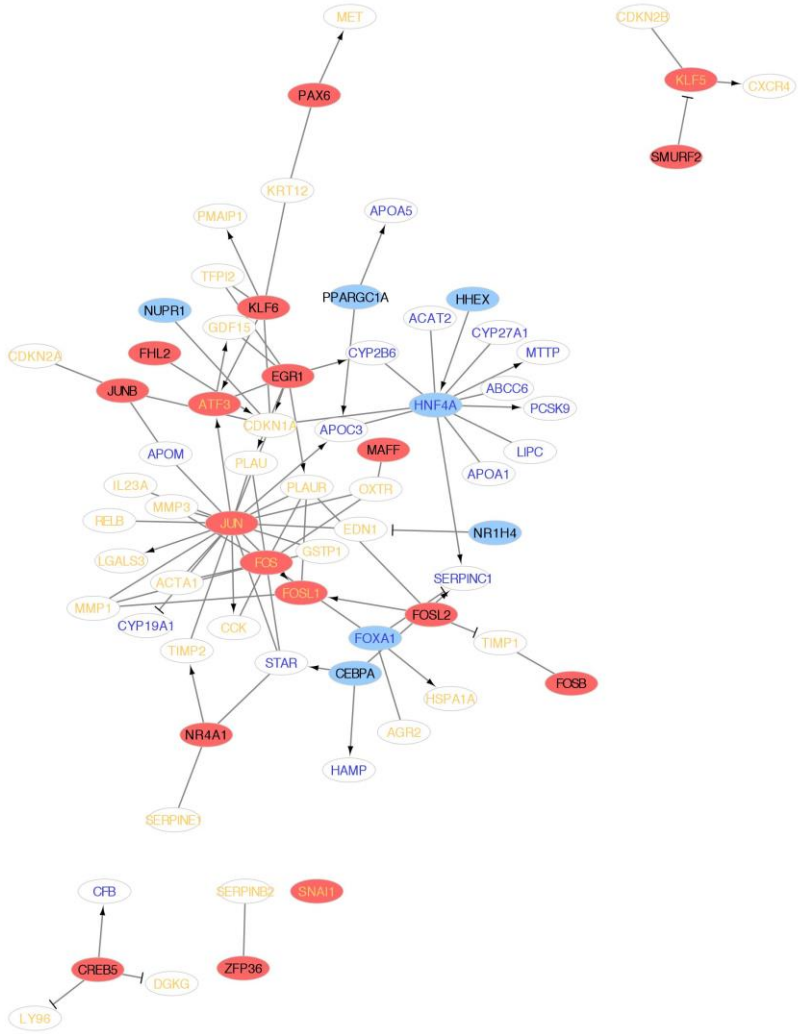

9.3.9 Comparing changes in gene expression elicited by different metal ions, i.e. cadmium and copper

Despite comparable chemical characteristics of copper and cadmium, copper is an essential metal involved in fundamental life processes. We thus wanted to identify, using copper-treated cells, which genes were specifically associated to the toxic cadmium response and which ones more broadly to similar metal ions and less relevant in playing a role in cadmium-based toxicity. The same approaches used for Cd to a dataset in which the HepG2 cell line was exposed to different Cu concentrations [76] compared to cadmium effects were applied.

In the lower concentration comparison (2 µM cadmium vs 100 µM Cu), 10 genes were up-regulated (Figure 9.6A): Six MTs, ASNS, PROP1, UCHL1 and PAQR7 with PROP1 and PAQR7 being up-regulated only at this stage. MT-1 and MT-2 isoforms were up-regulated by both lower concentrations (2 µM cadmium vs 100 µM Cu) to maintain metals homeostasis and higher concentrations (10 µM cadmium vs 400 µM Cu) to participate into metal detoxification (Figure 9.6B), as shown by previous studies regarding copper exposure alone [76 77]. By contrast, we found that MTs induction by copper cannot be comparable with that of cadmium. The expression level of MTs remained higher in cadmium samples than in copper for both comparisons (Figure 9.6A and B). The other genes above mentioned are distinct to cadmium 2 µM activity: Asparagine synthetase (ASNS) is involved in the conversion of aspartic acid to asparagine and increases cell proliferation and colony formation [78]; UCHL1 mediates the activation of HIF-1 and induces the antioxidant and radioresistant properties of cancer cells through the carbohydrate metabolic reprogramming with the activation of the pentose phosphate pathway [79]; PROP1, a marker of pituitary hormone cell types [80] and PAQR7, [81] were both identified as potential tumour suppressors.

In the higher concentration comparison (10 µM Cd vs 400 µM Cu), we identified [85] up- and [42] down-regulated genes. Among the up-regulated genes, zinc finger transcription factor SNAI1 and membrane protein MLC1, GTP-binding protein RRAD and Serine protease HTRA3 are specific to cadmium 10 µM (Figure 6B). Overexpression of SNAI1 promotes metastasis in most cancer types [82] including hepatocellular carcinoma [83], inhibits the activity of p53 [84] and up-regulates stemness factors that are involved in drug resistance [85]. In

hepatocellular carcinoma (HCC), RRAD promotes proliferation, apoptosis, and the Warburg effect [86].

We observed 16 other genes in addition to this group of proteins. HSPA6, EGR1 and IL11 were representative of the genes with the highest logFC. The Heat shock proteins (HSPs) 70 family are inducible proteins that defend cells from stress and are responsible for refolding of damaged proteins. At the same time, the overexpression of HSP70s is significantly associated with tumour transformation. High levels of expression of HSPA1A and HSPA6 are correlated with hepatoma progression [87]. Egr1 is a zinc-finger transcription factor that directly induces the transcription of p53. Studies on Egr1 revealed that this gene leads to cell cycle arrest, senescence, and transformation for all cells that survived after treatment with drugs or agents [88]. Interleukin (IL)-11 is able to confer hallmark capabilities to neoplastic cells, including survival and proliferation of cancer cells, stimulation of angiogenesis of the primary tumour and creation of metastasis [89]. We identified high level of NCF2 whose up-regulation may be in response to p53 induction [90]. One further difference between cadmium and copper concerned the down-regulation of the genes. We found that a high concentration of cadmium was able to reduce the level of expression of 13 genes compared to copper, despite the emerged conclusions are similar to the cadmium alone analysis. For example, the data also showed the down-regulation of fibrinogen gamma (FGG) and FGA that, together with FGB, acts forming an insoluble fibrin matrix. The down-regulation of Kallistatin (SERPINA4), that has anti-inflammatory and antioxidative properties, facilitates tumour progression [91]. Down-regulated SERPINA6 could be related to control of cortisol in the blood. This result underlined that, at the same concentration, cadmium was more toxic than copper, as expected since, unlike copper, cadmium is a non-essential element.

Figure 9.6. Volcano plot for differentially expressed genes cadmium for the pairwise comparison between cadmium 2 µM versus copper 100 µM (Figure 6A) and between cadmium 10 µM versus copper 400 µM (Figure 6B). The differential expression analysis was performed for low concentrations (Figure 6A) and high concentrations of both cadmium and copper (Figure 6B). The fold change is represented on the x-axis and the statistical significance i.e -log10 of the p-value on the y-axis. The upregulated genes are situated on the right part of the plot and colored in red. The downregulated genes are situated on the left part and are colored in green. The up- and downregulated genes found as a result are labeled in orange. Each single dot represents one gene with a detectable gene expression in both subtypes. The colored dots are statistically significantly ($p <= 0.05$) down-regulated and up-regulated genes respectively in green and red above the horizontal line that marks the threshold ($p < 0.05$). The vertical dashed lines represents a cutoff to retain significant DE genes with |logFC| >= 1.

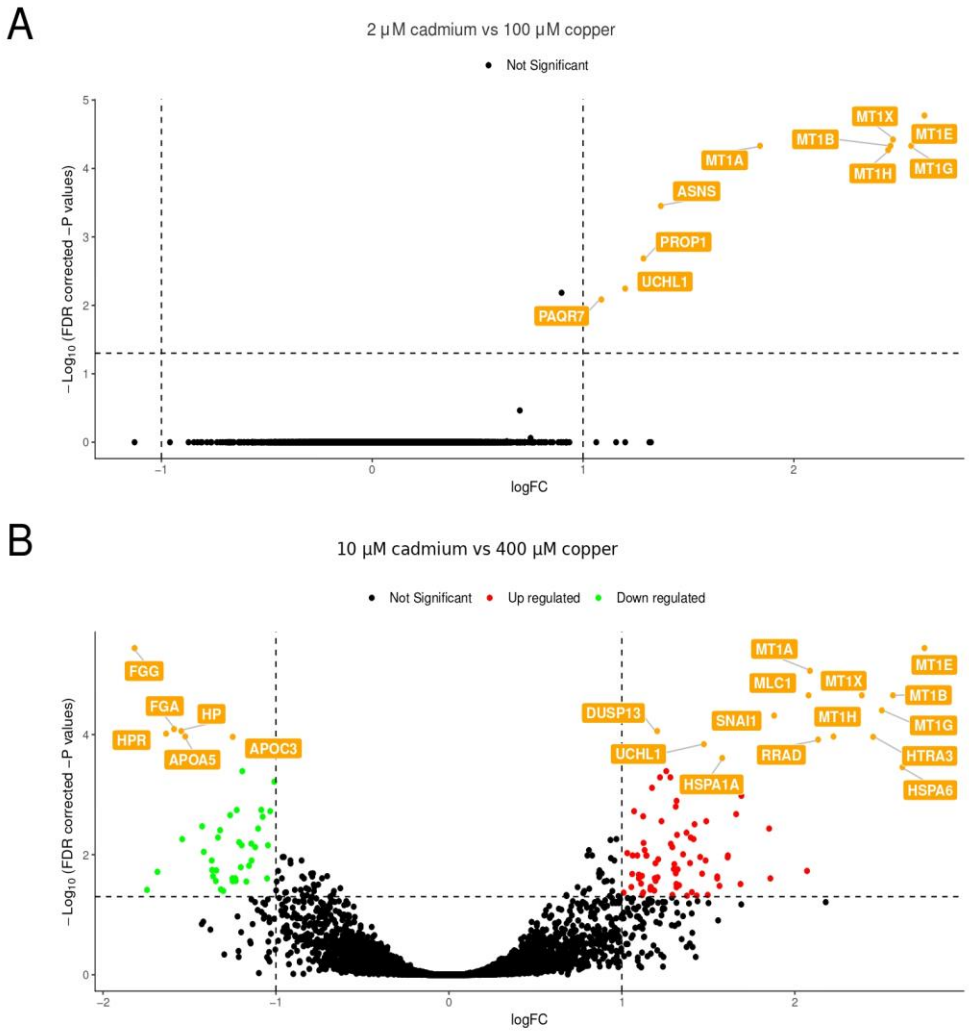

❖ 9.4. Discussion

Cadmium is a known human carcinogen, however it does not exhibit a simple mechanism of carcinogenesis. This metal exerts multiple toxic effects in mammalian cells and, since the mid 1960s, the researchers have been attempting to validate a variety of theories about its multi-stage model of tumour transformation [92]. In terms of toxicity, it has been shown that cadmium affected cell proliferation and differentiation, modified gene expression and disrupted cell to cell adhesion [93]. All these mechanisms were observed in HepG2 cell line, used as a hepatic model for this study and above all, the results of this study strongly support that Cd is able to modify gene expression in a cancer cell line. Besides, Cd can have an impact on transcriptional regulation in normal prokaryotic and eukaryotic cells [94]. The majority of evidence concerns cadmium ecotoxicity and genotoxicity in aquatic organisms and in varieties of plants, but actually, the accumulation of cadmium in the environment increases the concern for human health. In particular, since the main sources of cadmium are food and drinking water, we focused our attention on the liver and on the correlation between Cd and hepatic dysfunctions. Indeed, Cd is primarily accumulated in the liver after acute exposure, whereas chronic Cd exposure results principally in renal diseases [95]. In contrast, the excretion of cadmium through urine is the primary biomarker of chronic exposure and bioaccumulation of cadmium in the human body [96]. When cadmium reaches the liver, absorbed through ingestion or carried by the blood, it induces and binds metallothioneins (MTs), and it increases the levels of the heat shock proteins, as shown by our results and known under different experimental conditions [36]. Moreover, the formation of CdMT complex leads to an imbalance in zinc metabolism and to the loss of their antioxidant role against reactive oxygen species (ROS) [36 37 38]. Although cadmium is not able to directly stimulate the production of ROS, it interferes with antioxidant defence mechanisms, controlling glutathione and proteins involved in maintaining redox balance. For example, we found a down-regulation of cytochromes P450 and glutathione S-transferases. Glutathione (GSH) may provide another defence against oxidative damage and free radicals generation. Moreover, the imbalance in the homeostasis of metal ions chelated by MTs increases the concentration of free bivalent ions, that could be Fenton-reactive metals, such as Cu and Fe. In in vivo experiments, increased oxidative stress was closely related to the

inflammation stimulated by Cd-induced activation of Kupffer cells and direct damage to hepatocytes [97]. Nevertheless, induction of oxidative stress was also caused by DNA damage in preneoplastic lesions [98], whereas our results tried to describe another stage of cadmium-carcinogenicity: the tumour progression. In this work, among the biochemical changes induced by cadmium, we showed that the dysfunction and disruption of cell-to-cell adhesion were the main cause of tumour progression after cadmium exposure. We confirmed that at non-cytotoxic concentrations Cd stimulated the development of tumors. In addition, Waalkes et al. [99] showed that the tumour progression and metastasis in rats were enhanced after repeated Cd exposures. In the same work, they observed that low Cd exposure stimulated and enhanced the invasiveness of these tumors [99]. Additionally, we wondered whether the modification of the extracellular matrix and other biological effects that we described above were specific of cadmium toxicity. Thus, we compared cadmium to copper, another bivalent ion. Copper is an essential micronutrient for cellular homeostasis, whereas cadmium is a non-essential toxic element with no known functions in human cells. Song et al. illustrated that a toxic concentration of copper increased apoptosis and reduced cell cycle progression [28]. In fact, Song and colleagues [76] explained that a toxicological response did not appear when HepG2 were exposed to levels of copper that occurred in the environment. Indeed, only 10 genes (all MTs) were upregulated at 100 µM copper, and cells maintained metal homeostasis because they used copper as an essential micronutrient in fundamental life processes. Moreover, comparing the expression level of MTs, we found that MTs induced by copper were lower than by cadmium. Subsequently, Song and colleagues reported that the highest concentration of copper up-regulated all genes that were involved in apoptosis and in a reduction of cell proliferation. Instead, down-regulated genes were involved in the regulation of DNA repair and replication. The goal of this analysis was to underline that, despite some cancer types have changed the systemic copper distribution, copper was a metal whose damage was contained in only some aspects of tumour progression, and metastatic features occurred in rare cases. Consequently, this low copper toxicity could help the development of new therapies, as copper-specific chelators or copper-ionophores, to inhibit cancer progression 100 that were not available for cadmium intoxication. By contrast, we showed that cadmium is a heavy metal of significant toxicity with a destructive impact on the liver, promoting the

transformation of low deviation tumour HepG2 into metastatic cells, even at low concentrations. Cadmium did not act only as a positive regulator of cell migration modifying the extracellular matrix organization, but also by preventing the normal function of the liver cells. In conclusion, it became clear that various mechanisms of Cd toxicity which were involved in different stages of carcinogenicity existed. Precise therapeutics approaches are needed for both chronic and acute Cd intoxication and normal or cancer cells. In a previous work [101], analyzing the effect of Cd on a healthy cell line (C3H mouse fibroblasts), we found that the majority of DEGs were down-regulated; however, MT2 and Phosphatidylinositol-4-phosphate 5-kinase, type 1 alpha (Pip5k1a) were found to be among the top up-regulated genes after both [24] and [48] hrs Cd treatment, the up-regulation decreasing during the recovery phase. Pip5k1a catalyzes the phosphorylation of phosphatidylinositol 4-phosphate to form phosphatidylinositol 4,5-bisphosphate. Interestingly, in HepG2 cells treated with Cd, phospholipase Ce (epsilon) 2 (PLCH2), which cleaves phosphatidylinositol 4,5-bisphosphate to yield inositol 1,4,5-trisphosphate and diacylglycerol, is up-regulated. Both inositol 1,4,5-trisphosphate and diacylglycerol are second messengers inducing Ca2+ release into the cytoplasm and activating many downstream cascades like MEK/ ERK and Akt cascades [102]. Moreover, phosphatidylinositol 4,5-bisphosphate is also a second messenger, interacting with several proteins that regulate actin cytoskeleton [103]. In accordance with data obtained in Cd treated HepG2 cells, MTs and Hsp figured among the top regulated genes in healthy C3H cells after 24 h of Cd exposure, confirming that both these protein families represent the first line defence against metal dyshomeostasis, particularly against toxic metals like Cd. The down-regulation of cytochromes P450 and glutathione S-transferases, found in Cd treated HepG2 cells finds no counterpart in our previous study on Cd treated healthy C3H cells, as revealed by KEGG pathway enrichment analysis showing that three pathways related to detoxification mechanisms, drug metabolism, metabolism of xenobiotics by cytochrome P450 and glutathione metabolism, were significantly up-regulated in 24 hour Cd-treated cells. We can speculate that this reflects the fact that cancer cells are less efficient in the protection against ROS and xenobiotics and therefore more sensitive to Cd. This would in turn account for a different effect of Cd toxicity, leading healthy cells towards transformation and cancer cells towards metastasis.

References

- 1. IARC, CADMIUM AND CADMIUM COMPOUNDS (Group 1), 1993, 58, 119.
- 2. P. B. Tchounwou, C. G. Yedjou, A. K. Patlolla and D. J. Sutton, Heavy metal toxicity and the environment, Exp Suppl, 2012, 101, 133-164.
- 3. S. Wang and X. Shi, Molecular mechanisms of metal toxicity and carcinogenesis, Mol Cell Biochem, 2001, 222, 3-9.
- 4. K. T. Eriksen, J. Halkjaer, M. Sorensen, J. R. Meliker, J. A. McElroy, A. Tjonneland and O. Raaschou-Nielsen, Dietary cadmium intake and risk of breast, endometrial and ovarian cancer in Danish postmenopausal women: a prospective cohort study, PLoS One, 2014, 9, e100815.
- 5. O. Faroon, A. Ashizawa, S. Wright, P. Tucker, K. Jenkins, L. Ingerman and C. Rudisill, in Toxicological Profile for Cadmium, Atlanta (GA), 2012.
- 6. M. D. Waters and J. M. Fostel, Toxicogenomics and systems toxicology: aims and prospects, Nat Rev Genet, 2004, 5, 936-948.
- 7. M. A. Benton, J. E. Rager, L. Smeester and R. C. Fry, Comparative genomic analyses identify common molecular pathways modulated upon exposure to low doses of arsenic and cadmium, BMC Genomics, 2011, 12, 173.
- 8. S. Koizumi and H. Yamada, DNA microarray analysis of altered gene expression in cadmium-exposed human cells, J Occup Health, 2003, 45, 331-334.
- 9. J. A. Colacino, A. E. Arthur, K. K. Ferguson and L. S. Rozek, Dietary antioxidant and anti-inflammatory intake modifies the effect of cadmium exposure on markers of systemic inflammation and oxidative stress, Environ Res, 2014, 131, 6-12.
- 10. M. G. Permenter, J. A. Lewis and D. A. Jackson, Exposure to nickel, chromium, or cadmium causes distinct changes in the gene expression patterns of a rat liver derived cell line, PLoS One, 2011, 6, e27730.
- 11. M. S. Madejczyk, C. E. Baer, W. E. Dennis, V. C. Minarchick, S. S. Leonard, D. A. Jackson, J. D. Stallings and J. A. Lewis, Temporal changes in rat liver gene expression after acute cadmium and chromium exposure, PLoS One, 2015, 10, e0127327.
- 12. V. e. a. Arroyo, Liver and Cadmium Toxicity, J Drug Metab Toxicol 2012, S5.
- 13. W. C. Prozialeck, J. R. Edwards, D. W. Nebert, J. M. Woods, A. Barchowsky and W. D. Atchison, The vascular system as a target of metal toxicity, Toxicol Sci, 2008, 102, 207-218.
- 14. N. Ishihara and T. Matsushiro, Biliary and urinary excretion of metals in humans, Arch Environ Health, 1986, 41, 324-330.
- 15. H. H. Gerets, K. Tilmant, B. Gerin, H. Chanteux, B. O. Depelchin, S. Dhalluin and F. A. Atienzar, Characterization of primary human hepatocytes, HepG2 cells, and HepaRG cells at the mRNA level and CYP activity in response to inducers and their predictivity for the detection of human hepatotoxins, Cell Biol Toxicol, 2012, 28, 69-87.

- 16. D. J. Thiele, Metal-regulated transcription in eukaryotes, Nucleic Acids Res, 1992, 20, 1183-1191.
- 17. C. Luparello, A. Longo and M. Vetrano, Exposure to cadmium chloride influences astrocyte-elevated gene-1 (AEG-1) expression in MDA-MB231 human breast cancer cells, Biochimie, 2012, 94, 207-213.
- 18. C. Y. Chen, S. L. Zhang, Z. Y. Liu, Y. Tian and Q. Sun, Cadmium toxicity induces ER stress and apoptosis via impairing energy homoeostasis in cardiomyocytes, Biosci Rep, 2015, 35.
- 19. B. E. Tvermoes, G. S. Bird and J. H. Freedman, Cadmium induces transcription independently of intracellular calcium mobilization, PLoS One, 2011, 6, e20542.
- 20. A. Hartwig, Zinc finger proteins as potential targets for toxic metal ions: differential effects on structure and function, Antioxid Redox Signal, 2001, 3, 625-634.
- 21. K. S. Lund E., Petering D. , The Chemical Biology of Cadmium, 2018, n: Thévenod F., Petering D., M. Templeton D., Lee WK., Hartwig A. (eds) Cadmium Interaction with Animal Cells. Springer, Cham.
- 22. A. Hartwig, Cadmium and Its Impact on Genomic Stability, 2018.
- 23. G. Malgieri, L. Zaccaro, M. Leone, E. Bucci, S. Esposito, I. Baglivo, A. Del Gatto, L. Russo, R. Scandurra, P. V. Pedone, R. Fattorusso and C. Isernia, Zinc to cadmium replacement in the A. thaliana SUPERMAN Cys(2) His(2) zinc finger induces structural rearrangements of typical DNA base determinant positions, Biopolymers, 2011, 95, 801-810.
- 24. J. H. Laity, B. M. Lee and P. E. Wright, Zinc finger proteins: new insights into structural and functional diversity, Curr Opin Struct Biol, 2001, 11, 39-46.
- 25. S. A. Lambert, A. Jolma, L. F. Campitelli, P. K. Das, Y. Yin, M. Albu, X. Chen, J. Taipale, T. R. Hughes and M. T. Weirauch, The Human Transcription Factors, Cell, 2018, 175, 598-599.
- 26. M. Fabbri, C. Urani, M. G. Sacco, C. Procaccianti and L. Gribaldo, Whole genome analysis and microRNAs regulation in HepG2 cells exposed to cadmium, ALTEX, 2012, 29, 173-182.
- 27. C. Urani, P. Melchioretto, C. Canevali and G. F. Crosta, Cytotoxicity and induction of protective mechanisms in HepG2 cells exposed to cadmium, Toxicol In Vitro, 2005, 19, 887-892.
- 28. M. O. Song and J. H. Freedman, Expression of copper-responsive genes in HepG2 cells, Mol Cell Biochem, 2005, 279, 141-147.
- 29. A. S. Andrew, A. J. Warren, A. Barchowsky, K. A. Temple, L. Klei, N. V. Soucy, K. A. O'Hara and J. W. Hamilton, Genomic and proteomic profiling of responses to toxic metals in human lung cells, Environ Health Perspect, 2003, 111, 825-835.
- 30. S. Satarug and M. R. Moore, Adverse health effects of chronic exposure to low-level cadmium in foodstuffs and cigarette smoke, Environ Health Perspect, 2004, 112, 1099-1103.

- 31. M. E. Ritchie, B. Phipson, D. Wu, Y. Hu, C. W. Law, W. Shi and G. K. Smyth, limma powers differential expression analyses for RNA-sequencing and microarray studies, Nucleic Acids Res, 2015, 43, e47.
- 32. S. R. Davis and R. J. Cousins, Metallothionein expression in animals: a physiological perspective on function, J Nutr, 2000, 130, 1085-1088.
- 33. G. F. Nordberg, Historical perspectives on cadmium toxicology, Toxicol Appl Pharmacol, 2009, 238, 192-200.
- 34. C. D. Klaassen, J. Liu and B. A. Diwan, Metallothionein protection of cadmium toxicity, Toxicol Appl Pharmacol, 2009, 238, 215-220.
- 35. I. Sabolic, D. Breljak, M. Skarica and C. M. Herak-Kramberger, Role of metallothionein in cadmium traffic and toxicity in kidneys and other mammalian organs, Biometals, 2010, 23, 897-926.
- 36. M. L. Albert, A. Reches and R. Silverberg, Hemianopic colour blindness, J Neurol Neurosurg Psychiatry, 1975, 38, 546-549.
- 37. T. Nagamine and K. Nakajima, Significance of metallothionein expression in liver disease, Curr Pharm Biotechnol, 2013, 14, 420-426.
- 38. Y. Lian, J. Zhao, Y. M. Wang, J. Zhao and S. Q. Peng, Metallothionein protects against isoniazid-induced liver injury through the inhibition of CYP2E1-dependent oxidative and nitrosative impairment in mice, Food Chem Toxicol, 2017, 102, 32-38.
- 39. M. Si and J. Lang, The roles of metallothioneins in carcinogenesis, J Hematol Oncol, 2018, 11, 107.
- 40. J. M. Moulis, Cellular mechanisms of cadmium toxicity related to the homeostasis of essential metals, Biometals, 2010, 23, 877-896.
- 41. P. B. Dziegiel P., Kobierzycki C., Stasiolek M., Podhorska-Okolow M. , Metallothioneins in Normal and Cancer Cells, 2016, Metallothioneins and immune function. Springer International Publishing; Cham, Switzerland, 65-77.
- 42. K. Subramanian Vignesh and G. S. Deepe, Jr., Metallothioneins: Emerging Modulators in Immunity and Infection, Int J Mol Sci, 2017, 18.
- 43. W. You, B. Chen, X. Liu, S. Xue, H. Qin and H. Jiang, Farnesoid X receptor, a novel proto-oncogene in non-small cell lung cancer, promotes tumor growth via directly transactivating CCND1, Sci Rep, 2017, 7, 591.
- 44. F. Yang, X. Huang, T. Yi, Y. Yen, D. D. Moore and W. Huang, Spontaneous development of liver tumors in the absence of the bile acid receptor farnesoid X receptor, Cancer Res, 2007, 67, 863-867.
- 45. S. Dubaisi, K. G. Barrett, H. Fang, J. Guzman-Lepe, A. Soto-Gutierrez, T. A. Kocarek and M. Runge-Morris, Regulation of Cytosolic Sulfotransferases in Models of Human Hepatocyte Development, Drug Metab Dispos, 2018, 46, 1146-1156.

- 46. A. Cretu, X. Sha, J. Tront, B. Hoffman and D. A. Liebermann, Stress sensor Gadd45 genes as therapeutic targets in cancer, Cancer Ther, 2009, 7, 268-276.
- 47. H. Bulus, S. Oguztuzun, G. Guler Simsek, M. Kilic, A. O. Ada, S. Gol, A. K. Kocdogan, P. Kaygin, B. Bozer and M. Iscan, Expression of CYP and GST in human normal and colon tumor tissues, Biotech Histochem, 2019, 94, 1-9.
- 48. B. F. El-Rayes, S. Ali, L. K. Heilbrun, S. Lababidi, D. Bouwman, D. Visscher and P. A. Philip, Cytochrome p450 and glutathione transferase expression in human breast cancer, Clin Cancer Res, 2003, 9, 1705-1709.
- 49. M. Saitoh, Epithelial-mesenchymal transition is regulated at post-transcriptional levels by transforming growth factor-beta signaling during tumor progression, Cancer Sci, 2015, 106, 481-488.
- 50. Z. Y. Lin, Y. H. Chuang and W. L. Chuang, Cancer-associated fibroblasts up-regulate CCL2, CCL26, IL6 and LOXL2 genes related to promotion of cancer progression in hepatocellular carcinoma cells, Biomed Pharmacother, 2012, 66, 525-529.
- 51. Y. Zhang, H. X. Qiao, Y. T. Zhou, L. Hong and J. H. Chen, Fibrinogenlikeprotein 1 promotes the invasion and metastasis of gastric cancer and is associated with poor prognosis, Mol Med Rep, 2018, 18, 1465-1472.
- 52. H. JingSong, G. Hong, J. Yang, Z. Duo, F. Li, C. WeiCai, L. XueYing, M. YouSheng, O. YiWen, P. Yue and C. Zou, siRNA-mediated suppression of collagen type iv alpha 2 (COL4A2) mRNA inhibits triple-negative breast cancer cell proliferation and migration, Oncotarget, 2017, 8, 2585-2593.
- 53. K. H. Chiu, Y. H. Chang, Y. S. Wu, S. H. Lee and P. C. Liao, Quantitative secretome analysis reveals that COL6A1 is a metastasis-associated protein using stacking gel-aided purification combined with iTRAQ labeling, J Proteome Res, 2011, 10, 1110-1125.
- 54. K. Koshizuka, T. Hanazawa, N. Kikkawa, T. Arai, A. Okato, A. Kurozumi, M. Kato, K. Katada, Y. Okamoto and N. Seki, Regulation of ITGA3 by the anti-tumor miR-199 family inhibits cancer cell migration and invasion in head and neck cancer, Cancer Sci, 2017, 108, 1681-1692.
- 55. S. N. Jung, H. S. Lim, L. Liu, J. W. Chang, Y. C. Lim, K. S. Rha and B. S. Koo, LAMB3 mediates metastatic tumor behavior in papillary thyroid cancer by regulating c-MET/Akt signals, Sci Rep, 2018, 8, 2718.
- 56. Y. Kita, K. Mimori, F. Tanaka, T. Matsumoto, N. Haraguchi, K. Ishikawa, S. Matsuzaki, Y. Fukuyoshi, H. Inoue, S. Natsugoe, T. Aikou and M. Mori, Clinical significance of LAMB3 and COL7A1 mRNA in esophageal squamous cell carcinoma, Eur J Surg Oncol, 2009, 35, 52-58.
- 57. A. P. Mazar, Urokinase plasminogen activator receptor choreographs multiple ligand interactions: implications for tumor progression and therapy, Clin Cancer Res, 2008, 14, 5649-5655.
- 58. C. Bonnans, J. Chou and Z. Werb, Remodelling the extracellular matrix in development and disease, Nat Rev Mol Cell Biol, 2014, 15, 786-801.

- 59. M. A. Pavon, I. Arroyo-Solera, M. V. Cespedes, I. Casanova, X. Leon and R. Mangues, uPA/uPAR and SERPINE1 in head and neck cancer: role in tumor resistance, metastasis, prognosis and therapy, Oncotarget, 2016, 7, 57351-57366.
- 60. Y. T. Huang, Q. Lan, G. Lorusso, N. Duffey and C. Ruegg, The matricellular protein CYR61 promotes breast cancer lung metastasis by facilitating tumor cell extravasation and suppressing anoikis, Oncotarget, 2017, 8, 9200-9215.
- 61. S. Bakshi, X. Zhang, S. Godoy-Tundidor, R. Y. Cheng, M. A. Sartor, M. Medvedovic and S. M. Ho, Transcriptome analyses in normal prostate epithelial cells exposed to low-dose cadmium: oncogenic and immunomodulations involving the action of tumor necrosis factor, Environ Health Perspect, 2008, 116, 769-776.
- 62. J. S. Joyal, S. Nim, T. Zhu, N. Sitaras, J. C. Rivera, Z. Shao, P. Sapieha, D. Hamel, M. Sanchez, K. Zaniolo, M. St-Louis, J. Ouellette, M. Montoya-Zavala, A. Zabeida, E. Picard, P. Hardy, V. Bhosle, D. R. Varma, F. Gobeil, Jr., C. Beausejour, C. Boileau, W. Klein, M. Hollenberg, A. Ribeiro-da-Silva, G. Andelfinger and S. Chemtob, Subcellular localization of coagulation factor II receptor-like 1 in neurons governs angiogenesis, Nat Med, 2014, 20, 1165-1173.
- 63. H. Hauge, K. E. Fjelland, M. Sioud and H. C. Aasheim, Evidence for the involvement of FAM110C protein in cell spreading and migration, Cell Signal, 2009, 21, 1866-1873.
- 64. M. Nishioka, K. Ueno, S. Hazama, T. Okada, K. Sakai, Y. Suehiro, N. Okayama, H. Hirata, M. Oka, K. Imai, R. Dahiya and Y. Hinoda, Possible involvement of Wnt11 in colorectal cancer progression, Mol Carcinog, 2013, 52, 207-217.
- 65. A. Gont, M. Daneshmand, J. Woulfe, S. J. Lavictoire and I. A. Lorimer, PREX1 integrates G protein-coupled receptor and phosphoinositide 3-kinase signaling to promote glioblastoma invasion, Oncotarget, 2017, 8, 8559-8573.
- 66. Z. Yang, H. Wang, L. Xia, L. Oyang, Y. Zhou, B. Zhang, X. Chen, X. Luo, Q. Liao and J. Liang, Overexpression of PAK1 Correlates with Aberrant Expression of EMT Markers and Poor Prognosis in Non-Small Cell Lung Cancer, J Cancer, 2017, 8, 1484-1491.
- 67. S. C. Kim, Y. K. Shin, Y. A. Kim, S. G. Jang and J. L. Ku, Identification of genes inducing resistance to ionizing radiation in human rectal cancer cell lines: re-sensitization of radio-resistant rectal cancer cells through down regulating NDRG1, BMC Cancer, 2018, 18, 594.
- 68. F. Ren, D. Wang, Y. Wang, P. Chen and C. Guo, SPOCK2 Affects the Biological Behavior of Endometrial Cancer Cells by Regulation of MT1-MMP and MMP2, Reprod Sci, 2019, DOI: 10.1177/1933719119834341, 1933719119834341.
- 69. Y. Sasaki, M. Tamura, K. Takeda, K. Ogi, T. Nakagaki, R. Koyama, M. Idogawa, H. Hiratsuka and T. Tokino, Identification and characterization of the intercellular adhesion molecule-2 gene as a novel p53 target, Oncotarget, 2016, 7, 61426-61437.
- 70. K. Holmborn, J. Habicher, Z. Kasza, A. S. Eriksson, B. Filipek-Gorniok, S. Gopal, J. R. Couchman, P. E. Ahlberg, M. Wiweger, D. Spillmann, J. Kreuger and J. Ledin, On the roles

and regulation of chondroitin sulfate and heparan sulfate in zebrafish pharyngeal cartilage morphogenesis, J Biol Chem, 2012, 287, 33905-33916.

- 71. A. Hisado-Oliva, A. Ruzafa-Martin, L. Sentchordi, M. F. A. Funari, C. Bezanilla-Lopez, M. Alonso-Bernaldez, J. Barraza-Garcia, M. Rodriguez-Zabala, A. M. Lerario, S. Benito-Sanz, M. Aza-Carmona, A. Campos-Barros, A. A. L. Jorge and K. E. Heath, Mutations in C-natriuretic peptide (NPPC): a novel cause of autosomal dominant short stature, Genet Med, 2018, 20, 91-97.
- 72. A. Engstrom, K. Michaelsson, M. Vahter, B. Julin, A. Wolk and A. Akesson, Associations between dietary cadmium exposure and bone mineral density and risk of osteoporosis and fractures among women, Bone, 2012, 50, 1372-1378.
- 73. H. Han, J. W. Cho, S. Lee, A. Yun, H. Kim, D. Bae, S. Yang, C. Y. Kim, M. Lee, E. Kim, S. Lee, B. Kang, D. Jeong, Y. Kim, H. N. Jeon, H. Jung, S. Nam, M. Chung, J. H. Kim and I. Lee, TRRUST v2: an expanded reference database of human and mouse transcriptional regulatory interactions, Nucleic Acids Res, 2018, 46, D380-D386.
- 74. Z. Qin, R. M. Balimunkwe and T. Quan, Age-related reduction of dermal fibroblast size upregulates multiple matrix metalloproteinases as observed in aged human skin in vivo, Br J Dermatol, 2017, 177, 1337-1348.
- 75. E. Shaulian and M. Karin, AP-1 in cell proliferation and survival, Oncogene, 2001, 20, 2390-2400.
- 76. M. O. Song, J. Li and J. H. Freedman, Physiological and toxicological transcriptome changes in HepG2 cells exposed to copper, Physiol Genomics, 2009, 38, 386-401.
- 77. P. Muller, H. van Bakel, B. van de Sluis, F. Holstege, C. Wijmenga and L. W. Klomp, Gene expression profiling of liver cells after copper overload in vivo and in vitro reveals new copper-regulated genes, J Biol Inorg Chem, 2007, 12, 495-507.
- 78. Q. Yu, X. Wang, L. Wang, J. Zheng, J. Wang and B. Wang, Knockdown of asparagine synthetase (ASNS) suppresses cell proliferation and inhibits tumor growth in gastric cancer cells, Scand J Gastroenterol, 2016, 51, 1220-1226.
- 79. R. Nakashima, Y. Goto, S. Koyasu, M. Kobayashi, A. Morinibu, M. Yoshimura, M. Hiraoka, E. M. Hammond and H. Harada, UCHL1-HIF-1 axis-mediated antioxidant property of cancer cells as a therapeutic target for radiosensitization, Sci Rep, 2017, 7, 6879.
- 80. M. Orciani, S. Davis, G. Appolloni, R. Lazzarini, M. Mattioli-Belmonte, R. A. Ricciuti, M. Boscaro, R. Di Primio and G. Arnaldi, Isolation and characterization of progenitor mesenchymal cells in human pituitary tumors, Cancer Gene Ther, 2015, 22, 9-16.
- 81. A. C. V. Krepischi, M. Maschietto, E. N. Ferreira, A. G. Silva, S. S. Costa, I. W. da Cunha, B. D. F. Barros, P. E. Grundy, C. Rosenberg and D. M. Carraro, Genomic imbalances pinpoint potential oncogenes and tumor suppressors in Wilms tumors, Mol Cytogenet, 2016, 9, 20.
- 82. Z. Wang, P. Wade, K. J. Mandell, A. Akyildiz, C. A. Parkos, R. J. Mrsny and A. Nusrat, Raf 1 represses expression of the tight junction protein occludin via activation of the zinc-finger transcription factor slug, Oncogene, 2007, 26, 1222-1230.

- 83. J. Qi, T. Li, H. Bian, F. Li, Y. Ju, S. Gao, J. Su, W. Ren and C. Qin, SNAI1 promotes the development of HCC through the enhancement of proliferation and inhibition of apoptosis, FEBS Open Bio, 2016, 6, 326-337.
- 84. N. K. Kurrey, S. P. Jalgaonkar, A. V. Joglekar, A. D. Ghanate, P. D. Chaskar, R. Y. Doiphode and S. A. Bapat, Snail and slug mediate radioresistance and chemoresistance by antagonizing p53-mediated apoptosis and acquiring a stem-like phenotype in ovarian cancer cells, Stem Cells, 2009, 27, 2059-2068.
- 85. N. Hojo, A. L. Huisken, H. Wang, E. Chirshev, N. S. Kim, S. M. Nguyen, H. Campos, C. A. Glackin, Y. J. Ioffe and J. J. Unternaehrer, Snail knockdown reverses stemness and inhibits tumour growth in ovarian cancer, Sci Rep, 2018, 8, 8704.
- 86. Y. Yan, M. Xie, L. Zhang, X. Zhou, H. Xie, L. Zhou, S. Zheng and W. Wang, Ras-related associated with diabetes gene acts as a suppressor and inhibits Warburg effect in hepatocellular carcinoma, Onco Targets Ther, 2016, 9, 3925-3937.
- 87. C. W. Shu and C. M. Huang, HSP70s: From Tumor Transformation to Cancer Therapy, Clin Med Oncol, 2008, 2, 335-345.
- 88. V. Baron, E. D. Adamson, A. Calogero, G. Ragona and D. Mercola, The transcription factor Egr1 is a direct regulator of multiple tumor suppressors including TGFbeta1, PTEN, p53, and fibronectin, Cancer Gene Ther, 2006, 13, 115-124.
- 89. C. N. Johnstone, A. Chand, T. L. Putoczki and M. Ernst, Emerging roles for IL-11 signaling in cancer development and progression: Focus on breast cancer, Cytokine Growth Factor Rev, 2015, 26, 489-498.
- 90. D. Italiano, A. M. Lena, G. Melino and E. Candi, Identification of NCF2/p67phox as a novel p53 target gene, Cell Cycle, 2012, 11, 4589-4596.
- 91. K. S. Nallagangula, K. N. Shashidhar, V. Lakshmaiah and C. Muninarayana, Cirrhosis of liver: Interference of serpins in quantification of SERPINA4 - A preliminary study, Pract Lab Med, 2017, 9, 53-57.
- 92. J. Huff, R. M. Lunn, M. P. Waalkes, L. Tomatis and P. F. Infante, Cadmium-induced cancers in animals and in humans, Int J Occup Environ Health, 2007, 13, 202-212.
- 93. M. Waisberg, P. Joseph, B. Hale and D. Beyersmann, Molecular and cellular mechanisms of cadmium carcinogenesis, Toxicology, 2003, 192, 95-117.
- 94. D. Laukens, A. Waeytens, P. De Bleser, C. Cuvelier and M. De Vos, Human metallothionein expression under normal and pathological conditions: mechanisms of gene regulation based on in silico promoter analysis, Crit Rev Eukaryot Gene Expr, 2009, 19, 301-317.
- 95. S. A. Adefegha, O. S. Omojokun and G. Oboh, Modulatory effect of protocatechuic acid on cadmium induced nephrotoxicity and hepatoxicity in rats in vivo, Springerplus, 2015, 4, 619.

- 96. H. Welinder, S. Skerfving and O. Henriksen, Cadmium metabolism in man, Br J Ind Med, 1977, 34, 221-228.
- 97. T. Yamano, L. A. DeCicco and L. E. Rikans, Attenuation of cadmium-induced liver injury in senescent male fischer 344 rats: role of Kupffer cells and inflammatory cytokines, Toxicol Appl Pharmacol, 2000, 162, 68-75.
- 98. A. Kakehashi, M. Wei, S. Fukushima and H. Wanibuchi, Oxidative stress in the carcinogenicity of chemical carcinogens, Cancers (Basel), 2013, 5, 1332-1354.
- 99. M. P. Waalkes, S. Rehm and M. G. Cherian, Repeated cadmium exposures enhance the malignant progression of ensuing tumors in rats, Toxicol Sci, 2000, 54, 110-120.
- 100. D. Denoyer, S. Masaldan, S. La Fontaine and M. A. Cater, Targeting copper in cancer therapy: 'Copper That Cancer', Metallomics, 2015, 7, 1459-1476.
- 101. G. Callegaro, M. Forcella, P. Melchioretto, A. Frattini, L. Gribaldo, P. Fusi, M. Fabbri and C. Urani, Toxicogenomics applied to in vitro Cell Transformation Assay reveals mechanisms of early response to cadmium, Toxicol In Vitro, 2018, 48, 232-243.
- 102. A. Gericke, N. R. Leslie, M. Losche and A. H. Ross, PtdIns(4,5)P2-mediated cell signaling: emerging principles and PTEN as a paradigm for regulatory mechanism, Adv Exp Med Biol, 2013, 991, 85-104.
- 103. I. van den Bout and N. Divecha, PIP5K-driven PtdIns(4,5)P2 synthesis: regulation and cellular functions, J Cell Sci, 2009, 122, 3837-3850.
- 104. P. Langfelder and S. Horvath, WGCNA: an R package for weighted correlation network analysis, BMC Bioinformatics, 2008, 9, 559.
- 105. S. Durinck, P. T. Spellman, E. Birney and W. Huber, Mapping identifiers for the integration of genomic datasets with the R/Bioconductor package biomaRt, Nat Protoc, 2009, 4, 1184-1191.
- 106. C. Workman, L. J. Jensen, H. Jarmer, R. Berka, L. Gautier, H. B. Nielser, H. H. Saxild, C. Nielsen, S. Brunak and S. Knudsen, A new non-linear normalization method for reducing variability in DNA microarray experiments, Genome Biol, 2002, 3, research0048.
- 107. J. R. Conway, A. Lex and N. Gehlenborg, UpSetR: an R package for the visualization of intersecting sets and their properties, Bioinformatics, 2017, 33, 2938-2940.
- 108. A. Colaprico, T. C. Silva, C. Olsen, L. Garofano, C. Cava, D. Garolini, T. S. Sabedot, T. M. Malta, S. M. Pagnotta, I. Castiglioni, M. Ceccarelli, G. Bontempi and H. Noushmehr, TCGAbiolinks: an R/Bioconductor package for integrative analysis of TCGA data, Nucleic Acids Res, 2016, 44, e71.
- 109. A. Fabregat, K. Sidiropoulos, G. Viteri, P. Marin-Garcia, P. Ping, L. Stein, P. D'Eustachio and H. Hermjakob, Reactome diagram viewer: data structures and strategies to boost performance, Bioinformatics, 2018, 34, 1208-1214.

- 110. M. Milacic, R. Haw, K. Rothfels, G. Wu, D. Croft, H. Hermjakob, P. D'Eustachio and L. Stein, Annotating cancer variants and anti-cancer therapeutics in reactome, Cancers (Basel), 2012, 4, 1180-1211.
- 111. C. The Gene Ontology, Expansion of the Gene Ontology knowledgebase and resources, Nucleic Acids Res, 2017, 45, D331-D338.
- 112. M. Ashburner, C. A. Ball, J. A. Blake, D. Botstein, H. Butler, J. M. Cherry, A. P. Davis, K. Dolinski, S. S. Dwight, J. T. Eppig, M. A. Harris, D. P. Hill, L. Issel-Tarver, A. Kasarskis, S. Lewis, J. C. Matese, J. E. Richardson, M. Ringwald, G. M. Rubin and G. Sherlock, Gene ontology: tool for the unification of biology. The Gene Ontology Consortium, Nat Genet, 2000, 25, 25-29.
- 113. W. Walter, F. Sanchez-Cabo and M. Ricote, GOplot: an R package for visually combining expression data with functional analysis, Bioinformatics, 2015, 31, 2912-2914.
- 114. J. P. Pinto, R. K. Kalathur, D. V. Oliveira, T. Barata, R. S. Machado, S. Machado, I. Pacheco-Leyva, I. Duarte and M. E. Futschik, StemChecker: a web-based tool to discover and explore stemness signatures in gene sets, Nucleic Acids Res, 2015, 43, W72-77.
- 115. S. Davis and P. S. Meltzer, GEOquery: a bridge between the Gene Expression Omnibus (GEO) and BioConductor, Bioinformatics, 2007, 23, 1846-1847.

Supplementary

Figure 9.1S. Volcano plot for differentially expressed genes cadmium for the pairwise comparison between cadmium 10µM versus ctr. The fold change is represented on the x-axis and the statistical significance i.e -log10 of the p-value on the y-axis. The MTs genes are situated on the right part of the plot and colored in red. Each single dot represents one gene with a detectable gene expression in both subtypes. The colored dots are statistically significantly (p < = 0.05) down-regulated and up-regulated genes respectively in green and red above the horizontal line that marks the threshold (p < 0.05). The vertical dashed lines represents a cutoff to retain significant DE genes with |logFC| >= 1.

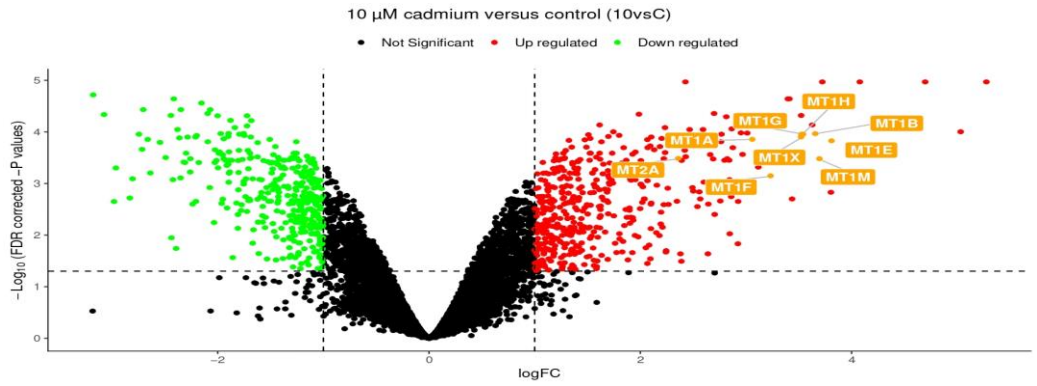

Figure 9.2S. Volcano plot for differentially expressed genes cadmium for the pairwise comparison between cadmium 10µM versus cadmium 2µM. The fold change is represented on the x-axis and the statistical significance i.e -log10 of the p-value on the y-axis. The upregulated genes are situated on the right part of the plot and colored in red. The downregulated genes are situated on the left part and are colored in green. The up- and downregulated genes found as a result are labeled in orange. Each single dot represents one gene with a detectable gene expression in both subtypes. The colored dots are statistically significantly (p < = 0.05) down-regulated and up-regulated genes respectively in green and red above the horizontal line that marks the threshold (p < 0.05). The vertical dashed lines represents a cutoff to retain significant DE genes with |logFC| >= 1.

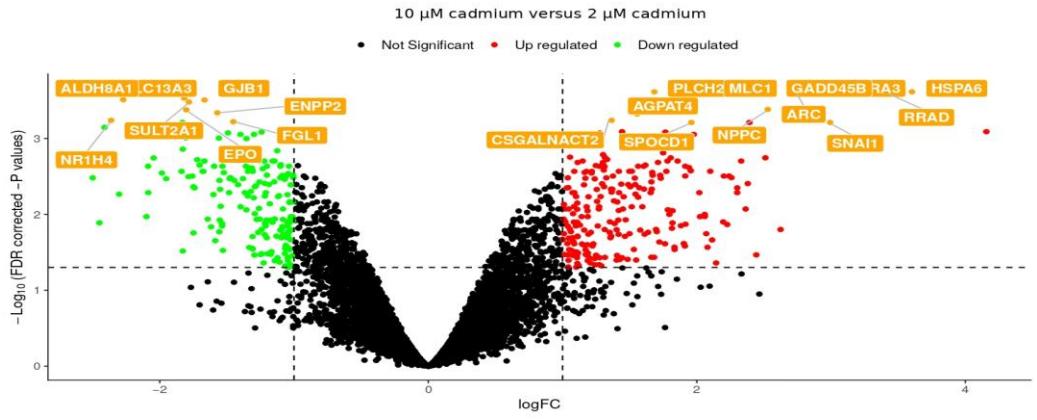

From tables S1A to S2B:

Table 1SA = upregulated genes cd10 vs ctrl
Table 12B = downregulated genes cd10 vs ctrl
Table 2SA = upregulated genes cd2 vs cd10
Table 2SB = downregulated genes cd2 vs cd10

Tables include logarithm 2 fold changes (logFC), standard errors, t-statistics and p-values as columns.

The **logFC** column gives the value of the contrast.

The **AveExpr** column gives the average log2 expression level for that gene across all the arrays and channels in the experiment.

Column **t** is the moderated t-statistic. Moderated t-statistic has the same interpretation as an ordinary t-statistic except that the standard errors have been moderated across genes. Moderated t-statistics lead to p-values in the same way that ordinary t-statistics do except that the degrees of freedom are increased, reflecting the greater reliability associated with the smoothed standard errors.

Column **P.Value** is the associated p-value and **adj.P.Value** is the p-value adjusted for multiple testing. The adjusted values are often called q-values if the intention is to control or estimate the false discovery rate. The most popular form of adjustment is Benjamini and Hochberg's method (BH) to control the false discovery rate. The adjusted values are often called q-values if the intention is to control or estimate the false discovery rate. For example, if all genes with q-value with a threshold < 0.05 are selected as differentially expressed, then the expected proportion of false discoveries in the selected group is controlled to be less than the threshold value, in this case 5%.

The **B-statistic (lods or B)** is the log-odds that the gene is differentially expressed. For example, a B-statistic of zero corresponds to a 50-50 chance that the gene is differentially expressed. The B-statistic is automatically adjusted for multiple testing by assuming that 1% of the genes, are expected to be differentially expressed. The p-values and B-statistics will normally rank genes in the same order. If the data contains no missing values or quality weights, the order will be precisely the same.

Column **dir**: if genes are upregulated = up and if downregulated = down.

Table 9.1SA . Upregulated genes cd10 vs ctrl

	logFC	AveExpr	t	P.Value	adj.P.Val	B
HTRA3	4,07784757	8,02348833	19,6634338	2,99E-09	1,07E-05	11,5712494
GADD45B	3,72248115	11,5635485	19,3660360	3,46E-09	1,07E-05	11,4496371
HSPA6	5,27601923	8,64410017	19,2117689	3,74E-09	1,07E-05	11,3854983
PLCH2	2,42650331	9,77222311	18,8789976	4,42E-09	1,07E-05	11,2446263
RRAD	4,69611672	10,4841599	18,8125316	4,58E-09	1,07E-05	11,2160697
MLC1	3,41115812	7,33706205	16,5588825	1,56E-08	2,28E-05	10,1574842
ARC	3,39682466	7,29933612	16,5283530	1,58E-08	2,28E-05	10,1418404
SPOCD1	2,69823218	8,37853143	14,4711716	5,63E-08	4,40E-05	8,99430147
AGPAT4	1,98725829	6,91698576	14,3275177	6,18E-08	4,53E-05	8,90670930
CCL26	3,52274047	7,87522468	13,9986805	7,70E-08	4,80E-05	8,70217953
IL11	3,15502342	10,3543552	13,8038263	8,79E-08	4,86E-05	8,57827348
NPPC	2,96806251	7,01127615	13,6985365	9,45E-08	4,86E-05	8,51046046
MMP3	2,81368139	8,14242453	13,5578804	1,04E-07	5,09E-05	8,41891139
SNAI1	3,62770182	9,32294120	12,8829893	1,68E-07	7,31E-05	7,96383459
CSGALNACT2	1,61521244	9,12409786	12,8287208	1,75E-07	7,33E-05	7,92606485
AXL	2,23355348	9,5592392	12,5287905	2,18E-07	8,26E-05	7,71402689
AKAP12	2,86504889	11,5677562	12,4131092	2,38E-07	8,73E-05	7,63072613
METRNL	2,46638201	11,1812189	12,3305187	2,53E-07	8,98E-05	7,57072554
GLIPR1	2,59351060	9,43448731	12,2883066	2,61E-07	8,98E-05	7,53988758
GADD45G	5,03247971	8,26588458	12,0883192	3,05E-07	9,94E-05	7,39218829
GPRC5A	1,74520249	7,46223817	12,0518969	3,13E-07	9,94E-05	7,36500128
KRTAP3-1	2,95260318	12,0040717	11,9543690	3,38E-07	0,00010446	7,29176018
HSPA1A	3,01203563	14,8732783	11,9114577	3,50E-07	0,00010524	7,25932923
MT1B	3,65621902	15,8875847	11,7513805	3,96E-07	0,00010823	7,13722534
EGR4	2,76787916	8,03595741	11,6519753	4,29E-07	0,00011091	7,06049806
MT1H	3,53995521	16,3200791	11,6091038	4,44E-07	0,00011091	7,02719088
MT1G	3,52530019	16,3988262	11,5795633	4,55E-07	0,00011113	7,00416429
S1PR4	1,50865887	8,39314716	11,5318108	4,72E-07	0,00011311	6,96680901
BIRC3	1,79956322	8,56992446	11,4661530	4,98E-07	0,00011686	6,91517806
AQP3	2,70490711	10,8680073	11,3396553	5,52E-07	0,00012215	6,81481787
KRT15	1,69775567	10,0737033	11,3027587	5,69E-07	0,00012275	6,78532279
RASD1	2,46950753	13,3734500	11,2740392	5,82E-07	0,00012275	6,76229451
SH2D5	2,10379786	12,8805187	11,1681576	6,35E-07	0,00012572	6,67686141
MT1X	3,52154208	16,2315007	11,1532722	6,43E-07	0,00012572	6,66478308
SLC6A6	1,52591717	8,94097966	11,0037733	7,28E-07	0,00013402	6,54253929
NR4A1	2,20255029	10,1331086	10,9821716	7,41E-07	0,00013402	6,52473380
MLLT11	2,38685028	9,35150723	10,9802436	7,4305E-07	0,00013402	6,52314282
MT1A	3,05992493	16,1830464	10,8713609	8,14E-07	0,00013965	6,43282552
JUNB	2,06673393	11,9568435	10,8300275	8,43E-07	0,00014123	6,39829635
RIN1	1,47474963	10,1064275	10,8029384	8,62E-07	0,00014248	6,37559341
PLEKHO1	1,32440175	11,6999649	10,7576934	8,96E-07	0,00014602	6,33754429

MT1E	3,80968670	16,0795110	10,7201707	9,25E-07	0,00014870	6,30586539
IGFBP1	2,76323659	11,9170603	10,6286504	1,00E-06	0,00015519	6,22812367
SVIL	1,63209699	9,54729707	10,6046573	1,02E-06	0,00015568	6,20763054
DOK7	2,37937310	7,77850221	10,5633603	1,05E-06	0,00015927	6,17224789
ADAMTS4	2,09324828	9,57961510	10,3398331	1,28E-06	0,00018645	5,97828903
LIF	2,18596129	9,45292714	10,2838192	1,35E-06	0,00019261	5,92902891
CLCF1	1,48975231	7,95644459	10,2243654	1,42E-06	0,00019740	5,87645189
TMEM54	1,35106944	8,33199959	10,2209733	1,43E-06	0,00019740	5,87344295
RGS2	2,87598714	8,63588675	10,1786011	1,48E-06	0,00020239	5,83577468
ARHGAP23	2,06970245	8,05682532	10,1615047	1,50E-06	0,00020239	5,82053241
DUSP6	1,84224112	11,3963777	10,1541310	1,51E-06	0,00020239	5,81395067
TUBB2B	2,13165549	11,1670360	10,0265956	1,70E-06	0,00022196	5,69936384
KRT37	4,12347927	9,08649256	9,99113645	1,75E-06	0,00022423	5,66725151
TFPI2	2,42015522	7,93031156	9,95150575	1,82E-06	0,00022750	5,63122985
TMEM217	1,29479657	7,18945093	9,93623492	1,84E-06	0,00022826	5,61731246
QSOX1	1,95360172	11,9876757	9,81317064	2,07E-06	0,00024519	5,50439333
PHLDA2	2,23453334	12,1300734	9,77310602	2,14E-06	0,00025188	5,46733669
CNN1	1,73327025	9,71600616	9,73381388	2,22E-06	0,00025862	5,43085257
KLF5	1,52299837	7,80133129	9,67895295	2,34E-06	0,00025876	5,37967568
STX1A	1,27226127	9,74432924	9,66157826	2,38E-06	0,00025876	5,36340996
OTUB2	1,61486724	8,03894345	9,65899995	2,38E-06	0,00025876	5,36099384
ITPRIP	1,52946325	9,78917289	9,65130456	2,40E-06	0,00025876	5,35377888
EDEM1	1,20238240	10,4016816	9,60065503	2,52E-06	0,00026643	5,30615435
PLAUR	1,92690711	8,35924416	9,57448721	2,58E-06	0,00027062	5,28145581
UCHL1	2,96826502	8,59013625	9,55463473	2,63E-06	0,00027328	5,26267529
BATF	2,66156534	10,2290690	9,53938033	2,67E-06	0,00027481	5,24821946
GALNT10	2,42970584	8,99678524	9,40191822	3,04E-06	0,00030247	5,11696150
TIMP1	1,58343123	10,1876879	9,36346226	3,15E-06	0,00030856	5,07991872
DYNC2H1	1,19703806	6,63752638	9,27889144	3,42E-06	0,00031899	4,99795392
NRP1	1,28461314	10,1396270	9,27549302	3,43E-06	0,00031899	4,99464572
MT2A	2,35892189	16,9740657	9,22430649	3,61E-06	0,00032659	4,94468166
ATP8A2	1,27959596	6,74198650	9,18674133	3,74E-06	0,00033045	4,90785024
PPP1R15A	2,82203734	9,55746438	9,17364302	3,79E-06	0,00033045	4,89497509
FHL2	2,22295934	14,1169281	9,15740423	3,85E-06	0,00033045	4,87898943
MT1M	3,69498154	14,9724285	9,14967930	3,883E-06	0,00033045	4,87137576
RIOK3	1,24677154	10,6661981	9,12764133	3,96E-06	0,00033463	4,84962267
TAGLN3	1,25367863	6,61244628	9,11967594	3,99E-06	0,00033483	4,84174839
MYLIP	2,68948665	7,80580891	9,11241740	4,02E-06	0,00033483	4,83456737
ARHGEF4	1,61932291	7,26017457	9,08948504	4,11E-06	0,00033765	4,81184541
EGR1	3,12035535	11,1217643	9,06836302	4,20E-06	0,00034217	4,79087070
SERTAD1	1,43128842	12,6790879	9,05360009	4,26E-06	0,00034258	4,77618420
NPPB	3,26234116	9,70139433	8,98634665	4,55E-06	0,00035488	4,70900138
ZBTB20	1,52040285	7,41171177	8,98362636	4,57E-06	0,00035488	4,70627434
CYTH3	1,22940461	7,39316982	8,97706040	4,60E-06	0,00035488	4,69968897
MYOF	2,79746463	9,63302392	8,96635852	4,65E-06	0,00035491	4,68894608

RAB3B	3,13210061	10,0002213	8,94372075	4,75E-06	0,00035491	4,66618323
FJX1	1,86678808	8,40113563	8,93823396	4,78E-06	0,00035491	4,66065826
FOS	2,84085789	7,47033941	8,93589278	4,79E-06	0,00035491	4,65829986
MMP1	2,39140314	7,64876442	8,91569713	4,89E-06	0,00035744	4,63793240
LARP6	2,00526950	8,77535273	8,89065234	5,01E-06	0,00035938	4,61261659
HAS3	1,18228220	7,13668015	8,85324119	5,20E-06	0,00036362	4,57468060
GDF15	1,41167904	16,4814262	8,84613672	5,24E-06	0,00036365	4,56746018
ATF3	1,41237891	9,82212624	8,79774264	5,50E-06	0,00037730	4,51813728
CTAG1A	1,07705336	6,87869667	8,74663163	5,79E-06	0,00039042	4,46578095
RAB3A	1,35729039	7,66438721	8,73298325	5,87E-06	0,00039286	4,45175385
PLEKHG5	1,71074427	9,53867461	8,67125815	6,25E-06	0,00040095	4,38807153
CREB5	1,36544816	7,37623144	8,66535208	6,29E-06	0,00040095	4,38195712
TEP1	1,82392782	11,0576083	8,65656520	6,34E-06	0,00040237	4,37285345
RAB7B	1,65033206	7,65207345	8,59309705	6,77E-06	0,00042249	4,30685356
ROBO4	1,35947763	6,95497497	8,58001661	6,86E-06	0,00042410	4,29319797
CAPN2	2,04893033	13,3730929	8,56604350	6,96E-06	0,00042757	4,27859022
CPEB4	1,24247941	10,0814408	8,41621112	8,13E-06	0,00048165	4,12062846
MYEOV	2,14922001	8,81110071	8,41063425	8,18E-06	0,00048203	4,11470189
ASB2	3,11711390	10,8642161	8,40522417	8,22E-06	0,00048233	4,10894932
SH3RF2	1,25512175	8,40799957	8,38518414	8,40E-06	0,00049008	4,08761265
NFATC1	1,21081357	6,66249361	8,35165970	8,70E-06	0,00050012	4,05182039
LHX6	1,40997755	8,38173101	8,32467356	8,95E-06	0,00050510	4,02291862
EMP1	1,37735351	7,01323632	8,32372933	8,96E-06	0,00050510	4,02190590
C2CD2L	1,17537202	11,2556736	8,29273878	9,25E-06	0,00051443	3,98861269
IL23A	1,57132692	8,36539478	8,23269828	9,86E-06	0,00053794	3,92380663
OSMR	1,40252760	9,06579619	8,21603824	1,00E-05	0,00054500	3,90575272
ZFP36L1	1,27580353	13,5060054	8,16499955	1,06E-05	0,00056401	3,85024942
KLF6	1,69392431	12,7073109	8,16232997	1,06E-05	0,00056401	3,84733823
TGM2	1,91786586	12,3075941	8,14690637	1,08E-05	0,00057080	3,83050287
ACSL5	1,21853218	11,0406871	8,11684598	1,11E-05	0,00058682	3,79761340
PLK2	1,39566355	11,6131451	8,10832187	1,12E-05	0,00058824	3,78826836
CCR7	2,15863913	7,26810769	8,10625954	1,12E-05	0,00058824	3,78600616
TIE1	1,10817074	6,68311427	8,01015047	1,25E-05	0,00062519	3,68004284
TRPV2	1,54775831	12,7536955	8,00212376	1,26E-05	0,00062746	3,67115053
IDS	1,54733933	9,20900206	7,99120352	1,27E-05	0,00062878	3,65902777
USP35	1,33287358	11,5318334	7,98761469	1,28E-05	0,00062878	3,65504252
MPP3	2,08051014	10,4470973	7,98468415	1,28E-05	0,00062878	3,65178718
SUSD2	1,18292198	11,8340666	7,97587940	1,29E-05	0,00063203	3,64200057
DUSP1	1,37639661	9,88973018	7,96538424	1,31E-05	0,00063203	3,63032330
ENDOD1	1,08180716	10,4546255	7,96507383	1,31E-05	0,00063203	3,62997773
MICAL1	1,64551603	9,93758682	7,92885152	1,36E-05	0,0006499	3,58957585
LETM2	1,40340256	7,95363434	7,92587199	1,37E-05	0,0006499	3,58624571
KYNU	1,13214571	13,1482473	7,92247314	1,37E-05	0,0006499	3,58244564
KLHL29	1,02519583	6,25773917	7,92051468	1,38E-05	0,0006499	3,58025539
WDR66	1,71661475	8,41384091	7,85183682	1,48E-05	0,00069233	3,50316481

SH3RF1	1,69730761	11,8231341	7,82716588	1,52E-05	0,00070578	3,47533631
MT1F	3,23232418	13,5010512	7,81747469	1,54E-05	0,00071056	3,46438509
DUSP4	1,27560418	8,55472504	7,78625074	1,59E-05	0,00072855	3,42902576
RGS20	1,70655635	8,50101294	7,71130696	1,73E-05	0,00078027	3,34368234
GPSM1	1,90137727	11,5519952	7,70916247	1,74E-05	0,00078027	3,34123038
IQCD	1,33192993	8,37539344	7,68202027	1,79E-05	0,00079466	3,31014880
FOSB	1,24280663	7,13697768	7,65150533	1,85E-05	0,00081003	3,27509896
OSCAR	1,31294405	8,68910803	7,64246240	1,87E-05	0,00081224	3,26469052
TUBB2A	1,41517159	15,1854917	7,62072939	1,92E-05	0,00082924	3,23963526
UBASH3B	1,06083475	7,13160808	7,59748923	1,97E-05	0,00084423	3,21277899
NCF2	2,84421443	10,5537084	7,58998889	1,99E-05	0,00084423	3,20409758
EMP3	1,95219733	10,1305256	7,58337002	2,00E-05	0,00084423	3,19643076
ADAP2	1,90865148	9,92225074	7,56897878	2,03E-05	0,00084984	3,17974253
INHBB	1,58510769	10,2657126	7,56051975	2,05E-05	0,00084996	3,16992153
TNFRSF25	1,72700590	9,2111074	7,55368435	2,07E-05	0,00083555	3,1619792
PROCR	1,91350195	10,9646792	7,54064581	2,10E-05	0,00086321	3,14681329
SOX4	2,06726675	14,2367970	7,51276464	2,17E-05	0,00088169	3,11431304
IQCG	1,09603737	7,15376714	7,50966817	2,18E-05	0,00088174	3,11069769
ESAM	2,60176633	11,5780206	7,44158308	2,35E-05	0,00093955	3,03090409
NPAS1	1,70463538	8,29670657	7,39331884	2,49E-05	0,00097350	2,97399156
PMAIP1	1,74024802	7,89564381	7,38380738	2,51E-05	0,00098093	2,96274151
GRB10	2,00420770	11,1488034	7,31803945	2,71E-05	0,00102793	2,88464167
DEFB103A	1,56114233	6,38556436	7,30566961	2,75E-05	0,00103900	2,86989162
ZNF280A	1,70944135	9,19525537	7,29739177	2,78E-05	0,00104565	2,86001017
RFTN1	1,12498995	6,70650968	7,29312261	2,79E-05	0,00104657	2,85491058
PFKP	2,00665796	11,2342639	7,29112399	2,80E-05	0,00104657	2,85252240
CDC42EP2	1,11540933	10,4367388	7,27685464	2,84E-05	0,00106068	2,83545709
CYR61	2,15690414	12,4853889	7,25942517	2,90E-05	0,00107825	2,81457747
TRIB1	1,30450715	14,1230530	7,24698143	2,95E-05	0,00108784	2,79964691
HK1	1,33945626	6,96720550	7,19383007	3,13E-05	0,00113610	2,73565151
RHBDF2	1,44395655	12,3562613	7,17034423	3,22E-05	0,00115712	2,70725905
TAGLN	1,17217839	13,2165101	7,16510836	3,24E-05	0,00116055	2,70091968
SERPINB8	2,02411761	10,6432162	7,16174714	3,26E-05	0,00116055	2,69684820
DISP2	1,25945542	9,60181808	7,16005156	3,26E-05	0,00116055	2,69479377
SPANXA1	1,58316879	6,36908129	7,14985435	3,30E-05	0,00117100	2,68243067
IER2	1,27988036	15,5041941	7,14415131	3,32E-05	0,00117380	2,67551048
TMCC1	1,57130911	9,05047147	7,14042717	3,34E-05	0,00117380	2,67098928
PREX1	1,17646575	7,02874452	7,14016400	3,34E-05	0,00117380	2,67066971
PLAU	2,49294490	9,33797366	7,11037205	3,46E-05	0,00120193	2,6344361
SLC38A2	1,18951083	13,6037473	7,10902464	3,46E-05	0,00120193	2,63279464
GEM	1,03406961	6,29825155	7,09980812	3,50E-05	0,00120578	2,62156049
KCNN4	1,13061019	7,64445659	7,07541226	3,60E-05	0,00123029	2,59177098
CXCR4	2,25980989	7,94966436	7,06824304	3,64E-05	0,00123362	2,58300207
C3orf52	1,42234601	8,05093973	7,04541667	3,74E-05	0,00125518	2,55503788
BICD1	1,01199951	8,41453311	7,04397312	3,74E-05	0,00125518	2,55326713

MAFF	1,66484110	8,58323358	7,01936660	3,85E-05	0,00128514	2,52304153
EGLN1	1,12147810	11,2751384	6,99934054	3,95E-05	0,00131249	2,49838404
SOHLH1	1,69146739	7,92383254	6,98814031	4,00E-05	0,00132194	2,48457066
TNFRSF12A	1,61447073	13,7037353	6,98625610	4,01E-05	0,00132194	2,48224523
HOMER2	1,12701915	8,43785313	6,93002866	4,29E-05	0,00140233	2,41263657
ASPH	2,50195681	11,9635730	6,92395247	4,32E-05	0,00140479	2,40508943
KRTAP1-5	1,25888537	6,45135325	6,90683066	4,41E-05	0,00142718	2,38379650
AREG	2,55818478	13,08952	6,88789285	4,51E-05	0,00145112	2,36020004
NDRG1	1,68598640	11,7342359	6,87186024	4,60E-05	0,00147145	2,34018631
CRYAB	3,80466079	10,2842281	6,86515391	4,64E-05	0,00147751	2,3318046
HIST2H2AA4	1,55812736	12,4098360	6,85160966	4,72E-05	0,00149279	2,31485849
MLF1	1,45357459	7,66371593	6,83926637	4,79E-05	0,00151014	2,29939373
C16orf45	1,52858074	7,94292072	6,83608044	4,81E-05	0,00151193	2,29539882
KREMEN2	1,25902996	10,6820445	6,82754821	4,86E-05	0,00152283	2,28469341
NAV3	1,31665779	6,37978477	6,81039185	4,96E-05	0,00153925	2,26313791
GABARAPL1	1,32099883	9,52965349	6,80516288	4,99E-05	0,00154499	2,25656034
DUSP18	1,12706232	9,17020359	6,69188025	5,73E-05	0,00173537	2,11316058
LDHB	1,06005817	6,54351367	6,66376343	5,94E-05	0,00177659	2,07730064
ITGA6	1,08137555	11,7713014	6,65593196	5,99E-05	0,00178475	2,06729337
RELB	1,36914535	12,2800479	6,65157181	6,03E-05	0,00178745	2,06171824
EPS8L1	1,03270212	9,39087781	6,63879164	6,12E-05	0,00179725	2,04536195
VCX3A	2,86027290	7,84358422	6,63535959	6,15E-05	0,00179881	2,04096578
ASAP2	1,63645709	10,6127195	6,61349948	6,32E-05	0,00183906	2,01292711
FOSL1	1,41930030	8,78363185	6,59880158	6,43E-05	0,00186831	1,99403838
VGF	1,27633734	7,45882408	6,59426930	6,47E-05	0,00187423	1,98820785
LRP10	1,05139124	12,0093329	6,57923709	6,59E-05	0,00189559	1,96884969
ITPR3	1,41546924	12,5916918	6,55169680	6,82E-05	0,00193809	1,93330367
RELT	1,26800092	10,9618551	6,53433284	6,97E-05	0,00197507	1,91083871
LAMB3	3,43644638	9,59258228	6,52372032	7,07E-05	0,00199150	1,89708817
FRMD5	2,03592983	10,7123045	6,51956261	7,10E-05	0,00199150	1,89169686
SPANXD	1,36025924	6,26850163	6,51762857	7,12E-05	0,00199150	1,88918816
CD109	2,03982398	9,82840530	6,51492628	7,14E-05	0,00199150	1,88568209
VCX2	2,56730342	7,35166203	6,51274869	7,16E-05	0,00199150	1,88285607
SAMD4A	1,16435168	10,2461694	6,49931585	7,29E-05	0,00201831	1,86540878
DUSP13	1,65402169	11,5786399	6,45129566	7,74E-05	0,00209207	1,80283409
SMURF2	1,06340034	8,80543671	6,42096916	8,04E-05	0,00213446	1,76315157
SPRY4	1,41362676	8,67428709	6,41599271	8,09E-05	0,00213893	1,75662764
ZFP36	1,68421170	9,29086607	6,38846988	8,38E-05	0,00216069	1,72048423
CHI3L2	1,18422027	6,73823674	6,38402442	8,43E-05	0,00216816	1,71463650
AMPD3	2,75738965	8,15917924	6,37688327	8,50E-05	0,00218314	1,705237
GFPT2	2,34715799	7,43137116	6,35927686	8,70E-05	0,00221333	1,68203227
AHNAK2	1,12712934	6,51846896	6,35524175	8,74E-05	0,00221525	1,67670803
EDN1	2,92586627	9,11634507	6,34263528	8,88E-05	0,00222687	1,66005941

TM4SF1	1,05055567	15,8866543	6,32994095	9,03E-05	0,00223641	1,64327232
RAB31	1,08626034	8,09227298	6,32580073	9,08E-05	0,00224173	1,63779239
PALLD	1,32605506	7,94966859	6,30305785	9,35E-05	0,00229266	1,60764743
INPP1	1,16631715	9,76998471	6,30058479	9,38E-05	0,00229266	1,60436511
NRG1	2,01921430	7,13060758	6,28399793	9,58E-05	0,00232104	1,58232827
IER3	1,69482421	13,1134047	6,28055011	9,62E-05	0,00232653	1,57774275
COL4A2	1,35480796	9,10769004	6,27370630	9,70E-05	0,00234224	1,56863570
NOSTRIN	1,31526667	7,05284162	6,24873729	0,00010026	0,00237979	1,53535359
FOXC1	1,36167737	11,0496741	6,24619044	0,00010059	0,00237979	1,53195387
FRG2	1,30142979	6,55466703	6,24551444	0,00010068	0,00237979	1,53105134
MICALL2	1,06494666	11,2862308	6,23881495	0,00010155	0,00239434	1,52210337
LAIR2	2,10323629	8,95437425	6,23584098	0,00010194	0,00239434	1,51812925
MTMR11	1,14781469	9,17964562	6,2269288	0,00010312	0,00239883	1,50621243
SNAPC4	1,15736662	12,7654467	6,22467461	0,00010342	0,00240106	1,50319649
GLRX	1,27879987	13,3357600	6,17913885	0,00010970	0,00250380	1,44211934
VCX	2,64385401	7,41269372	6,17742350	0,00010994	0,00250380	1,43981282
EREG	2,10006406	7,65984483	6,16949476	0,00011108	0,00251605	1,42914608
CCK	2,26623746	6,96534598	6,15838448	0,00011269	0,00254580	1,41418416
PLK3	1,49537801	12,2775372	6,14674502	0,00011441	0,00257316	1,39849083
JUN	2,22262530	11,2669386	6,14573626	0,00011456	0,00257316	1,39712982
SPSB1	1,52959060	11,1439169	6,11908367	0,00011861	0,00263884	1,36111824
GRB14	1,50530124	9,04994895	6,10611688	0,00012064	0,00265869	1,34356168
NES	1,62389986	11,7187057	6,08478362	0,00012405	0,00272736	1,31462514
SPEG	1,60927102	7,70975982	6,06168506	0,00012787	0,00279177	1,28322099
F2RL1	2,54054257	10,1833238	6,05580083	0,00012886	0,00280299	1,27520880
FBXL19	1,17352535	10,5235042	6,03406191	0,00013260	0,00287133	1,24556533
SMYD3	1,08493565	13,3233640	6,03326241	0,00013274	0,00287133	1,24447384
KRT23	1,23721299	15,2147607	6,02635557	0,00013395	0,00289223	1,23504065
SLC25A12	1,38596327	10,7733893	6,01357622	0,00013623	0,00293058	1,21756893
UPP1	1,47330760	9,81379280	6,00038654	0,00013862	0,00296033	1,19951171
CSAG1	1,89679456	7,20592819	5,99066878	0,00014041	0,00298230	1,18619172
SDCBP2	1,11423899	7,37221901	5,98886058	0,00014075	0,00298403	1,18371767
CDC42SE1	1,00112995	10,7934906	5,96307387	0,00014564	0,00306672	1,14829397
SLC43A2	1,14308120	10,8825551	5,96176390	0,00014589	0,00306672	1,14649220
SLC16A4	1,07971991	7,34545447	5,96142738	0,00014596	0,00306672	1,14602930
NUAK1	1,99841121	10,4182462	5,95711436	0,00014679	0,00306782	1,14009506
MAP3K14	1,02050892	9,35187795	5,91480804	0,00015529	0,00319411	1,08174453
GGT5	1,86236557	8,48791818	5,91049742	0,00015618	0,00319722	1,07578469
STK10	1,62256670	10,1546966	5,90492448	0,00015735	0,00319722	1,06807561
HIVEP2	1,40127438	7,65508599	5,88714337	0,00016113	0,00325526	1,04344898
FADS3	1,14883162	10,0230286	5,88329692	0,00016196	0,00325863	1,03811568
ANTXR2	1,10237982	11,1916942	5,88164790	0,00016232	0,00325863	1,03582859
SCHIP1	1,89680844	8,31350280	5,86556305	0,00016585	0,00330689	1,01349920
PSG6	1,45561199	6,60932318	5,83001518	0,00017395	0,00342763	0,96401822
MCL1	1,27766464	13,5532627	5,82180787	0,00017588	0,00345406	0,95256806

DOCK4	1,01539981	9,85844368	5,79344187	0,00018273	0,00355189	0,912919
KRT80	2,19699947	9,43041860	5,78113796	0,00018579	0,00359453	0,89568489
PDLIM7	1,07930714	9,60474846	5,73628450	0,00019743	0,00376031	0,83267230
TICAM1	1,06984611	11,7965190	5,72897815	0,00019939	0,00378889	0,82238029
ANKRD1	1,69583369	10,5217745	5,70948464	0,00020475	0,00386558	0,79488300
CILP	1,50253276	6,32959587	5,69337240	0,00020929	0,00390661	0,77211359
S100A2	2,70384053	11,0673401	5,67588181	0,00021435	0,00397632	0,74735359
S100A16	1,29843050	12,9165072	5,67455443	0,00021473	0,00397724	0,74547271
CCNO	1,18777261	7,04140926	5,65217996	0,00022140	0,00407503	0,71372978
BIK	1,62355579	8,59837046	5,61667738	0,00023245	0,00420569	0,66321219
MOSPD1	1,74882429	10,0460137	5,60844140	0,0002351	0,00424047	0,65146675
ZNF655	1,01837905	10,8296221	5,59827930	0,00023840	0,00428697	0,63696079
TIMP2	1,90618993	12,2040532	5,55524488	0,00025298	0,00450701	0,57536413
PDLIM4	1,87277754	10,3097278	5,54741830	0,00025574	0,00452917	0,56413264
POMC	1,61574143	7,05294457	5,53699430	0,00025945	0,00456739	0,54915984
NKAIN1	1,92775975	9,13142662	5,53259911	0,00026104	0,00458549	0,54284193
RRP12	1,19082783	11,0450664	5,53197345	0,00026126	0,00458549	0,54194234
NAGS	1,35545739	10,8328031	5,52636358	0,00026330	0,00460062	0,53387377
NTSR1	1,24122001	6,84532275	5,49338147	0,00027564	0,00475249	0,48634330
RNF183	1,44156354	8,10653084	5,48394459	0,00027929	0,00478016	0,47271460
KRT33A	1,31104347	9,82294013	5,47954724	0,00028100	0,00480252	0,46635952
TNFRSF21	1,15520730	13,0790987	5,45393012	0,00029122	0,00490569	0,42928134
CCDC84	1,10449753	10,9611819	5,42563244	0,00030298	0,00507173	0,38821187
GPR157	1,16669159	9,08320084	5,41270998	0,00030852	0,00513066	0,36941812
MAP1B	1,93176054	10,4670001	5,40791400	0,00031060	0,00515068	0,36243689
VASP	1,11844336	11,7732952	5,39258933	0,00031736	0,0052252	0,34010714
LCK	1,36986595	7,24565661	5,32332867	0,00034992	0,00564300	0,23875880
VCY	1,12506182	7,45550615	5,29438350	0,00036457	0,00579950	0,19619617
COTL1	1,90306579	12,5754530	5,27704782	0,00037366	0,00589608	0,17064628
ARHGEF18	1,21518871	13,2545803	5,25032467	0,00038814	0,00607564	0,13117498
TLE3	1,02292336	8,35648264	5,24513150	0,00039103	0,00608186	0,12349236
TRMT1	1,08230391	12,2191755	5,24398026	0,00039167	0,00608195	0,12178872
TMSB4X	2,19329693	9,23736627	5,24289326	0,00039228	0,00608195	0,12017996
FBXL16	1,42887074	9,43604877	5,23702446	0,00039558	0,00611848	0,11149119
SGCB	1,03329450	10,2454635	5,21390732	0,00040886	0,00624977	0,07721742
ANXA3	1,84933329	11,2705995	5,17823868	0,00043031	0,00652651	0,02418207
GCLM	1,22088656	10,8962416	5,17147240	0,00043451	0,00655809	0,01410048
CORO2B	1,07917139	6,88478582	5,14211453	0,00045326	0,00674241	-0,02971901
TSPAN1	1,16547666	9,9811825	5,14165060	0,00045356	0,00674241	-0,03041248
ZBED2	1,11590090	6,40549278	5,12317387	0,00046581	0,00685223	-0,05805619
NFE2L3	1,46851912	11,3620950	5,11849622	0,00046897	0,00687280	-0,06506243
PPP1R13L	1,19374325	9,69766843	5,11101541	0,00047407	0,00693017	-0,07627390
CARD10	1,37387622	13,5965050	5,09904163	0,00048235	0,00699586	-0,09423582
PAQR3	1,34028414	9,86968347	5,09845423	0,00048276	0,00699586	-0,09511754
WNK4	1,23924792	7,79576850	5,09787430	0,00048316	0,00699586	-0,09598804

IER5L	1,52036190	10,8247569	5,09740377	0,00048349	0,00699586	-0,0966944
SPINT2	1,58654590	8,34388292	5,09077896	0,00048815	0,00704645	-0,1066427
S100A3	2,21005507	9,35892807	5,08883794	0,00048953	0,00705067	-0,10955880
PLEKHA6	1,47995956	9,69514219	5,08606360	0,00049150	0,00706269	-0,11372765
ARID3B	1,04468072	12,3800893	5,06364188	0,00050775	0,00723597	-0,14746045
ADM	1,61826063	11,6054832	5,05954665	0,00051078	0,00724839	-0,15362946
PPFIBP1	1,21091534	9,63054300	5,05898063	0,0005112	0,00724839	-0,15448229
CHIC2	1,26283778	9,85605804	5,05885258	0,00051129	0,00724839	-0,15467524
CATSPER1	1,50932169	7,06927636	5,05516911	0,00051403	0,00726096	-0,16022640
CDA	1,44534928	8,21221471	5,05187338	0,00051650	0,00726955	-0,16519488
LRRC8A	1,45534834	13,6438066	5,04827091	0,00051922	0,00728343	-0,17062759
ICAM2	1,50341216	11,7549449	5,04808961	0,00051935	0,00728343	-0,17090104
RIT1	1,27488081	10,6525497	5,04606320	0,00052089	0,00729307	-0,17395784
LY6K	2,09980131	7,08265960	5,02068499	0,00054050	0,00748963	-0,21229052
DBN1	1,00028127	13,5732268	4,99583153	0,00056048	0,00769447	-0,24992047
TES	1,05584377	10,2432756	4,97539396	0,00057749	0,00786362	-0,28093096
ZNF556	1,01063719	10,0706379	4,97143986	0,00058085	0,00789365	-0,28693754
ABR	1,37779226	12,6699479	4,96895887	0,00058296	0,00791056	-0,29070751
LIMS3	1,08623736	7,56186521	4,96595485	0,00058554	0,00791798	-0,29527342
GAL	1,31968915	6,98823793	4,94742287	0,00060168	0,00809725	-0,32346936
BAAT	1,27624414	10,4033201	4,93707390	0,00061090	0,00819418	-0,33923644
HES2	1,07901286	6,81188849	4,91363068	0,00063235	0,00843431	-0,37500978
TMEM173	1,10944142	9,82700966	4,91246725	0,00063344	0,00843919	-0,37678716
SAT1	1,35050989	15,1942337	4,90918596	0,00063651	0,00845130	-0,38181072
AP1S3	1,56027396	10,4301660	4,89035495	0,00065445	0,00861144	-0,41060505
WSB2	1,31270949	12,6561310	4,88510789	0,00065954	0,00864933	-0,41863997
ELK3	1,41498044	7,14729119	4,87778390	0,00066672	0,00869868	-0,42986186
HSPB8	1,45993215	7,30426239	4,87566844	0,00066881	0,00869908	-0,43310462
MPZL3	1,66716609	11,5803685	4,87156182	0,00067289	0,00873640	-0,43940139
ACTG2	1,34325532	8,18248387	4,85819110	0,00068634	0,00884255	-0,45991962
SERPINB2	1,34858468	7,38189917	4,85306160	0,00069158	0,00888076	-0,46779789
FAT1	1,42481010	11,7986094	4,84752786	0,00069728	0,00891488	-0,47630120
COL7A1	1,34878139	8,54553614	4,84154092	0,00070350	0,00896973	-0,48550579
SERPINE2	2,15157892	11,3681595	4,84099075	0,00070407	0,00896973	-0,48635190
MAP3K6	1,02137486	10,6416761	4,82756499	0,00071825	0,00908400	-0,50701274
CLTB	1,35289275	12,1501269	4,81603142	0,00073068	0,00919156	-0,52478204
TM4SF19	1,08348366	6,29212480	4,80559402	0,00074212	0,00930553	-0,54087868
GCNT3	1,80220876	13,1377088	4,79285934	0,00075634	0,00939543	-0,56053897
PRSS23	2,84640325	8,39768338	4,78885917	0,00076086	0,00943961	-0,56671929
ZFHX2	1,30713129	7,95304367	4,76518005	0,00078825	0,00969547	-0,60334988
FAM110B	1,31695006	8,79235712	4,76212320	0,00079186	0,00971116	-0,60808442
UBR4	1,13530973	11,2490224	4,74721193	0,00080973	0,0098992	-0,63119819
FOSL2	1,15353414	9,26634482	4,74056651	0,00081784	0,00996712	-0,64150917
FOLR1	1,26009429	7,77725161	4,72528434	0,00083680	0,01014547	-0,6652442
S100A6	1,94924583	14,2684879	4,72350384	0,00083904	0,01016211	-0,66801169

LTBP1	1,34253192	7,18817299	4,71765801	0,00084643	0,01022571	-0,67710101
MICAL2	2,18047781	9,99227581	4,71728819	0,00084690	0,01022571	-0,67767619
KIF3C	1,53733592	9,46201258	4,69550034	0,00087511	0,01048712	-0,71159571
STK17B	1,98031646	9,11013003	4,66499456	0,00091629	0,01084015	-0,75919777
LGALS1	1,59736462	14,4591686	4,65288383	0,00093320	0,01098484	-0,77813127
SLC16A5	1,18204982	12,3734292	4,64218602	0,00094842	0,01108605	-0,79487263
STEAP1	1,15530833	12,6179908	4,62312434	0,00097619	0,01130919	-0,82474176
IFRD1	1,16256178	11,2414701	4,60982827	0,00099607	0,01150541	-0,84560574
SH3BGRL3	1,20933728	11,4968461	4,60888909	0,00099749	0,01151048	-0,84708039
AHNAK	1,52465834	10,2389459	4,60311822	0,00100627	0,01158894	-0,85614418
PFKFB3	1,02956894	9,42966450	4,60055775	0,00101019	0,01162267	-0,86016714
PLXND1	1,21269306	11,9504358	4,59572261	0,00101764	0,01167398	-0,86776643
MTHFD1L	1,09792653	11,9299133	4,59440149	0,00101968	0,01167459	-0,86984336
COL1A1	1,8046243	7,18783296	4,58036322	0,00104168	0,01185617	-0,89192755
ORAI2	1,17079659	10,7577611	4,50383561	0,00117081	0,01290091	-1,01278342
FILIP1L	1,2397975	10,1511445	4,48440289	0,00120623	0,0131516	-1,04359708
ITGA2	1,83628332	9,83680507	4,47401453	0,00122563	0,01326269	-1,0600899
GOLT1A	1,16266553	9,41048049	4,4731434	0,00122727	0,01326269	-1,06147367
SLC16A6	1,24084243	8,97073265	4,45691620	0,00125828	0,01347227	-1,08726686
GPC1	1,36008157	12,3204206	4,45148062	0,00126885	0,01354835	-1,09591450
PPP1R2	1,10776112	11,8742483	4,43507555	0,00130134	0,01379470	-1,12203728
MET	1,44478581	12,4033833	4,41119283	0,00135021	0,01415917	-1,16012998
AGAP2	1,02712197	8,03448488	4,40497392	0,00136326	0,01425769	-1,17006124
CYB5R2	1,15724402	9,22118630	4,39821214	0,00137759	0,01435636	-1,18086512
RNF128	1,01448621	13,3169241	4,39332340	0,00138805	0,01442713	-1,18867996
CYP24A1	1,76145682	12,3080459	4,39274144	0,00138930	0,01442713	-1,18961045
SERPINB9	1,30225311	7,92608523	4,37908994	0,00141899	0,01467048	-1,21145024
ITGA3	1,27413412	6,80372532	4,37789442	0,00142163	0,01467182	-1,21336399
TNS4	2,92328485	12,2499324	4,37266555	0,00143320	0,01472643	-1,22173631
KRT12	1,08276291	6,76277235	4,36885925	0,00144168	0,01478771	-1,22783308
CDKN1A	1,06124615	12,9442247	4,36076947	0,00145990	0,01490931	-1,24079708
CLCN5	1,03810444	8,79907877	4,35749962	0,00146733	0,01495082	-1,24603945
DCBLD2	2,08342653	13,9539918	4,32143085	0,00155200	0,01562060	-1,30395659
EPHA2	1,39445735	10,1813309	4,30363369	0,00159567	0,01590791	-1,33259475
DSP	1,19219619	13,6376658	4,29758760	0,00161080	0,01603148	-1,34233281
EIF5A2	1,41826913	10,2812227	4,25391559	0,00172468	0,01696330	-1,41280761
AK5	1,28346519	6,37418710	4,22124023	0,00181544	0,01759994	-1,46569029
RGS10	2,05266495	11,0598669	4,21792841	0,00182491	0,01763728	-1,47105748
S100A11	1,55324460	10,7082405	4,20571204	0,00186032	0,01778992	-1,49086700
BCAR3	1,10484855	9,93131141	4,19528903	0,00189110	0,01796703	-1,50778271
STK17A	1,04136165	11,1435774	4,19300465	0,00189792	0,01801721	-1,51149183
SYT11	1,02497564	6,65970892	4,18052351	0,00193563	0,01824226	-1,53176826
GSTP1	1,18504612	7,78152456	4,16322103	0,00198922	0,01855343	-1,55990795
HIST1H2AD	1,36173801	10,5014440	4,15959235	0,00200066	0,01863045	-1,56581391

ARRDC4	1,35238251	9,09423865	4,15854537	0,00200397	0,01864648	-1,56758256
PAK1	1,13081234	7,47974281	4,15281267	0,00202221	0,01875666	-1,57685254
SLCO4A1	1,06456502	7,76793771	4,14896520	0,00203455	0,01884130	-1,58311937
SMOX	1,14241815	12,2109878	4,11566574	0,00214472	0,01964433	-1,63743034
HSPBAP1	1,00064776	8,69073512	4,10890901	0,00216783	0,0197882	-1,64846617
RBP1	1,44594802	11,6901990	4,10860833	0,00216887	0,0197882	-1,64895740
ITPRIPL2	1,34688679	11,2688231	4,10406513	0,00218456	0,01985621	-1,65638097
SERPINE1	2,24400992	8,70224824	4,09575823	0,00221357	0,02005559	-1,66996052
RND3	1,82886091	7,47958708	4,04925287	0,00238363	0,02123120	-1,74612898
TMC7	1,01407451	9,55903325	4,04827032	0,00238737	0,02123637	-1,74774086
TSPAN5	2,24298327	9,98887701	4,04656367	0,00239387	0,02126199	-1,75054089
RHOC	1,39923747	13,6231857	4,03440210	0,00244079	0,02153081	-1,77050324
TGFB1I1	1,42178770	7,73728188	4,03396149	0,00244250	0,02153081	-1,77122679
GLIPR2	1,08803347	7,59624342	4,02387429	0,00248218	0,02176597	-1,78779710
VCAN	1,77479608	9,08693379	4,02305736	0,00248542	0,02177812	-1,78913957
MACF1	1,01492982	9,94051911	4,01645143	0,00251181	0,02186947	-1,7999978
ACTA1	1,92436276	13,5902996	4,0162448	0,00251263	0,02186947	-1,80033740
GULP1	1,18639640	7,02199245	3,99300893	0,00260783	0,02239876	-1,83856889
LOXL2	2,64004079	8,48521667	3,96502843	0,00272752	0,02306324	-1,88468393
BHLHE40	1,18079422	9,12756592	3,96170198	0,00274213	0,02312205	-1,89017181
CYP1A1	2,38008738	9,72070529	3,96143169	0,00274332	0,02312205	-1,89061779
DGKG	1,08639367	8,32890485	3,95946997	0,00275198	0,02317835	-1,89385479
SLC2A1	1,37855292	14,6342480	3,94489978	0,00281718	0,02350799	-1,91790948
SDC4	1,32961640	12,5437538	3,93084940	0,00288160	0,02389244	-1,94112693
EPPK1	1,27841579	11,9041881	3,89892359	0,00303377	0,02463564	-1,99395794
B3GNT3	1,63386769	11,1827172	3,89559004	0,00305014	0,02471313	-1,99948027
MYH9	1,02106096	12,2980254	3,88884149	0,00308356	0,02491504	-2,01066329
ADAMTS14	1,51805279	7,40911969	3,86468458	0,00320637	0,02561136	-2,05073089
SLC39A10	1,17767438	9,39578444	3,86458671	0,00320688	0,02561136	-2,05089334
OAS1	1,49499397	8,98331098	3,83470995	0,00336591	0,0264668	-2,10052738
GRAP	1,25122409	8,78765371	3,80483205	0,00353322	0,02729304	-2,15024865
C19orf33	2,09517559	10,5295576	3,75336297	0,00384215	0,02879873	-2,23609429
OXTR	1,13178726	7,2535991	3,75302830	0,00384425	0,02879873	-2,23665326
FBLIM1	1,69192341	10,993704	3,72787396	0,00400546	0,02959047	-2,27869509
BDH1	1,06934358	9,07022519	3,71034036	0,00412200	0,03025897	-2,30803225
SOCS2	1,88321654	11,0597258	3,70758233	0,00414065	0,03025897	-2,31264934
FAM110C	1,56053795	9,45768367	3,69215274	0,00424662	0,03063841	-2,33849112
NDRG4	1,59207299	10,5751031	3,65877062	0,00448569	0,03177659	-2,39446692
MALT1	1,15281563	10,6370549	3,65649229	0,00450251	0,03184483	-2,39829053
ADAM19	2,38871077	10,6793609	3,64917985	0,00455694	0,03218407	-2,41056540
BAIAP2L2	1,04057872	11,0557982	3,64810168	0,00456502	0,03222174	-2,41237561
MEI1	1,08032730	8,04312182	3,62630323	0,00473168	0,03296152	-2,44899361
NEXN	1,28223473	8,37836550	3,59021222	0,00502167	0,03427430	-2,50969958
SPOCK2	1,00323071	14,9837047	3,57566893	0,00514370	0,03493903	-2,53418853
MLPH	1,24236550	6,58994739	3,57095594	0,00518390	0,03506988	-2,54212778

ELF4	1,03940890	11,6220665	3,56290529	0,00525333	0,03531543	-2,55569306
GLCCI1	2,06673985	10,2727515	3,55600799	0,00531358	0,03550064	-2,56731849
AGR2	1,06861086	7,87162042	3,55593889	0,00531419	0,03550064	-2,56743497
FSTL3	1,04671192	9,81127489	3,51095046	0,00572526	0,03736838	-2,64334115
LY96	1,47074009	7,35900277	3,51069883	0,00572765	0,03736838	-2,64376607
FXYD5	1,35648758	7,24823976	3,49996676	0,00583054	0,03787108	-2,66189296
PAX6	1,09060504	7,78786647	3,49637533	0,00586540	0,03801326	-2,66796061
TTC9	1,56222583	8,46624172	3,47746918	0,00605250	0,03890328	-2,69991505
WNT11	1,26306841	9,80979744	3,45946405	0,00623644	0,0398019	-2,73036612
LGALS3	1,36775040	11,2638202	3,44691145	0,0063681	0,04029120	-2,75160647
DEFB1	1,58723917	7,24769795	3,43655780	0,00647885	0,04073882	-2,76913249
BAZ1A	1,03876612	10,0995565	3,42926408	0,00655807	0,04109398	-2,78148228
DNAJB5	1,09621136	9,81255403	3,42889778	0,00656207	0,04109711	-2,78210257
CCNJL	1,02582244	7,26546413	3,42534458	0,00660105	0,04119354	-2,78811997
CDKN2B	1,2609676	7,30187208	3,39789462	0,00691037	0,04235085	-2,83462852
ARL4A	1,34732919	9,21419430	3,38034183	0,00711598	0,04294154	-2,86438750
PPP1R1C	1,00518623	7,97888544	3,36732026	0,00727258	0,04361320	-2,88647344
CDKN2A	1,33905092	12,1637746	3,35092910	0,00747479	0,04439436	-2,91428513
PMEPA1	1,58369072	8,68135386	3,33857312	0,00763105	0,04500323	-2,93525756
LRRN4	1,25885040	8,10788291	3,32666346	0,00778485	0,04556644	-2,95547822
TMSB10	1,38634092	13,4695241	3,31695943	0,00791253	0,04606083	-2,97195810
COL6A1	1,12641495	10,0257351	3,29648866	0,008189	0,04719013	-3,00673380
ISG20	1,02871782	11,5982017	3,29497558	0,00820982	0,04725184	-3,00930480
S100A13	1,13630304	13,4605362	3,28362257	0,00836783	0,04780922	-3,02859802
TPM2	1,01363714	9,66156815	3,26882019	0,00857857	0,04868112	-3,05375919

Table 9.1SB . Downregulated genes cd10 vs ctrl

	logFC	AveExpr	t	P.Value	adj.P.Val	B
ALDH8A1	-3,17885738	8,76352656	-17,379334	9,81E-09	1,91E-05	10,5642119
SULT2A1	-2,41661705	10,1506702	-16,356203	1,75E-08	2,28E-05	10,0529198
GJB1	-2,15355367	12,4977832	-15,864475	2,34E-08	2,75E-05	9,79213373
SERPINA6	-2,70556123	12,4190576	-15,092583	3,77E-08	3,7E-05	9,36139251
EPO	-2,34901311	9,02131987	-15,051994	3,87E-08	3,7E-05	9,33798464
ENPP2	-2,07171246	8,28598451	-14,962205	4,10E-08	3,7E-05	9,28592601
SLC13A3	-2,09537742	10,6022719	-14,573809	5,26E-08	4,40E-05	9,05624396
NR1H4	-3,07643152	9,85984144	-14,209798	6,69E-08	4,61E-05	8,83414069
APOA5	-2,44359791	9,63704706	-13,984254	7,78E-08	4,80E-05	8,69307639
F7	-2,00122478	8,97572929	-13,714756	9,35E-08	4,86E-05	8,52094700
IL22RA1	-1,72250540	9,78477559	-13,685046	9,54E-08	4,86E-05	8,50172773
MRAP	-1,87895783	7,16378364	-13,267862	1,27E-07	5,99E-05	8,22661439
HADH	-1,68192412	12,7899929	-13,198813	1,34E-07	6,05E-05	8,18011599
FGL1	-1,72296698	14,7918413	-12,724880	1,89E-07	7,64E-05	7,85328902
RGN	-1,83795631	12,2292503	-12,532465	2,18E-07	8,26E-05	7,71665924
PAH	-2,38070239	11,2614476	-12,257437	2,68E-07	8,98E-05	7,51726260

KNG1	-1,89778855	7,63898593	-11,851536	3,66E-07	0,00010745	7,21383069
IDH1	-1,75492214	14,3081583	-11,821010	3,75E-07	0,00010745	7,19055698
SAMD11	-1,97203211	8,31966651	-11,787467	3,85E-07	0,0001077	7,16490719
CASP1	-1,79531557	7,60363963	-11,612597	4,43E-07	0,00011091	7,02990969
FGA	-2,7454933	11,725599	-11,608420	4,44E-07	0,00011091	7,02665907
SLC13A5	-2,19951086	11,1655346	-11,422415	5,16E-07	0,00011768	6,88061084
PIP5K1B	-1,74873783	8,40152257	-11,409008	5,21E-07	0,00011768	6,86998639
LGALS2	-1,90138249	11,1943020	-11,266276	5,86E-07	0,00012275	6,75605982
ACSF2	-1,68637308	10,5989966	-11,195881	6,21E-07	0,00012572	6,69931272
ACSM2B	-2,20977414	8,69361098	-11,160705	6,39E-07	0,00012572	6,67081687
SPTLC3	-2,28559471	9,07112860	-11,130200	6,55E-07	0,00012605	6,64602887
DIO1	-2,36298307	8,63630129	-11,068482	6,90E-07	0,00013053	6,59566127
C2orf72	-1,94339875	10,4821436	-10,942409	7,67E-07	0,00013624	6,49186479
ACSM2A	-1,50816115	7,15426976	-10,882174	8,06E-07	0,00013965	6,44183691
SLC30A10	-2,66239201	9,20861255	-10,860333	8,21E-07	0,00013965	6,42362657
APOC3	-2,09415182	12,2914252	-10,624644	1,00E-06	0,00015519	6,22470493
FOXD2	-1,25651816	7,35257573	-10,623502	1,00E-06	0,00015519	6,22373087
SERPINF2	-2,54644786	10,0672150	-10,543544	1,07E-06	0,00015998	6,15522074
TCEA3	-1,6219239	12,9892920	-10,516361	1,10E-06	0,00016175	6,13180954
SLC37A4	-1,45448196	11,8906092	-10,275444	1,36E-06	0,00019261	5,92164129
KLB	-2,71636267	10,9384900	-10,060036	1,65E-06	0,00021778	5,72954657
ANG	-2,02564316	13,2457579	-10,009935	1,72E-06	0,00022286	5,68429006
GDPD5	-1,79898648	10,9138055	-9,9564705	1,81E-06	0,00022750	5,63575012
GLUD1	-1,71486189	14,2238766	-9,9243466	1,86E-06	0,00022835	5,60646341
HPN	-1,89339530	10,3749482	-9,8417903	2,01E-06	0,00024374	5,53077522
FZD4	-1,98199042	13,6331893	-9,8228728	2,05E-06	0,00024519	5,51334519
SLC47A1	-1,25392616	12,7542939	-9,7165434	2,26E-06	0,00025876	5,41477168
ITIH3	-1,28065471	12,0429915	-9,7055592	2,28E-06	0,00025876	5,40452979
GNMT	-2,29992494	8,12874469	-9,6895090	2,32E-06	0,00025876	5,38954442
SLC38A3	-1,69572093	8,4319012	-9,6823013	2,33E-06	0,00025876	5,38280714
METTL7A	-1,98856396	11,4176064	-9,6323532	2,44E-06	0,00026099	5,33598734
ACADSB	-1,47356368	10,1360433	-9,5219746	2,71E-06	0,00027693	5,23169827
ZCCHC2	-1,95362993	10,0542584	-9,5105505	2,74E-06	0,00027752	5,22083911
APOH	-1,15536613	16,6138360	-9,4368774	2,94E-06	0,00029506	5,15051316
IFIT1	-1,62312616	7,71255759	-9,3837295	3,09E-06	0,00030518	5,09945895
IL1RAP	-1,42730164	7,95937508	-9,3463766	3,21E-06	0,00031106	5,06341538
AIF1L	-1,68389539	12,5392650	-9,3239811	3,28E-06	0,00031384	5,04174034
FGB	-2,49273968	11,3895168	-9,3200154	3,29E-06	0,00031384	5,03789724
ASF1B	-1,30345410	11,1022642	-9,3006975	3,35E-06	0,00031715	5,01915443
NEK10	-1,27119378	7,68471753	-9,2698819	3,45E-06	0,00031899	4,98918109
GPX2	-1,24847908	13,0051796	-9,2368635	3,56E-06	0,00032659	4,95696250
CFB	-1,69267299	11,4778766	-9,2213990	3,62E-06	0,00032659	4,94183593
ANXA9	-1,28469739	10,5193376	-9,1959364	3,71E-06	0,00033045	4,91687860
KHK	-1,10210540	12,4722405	-9,1641205	3,82E-06	0,00033045	4,88560423
CDC42EP4	-1,94223042	11,3165949	-9,1519445	3,87E-06	0,00033045	4,87360897

SLC5A9	-2,25877543	9,00372196	-9,1479184	3,88E-06	0,00033045	4,86963940
IMPA2	-1,41977508	13,3940078	-9,1010240	4,07E-06	0,00033621	4,82328510
ALDH3A2	-1,76578386	10,6605331	-9,0617999	4,23E-06	0,00034217	4,78434428
CFI	-1,32245148	13,2032987	-9,0349017	4,34E-06	0,00034657	4,75755126
HPX	-1,86713	9,13044459	-8,9823021	4,57E-06	0,00035488	4,70494654
KLHDC2	-1,36840400	11,8947744	-8,9811131	4,58E-06	0,00035488	4,70375420
PRODH2	-1,92699744	9,20112591	-8,9514107	4,71E-06	0,00035491	4,67392154
TMEM86B	-1,89365915	10,0236037	-8,9364028	4,79E-06	0,00035491	4,65881374
TIGD3	-1,3779762	8,78773103	-8,9316132	4,81E-06	0,00035491	4,65398740
EPHX2	-2,01254629	10,6867020	-8,9119256	4,90E-06	0,00035744	4,63412420
SLC6A14	-1,80596410	8,31724770	-8,8968356	4,98E-06	0,00035938	4,61887274
HAAO	-1,22951178	9,04889075	-8,8823978	5,05E-06	0,00035938	4,60425867
GPAM	-1,14208259	12,5679377	-8,8814770	5,05E-06	0,00035938	4,60332590
SLC39A5	-1,56610752	10,6933646	-8,8758473	5,08E-06	0,00035938	4,59762113
GAMT	-1,22990360	13,6681909	-8,8521618	5,21E-06	0,00036362	4,57358400
C4BPA	-1,52755178	10,4665956	-8,8044433	5,46E-06	0,00037697	4,52498105
ITIH1	-2,32076162	8,40521181	-8,7728209	5,64E-06	0,00038465	4,49264238
PECR	-1,48655378	11,7552916	-8,7532780	5,75E-06	0,00039005	4,47260474
ACOT2	-1,08675087	14,1822077	-8,7181926	5,96E-06	0,00039286	4,43653079
CPN2	-1,44292148	9,28215266	-8,7150568	5,98E-06	0,00039286	4,43330033
PCYT2	-1,49231125	11,7823765	-8,7102428	6,011E-06	0,00039286	4,42833899
SERPINC1	-2,17948274	12,0119853	-8,7087447	6,02E-06	0,00039286	4,42679463
DDC	-2,30999909	13,3207231	-8,7041785	6,04E-06	0,00039286	4,42208567
LIME1	-2,02712532	9,90366766	-8,7015552	6,06E-06	0,00039286	4,41937944
SPC24	-1,11872836	10,7293937	-8,6656872	6,29E-06	0,00040095	4,38230426
FOXA1	-1,49752304	13,0658856	-8,6479663	6,40E-06	0,00040373	4,36393664
GRB7	-1,43686932	9,60354382	-8,5943591	6,76E-06	0,00042249	4,30817024
MMP11	-1,90181209	8,37111149	-8,5790810	6,87E-06	0,00042410	4,29222055
MMAB	-1,42579225	12,6040817	-8,5585149	7,01E-06	0,00042865	4,27071106
ANTXR1	-1,08423120	7,76530030	-8,5340651	7,19E-06	0,00043730	4,24508056
ALDH6A1	-1,91480338	10,0792627	-8,5073518	7,40E-06	0,00044721	4,21700375
TMPRSS6	-1,23749292	7,45567208	-8,4513257	7,84E-06	0,00047151	4,15786684
TMEM97	-1,17344902	12,4005257	-8,4303887	8,015E-06	0,00047797	4,13567976
CHST13	-1,37853840	12,6617487	-8,4284453	8,03E-06	0,00047797	4,13361796
ENPP3	-1,99760481	8,90266969	-8,3652227	8,57E-06	0,00049794	4,06631582
HP	-2,96397909	14,5565433	-8,3529192	8,69E-06	0,00050012	4,05316740
SFXN2	-1,39738676	10,0546917	-8,3451572	8,76E-06	0,00050109	4,04486372
SLC25A33	-1,29090341	13,8741276	-8,3264736	8,93E-06	0,00050510	4,02484903
ARSE	-1,06961799	9,74419289	-8,3166745	9,02E-06	0,00050642	4,01433629
MVK	-1,36400629	14,2803273	-8,2838651	9,34E-06	0,00051682	3,97906004
STAR	-1,70966487	10,0387550	-8,2776773	9,40E-06	0,00051776	3,97239356
CYP27A1	-1,48028979	10,9642309	-8,2709894	9,47E-06	0,00051899	3,96518358
SHPK	-1,11905904	11,6707592	-8,1817865	1,04E-05	0,00056004	3,86853734
IL11RA	-1,17964665	8,62942756	-8,1630907	1,06E-05	0,00056401	3,84816799
TCEA2	-1,25174305	8,98893459	-8,0889952	1,15E-05	0,00059625	3,76704971

SLCO4C1	-1,88700160	8,68693893	-8,0854258	1,15E-05	0,00059625	3,76312620
GRTP1	-1,15181092	9,11012197	-8,0731048	1,16E-05	0,00059973	3,74957178
VAV3	-2,26110906	11,9774035	-8,0718517	1,17E-05	0,00059973	3,74819220
ADH6	-1,80332159	8,89445635	-8,0459702	1,20E-05	0,00061211	3,71965923
CYP4F12	-1,19403616	8,99896539	-8,0448370	1,20E-05	0,00061211	3,71840821
KANK4	-2,63826305	10,4178948	-8,0205049	1,23E-05	0,00062507	3,69150997
LIPC	-1,48981358	9,82401653	-8,0174574	1,24E-05	0,00062507	3,68813630
SLC2A4RG	-1,10451480	15,6096575	-8,0093866	1,25E-05	0,00062519	3,67919644
TRIM50	-1,89263662	8,34784918	-7,9647198	1,31E-05	0,00063203	3,62958362
CYP4F8	-1,13870841	9,40852296	-7,9530260	1,33E-05	0,00063751	3,61655674
DHCR24	-1,21032166	12,9772425	-7,9120431	1,39E-05	0,00065331	3,57077604
VTN	-1,38169303	10,9103814	-7,8683199	1,46E-05	0,00068262	3,52171762
TNFRSF11A	-1,1320178	8,42529909	-7,8456799	1,49E-05	0,00069428	3,49622671
ABCC6	-1,1998048	13,6346845	-7,7842507	1,60E-05	0,00072855	3,42675693
CRYL1	-1,17746323	13,0463609	-7,7494933	1,66E-05	0,00075423	3,38725151
HAMP	-2,35256061	11,7339084	-7,7086145	1,74E-05	0,00078027	3,34060384
EHHADH	-1,10148133	7,56003669	-7,6899332	1,78E-05	0,00079303	3,31921935
RBP4	-1,40883278	15,7037877	-7,6872445	1,78E-05	0,00079303	3,31613815
FGG	-2,80602109	14,8033755	-7,6574124	1,84E-05	0,00081003	3,28189276
AFMID	-1,08516438	10,3235271	-7,6558382	1,84E-05	0,00081003	3,28008263
PPP1R3C	-1,73312734	9,75955494	-7,6529344	1,85E-05	0,00081003	3,27674301
A1CF	-1,66993823	10,8109417	-7,6425048	1,87E-05	0,00081224	3,26473940
SERPINA1	-1,60576578	7,52348894	-7,6134086	1,93E-05	0,00083303	3,23118248
MID1IP1	-1,44980934	10,0223903	-7,5947229	1,98E-05	0,00084423	3,20957794
GSTA2	-2,42399040	9,64390288	-7,5864532	1,99E-05	0,00084423	3,20000281
PCSK6	-1,42542168	9,40714269	-7,5822429	2,00E-05	0,00084423	3,19512473
ERBB3	-1,58457339	9,55620680	-7,5700710	2,03E-05	0,00084984	3,18101005
SLA2	-1,10486800	7,73485563	-7,5669022	2,04E-05	0,00084984	3,17733249
RAB26	-1,05944573	7,62296557	-7,5610481	2,05E-05	0,00084996	3,17053528
DMGDH	-1,02864378	6,90578135	-7,5291016	2,13E-05	0,00086888	3,13336814
SULT1C2	-1,13138165	7,44242714	-7,5287133	2,13E-05	0,00086888	3,13291563
TRIM74	-1,75339454	8,45020884	-7,4737659	2,27E-05	0,00091222	3,06869289
CEBPA	-1,89569125	14,5718797	-7,4301761	2,38E-05	0,00094583	3,01747939
RPS6KA3	-1,19762622	13,3557188	-7,4205601	2,41E-05	0,00095308	3,00614975
TMEM135	-1,46625271	10,7711808	-7,3753119	2,54E-05	0,00098499	2,95268359
FAM20C	-1,25556146	11,7221359	-7,3744638	2,54E-05	0,00098499	2,95167905
CHEK2	-1,05412079	10,3374600	-7,3686137	2,56E-05	0,00098838	2,94474716
GLUL	-1,20899342	10,9650592	-7,3541656	2,60E-05	0,00099841	2,92760895
CCDC34	-1,10658615	11,5303549	-7,3422053	2,64E-05	0,00100898	2,91340198
SECTM1	-1,21796057	7,76750471	-7,3251531	2,69E-05	0,00102572	2,89311547
GLUD2	-1,75411755	13,5332843	-7,3176970	2,71E-05	0,00102793	2,88423362
C8B	-1,49176307	6,96203594	-7,2572858	2,91E-05	0,00107825	2,81201202
TMCO6	-1,21187529	9,35228229	-7,2203843	3,04E-05	0,00111861	2,76766843
MPV17L	-1,44634889	8,36903728	-7,2116629	3,07E-05	0,00112654	2,75716290

HNMT	-1,33575809	11,6538158	-7,2050884	3,09E-05	0,00113171	2,74923698
HMGCR	-1,37044974	13,7387217	-7,1984838	3,12E-05	0,00113610	2,74126911
TMEM143	-1,04191816	10,8101370	-7,1850891	3,17E-05	0,00114076	2,72509267
ORM1	-1,06028690	15,5102513	-7,1263175	3,39E-05	0,00118955	2,65384363
IGSF1	-2,07552129	9,90439860	-7,1138827	3,44E-05	0,00120193	2,63871188
MAT1A	-1,53740950	13,5752815	-7,1074860	3,47E-05	0,00120193	2,63091996
DHFR	-1,15901216	12,9808521	-7,0902468	3,54E-05	0,00121593	2,60989447
UPB1	-1,26221040	7,70891817	-7,0800386	3,59E-05	0,00122713	2,59742612
CIDEB	-1,08987855	8,98359737	-7,0687426	3,63E-05	0,00123362	2,58361333
KLC4	-1,32971729	8,34831415	-7,0563232	3,69E-05	0,00124558	2,56840776
FAM151A	-1,42736578	7,10710571	-7,0552533	3,69E-05	0,00124558	2,56709694
GALM	-1,01702321	11,2516854	-7,0403376	3,76E-05	0,00125702	2,54880644
LDHD	-1,47632808	8,11711114	-6,9888247	4,00E-05	0,00132194	2,48541528
GSTA1	-1,80377893	8,07899360	-6,9826152	4,03E-05	0,00132399	2,47775042
F11	-1,25566469	10,3691727	-6,9567054	4,15E-05	0,00136191	2,44571379
HMGB2	-1,18127231	14,7526350	-6,8882660	4,51E-05	0,00145112	2,36066544
ASB9	-1,42146389	9,10920928	-6,8639748	4,65E-05	0,00147751	2,33033036
NDRG2	-1,58592412	12,4694424	-6,8510184	4,72E-05	0,00149279	2,31411826
EFNA1	-1,52433574	14,0224052	-6,8257605	4,87E-05	0,00152283	2,28244923
CDC25C	-1,12790089	10,0727399	-6,8173807	4,92E-05	0,00153434	2,27192364
TMEM121	-1,11027489	11,6793873	-6,7688875	5,22E-05	0,00160521	2,2108285
APOA4	-1,27665148	8,48903314	-6,7182525	5,55E-05	0,00170031	2,14669841
PCOLCE	-1,33800791	9,96221629	-6,7071648	5,63E-05	0,00171457	2,13260955
AMDHD1	-1,27161439	8,98714826	-6,6911126	5,74E-05	0,00173537	2,11218296
SLC35D1	-1,00286958	9,35445186	-6,6887209	5,76E-05	0,00173601	2,10913653
ACAD11	-1,19656656	7,96739237	-6,6822547	5,80E-05	0,00174541	2,10089632
SHMT1	-1,14641233	10,3042211	-6,6604146	5,96E-05	0,00177941	2,07302244
FDFT1	-1,07042757	13,9164163	-6,6506144	6,03E-05	0,00178745	2,06049378
ATP6V0E2	-1,42568275	10,8481188	-6,6397699	6,11E-05	0,00179725	2,04661473
MAP2K6	-1,73715836	9,60580234	-6,6381141	6,13E-05	0,00179725	2,04449423
ACSS1	-1,59305928	11,4921469	-6,6380768	6,13E-05	0,00179725	2,04444644
CYP19A1	-1,11177476	6,93093405	-6,6179928	6,28E-05	0,00183338	2,01869576
SLC25A1	-1,01676053	12,6044222	-6,5825976	6,56E-05	0,00189559	1,97318002
ACAT2	-1,17122420	15,3209551	-6,5730171	6,64E-05	0,00190567	1,96083069
LEAP2	-2,83220551	10,6546416	-6,5679544	6,69E-05	0,00191305	1,95429982
CCDC69	-1,56161937	7,35117107	-6,5558687	6,79E-05	0,00193269	1,93869503
PRPSAP1	-1,06630836	13,2595789	-6,5142076	7,15E-05	0,00199150	1,88474953
PNPLA3	-1,70015366	10,7322259	-6,5135430	7,16E-05	0,00199150	1,88388706
SERPINA4	-1,62278838	8,40170305	-6,4959914	7,32E-05	0,00201831	1,86108705
MLXIPL	-1,95237798	12,1012226	-6,4945811	7,33E-05	0,00201831	1,85925311
CLGN	-1,08157000	9,30164362	-6,4647253	7,61E-05	0,00207607	1,82036634
ACSM5	-1,02791981	7,02984256	-6,4519976	7,73E-05	0,00209207	1,80375114
CAT	-1,09778288	11,9427304	-6,4299920	7,95E-05	0,00212729	1,77497139
ACSL4	-1,20123825	11,5207267	-6,4291469	7,96E-05	0,00212729	1,77386478
ERP27	-1,70910541	9,17449310	-6,4290117	7,96E-05	0,00212729	1,77368783

EPN3	-1,69473769	9,36077236	-6,4223875	8,03E-05	0,00213446	1,76501043
TMEM37	-1,42519288	11,1143591	-6,4223852	8,03E-05	0,00213446	1,76500731
PGM1	-1,25070251	12,2712263	-6,4112613	8,14E-05	0,00213893	1,75042183
GSTM4	-1,03027829	8,40149421	-6,4110644	8,14E-05	0,00213893	1,75016353
PKLR	-1,29659430	7,78642947	-6,4095265	8,16E-05	0,00213893	1,74814568
CDCA3	-1,04027803	11,4998849	-6,4086721	8,17E-05	0,00213893	1,74702449
KCNK7	-1,24611850	12,1317612	-6,4053404	8,20E-05	0,00214319	1,74265135
TM7SF2	-1,13472194	14,2829436	-6,4001262	8,26E-05	0,00214863	1,73580435
SERPIND1	-1,70718575	12,315812	-6,3998381	8,26E-05	0,00214863	1,73542599
MCM2	-1,25135934	13,2670654	-6,3902421	8,36E-05	0,00216058	1,7228148
SLC22A7	-1,49882673	8,44272355	-6,3677532	8,60E-05	0,00220382	1,69320927
PHGDH	-1,51859073	12,1198326	-6,3592413	8,70E-05	0,00221333	1,68198541
PCSK9	-2,20657794	12,5165885	-6,3489743	8,81E-05	0,00222319	1,66843381
ECH1	-1,17329684	11,9062365	-6,3453862	8,85E-05	0,00222604	1,66369437
RARRES2	-1,08615495	12,6407205	-6,3446034	8,86E-05	0,00222604	1,66266010
HPR	-2,98124088	10,6451656	-6,3384481	8,93E-05	0,00223403	1,65452478
ST6GAL1	-1,20371603	11,9724420	-6,3330349	8,99E-05	0,00223522	1,64736592
HNF4A	-1,05994621	7,52632829	-6,3293099	9,04E-05	0,00223641	1,64243723
FNTB	-1,06506334	10,0312551	-6,3000613	9,38E-05	0,00229266	1,60367030
KIF22	-1,18802937	12,6634725	-6,2489657	0,00010023	0,00237979	1,53565851
SKP2	-1,15268402	10,2835080	-6,2326633	0,00010236	0,00239434	1,51388158
LRP11	-1,43311411	8,80363629	-6,2322050	0,00010242	0,00239434	1,51326887
GSTA3	-1,82259210	8,05274811	-6,2304831	0,00010265	0,00239434	1,51096648
GSTA5	-1,96252516	8,56433142	-6,2101889	0,00010537	0,00243533	1,48379863
SLC22A3	-1,28956454	10,0447495	-6,2059269	0,00010596	0,00244061	1,47808567
GLTPD2	-1,07447518	10,3367924	-6,1964091	0,00010727	0,00246602	1,46531848
SLC23A1	-1,32547012	6,98352173	-6,1865407	0,00010865	0,00249286	1,45206747
C8A	-2,23732760	8,77189417	-6,1771524	0,00010998	0,00250380	1,43944829
SCRN2	-1,21601984	10,1834888	-6,1720075	0,00011072	0,00251569	1,43252759
AMT	-1,22555952	12,2118530	-6,1544077	0,00011328	0,00255408	1,40882453
C1orf115	-1,77417441	10,6516891	-6,1417086	0,00011517	0,00258174	1,39169441
SLCO2B1	-1,06405673	9,84095779	-6,1140609	0,00011939	0,00264117	1,35432049
ACAA1	-1,02817848	13,6382488	-6,0743015	0,00012577	0,00275621	1,30038339
PGLYRP2	-1,57423708	6,77078045	-6,0651882	0,00012728	0,00278415	1,28798868
SELENBP1	-1,21161564	12,6043733	-6,0426629	0,00013111	0,00284653	1,25730195
DUSP9	-1,91224373	13,8040972	-5,9868850	0,00014112	0,00298644	1,18100182
HLF	-1,11977084	12,8360793	-5,9479704	0,00014859	0,00309426	1,12750520
FADS1	-1,02660930	13,5255585	-5,9347035	0,00015123	0,00313261	1,10921728
KIF20B	-1,144404	8,30484836	-5,9303303	0,00015211	0,00314532	1,10318336
SERPINF1	-1,2113652	14,7289938	-5,9087908	0,00015654	0,00319722	1,07342448
IDI1	-1,27966168	13,3482696	-5,8738434	0,00016402	0,00328572	1,02499892
ANGPTL1	-1,10300158	7,18376522	-5,8729031	0,00016423	0,00328572	1,02369355
SGK3	-1,10262445	10,1264134	-5,8708278	0,00016468	0,00328925	1,02081206
GALK1	-1,20479808	10,8508990	-5,8574293	0,00016767	0,00333179	1,00219353
ASS1	-1,77841819	10,5027084	-5,8558792	0,00016801	0,00333307	1,00003790

ESPN	-1,23833428	8,54805310	-5,8465026	0,00017014	0,00336955	0,98699076
AUH	-1,08241354	10,9049079	-5,8388049	0,00017191	0,00339739	0,97627012
EPHA1	-1,43875915	8,30786961	-5,8378621	0,00017213	0,00339739	0,97495658
KAZALD1	-1,17310588	10,2685243	-5,8236475	0,00017545	0,00345130	0,95513542
C5	-1,72347917	10,0951013	-5,8132407	0,00017792	0,00348827	0,94060555
TJP3	-1,09375213	7,05727229	-5,7829786	0,00018533	0,00359153	0,89826454
PAQR8	-1,38619684	11,2815417	-5,7721636	0,00018806	0,00362047	0,88310064
WFIKKN1	-1,18501224	8,57756852	-5,6951129	0,0002088	0,00390661	0,77457515
HSDL2	-1,05416157	10,5772361	-5,6900948	0,00021023	0,00390661	0,76747725
FAM3B	-1,80916209	11,8590188	-5,6696526	0,00021618	0,00399764	0,73852472
HIST1H2BD	-1,28820206	10,8790292	-5,6594817	0,00021920	0,00404087	0,72409691
HHEX	-1,57700223	10,9264934	-5,6191972	0,00023165	0,00420569	0,66680384
C1S	-1,31879764	10,4819973	-5,6175054	0,00023219	0,00420569	0,66439256
USP18	-1,09261547	11,8495505	-5,6172607	0,00023226	0,00420569	0,66404375
FETUB	-1,05793392	7,53928307	-5,5904528	0,00024099	0,00432016	0,62577857
SMAD9	-1,23202642	8,52139768	-5,5858091	0,00024253	0,00434125	0,61913958
NFE2	-1,25952291	9,71953124	-5,5542483	0,00025333	0,00450701	0,57393452
PIPOX	-1,54679527	11,3904808	-5,5450306	0,00025658	0,00453288	0,56070439
NUDT7	-1,04221780	9,08744912	-5,5446450	0,00025672	0,00453288	0,56015071
CABLES2	-1,23720753	9,27983683	-5,5124350	0,00026844	0,00466259	0,51382069
IFIH1	-1,19359314	8,10035212	-5,5103367	0,00026922	0,00466928	0,51079743
KIF15	-1,22530643	10,6014997	-5,4890486	0,00027731	0,00476720	0,48008752
SORBS2	-1,04134864	10,3078613	-5,4687844	0,00028525	0,00484710	0,45079315
CENPM	-1,02146611	10,0977838	-5,4592045	0,00028909	0,00489078	0,43692335
RHBG	-1,16348701	12,5225043	-5,4558893	0,00029043	0,00490568	0,43212044
DAO	-1,11923026	8,50865090	-5,4402194	0,00029686	0,00499342	0,40939720
FAM117A	-1,30378939	10,9832881	-5,3975926	0,00031513	0,00520376	0,34740133
FRAT2	-1,17737121	11,4351164	-5,3916660	0,00031777	0,0052252	0,33876074
RAB11FIP4	-1,26097568	13,6361768	-5,3523143	0,00033587	0,0054921	0,28125843
ONECUT1	-1,61658441	8,27004697	-5,3352806	0,00034405	0,00561249	0,25629799
SEMA6B	-1,09165865	10,6468388	-5,3344934	0,00034443	0,00561249	0,25514348
CDKN2C	-1,57457914	11,9505845	-5,3340031	0,00034467	0,00561249	0,25442428
HOXD1	-1,61833686	8,89772192	-5,3317348	0,00034578	0,00561492	0,2510968
SQLE	-1,09735833	14,1442559	-5,3272510	0,00034798	0,00563502	0,24451707
AGT	-1,18411719	15,2275381	-5,3239270	0,00034962	0,00564300	0,23963736
NRTN	-1,26289282	8,34167943	-5,3176507	0,00035274	0,00568072	0,23041934
KRTAP4-7	-1,00520879	7,68349304	-5,3115307	0,00035581	0,00571259	0,22142529
H1FX	-1,02280094	10,3398339	-5,3104380	0,00035636	0,00571259	0,21981879
MIXL1	-2,03511864	8,80627018	-5,3098318	0,00035667	0,00571259	0,21892747
ITIH2	-1,23504249	13,9851867	-5,3069970	0,00035810	0,00572776	0,21475894
CA5A	-1,35702553	9,70515499	-5,3024159	0,00036044	0,00574962	0,20801981
A1BG	-1,4777146	10,9968135	-5,2639138	0,00038070	0,00599115	0,15125982
SLC29A4	-1,08367011	7,87555911	-5,2489426	0,00038891	0,00607950	0,12913087

TMEM141	-1,12637953	13,5353446	-5,2276234	0,00040092	0,00616054	0,09756251
PANK1	-1,03231997	8,41098739	-5,2045028	0,00041441	0,00631799	0,06325199
DLK1	-1,18850626	14,5390109	-5,1712844	0,00043463	0,00655809	0,01382038
EPHX1	-1,00317719	9,86169891	-5,1672464	0,00043716	0,00657932	0,00780060
HMGCS1	-1,06215277	13,1607547	-5,1395522	0,00045494	0,00674701	-0,03354948
SERPINA7	-1,12945981	11,8105556	-5,1382638	0,00045578	0,00674701	-0,03547581
HSD17B4	-1,12808475	12,4408038	-5,0967780	0,00048393	0,00699586	-0,09763376
ALDH7A1	-1,04288820	13,3341669	-5,0807572	0,00049529	0,00710753	-0,12170439
MOGAT2	-1,04585172	9,91930815	-5,0755516	0,00049904	0,00715263	-0,12953359
ADH4	-1,55243101	10,1143217	-5,0746654	0,00049969	0,00715309	-0,13086682
CEBPE	-1,19328465	9,63959617	-5,0706850	0,00050258	0,00718574	-0,13685646
SLC25A42	-1,06761857	8,74249042	-5,0698013	0,00050323	0,00718620	-0,13818650
CYP2B6	-1,01455063	8,96985411	-5,0401123	0,00052542	0,00732371	-0,18293796
GYG2	-1,29571539	10,2458814	-5,0398345	0,00052563	0,00732371	-0,18335742
SEMA4G	-1,20820618	10,8608289	-5,0396451	0,00052577	0,00732371	-0,1836432
RNASE4	-1,80958087	11,6228145	-5,0312107	0,00053227	0,00738730	-0,19638051
IGFALS	-1,39754820	8,70657446	-5,0310056	0,00053243	0,00738730	-0,19669038
DAPK1	-1,11732180	8,53968946	-5,0124335	0,00054705	0,00756325	-0,22477390
TNFAIP8L1	-1,19981573	9,89247145	-5,0091686	0,00054966	0,00758150	-0,22971601
CDO1	-1,66149129	7,65451465	-4,9712089	0,00058105	0,00789365	-0,28728846
PZP	-1,46587274	7,93268742	-4,9018953	0,00064339	0,00850414	-0,39294676
FBXW2	-1,17039463	10,1620556	-4,8870375	0,00065766	0,00863445	-0,41568466
GLYCTK	-1,28766228	10,7829923	-4,8777698	0,00066673	0,00869868	-0,42988346
MASP2	-1,18720923	9,83582481	-4,8760668	0,00066842	0,00869908	-0,43249388
HIST3H2BB	-1,21061578	10,7857201	-4,8533651	0,00069127	0,00888076	-0,46733156
USP41	-1,05801395	9,32637404	-4,8343983	0,00071100	0,00902144	-0,49649371
OBSL1	-1,09539978	11,8571937	-4,7962656	0,00075251	0,00938592	-0,55527801
NEDD4L	-1,09947132	13,0360433	-4,7954974	0,00075337	0,00938635	-0,55646429
CCDC142	-1,11277449	9,56172623	-4,7853458	0,00076486	0,00946918	-0,57214926
SERPINA1	-1,07147029	15,4389563	-4,7725989	0,00077956	0,00962065	-0,59186471
SHROOM1	-1,26983125	10,6404786	-4,7326648	0,00082758	0,01004665	-0,65377737
CGREF1	-1,03401374	11,7056428	-4,6950422	0,00087571	0,01048712	-0,71230952
NUPR1	-1,30086280	13,7297211	-4,6660770	0,00091479	0,01083339	-0,75750637
SCARA3	-1,44469935	9,35107867	-4,6633029	0,00091863	0,01085191	-0,76184117
TET1	-1,32308211	8,63266307	-4,6458738	0,00094314	0,01105746	-0,78909967
TNFAIP8L3	-1,00470123	7,21558663	-4,6330904	0,00096156	0,01118395	-0,8091189
PPP1R1A	-2,43848600	8,74294348	-4,6275470	0,00096967	0,01126356	-0,81780710
LSS	-1,01237641	13,3849298	-4,5891576	0,00102784	0,01174507	-0,87808962
KIRREL2	-1,31164816	7,56166257	-4,5839918	0,00103595	0,01180318	-0,88621671
PBK	-1,03079329	12,6026101	-4,5797713	0,00104262	0,01185617	-0,89285922
FGFR2	-1,37779994	7,66994528	-4,5432455	0,00110231	0,01237623	-0,95044719
SOAT2	-1,12985701	9,63496666	-4,5010605	0,0011758	0,01292547	-1,01718058
SERPINA3	-1,27518997	14,0199481	-4,4847417	0,00120560	0,0131516	-1,04305934
C3	-1,03072097	14,8265054	-4,4762518	0,00122142	0,01325925	-1,05653668

A2M	-1,23352283	14,4040118	-4,4135037	0,00134540	0,01415917	-1,15644090
SOBP	-1,22283662	9,50188497	-4,4123676	0,00134776	0,01415917	-1,15825442
PEG10	-1,66950414	12,7082859	-4,3982850	0,00137743	0,01435636	-1,18074865
CYP8B1	-1,01139677	6,61946552	-4,3734417	0,00143147	0,01472162	-1,22049332
FMO5	-1,03938393	9,00161296	-4,3448125	0,00149654	0,01520408	-1,26639285
TMEM170B	-1,10041094	8,36280290	-4,2413154	0,00175910	0,01715785	-1,43318455
CYP2W1	-1,32191167	10,8118897	-4,2244631	0,00180627	0,01754492	-1,46046849
MTTP	-2,39367132	9,39398738	-4,1875489	0,00191431	0,01813431	-1,5203527
PPARGC1A	-1,18102395	7,84969806	-4,1703972	0,00196681	0,01841764	-1,54823277
POLR2J2	-1,00929687	11,1007804	-4,1644492	0,00198536	0,01853221	-1,55790927
HS3ST3B1	-1,06403768	9,78155006	-4,0861551	0,00224761	0,02033258	-1,68566878
SORBS3	-1,08520733	9,79327537	-4,0443868	0,00240220	0,02131980	-1,75411275
MYL5	-1,23432751	9,92174423	-4,0247084	0,00247887	0,02175325	-1,78642633
TNNI2	-1,61171002	14,7823838	-3,9755918	0,00268167	0,02279913	-1,86726442
AATK	-1,03083135	10,8209103	-3,9295684	0,00288755	0,02390795	-1,94324474
PLA2G12B	-1,23776605	10,6502750	-3,9177345	0,00294312	0,02423116	-1,96281684
E2F8	-1,30848975	9,27360208	-3,9093813	0,00298302	0,02445662	-1,97664093
STOX1	-1,03505098	7,97889583	-3,8519267	0,00327328	0,02598241	-2,07191473
LDLRAD1	-1,32129035	8,72528819	-3,8185753	0,00345521	0,02702395	-2,12736729
BHMT	-1,85777234	8,40730971	-3,8043191	0,00353617	0,02729304	-2,15110295
TLN2	-1,03596630	8,78908803	-3,8011978	0,00355416	0,02737781	-2,15630215
PFKL	-1,02572277	10,9307745	-3,7992353	0,00356552	0,02741129	-2,15957166
AVPI1	-1,26709341	11,9590119	-3,7968055	0,00357964	0,02746579	-2,16362017
IGDCC3	-1,13441508	12,5026690	-3,7897655	0,00362087	0,02763747	-2,17535320
FNDC5	-1,38312899	8,10396394	-3,7638075	0,00377725	0,02849713	-2,21865427
INHBE	-1,53365467	9,06480468	-3,7449046	0,00389556	0,02906118	-2,25022468
ALDH1A1	-1,01174657	14,5737805	-3,7374364	0,00394336	0,02922376	-2,26270624
SERPINA5	-1,44829043	14,5028498	-3,7022550	0,00417692	0,03035974	-2,32156941
MVD	-1,15754881	11,6177804	-3,6212295	0,00477137	0,03315921	-2,45752178
TCP10L	-1,01248527	9,13743995	-3,6189703	0,00478915	0,03324339	-2,46131982
APOA1	-1,20868429	16,3432853	-3,5521272	0,00534780	0,03568376	-2,57386085
MCEE	-1,13975278	10,7430515	-3,4975727	0,00585375	0,03795876	-2,66593757
CREB3L3	-1,28653629	9,31908441	-3,4211730	0,00664712	0,04140454	-2,79518528
GM2A	-1,00785548	8,56439491	-3,4197880	0,00666249	0,04143823	-2,79753135
GAL3ST1	-1,05153457	10,6196806	-3,3524465	0,00745583	0,04434915	-2,91170992
APOM	-1,21634639	12,0307138	-3,3450992	0,00754810	0,04469119	-2,92417972
TSPAN7	-1,03481515	7,57480528	-3,3433721	0,00756996	0,04477813	-2,92711122

Table 9.2SA . Upregulated genes cd10 vs cd2

	logFC	AveExpr	t	P.Value	adj.P.Val	B
HTRA3	3,15902882	8,02348833	15,2328779	3,45E-08	0,00021434	9,08871159
GADD45B	2,91104712	11,5635485	15,1445880	3,65E-08	0,00021434	9,04411244
RRAD	3,40548210	10,4841599	13,6422801	9,83E-08	0,00024276	8,22495205
ARC	2,74206644	7,29933612	13,3424143	1,21E-07	0,00024276	8,04673553
HSPA6	3,60204870	8,64410017	13,1162765	1,42E-07	0,00024276	7,90882390
PLCH2	1,68335369	9,77222311	13,0970480	1,44E-07	0,00024276	7,89695471
MLC1	2,69671599	7,33706205	13,0907456	1,44E-07	0,00024276	7,89305955
NPPC	2,52840822	7,01127615	11,6693945	4,23E-07	0,00041384	6,94869894
AGPAT4	1,55581822	6,91698576	11,2169682	6,10E-07	0,00047719	6,61825515
CSGALNACT2	1,36482127	9,12409786	10,8400050	8,36E-07	0,00057667	6,33080172
SNAI1	2,99303824	9,32294120	10,6291204	1,00E-06	0,00061546	6,16495747
SPOCD1	1,96007981	8,37853143	10,5123093	1,10E-06	0,00061546	6,07149081
IL11	2,39174186	10,3543552	10,4643246	1,15E-06	0,00061546	6,03275881
GADD45G	4,15688318	8,26588458	9,98508368	1,76E-06	0,00081294	5,63484484
GPRC5A	1,44291646	7,46223817	9,96439130	1,80E-06	0,00081294	5,61719883
AXL	1,76570890	9,5592392	9,90448501	1,90E-06	0,00082382	5,56588942
S1PR4	1,27660697	8,39314716	9,75806422	2,17E-06	0,00084406	5,43907345
MMP3	1,97737296	8,14242453	9,52808174	2,70E-06	0,00088317	5,23577068
HSPA1A	2,40825802	14,8732783	9,52374642	2,71E-06	0,00088317	5,23188918
STX1A	1,22966796	9,74432924	9,33812377	3,23E-06	0,00098839	5,06395991
TMEM217	1,17475225	7,18945093	9,01501797	4,43E-06	0,00126720	4,76336086
METRNL	1,74928718	11,1812189	8,74544912	5,80E-06	0,00154579	4,50422041
KRT15	1,30217081	10,0737033	8,66916404	6,26E-06	0,00163309	4,42946542
PLEKHO1	1,05562241	11,6999649	8,57448452	6,90E-06	0,00176003	4,33579564
SVIL	1,3152914	9,54729707	8,54619243	7,10E-06	0,00177345	4,30761242
MYLIP	2,51078971	7,80580891	8,50696317	7,40E-06	0,00179657	4,26838621
TUBB2B	1,80567268	11,1670360	8,49328139	7,5087E-06	0,00179657	4,25466493
ROBO4	1,33208374	6,95497497	8,40712665	8,21E-06	0,00188775	4,16777637
ATP8A2	1,14913517	6,74198650	8,25011009	9,68E-06	0,00198138	4,00724440
RGS2	2,33077382	8,63588675	8,24899970	9,69E-06	0,00198138	4,00609903
DOK7	1,85740356	7,77850221	8,24604731	9,72E-06	0,00198138	4,00305292
MLLT11	1,78155204	9,35150723	8,19568597	1,02E-05	0,00198138	3,95093664
ATF3	1,30145923	9,82212624	8,10682124	1,12E-05	0,00206931	3,85825041
GLIPR1	1,71074785	9,43448731	8,10569048	1,12E-05	0,00206931	3,85706502
TAGLN3	1,11216643	6,61244628	8,09026907	1,14E-05	0,00207149	3,84088350
ADAMTS4	1,61711322	9,57961510	7,987911	1,28E-05	0,00224334	3,73276264
BIRC3	1,24754592	8,56992446	7,94890243	1,33E-05	0,00227380	3,69122735
ARHGAP23	1,60478966	8,05682532	7,87894789	1,44E-05	0,00232439	3,61628050
TFPI2	1,91365711	7,93031156	7,86882164	1,46E-05	0,00232439	3,60538228
OTUB2	1,30806432	8,03894345	7,82392068	1,53E-05	0,00232439	3,55690728
NR4A1	1,56334656	10,1331086	7,79502760	1,58E-05	0,00232439	3,52558355
DUSP4	1,27463916	8,55472504	7,78036031	1,61E-05	0,00232439	3,50964301

ZBTB20	1,31233825	7,41171177	7,75423204	1,65E-05	0,00234122	3,48118075
CCL26	1,94151688	7,87522468	7,71520774	1,73E-05	0,00241589	3,43851289
PLK2	1,30735516	11,6131451	7,59528073	1,97E-05	0,00260793	3,30619792
GALNT10	1,95547011	8,99678524	7,56682961	2,04E-05	0,00266306	3,27454211
PLAUR	1,51618727	8,35924416	7,53368729	2,12E-05	0,00270640	3,23753719
BATF	2,10007131	10,2290690	7,52691607	2,13E-05	0,00270640	3,22995963
QSOX1	1,49779448	11,9876757	7,52359741	2,14E-05	0,00270640	3,22624363
FOSB	1,21776242	7,13697768	7,49731733	2,21E-05	0,00271374	3,19676742
EGR4	1,77313017	8,03595741	7,46436812	2,29E-05	0,00271374	3,15968611
CLCF1	1,08697202	7,95644459	7,46003152	2,30E-05	0,00271374	3,15479529
SERTAD1	1,17782471	12,6790879	7,45031805	2,33E-05	0,00271374	3,14383165
JUNB	1,41938682	11,9568435	7,43782163	2,36E-05	0,00271374	3,12970904
LARP6	1,66785138	8,77535273	7,39466031	2,48E-05	0,0028025	3,08077597
CREB5	1,16397289	7,37623144	7,38675787	2,50E-05	0,0028025	3,07179066
EMP1	1,21557626	7,01323632	7,34606451	2,63E-05	0,00285539	3,02539271
AQP3	1,72742646	10,8680073	7,24180902	2,96E-05	0,00305835	2,90553478
AKAP12	1,67111412	11,5677562	7,24026811	2,97E-05	0,00305835	2,90375256
CCR7	1,91405633	7,26810769	7,18778660	3,16E-05	0,0031203	2,84286443
MYOF	2,24014763	9,63302392	7,18006104	3,19E-05	0,0031203	2,83387054
RAB7B	1,37517632	7,65207345	7,16039147	3,26E-05	0,00312697	2,81093591
PPP1R15A	2,20149252	9,55746438	7,15642782	3,28E-05	0,00312697	2,80630807
CXCR4	2,25827634	7,94966436	7,06344641	3,66E-05	0,00327685	2,69714288
CPEB4	1,03924811	10,0814408	7,03957866	3,76E-05	0,00329977	2,66893343
SH2D5	1,32587974	12,8805187	7,03852506	3,77E-05	0,00329977	2,66768641
RASD1	1,53872418	13,3734500	7,02473529	3,83E-05	0,00332954	2,65135116
USP35	1,17019191	11,5318334	7,01269963	3,88E-05	0,00333937	2,63707278
KRTAP3-1	1,73121269	12,0040717	7,00925730	3,90E-05	0,00333937	2,63298540
ARHGEF4	1,23979836	7,26017457	6,95916085	4,14E-05	0,00339952	2,57331935
FHL2	1,66215437	14,1169281	6,84718752	4,74E-05	0,00373425	2,43871649
RAB3B	2,37951112	10,0002213	6,79469966	5,05E-05	0,00392758	2,37502653
IL23A	1,29514445	8,36539478	6,78568756	5,11E-05	0,00394486	2,36405263
LIF	1,43675073	9,45292714	6,75917036	5,28E-05	0,00399588	2,33169757
TNFRSF25	1,54121017	9,2111074	6,74103960	5,40E-05	0,00404548	2,30951889
RGS20	1,48931012	8,50101294	6,72965035	5,47E-05	0,00404548	2,29556338
DUSP1	1,15967393	9,88973018	6,71118225	5,60E-05	0,00408012	2,27289547
PLEKHG5	1,30917285	9,53867461	6,63581104	6,14E-05	0,00432263	2,17988809
HIST2H2AA4	1,50458171	12,4098360	6,61615148	6,30E-05	0,00433026	2,15549683
ITPRIP	1,04302365	9,78917289	6,58174617	6,57E-05	0,00443935	2,11267927
CAPN2	1,57182300	13,3730929	6,57138216	6,66E-05	0,00446290	2,09974833
PLAU	2,30082154	9,33797366	6,56239822	6,73E-05	0,00447378	2,08852694
KLF5	1,03119936	7,80133129	6,55347393	6,81E-05	0,00448683	2,07736870
FJX1	1,36117237	8,40113563	6,51733167	7,12E-05	0,00464852	2,03206330
MYEOV	1,66431467	8,81110071	6,51303353	7,16E-05	0,00464852	2,02666307
GPSM1	1,60606900	11,5519952	6,51183070	7,17E-05	0,00464852	2,02515135
TEP1	1,36999482	11,0576083	6,50214845	7,26E-05	0,00465392	2,01297511

TRPV2	1,25472441	12,7536955	6,48709812	7,40E-05	0,00469148	1,99402148
DEFB103A	1,36504943	6,38556436	6,38801467	8,39E-05	0,00509681	1,86842951
MPP3	1,65623819	10,4470973	6,35639241	8,73E-05	0,00516959	1,82804930
C16orf45	1,42076396	7,94292072	6,35390494	8,76E-05	0,00516959	1,82486677
FOS	2,01833213	7,47033941	6,34864544	8,82E-05	0,00516959	1,81813470
LHX6	1,07437019	8,38173101	6,34320814	8,88E-05	0,00516959	1,81117084
NPPB	2,30061470	9,70139433	6,33720392	8,95E-05	0,00516959	1,80347590
OSCAR	1,08765832	8,68910803	6,33110591	9,02E-05	0,00517234	1,79565542
NDRG1	1,54337788	11,7342359	6,29060656	9,50E-05	0,00540728	1,74357937
CNN1	1,10159676	9,71600616	6,18642005	0,00010867	0,00582330	1,60851203
KLF6	1,28370770	12,7073109	6,18566354	0,00010877	0,00582330	1,60752548
NAV3	1,19357510	6,37978477	6,17374856	0,00011047	0,00586158	1,59197627
PMAIP1	1,45502217	7,89564381	6,17360474	0,00011049	0,00586158	1,59178846
PROCR	1,56299919	10,9646792	6,15939967	0,00011255	0,00593787	1,57322311
PHLDA2	1,38346783	12,1300734	6,05082840	0,00012971	0,00664068	1,43034301
FRG2	1,25700533	6,55466703	6,03232308	0,00013290	0,00674541	1,40581603
ZNF280A	1,40729337	9,19525853	6,00755974	0,00013731	0,0068631	1,37291515
HK1	1,11017908	6,96720550	5,96244900	0,00014576	0,00709093	1,31274610
DAND5	1,01011220	6,59364251	5,91859360	0,00015451	0,00739382	1,25396068
CHI3L2	1,08503823	6,73823674	5,84934301	0,00016949	0,00788567	1,1605491
C3orf52	1,17889258	8,05093973	5,83949993	0,00017175	0,00793947	1,14721352
IGFBP1	1,51514415	11,9170603	5,82792575	0,00017444	0,00793947	1,13151402
GRB10	1,59436148	11,1488034	5,82155243	0,00017594	0,00793947	1,12286052
WDR66	1,27262550	8,41384091	5,82101939	0,00017607	0,00793947	1,12213649
ADAP2	1,44983508	9,92225074	5,74948915	0,00019392	0,00848965	1,02459019
AHNAK2	1,01950538	6,51846896	5,74841140	0,00019421	0,00848965	1,02311456
SPANXA1	1,27097008	6,36908129	5,73991287	0,00019646	0,00849034	1,01147249
KRTAP1-5	1,04533100	6,45135325	5,73517208	0,00019772	0,00849034	1,00497337
KRT37	2,36350331	9,08649256	5,72673768	0,00020000	0,00849591	0,99340237
RELT	1,10920493	10,9618551	5,71601654	0,00020294	0,00856913	0,97867872
CD109	1,78425923	9,82840530	5,69868649	0,00020778	0,00870028	0,95484222
CSAG1	1,79842986	7,20592819	5,68000239	0,00021314	0,00886148	0,92909249
SPSB1	1,41899927	11,1439169	5,67666619	0,00021412	0,00887048	0,92448913
NRG1	1,81951148	7,13060758	5,66250269	0,00021830	0,00896026	0,90492725
INHBB	1,18602481	10,2657126	5,65700617	0,00021995	0,00898505	0,89732760
VGF	1,07875495	7,45882408	5,57344869	0,00024670	0,00980475	0,78123553
SCHIP1	1,79576962	8,31350280	5,55311738	0,00025373	0,01000178	0,75282797
ASB2	2,05887906	10,8642161	5,55171888	0,00025422	0,01000178	0,75087163
NCF2	2,05909431	10,5537084	5,49483991	0,00027508	0,01065045	0,67105360
GFPT2	2,02362444	7,43137116	5,48271063	0,00027977	0,01071020	0,65396916
SH3RF1	1,18794650	11,8231341	5,47823758	0,00028152	0,01071020	0,64766312
SPANXD	1,14244581	6,26850163	5,47398414	0,00028319	0,01071020	0,64166385
ANTXR2	1,00898925	11,1916942	5,38337098	0,0003215	0,01155522	0,51320640
SOX4	1,47031615	14,2367970	5,34335455	0,00034015	0,01179868	0,45608066
SPEG	1,41537473	7,70975982	5,33133062	0,00034598	0,01189492	0,43886834

GABARAPL1	1,02102929	9,52965349	5,25986130	0,00038291	0,01250484	0,33610728
EMP3	1,35285591	10,1305256	5,25521001	0,00038545	0,01255300	0,32939267
TMSB4X	2,19674509	9,23736627	5,25113580	0,0003877	0,01256806	0,32350844
GLRX	1,08448821	13,3357600	5,24022827	0,00039377	0,01262890	0,30774272
MICAL1	1,08640774	9,93758682	5,23481115	0,00039683	0,01267707	0,29990613
ANGPTL4	1,10994711	7,53134610	5,22836303	0,00040050	0,01269991	0,29057228
ESAM	1,81849656	11,5780206	5,20127156	0,00041633	0,01295208	0,25128777
MMP1	1,38824281	7,64876442	5,17568630	0,00043189	0,01322068	0,21408547
AREG	1,91541726	13,08952	5,15724627	0,00044349	0,01347029	0,18721138
AMPD3	2,22624859	8,15917924	5,14853945	0,00044908	0,01360493	0,17450441
TMCC1	1,12951097	9,05047147	5,13278439	0,00045940	0,01384581	0,15148196
CCK	1,88145692	6,96534598	5,11276303	0,00047287	0,01410681	0,12217129
ASAP2	1,26220446	10,6127195	5,10101278	0,00048097	0,01419851	0,10494116
GPR157	1,09936277	9,08320084	5,10034690	0,00048144	0,01419851	0,10396411
CCDC84	1,03776186	10,9611819	5,09780625	0,00048321	0,01419851	0,10023560
ASPH	1,81482557	11,9635730	5,02237525	0,00053917	0,01523690	-0,01090444
NOSTRIN	1,05304445	7,05284162	5,00293838	0,00055469	0,01552072	-0,03968104
EREG	1,69652983	7,65984483	4,98400601	0,00057026	0,01580552	-0,06776505
LAMB3	2,62398451	9,59258228	4,98134968	0,00057248	0,01582968	-0,07170971
CILP	1,31343309	6,32959587	4,97683907	0,00057627	0,01584340	-0,07841037
SERPINB8	1,40277633	10,6432162	4,96331306	0,00058781	0,01591580	-0,09852193
ADM	1,57866916	11,6054832	4,93576258	0,00061208	0,01610808	-0,13957059
TGM2	1,16144130	12,3075941	4,93368892	0,00061395	0,01610808	-0,14266480
NKAIN1	1,70196767	9,13142662	4,88458421	0,00066005	0,01685946	-0,21612298
ZBED2	1,06236039	6,40549278	4,87736592	0,00066713	0,01689314	-0,22695131
CHIC2	1,21091008	9,85605804	4,85083330	0,00069387	0,01724183	-0,26681974
COL7A1	1,35129673	8,54553614	4,85056991	0,00069414	0,01724183	-0,26721604
PDLIM4	1,63674988	10,3097278	4,8482727	0,00069651	0,01725368	-0,27067286
VCX3A	2,07026496	7,84358422	4,80267196	0,00074536	0,01795528	-0,33945301
FRMD5	1,49878585	10,7123045	4,79949164	0,00074890	0,01795528	-0,34426133
CD59	1,01024894	13,5179807	4,79810676	0,00075045	0,01795566	-0,34635559
PSG6	1,19271028	6,60932318	4,77704158	0,00077440	0,01824365	-0,3782456
LAIR2	1,61105634	8,95437425	4,77658700	0,00077493	0,01824365	-0,37893451
CYR61	1,41738783	12,4853889	4,77045814	0,00078206	0,01833781	-0,38822543
BIK	1,36192255	8,59832704	4,71155940	0,00085423	0,01937136	-0,47779074
GCLM	1,11129015	10,8962416	4,70724023	0,00085979	0,01938341	-0,48437856
MOSPD1	1,46466015	10,0460137	4,69713318	0,00087296	0,01949455	-0,49980495
MAFF	1,11162222	8,58323358	4,68686405	0,00088656	0,01968581	-0,51549381
TNFRSF12A	1,07487079	13,7037353	4,65125968	0,00093549	0,02032120	-0,57000671
POMC	1,35658074	7,05294457	4,64887492	0,00093887	0,02032120	-0,57366446
TMEM173	1,04722822	9,82700966	4,63699499	0,00095590	0,02056328	-0,59189805
PDE4C	1,04966766	11,0496514	4,62975626	0,00096643	0,02071387	-0,60301812
FOXC1	1,00205786	11,0496741	4,59656918	0,00101633	0,02143070	-0,65409539
EDN1	2,11395955	9,11634507	4,58259987	0,00103814	0,02173433	-0,67564196
HIVEP2	1,08019513	7,65508599	4,53820017	0,00111084	0,02288967	-0,74430795

KRT80	1,72106937	9,43041860	4,52878556	0,00112694	0,02309833	-0,75890363
STK17B	1,90406381	9,11013003	4,48536763	0,00120444	0,02424940	-0,82637544
RNF128	1,03556527	13,3169241	4,48460816	0,00120585	0,02424940	-0,82755800
VCX2	1,76313187	7,35166203	4,47272211	0,00122806	0,02438431	-0,84607590
PFKP	1,22934419	11,2342639	4,46678063	0,00123933	0,02442130	-0,85533974
PLK3	1,08666919	12,2775372	4,46674914	0,00123939	0,02442130	-0,85538886
DUSP13	1,14407129	11,5786399	4,46230068	0,00124790	0,02454769	-0,86232801
FOLR1	1,18430543	7,77725161	4,44108028	0,00128935	0,02506859	-0,89546721
ZFAND2A	1,15918432	12,374905	4,42572757	0,00132024	0,02550011	-0,91948148
S100A3	1,91103478	9,35892807	4,40031854	0,00137311	0,02613821	-0,95929611
SERPINB2	1,22274403	7,38189917	4,40020727	0,00137334	0,02613821	-0,95947066
F2RL1	1,83366869	10,1833238	4,37085075	0,00143724	0,02703171	-1,00558001
S100A2	2,07933700	11,0673401	4,36492866	0,00145050	0,02714726	-1,01489569
MAP1B	1,53109398	10,4670001	4,28625825	0,00163956	0,02899766	-1,13908979
VCX	1,83441520	7,41269372	4,28615179	0,00163983	0,02899766	-1,13925840
NAGS	1,04975811	10,8328031	4,27999067	0,00165570	0,02914641	-1,14901922
ZFHX2	1,17191447	7,95304367	4,27224373	0,00167589	0,02932561	-1,16129941
HIST1H2AE	1,06334923	9,12279619	4,26278499	0,00170089	0,02963037	-1,17630364
LCK	1,08525523	7,24565661	4,21732529	0,00182664	0,03085826	-1,24856411
RNF183	1,10559255	8,10653084	4,20585573	0,00185990	0,03132975	-1,26685267
NES	1,11509046	11,7187057	4,17826513	0,00194254	0,03218448	-1,31088519
GSTP1	1,18837716	7,78152456	4,17492340	0,00195281	0,03228917	-1,31622483
LTBP1	1,17318413	7,18817299	4,12256978	0,00212137	0,03379214	-1,40005985
GRB14	1,01599472	9,04994895	4,12128969	0,00212568	0,03381483	-1,40211392
RIT1	1,03865458	10,6525497	4,11106402	0,00216043	0,03413134	-1,41852941
PRSS23	2,44308234	8,39768338	4,11030211	0,00216304	0,03413134	-1,41975303
GLIPR2	1,10762467	7,59624342	4,09632844	0,00221157	0,03438785	-1,44220708
GPC1	1,25036319	12,3204206	4,09237772	0,00222549	0,03451282	-1,44855968
EGR1	1,40604215	11,1217643	4,08623351	0,00224733	0,03466769	-1,45844308
PAQR3	1,07397550	9,86968347	4,08541350	0,00225026	0,03466769	-1,45976246
ITGA3	1,18582871	6,80372532	4,07447913	0,00228974	0,03501223	-1,47736344
S100A6	1,66116036	14,2684879	4,02540163	0,00247613	0,03669103	-1,55653739
LY6K	1,68226120	7,08265960	4,02233464	0,00248829	0,03678789	-1,56149455
KIF3C	1,31551248	9,46201258	4,01798282	0,00250566	0,03685877	-1,56853025
COTL1	1,44399971	12,5754530	4,00409464	0,00256195	0,03725658	-1,59099822
ACTG2	1,10692097	8,18283873	4,00343368	0,00256466	0,03725658	-1,59206807
AP1S3	1,27608354	10,4301660	3,99961906	0,00258037	0,03725658	-1,59824343
AGR2	1,19996272	7,87162042	3,99302896	0,00260775	0,03751328	-1,60891585
SPINT2	1,23896892	8,34388292	3,97550230	0,00268206	0,03815559	-1,63732364
GCNT3	1,48487753	13,1377088	3,94893715	0,00279896	0,03915872	-1,68044717
JUN	1,42539131	11,2669386	3,94132068	0,00283345	0,03945297	-1,69282556
COL1A1	1,54861222	7,18783296	3,93057241	0,00288288	0,03995152	-1,71030465
ANXA3	1,40249006	11,2705995	3,92705215	0,00289927	0,04008385	-1,71603213
GAL	1,04505357	6,98823793	3,91783317	0,00294265	0,04020943	-1,73103787
AK5	1,18816994	6,37418710	3,90781987	0,00299054	0,04072142	-1,74734696

C19orf33	2,14396054	10,5295576	3,84075785	0,00333306	0,04366134	-1,85684826
GGT5	1,20941732	8,48791818	3,83826788	0,00334655	0,04378903	-1,86092299
ELK3	1,11063800	7,14729119	3,82864102	0,00339921	0,04432973	-1,87668287
NUAK1	1,27234286	10,4182462	3,79275893	0,00360328	0,04598225	-1,93550669
EPPK1	1,24219992	11,9041881	3,78847210	0,00362850	0,04613418	-1,9425429
SERPINB9	1,11877203	7,92608523	3,76209764	0,00378780	0,04684408	-1,98587210
LGALS1	1,28783522	14,4591686	3,75127109	0,00385529	0,04751986	-2,00367781
IER5L	1,11808120	10,8247569	3,74865439	0,00387179	0,04751986	-2,00798299
CLTB	1,04243086	12,1501269	3,71084831	0,00411857	0,04917125	-2,07025543
ICAM2	1,10176863	11,7549449	3,69946906	0,00419602	0,04974136	-2,08902444

Table 9.2SB . Downregulated genes cd10 vs cd2

	logFC	AveExpr	t	P.Value	adj.P.Val	B
SLC13A3	-1,81831595	10,6022719	-12,6467862	2,00E-07	0,00029350	7,61244780
ALDH8A1	-2,27259771	8,76352656	-12,4246641	2,36E-07	0,00030788	7,46731333
GJB1	-1,66587068	12,4977832	-12,2718855	2,65E-07	0,000311	7,36558886
SULT2A1	-1,78290234	10,1506702	-12,0670808	3,10E-07	0,00033071	7,22673505
EPO	-1,80256222	9,02131987	-11,5504489	4,65E-07	0,00042003	6,86331419
ENPP2	-1,57148847	8,28598451	-11,3495155	5,47E-07	0,00045874	6,71667300
NR1H4	-2,36213676	9,85984144	-10,9105268	7,87E-07	0,00057667	6,38544471
FGL1	-1,45221941	14,7918413	-10,7252883	9,21E-07	0,00060046	6,24104386
APOA5	-1,83093987	9,63704706	-10,4781271	1,14E-06	0,00061546	6,04392009
PAH	-1,99889088	11,2614476	-10,2916189	1,34E-06	0,00068519	5,89170653
FGA	-2,41156084	11,725599	-10,1964963	1,46E-06	0,00071455	5,81290006
IL22RA1	-1,24214620	9,78477559	-9,86866469	1,96E-06	0,00082382	5,53505057
C2orf72	-1,73132032	10,4821436	-9,74829088	2,19E-06	0,00084406	5,43053688
PIP5K1B	-1,49168451	8,40152257	-9,73195698	2,23E-06	0,00084406	5,41624974
GPX2	-1,29754387	13,0051796	-9,59986903	2,52E-06	0,00088317	5,29977723
RGN	-1,39861817	12,2292503	-9,53675229	2,67E-06	0,00088317	5,24352810
SERPINA6	-1,70936052	12,4190576	-9,53542160	2,68E-06	0,00088317	5,24233803
SLC13A5	-1,80626820	11,1655346	-9,38024317	3,10E-06	0,00098481	5,10236438
SAMD11	-1,55948083	8,31966651	-9,32151607	3,28E-06	0,00098839	5,04876818
F7	-1,35405704	8,97572929	-9,27959873	3,42E-06	0,00100336	5,01030133
ZCCHC2	-1,82870950	10,0542584	-8,90241996	4,95E-06	0,00138323	4,65606071
HADH	-1,12520184	12,7899929	-8,82996379	5,32E-06	0,00145263	4,58630184
SERPINF2	-2,04527937	10,0672150	-8,46846117	7,70E-06	0,00180650	4,22971930
SPTLC3	-1,72079158	9,07112860	-8,37976879	8,44E-06	0,00190511	4,14000936
ANXA9	-1,15921692	10,5193376	-8,29774018	9,20E-06	0,00198138	4,05624067
FZD4	-1,66947565	13,6331893	-8,27402941	9,44E-06	0,00198138	4,03188263
IDH1	-1,22151269	14,3081583	-8,22800890	9,91E-06	0,00198138	3,98441990
SLC6A14	-1,66711386	8,31724770	-8,21280888	1,00E-05	0,00198138	3,96868942
TCEA3	-1,26138269	12,9892920	-8,17865451	1,04E-05	0,00198138	3,93324465
ASF1B	-1,14583069	11,1022642	-8,17598772	1,04E-05	0,00198138	3,93047135
NEK10	-1,09874215	7,68471753	-8,01231894	1,24E-05	0,00221901	3,75865849
DIO1	-1,70250504	8,63630129	-7,97472784	1,30E-05	0,00224334	3,71874607
ANG	-1,59470003	13,2457579	-7,88038330	1,44E-05	0,00232439	3,61782433
ITIH3	-1,03737614	12,0429915	-7,86185029	1,47E-05	0,00232439	3,59787219
C4BPA	-1,35831791	10,4665956	-7,82901975	1,52E-05	0,00232439	3,56242467
FGB	-2,08697788	11,3895168	-7,80292717	1,57E-05	0,00232439	3,53415788
SLC37A4	-1,10109421	11,8906092	-7,77887457	1,61E-05	0,00232439	3,50802682
APOC3	-1,53252601	12,2914252	-7,77524495	1,61E-05	0,00232439	3,50407736
CASP1	-1,20150677	7,60363963	-7,77167769	1,62E-05	0,00232439	3,50019416
GLUD1	-1,32651441	14,2238769	-7,67687991	1,80E-05	0,00245552	3,39642196
FOXA1	-1,32906707	13,0658856	-7,67515885	1,81E-05	0,00245552	3,39452765
PCYT2	-1,31394772	11,7823765	-7,66918008	1,82E-05	0,00245552	3,38794400

RPS6KA3	-1,23332904	13,3557188	-7,64177685	1,87E-05	0,00250327	3,35771119
ADH6	-1,67548166	8,89445635	-7,47558039	2,26E-05	0,00271374	3,17232011
SLC38A3	-1,30700425	8,4319012	-7,46278988	2,30E-05	0,00271374	3,15790644
EPHX2	-1,68079529	10,6867020	-7,44287111	2,35E-05	0,00271374	3,13541804
SLC5A9	-1,83764821	9,00372196	-7,44237590	2,35E-05	0,00271374	3,13485830
GDPD5	-1,34277685	10,9138055	-7,43158342	2,38E-05	0,00271374	3,12265150
METTL7A	-1,52223968	11,4176064	-7,37353723	2,54E-05	0,00281859	3,05674030
KLB	-1,98441420	10,9384900	-7,34926847	2,62E-05	0,00285539	3,02905364
GRTP1	-1,04379488	9,11012197	-7,31601465	2,72E-05	0,00290256	2,99099183
ACSM2A	-1,00721444	7,15426976	-7,26758115	2,88E-05	0,00304228	2,93529665
CPN2	-1,20200998	9,28215266	-7,25998296	2,90E-05	0,00304228	2,92653130
CFI	-1,05653312	13,2032987	-7,21816501	3,05E-05	0,00306411	2,87815337
ACSF2	-1,08696713	10,5989966	-7,21640750	3,05E-05	0,00306411	2,87611510
SLC30A10	-1,75729855	9,20861255	-7,16830891	3,23E-05	0,00312697	2,82017380
SERPINC1	-1,78535871	12,0119853	-7,13390982	3,36E-05	0,00318507	2,77997697
MRAP	-1,00484835	7,16378364	-7,09552369	3,52E-05	0,00327685	2,73493434
HPX	-1,47328569	9,13044459	-7,08761427	3,55E-05	0,00327685	2,72562880
IMPA2	-1,10281697	13,3940078	-7,06926322	3,63E-05	0,00327685	2,70400616
HP	-2,49955220	14,5565433	-7,04409751	3,74E-05	0,00329977	2,67428020
KLHDC2	-1,06640488	11,8947744	-6,99903164	3,95E-05	0,00333937	2,62083410
ACSM2B	-1,38039729	8,69361098	-6,97184733	4,08E-05	0,00338328	2,58846153
CDC42EP4	-1,47949086	11,3165949	-6,97147849	4,08E-05	0,00338328	2,58802159
VAV3	-1,95217878	11,9774035	-6,96901269	4,09E-05	0,00338328	2,58508009
TIGD3	-1,07059356	8,78773103	-6,93925460	4,24E-05	0,00345754	2,54951564
ALDH6A1	-1,55477620	10,0792627	-6,90777359	4,41E-05	0,00356626	2,51176037
ERBB3	-1,44438376	9,55620680	-6,90033531	4,45E-05	0,00357374	2,50281979
GRB7	-1,14699643	9,60354382	-6,86053991	4,66E-05	0,00372431	2,45485782
CFB	-1,25740007	11,4778766	-6,85010506	4,72E-05	0,00373425	2,44224552
CYP27A1	-1,21766005	10,9642309	-6,80356884	5,00E-05	0,00391127	2,38581538
SLC39A5	-1,18718227	10,6933646	-6,72830471	5,48E-05	0,00404548	2,29391334
SERPINA1	-1,41682738	7,52348894	-6,71759600	5,55E-05	0,0040734	2,28077318
IL1RAP	-1,02385321	7,95937508	-6,70448174	5,64E-05	0,00408848	2,26465940
HPN	-1,28452384	10,3749482	-6,67690170	5,84E-05	0,00420381	2,23069256
ALDH3A2	-1,29103787	10,6605331	-6,62545806	6,22E-05	0,00432263	2,16705015
ITIH1	-1,74848461	8,40521181	-6,60952949	6,35E-05	0,00433026	2,14726875
DDC	-1,74104132	13,3207231	-6,56032053	6,75E-05	0,00447378	2,08593018
ENPP3	-1,55064462	8,90266969	-6,49352040	7,34E-05	0,00467905	2,00211335
C8B	-1,32159305	6,96203594	-6,42942487	7,96E-05	0,00499141	1,92109019
LIME1	-1,48365288	9,90366766	-6,36866767	8,59E-05	0,00516959	1,84374142
PRODH2	-1,36598386	9,20112591	-6,34535486	8,85E-05	0,00516959	1,81392078
KANK4	-2,08610876	10,4178948	-6,34191710	8,89E-05	0,00516959	1,80951670
MID1IP1	-1,20988402	10,0223903	-6,33789130	8,94E-05	0,00516959	1,80435711
FGG	-2,30286504	14,8033755	-6,28433889	9,57E-05	0,00542460	1,73549878
CEBPA	-1,60015603	14,5718797	-6,27182365	9,73E-05	0,00548599	1,71934638
SFXN2	-1,04847953	10,0546917	-6,26149238	9,86E-05	0,00550640	1,70599543

UPB1	-1,11147914	7,70891817	-6,23455112	0,00010211	0,00567383	1,67110637
MCM2	-1,21743145	13,2670654	-6,21698461	0,00010445	0,00573253	1,64830049
MAT1A	-1,34449685	13,5752815	-6,21564558	0,00010463	0,00573253	1,64656024
AIF1L	-1,11850770	12,5392650	-6,19334475	0,0001077	0,00581877	1,61753849
TMEM86B	-1,30018346	10,0236037	-6,13572044	0,00011607	0,00604812	1,54220949
TMCO6	-1,00808162	9,35228229	-6,00617631	0,00013756	0,00686316	1,37107442
SHMT1	-1,03248243	10,3042211	-5,99850583	0,00013896	0,00686358	1,36086327
IFIT1	-1,03413519	7,71255759	-5,97861411	0,00014267	0,00696958	1,33434207
TMEM135	-1,18039055	10,7711808	-5,93741338	0,00015068	0,00724049	1,27922257
EPN3	-1,54666142	9,36077236	-5,86123689	0,00016681	0,00782301	1,17664374
GLUD2	-1,39824053	13,5332843	-5,83307580	0,00017324	0,00793947	1,13850216
A1CF	-1,26055753	10,8109417	-5,76896611	0,00018887	0,00833747	1,05122733
KLC4	-1,08231968	8,34831415	-5,74347459	0,00019551	0,00848965	1,01635299
TRIM50	-1,35467506	8,34784918	-5,70083406	0,00020717	0,00870028	0,95779854
NDRG2	-1,29096256	12,4694424	-5,57681685	0,00024556	0,00979249	0,78593558
LIPC	-1,01789283	9,82401653	-5,47780780	0,00028168	0,01071020	0,64705705
MIXL1	-2,09928114	8,80627018	-5,47723831	0,00028191	0,01071020	0,64625394
ACSL4	-1,02315415	11,5207267	-5,47602304	0,00028239	0,01071020	0,64453996
SKP2	-1,01124738	10,2835080	-5,46790304	0,00028560	0,01076340	0,63308201
ESPN	-1,14290187	8,54805310	-5,39594108	0,00031587	0,01150079	0,53110079
HAMP	-1,64281372	11,7339084	-5,38299321	0,00032167	0,01155522	0,51266825
SLCO4C1	-1,25446474	8,68693893	-5,37513146	0,00032524	0,01155522	0,50146388
PHGDH	-1,27842163	12,1198326	-5,35351066	0,00033531	0,01167021	0,47060209
PKLR	-1,08291021	7,78642947	-5,35321018	0,00033545	0,01167021	0,47017268
KIF20B	-1,0306736	8,30484836	-5,34097652	0,00034129	0,01180345	0,45267823
IGSF1	-1,55260528	9,90439860	-5,32157970	0,00035078	0,01189876	0,42489375
PPP1R3C	-1,20447011	9,75955494	-5,31855370	0,00035229	0,01189876	0,42055409
SMAD9	-1,17225407	8,52139768	-5,31481095	0,00035416	0,01189876	0,41518459
KIF22	-1,00717608	12,6634725	-5,29768790	0,00036286	0,01212035	0,39059214
MPV17L	-1,05091948	8,36903728	-5,24000619	0,00039390	0,01262890	0,30742153
NR6A1	-1,16037275	7,69534389	-5,22973807	0,00039972	0,01269991	0,29256321
ITIH2	-1,21233279	13,9851867	-5,20941311	0,00041150	0,01290650	0,26310525
HPR	-2,44915836	10,6451656	-5,2071818	0,00041282	0,01290650	0,25986749
AMT	-1,03533533	12,2118530	-5,19915654	0,00041759	0,01295208	0,24821617
C5	-1,53698051	10,0951013	-5,18418668	0,00042665	0,01313450	0,22645644
TRIM74	-1,21617440	8,45020884	-5,18388913	0,00042683	0,0131345	0,22602359
MLXIPL	-1,53557720	12,1012226	-5,10809422	0,00047607	0,01416629	0,11532761
GNMT	-1,21181600	8,12874469	-5,10534144	0,00047797	0,01418678	0,11129096
DAO	-1,04701846	8,50865090	-5,08922108	0,00048925	0,01426882	0,08762934
SLC23A1	-1,08689886	6,98352173	-5,07302579	0,00050088	0,01449958	0,06381835
DUSP9	-1,61775349	13,8040972	-5,06489006	0,00050683	0,01459972	0,05184199
SERPINA7	-1,09283788	11,8105556	-4,97165928	0,00058066	0,01587039	-0,08610887
SERPINA4	-1,24197241	8,40170305	-4,97159230	0,00058072	0,01587039	-0,08620846
STAR	-1,02193898	10,0387550	-4,94791773	0,00060124	0,01607601	-0,12144617
KIF15	-1,10174284	10,6014997	-4,93551649	0,00061230	0,01610808	-0,13993775

GSTA2	-1,55667783	9,64390288	-4,87199273	0,00067246	0,01698526	-0,23501676
ATP6V0E2	-1,04440999	10,8481188	-4,86408495	0,00068038	0,01704440	-0,24689455
GTSE1	-1,03898923	10,3308075	-4,84300600	0,00070197	0,01728986	-0,27860104
MAP2K6	-1,26680342	9,60580234	-4,84077093	0,00070430	0,01731094	-0,28196683
C8A	-1,74866065	8,77189417	-4,82796682	0,00071783	0,01753301	-0,30126269
CA5A	-1,21841443	9,70515499	-4,76080955	0,00079342	0,01853013	-0,40286312
HIST1H2BD	-1,08254953	10,8790292	-4,7559847	0,00079917	0,01856527	-0,41018791
MMP11	-1,04643537	8,37111149	-4,72047364	0,00084286	0,01926894	-0,46420279
ACSS1	-1,13038619	11,4921469	-4,71017650	0,00085600	0,01937193	-0,47989971
PIPOX	-1,30865499	11,3904808	-4,69133317	0,00088062	0,01959086	-0,50866416
GSTA1	-1,20286366	8,07899360	-4,65640990	0,00092824	0,02030329	-0,56211007
NFE2	-1,05584690	9,71953124	-4,65607717	0,00092871	0,02030329	-0,56262013
SLC22A7	-1,09468211	8,44272355	-4,65074810	0,00093622	0,02032120	-0,57079130
EFNA1	-1,02438945	14,0224052	-4,58707155	0,00103111	0,02162563	-0,66874173
PCSK9	-1,58643063	12,5165885	-4,56462796	0,00106694	0,02221821	-0,70340280
PAQR8	-1,06149208	11,2815417	-4,42008364	0,0013318	0,02559676	-0,92831765
ADH4	-1,33309593	10,1143217	-4,35769175	0,00146689	0,02729822	-1,02628602
TNFAIP8L	-1,04217406	9,89247145	-4,35102287	0,00148217	0,02747803	-1,03678852
ONECUT1	-1,31046731	8,27004697	-4,32498968	0,00154342	0,02807799	-1,07784359
EPHA1	-1,06535824	8,30786961	-4,32276282	0,00154879	0,02810838	-1,08135958
ASS1	-1,30955160	10,5027084	-4,31202072	0,00157493	0,02839669	-1,09832949
HOXD1	-1,30736843	8,89772192	-4,30722551	0,00158675	0,02853246	-1,10590967
FAM117A	-1,0333663	10,9832881	-4,27806083	0,00166071	0,02915665	-1,15207760
RNASE4	-1,52975347	11,6228145	-4,25320155	0,00172662	0,02981901	-1,19151748
LEAP2	-1,82827500	10,6546416	-4,23981481	0,00176325	0,03035589	-1,21278895
SOBP	-1,16803132	9,50188497	-4,21461339	0,00183445	0,03094554	-1,25289620
HHEX	-1,17355467	10,9264934	-4,18162704	0,00193226	0,03208770	-1,30551471
GYG2	-1,06804531	10,2458814	-4,15428544	0,00201751	0,03280622	-1,34923239
PZP	-1,23954198	7,93268742	-4,14504271	0,00204721	0,03304213	-1,36403200
C1orf115	-1,19723851	10,6516891	-4,14451369	0,00204892	0,03304213	-1,36487938
SERPINA3	-1,17417701	14,0199481	-4,12948719	0,00209825	0,03346925	-1,38896349
FGFR2	-1,24896444	7,66994528	-4,11841518	0,00213539	0,03387734	-1,40672715
GSTA5	-1,29486164	8,56433142	-4,09744322	0,00220765	0,03437260	-1,44041489
HIST3H2BB	-1,01490972	10,7857201	-4,06878517	0,00231061	0,03522714	-1,48654533
PNPLA3	-1,04614769	10,7322259	-4,00794832	0,00254620	0,03720497	-1,58476161
A1BG	-1,12312492	10,9968135	-4,00079455	0,00257552	0,03725658	-1,59634028
SERPIND1	-1,04627798	12,315812	-3,92225025	0,00292178	0,04016088	-1,72384704
GSTA3	-1,14243745	8,05274811	-3,90539238	0,00300227	0,04083375	-1,75130234
KIRREL2	-1,10697540	7,56166257	-3,86869463	0,00318563	0,04244138	-1,81117473
FAM3B	-1,22656946	11,8590188	-3,84389151	0,00331618	0,04358623	-1,85172106
ALDH1A1	-1,03022986	14,5737805	-3,80571455	0,00352816	0,04536256	-1,91425290
TET1	-1,06513406	8,63266307	-3,74011439	0,00392615	0,04774919	-2,02203808
PPARGC1	-1,04922336	7,84969806	-3,70498682	0,00415828	0,04949411	-2,07992196

Chapter 10

"Neuronal specific and non-specific responses to cadmium possibly involved in neurodegeneration: a toxicogenomics study in a human neuronal cell model."

ABSTRACT

Epidemiological data have linked cadmium exposure to neurotoxicity and to neurodegenerative diseases (e.g., Alzheimer's and Parkinson's disease), and to increased risk of developing ALS. Even though the brain is not a primary target organ, this metal can bypass the blood brain barrier, thus exerting its toxic effects. The coordination chemistry of cadmium is of strong biological relevance, as it resembles to zinc(II) and calcium(II), two ions crucial for neuronal signaling. A toxicogenomics approach applied to a neuronal human model (SH-SY5Y cells) exposed to cadmium (10 and 20 µM) allowed the identification of early deregulated genes and altered processes, and the discrimination between neuronal-specific and unspecific responses as possible triggers of neurodegeneration. Cadmium confirmed its recognized carcinogenicity even on neuronal cells by activating the p53 signaling pathway and genes involved in tumor initiation and cancer cell proliferation, and by down-regulating genes coding for tumor suppressors and for DNA repair enzymes. Two cadmium-induced stress responses were observed: the activation of different members of the heat shock family, as a mechanism to restore protein folding in response to proteotoxicity, and the activation of metallothioneins (MTs), involved in zinc and copper homeostasis, protection against metal toxicity and oxidative damage. Perturbed function of essential metals is suggested by the mineral absorption pathway, with MTs, HMOX1, ZnT-1, and Ferritin genes highly up-regulated. Cadmium interferes also with Ca^{2+} regulation as S100A2 is one of the top up-regulated genes, coding for a highly specialized family of regulatory Ca^{2+}-binding proteins. Other neuronal-related functions altered in SH-SY5Y cells by cadmium are microtubules dynamics, microtubules motor-based proteins and neuroprotection by down-regulation of NEK3, KIK15, and GREM2 genes, respectively.

Matilde Forcella, Pierre Lau, Monica Oldani, Pasquale Melchioretto, Alessia Bogni, Laura Gribaldo, Paola Fusi and Chiara Urani

Keywords: Cadmium; Neurotoxicity; SH-SY5Y human neuronal cells; Toxicogenomics

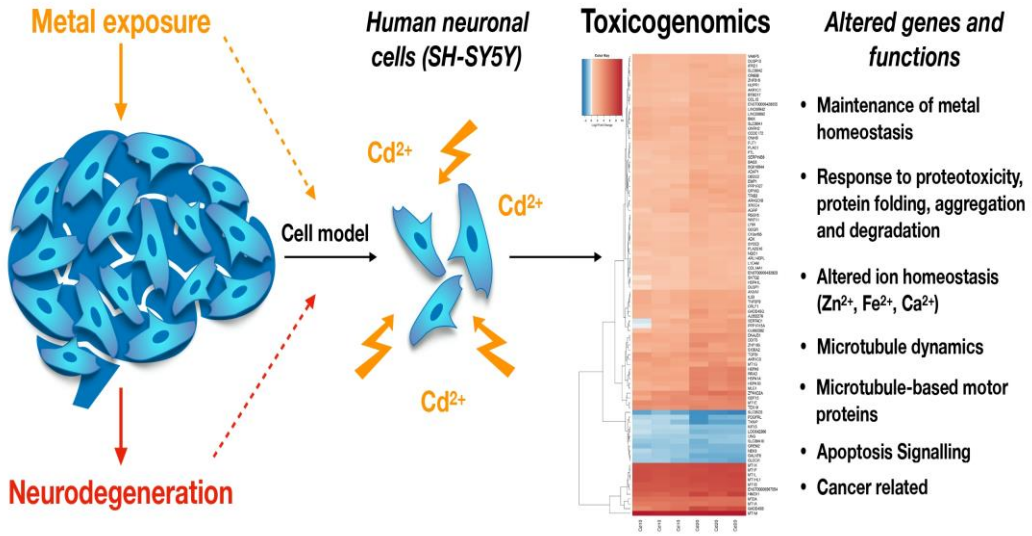

This chapter is an extract of the submitted and accepted paper in Neurotoxicology, (2019)

❖ 10.1. Introduction

Among the toxic metals, cadmium (Cd) is of particular concern for its environmental, chemical and biological features; it is ubiquitously distributed in the environment by natural sources (e.g. volcanic activities and forest fires), and huge anthropogenic release (~30,000 tons/year). Due to its slow excretion from the human body, and a very long biological half-life (10-30 years), Cd is heavily accumulated in the organism (e.g. 2 μg/g liver, and 70 μg/g kidney) reaching its plateau in the kidney at 50 years of age. Consequently, Cd has been listed as the seventh most hazardous chemical for human health, considering both toxicity and exposure frequency (ATDSR, 2017). Cd exposure for non-occupational reasons can primarily occur through food, drinking water, air particles, cosmetics and cigarette smoking (Bocca et al., 2014; Hartwig and Jahnke, 2017; Satarung and Moore, 2004). Being an integral constituent of tobacco with a typical content of 0.5-1 μg/cigarette, Cd is accumulated in smokers blood at concentrations 4-5 times higher than in non-smokers, and can deposit in the aortic wall of heavy smokers at concentrations up to 20 μM (Satarug and Moore, 2004). In addition, brain Cd bioaccumulation data are available in wild animals (see e.g., Gajdosechova et al., 2016), and Cd was also found in locus ceruleus neurons from human autopsies of individuals with diverse clinicopathological conditions and causes of death (Pamphlett et al., 2018), and in the olfactory bulbs of experimental animals exposed to Cd through diet or inhalation (Sunderman, 2001).

Moreover, Cd is considered a neurotoxin, although the mechanisms remain poorly understood. One of the first evidences for a cause-effect relationship between Cd uptake and a neurodegenerative disease, was reported in 2001 in a patient with Amyotrophic Lateral Sclerosis-like syndrome after occupational Cd intoxication (Bar-Sela et al., 2001). Amyotrophic lateral sclerosis (ALS) is a progressive and invariably fatal neurodegenerative disease involving the motor system. Five to 10% of ALS cases are familial and a number of mutated genes have been identified (Aude et al., 2018), while the majority of ALS cases (90-95%) are sporadic. Despite its identification as a neurological condition 150 years ago, the etiology of motor neuron degeneration in ALS still remains largely unknown.

The general hypothesis is that sporadic ALS is a complex multi-factorial disease, and many genetic and environmental factors are under investigation as possible culprits (Ingre et al., 2015; Wang et al., 2017). Among these factors, various toxic metals and the unbalance of essential trace elements contributing to the development of ALS have been proposed: *i)* lead involvement is a long-standing hypothesis; *ii)* manganese is well known for its neurotoxic properties; *iii)* iron accumulation has been reported in ALS patients; and *iv)* the potential role of selenium has been investigated. Many other metals with potential significance for ALS have been evidenced e.g. copper, aluminium, arsenic, cobalt, zinc and cadmium, all of which have been found at elevated concentrations in ALS patients, when compared to healthy controls (Roos et al., 2013). It is noteworthy that cigarette smoking is the only factor recently identified and related to negative survival in ALS patients (Calvo et al., 2016).

Very interestingly, Cd is transported along the primary olfactory neurons to their terminations in the olfactory bulb, thereby bypassing the intact blood brain barrier, and representing therefore a likely way for Cd to reach the brain. In the nervous system, Cd tends to accumulate in the choroids plexus at concentrations much greater than those found in the cerebrospinal fluid (CSF) and in other brain areas (Wang and Du, 2013). In addition, Cd-induced apoptosis of motor neurons in cultured explants from human fetal spinal cords was observed (Sarchielli et al., 2012).

To the understanding of Cd toxic mechanisms, the coordination chemistry of cadmium(II) is of strong biological relevance as it resembles zinc(II) and calcium(II), both being crucial for neuronal signaling. Cd neurotoxicity is further described for its alterations in the release of neurotransmitters, oxidative stress, mitochondrial damage and induction of apoptosis (Maret and Moulis, 2013; Choong et al., 2014). This metal can also affect proteasomal functions and prion protein aggregation along with features responsible for axonal transport, such as microtubule disassembly, inhibition of microtubule formation, and kinesin- and dynein-dependent motility (Böhm, 2014; Méndez-Armenta and Ríos, 2007). However, the gathered knowledge on Cd (neuro)toxicity has not yet clarified the overall vision of the key events and processes necessary to untangle causes and consequences in a complex disease progression such as neurodegeneration.

We have applied a toxicogenomics approach to identify deregulated pathways in SH-SY5Y cells exposed to Cd, to unravel neuronal specific and non-specific

responses to this toxic metal, and to recognize early genes and processes involved upon Cd exposure. SH-SY5Y is a neuroblastoma cell line, widely used as *in vitro* model for neurotoxicity studies and neurodegenerative diseases (Cheung et al., 2009; Rossi et al., 2015). In addition, following the recommendations of the National Research Council of the National Academy of Sciences described in a recent report on toxicity testing in the 21st century, SH-SY5Y cells were used in this work as they are from human.

❖ 10.2. Materials and Methods

10.2.1 Cell culture and treatments

Human SH-SY5Y neuroblastoma cells (ATCC® CRL-2266™) were cultured with Eagle Minimum Essential Medium (EMEM) and F12 medium (1:1) completed with 10% heat inactivated foetal bovine serum and 1% antibiotics (streptomycin/penicillin) at 37°C under an atmosphere of 5% CO_2 in air. All culture reagents and media were from Euroclone, Italy. Neuroblastoma cells were seeded either in 100 mm Ø Petri dish for RNA extraction at a density of $2{\cdot}10^6$ cells/dish, or in 162 cm^2 growth area flasks for SDS-PAGE and western blotting at a density of $3{\cdot}10^6$ cells/flask, with three flasks for each treatment. Twenty four hours after seeding, the cells were exposed to 10 and 20 µM $CdCl_2$ (Cd) for 48 h. The stock solution (1 mM) of $CdCl_2$ (97% purity, BDH Laboratory, Milan, Italy) was prepared in ultra-pure water (0.22 µm filtered Milli-Q water, Millipore, Vimodrone, Milan, Italy) and stored at 4°C. Both Cd concentrations are below the cytotoxicity threshold (IC_{50}), as demonstrated by MTT assays (data not shown), displaying a mean cell viability of 93% at 10 µM, and a decrease at around 70% at 20 µM.

10.2.2 Microarray expression profiling

Total RNA was purified from SH-SY5Y cells using the RNeasy Plus kit (Qiagen). RNA was quantified using an ND-1000 UV-Vis spectrophotometer (Thermo Scientific, Wilmington, DE, USA), and the RNA integrity was assessed with the Agilent 2100 Bioanalyzer (Agilent Technologies Inc.) according to the manufacturer's instructions. The RNA samples used in this study exhibited a 260/280 ratio above 1.9 and a RNA Integrity Number (RIN) above 9.0.

The microarray experiment included two biological replicates for the controls, and three for the treatments. All sample-labeling, hybridization, washing, and scanning steps were conducted according to the manufacturer's specifications. Briefly, Cy3-labelled cRNA was generated from 50 ng of total RNA using the One Color Quick Amp Labeling Kit (Agilent Technologies Inc.). For every sample, 600 ng cRNA from each labeling reaction (with a specific activity above 9.0) was hybridized using the Gene Expression Hybridization Kit (Agilent Technologies Inc.) to the SurePrint G3 Human Gene Expression v2 Microarray (Agilent Technologies Inc.), an eight high-definition 60K arrays format. After hybridization, the slides were washed and then scanned with the Agilent G2565BA Microarray Scanner (Agilent Technologies Inc.). The fluorescence intensities of the scanned images were extracted and pre-processed using the Agilent Feature Extraction Software (version 10.7.3.1). The Agilent data were processed with limma (version 3.34.9). The signal from the green channel was collected and the background subtracted using the normexp method. Normalization between arrays was performed using quantile normalization and signals from replicated spots were averaged. The intensities corresponding to the same gene were also averaged and differentially expressed genes were found using F-statistics implemented in limma by testing all contrasts (i.e concentrations) simultaneously and adjusting for multiple tests with the Benjamini and Hochberg False Discovery Rate procedure. A collection of 285 KEGG pathways (release March 1, 2017) with a minimum size of 5 genes was considered for EGSEA (version 1.12.0). The limma test was used to determine the log2 fold changes of genes after Cd treatment. The ten methods considered for EGSEA were: camera (limma:3.40.2), safe (safe:3.24.0), gage (gage:2.34.0), padog (PADOG:1.26.0), plage (GSVA:1.32.0), zscore (GSVA:1.32.0), gsva (GSVA:1.32.0), ssgsea (GSVA:1.32.0), globaltest (globaltest:5.38.0), fry (limma:3.40.2) (Alhamdoosh et al., 2017).

10.2.3 qPCR validation of transcriptomics data

The total RNA was isolated using the Quick-RNATM MiniPrep (Zymo Research, Irvine, CA, USA), according to manufacturer's instructions. Total RNA was reverse-transcribed using SuperScript II RT (Invitrogen, Carlsbad, CA, USA), oligo dT and random primers, according to the manufacturer's protocol. For quantitative real-time PCR (qPCR), SYBR Green method was used to evaluate growth arrest and DNA damage-inducible protein GADD45β, heme oxygenase 1 and S100 calcium binding protein A2 expression. The genes were chosen as GADD45β and heme oxygenase 1 show the highest up-regulation, just after the metallothioneins, and S100 calcium binding protein A2 is the transcript with the lowest log2 fold change among the top up-regulated genes. Other transcripts (i.e. metallothioneins and heat shock proteins) were validated by immunochemical analyses. Briefly, 50 ng cDNA was PCR amplified with Luna® Universal qPCR Master Mix (New England BioLabs, Hitchin, Hertfordshire, UK) and specific primers, using an initial denaturation step at 95°C for 10 min, followed by 40 cycles of 95°C for 15 sec and 59°C annealing/polymerization for 1 min. Each sample was normalized using β-actin gene as internal reference control. The relative expression level was calculated with the Livak method (2[-ΔΔC(T)]) and expressed as a relative fold change between Cd treated and untreated cells. The primers used for qPCR are the following: GADD45β Fw 5'-CAGAAGATGCAGACGGTGAC-3' and Rv 5'-AGGACTGGATGAGCGTGAAG-3'; HMOX1 Fw 5'-TGCCCCAGGATTTGTCAGAG-3' and Rv 5'-AAGTAGACAGGGGCGAAGAC-3'; S100A2 Fw 5'- GCGACAAGTTCAAGCTGAGTA-3' and Rv 5'-ACAGTGATGAGTGCCAGGAAA-3'; β-ACT Fw 5'-CGACAGGATGCAGAAGGAG-3' and Rv 5'-ACATCTGCTGGAAGGTGGA-3'.

10.2.4 Cell extract preparation and immunochemical analysis of metallothioneins and heat shock proteins

10.2.4.1 Metallothioneins (MT)

At the end of the treatment period (48 h), cells were processed essentially according to Callegaro et al., 2018. Briefly, cells were harvested by trypsinisation, washed with ice-cold PBS, centrifuged and lysed in 10 mM Tris-HCl buffer (pH 7) containing 5mM EDTA, 1mM PMSF and protease inhibitors. All samples were immediately frozen (-20°C) to obtain cell lysates. Low molecular weight proteins, including metallothioneins (MT), were separated by high-speed centrifugation (20000 *g* for 45 min). A small aliquot of clarified samples (supernatants) was used for protein content quantification by the Bradford assay. The remaining volume of clarified samples was diluted 1:1 in sample buffer (0.25 M Tris-HCl, pH 6.8, 2% SDS, 30% glycerol, 10% β-mercaptoethanol, 0.01% bromophenol blue) and stored at -20 °C. Total proteins (20 µg) were separated by SDS-PAGE in 12% NuPAGE gels (Invitrogen, Italy) and transferred using a transfer buffer (CAPS buffer: 10 mM 3-cyclohexylamino-1-propanesulfonic acid pH 10.8 in 10% methanol containing 2mM $CaCl_2$). Western blotting and immunoreactions were performed according to previously published protocols (Urani et al., 2010) using a mouse anti-metallothionein antibody (Zymed, Invitrogen, Corp. cat. n. 18-0133) that recognizes both MT-1 and MT-2 isoforms. Gels of the same samples were stained with Coomassie Blue for visualization of correct sample loading.
The expression of MT in controls and Cd-treated samples was analyzed by comparing bands intensities of different samples.

10.2.4.2 Heat shock proteins (Hsp70)

Treated and control cells were collected in PBS buffer containing protease inhibitors (aprotinin, leupeptin, pepstatin, PMSF), passed through a syringe needle (22-23 ga Ø) and incubated on ice for 15 min. The cells were homogenized by sonication (10-15 sec on ice), centrifuged, and the supernatants collected for total protein content analysis and stored at -80°C in the sample buffer. Hsp70 expression was determined according to Urani and co-workers (2007) by immunochemical analysis separating 30 µg of proteins on

7% Tris-acetate NuPAGE gels (Invitrogen, Carlsbad, CA, USA). Separated proteins were transferred onto nitrocellulose membranes, and the membranes were blocked for 2 h in Tween buffer (0.1% Tween-20, 8 mM NaN_3, in PBS) containing 5% BSA. A mouse monoclonal anti-hsp70 antibody (Enzo Life Sciences, Switzerland cat. ADI-SPA-810-D) was used for protein detection. The protein bands were visualized after the secondary antibody (goat anti-mouse phosphatase-conjugate) reaction and addition of the colorimetric substrate. The equal sample loading was assessed by staining the gels of the same samples with Coomassie Blue.

Protein levels were quantified by densitometric analysis using the Scion Image software (Scion Corp., Frederick, MD, USA). Densitometric data of MT and Hsp70 proteins of at least three biological replicates were analyzed and the statistical comparison performed.

10.2.5 Statistical analysis

Densitometric data from western blot and the relative fold changes from qPCR were tested by Dunnett's multiple comparison procedure. All calculations were conducted using the R statistical programming environment. All treated samples were compared to their reference controls.

❖ 10.3. Results

10.3.1 Cadmium induces a strong deregulation of specific transcripts

A total of 85 genes were significantly up-regulated, and 11 genes were down-regulated (ANOVA limma, p value adjusted by the Benjamini and Hochberg's method equals or smaller than 0.05) (Smyth, 2004). The first 25 up-regulated genes are shown in Table 10.1 with log2 fold changes values and statistical significance (adjusted p value). Table 10.2 shows all down-regulated genes. The complete list and description of 96 differentially expressed genes is found in supplementary materials (Table 10.1S). A major group of up-regulated genes is the metallothioneins (*MT*) family, with (sub)isoforms of *MT-1* and *MT-2* highly up-regulated (up to around 10 log2 fold change, FC) by both 10 and 20 µM Cd. MTs are proteins involved in metalloregulatory processes, and highly inducible by Zn and Cd (Choi and Bird, 2014). *HMOX1* is amongst the top up-regulated genes with *MT* in SH-SY5Y cells exposed to Cd. This gene encodes for heme-oxygenase-1 (HO-1), which is of keen research interest as it is considered to be a major protein in diseases caused by oxidative and inflammatory insults, with a role in contrasting stressful events. HO-1, which is the stress-inducible isozyme of heme oxygenase, catalyzes the breakdown of heme into free ferrous iron (Fe^{2+}), biliverdin, and carbon monoxide. Fe^{2+} stimulates the synthesis of ferritin (iron-bound-compound), biliverdin is converted to bilirubin, all being cytoprotective compounds. A group of up-regulated and stress-related genes is represented by *ZFAND2A, HSPA1A, HSPA6, HSPA1B, DNAJB1* coding for heat shock-related proteins, belonging to a superfamily of cytoprotective chaperones, dealing with proteotoxic stress (Kostenko et al., 2014; Rossi et al., 2010). Furthermore, the product of growth arrest and DNA damage response 45*β* (*GADD45β*) gene involved in cell growth arrest and DNA repair, and recently described as a regulatory protein, controlling autophagy and apoptosis in rat cerebral neurons (He et al., 2016), is among the highest up-regulated genes. Another protein with pro-apoptotic properties is encoded by *DDIT3* gene, also known as CCAAT/enhancer binding homologous protein (CHOP)/GADD153 (Syk-Mazurek et al., 2017).

TEX19, AKR1C3, TGFBI, GDF15 and RRAD up-regulated genes are all coding for proteins related to cancer, cancer cell proliferation, and enhancement of tumor initiation representing, in some cases, prognostic biomarkers (see as examples Planells-Palop et al., 2017; Karunasinghe et al., 2017; Pan et al., 2018, Li et al., 2016; Yeom et al., 2014). *S100A2* is a gene coding for a member of the S100 proteins, a family of regulatory, calcium-binding-proteins that mediate signal transduction in the nervous system. S100 family members are involved in different diseases such as psoriasis, rheumatoid arthritis, cystic fibrosis, cardiomyopathy, multiple sclerosis, amyotrophic lateral sclerosis, Down's syndrome, Alzheimer's disease and cancer (Zimmer et al., 2005). All down-regulated genes are shown in Table 10.2. Even though 10 µM Cd has a weak effect on gene down-regulation, it is interesting to note the trend of increasing down-regulation relevant at the highest concentration used. Analyzing all down-regulated genes, *SLC35D* is the top down-regulated with a log2 fold change of -2,15 at 20 µM Cd concentration. This gene in mouse is specifically expressed in the brain, suggesting a functional role in the central nervous system. The gene is predicted to code for an orphan nucleotide sugar transporter or a fringe connection-like protein with transmembrane domains (Zhang et al., 2014). Another down-regulated gene related to transporter functions is *SLC39A10*. This gene encodes for a member of the Zip proteins, a family of import Zn^{2+} transporters (Landry et al., 2019). *GALNT6* encodes for the polypeptide *N*-acetylgalactosaminyltransferase 6, critical for the stability, subcellular localization, and anti-apoptotic function of GRP78 protein in cancer cells (Lin et al., 2017). Little is known about *GLCCI1,* glucocorticoid-induced transcript 1, in the central nervous system, recently proposed as a tool to identify progenitors in the ventricular zone during telencephalon development (Kohli et al., 2018). Even though the general functions of this gene are unclear, this cortical-response gene plays a role in regulating the sensitivity to endogenous cortisol in humans (Liu et al., 2017 and references therein). Very interestingly, among the down-regulated genes, a group of Cd-targeted genes encodes for neuronal-related proteins: *GREM2* codes for a member of the gremlin protein family, described as neuroprotective factors in dopaminergic neurons both *in vivo* and *in vitro* (Phani et al., 2013); the product of *Nek3* influences neuronal morphogenesis and polarity through effects on microtubules as this protein belongs to a Ser/Thr kinases involved in coordinating microtubule dynamics (Chang et al., 2009); *Kif15* product belongs

to the kinesins superfamily of microtubule-based motor proteins, particularly expressed in neurons undergoing migration and in the developing brain (Klejnot et al., 2014). Finally, a group of down-regulated genes produces transcripts related to carcinogenesis: *UNG*, that encodes for uracil-DNA glycosylase protein responsible for the initial step in the base excision repair pathway (Gokey et al., 2016); *PDGFRL*, the platelet-derived growth factor receptor-like gene is regarded as a tumor suppressor, although the precise biological function is not known (Kawata et al., 2017); *TXNIP* gene encodes for a potent tumor suppressor protein, and its down-regulation leads to increased proliferation of certain types of cancer cells (Park et al., 2018).

Table 10.1. Top up-regulated genes in SH-SY5Y cells treated with 10 or 20 μM Cd for 48 h

Gene	Cd10 μM log2 fold change	Cd20 μM log2 fold change	adj.P.Value	Description
MT1M	9,71	9,92	2,61E-05	metallothionein 1M
MT1X	7,11	7,53	7,53E-05	metallothionein 1X
MT1F	7,10	7,37	8,98E-05	metallothionein 1F
MT1L	7,04	7,43	3,84E-05	metallothionein 1L (gene/pseudogene)
MT1HL1	6,95	7,42	3,84E-05	Metallothionein 1H-like protein 1
MT1B	6,74	7,25	2,61E-05	metallothionein 1B
ENST00000567054	6,63	7,02	3,84E-05	metallothionein 1C (pseudogene)
HMOX1	6,08	7,26	0,001731748	heme oxygenase (decycling) 1
MT2A	5,42	5,45	0,000160204	metallothionein 2A
MT1A	4,92	5,29	0,00014948	metallothionein 1A
GADD45β	4,82	7,05	0,000545108	growth arrest and DNA-damage-inducible, beta
MT1E	3,95	4,15	0,000250941	metallothionein 1E
ZFAND2A	3,64	5,20	0,006524353	zinc finger, AN1-type domain 2A
TEX19	3,47	4,15	0,003753672	testis expressed 19
GDF15	3,24	4,22	0,002993824	growth differentiation factor 15
AKR1C3	2,94	3,14	0,002993824	aldo-keto reductase family 1, member C3 (3-alpha hydroxysteroid dehydrogenase, type II)
TGFBI	2,90	3,59	0,013115332	transforming growth factor, beta-induced, 68kDa
MT1G	2,70	3,36	0,034682665	metallothionein 1G
HSPA1A	2,67	4,38	0,005651168	heat shock 70kDa protein 1A
HSPA6	2,53	4,36	0,000545108	heat shock 70kDa protein 6 (Hsp70B')
RRAD	2,53	4,24	0,00208082	Ras-related associated with diabetes
HSPA1B	2,29	4,10	0,014428639	heat shock 70kDa protein 1B
DNAJB1	2,23	3,57	0,001731748	DnaJ (Hsp40) homolog, subfamily B, member 1
DDIT3	2,21	3,45	0,000545108	DNA-damage-inducible transcript 3
S100A2	1,98	2,91	0,001731748	S100 calcium binding protein A2

Table 10.2. Complete list of down-regulated genes in SH-SY5Y cells treated with 10 or 20 µM Cd for 48 h.

Gene	Cd10 µM log2 fold change	Cd20 µM log2 fold change	adj.P.Value	Description
SLC35D3	-1,41	-2,15	0,03018534	solute carrier family 35, member D3
GREM2	-1,02	-1,32	0,02198818	gremlin 2
SLC39A10	-0,88	-1,07	0,04704006	solute carrier family 39 (zinc transporter), member 10
GLCCI1	-0,84	-1,42	0,02971039	glucocorticoid induced transcript 1
GALNT6	-0,82	-1,48	0,03741771	UDP-N-acetyl-alpha-D-galactosamine:polypeptide N-acetylgalactosaminyltransferase 6 (GalNAc-T6)
NEK3	-0,77	-1,28	0,04518064	NIMA (never in mitosis gene a)-related kinase 3
UNG	-0,72	-1,00	0,04826738	uracil-DNA glycosylase
TXNIP	-0,65	-1,77	0,01403976	thioredoxin interacting protein
LOC642366	-0,53	-1,24	0,04997033	uncharacterized LOC642366
PDGFRL	-0,51	-1,53	0,02586179	platelet-derived growth factor receptor-like
KIF15	-0,42	-1,09	0,03768701	kinesin family member 15

10.3.2 Most deregulated genes show a concentration-dependence profile

All deregulated genes and their trends are shown in Figure 1. The ninety-six differentially expressed genes (p adj ≤ 0.05, ANOVA limma) in Cd-treated *vs* control samples are shown in the heat map of Figure 10.1A. After clustering these significant genes, a first cluster of 11 highly down-regulated genes (*SLC35D3*, *PDGFRL*, *TXNIP*, *KIF15*, *LOC6442366*, *UNG*, *SLC39A10*, *GREM2*, *NEK3*, *GALNT6* and *GLCCI1*) was observed. A second cluster of 11 strongly up-regulated genes (*MT1X*, *MT1F*, *MT1L*, *MT1HL1*, *MT1B*, *MT1A*, *MT2A*, *MT1M*, GADD45β, *HMOX1* and *ENST00000567054*) was also found. In addition to these highly significant genes, a third cluster was made of 74 genes found to be up-regulated with lower log2 fold changes (Figure 10.1A). It is worth noting that a Cd concentration-dependence was observed for most of these 96 deregulated genes (Figure 10.1B). The highest Cd concentration tested (i.e 20 µM) resulted in a more pronounced log2 fold change when compared to 10 µM Cd-treatment. When using a cut-off at an absolute log2 fold change of 3 (for any of the two tested concentrations), the highly significant genes in clusters 1 and 2 (Figure 10.1A) showed such concentration-dependence (Figure 10.1B). In addition, 15 up-regulated genes from cluster 3 also showed a concentration-dependence profile (namely, *MT1E*, *MT1G*, *HSPA1A*, *HSPA1B*, *HSPA6*, *ZFAND2A*, *RRAD*, *GDF15*, *TEX19*, *MLC1*, *TGFBI*, *DNAJB1*, *ZNF165*, *DDIT3* and *AKRC3*).

Figure 10.1. Toxicogenomics analysis of cadmium on SH-SY5Y cells. (A) Heatmap of differentially expressed genes after cadmium treatment The log2 fold changes of differentially expressed genes (p adj ≤ 0.05, ANOVA-limma adjusted for multiple comparisons according to the Benjamini-Hochberg method), are represented in the heatmap for three replicates of Cd-treated samples (10 and 20 µM 48 h). Red color represents up-regulated genes when compared to control conditions, whereas blue color is used for down-regulated genes. The gene names are shown on the right side of the heatmap and the treatment conditions are indicated at the bottom part. On the left, the hierarchical clustering of the genes (see the text for details).(B) Dose dependence of 96 differentially expressed genes. The log2 fold changes of the ninety-six genes found to be differentially expressed after cadmium treatment (p adj ≤ 0.05, ANOVA-limma) are plotted, with the cadmium concentration on the x-axis and the log2 fold change on the y-axis. Each line connects the log2 fold changes observed at the two concentrations tested (10 and 20 µM). The name of genes with an absolute log2 fold change that are higher than 3, are indicated, corresponding to eleven down-regulated and twenty-six up-regulated genes. The up-regulated genes are separated from the down-regulated genes by a horizontal dashed line at log2 fold change = 0. Figure in the next page.

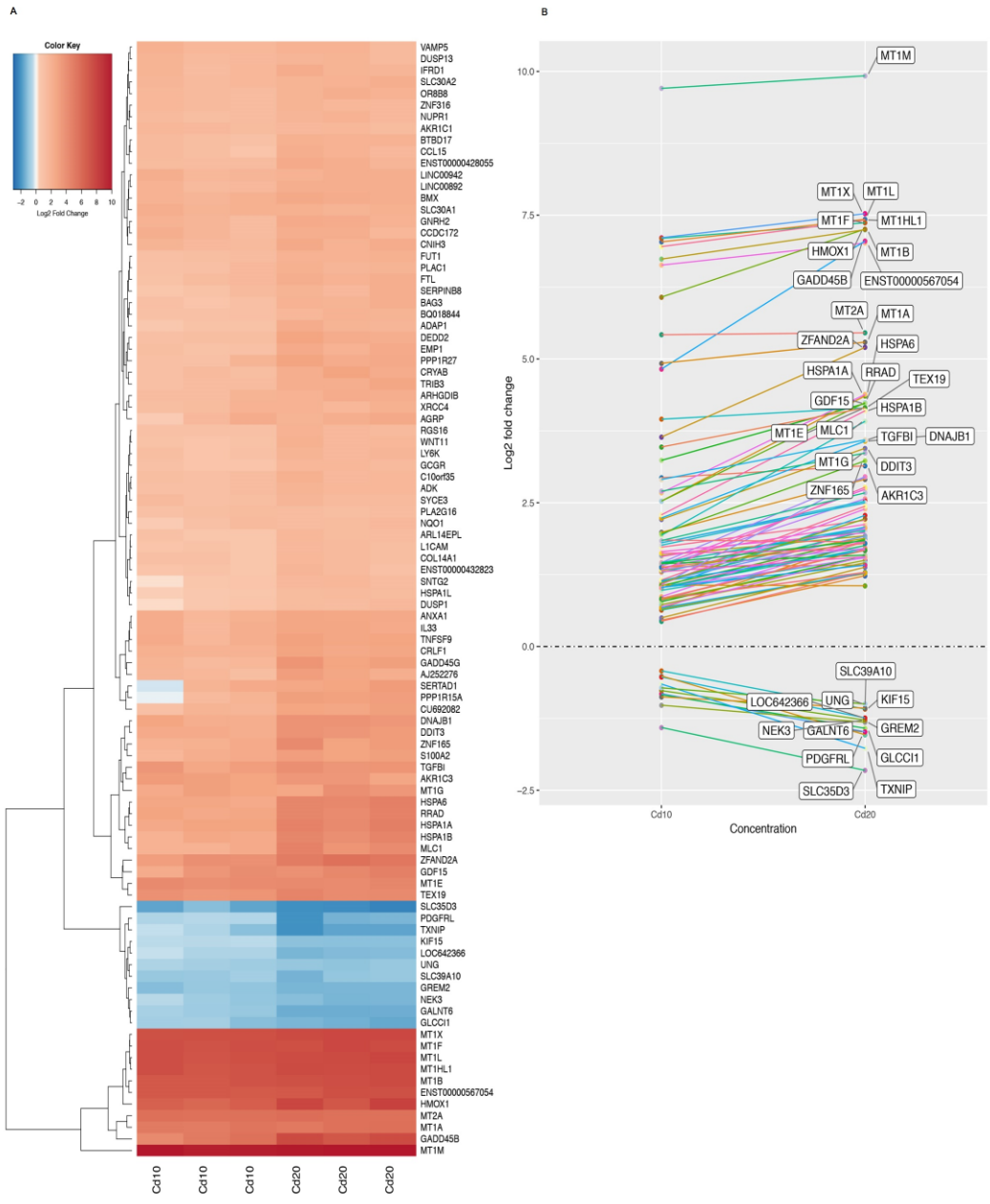
A
Color Key
−2 0 2 4 6 8 10
Log2 Fold Change
VAMP5
DUSP13
IFRD1
SLC30A2
OR8B8
ZNF316
NUPR1
AKR1C1
BTBD17
CCL15
ENST00000428055
LINC00942
LINC00892
BMX
SLC30A1
GNRH2
CCDC172
CNIH3
FUT1
PLAC1
FTL
SERPINB8
BAG3
BQ018844
ADAP1
DEDD2
EMP1
PPP1R27
CRYAB
TRIB3
ARHGDIB
XRCC4
AGRP
RGS16
WNT11
LY6K
GCGR
C10orf35
ADK
SYCE3
PLA2G16
NQO1
ARL14EPL
L1CAM
COL14A1
ENST00000432823
SNTG2
HSPA1L
DUSP1
ANXA1
IL33
TNFSF9
CRLF1
GADD45G
AJ252276
SERTAD1
PPP1R15A
CU692082
DNAJB1
DDIT3
ZNF165
S100A2
TGFBI
AKR1C3
MT1G
HSPA6
RRAD
HSPA1A
HSPA1B
MLC1
ZFAND2A
GDF15
MT1E
TEX19
SLC35D3
PDGFRL
TXNIP
KIF15
LOC642366
UNG
SLC39A10
GREM2
NEK3
GALNT6
GLCCI1
MT1X
MT1F
MT1L
MT1HL1
MT1B
ENST00000567054
HMOX1
MT2A
MT1A
GADD45B
MT1M
Cd10
Cd10
Cd10
Cd20
Cd20
Cd20
B
10.0
7.5
5.0
2.5
0.0
−2.5
Log2 fold change
MT1M
MT1X
MT1L
MT1F
MT1HL1
HMOX1
MT1B
GADD45B
ENST00000567054
MT2A
MT1A
ZFAND2A
HSPA6
HSPA1A
RRAD
TEX19
GDF15
HSPA1B
MT1E
MLC1
TGFBI
DNAJB1
MT1G
DDIT3
ZNF165
AKR1C3
SLC39A10
LOC642366
UNG
KIF15
NEK3
GALNT6
GREM2
PDGFRL
GLCCI1
SLC35D3
TXNIP
Cd10
Cd20
Concentration

10.3.3 Mineral absorption, cancer related and glycosphingolipid biosynthesis pathways are the main pathways perturbed by cadmium

Ensemble of Gene Set Enrichment Analyses (EGSEA) was applied to determine the KEGG pathways perturbed by Cd treatment. At 10 µM, the five most important pathways, as determined by their low median ranks across ten methods performed by EGSEA, were: p53 signaling pathway, mineral absorption, glycosphingolipid biosynthesis, basal cell carcinoma and endometrial cancer (p adj ≤ 0.05, Wilcoxon rank sum test adjusted by the Benjamini and Hochberg's procedure) (Figure 10.2A). The individual ranks attributed to the KEGG pathways by each method are reported in Supplementary Table 10.2S. At 20 µM Cd, the seven most perturbed KEGG pathways were: Fanconi anemia pathway, mineral absorption, p53 signaling pathway, legionellosis, rheumatoid arthritis, homologous recombination and glycosphingolipid biosynthesis (Figure 10.2B). The ranks of the KEGG pathways are detailed in Supplementary Table 10.3S.

Figure 10.2. EGSEA of KEGG pathways after cadmium treatment. The x-axis shows the -log10 of the EGSEA Wilcoxon p value adjusted for multiple comparisons of the KEGG pathways, and the y-axis represents the average of the absolute log2 fold changes of the genes present in each of these pathways. A collection of 285 KEGG pathways with a minimum size of 5 genes was considered for EGSEA. The limma test was used by EGSEA to determine the log2 fold changes of genes after treatment with 10 (**panel A**) or 20 (**panel B**) µM of cadmium. A bigger dot is used for KEGG pathways of lower median ranks observed across ten methods performed by EGSEA. The vertical dashed line at -log10 (padj) = 1.3 corresponds to a false discovery rate of 0.05. Red color is used for up-regulated KEGG pathways whereas blue color represents down-regulated pathways. Figures in the next page.

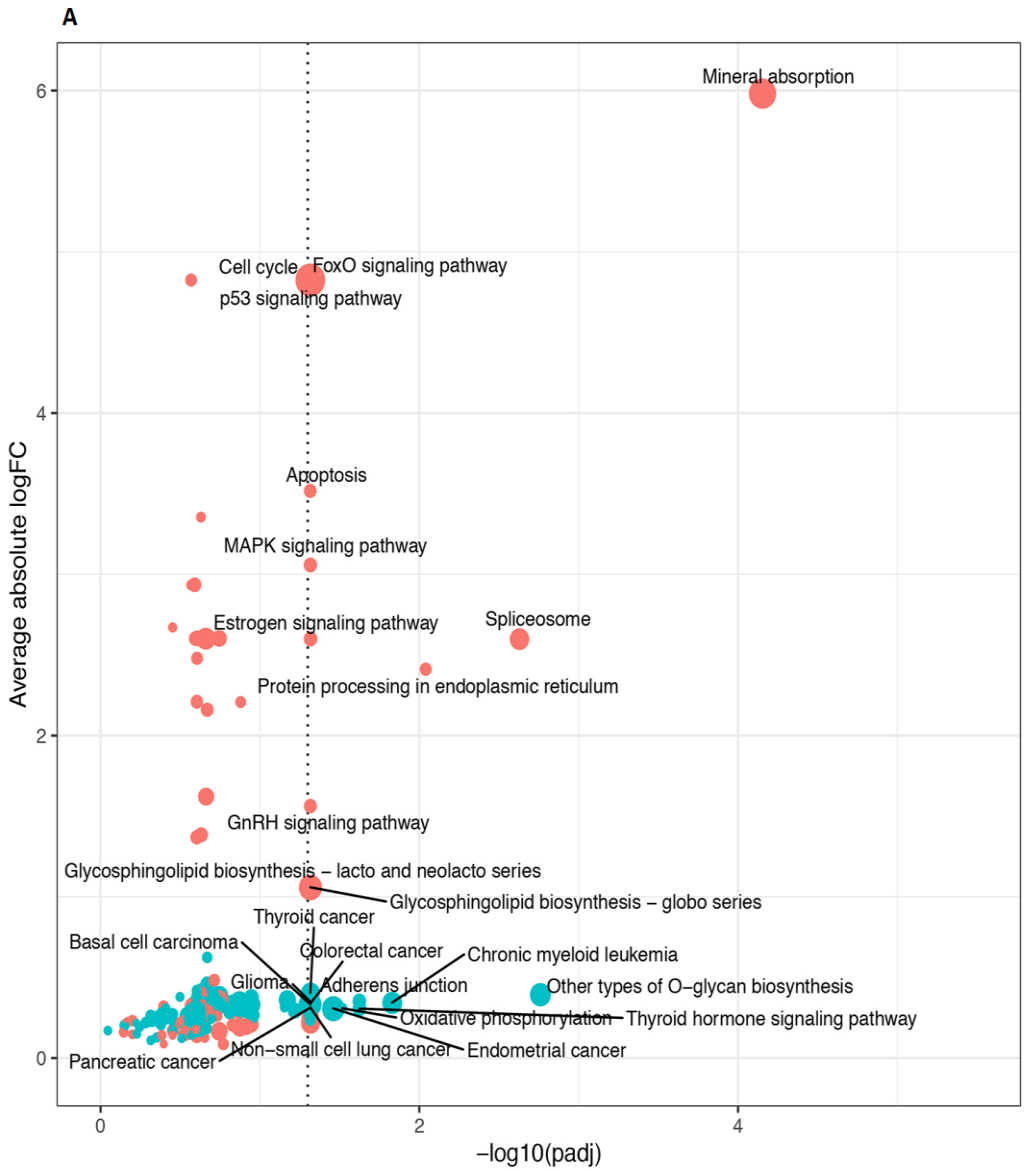
A
Mineral absorption
Cell cycle
FoxO signaling pathway
p53 signaling pathway
Apoptosis
MAPK signaling pathway
Estrogen signaling pathway
Spliceosome
Protein processing in endoplasmic reticulum
GnRH signaling pathway
Glycosphingolipid biosynthesis – lacto and neolacto series
Glycosphingolipid biosynthesis – globo series
Thyroid cancer
Basal cell carcinoma
Colorectal cancer
Chronic myeloid leukemia
Glioma
Adherens junction
Other types of O–glycan biosynthesis
Oxidative phosphorylation
Thyroid hormone signaling pathway
Pancreatic cancer
Non–small cell lung cancer
Endometrial cancer
Average absolute logFC
–log10(padj)
0
2
4
6
0
2
4

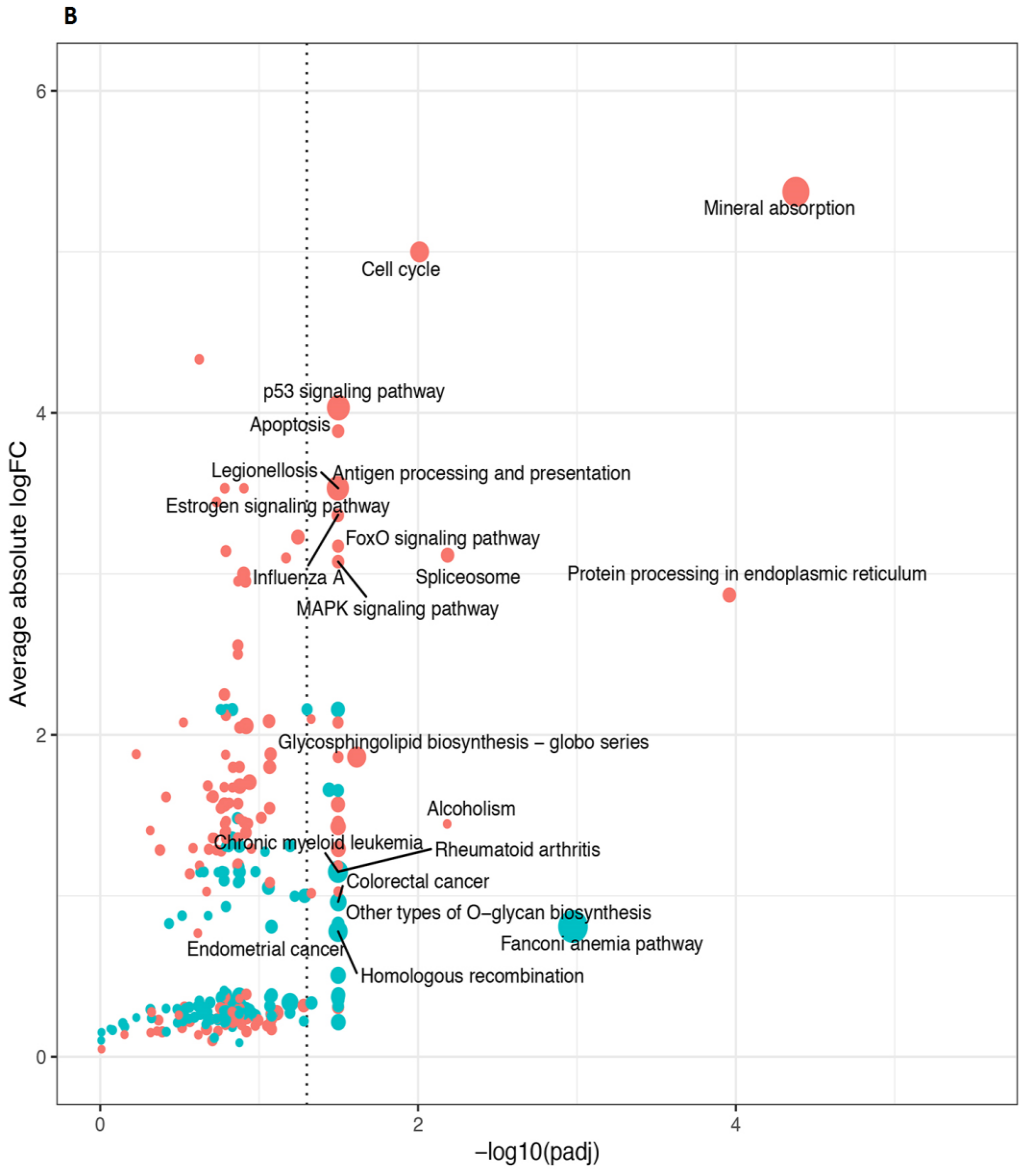
B
Average absolute logFC
−log10(padj)
0
2
4
6
Mineral absorption
Cell cycle
p53 signaling pathway
Apoptosis
Legionellosis
Antigen processing and presentation
Estrogen signaling pathway
FoxO signaling pathway
Influenza A
Spliceosome
Protein processing in endoplasmic reticulum
MAPK signaling pathway
Glycosphingolipid biosynthesis – globo series
Alcoholism
Chronic myeloid leukemia
Rheumatoid arthritis
Colorectal cancer
Other types of O–glycan biosynthesis
Fanconi anemia pathway
Endometrial cancer
Homologous recombination

Three KEGG pathways are in common when comparing the two Cd concentrations used. The path views for these three pathways, mineral absorption, p53 signaling pathway and glycosphingolipid biosynthesis, highlight some important genes that are altered by Cd (Figure 10.3). For the mineral absorption, the up-regulation of metallothioneins (*MT1 and MT2 isoforms*), HMOX (*HMOX1*), ZnT1 (*SLC30A1*), Zip4 (*SLC39A4*) and ferritin heavy chain 1 (*FTH1*) was observed, whereas down-regulation of heme carrier protein 1 (*HCP1/SLC46A1*) and ferroportin (*FPN1/SLC40A1*) was found (Figure 10.3A). In the p53 signaling pathway, there is up-regulation of Gadd45 (*GADD45A/B/G*), p21 (*CDKN1A*), Noxa (*PMAIP1*) and the Sestrins (*SESN2*) (Figure 10.3B). In addition to *p21*, *CDK6* is another gene present in the cell cycle module of the p53 signaling pathway and found to be down-regulated. When looking at the cell cycle pathway itself, we observed down-regulation of additional genes such as *EP300*, *MCM* (2 to 10), and *E2F* (1 to 8) (Supplementary Figure 10.1S). The importance of cancer related pathways is further highlighted by the endometrial cancer pathway, containing the p53 signaling and cell cycle modules but also the PI3K-Akt signaling pathway. In this latter pathway, there was down-regulation of PI3K (*PIK3CA*) and PKB (*AKT1*) (Supplementary Figures 10.1S). Of interest, the homologous recombination pathway was also found significant, driven by down-regulation of *RAD50*, *RAD51* and *RAD54L* subunits, and of the catalytic subunit of DNA polymerase epsilon (*POLE*) (Supplementary Figure 10.1S). Another cancer related pathway, i.e basal cell carcinoma, was also revealed by EGSEA. This pathway contains the p53 signaling and the cell cycle modules, but also the Wnt signaling pathway (Supplementary Figure 10.1S). In this pathway, Wnt (*WNT2, 7A, 8A, 10B, 11*) were up-regulated after Cd treatment, whereas Frizzled (*FZD1*), TCF/LEF (*TCF7, TCF7L1, TCF4, LEF1*) were down-regulated. In the glycosphingolipid biosynthesis pathway, we found up-regulation of fucosyltransferase 1 (*FUT1*/ KEGG enzyme 2.4.1.69), beta-hexoaminidase (*HEXA* and *HEXB*, KEGG enzyme 3.2.1.52) and alpha-galactosidase (*GLA*/KEGG enzyme 3.2.1.22). This large group of complex lipids is particularly abundant in the outer layer of neuronal plasma membranes. Overall, the EGSEA shows that Cd is targeting three important pathways (mineral absorption, p53 signaling and glycosphingolipid biosynthesis pathways), with “mineral absorption” likely representing the most direct effects of Cd on human neuronal cells.

Figure 10.3. Path views of three significant KEGG pathways altered by 20 µM cadmium. The comparison of microarray data between cells treated with 20 µM cadmium and controls was made using limma. The mineral absorption (A), p53 signaling pathway (B), and glycosphingolipid biosynthesis pathway (C), are shown with the log2 fold changes of genes layered onto the native KEGG pathway views. A red color illustrates up-regulated genes, whereas blue represents down-regulated genes, when compared to control cells.

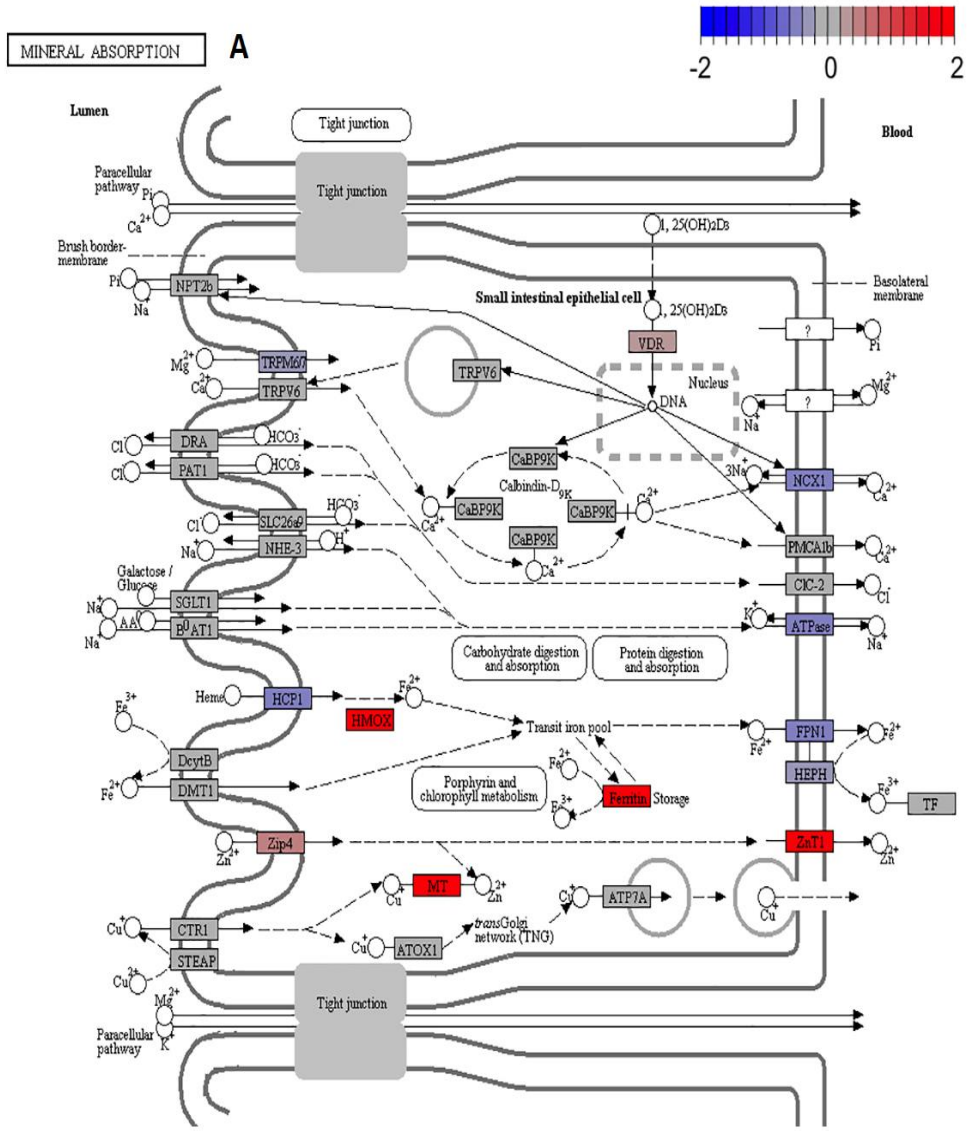

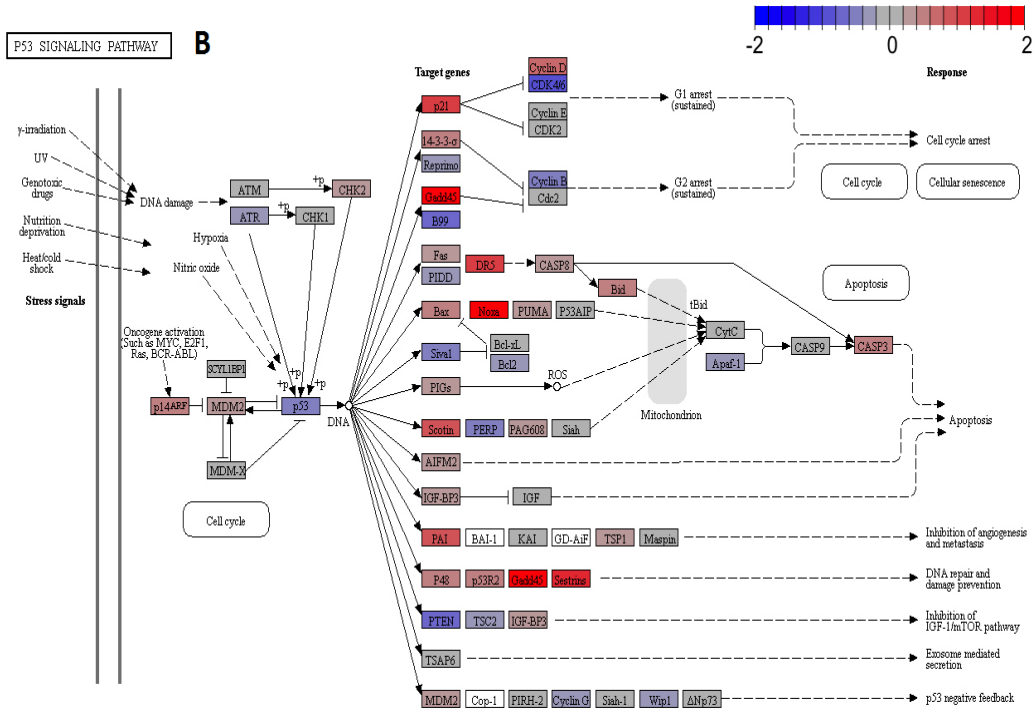
P53 SIGNALING PATHWAY
B
-2
0
2
Target genes
Response
γ-irradiation
UV
Genotoxic drugs
Nutrition deprivation
Heat/cold shock
Stress signals
DNA damage
ATM
ATR
CHK2
CHK1
Hypoxia
Nitric oxide
Oncogene activation (Such as MYC, E2F1, Ras, BCR-ABL)
p14ARF
MDM2
p53
DNA
MDM-X
Cell cycle
Cyclin D
CDK4/6
p21
Cyclin E
CDK2
14-3-3-σ
Reprimo
Gadd45
B99
Cyclin B
Cdc2
G1 arrest (sustained)
G2 arrest (sustained)
Cell cycle arrest
Cell cycle
Cellular senescence
Fas
PIDD
DR5
CASP8
Bid
Apoptosis
Bax
Noxa
PUMA
P53AIP
tBid
CytC
Apaf-1
CASP9
CASP3
Sivai
Bcl-xL
Bcl2
PIGs
ROS
Mitochondrion
Scotin
PERP
PAG608
Siah
Apoptosis
AIFM2
IGF-BP3
IGF
PAI
BAI-1
KAI
GD-AIF
TSP1
Maspin
Inhibition of angiogenesis and metastasis
P48
p53R2
Gadd45
Sestrins
DNA repair and damage prevention
PTEN
TSC2
IGF-BP3
Inhibition of IGF-1/mTOR pathway
TSAP6
Exosome mediated secretion
MDM2
Cop-1
PIRH-2
Cyclin G
Siah-1
Wip1
ΔNp73
p53 negative feedback

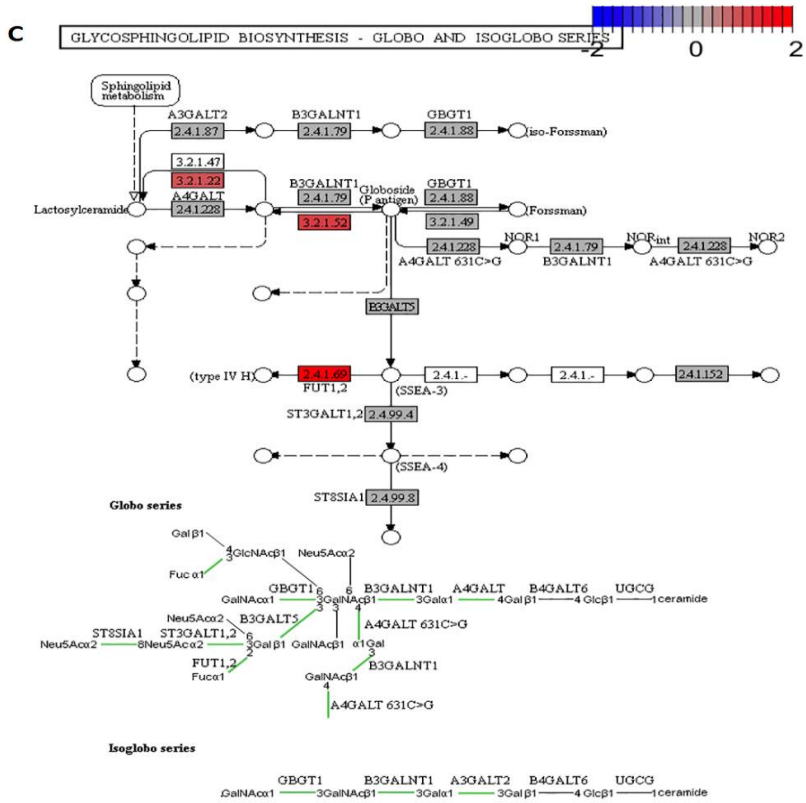
C
GLYCOSPHINGOLIPID BIOSYNTHESIS - GLOBO AND ISOGLOBO SERIES
-2
0
2
Sphingolipid metabolism
A3GALT2
2.4.1.87
B3GALNT1
2.4.1.79
GBGT1
2.4.1.88
(iso-Forssman)
3.2.1.47
3.2.1.22
A4GALT
2.4.1.228
Lactosylceramide
Globoside (P antigen)
(Forssman)
3.2.1.52
3.2.1.49
NOR1
NOR int
NOR2
A4GALT 631C>G
B3GALT5
(type IV H)
FUT1,2
(SSEA-3)
ST3GALT1,2
2.4.99.4
(SSEA-4)
ST8SIA1
2.4.99.8
Globo series
Isoglobo series
GalNAcα1
GalNAcβ1
Galα1
Galβ1
GlcNAcβ1
Glcβ1
ceramide
Neu5Acα2
Fucα1
A4GALT
B4GALT6
UGCG

10.3.4 Metallothioneins and the heat shock response are the earliest cytoprotective mechanisms against cadmium

MT-I and –II are highly inducible isoforms of cytoprotective proteins, as clearly demonstrated by our transcriptomics data (see Table 10.1) and protein expression (Figure 10.4). Western blots, followed by densitometric analyses of MT-I and –II protein levels revealed a strong a dose-dependent increase with 25 and 40 mean fold changes after treatment with 10 and 20 μM Cd, respectively (Figure 10.4).

Figure 10.4. Metallothioneins expression in cadmium-treated SH-SY5Y cells. Metallothionein (MT-I, -II) expression (A) is highly induced in SH-SY5Y cells exposed to 10 and 20 μM Cd for 48 h. Very low, undetectable levels of MT are present in the controls (CTR), whereas Cd treated cells show a dose-dependent increase of protein expression, confirmed by the relative protein expression measured by densitometry analyses (B). ***Significantly different from control ($p<0.001$) (Dunnett's test).

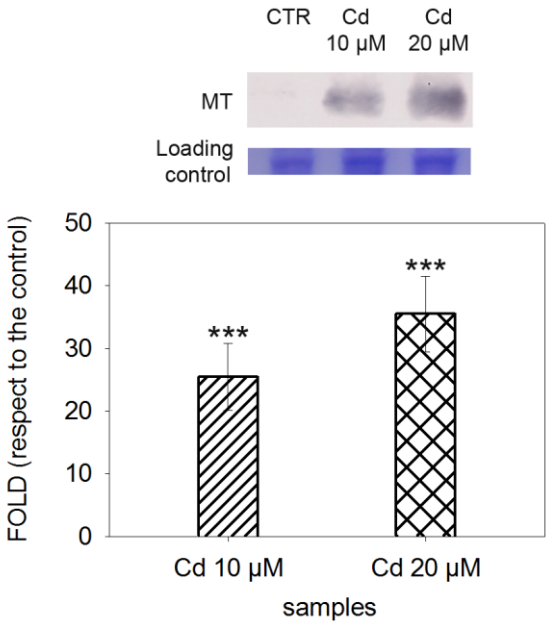

We observed a similar response for Hsp70, which represents one of the highly conserved and inducible heat shock family members. As for MTs, Hsp70 protein expression (Figure 10.5) follows a dose-dependent pattern. In accordance with previous data (Kostenko et al., 2014), showing that members of DNAJ/Hsp40 family are involved in recruiting chaperone Hsp70, we found *DNAJB1*, a *DNAJ/Hsp40 homolog*, to be upregulated following treatment with both 10 and 20 μM Cd (see par. 10.3.1, and Table 10.1).

Figure 10.5. Heat shock protein 70 expression in cadmium-treated SH-SY5Y cells. (A) High constitutive levels of Hsp70 are present in controls (CTR), and are increased by Cd treatment (10 and 20 μM). (B) The increased expression is confirmed by densitometry analysis and reveals a significant difference between CTR and treated samples. ***Significantly different from control ($p<0.001$) (Dunnett's test).

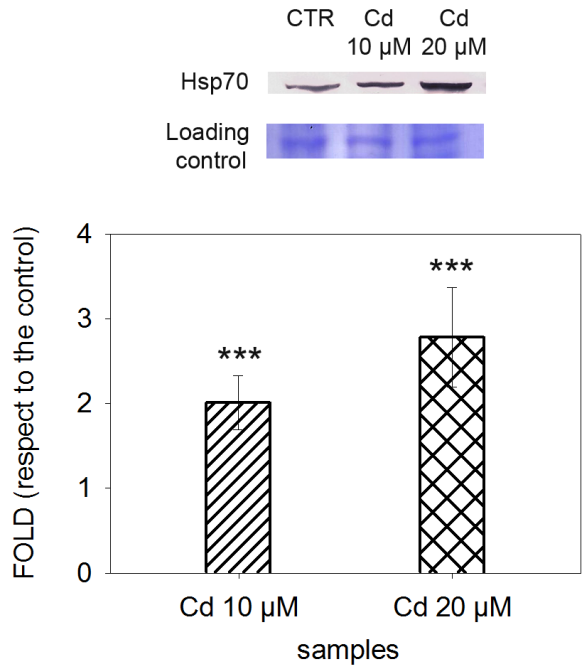

Along with immunochemical results on MT and Hsp70 protein expression, the expression of *GADD45β*, *HMOX-1*, and *S100A2* genes assessed by qPCR (Figure 10.6), strongly supports and validates transcriptomics results, showing an increased expression of both *GADD45β*, *HMOX-1* and, to a less extent, of *S100A2 mRNA.*

Figure 10.6. Relative quantification of GADD45β, HMOX1 and S100A2 mRNA levels by real time quantitative PCR. The relative expression levels were expressed as a fold change ± SE, using β-ACT gene as internal reference control and SHSH5Y cells not treated with Cd (control) as calibrator. Values are presented as means of three different experiments. ** Significantly different from control ($p<0.01$); ***significantly different from control ($p<0.001$) (Dunnett's test).

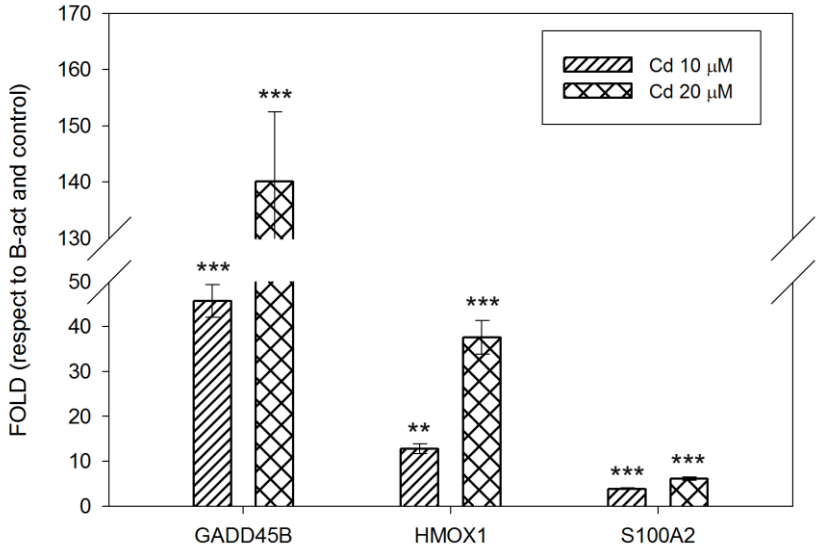

❖ 10.4. Discussion and Conclusions

Epidemiological and experimental studies have linked cadmium exposure to impaired functions of the nervous system and to neurodegenerative diseases, such as Alzheimer's disease and Parkinson's disease (Wang and Du, 2013), and to increased risk of developing ALS (Wang et al., 2017; Sheykhansari et al., 2018). However, its involvement in neurodegeneration and neurodegenerative-related mechanisms has been highly neglected, despite the increasing number of papers referring to Cd toxic effects on the neuronal system. Our results on SH-SY5Y cells, a human neuronal model, provide the evidence of neurotoxic mechanisms of cadmium, which could represent key triggers in the neurodegenerative process. This toxic metal is widely studied to unravel the mechanisms of its carcinogenicity (see for example Chen et al., 2019; Fabbri et al., 2012; Forcella et al., 2016; Hartwig, 2018). Our results on human SH-SY5Y neuronal cells confirm that cadmium induces the expression of genes belonging to a carcinogenic effect even on brain-derived cells. These cells respond to Cd exposure by activating e.g., the p53 signaling pathway, involved in cell cycle arrest upon stress signals and associated with cancer (see for example Joerger and Fersht, 2016), and genes involved in tumor initiation and cancer cell proliferation (*TEX19, AKR1C3, TGFB1,* and *RRAD)*, or down-regulating tumor suppressors (*PDGFRL, TXNIP*), or enzymes involved in the initial step of DNA repair (*UNG*). All these conditions create an environment susceptible to carcinogenesis. The SH-SH5Y neuronal cells exposed to Cd respond to the metal-induced stress by activating two major defense mechanisms, namely the heat shock proteins (Hsp), and the metallothioneins (MT). Both MT and Hsp represent the first line of defense against cadmium and metals in general. Multiple functions, including the involvement of Zn and Cu homeostasis, protection against metal toxicity and oxidative damage, are associated to MT (Babula et al., 2012). The heat shock response has evolutionary evolved as a cell defense mechanism to maintain proteostasis and restore perturbed protein homeostasis. The Hsp are mainly involved in the assistance of refolding or degrading intracellular proteins injured upon stress. The modulation of these defense mechanisms is a response evidenced in mammalian cells, both in cadmium target (e.g., hepatic, kidney and bronchial cell models) and in non-target tissues, such as Sertoli and brain cells (Bonham et al., 2003; Han et al.,

2007; Hung et al., 1998; Luparello et al., 2011; Kusakabe et al., 2008; Urani et al., 2007, 2010). The high response of different family members of heat shock proteins, visualized both as increased protein (Hsp70) expression and as transcripts (*HSPA1A*, *HSPA6*, *HSPA1B*, *DNAJB1*) in our samples exposed to cadmium, shows the need of these molecular chaperones to refold mis-folded proteins and/or degrade damaged or aggregated ones. The perturbation of protein homeostasis and protein folding, aggregation and degradation may lead to accelerated ageing and the incidence of proteotoxicity-triggered disorders, all hallmarks of a number of neurodegenerative diseases, including ALS (Barna et al., 2018; Kalmar et al., 2014). In addition, many proteins arising and/or aggregating during neurodegeneration include, among others, beta-amyloid, tau and heat shock proteins, which act as danger-associated molecular patterns that compromise neuronal functions and cause cell death (Ardura-Fabregat et al., 2017). MT are Zn-bound low molecular weight proteins (<7 KDa), which have a major role in the maintenance of metal homeostasis, mainly Zn and Cu, with their α- and β-cluster domains responsible for the binding of up to seven metals. The Zn-bound form of MT is an anti-oxidant agent, as the Zn-sulphur cluster is sensitive to changes in the redox state, thus having also a protective role against reactive oxygen species. Zn, after iron, is the second most abundant metal in organisms, playing pivotal roles as structural, catalytic, and signaling component, and as a modulator of synaptic activity and neuronal plasticity. Thus, due to the relative abundance of Zn in the brain, which is protein-bound or compartmentalized to be maintained at very low concentrations, MT are also expected to regulate the intracellular Zn pools in the brain. This function is coordinated with two zinc transporter families, Zrt- and Irt-like proteins (SLC39A), and Zn transporters (ZnT family members) (Méndez-Armenta and Rìos, 2007; Prakash et al., 2015; Kimura and Kambe, 2016). In our model of SH-SY5Y neuronal cells, the highly dose-dependent up-regulation of MT-I and –II proteins represents the immediate response to Cd exposure. In addition, the mineral absorption pathway is the one most significantly perturbed by both Cd concentrations used. Notably, highly up-regulated genes in this pathway are represented by *MTs*, *HMOX1*, *Ferritin*, and *ZnT-1*. The membrane protein encoded by *ZnT-1* gene belongs to a family of Zn transporters, specifically responsible for Zn transport to the extracellular compartments (Kimura and Kambe, 2016), to restore Zn homeostasis and physiological levels. An increased expression of ZnT-1

transporter and of intracellular zinc levels upon Cd exposure were previously demonstrated by our group in human hepatoma cells (Urani et al., 2010 and 2015). In neurons, a role of ZnT-1 transporter in attenuating cadmium and zinc permeation and toxicity, and the increase of Cd^{2+}-induced neuronal death in ZnT-1 siRNA transfected cells was evidenced (Ohana et al., 2006). Very interestingly, strictly linked to Cd effect on Zn transporter discussed above, our results demonstrate that Cd deregulates the expression of genes involved in specific neuronal functions and pathways, giving an overall picture strongly associated to a metal dyshomeostasis and to a damage of neuronal functions and dynamics. Among the top up-regulated genes in our Cd-exposed cells is *HMOX1*, encoding for heme-oxygenase-1 (HO-1). Although beneficial effects of HO-1 as a cytoprotective and anti-inflammatory agent are recognized, an emerging role of increased HO-1 expression in neurodegenerative diseases is evidenced. HO-1 hyperactivity leads to the pathological iron (Fe) deposition recently observed in various neurodegenerative diseases (Wang et al., 2017, and references therein). Other Fe-related functions that we found altered in Cd treated SH-SY5Y cells are related to the increased level of *Ferritin*, as highlighted by path views of mineral absorption. In neuronal cells, iron is mostly bound to ferritin or stored in the lysosomes. A variety of neurodegenerative disorders show disturbances in Fe and/or Cu metabolism and excess loading of these metals. The role of Fe, Cu and Zn in the pathophysiology of ALS was previously highlighted. Both animal and *in vitro* models (Lovejoy and Guillemin, 2014), as well as population studies (Qureshi et al., 2008), evidenced elevated ferritin levels in neurodegenerative processes, and a correlation with toxic metal levels (e.g., As, Pb, Hg, Cd) in human samples from ALS patients, suggesting perturbation in iron metabolism by autophagy dysregulation (Biasiotto et al., 2016). In addition, interference of Cd with Fe ions can be mediated by divalent metal transporter 1 protein (DMT1) and transferrin, two Fe^{2+} transporters which can be used by Cd (Kozlowski et al., 2014). Remarkably, as the mechanisms underlying iron absorption are similar to those of Cd, an iron deficiency leads to increased Cd levels, as demonstrated by population studies (see Lee et al., 2014 and references therein). The interplay and the interference of Cd with other essential metals and ions, are of particular relevance with zinc and calcium, due to their roles in neurotransmission and as signaling elements. Elevation of $[Ca^{2+}]_i$ by Cd in neuronal cells (PC12 and SH-SY5Y), both by extracellular influx and by

intracellular release from Ca^{2+} storage, was previously demonstrated and related to neuronal apoptosis (Xu et al., 2011). One of the 25 top up-regulated genes (*S100A2*) in our cells exposed to cadmium belongs to the highly specialized family of regulatory Ca^{2+}-binding proteins that mediate signal transduction and diseases of the nervous system. Six brain S100 family members, among which is S100A2, are hallmarks of normal aging, and they increase in neurodegenerative disorders (Zimmer eta al., 2005). Notably, an increase of S100B, a S100 family member, has been described in neurodegenerative diseases such as Alzheimer's disease, Parkinson's disease and ALS, and new functions as sensors and regulators of zinc levels, as well as a metal-buffering activity of these binding proteins are emerging (Hagmeyer et al., 2018). Moreover, S100A2 is present in the human genome but not in rat/mouse genomes, illustrating the importance of using human models in neurotoxicity studies (Zimmer et al., 2005). Due to the role of glycosphingolipids in neuronal plasma membrane, the dysregulation of this pathway in SH-SY5Y cells suggests possible modifications in neuronal membrane composition and it is tempting to speculate that it may have consequences on recognition of external messenger(s) and their signal transduction pathways (Aureli et al., 2014). Other remarkable altered genes in our cells exposed to cadmium with neuronal-related functions are *NEK3* and *KIF15*. Nek3 protein belongs to a family of Ser-Thr kinases expressed in neurons with critical roles in coordinating microtubule dynamics. In particular, Nek3 was found to have a role in neuronal morphogenesis and polarity through microtubules effects, suggesting that it could be involved in processes related to axonal projections and degeneration (Chang et al., 2009). Kif15 is a kinesin-related protein, a superfamily of microtubule-based motor proteins with functions ranging from intracellular transport and division. Noteworthy, one member of the kinesin family (KIF5A) was recently identified as a novel gene associated to ALS (Nicolas et al., 2018), strengthening the role of cytoskeletal defects in ALS pathogenesis. The inhibition of microtubule assembly and motility activity of neuronal kinesin were previously demonstrated as consequences of both *in vitro* cadmium exposure and of elevated non-physiological zinc levels, and are proposed as molecular causes contributing to neuronal disorders (Böhm, 2014 and 2017). Other genes that we found among the top up-regulated in SH-SY5Y cells exposed to Cd and relevant for their link to neurodegeneration are *RRAD*, *DDIT3 (*known also as *CHOP)*, and *GDF15*.

RRAD was recently found up-regulated in the *motor cortex* of sporadic ALS patients, *CHOP* has been linked to the activation of apoptosis signaling in neuroblastoma cells, and GDF15 levels in the cerebrospinal fluid is proposed as a potential marker in disorders such as Parkinson's disease and dementia (Sanfilippo et al., 2017; Soo et al., 2012; Maetzler et al., 2016). The results of this study on different molecular components and processes altered provide new insights and links on Cd-induced neurotoxicity, and suggest further in depth studies on remedies to counteract the induced essential metal dyshomeostasis. As concluding remarks, we highlight that toxicogenomics approach is invaluable for mechanistic studies as it provides information on all possible dysregulated genes upon a specific environmental insult. The identification and systematic analysis of up- and down-regulated genes not only provide evidence on functions related to neurodegeneration at a single gene level, but also give a comprehensive vision of possible altered processes. In addition, this analysis will help to clarify whether metal-induced cell deregulations are the consequence rather than the cause of neurodegeneration. Deregulated pathways, even not cell-specific, could represent the early triggers for subsequent metabolic and structural unbalances and for neurodegeneration. Finally, the analysis in a controlled environment and standardized neuronal cell model, and further investigations in more complex models such as co-cultures or 3D models, could help in identifying potential biomarkers to be studied in exposed individuals or in the general population.

Acknowledgements

The Authors acknowledge the University of Milan Bicocca (grant 2016-ATE-0411 to CU and 2017-ATE-0273 to PF) for partial support, and the European Commission. The funding sources had no involvement in data collection, analysis and interpretation, nor in writing and in the decision to submit the article for publication.

References

- Alhamdoosh M, Ng M, Wilson NJ, Sheridan JM, Huynh H, Wilson MJ, Ritchie ME (2017) Combining multiple tools outperforms individual methods in gene set enrichment analyses. Bioinformatics, 33: 414-424. doi: 10.1093/bioinformatics/btw623
- Ardura-Fabregat A, Boddeke EWGM, Boza-Serrano A, Brioschi S, Castro-Gomez S, Ceyzériat K, Dansokho C, Dierkes T, Gelders G, Heneka MT, Hoeijmakers L, Hoffman A, Iaccarino L, Jahnert S, Kuhbandner K, Landreth G, Lonnemann N, Löschmann PA, McManus RM, Paulus A, Reemst K, Sanchez-Caro JM, Tiberi A, Van der Perren A, Vauthney A, Venegas C, Webers A, Weydt P, Wijasa TS, Xiang X, Yang Y (2017) Targeting neuroinflammation to treat Alzheimer's disease. CNS Drugs, 31: 1057-1082. doi: 10.1007/s40263-017-0483-3
- ATDSR (2018) Substance Priority List. https://www.atsdr.cdc.gov/spl/resources/index.html (accessed June 10, 2019)
- Aude N, Kenna KP, Renton AE, Ticozzi N, et al., (2018) Genome-wide analyses identify KIF5A as a novel ALS gene. Neuron, 97: 1268-1283. doi: 10.1016/j.neuron.2018.02.027
- Aureli M, Samarani M, Loberto N, Bassi R, Murdica V, Prioni S, Prinetti A, Sonnino S (2014) The glycosphingolipid hydrolases in the central nervous system. Mol Neurobiol 50: 76-87. doi: 10.1007/s12035-013-8592-6
- Babula P, Masarik M, Adam V, Eckschlanger T, Stiborova M, Trnkova L, Skutkova H, Provaznik I, Hubalek J and Kizek R (2012) Mammalian metallothioneins: properties and functions. Metallomics, 4: 739-750. doi: 10.1039/c2mt20081c
- Barna J, Csermely P, Vellai T (2018) Roles of heat shock factor 1 beyond the heat shock response. Cellular and Molecular Life Sciences 75: 2897-2916. doi: 10.1007/s00018-018-2836-6
- Bar-Sela S, Reingold S, Richter ED (2001) Amyotrophic lateral sclerosis in a battery-factory worker exposed to cadmium. Int J Occup Environ Health 7: 109-112. doi:10.1179/107735201800339470
- Biasiotto G, Di Lorenzo D, Archetti S, Zanella I (2016) Iron and neurodegeneration: Is ferritinophagy the link? Mol Neurobiol, 53: 5542-5574. doi: 10.1007/s12035-015-9473-y
- Bocca B, Pino A, Alimonti A, Forte G (2014) Toxic metals contained in cosmetics: A status report. Reg Toxicol Pharmacol, 68: 447-467. doi: 10.1016/j.yrtph.2014.02.003
- Böhm KJ (2014) Kinesin-dependent motility generation as target mechanism of cadmium intoxication. Toxicology Letters 224: 356-361. doi: 10.1016/j.toxlet.2013.11.004
- Böhm KJ (2017) Toxic effects of zinc ions on kinesin – Potential molecular cause of impaired intracellular transport. Toxicology Letters 268: 58-62. doi: 10.1016/j.toxlet.2017.01.013
- Bonham RT, Fine MR, Pollock FM, Shelden EA (2003) Hsp27, Hsp70, and metallothioneins in MDCK and LLC-PK1 renal epithelial cells: effects of prolonged exposure to cadmium. Toxicol Appl Pharmacol 191: 63-73. doi: 10.1016/s0041-008x(03)00226-6

- Callegaro G, Forcella M, Melchioretto P, Frattini A, Gribaldo L, Fusi P, Fabbri M, Urani C (2018) Toxicogenomics applied to *in vitro* Cell Transformation Assay reveals mechanisms of early response to cadmium. Toxicol in Vitro, 48: 232-243. doi: 10.1016/j.tiv.2018.01.025
- Calvo A, Canosa A, Bertuzzo D, Cugnasco P, Solero L, Clerico M, De Mercanti M, Bersano E, Cammarosano S, Ilardi A, Manera U, Moglia C, Marinou K, Bottacchi E, Pisano F, Mora G, Mazzini L, Chiò A (2016) Influence of cigarette smoking on ALS outcome: a population-based study. J Neurol Neurosurg Psychiatry, 87: 1229-1233. doi: 10.1136/jnnp-2016-313793
- Chang J, Baloh RH, Mildbrandt J (2009) The NIMA-family kinase Nek3 regulates microtubule acetylation in neurons. Journal of Cell Science, 122: 2274-2282. doi: 10.1242/jcs.048975
- Chen QY, DesMarais T, Costa M (2019) Metals and mechanisms of carcinogenesis. Ann Rev Pharmacol Toxicol 59: 537-554. doi: 10.1146/anurev-pharmtox-010818-021031
- Cheung Y-T, Lau WK-W, Yu M-S, Lai CS-W, Yeung S-C, So K-F, Chang RC-C (2009) Effects of all-*trans*-retinoic acid on human SH-SY5Y neuroblastoma as *in vitro* model in neurotoxicity research. NeuroToxicol, 30: 127-135. doi: 10.1016/j.neuro.2008.11.001
- Choi S, and Bird AJ (2014) Zinc'ing sensibly: controlling zinc homeostasis at the transcriptional level. Metallomics doi: 10.1039/c4mt00064a
- Choong G, Liu Y, Templeton DM (2014) Interplay of calcium and cadmium in mediating cadmium toxicity. Chemico-Biol Interac, 211: 54-65. doi: 10.1016/j.cbi.2014.01.007
- Fabbri M, Urani C, Sacco MG, Procaccianti C, Gribaldo L (2012) Whole genome analysis and microRNAs regulation in HepG2 cells exposed to cadmium. ALTEX, 29: 173-182. doi: 10.14573/altex.2012.2.173
- Forcella M, Callegaro G, Melchioretto P, Gribaldo L, Frattini M, Stefanini FM, Fusi P, Urani C (2016) Cadmium-transformed cells in the in vitro cell transformation assay reveal different proliferative behaviours and activated pathways. Toxicol in Vitro, 36: 71-80. doi: 10.1016/j.tiv.2016.07.006
- Gajdosechova Z, Brownlow A, Cottin NT, Fernandes M, Read FL, Urgast DS, Raab A, Feldmann J, Krupp EM (2016) Possible link between Hg and Cd accumulation in the brain of long-finned pilot whales (*Globicephala melas*). Sc Total Environ, 545-546: 407-413. doi: 10.1016/j_scitotenv.2015.12082
- Gokey T, Hang B, Guliaev AB (2016) Cadmium(II) inhibition of human uracil-DNA glycosylase by catalytic water supplantation. Scientific Reports, 6: 39137. doi: 10.1038/srep39137
- Hagmeyer S, Cristòväo JS, Mulvhill JJE, Boeckers T, Gomes CM, Grabrucker AM (2018) Zinc binding to S100B affords regulation of trace metal homeostasis and excitotoxicity in the brain. Front Mol Neurosci 10: 456 doi: 10.3389/fnmol.2017.00456
- Han SG, Castranova V, Vallyathan V (2007) Comparative cytotoxicity of cadmium and mercury in a human bronchial epithelial cell line (Beas-2B) and its role in oxidative stress and induction of heat shock protein 70. J Toxicol Environ Health A, 70: 852-860. doi: 10.1080/15287390701212695

- Hartwig A (2018) Cadmium and its impact on genomic stability. In “Cadmium interaction with animal cells“ Thévenod et al., Eds., Chapter 5, pagg 107-125. doi: 10.1007/978-3-319-89623-6
- Hartwig A, and Jahnke G (2017) Toxic metals and metalloids in food. In “Chemical contaminants and residues in food” second edition (Screnk D and Cartus A, Eds.), Chapter 10, pages 209-222. doi: 10.1016/B978-0-08-100674-0.00010-2
- He G, Xu W, Tong L, Li S, Su S, Tan X, Li C (2016) Gadd45b prevents autophagy and apoptosis against rat cerebral neuron oxygen-glucose deprivation/reperfusion injury. Apoptosis 21: 390-403. doi: 10.1007/s10495-016-1213-x
- Hung J-J, Cheng T-J, Chang MD-T, Chen K-D, Huang H-L, Lai Y-K (1998) Involvement of heat shock elements and basal transcription elements in the differential induction of the 70kDa heat shock protein and its cognate by cadmium chloride in 9L rat brain tumor cells. J Cell Biochem 71: 21-35.
- Joerger AC and Fersht AR (2016) The p53 pathway: Origins, inactivation in cancer, and emerging therapeutic approaches. Annu. Rev. Biochem, 85: 375-404. 10.1146/annurev-biochem-060815-014710
- Kalmar B, Lu C-H, Greensmith L (2014) The role of heat shock proteins in Amyotrophic Lateral Sclerosis: The therapeutic potential of Arimoclomol. Pharmacology & Therapeutics, 141: 40-54. doi: 10.1016/j.pharmthera.2013.08.003
- Karunasinghe N, Masters J, Flanagan JU, Ferguson LR (2017) Influence of aldo-keto reductase 1C3 in prostate cancer – A mini review. Current Cancer Drug Targets, 17: 603-616. doi: 10.2174/1568009617666170330115722
- Kawata K, Kubota S, Eguchi T, Aoyama E, Moritani NH, Oka M, Kawaki H, Tagigawa M (2017) A tumor suppressor gene product, platelet-derived growth factor receptor-like protein controls chondrocyte proliferation and differentiation. Journal of Cellular Biochemistry, 118: 4033-4044. doi: 10.1002/jcb.26059
- Kimura T and Kambe T (2016) The functions of metallothioneins and ZIP and ZnT transporters: An overview and perspective. International Journal of Molecular Sciences, 17: 336-357. doi: 10.3390/ijms17030336
- Klejnot M, Falnikar A, Ulaganathan V, Cross RA, Baas PW, Kozielski F (2014) The crystal structure and biochemical characterization of Kif15: a bifunctional molecular motor involved in bipolar spindle formation and neuronal development. Acta Crystallographica, D70: 123-133. doi: 10.1107/S1399004713028721
- Kohli V, Nardini N, Ehrman LA, Waclaw RR (2018) Characterization of Glcci1 expression in a subpopulation of lateral ganglionic eminence progenitors in the mouse telencephalon. Dev Dyn 247: 222-228. doi: 10.1002/dvdy.24556
- Kostenko S, Jensen KL, Moens U (2014) Phosphorylation of heat shock protein 40 (Hsp40/DnaJB1) by mitogen-activated protein kinase-activated protein kinase 5

(MK5/PRAK). The International Journal of Biochemistry and Cell Biology, 47: 29-37. doi: 10.1016/j.biocel.2013.11.004

- Kozlowski H, Kolkowska P, Watly J, Krzywoszynska K, Potocki S (2014) General aspects of metal toxicity. Curr Med Chem 21: 3721-3740.
- Kusakabe T, Nakajima K, Nakazato K, Suzuki S, Takada H, Satoh T, Oikawa M, Arakawa K, Nagamine T (2008) Changes of heavy metal, metallothioneins and heat shock proteins in Sertoli cells induced by cadmium. Toxicol in Vitro 22: 1469-1475. doi: 10.1016/j.tiv.2008.04.021
- Ingre C, Roos PM, Piehl F, Kamel F, Fang F (2015) Risk factors for amyotrophic lateral sclerosis. Clin Epidemiol, 7: 181-193. doi: 10.2147/CLEP.S37505
- Landry GM, Furrow E, Holmes HL, Hirata T, Kato A, Williams P et al., (2019) Cloning, function, and localization of human, canine, and *Drosophila* ZIP10 (SLC39A10), a Zn^{2+} transporter. Am J Renal Physiol 316: F263-F273. doi: 10.1152/ajprenal.00573.2017
- Lee B-K, Kim SH, Kim N-S, Ham J-O, Kim Yh (2014) Iron deficiency increases blood cadmium levels in adolescents surveyed in KNHANES 2010-2011. Biol Trace Elem Res, 159: 52-58. doi: 10.1007/s12011-014-9982-y
- Li C, Wang X, Casal I, Wang J, Li P, Zhang W, Xu E, Lai M, Zhang H (2016) Growth differentiation factor 15 is a promising diagnostic and prognostic biomarker in colorectal cancer. Journal Cell and Molecular Medicine, 20: 1420-1426. doi: 10.1111/jcmm.12830
- Lin J, Chung S, Ueda K, Matsuda K, Nakamura Y, Park J-H (2017) GALNT6 stabilizes GRP78protein by O-glycosylation and enhances its activity to suppress apoptosis under stress condition. Neoplasia, 19: 43-53. doi: 10.1016/j.neo.2016.11.007
- Liu X-H, Wang Z-J, Jin L, Huang J, Pu D-Y, Wand D-S, Zhang Y-G (2017) Effects of subchronic exposure to waterborne cadmium on H-P-I axis hormones and related genes in rare minnows (*Gobiocypris rarus*). Comparative Biochemistry and Physiology, Part C 202: 1-11. doi: 10.1016/j.cbpc.2017.07.002
- Lovejoy DB and Guillemin GJ (2014) The potential for transition metal-mediated neurodegeneration in amyotrophic lateral sclerosis. Frontiers in Aging Neuroscience, 6 article 173, 13 pages doi: 103389/fnagi.2014.00173
- Luparello C, Sirchia R, Longo A (2011) Cadmium as a transcriptional modulator in human cells. Crit Rev Toxicol 41: 73-80. doi: 10.3109/10408444.2010.529104
- Maetzler W, Deleersnijder W, Hanssens V, Bernard A, Brockmann K, Marquetand J, Wurster I, Rattay TW, Roncoroni L, Schaeffer E, Lerche S, Apel A, Deuschle C, Berg D (2016) GDF15/MIC1 and MMP9 cerebrospinal fluid levels in Parkinson's disease and Lewy body dementia. PLoS ONE 11(3): e0149349. doi:10.1371/journal.pone.0149349
- Maret W and Moulis J-M (2013) The bioinorganic chemistry of cadmium in the context of its toxicity. In "Cadmium: From toxicity to essentiality – Metal Ions in Life Sciences" (Sigel A, Sigel H, and Sigel RKO Eds.), Chapter 1, pages 1-29. doi: 10.1007/978-94-007-51798_1

- Méndez-Armenta M and Rìos C (2007) Cadmium neurotoxicity. Environmental Toxicology and Pharmacology, 23: 350-358. 10.1016/j.etap.2006.11.009
- Nicolas A, Kenna KP, Renton AE, Ticozzi N, Faghri F, Chia R, Dominov JA, Kenna BJ, Nalls MA, Keagle P, Rivera AM, van Rheenen W, Murphy NA, van Vugt JJFA, Geiger JT, Van der Spek RA, Pliner HA, Shankaracharya, Smith BN, Marangi G, Topp SD, Abramzon Y, Gkazi AS, Eicher JD, Kenna A; ITALSGEN Consortium, Mora G, Calvo A, Mazzini L, et al., (2018) Genome-wide analyses identify KIF5A as a novel ALS gene. Neuron, 97: 1268-1283. doi: 10.1016/j.neuron.2018.02.027
- Ohana E, Sekler I, Kaisman T, Kahn N, Cove J, Silverman WF, Amsterdam A, Hershfinkel M (2006) Silencing of ZnT-1 expression enhances heavy met influx and toxicity. J Mol Med 84: 753-763. doi: 10.1007/s00109-006-0062-4
- Pamphlett R, Bishop DP, Jew SK, Doble PA (2018) Age-related accumulation of toxic metals in the human locus ceruleus. PLOS One, 13(9): e0203627. doi 10.1371/journal.pone.0203627
- Pan YB, Zhan CH, Wang SQ, Ai PH, Chen K, Zhu L, Sun ZL, Feng DF (2018) Transforming growth factor beta induced (TGFBI) is a potential signature gene for mesenchymal subtype high-grade glioma. Journal of Neurooncology, 137: 395-407. doi: 10.1007/s11060-017-2729-9
- Park JW, Lee SH, Woo G-H, Kwon H-J, Kim D-Y (2018) Downregulation of TXNIP leads to high proliferative activity and estrogen-dependent cell growth in breast cancer. Biochemical and Biophysical Research Communications, 498: 566-572. doi: 10.1016/j.bbrc.2018.03.020
- Phani S, Jablonski M, Pelta-Heller J, Cai J, Iacovitti L (2013) Gremlin is a novel VTA derived neuroprotective factor for dopamine neurons. Brain Research 1500: 88-98. doi: 10.1016/j.brainres.2013.01.017
- Planells-Palop V, Hazazi A, Feichtinger J, Jezkova J, Thallinger G, Olsiwiheri NO, et al., (2017) Human germ/stem cell-specific gene *TEX19* influences cancer cell proliferation and cancer prognosis. Molecular Cancer, 16: 84-101. doi: 10.1186/s12943-017-0653-4
- Prakash A, Bharti K, Bakar A, Majeed ABA (2015) Zinc: indications in brain disorders. Fundamental & Clinical Pharmacology, 29: 131-149. doi: 10.1111/fcp.12110 Qureshi M, Brown Jr RH, Rogers JT, Cudkowicz ME (2008) Serum ferritin and metal levels as risk factors for amyotrophic lateral sclerosis. The Open Neurology Journal, 2: 51-54. doi: 10.2174/1874205X00802010051
- Roos PM, Vesterberg O, Syversen T, Flaten TP, Nordberg M (2013) Metal concentrations in cerebrospinal fluid and blood plasma from patients with amyotrophic lateral sclerosis. Biol Trace Elem Res, 151: 159-170. doi: 10.1007/s12011-012-9547-x
- Rossi A, Trotta E, Brandi R, Arisi I, Coccia M, Santoro MG (2010) *AIRAP,* a new human heat shock gene regulated by heat shock factor 1. Journal of Biological Chemistry, 285: 13607-13615. doi: 10.1074/jbc.M109.082693

- Rossi S, Serrano A, Gerbino V, Giorgi A, Di Francesco L, Nencini M, Bozzo F, Schininà ME, Bagni C, Cestra G, Carrì MT, Achsel T, Cozzolino M (2015) Nuclear accumulation of mRNAs underlies G4C2-repeat-induced translational repression in a cellular model of *C9orf72* ALS. J Cell Sci, 128: 1787-1799. doi: 10.1242/jcs.165332
- Sanfilippo C, Longo A, Lazzara F, Cambria D, Distefano G, Palumbo M, Cantarella A, Malaguarnera I, Di Rosa M (2017) *Chi3L1* and *CHI3L2* overexpression in motor cortex and spinal cord of sALS patients. Molecular and Cellular Neuroscience 85: 162-169. doi: 10.1016/j.mcn.2017.10.001
- Sarchielli E, Pacini S, Morussi G, Punzi T, Marini M, Vannelli GB, Gulisano M (2012) Cadmium induces alterations in the human spinal cord morphogenesis. Biometals 25: 63-74. doi: 10.1007/s10534-011-9483-9
- Satarung S and Moore MR (2004) Adverse health effects of chronic exposure to low-level cadmium in foodstuff and cigarette smoke. Environ Health Persp 112: 1099-1103. doi: 10.1289/ehp.6751
- Sheykhansari S, Kozielski K, Bill J, Sitti M, Gemmati D, Zamboni P and Singh AV (2018) Redox metals homeostasis in multiple sclerosis and amyotrophic lateral sclerosis: a review. Cell Death & Disease 9: 348-363. doi: 10.1038/s41419-018-0379-2
- Smyth, GK. (2004) Linear models and empirical bayes methods for assessing differential expression in microarray experiments. Stat Appl Genet Mol Biol 3, Article3. doi:10.2202/1544-6115.1027
- Soo KY, Atkin JD, Farg M, Walker AK, Horne MK, Nagley P (2012) Bim links ER stress and apoptosis in cells expressing mutant SOD1 associate with amyotrophic lateral sclerosis. PLoS ONE 7(4): e35413. doi: 10.1371/journal.pone.0035413
- Sunderman, FW Jr (2001) Nasal toxicity, carcinogenicity, and olfactory uptake of metals. Ann Clin Lab Sci, 31: 3-24.
- Syk-Mazurek SB, SB, Fernandes KA, Wilson MP, Shrager P, and Libby RT (2017) Together JUN and DDIT3 (CHOP) control retinal ganglion cell death after axonal injury. Molecular Neurodegeneration, 12: 71-84. doi: 10.1186/s13024-017-0214-8
- Urani C, Melchioretto P, Gribaldo L (2010) Regulation of metallothioneins and ZnT-1 transporter expression in human hepatoma cells HepG2 exposed to zinc and cadmium. Toxicol In Vitro, 24: 370-374. doi: 10.1016/j.tiv.2009.11.003
- Urani C, Melchioretto P, Canevali C, Morazzoni F, Gribaldo L (2007) Metallothionein and hsp70 expression in HepG2 cells after prolonged cadmium exposure. Toxicol. In Vitro 21: 314-319. doi: 10.1016/j.tiv.2006.08.014
- Urani C, Melchioretto P, Bruschi M, Fabbri M, Sacco MG, Gribaldo L (2015) Impact of Cadmium on Intracellular Zinc Levels in HepG2 Cells: Quantitative Evaluations and Molecular Effects. Biomed Res Int, article ID 949514, pages 1-11. doi: 10.1155/2015/949514
- Wang B and Du Y (2013) Cadmium and its neurotoxic effects. Oxidative Medicine and Cellular Longevity, Article ID 898034, 12 pp. doi: 10.1155/2013/898034

- Wang M-D, Little J, Gomes J, Cashman NR, Krewski D (2017) Identification of risk factors associated with onset and progression of amyotrophic lateral sclerosis using systematic review and meta-analysis. NeuroToxicol, 61: 101-130. doi: 10.1016/j.neuro.2016.06.015
- Xu B, Chen S, Luo Y, Chen Z, Liu L, Zhou H, Chen W, Han X, Chen L, Huang S (2011) Calcium signaling is involved in cadmium-induced neuronal apoptosis via induction of reactive oxygen species and activation of MAPK/mTOR network. PLoS ONE 64: e19052 doi: 10.1371/journal.pone.0019052.
- Yeom S-Y, Nam D-H, Park C (2014) RRAD promotes EGFR-mediated STAT3 activation and induces Temozolomide resistance of malignant glioblastoma. Molecular Cancer Therapeutics, 13: 3049-3061. doi: 10.1158/1535-7163.MCT-14-0244
- Zhang Z, Hao C-J, Li C-G, Zang D-J, Zhao J, Li X-N, Wei A-H, Wei Z-B, Yang L, Zhen X-C, Gao X, Speakman JR, Li W (2014) Mutation of SLC35D causes metabolic syndrome by impairing dopamine signaling in striatal D1 neurons. PLOS Genetics 10: e1004124. doi: 10.1371/journal.pgen.1004124
- Zimmer DB, Chaplin J, Baldwin A, Rast M (2005) S100-mediated signal transduction in the nervous system and neurological diseases. Cellular and Molecular Biology, 51: 201-214

Supplementary

Table 10.1S. One-way ANOVA of gene expression changes at two concentrations of cadmium chloride in LogFC

Gene	C10	C20	AveExpr	F statistic value	P.Value	adj.P.Val	Description
MT1M	9,71	9,92	11,63	2933,37627	1,01E-09	2,61E-05	metallothionein 1M
MT1X	7,11	7,53	13,10	1140,07147	1,72E-08	7,53E-05	metallothionein 1X
MT1F	7,10	7,37	11,71	1021,05166	2,40E-08	8,98E-05	metallothionein 1F
MT1L	7,04	7,43	13,96	1681,188	5,36E-09	3,84E-05	metallothionein 1L (gene/pseudogene)
MT1HL1	6,95	7,42	13,45	1515,4634	7,33E-09	3,84E-05	Metallothionein 1H-like protein 1
MT1B	6,74	7,25	13,66	2336,76535	1,99E-09	2,61E-05	metallothionein 1B
ENST00000567054	6,63	7,02	10,45	1568,61367	6,61E-09	3,84E-05	NA
HMOX1	6,08	7,26	12,29	300,938368	9,28E-07	0,001731748	heme oxygenase (decycling) 1
MT2A	5,42	5,45	15,06	774,275103	5,50E-08	0,000160204	metallothionein 2A
MT1A	4,92	5,29	14,89	824,119568	4,56E-08	0,00014948	metallothionein 1A
GADD45B	4,82	7,05	9,13	464,071108	2,55E-07	0,000545108	growth arrest and DNA-damage-inducible, beta
MT1E	3,95	4,15	9,27	643,569989	9,57E-08	0,000250941	metallothionein 1E
ZFAND2A	3,64	5,20	10,00	156,440534	6,47E-06	0,006524353	zinc finger, AN1-type domain 2A
TEX19	3,47	4,15	8,55	206,040107	2,86E-06	0,003753672	testis expressed 19
GDF15	3,24	4,22	11,51	226,22906	2,17E-06	0,002993824	growth differentiation factor 15
AKR1C3	2,94	3,14	9,50	228,184774	2,11E-06	0,002993824	aldo-keto reductase family 1, member C3 (3-alpha hydroxysteroid dehydrogenase, type II)
TGFBI	2,90	3,59	8,35	113,991715	1,64E-05	0,013115332	transforming growth factor, beta-induced, 68kDa

MT1G	2,70	3,36	7,17	61,0783969	0,00010053	0,034682665	metallothionein 1G
HSPA1A	2,67	4,38	11,94	171,190293	4,96E-06	0,005651168	heat shock 70kDa protein 1A
HSPA6	2,53	4,36	7,82	454,94865	2,70E-07	0,000545108	heat shock 70kDa protein 6 (HSP70B')
RRAD	2,53	4,24	7,40	265,41965	1,35E-06	0,00208082	Ras-related associated with diabetes
HSPA1B	2,29	4,10	12,08	100,625577	2,37E-05	0,014428639	heat shock 70kDa protein 1B
DNAJB1	2,23	3,57	10,53	288,112061	1,06E-06	0,001731748	DnaJ (Hsp40) homolog, subfamily B, member 1
DDIT3	2,21	3,45	7,76	455,79828	2,69E-07	0,000545108	DNA-damage-inducible transcript 3
S100A2	1,98	2,91	8,16	289,591039	1,04E-06	0,001731748	S100 calcium binding protein A2
ZNF165	1,96	3,23	7,97	73,747117	5,84E-05	0,026555804	zinc finger protein 165
MLC1	1,93	3,92	6,78	123,771732	1,29E-05	0,010910173	megalencephalic leukoencephalopathy with subcortical cysts 1
SLC30A1	1,85	1,82	8,48	111,669724	1,74E-05	0,013115332	solute carrier family 30 (zinc transporter), member 1
TNFSF9	1,84	2,67	6,34	70,1096944	6,76E-05	0,026908221	tumor necrosis factor (ligand) superfamily, member 9
ANXA1	1,80	2,50	7,07	102,391445	2,25E-05	0,014039758	annexin A1
CRLF1	1,80	2,53	9,01	179,177828	4,33E-06	0,005162278	cytokine receptor-like factor 1
IL33	1,76	2,50	7,13	65,6295774	8,18E-05	0,030185338	interleukin 33
BMX	1,73	2,20	6,73	146,387928	7,87E-06	0,007643074	BMX non-receptor tyrosine kinase
LINC00942	1,65	1,98	6,71	107,931956	1,93E-05	0,014039 15	NA
VAMP5	1,62	1,68	8,45	72,5542878	6,12E-05	0,026758556	vesicle-associated membrane protein 5 (myobrevin)
CCDC172	1,58	1,92	8,01	73,5787431	5,88E-05	0,026555804	Coiled-Coil Domain Containing 172
GNRH2	1,56	2,12	6,75	112,324168	1,71E-05	0,013115332	gonadotropin-releasing hormone 2
LINC00892	1,46	2,02	6,13	104,363409	2,13E-05	0,014039758	NA

GADD45G	1,46	2,95	7,93	83,8746951	4,02E-05	0,019900516	growth arrest and DNA-damage-inducible, gamma
CNIH3	1,45	2,07	7,00	70,4810714	6,66E-05	0,026908221	cornichon homolog 3 (Drosophila)
SLC30A2	1,45	1,84	6,33	131,560782	1,08E-05	0,009421853	solute carrier family 30 (zinc transporter), member 2
DUSP13	1,44	1,59	6,13	70,4592995	6,66E-05	0,026908221	dual specificity phosphatase 13
CU692082	1,42	2,73	9,10	106,755892	1,99E-05	0,014039758	NA
AJ252276	1,40	2,57	6,49	195,287551	3,36E-06	0,004190739	NA
AKR1C1	1,39	1,42	6,61	92,4163554	3,03E-05	0,016922653	aldo-keto reductase family 1, member C1 (dihydrodiol dehydrogenase 1; 20-alpha (3-alpha)-hydroxysteroid dehydrogenase)
IFRD1	1,37	1,79	8,37	50,2215322	0,00017575	0,049025169	interferon-related developmental regulator 1
AGRP	1,37	2,05	7,07	140,523834	8,88E-06	0,008027401	agouti related protein homolog (mouse)
XRCC4	1,34	1,71	8,04	71,2771788	6,45E-05	0,026908221	X-ray repair complementing defective repair in Chinese hamster cells 4
SERTAD1	1,33	2,77	10,87	63,7049111	8,91E-05	0,031691269	SERTA domain containing 1
OR8B8	1,32	1,88	7,58	68,9066357	7,11E-05	0,027810656	olfactory receptor, family 8, subfamily B, member 8
ZNF316	1,30	1,56	6,86	90,2926879	3,25E-05	0,017022155	Zinc Finger Protein 316
ARHGDIB	1,29	2,08	7,96	111,536678	1,75E-05	0,013115332	Rho GDP dissociation inhibitor (GDI) beta
CRYAB	1,15	2,44	6,69	58,4263822	0,00011416	0,037417706	crystallin, alpha B
ENST00000428055	1,14	2,00	6,04	163,411007	5,69E-06	0,006030439	NA
NUPR1	1,13	1,67	6,15	73,169698	5,98E-05	0,026555804	nuclear protein, transcriptional regulator, 1
FTL	1,13	1,92	12,64	99,4789025	2,45E-05	0,014580907	ferritin, light polypeptide

TRIB3	1,11	2,22	12,29	85,2845733	3,83E-05	0,019323964	tribbles homolog 3 (Drosophila)
PPP1R27	1,09	2,39	6,42	60,5261238	0,00010318	0,035135668	protein phosphatase 1, regulatory subunit 27
PPP1R15A	1,07	2,95	7,82	104,995933	2,09E-05	0,014039758	protein phosphatase 1, regulatory subunit 15A
PLA2G16	1,07	1,06	10,34	56,4708369	0,00012583	0,037925488	phospholipase A2, group XVI
FUT1	1,06	1,86	7,75	144,404882	8,19E-06	0,007672561	fucosyltransferase 1 (galactoside 2-alpha-L-fucosyltransferase, H blood group)
SYCE3	1,03	1,41	6,79	57,1940505	0,00012134	0,037687006	synaptonemal complex central element protein 3
C10orf35	1,02	1,54	10,33	49,8736206	0,00017925	0,049476003	chromosome 10 open reading frame 35
CCL15	1,02	1,76	6,88	102,597128	2,24E-05	0,014039758	chemokine (C-C motif) ligand 15
PLAC1	1,02	1,70	6,06	96,7605418	2,65E-05	0,015458328	placenta-specific 1
BTBD17	1,02	1,83	5,93	162,812866	5,75E-06	0,006030439	BTB (POZ) domain containing 17
DEDD2	1,01	2,28	9,24	95,5253541	2,75E-05	0,015700046	death effector domain containing 2
ADK	0,98	1,55	9,32	63,6158239	8,94E-05	0,031691269	adenosine kinase
EMP1	0,87	2,06	6,03	66,7130321	7,80E-05	0,029710392	epithelial membrane protein 1
BQ018844	0,84	1,68	5,84	86,9353139	3,62E-05	0,01863447	NA
SERPINB8	0,83	1,67	6,01	50,3242348	0,00017473	0,049025169	serpin peptidase inhibitor, clade B (ovalbumin), member 8
NQO1	0,82	1,28	7,23	71,1725213	6,47E-05	0,026908221	NAD(P)H dehydrogenase, quinone 1
COL14A1	0,82	1,29	6,01	56,8250188	0,00012361	0,037687006	collagen, type XIV, alpha 1
RGS16	0,81	1,50	9,01	91,2615374	3,15E-05	0,017022155	regulator of G-protein signaling 16
BAG3	0,80	1,83	6,85	65,3215107	8,29E-05	0,030185338	BCL2-associated athanogene 3
LY6K	0,78	1,57	5,82	50,4994012	0,00017302	0,049025169	lymphocyte antigen 6 complex, locus K
GCGR	0,73	1,46	6,08	70,063366	6,77E-05	0,026908221	glucagon receptor

WNT11	0,69	1,57	5,67	75,3386017	5,49E-05	0,025861792	wingless-type MMTV integration site family, member 11
L1CAM	0,67	1,28	6,34	54,8953935	0,00013642	0,040649584	L1 cell adhesion molecule
ADAP1	0,66	1,83	6,87	90,8893859	3,18E-05	0,017022155	ArfGAP with dual PH domains 1
ENST00000432823	0,65	1,27	6,66	61,4893483	9,86E-05	0,034475443	NA
ARL14EPL	0,63	1,28	5,44	57,045369	0,00012225	0,037687006	ADP Ribosylation Factor Like GTPase 14 Effector Protein Like
SNTG2	0,50	1,38	5,53	57,3005422	0,0001207	0,037687006	syntrophin, gamma 2
DUSP1	0,46	1,23	8,15	58,4877078	0,00011382	0,037417706	dual specificity phosphatase 1
HSPA1L	0,44	1,29	6,06	56,8266047	0,0001236	0,037687006	heat shock 70kDa protein 1-like
KIF15	-0,42	-1,09	7,79	57,4032177	0,00012008	0,037687006	kinesin family member 15
PDGFRL	-0,51	-1,53	7,13	75,1870684	5,52E-05	0,025861792	platelet-derived growth factor receptor-like
LOC642366	-0,53	-1,24	9,92	49,5161687	0,00018295	0,049970328	uncharacterized LOC642366
TXNIP	-0,65	-1,77	10,21	102,719688	2,23E-05	0,014039758	thioredoxin interacting protein
UNG	-0,72	-1,00	10,92	51,0775074	0,00016751	0,048267377	uracil-DNA glycosylase
NEK3	-0,77	-1,28	6,99	52,6880002	0,00015335	0,045180638	NIMA (never in mitosis gene a)-related kinase 3
GALNT6	-0,82	-1,48	8,29	58,5499091	0,00011347	0,037417706	UDP-N-acetyl-alpha-D-galactosamine:polypeptide N-acetylgalactosaminyltransferase 6 (GalNAc-T6)
GLCCI1	-0,84	-1,42	8,22	66,6607567	7,82E-05	0,029710392	glucocorticoid induced transcript 1
SLC39A10	-0,88	-1,07	6,28	51,7429939	0,00016146	0,047040057	solute carrier family 39 (zinc transporter), member 10
GREM2	-1,02	-1,32	6,26	80,5217315	4,53E-05	0,021988176	gremlin 2
SLC35D3	-1,41	-2,15	7,43	65,6530468	8,17E-05	0,030185338	solute carrier family 35, member D3

Table 10.2S. KEGG pathways and individual ranks attributed by each method

KEGG.pathway	p.value	p.adj
p53 signaling pathway	0,00525071	0,04827266
Mineral absorption	2,47E-07	7,03E-05
Glycosphingolipid biosynthesis - globo series	0,0030785	0,04827266
Basal cell carcinoma	0,00525071	0,04827266
Endometrial cancer	0,00109454	0,03466032
Other types of O-glycan biosynthesis	1,22E-05	0,00173792
Lysine degradation	0,02473284	0,14685123
Aminoacyl-tRNA biosynthesis	0,05649969	0,21469881
Chronic myeloid leukemia	0,00025981	0,01480927
Legionellosis	0,05870768	0,21781846
Spliceosome	2,47E-05	0,00234734
Riboflavin metabolism	0,01647909	0,11741351
Complement and coagulation cascades	0,00401506	0,04827266
Thyroid cancer	0,00525071	0,04827266
DNA replication	0,03570263	0,17947859
Biosynthesis of amino acids	0,0213319	0,1349358
MicroRNAs in cancer	0,00525071	0,04827266
Proteasome	0,03539822	0,17947859
Primary bile acid biosynthesis	0,00312985	0,04827266
Cell cycle	0,00207235	0,04827266
Notch signaling pathway	0,0077676	0,06708381
mRNA surveillance pathway	0,01383631	0,11235451
Allograft rejection	0,02055491	0,13313978
Autoimmune thyroid disease	0,03436	0,17947859
SNARE interactions in vesicular transport	0,05961347	0,21781846
Glutathione metabolism	0,06652991	0,22844609
Fanconi anemia pathway	0,01992966	0,13209196
Colorectal cancer	0,00415498	0,04827266
Glycosylphosphatidylinositol(GPI)-anchor biosynthesis	0,08254799	0,23419013
Ubiquinone and other terpenoid-quinone biosynthesis	0,10974673	0,24896242
Graft-versus-host disease	0,01551788	0,11339989
RNA degradation	0,04297022	0,19438908
Insulin signaling pathway	0,01419215	0,11235451
Bacterial invasion of epithelial cells	0,02729347	0,15252233
Intestinal immune network for IgA production	0,01745695	0,12134707

Phosphatidylinositol signaling system	0,11908382	0,24896242
RNA transport	0,01548413	0,11339989
Non-small cell lung cancer	0,00525071	0,04827266
Wnt signaling pathway	0,03709095	0,17947859
Endocytosis	0,0370914	0,17947859
Cysteine and methionine metabolism	0,03715522	0,17947859
HIF-1 signaling pathway	0,09869196	0,24458443
Shigellosis	0,14429294	0,24896242
Amino sugar and nucleotide sugar metabolism	0,07126163	0,23419013
Hedgehog signaling pathway	0,01477996	0,11339989
Glioma	0,00525071	0,04827266
Phenylalanine, tyrosine and tryptophan biosynthesis	0,07254505	0,23419013
Fc gamma R-mediated phagocytosis	0,10327182	0,24737929
Circadian rhythm	0,16142537	0,25259201
Renal cell carcinoma	0,19517685	0,2587228
Prostate cancer	0,05202249	0,21423606
Central carbon metabolism in cancer	0,11069018	0,24896242
Mismatch repair	0,08641081	0,23419013
Acute myeloid leukemia	0,00678764	0,06045242
Epstein-Barr virus infection	0,07331502	0,23419013
Neurotrophin signaling pathway	0,12183378	0,24896242
Toxoplasmosis	0,10379807	0,24737929
Homologous recombination	0,12831858	0,24896242
Inositol phosphate metabolism	0,15223581	0,24896242
Non-homologous end-joining	0,07096523	0,23419013
2-Oxocarboxylic acid metabolism	0,05277669	0,21423606
Thyroid hormone signaling pathway	0,00049996	0,02374831
Melanogenesis	0,00525071	0,04827266
Carbon metabolism	0,05450977	0,21423606
Rheumatoid arthritis	0,02268061	0,13753135
Chemical carcinogenesis	0,1069149	0,24896242
Adherens junction	0,00058585	0,02385227
Pancreatic cancer	0,00525071	0,04827266
N-Glycan biosynthesis	0,07281647	0,23419013
Metabolism of xenobiotics by cytochrome P450	0,0807146	0,23419013
Estrogen signaling pathway	0,00525071	0,04827266
Oxytocin signaling pathway	0,11459114	0,24896242

AMPK signaling pathway	0,02177911	0,1349358
Choline metabolism in cancer	0,0836505	0,23419013
MAPK signaling pathway	0,00525071	0,04827266
Herpes simplex infection	0,08188051	0,23419013
Arachidonic acid metabolism	0,186794	0,2559437
Arginine and proline metabolism	0,05562621	0,21423606
Melanoma	0,00525071	0,04827266
cGMP-PKG signaling pathway	0,13868838	0,24896242
Selenocompound metabolism	0,21049526	0,27022173
Adipocytokine signaling pathway	0,13130425	0,24896242
GnRH signaling pathway	0,00525071	0,04827266
Staphylococcus aureus infection	0,13925788	0,24896242
Signaling pathways regulating pluripotency of stem cells	0,14776301	0,24896242
Antigen processing and presentation	0,18430478	0,2546032
Galactose metabolism	0,08602144	0,23419013
Endocrine and other factor-regulated calcium reabsorption	0,11542042	0,24896242
Pathways in cancer	0,14394975	0,24896242
Steroid hormone biosynthesis	0,05187933	0,21423606
Protein export	0,07932739	0,23419013
Fc epsilon RI signaling pathway	0,00525071	0,04827266
Base excision repair	0,13961445	0,24896242
Pentose phosphate pathway	0,0871023	0,23419013
HTLV-I infection	0,13204983	0,24896242
Biosynthesis of unsaturated fatty acids	0,21307683	0,27022173
Cholinergic synapse	0,12670297	0,24896242
Glucagon signaling pathway	0,24392739	0,29209792
Apoptosis	0,00525071	0,04827266
Sphingolipid signaling pathway	0,15637376	0,25029705
ErbB signaling pathway	0,11486707	0,24896242
Ubiquitin mediated proteolysis	0,13924012	0,24896242
Transcriptional misregulation in cancer	0,1092214	0,24896242
Small cell lung cancer	0,16362405	0,25259201
Ribosome biogenesis in eukaryotes	0,04287116	0,19438908
Pentose and glucuronate interconversions	0,1931927	0,25728934
Glycolysis / Gluconeogenesis	0,10069783	0,24737929
TGF-beta signaling pathway	0,14465908	0,24896242

Hepatitis B	0,12478877	0,24896242
Chemokine signaling pathway	0,13318509	0,24896242
Prolactin signaling pathway	0,17457235	0,25259201
Valine, leucine and isoleucine degradation	0,19706261	0,26001317
Drug metabolism - cytochrome P450	0,21591937	0,27022173
Regulation of actin cytoskeleton	0,17289638	0,25259201
Protein processing in endoplasmic reticulum	0,00012778	0,00910441
Glycosaminoglycan degradation	0,09233154	0,2383394
Glycosaminoglycan biosynthesis - chondroitin sulfate / dermatan sulfate	0,09327667	0,2383394
Hippo signaling pathway	0,15821714	0,25051047
Hepatitis C	0,14105294	0,24896242
Type I diabetes mellitus	0,02604226	0,14844086
Gap junction	0,21686196	0,27022173
Influenza A	0,1041597	0,24737929
Glycerophospholipid metabolism	0,14436134	0,24896242
Histidine metabolism	0,31865703	0,3522572
Alanine, aspartate and glutamate metabolism	0,15546827	0,25029705
cAMP signaling pathway	0,18297911	0,2546032
NF-kappa B signaling pathway	0,20839664	0,27022173
Axon guidance	0,24055866	0,29050516
Glycosphingolipid biosynthesis - ganglio series	0,06885482	0,23361456
Proteoglycans in cancer	0,18222889	0,2546032
Sulfur relay system	0,04202981	0,19438908
mTOR signaling pathway	0,24760384	0,29402956
Phenylalanine metabolism	0,11206731	0,24896242
Synaptic vesicle cycle	0,02589236	0,14844086
Cytokine-cytokine receptor interaction	0,1792503	0,2546032
Vitamin digestion and absorption	0,05451621	0,21423606
Insulin secretion	0,23780387	0,28858101
Morphine addiction	0,12898461	0,24896242
Fructose and mannose metabolism	0,13067557	0,24896242
Purine metabolism	0,12820972	0,24896242
Epithelial cell signaling in Helicobacter pylori infection	0,11482174	0,24896242
Regulation of autophagy	0,17459869	0,25259201
Arrhythmogenic right ventricular cardiomyopathy (ARVC)	0,31353995	0,3522572
Progesterone-mediated oocyte maturation	0,16275591	0,25259201

Asthma	0,03113202	0,16941738
Renin-angiotensin system	0,09590332	0,23975829
B cell receptor signaling pathway	0,20432097	0,26711686
Pantothenate and CoA biosynthesis	0,05904644	0,21781846
Systemic lupus erythematosus	0,05494306	0,21423606
Gastric acid secretion	0,43483336	0,45899077
Pancreatic secretion	0,21153418	0,27022173
Pathogenic Escherichia coli infection	0,1403571	0,24896242
Thiamine metabolism	0,14673935	0,24896242
Pyruvate metabolism	0,13561917	0,24896242
Viral carcinogenesis	0,14950752	0,24896242
Porphyrin and chlorophyll metabolism	0,29491616	0,33353613
Carbohydrate digestion and absorption	0,43263124	0,45836395
Neuroactive ligand-receptor interaction	0,21437856	0,27022173
Ras signaling pathway	0,14395021	0,24896242
Adrenergic signaling in cardiomyocytes	0,13862766	0,24896242
Alcoholism	0,37104389	0,40208179
Glycosaminoglycan biosynthesis - heparan sulfate / heparin	0,32012146	0,3522572
Non-alcoholic fatty liver disease (NAFLD)	0,01952766	0,13209196
Cytosolic DNA-sensing pathway	0,06596092	0,22844609
Dorso-ventral axis formation	0,38867294	0,41652315
Vasopressin-regulated water reabsorption	0,0936632	0,2383394
Folate biosynthesis	0,14969098	0,24896242
Starch and sucrose metabolism	0,06551937	0,22844609
Platelet activation	0,17326361	0,25259201
One carbon pool by folate	0,23795276	0,28858101
Fatty acid metabolism	0,36700292	0,40075031
FoxO signaling pathway	0,00525071	0,04827266
Phosphonate and phosphinate metabolism	0,08608651	0,23419013
Rap1 signaling pathway	0,1913215	0,25599356
Pertussis	0,14774522	0,24896242
Vascular smooth muscle contraction	0,25765187	0,30218429
Basal transcription factors	0,18165285	0,2546032
Cardiac muscle contraction	0,10360706	0,24737929
Glycosphingolipid biosynthesis - lacto and neolacto series	0,00525071	0,04827266
alpha-Linolenic acid metabolism	0,12435887	0,24896242

Maturity onset diabetes of the young	0,62055005	0,6316313
Glycosaminoglycan biosynthesis - keratan sulfate	0,15006789	0,24896242
Bladder cancer	0,00525071	0,04827266
VEGF signaling pathway	0,17712146	0,2546032
Dilated cardiomyopathy	0,18355332	0,2546032
Long-term depression	0,49856671	0,51858216
Glycine, serine and threonine metabolism	0,03896716	0,185094
Other glycan degradation	0,05280441	0,21423606
Glycerolipid metabolism	0,15720412	0,25029705
Measles	0,08505479	0,23419013
Proximal tubule bicarbonate reclamation	0,46532813	0,48578211
Citrate cycle (TCA cycle)	0,03150569	0,16941738
Pyrimidine metabolism	0,11301881	0,24896242
Bile secretion	0,08331535	0,23419013
Fatty acid biosynthesis	0,39855953	0,42542871
Aldosterone-regulated sodium reabsorption	0,70245521	0,70741956
Tyrosine metabolism	0,15256185	0,24896242
Circadian entrainment	0,17441566	0,25259201
Dopaminergic synapse	0,09558419	0,23975829
Oocyte meiosis	0,13297608	0,24896242
Phagosome	0,17148538	0,25259201
RNA polymerase	0,17060244	0,25259201
Lysosome	0,08673411	0,23419013
Mucin type O-Glycan biosynthesis	0,12406016	0,24896242
Natural killer cell mediated cytotoxicity	0,15036165	0,24896242
Cocaine addiction	0,08202201	0,23419013
Focal adhesion	0,24756848	0,29402956
Nucleotide excision repair	0,09227717	0,2383394
Toll-like receptor signaling pathway	0,09322382	0,2383394
Oxidative phosphorylation	0,00085457	0,03044413
Vibrio cholerae infection	0,14542213	0,24896242
Tryptophan metabolism	0,18820925	0,25599356
Sulfur metabolism	0,27582857	0,3157074
Huntington's disease	0,09135741	0,2383394
Ovarian steroidogenesis	0,21031701	0,27022173
Synthesis and degradation of ketone bodies	0,71296408	0,71547452
PI3K-Akt signaling pathway	0,14285485	0,24896242

Peroxisome	0,08639198	0,23419013
Inflammatory mediator regulation of TRP channels	0,18411467	0,2546032
Fatty acid elongation	0,17104664	0,25259201
Metabolic pathways	0,08145832	0,23419013
Ether lipid metabolism	0,18865804	0,25599356
beta-Alanine metabolism	0,19101501	0,25599356
Tight junction	0,15089743	0,24896242
Amoebiasis	0,21919928	0,2716165
Viral myocarditis	0,0633249	0,22559497
Leukocyte transendothelial migration	0,1999037	0,26254633
Salmonella infection	0,16592629	0,25259201
Fat digestion and absorption	0,38875494	0,41652315
NOD-like receptor signaling pathway	0,17292823	0,25259201
African trypanosomiasis	0,26501206	0,30578315
Nitrogen metabolism	0,31697271	0,3522572
Drug metabolism - other enzymes	0,25003806	0,29568816
Chagas disease (American trypanosomiasis)	0,15525642	0,25029705
Nicotine addiction	0,06157221	0,22212758
Leishmaniasis	0,07452855	0,23419013
Jak-STAT signaling pathway	0,17191093	0,25259201
Calcium signaling pathway	0,11875018	0,24896242
Amphetamine addiction	0,15287166	0,24896242
Cell adhesion molecules (CAMs)	0,18427826	0,2546032
Salivary secretion	0,26302101	0,30578315
Terpenoid backbone biosynthesis	0,35542054	0,3895956
Steroid biosynthesis	0,55049769	0,5684487
Phototransduction	0,41764335	0,44413565
Ascorbate and aldarate metabolism	0,38201988	0,41240782
Malaria	0,22663102	0,27960971
Long-term potentiation	0,45327558	0,47669203
Prion diseases	0,31854538	0,3522572
Type II diabetes mellitus	0,22814637	0,28026601
Glutamatergic synapse	0,19018148	0,25599356
Ribosome	0,0829876	0,23419013
Taste transduction	0,24193819	0,29093833
Parkinson's disease	0,00834864	0,06998124
Thyroid hormone synthesis	0,16714104	0,25259201

Taurine and hypotaurine metabolism	0,21553664	0,27022173
Hypertrophic cardiomyopathy (HCM)	0,23261545	0,28452963
Protein digestion and absorption	0,26497836	0,30578315
Serotonergic synapse	0,21189949	0,27022173
Vitamin B6 metabolism	0,27944978	0,3181326
TNF signaling pathway	0,11813559	0,24896242
T cell receptor signaling pathway	0,25931368	0,30288688
Collecting duct acid secretion	0,66942484	0,67895402
GABAergic synapse	0,04515669	0,20108839
Inflammatory bowel disease (IBD)	0,05455044	0,21423606
Retinol metabolism	0,25203128	0,2968137
Butanoate metabolism	0,05513529	0,21423606
Tuberculosis	0,13470703	0,24896242
Hematopoietic cell lineage	0,46182053	0,48389283
Alzheimer's disease	0,11619792	0,24896242
RIG-I-like receptor signaling pathway	0,12931346	0,24896242
Olfactory transduction	0,61861787	0,6316313
Osteoclast differentiation	0,21712553	0,27022173
Linoleic acid metabolism	0,26989794	0,31016498
Primary immunodeficiency	0,575344	0,59196043
Nicotinate and nicotinamide metabolism	0,89914189	0,89914189
PPAR signaling pathway	0,54885193	0,5684487
Propanoate metabolism	0,31643502	0,3522572
Retrograde endocannabinoid signaling	0,18492232	0,2546032
ABC transporters	0,16920288	0,25259201
Amyotrophic lateral sclerosis (ALS)	0,31946843	0,3522572
Sphingolipid metabolism	0,16465101	0,25259201
Glyoxylate and dicarboxylate metabolism	0,28017994	0,3181326
Butirosin and neomycin biosynthesis	0,36975059	0,40208179
ECM-receptor interaction	0,58244167	0,59710747
Fatty acid degradation	0,68851887	0,69584354

Table 10.3S. KEGG pathways and individual ranks attributed by each method

KEGG pathways	p.value	p.adj
Fanconi anemia pathway	1,12E-05	0,00106057
Mineral absorption	1,46E-07	4,17E-05
p53 signaling pathway	0,00117542	0,03183941
Legionellosis	0,00525071	0,03183941
Rheumatoid arthritis	0,00140025	0,03183941
Homologous recombination	0,00525071	0,03183941
Glycosphingolipid biosynthesis - globo series	0,00059473	0,0242141
Cell cycle	0,00020634	0,00980122
Antigen processing and presentation	0,00525071	0,03183941
Endometrial cancer	0,00525071	0,03183941
Chronic myeloid leukemia	0,00181279	0,03183941
Lysine degradation	0,01340178	0,06393485
Colorectal cancer	0,00525071	0,03183941
Other types of O-glycan biosynthesis	0,00525071	0,03183941
Thyroid cancer	0,00525071	0,03183941
Complement and coagulation cascades	0,00119431	0,03183941
Arachidonic acid metabolism	0,04147603	0,12061905
Riboflavin metabolism	0,0034425	0,03183941
Selenocompound metabolism	0,00525071	0,03183941
RNA degradation	0,05700431	0,13288458
Wnt signaling pathway	0,00525071	0,03183941
Histidine metabolism	0,01684419	0,07742893
Hedgehog signaling pathway	0,05674414	0,13288458
Prostate cancer	0,00525071	0,03183941
Non-small cell lung cancer	0,00525071	0,03183941
Non-homologous end-joining	0,03663046	0,1151377
SNARE interactions in vesicular transport	0,05824827	0,13288458
RNA transport	0,0035742	0,03183941
Mismatch repair	0,00403428	0,03183941
Porphyrin and chlorophyll metabolism	0,01122086	0,05710617
Chemical carcinogenesis	0,04054936	0,12038092
Protein processing in endoplasmic reticulum	7,70E-07	0,00010978
Spliceosome	0,00011466	0,0065356

Toxoplasmosis	0,04481122	0,12493339
Ubiquitin mediated proteolysis	0,08167849	0,15018304
MicroRNAs in cancer	0,00610463	0,03624623
Phosphatidylinositol signaling system	0,0966969	0,16178549
Base excision repair	0,00963752	0,05182442
Basal cell carcinoma	0,10897457	0,16560238
Valine, leucine and isoleucine degradation	0,02458434	0,08758171
Aminoacyl-tRNA biosynthesis	0,00525071	0,03183941
Pancreatic cancer	0,00525071	0,03183941
Pentose and glucuronate interconversions	0,0225799	0,08564671
Acute myeloid leukemia	0,00525071	0,03183941
Butanoate metabolism	0,02006808	0,08353923
Adherens junction	0,02038334	0,08353923
Cytokine-cytokine receptor interaction	0,02407888	0,08686686
Inositol phosphate metabolism	0,08280745	0,15128284
DNA replication	0,01883614	0,08353923
Influenza A	0,00525071	0,03183941
Steroid hormone biosynthesis	0,02135874	0,08454502
MAPK signaling pathway	0,00091011	0,03183941
Apoptosis	0,00361371	0,03183941
beta-Alanine metabolism	0,02000468	0,08353923
Glutathione metabolism	0,01005756	0,05239124
Fatty acid metabolism	0,05483673	0,13288458
Biosynthesis of unsaturated fatty acids	0,04140615	0,12061905
Notch signaling pathway	0,09147456	0,16159352
Glucagon signaling pathway	0,00525071	0,03183941
Staphylococcus aureus infection	0,05870517	0,13288458
Insulin signaling pathway	0,06063584	0,13500949
Glioma	0,00525071	0,03183941
Melanoma	0,00525071	0,03183941
Thyroid hormone signaling pathway	0,00818135	0,04701907
Primary bile acid biosynthesis	0,00128347	0,03183941
Glycosylphosphatidylinositol(GPI)-anchor biosynthesis	0,19582035	0,23548017
FoxO signaling pathway	0,00184517	0,03183941
Intestinal immune network for IgA production	0,02230455	0,08564671

mRNA surveillance pathway	0,10446989	0,1646963
Pentose phosphate pathway	0,03181937	0,10566958
Bladder cancer	0,00525071	0,03183941
Choline metabolism in cancer	0,07800692	0,1475445
Phagosome	0,0184556	0,0834896
HTLV-I infection	0,00457522	0,03183941
Arginine and proline metabolism	0,0420879	0,12116215
Hematopoietic cell lineage	0,0428686	0,12217552
Phenylalanine, tyrosine and tryptophan biosynthesis	0,02324673	0,08564671
Metabolism of xenobiotics by cytochrome P450	0,06471401	0,13587126
Progesterone-mediated oocyte maturation	0,06847564	0,13727252
Pathogenic Escherichia coli infection	0,14815399	0,19548096
ErbB signaling pathway	0,00525071	0,03183941
Amino sugar and nucleotide sugar metabolism	0,11659457	0,16867743
Hippo signaling pathway	0,04998669	0,13190933
Prion diseases	0,01345997	0,06393485
Cysteine and methionine metabolism	0,0764084	0,14615029
Small cell lung cancer	0,1072196	0,16560238
Protein export	0,06248274	0,13587126
Vibrio cholerae infection	0,08360108	0,15175993
Pathways in cancer	0,07968559	0,1475445
Pantothenate and CoA biosynthesis	0,03676326	0,1151377
Drug metabolism - other enzymes	0,02264402	0,08564671
Graft-versus-host disease	0,17254971	0,21427148
Renal cell carcinoma	0,11829582	0,17027428
Phenylalanine metabolism	0,02344015	0,08564671
Collecting duct acid secretion	0,02081153	0,08353923
Circadian rhythm	0,07476133	0,14615029
Neurotrophin signaling pathway	0,00525071	0,03183941
Signaling pathways regulating pluripotency of stem cells	0,10226615	0,16445436
Central carbon metabolism in cancer	0,0090902	0,04982129
Mucin type O-Glycan biosynthesis	0,06887709	0,13727252
Dorso-ventral axis formation	0,05778095	0,13288458
Transcriptional misregulation in cancer	0,06546427	0,13587126
AMPK signaling pathway	0,11258365	0,16625046

Synthesis and degradation of ketone bodies	0,00525071	0,03183941
Natural killer cell mediated cytotoxicity	0,03001189	0,10182605
cGMP-PKG signaling pathway	0,12162129	0,1732775
Melanogenesis	0,00525071	0,03183941
Glycosphingolipid biosynthesis - lacto and neolacto series	0,00525071	0,03183941
Drug metabolism - cytochrome P450	0,07619391	0,14615029
Adipocytokine signaling pathway	0,05118631	0,13261907
Pertussis	0,08680228	0,15558898
Tryptophan metabolism	0,01337449	0,06393485
Estrogen signaling pathway	0,0020809	0,03183941
Glycerolipid metabolism	0,05797451	0,13288458
Propanoate metabolism	0,04556136	0,12493339
Shigellosis	0,12281423	0,1732775
Fc gamma R-mediated phagocytosis	0,15800402	0,20376084
mTOR signaling pathway	0,02820683	0,09685478
Ovarian steroidogenesis	0,09468813	0,16159352
Oxytocin signaling pathway	0,05257381	0,13288458
Peroxisome	0,03434061	0,11121676
Autoimmune thyroid disease	0,0202802	0,08353923
Glycosphingolipid biosynthesis - ganglio series	0,12691389	0,17558475
One carbon pool by folate	0,00525071	0,03183941
Gap junction	0,09289625	0,16159352
Cell adhesion molecules (CAMs)	0,04485164	0,12493339
Pyrimidine metabolism	0,12384148	0,17386612
Serotonergic synapse	0,0663696	0,13587126
Allograft rejection	0,03902227	0,11958437
Epithelial cell signaling in Helicobacter pylori infection	0,05217559	0,13288458
Hepatitis B	0,05884488	0,13288458
Ubiquinone and other terpenoid-quinone biosynthesis	0,39392018	0,4204766
Other glycan degradation	0,03978596	0,12038092
Long-term potentiation	0,06645574	0,13587126
Morphine addiction	0,06316628	0,13587126
GnRH signaling pathway	0,09783321	0,16178549
Amphetamine addiction	0,04040872	0,12038092
Tyrosine metabolism	0,02529776	0,08901065

Proteoglycans in cancer	0,05326651	0,13288458
Osteoclast differentiation	0,03795632	0,11758207
Prolactin signaling pathway	0,11156371	0,16560238
Asthma	0,15016317	0,19631423
Vascular smooth muscle contraction	0,13282648	0,181319
Ribosome	0,09447945	0,16159352
Neuroactive ligand-receptor interaction	0,09397818	0,16159352
Bacterial invasion of epithelial cells	0,20004343	0,23755157
Retinol metabolism	0,02317991	0,08564671
Proteasome	0,26056838	0,29469043
Axon guidance	0,12119061	0,1732775
Cholinergic synapse	0,11018189	0,16560238
Primary immunodeficiency	0,01196018	0,05980091
Maturity onset diabetes of the young	0,23736594	0,27277941
Amyotrophic lateral sclerosis (ALS)	0,05921523	0,13288458
Nucleotide excision repair	0,15431804	0,20082484
Type I diabetes mellitus	0,38138785	0,40862983
Malaria	0,03188626	0,10566958
Galactose metabolism	0,07481181	0,14615029
Cytosolic DNA-sensing pathway	0,06722052	0,13587126
Fatty acid elongation	0,01974021	0,08353923
Protein digestion and absorption	0,16098993	0,20667626
Arrhythmogenic right ventricular cardiomyopathy (ARVC)	0,23930168	0,27389951
Pyruvate metabolism	0,0618303	0,13587126
Glycine, serine and threonine metabolism	0,2368637	0,27277941
HIF-1 signaling pathway	0,11470502	0,1676458
Terpenoid backbone biosynthesis	0,1801802	0,22134205
Fatty acid degradation	0,04587984	0,12493339
Sphingolipid signaling pathway	0,20879517	0,2438796
Glycosaminoglycan biosynthesis - heparan sulfate / heparin	0,33908241	0,36884918
Adrenergic signaling in cardiomyocytes	0,09820663	0,16178549
RNA polymerase	0,46268027	0,48301786
Regulation of autophagy	0,10271185	0,16445436
Oocyte meiosis	0,11075905	0,16560238
Alanine, aspartate and glutamate metabolism	0,00525071	0,03183941

Epstein-Barr virus infection	0,01448885	0,06769382
Lysosome	0,16630978	0,21027834
Oxidative phosphorylation	0,11043611	0,16560238
Endocrine and other factor-regulated calcium reabsorption	0,21965741	0,25551985
Fc epsilon RI signaling pathway	0,09806237	0,16178549
Ribosome biogenesis in eukaryotes	0,06716898	0,13587126
Purine metabolism	0,13785515	0,1852729
Folate biosynthesis	0,10004002	0,16280344
Tuberculosis	0,04982109	0,13190933
Hypertrophic cardiomyopathy (HCM)	0,06298752	0,13587126
Dilated cardiomyopathy	0,10545667	0,1651382
ECM-receptor interaction	0,35728701	0,38570757
Steroid biosynthesis	0,25510515	0,28966123
TGF-beta signaling pathway	0,18186921	0,22245804
Cocaine addiction	0,1045966	0,1646963
Ascorbate and aldarate metabolism	0,01011059	0,05239124
PI3K-Akt signaling pathway	0,05418051	0,13288458
Regulation of actin cytoskeleton	0,12222175	0,1732775
Herpes simplex infection	0,09583491	0,16178549
Basal transcription factors	0,19872047	0,23755157
PPAR signaling pathway	0,14926847	0,19604384
Inflammatory mediator regulation of TRP channels	0,08514472	0,15358384
2-Oxocarboxylic acid metabolism	0,12490386	0,17449803
Viral myocarditis	0,27547789	0,30549105
Endocytosis	0,10404705	0,1646963
Thyroid hormone synthesis	0,09459515	0,16159352
B cell receptor signaling pathway	0,16674704	0,21027834
Chemokine signaling pathway	0,09421964	0,16159352
cAMP signaling pathway	0,11333228	0,1664933
Toll-like receptor signaling pathway	0,03501162	0,11211588
Synaptic vesicle cycle	0,40544661	0,43116524
Glycosaminoglycan biosynthesis - chondroitin sulfate / dermatan sulfate	0,29883119	0,32665184
Non-alcoholic fatty liver disease (NAFLD)	0,13753882	0,1852729
NF-kappa B signaling pathway	0,20120674	0,23794158
RIG-I-like receptor signaling pathway	0,03229715	0,10580101

VEGF signaling pathway	0,13573721	0,18421478
Jak-STAT signaling pathway	0,06671353	0,13587126
Butirosin and neomycin biosynthesis	0,05067426	0,13249692
Proximal tubule bicarbonate reclamation	0,27708421	0,30608139
Taurine and hypotaurine metabolism	0,13217886	0,181319
Salmonella infection	0,0797258	0,1475445
Circadian entrainment	0,00525071	0,03183941
Platelet activation	0,1939176	0,23517666
Measles	0,04602809	0,12493339
Tight junction	0,11152209	0,16560238
Phototransduction	0,00825176	0,04701907
Carbohydrate digestion and absorption	0,7077166	0,7203544
NOD-like receptor signaling pathway	0,02645529	0,09194827
Calcium signaling pathway	0,11073991	0,16560238
Rap1 signaling pathway	0,12610924	0,1753226
Leukocyte transendothelial migration	0,22505203	0,26073101
African trypanosomiasis	0,07950215	0,1475445
Leishmaniasis	0,19550203	0,23548017
Citrate cycle (TCA cycle)	0,16883721	0,21197624
Sphingolipid metabolism	0,11155059	0,16560238
Fructose and mannose metabolism	0,02076666	0,08353923
N-Glycan biosynthesis	0,44992828	0,4749243
Biosynthesis of amino acids	0,19963861	0,23755157
Gastric acid secretion	0,26268885	0,29591431
Inflammatory bowel disease (IBD)	0,13296726	0,181319
Metabolic pathways	0,09930494	0,16265464
Taste transduction	0,14403	0,19102817
TNF signaling pathway	0,05735106	0,13288458
Chagas disease (American trypanosomiasis)	0,06671024	0,13587126
ABC transporters	0,04777064	0,12843992
Pancreatic secretion	0,29914432	0,32665184
Starch and sucrose metabolism	0,06690407	0,13587126
Olfactory transduction	0,57169508	0,592484
Hepatitis C	0,07829153	0,1475445
Parkinson's disease	0,45242764	0,47580029

Glycosaminoglycan biosynthesis - keratan sulfate	0,26920641	0,29987652
T cell receptor signaling pathway	0,0758429	0,14615029
Vasopressin-regulated water reabsorption	0,26936276	0,29987652
Ras signaling pathway	0,07623999	0,14615029
Carbon metabolism	0,14410897	0,19102817
Thiamine metabolism	0,35390589	0,38351019
Cardiac muscle contraction	0,24334657	0,27741509
Renin-angiotensin system	0,10053827	0,16280344
Dopaminergic synapse	0,11569918	0,16823606
Vitamin digestion and absorption	0,82367461	0,83539952
Retrograde endocannabinoid signaling	0,09700912	0,16178549
Nicotinate and nicotinamide metabolism	0,68041738	0,70006842
Phosphonate and phosphinate metabolism	0,17037257	0,21296571
Insulin secretion	0,13846712	0,1852729
Viral carcinogenesis	0,00841394	0,04701907
Glycolysis / Gluconeogenesis	0,08977008	0,15990295
Glyoxylate and dicarboxylate metabolism	0,68724133	0,70202072
Amoebiasis	0,18727611	0,2280927
Fatty acid biosynthesis	0,35865487	0,38572317
Salivary secretion	0,17551823	0,21654847
Type II diabetes mellitus	0,17292084	0,21427148
Bile secretion	0,16437875	0,21008046
Huntington's disease	0,20758074	0,24345889
Focal adhesion	0,1558888	0,20194685
GABAergic synapse	0,11003023	0,16560238
Aldosterone-regulated sodium reabsorption	0,46686698	0,48560982
Alcoholism	0,00010182	0,0065356
Long-term depression	0,20465895	0,24102397
Fat digestion and absorption	0,41492063	0,43959993
alpha-Linolenic acid metabolism	0,45955602	0,48152009
Systemic lupus erythematosus	0,05684105	0,13288458
Glycerophospholipid metabolism	0,26860279	0,29987652
Alzheimer's disease	0,29074158	0,31992799
Glutamatergic synapse	0,16655226	0,21027834
Sulfur relay system	0,05495002	0,13288458

Nicotine addiction	0,68701124	0,70202072
Vitamin B6 metabolism	0,05829622	0,13288458
Glycosaminoglycan degradation	0,57388245	0,59259601
Ether lipid metabolism	0,98265847	0,98265847
Nitrogen metabolism	0,97428417	0,98116957
Linoleic acid metabolism	0,97943556	0,98265847
Sulfur metabolism	0,85750081	0,86662316

Chapter 11

11. Discussion

The identification of chemical hazards, the evaluation of their risks and the setting up of control measures to reduce chemical exposure for humans are all critical steps to secure the health and safety of the people. Hence, one of the goals of chemical risk assessment is a full understanding of the nature, magnitude and probability of potential adverse health or environmental effect of a chemical. In particular, the assessment of chemical carcinogenesis, also for innovative drug development, is one of the crucial issues for modern society that uses several chemical compounds daily and it is characterised by a dramatic environmental pollution. In this context, the principal aim of this thesis was to obtain a better knowledge of carcinogenesis induced by cadmium, especially using alternative methods to animal experimentation. Indeed, Cd is a source of occupational and environmental concerns, due to its spread in all environmental compartments (air, soil and water), its many adverse effects in almost all living species; and, especially for humans, its extremely long biological half-life in the body and the absence of proven effective treatments for chronic Cd intoxication. Furthermore, Cd has been classified as a human carcinogen by the World Health Organization's International Agency for Research on Cancer and the United States National Toxicology Program. Thus, to study the mechanisms underpinning Cd-induced carcinogenesis, that are still largely unknown, we have chosen to use the Cell Transformation Assay (CTA), one of the most advanced in vitro tests for screening the potential chemical carcinogens. CTA was used not only because it can provide useful information on the steps of chemical carcinogenesis, but also because it is one of the building blocks of the IATA approaches in the 3Rs context. In this respect one of the aims of this thesis was to improve the CTA towards a more quantitive test, with the biochemical characterisation and the transcriptome analysis of cells. These were performed both in the early stage of the transformation (after 24 hr treatment) and on completely transformed cells (the foci). In addition, two human cell lines, HepG2 and SHSY5Y, were used as models to understand the common and the tissue-specific mechanisms of action of Cd in liver and brain, respectively. In particular, in Chapter 9 and 10, the results of a whole-genome analysis of these two cell lines after treatment with two different sublethal concentrations of Cd are described. In this case,

one of the possible future perspectives can be a more in-depth biochemical characterisation of Cd effects in both the cell lines (see Paragraph 11.3).

The results of the three parts of this thesis are now summarised in three paragraphs. The first one (Paragraph 11.1) is a detailed description of the whole genome transcriptomic analyses of C3H cell lines after 24 hr of Cd treatment respect to the three foci; the second one (Paragraph 11.2) is a critical consideration of the early and late effects of Cd in carcinogenesis. The third paragraph (Paragraph 11.3) is a comparison between the transcription analyses in two Cd target organs: liver and brain.

11.1 Differentially expressed genes (DEGs) after Cd treatment in C3H cell lines and foci

To understand the early events responsible for Cd carcinogenesis, and to evaluate the events maintained until the end of the transformation process, the identity of several DEGs was analysed through microarray-based toxicogenomics in different conditions. For example, in the investigation of the early phases of carcinogenesis, at first, we used a single $CdCl_2$ concentration (1 µM $CdCl_2$) and different times of exposure (Callegaro et al., 2018), subsequently, we used two different Cd concentrations in a 24 hr treatment (Chapter 5). In more details, Callegaro et al. (2018) used cells exposed to complete medium for 24 or 48 hr as control samples (CTR24-48), cells exposed to 1 µM Cd for 24 hr and harvested as Cd24, cells treated for 24 h with 1 µM Cd and collected after 24 h of recovery in control medium (Cd24R), and cells treated for 24 h with 1 µM Cd and collected after 48 h of recovery in control medium (Cd48R). In Chapter 5, we treated cells with 1 and 2 µM $CdCl_2$ for 24 hr and used cells exposed to complete medium for 24 hr as a control. Results showed that, after 24 hr of treatment, 1 µM $CdCl_2$ is able to induce the upregulation of the same genes (only 13) in both the experiments. These genes are Mt2, Mt1, Gm10639, Pip5k1a, Prl2c5, Gsta1, Gsta2, Gsta3, Gdf15, Ccr8, Slc30a1, Aldoc. Among these, Mt1 gene and the three genes coding for three isoforms of glutathione S-transferase (Gstα1–3) showed a remarkable upregulation in 24 hr $CdCl_2$ treated samples (Cd24). Furthermore, Mt2 and

Gstα3 genes were still upregulated after 24 hr recovery. These results indicated the importance of metal chelation and the response to oxidative stress set up soon after CdCl2 exposure, which was also confirmed by the biochemical characterisation presented in Paragraph 11.2. However, DEGs changed their number after 24 hr of recovery (47 DEGs were identified in the comparison Cd24R versus control), and after 48 hr of recovery (49 DEGs for the Cd48R versus control) with a different proportion of up- and downregulated genes. Notably, the majority of DEGs obtained during the recovery were downregulated and related with zinc homeostasis. The increasing number of dysregulated genes found after one of two days of recovery also demonstrated how Cd-induced carcinogenesis is a step process: although it was removed from the medium, Cd enhanced its effects on the transcriptome of treated cells with time. Consequently, if a perfect experiment were possible, in which transcriptomic analyses were carried out every day, it would be possible to understand which and how many genes were essential for each step of carcinogenesis. On the other hand, the treatment with 2 µM CdCl2 for 24 hr (Chapter 5) demonstrated that acute administration of this metal, although in a sublethal dose (IC50 = 8 in an MTT assay), was more toxic than 1 µM CdCl2. Indeed, around 2000 of DEGs were analysed after the treatment with a 2 µM CdCl2 respect the ca. 50 genes annotated after 48 hr of recovery. Among the 2000 DEGS, a high number of downregulated genes were related to the decrease of cell proliferation, a decrease of matrix cross-linking and to enhanced epithelial-mesenchymal transition (EMT) process. Also, we noticed the downregulation of genes involved in the PI3K-AKT signalling pathway and the down regulation of cyclin D (CycD) and Jun Proto- Oncogene (c-Jun). Hence, it seems be possible that Cd can lead to cell cycle arrest in C3H cell line and in this particular condition (also confirmed in preliminary results obtained with a cytoflex analysis, data not shown). In this regard, we have assumed that the cell cycle arrest induced by Cd was only transitional and it was not related to cell apoptosis. On the contrary, some cells that escaped cell cycle arrest could acquire elevated proliferative behaviours in the process of malignant transformation, leading to highly proliferative foci, like F1 *focus*. Furthermore, the cells seemed to lose their morphology, considering that a diverse group of cytoskeletal proteins, such as Vinculin, Actin, Actinin, Zyxin and Filamin, were down-regulated. More interestingly, the genes involved in mitochondrial functions were all upregulated, especially genes involved in OXPHOS, such as

ATP Synthase(ATP)5h, ATP5k, ATP5e, cytochrome c (Cycs), some NADH: Ubiquinone Oxidoreductase (NUDF) and Ubiquinol- Cytochrome C Reductase (UQCR). This result was the starting point of the biochemical analysis, reported in Paragraph 11.2. Several genes coding for proteins with Zinc finger (Znf) domains seem to be deregulated. In this purpose, some deeper analyses regarding the identification of genes condign for Zn-proteins are still ongoing. As a conclusion of these two works, Cd-induced carcinogenesis seems to involve the loss of the homeostasis of other divalent ions, such as Zn^{2+}, the new moonlighting activities of proteins, the deregulation of genes related to oxidative stress response and involved in rearrangements of the cytoskeleton. Mitochondria seems to be other important players in the early response against cadmium treatment. Thus, although just after the Cd treatment, most cells show efficient defense mechanisms, including metallothioneins and Hsp70 upregulation, we can speculate that a few cells, which are not able to fully neutralise the metal, can develop different metabolic alterations and become transformed foci at the end of CTA (Forcella et al., 2016). We also compared the lists of DEGs of three different fully transformed *foci* (F1, F2 and F3) looking for differences and similarities in transcriptome modifications. It was evident that a common stimulus (1 µM Cd for 24h) administered to the healthy C3H10T1/2 cells led to different cellular responses. However, among the 34 DEGs, common to all *foci*, most deregulated genes were mediators of inflammation, organ development, angiogenesis, and tumorigenesis. On the other hand, the most common downregulated DEGs code for proteins of the extracellular matrix or involved in cell growth. However, in F1 *focus*, a lot of upregulated genes are connected with an increase in cell growth and extracellular matrix rearrangement. Indeed, the ERK proliferative pathway is activated in F1 *focus*, while the survival pathway mediated by Akt is activated in F3 *focus* (Forcella et al., 2016). Moreover, F1 and F2 *foci* are more similar to each other than to F3 *focus*. In conclusion, the features of deregulated genes in all foci suggest that different proteins and/or processes are involved in the complex mechanism of cell transformation, but the control of the inflammatory response seems to be the most critical feature of Cd-induced cell transformation. In addition, in F3 *focus*, the inflammatory response appears to be related to mitochondrial damage.

11.2 Biochemical characterisation of foci and C3H after Cd treatment

On the basis of the transcriptomic analyses, we have chosen to investigate the role of oxidative stress and mitochondria in Cd-induced carcinogenesis. Moreover, since cells metabolism and mitochondrial functions are firmly connected, the Warburg effect was also studied. In particular, we analysed the same conditions of the transcriptomic analyses (C3H after 24 hr of treatment and foci), but, to study the early stage of carcinogenesis, we treated cells with 1 and 4 µM of CdCl2 for 24 hr, both sublethal doses of Cd (EC12 and EC25, respectively) for the C3H cell line. The choice of 4 µM CdCl2 was dictated by the need to intensify Cd effects in cells until their accurate detection in a multilevel approach. In this regard, many parameters and processes were analysed at different levels of biological organisation. For example, we have investigated the DNA damage with the comet assay, or the oxidative stress via the detection of reactive free oxygen species, the activity of the main detoxifying enzymes, and the identification of the reduced/oxidised glutathione ratio. As a result, we showed that Cd-induced carcinogenesis is connected with DNA damage, especially after the treatment with the highest Cd concentration (4 µM). Since Cd is not able to directly cause alterations in DNA structure or in the genetic information, DNA damage can be attributed to the oxidative stress induced by this metal. This is confirmed by the fact that Cd triggers the production of high levels of superoxide anion, which, transformed in hydroxyl radical through the Haber-Weiss reaction, can lead to DNA damage. This assumption is also supported by the discovery of the decreased activity of superoxide dismutase 1, the main enzyme responsible for the detoxification of superoxide anion. We also investigated mitochondrial damage after Cd treatment. Results showed that, although no difference in mitochondrial coupling between electron transport and ATP synthesis was observed in F1 focus, Cd increased basal mitochondrial respiration, ATP production and mitochondrial spare respiratory capacity. However, the enhanced mitochondrial metabolic efficiency was not connected with an increase in lactate production or *Krebs cycle* functionality. In this regard, the analysis of the activity of enzymes involved in the tricarboxylic acid (TCA) cycle showed that they were mostly downregulated (Figure 11.1).

Figure 11.1. Glycolytic metabolism and Krebs cycle enzymes activities in C3H cells after Cd treatment for 24 hrs. Results are expressed as Fold respect to control and are shown as mean ± SEM obtained in three independent experiments. Statistically significant: * $p < 0.05$ (Dunnett's test).

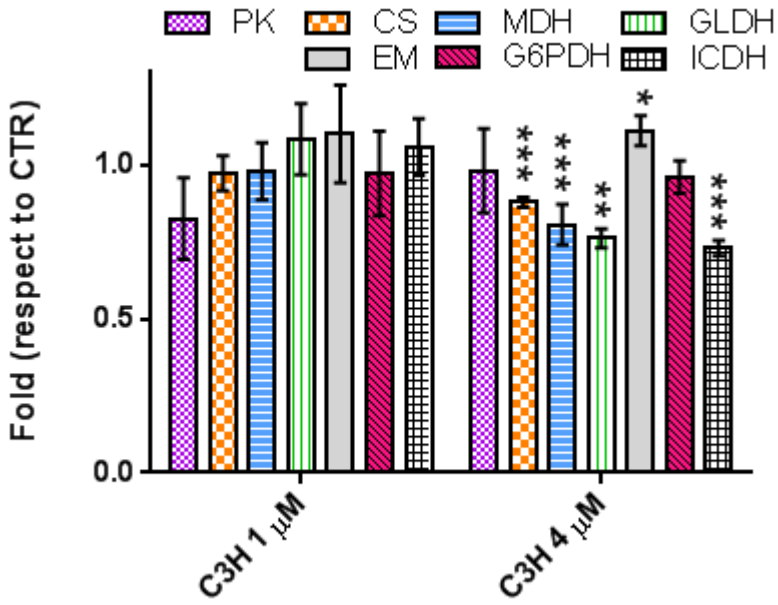

Consequently, we have assumed that the higher efficiency of mitochondrial respiration could not be related with the Warburg effect, but to the change in morphology and subcellular localisation of these organelles, as observed by confocal microscopy. On the contrary, considering the alterations analysed in *focus* F1 and F3, we have shown that some of the modifications observed after 24 hr treatment were maintained. In F1 *focus*, we observed high glycolytic, TCA and OxPhos rates to sustain its higher proliferative rate. In addition, as shown in C3H after 24 hr Cd treatment, mitochondria were rearranged in networks around the nucleus. However, in F1 *focus*, in contrast to what observed in the early stages of transformation, the enhanced of mitochondrial metabolic efficiency was accompanied with an increase in lactate production. Thus, we supposed that F1 high glycolytic rate could support the synthesis of many essential metabolites. In F3 *focus*, glycolysis is hyperactivated to compensate the decreased mitochondrial ATP production, although it is less active (as

shown by lower PFKFB3, PKM2 and GAPDH expression), than in F1 *focus*, justifying F3 lower proliferation rate. Consequently, in a different way, both F1 and F3 *foci* show alterations in glycolysis, TCA and OxPhos. These observations suggest that mitochondrial functions modifications can be the most significant Cd effect in inducing carcinogenesis; however, after this early hazardous outcome, each cell can react in its own peculiar way to endure cadmium intoxication.

To conclude, other experiments are in progress to deepen our knowledge of Cd-induced damage on mitochondria. In more details, we are studying in all these cell lines and through flow cytometric analysis the production of superoxide anion and hydrogen peroxide at the level of these organelles.

11.3 Cd effects in human liver and brain

Whole-genome analyses were carried out in two different human cells lines. The first one, the human hepatoma cell line HepG2, was chosen to investigate the Cd effects in the liver; the neuroblastoma cell line SHSY5Y was selected to provide evidence of Cd neurotoxic mechanisms. In particular, we treated these two cell lines with the same dose of Cd (10 µM), and with a second Cd concentration to study the possible dose-effect of this metal on cells. HepG2 cell line being more sensitive than SHSY5Y cells to Cd treatment, a 20 µM CdCl2 concentration represents the EC50 for the HepG2 cell line and the EC25 for the SHSY5Y cell line. However, despite this different sensitivity, both cell lines showed the same response to the metal-induced stress, by activating heat shock proteins (Hsps) and metallothioneins (MTs). Indeed, independently from the stimulus, MTs and Hsps always represent the first line of defense against metals in general and oxidative damage. In particular, MTs are involved in the control of Zn and Cu homeostasis, while the heat shock proteins maintain proteostasis and restore perturbed protein homeostasis. However, if in the liver Cd-MT complexes seems to have a major role in the maintenance of metal homeostasis, in the brain, the perturbation of protein homeostasis and protein folding, aggregation and degradation may accelerate the development of proteotoxicity-triggered disorders and neurodegenerative diseases, including

ALS. At the same time, strictly linked to Cd effect discussed in Chapter 9 and 10 of this thesis, our results have demonstrated some Cd tissue-specific effects. For example, in SHSY5Y cell lines, we have seen the deregulation of the expression of genes involved in specific neuronal functions and pathways; and in HepG2 cell lines, all the pathways related with the specific function of the liver were downregulated. In both cases, Cd leads to the loss of specific cell functions in a tissue, and consequently, to their malignant transformation. In HepG2 cell lines, for example, this event was more evident: in fact, many genes related to the development of metastasis resulted upregulated. Moreover, the assumption that Cd causes metastatic features in the HepG2 was also supported by the detection of upregulated genes, like MMP, involved in the extracellular matrix organisation. Besides, our results on human SH-SY5Y neuronal cells confirmed that Cd induces the expression of genes involved in carcinogenesis even on brain-derived cells: Cd can activate p53 signalling pathway, as well as genes involved in tumour initiation and cancer cell proliferation, such as TEX19, AKR1C3, TGFB1, and RRAD, or can downregulate tumour suppressors genes or genes that encode for enzymes involved in the DNA repair. All these conditions create an environment susceptible to the development of cancer, as a possible cause of transformation from normal to malignant cells, and also from a primary tumor to metastasis. Besides, in order to obtain more information about the comparison between Cd effects in liver and brain, we carried out a preliminary analysis comparing the up or down-regulated genes in HepG2 and SHSY5Y cell lines. When we compared the modulation of gene expression after the higher dose Cd treatment, we observed that only two genes were downregulated in both the cell lines (C5 and KIF15). The first gene (complement C5) encodes a component of the complement system, a part of the innate immune system that plays an important role in inflammation, host homeostasis, and host defense against pathogens. The second one, the Kinesin Family Member 15, is a gene that encodes a motor protein involved in mitosis and the regulation of microtubule motor activity. Consequently, we can speculate that Cd effects, as regards to the downregulation of genes, is tissue-specific. On the other hand, concerning the results of upregulated genes, we obtained a list of 53 DEGs shared by the two cell lines (data not shown). Except for metallothioneins and heat shock proteins, which we referred to earlier, we identified GADD45B and GADD45G, as the most upregulated genes in both the cell lines. The Growth Arrest and

DNA Damage-inducible 45 (GADD45) genes, as GADD45B (originally termed MyD118), and GADD45G (originally termed CR6), encode proteins that are implicated in the regulation of many cellular functions including DNA repair, cell cycle control, senescence and genotoxic stress. Also, GADD45B and G are considered as tumour suppressors, that if damaged, can be related to the initiation and progression of malignancies. The upregulation of these two transcripts hence underlined and confirmed that Cd, among others, could lead to genotoxic stress and DNA damage that the cells need to repair (Paragraph 3.2.2). The same can be applied at PPP1R15A (Protein Phosphatase 1 Regulatory Subunit 15A), a gene whose transcript levels are increased following stressful growth arrest conditions and treatment with DNA-damaging agents; and PLK3 (Polo Like Kinase 3) that is implicated in stress responses and double-strand break repair. At the same time, the list of shared DEGs is composed of several genes that encode for proteins that have a role in metal homeostasis or that bind bivalent cation in their domains. First of all, RRAD and his paralog GEM that regulate voltage-dependent L-type calcium channel subunit alpha-1C trafficking to the cell membrane, as well as S100A2, S100A3 and S100A16 genes that encoded members of the S100 family of proteins with 2 EF-hand calcium-binding motifs. In addition, S100A3 is one of the S100 proteins with the highest content of cysteines and, consequently, has a high affinity for zinc. Still, we illustrated the upregulation of genes for moonlight proteins, such as CRYAB, called also Heat Shock Protein Beta-5. As concluding remarks, the toxicogenomics approach used in this thesis can be defined as an invaluable step for mechanistic studies. Indeed, the identification and the systematic analysis of up- and downregulated genes gave a quick and comprehensive vision of possible altered processes involved in metal (Cd)-induced cells deregulations. However, other experiments are needed to confirm transcriptomic results on these cell lines. For this reason, a possible future perspective of this research can be the experimental validation of the deregulation of some specific pathways.

Another future approach to understand cadmium-induced carcinogenesis could be studying in more details the transcription factors that are deregulated in all the cell lines after cadmium treatment. Indeed, although several pathways involved in cadmium-induced carcinogenesis have been reported and described in previous chapters of this thesis, the factors initiating these

pathways remain to be fully elucidated. To this purpose, toxicogenomic applicable methods could be protein/DNA-binding arrays and/or small interfering RNA (siRNA), but at the moment, we have exclusively extracted the name of known transcription factors and their targets by comparing the TRRUST database with the list of our DEGs. Furthermore, although they seem not to be present among the list of our deregulated transcription factors, two factors that are normally activated in response to cadmium intoxication are the nuclear factor erythroid 2-related factor 2 (Nrf2) and the metal-responsive transcription factor 1 (MTF-1). In more details, these two genes need to be to taken into consideration because Nrf2 is able to coordinate mammalian oxidative stress response, while MTF-1 induces metallothionein genes. Nrf2 expression level could be interesting also because its activation dramatically increases the transcriptional expression of genes such as those encoding heme oxygenase-1 (HMOX1), NAD(P)H quinone oxidoreductase (NQO1), and glutathione-S transferase A2 (GSTA2), that we have observed to be upregulated in C3H cell line. Indeed, all the products of these genes can neutralize reactive oxygen species and electrophiles, biosynthesize glutathione and recycle oxidized proteins to detoxify the cell. Moreover, Nrf2 activation has been demonstrated in response to a variety of metals, including cadmium, in HepG2 cell line. A possible explanation of the lack of Nrf2 in our list of DEGs could be that stabilization and activation of Nrf2 is not always connected with an increase of transcript of the Nrf2 gene; sometimes metal exposure can exert a positive effects on the Nrf2 pathway through the reduction of sulfhydryl groups in Keap-1, the protein that normally keeps Nrf2 inactive, MAPK activation and resultant Nrf2 phosphorylation, or the inhibition of proteasomal pathways. The cumulative impact of these events leads to the stabilization and activation of Nrf2 without changing the expression of this transcription factor. Naturally, all these hypotheses need to be verified. In addition, results obtained in kidney cells have suggested that the activation of Nrf2 is not only an adaptive intracellular response to cadmium-induced oxidative stress but also a protection against cadmium-induced apoptosis. On the other hand, MTF-1 can act as an intracellular zinc sensor, since in a competitive situation, it requires a higher zinc concentration for DNA binding/function than other zinc-binding factors. This suggests a molecular mechanism, which explains why MTF-1-dependent genes are transcriptionally activated by a zinc load. However, it was reported that the activity of mammalian MTF-1 expressed in Saccharomyces

cerevisiae was induced by zinc but not by cadmium nor H_2O_2. It was thus speculated that other stress conditions (except zinc load) that activate MTF-1 in vivo occur indirectly, by freeing zinc from intracellular stores. Consequently, the cadmium-induced increase of zinc concentration in the cytoplasm, which we have observed in our experiments may, therefore, be a possible explanation for MTF-1 activation.

To conclude, our present work, especially Chapter 5,6,7, and 8 has emphasised the relevance of the cell transformation assays (CTAs) not only as in vitro methods for the evaluation of the carcinogenesis potential of chemicals, but also as powerful tools for the comprehension of the mechanisms underlying the process of cell transformation. In particular, the combination of in vitro and the bioinformatic mechanistic-based approach of this work, along with the analysis of different cellular endpoints during the early and the late stage of transformation process is in agreement with the idea of the Integrated Approaches to Testing and Assessment (IATA). Further, the possibility of the identification of specific structures/processes deregulated in transformed cells represents another essential advantage of this approach; especially, if this information can be used as a starting point for the development of specific anti-tumour agents. In this context, the use of CTAs represents an invaluable tool to perform preliminary studies without the use of animals.